Experimental Investigation into a Passive Auto-Tuning Mass Damper for structural vibration control of a MDOF system

Elizabeth Nicole Naicker

A research report submitted to the Faculty of Civil and Environmental Engineering, University of the Witwatersrand, Johannesburg, in partial fulfilment of the requirements for the degree of Master of Science in Engineering.
13 October, 2016

The financial assistance of the National Research Foundation (NRF) towards this research is hereby acknowledged. Opinions expressed and conclusions arrived at, are those of the author and are not necessarily to be attributed to the NRF.

The copyright in this thesis is owned by the author. Any quotation from the thesis or use of any of the information contained in it must acknowledge this thesis as the source of the quotation or information.

DECLARATION

I declare that this research report is my own unaided work. It is being submitted to the Degree of Master of Science to the University of the Witwatersrand, Johannesburg. It has not been submitted before for any degree or examination to any other University.

.....

Elizabeth Nicole Naicker

13th day of October 2016

ABSTRACT

A Passive Auto-Tuning Mass Damper with Pulley connections (PATPD) is a vibration control device that consists of a box filled with silica sand on roller supports. The silica sand provides the mass of the damper. The PATPD is connected to the structure to be controlled by a group of ropes and pulleys; it is free to move in any translational direction. The pulleys and rope transfer a driving force to the damper, caused by the movement of the structure. The mass provides an inertial force which, in addition to the driving force of pulleys, dissipates energy providing the vibration control of the structure.

Firstly, the test model underwent 'PATPD Efficiency tests' where the model was subjected to free translational, torsional and coupled vibration both with and without damper. This procedure was then repeated for forced harmonic excitation and the control effect for both analysed. These tests aimed to demonstrate the effectiveness of the PATPD at controlling structural vibrations. The results indicate that the PATPD provided at least 99% reduction to first natural frequency Power Spectral Density (PSD) peak for all tests, with relatively minimal increases for others.

The model then underwent 'Parameter Tests' where the damper characteristics were changed and test procedure above repeated. These tests aimed to investigate the effect of the property changes of the PATPD on its ability to control free and forced vibration. The results indicate that (a) the PATPD provided significant reduction to first natural frequency PSD peak for all tests and (b) the properties of the PATPD affected the amount of control provided to the structure thus optimization of the PATPD could result in improved control effect.

The models' 'Dynamic Properties' namely model mass and stiffness were changed and test procedure repeated. These tests aimed to demonstrate the auto-tuning or adaptivity of the PATPD in its ability to control free and forced vibration. The results indicate that for all tests performed the PATPD provided significant reduction to first natural frequency PSD peak for all tests, with relatively minimal increases for others. The PATPD worked over a wide frequency band and was able to adapt to frequency changes providing significant control effect.

Additional forced vibration tests under specific frequencies close to and far away from the models' natural frequency demonstrates PATPD adaptability and efficiency. In addition tests under random excitation (as could be expected for earthquake loading) demonstrated PATPD positive control effect, adaptability and efficiency.

ACKNOWLEGMENTS

First and foremost, I would like to thank God for His blessings in my academic studies.

Thank you to my supervisor Dr. Kuinain Li for his continuous guidance and support.

In addition I want to thank all the Wits Lab and technical staff for their help: Ralph Mulder and Eric Rood - without your timeous help I would still be testing.

Finally, thank you to my parents and sister for supporting me throughout my studies, financially and emotionally, and to my fiancé for all your support, encouragement, advice and help with my studies- I could not have done it without you.

Table of Contents

DECLARATION 1
ABSTRACT 2
ACKNOWLEGMENTS 3
LIST OF FIGURES 9
LIST OF TABLES 22
CHAPTER 1 23
Introduction 23
1.1 General 23
1.2 Objectives of Study 24
CHAPTER 2 27
Literature Review 27
2.1 Background 27
2.2 Vibration control in buildings 28
2.3 Brief history of Dampers Background **34**
2.4.0 Dampers types and Application **35**
2.4.1 Active structural vibration control **35**
2.4.2 Passive structural vibration control **38**
2.4.3 Semi-Active structural vibration control 47
2.5 Conclusions 50
CHAPTER 3 51
Experimental Method 51
3.1 Introduction 51
3.2.0 Experimental set-up and details 51
3.2.1 PATPD Efficiency Tests 51
3.2.2 Parameter Study 54
3.2.2.1 Changing the PATPD Mass Ratio 54
3.2.2.2 Changing the friction of PATPD support 55
3.2.2.3 Changing the PATPD connection configuration 56
(a) Configuration 1 56
(b) Configuration 2 57
(c) Configuration 3 57
(d) Configuration 4 57

(e) Configuration 5 58
(f) Configuration 6 58
3.2.3.0 Changing Dynamic Properties 58
3.2.3.1 Changing model mass 59
3.2.3.2 Changing model stiffness 60
3.3.0 Experimental procedure 60
3.3.1 Free Vibration tests 60
3.3.1 Forced Vibration tests 61
CHAPTER 4 62
Experimental results: Primary Model PATPD Efficiency tests 62
4.1 Damper optimization 62
4.2 Free Vibration 63
4.2.1 Translation in the X-direction 63
4.2.2 Translation in the Y-direction 66
4.2.3 Torsional Vibration 70
4.2.4 Coupled Vibration 75
4.3.0 Forced Vibration 82
4.3.1 Translational Vibration in the X-Direction 82
4.3.2 Translational Vibration in the Y-Direction 83
4.4.0 Summary and Conclusions 85
CHAPTER 5 87
Experimental results: Parameter Study 87
5.1 Parameter Test 1: Effect of changing damper mass ratio 87
5.1.1 Free Vibration 88
5.1.1.1 Translational Vibration in the X-direction 88
5.1.1.2 Translational Vibration in the Y-direction 91
5.1.1.3 Torsional Vibration (acceleration measured in the X-direction) 94
5.1.1.4 Torsional Vibration (acceleration measured in the Y-direction) 97
5.1.1.5 Coupled Vibration (Translation in X-direction and torsion) 100
5.1.1.6 Coupled Vibration (Translation in Y-direction and torsion) 103
5.1.2.0 Forced Vibration 106
5.1.2.1 Translational Vibration in the X-direction 106
5.1.2.2 Translational Vibration in the Y-direction 108

5.1.3.0 Summary 110
5.2 Parameter Test 2: Effect of changing friction 111
5.2.1 Free Vibration 111
5.2.1.1 Translational Vibration in the X-direction 111
5.2.1.2 Translational Vibration in the Y-direction 115
5.2.1.3 Torsional Vibration (acceleration measured in the X-direction) 118
5.2.1.4 Torsional Vibration (acceleration measured in the Y-direction) 120
5.2.1.5 Coupled Vibration (Translation in X-direction and torsion) 124
5.2.1.6 Coupled Vibration (Translation in Y-direction and torsion) 127
5.2.2.0 Forced Vibration 130
5.2.2.1 Translational Vibration in the X-direction 130
5.2.2.2 Translational Vibration in the Y-direction 131
5.2.3.0 Summary 134
5.3 Parameter Test 3: Effect of changing rope type 135
5.3.1 Free Vibration 135
5.3.1.1 Translational Vibration in the X-direction 135
5.3.1.2 Translational Vibration in the Y-direction 138
5.3.1.3 Torsional Vibration (acceleration measured in the X-direction) 142
5.3.1.4 Torsional Vibration (acceleration measured in the Y-direction) 145
5.3.1.5 Coupled Vibration (Translation in X-direction and torsion) 148
5.3.1.6 Coupled Vibration (Translation in Y-direction and torsion) 151
5.3.2.0 Forced Vibration 154
5.3.2.1 Translational Vibration in the X-direction 154
5.3.2.2 Translational Vibration in the Y-direction 156
5.3.3.0 Summary 158
5.4 Parameter Test 4: Effect of changing connections 159
5.4.1 Free Vibration 159
5.4.1.1 Translational Vibration in the X-direction 159
5.4.1.2 Translational Vibration in the Y-direction 163
5.4.1.3 Torsional Vibration (acceleration measured in the X-direction) 166
5.4.1.4 Torsional Vibration (acceleration measured in the Y-direction) 169
5.4.1.5 Coupled Vibration (Translation in X-direction and torsion) 172
5.4.1.6 Coupled Vibration (Translation in Y-direction and torsion) 175

5.4.2.0 Forced Vibration 178
5.4.2.1 Translational Vibration in the X-direction 178
5.4.2.2 Translational Vibration in the Y-direction 180
5.4.3.0 Summary 182
5.5 Parameter Test 5: Effect of changing connection height 183
5.5.1 Free Vibration 183
5.5.1.1 Translational Vibration in the X-direction 183
5.5.1.2 Translational Vibration in the Y-direction 187
5.5.1.3 Torsional Vibration (acceleration measured in the X-direction) 190
5.5.1.4 Torsional Vibration (acceleration measured in the Y-direction) 193
5.5.1.5 Coupled Vibration (Translation in X-direction and torsion) 196
5.5.1.6 Coupled Vibration (Translation in Y-direction and torsion) 199
5.5.2.0 Forced Vibration 202
5.5.2.1 Translational Vibration in the X-direction 202
5.5.2.2 Translational Vibration in the Y-direction 204
5.5.3.0 Summary 206
CHAPTER 6 207
Experimental results: Changing Dynamic Properties of model 207
6.1 Changing Dynamic Properties: Effect of changing model mass 207
6.1.1 Free Vibration 208
6.1.1.1Translational Vibration in the X-direction 208
6.1.1.2 Translational Vibration in the Y-direction 213
6.1.1.3 Torsional Vibration (acceleration measured in X-direction) 218
6.1.1.4 Torsional Vibration (acceleration measured in Y-direction) 223
6.1.1.5 Coupled Vibration (translation in X-direction and torsion) 228
6.1.1.6 Coupled Vibration (translation in Y-direction and torsion) 233
6.1.2.0 Forced Vibration 238
6.1.2.1 Translational Vibration in the X-Direction 238
6.1.2.2 Translational Vibration in the Y-Direction 240
6.1.3.0 Summary and Conclusions 242
6.2 Changing Dynamic Properties: Effect of changing model stiffness 244
6.2.1 Free Vibration 245
6.2.1.1 Translational Vibration in the X-direction 245

6.2.1.2 Translational Vibration in the Y-direction 250
6.2.1.3 Torsional Vibration (acceleration measured in X-direction) 255
6.2.1.4 Torsional Vibration (acceleration measured in Y-direction) 260
6.2.1.5 Coupled Vibration (translation in X-direction and torsion) 265
6.2.1.6 Coupled Vibration (translation in Y-direction and torsion) 270
6.2.2.0 Forced Vibration 275
6.2.2.1 Translational Vibration in the X-Direction 275
6.2.2.2 Translational Vibration in the Y-Direction 277
6.2.3.0 Summary and Conclusions 279
6.3 Changing Dynamic Properties: Comparison showing Auto-tuning characteristic of PATPD 282
CHAPTER 7 284
Experimental results: Additional Forced vibration tests 284
7.1 Tests under specific forced vibration frequency using sin curve wave shape 284
7.1.1 Forced frequency of 5.4Hz (structures second natural frequency for free vibration) 284
7.1.2 Forced frequency of 15Hz (structures second natural frequency for free vibration) . 286
7.1.3 Random excitation 288
CHAPTER 8 291
8. 1 Conclusions 291
8.2 Further Research 296
REFERENCES 297
APPENDIX A: ADDITONAL PATPD PHOTOS 304
APPENDIX B: SAP SIMULATION 306
APPENDIX C: Earthquake profile extrapolation 309

LIST OF FIGURES

Figure 1: Aftermath of the earthquake in Kanto, Japan, 1923 (Anon., n.d.) 27
Figure 2: (CUREE, 1998) 27
Figure 3: Number of 200m+ buildings completed each year from 1960 to 2016 (CTBUH, 2014) 29
Figure 4: (Kareem, et al., 1999) 30
Figure 5: Aerodynamic modifications to Square building shape (Amin & Ahuja, 2010) 31
Figure 6: (a) Jan Mao Building China, (b) Petronas Towers Malaysia (Kareem, et al., 1999), (c) Burj Khalifa (World, n.d.) 31
Figure 7: Building elevation plan of Shangai World Financial Center (Katz, et al., 2008) 32
Figure 8: Left - Primary model set-up, Top right - Data Logger and Bottom right – computer used 52
Figure 9: PATPD configuration 53
Figure 10: Schematic of 1.5% mass ratio (N.T.S) 54
Figure 11: Schematic of 3% mass ratio (N.T.S), primary model mass ratio 54
Figure 12: Schematic of 5% mass ratio (N.T.S) 55
Figure 13: Steel rolling surface, primary model 55
Figure 14: Rubber rolling surface 56
Figure 15: Sandpaper rolling surface 56
Figure 16: Primary configuration 57
Figure 17: only diagonal connection 57
Figure 18: transverse connection only 57
Figure 19: The height to connection 15cm 58
Figure 20: Nylon rope 58
Figure 21: Ski rope 58
Figure 22: Primary model with mass 42.09kg 59
Figure 23: Model with mass 54.09kg 59
Figure 24: Model with mass 66.09kg 59
Figure 25: (a) primary model original height ho = 37.00cm, (b) height change 1 h1 = 32.00cm, (c) height change 2 h2 = 27.75cm 60
Figure 26: Direction definition used for testing 61
Figure 27: Time history of acceleration response for free translational vibration in the x-direction 62
Figure 28: Time history of acceleration response per storey for free translational vibration in the x-direction, primary model 64
Figure 29: Power Spectral Density (PSD) per storey of the acceleration response for free translational vibration in the x-direction, primary model 65
Figure 30: Magnified Power Spectral Density (PSD) per storey of the acceleration response for free translational vibration in the x-direction, primary model 66
Figure 31: Time history of acceleration response per storey for free translational vibration in the y-direction, primary model 67
Figure 32: Power Spectral Density (PSD) per storey of the acceleration response for free translational vibration in the y-direction, primary model 68

Figure 33: Magnified Power Spectral Density (PSD) of the acceleration response for free translational vibration in the y-direction, primary model 68
Figure 34: Time history of acceleration response per storey for free torsional vibration in the x-direction, primary model 70
Figure 35: Power Spectral Density (PSD) per storey of the acceleration response for free torsional vibration in the x-direction, primary model 71
Figure 36: Magnified Power Spectral Density (PSD) per storey of the acceleration response for free torsional vibration in the x-direction, primary model 72
Figure 37: Time history of acceleration response per storey for free torsional vibration in the y-direction, primary model 73
Figure 38: Power Spectral Density (PSD) per storey of the acceleration response for free torsional vibration in the y-direction, primary model 74
Figure 39: Magnified Power Spectral Density (PSD) per storey of the acceleration response for free torsional vibration in the y-direction, primary model 75
Figure 40: Time history of acceleration response per storey for free coupled vibration (translation in the x-direction and torsion), primary model 76
Figure 41: Power Spectral Density (PSD) per storey of the acceleration response for free coupled vibration (translation in the x-direction and torsion) , primary model 77
Figure 42: Magnified Power Spectral Density (PSD) per storey of the acceleration response for free coupled vibration (translation in the x-direction and torsion), primary model 78
Figure 43: Time history of acceleration response per storey for free coupled vibration (translation in the y-direction and torsion), primary model 79
Figure 44: Power Spectral Density (PSD) per storey of the acceleration response for free coupled vibration (translation in the y-direction and torsion), primary model 80
Figure 45: Magnified Power Spectral Density (PSD) per storey of the acceleration response for free coupled vibration (translation in the y-direction and torsion), primary model 81
Figure 46: Time history of acceleration response per storey for forced translational excitation in the x-direction, primary model 82
Figure 47: Power Spectral Density (PSD) of the acceleration response per storey under forced excitation in the x-direction, primary model 83
Figure 48: Time history of acceleration response per storey for forced translational excitation in the y-direction, primary model 84
Figure 49: Power Spectral Density (PSD) of the acceleration response per storey under forced excitation in the y-direction, primary model 85
Figure 50: Time history of acceleration response per storey for free translational vibration in x-direction, mass ratios 1.5%, 3% and 5% 88
Figure 51: Magnified Power Spectral Density (PSD) storey 3 of the acceleration of the model under free translational vibration in the x-direction, mass ratios 1.5%, 3% and 5%..... 89
Figure 52: Magnified Power Spectral Density (PSD) storey 2 of the acceleration of the model under free translational vibration in the x-direction, mass ratios 1.5%, 3% and 5%..... 89
Figure 53: Magnified Power Spectral Density (PSD) storey 1 of the acceleration of the model under free translational vibration in the x-direction, mass ratios 1.5%, 3% and 5%..... 90

Figure 54: Time history of acceleration response per storey for free translational vibration in y-direction, mass ratios 1.5%, 3% and 5% 91
Figure 55: Magnified Power Spectral Density (PSD) storey 3 of the acceleration of the model under free translational vibration in the y-direction, mass ratios 1.5%, 3% and 5% 92
Figure 56: Magnified Power Spectral Density (PSD) storey 2 of the acceleration of the model under free translational vibration in the y-direction, mass ratios 1.5%, 3% and 5% 92
Figure 57: Magnified Power Spectral Density (PSD) storey 1 of the acceleration of the model under free translational vibration in the y-direction, mass ratios 1.5%, 3% and 5%..... 93
Figure 58: Time history of acceleration response in x-direction per storey for free torsional vibration, mass ratios 1.5%, 3% and 5% 94
Figure 59: Magnified Power Spectral Density (PSD) storey 3 of the acceleration in the x-direction of the model under free torsional vibration, mass ratios 1.5%, 3% and 5% 95
Figure 60: Magnified Power Spectral Density (PSD) storey 2 of the acceleration in the x-direction of the model under free torsional vibration, mass ratios 1.5%, 3% and 5% 95
Figure 61: Magnified Power Spectral Density (PSD) storey 1 of the acceleration in the x-direction of the model under free torsional vibration, mass ratios 1.5%, 3% and 5% 96
Figure 62: Time history of acceleration response in y-direction per storey for free torsional vibration, mass ratios 1.5%, 3% and 5% 97
Figure 63: Magnified Power Spectral Density (PSD) storey 3 of the acceleration in the y-direction of the model under free torsional vibration, mass ratios 1.5%, 3% and 5% 98
Figure 64: Magnified Power Spectral Density (PSD) storey 2 of the acceleration in the y-direction of the model under free torsional vibration, mass ratios 1.5%, 3% and 5% 98
Figure 65: Magnified Power Spectral Density (PSD) storey 1 of the acceleration in the y-direction of the model under free torsional vibration, mass ratios 1.5%, 3% and 5% 99
Figure 66: Time history of acceleration response in x-direction per storey for free coupled vibration, mass ratios 1.5%, 3% and 5% 100
Figure 67: Magnified Power Spectral Density (PSD) storey 3 of the acceleration in the x-direction of the model under free coupled vibration, mass ratios 1.5%, 3% and 5%..... 101
Figure 68: Magnified Power Spectral Density (PSD) storey 2 of the acceleration in the x-direction of the model under free coupled vibration, mass ratios 1.5%, 3% and 5%..... 101
Figure 69: Magnified Power Spectral Density (PSD) storey 1 of the acceleration in the x-direction of the model under free coupled vibration, mass ratios 1.5%, 3% and 5%..... 102
Figure 70: Time history of acceleration response in y-direction per storey for free coupled vibration, mass ratios 1.5%, 3% and 5% 103
Figure 71: Magnified Power Spectral Density (PSD) storey 3 of the acceleration in the y-direction of the model under free coupled vibration, mass ratios 1.5%, 3% and 5%..... 104
Figure 72: Magnified Power Spectral Density (PSD) storey 2 of the acceleration in the y-direction of the model under free coupled vibration, mass ratios 1.5%, 3% and 5%..... 104
Figure 73: Magnified Power Spectral Density (PSD) storey 1 of the acceleration in the y-direction of the model under free coupled vibration, mass ratios 1.5%, 3% and 5%..... 105
Figure 74: Time history of acceleration response per storey for forced translational vibration in x-direction, mass ratios 1.5%, 3% and 5% 106

Figure 75: Power Spectral Density (PSD) of the acceleration response per storey under forced excitation in the x-direction, mass ratios 1.5%, 3% and 5% 107
Figure 76: Time history of acceleration response per storey for forced translational vibration in y-direction, mass ratios 1.5%, 3% and 5% 108
Figure 77: Power Spectral Density (PSD) of the acceleration response per storey under forced excitation in the y-direction, mass ratios 1.5%, 3% and 5% 109
Figure 78: Time history of acceleration response per storey for free translational vibration in x-direction, steel, rubber and sandpaper surfaces 112
Figure 79: Magnified Power Spectral Density (PSD) storey 3 of the acceleration of the model under free translational vibration in the x-direction , steel, rubber and sandpaper surfaces 113
Figure 80: Magnified Power Spectral Density (PSD) storey 2 of the acceleration of the model under free translational vibration in the x-direction, steel, rubber and sandpaper surfaces .. 113
Figure 81: Magnified Power Spectral Density (PSD) storey 1 of the acceleration of the model under free translational vibration in the x-direction, steel, rubber and sandpaper surfaces .. 114
Figure 82: Time history of acceleration response per storey for free translational vibration in y-direction, steel, rubber and sandpaper surfaces 115
Figure 83: Magnified Power Spectral Density (PSD) storey 3 of the acceleration of the model under free translational vibration in the y-direction, steel, rubber and sandpaper surfaces . 116
Figure 84: Magnified Power Spectral Density (PSD) storey 2 of the acceleration of the model under free translational vibration in the y-direction, steel, rubber and sandpaper surfaces . 116
Figure 85: Magnified Power Spectral Density (PSD) storey 1 of the acceleration of the model under free translational vibration in the y-direction, steel, rubber and sandpaper surfaces . 117
Figure 86: Time history of acceleration response in x-direction per storey for free torsional vibration, steel, rubber and sandpaper surfaces 118
Figure 87: Magnified Power Spectral Density (PSD) storey 3 of the acceleration in the x-direction of the model under free torsional vibration, steel, rubber and sandpaper surfaces 119
Figure 88: Magnified Power Spectral Density (PSD) storey 2 of the acceleration in the x-direction of the model under free torsional vibration, steel, rubber and sandpaper surfaces 119
Figure 89: Magnified Power Spectral Density (PSD) storey 1 of the acceleration in the x-direction of the model under free torsional vibration, steel, rubber and sandpaper surfaces120
Figure 90: Time history of acceleration response in y-direction per storey for free torsional vibration, steel, rubber and sandpaper surfaces 121
Figure 91: Magnified Power Spectral Density (PSD) storey 3 of the acceleration in the y-direction of the model under free torsional vibration, steel, rubber and sandpaper surfaces 122
Figure 92: Magnified Power Spectral Density (PSD) storey 2 of the acceleration in the y-direction of the model under free torsional vibration, steel, rubber and sandpaper surfaces 122
Figure 93: Magnified Power Spectral Density (PSD) storey 1 of the acceleration in the y-direction of the model under free torsional vibration, steel, rubber and sandpaper surfaces123
Figure 94: Time history of acceleration response in x-direction per storey for free coupled vibration, steel, rubber and sandpaper surfaces 124
Figure 95: Magnified Power Spectral Density (PSD) storey 3 of the acceleration in the x-direction of the model under free coupled vibration, steel, rubber and sandpaper surfaces 125

Figure 96: Magnified Power Spectral Density (PSD) storey 2 of the acceleration in the x-direction of the model under free coupled vibration, steel, rubber and sandpaper surfaces 125
Figure 97: Magnified Power Spectral Density (PSD) storey 1 of the acceleration in the x-direction of the model under free coupled vibration, steel, rubber and sandpaper surfaces 126
Figure 98: Time history of acceleration response in y-direction per storey for free coupled vibration, steel, rubber and sandpaper surfaces 127
Figure 99: Magnified Power Spectral Density (PSD) storey 3 of the acceleration in the y-direction of the model under free coupled vibration, steel, rubber and sandpaper surfaces 128
Figure 100: Magnified Power Spectral Density (PSD) storey 2 of the acceleration in the y-direction of the model under free coupled vibration, steel, rubber and sandpaper surfaces 128
Figure 101: Magnified Power Spectral Density (PSD) storey 1 of the acceleration in the y-direction of the model under coupled vibration, , steel, rubber and sandpaper surfaces..... 129
Figure 102: Time history of acceleration response per storey for forced translational vibration in x-direction, steel, rubber and sandpaper surfaces 130
Figure 103: Power Spectral Density (PSD) of the acceleration response per storey under forced excitation in the x-direction, steel, rubber and sandpaper surfaces 131
Figure 104: Time history of acceleration response per storey for forced translational vibration in y-direction, steel, rubber and sandpaper surfaces 132
Figure 105: Power Spectral Density (PSD) of the acceleration response per storey under forced excitation in the y-direction, steel, rubber and sandpaper surfaces 133
Figure 106: Time history of acceleration response per storey for free translational vibration in x-direction, cotton rope, nylon rope and ski-rope 136
Figure 107: Magnified Power Spectral Density (PSD) storey 3 of the acceleration of the model under free translational vibration in the x-direction , cotton rope, nylon rope and ski-rope 137
Figure 108: Magnified Power Spectral Density (PSD) storey 2 of the acceleration of the model under free translational vibration in the x-direction, cotton rope, nylon rope and ski-rope. 137
Figure 109: Magnified Power Spectral Density (PSD) storey 1 of the acceleration of the model under free translational vibration in the x-direction, cotton rope, nylon rope and ski-rope 138
Figure 110: Time history of acceleration response per storey for free translational vibration in y-direction, cotton rope, nylon rope and ski-rope 139
Figure 111: Magnified Power Spectral Density (PSD) storey 3 of the acceleration of the model under free translational vibration in the y-direction, cotton rope, nylon rope and ski-rope s 140
Figure 112: Magnified Power Spectral Density (PSD) storey 2 of the acceleration of the model under free translational vibration in the y-direction, cotton rope, nylon rope and ski-rope.. 140
Figure 113: Magnified Power Spectral Density (PSD) storey 1 of the acceleration of the model under free translational vibration in the y-direction, cotton rope, nylon rope and ski-rope 141
Figure 114: Time history of acceleration response in y-direction per storey for free torsional vibration, cotton rope, nylon rope and ski-rope 142
Figure 115: Magnified Power Spectral Density (PSD) storey 3 of the acceleration in the x-direction of the model under free torsional vibration, cotton rope, nylon rope and ski-rope 143

Figure 116: Magnified Power Spectral Density (PSD) storey 2 of the acceleration in the x-direction of the model under free torsional vibration, cotton rope, nylon rope and ski-rope 143
Figure 117: Magnified Power Spectral Density (PSD) storey 1 of the acceleration in the x-direction of the model under free torsional vibration, cotton rope, nylon rope and ski-rope 144
Figure 118: Time history of acceleration response in y-direction per storey for free torsional vibration, cotton rope, nylon rope and ski-rope..... 145
Figure 119: Magnified Power Spectral Density (PSD) storey 3 of the acceleration in the y-direction of the model under free torsional vibration, cotton rope, nylon rope and ski-rope 146
Figure 120: Magnified Power Spectral Density (PSD) storey 2 of the acceleration in the y-direction of the model under free torsional vibration, cotton rope, nylon rope and ski-rope 146
Figure 121: Magnified Power Spectral Density (PSD) storey 1 of the acceleration in the y-direction of the model under free torsional vibration , cotton rope, nylon rope and ski-rope 147
Figure 122: Time history of acceleration response in x-direction per storey for free coupled vibration, cotton rope, nylon rope and ski-rope..... 148
Figure 123: Magnified Power Spectral Density (PSD) storey 3 of the acceleration in the x-direction of the model under free coupled vibration, cotton rope, nylon rope and ski-rope149
Figure 124: Magnified Power Spectral Density (PSD) storey 2 of the acceleration in the x-direction of the model under free coupled vibration, cotton rope, nylon rope and ski-rope 149
Figure 125: Magnified Power Spectral Density (PSD) storey 1 of the acceleration in the x-direction of the model under free coupled vibration, cotton rope, nylon rope and ski-rope 150
Figure 126: Time history of acceleration response in y-direction per storey for free coupled vibration, cotton rope, nylon rope and ski-rope..... 151
Figure 127: Magnified Power Spectral Density (PSD) storey 3 of the acceleration in the y-direction of the model under free coupled vibration, cotton rope, nylon rope and ski-rope152
Figure 128: Magnified Power Spectral Density (PSD) storey 2 of the acceleration in the y-direction of the model under free coupled vibration, cotton rope, nylon rope and ski-rope152
Figure 129: Magnified Power Spectral Density (PSD) storey 1 of the acceleration in the y-direction of the model under free coupled vibration, cotton rope, nylon rope and ski-rope153
Figure 130: Time history of acceleration response per storey for forced translational vibration in x-direction, steel, cotton rope, nylon rope and ski-rope 154
Figure 131: Power Spectral Density (PSD) of the acceleration response per storey under forced excitation in the x-direction, cotton rope, nylon rope and ski-rope 155
Figure 132: Time history of acceleration response per storey for forced translational vibration in y-direction, cotton rope, nylon rope and ski-rope..... 156
Figure 133: Power Spectral Density (PSD) of the acceleration response per storey under forced excitation in the y-direction, cotton rope, nylon rope and ski-rope 157
Figure 134: Time history of acceleration response per storey for free translational vibration in x-direction, configuration 1, 2 and 3..... 160
Figure 135: Magnified Power Spectral Density (PSD) storey 3 of the acceleration of the model under free translational vibration in the x-direction , configuration 1,2 and 3..... 161

Figure 136: Magnified Power Spectral Density (PSD) storey 2 of the acceleration of the model under free translational vibration in the x-direction, configuration 1, 2 and 3 161
Figure 137: Magnified Power Spectral Density (PSD) storey 1 of the acceleration of the model under free translational vibration in the x-direction, configuration 1,2 and 3 162
Figure 138: Time history of acceleration response per storey for free translational vibration in y-direction, configuration 1, 2 and 3..... 163
Figure 139: Magnified Power Spectral Density (PSD) storey 3 of the acceleration of the model under free translational vibration in the y-direction, configuration 1, 2 and 3..... 164
Figure 140: Magnified Power Spectral Density (PSD) storey 2 of the acceleration of the model under free translational vibration in the y-direction, configuration 1,2 and 3..... 164
Figure 141: Magnified Power Spectral Density (PSD) storey 1 of the acceleration of the model under free translational vibration in the y-direction, configuration 1, 2 and 3..... 165
Figure 142: Time history of acceleration response in x-direction per storey for free torsional vibration, configuration 1, 2 and 3 166
Figure 143: Magnified Power Spectral Density (PSD) storey 3 of the acceleration in the x-direction of the model under free torsional vibration, configuration 1,2 and 3 167
Figure 144: Magnified Power Spectral Density (PSD) storey 2 of the acceleration in the x-direction of the model under free torsional vibration, configuration 1,2 and 3 167
Figure 145: Magnified Power Spectral Density (PSD) storey 1 of the acceleration in the x-direction of the model under free torsional vibration, configuration 1,2 and 3 168
Figure 146: Time history of acceleration response in y-direction per storey for free torsional vibration, configuration 1, 2 and 3 169
Figure 147: Magnified Power Spectral Density (PSD) storey 3 of the acceleration in the y-direction of the model under free torsional vibration , configuration 1,2 and 3 170
Figure 148: Magnified Power Spectral Density (PSD) storey 2 of the acceleration in the y-direction of the model under free torsional vibration , configuration 1,2 and 3 170
Figure 149: Magnified Power Spectral Density (PSD) storey 1 of the acceleration in the y-direction of the model under free torsional vibration , configuration 1, 2 and 3 171
Figure 150: Time history of acceleration response in x-direction per storey for free coupled vibration, configuration 1, 2 and 3 172
Figure 151: Magnified Power Spectral Density (PSD) storey 3 of the acceleration in the x-direction of the model under free coupled vibration, configuration 1,2 and 3..... 173
Figure 152: Magnified Power Spectral Density (PSD) storey 2 of the acceleration in the x-direction of the model under free coupled vibration, configuration 1,2 and 3..... 173
Figure 153: Magnified Power Spectral Density (PSD) storey 1 of the acceleration in the x-direction of the model under free coupled vibration, configuration 1,2 and 3..... 174
Figure 154: Time history of acceleration response in y-direction per storey for free coupled vibration, configuration 1, 2 and 3 175
Figure 155: Magnified Power Spectral Density (PSD) storey 3 of the acceleration in the y-direction of the model under free coupled vibration, configuration 1,2 and 3..... 176
Figure 156: Magnified Power Spectral Density (PSD) storey 2 of the acceleration in the y-direction of the model under free coupled vibration, configuration 1, 2 and 3..... 176

Figure 157: Magnified Power Spectral Density (PSD) storey 1 of the acceleration in the y-direction of the model under free coupled vibration, configuration 1,2 and 3..... 177
Figure 158: Time history of acceleration response per storey for forced translational vibration in x-direction, configuration 1, 2 and 3..... 178
Figure 159: Power Spectral Density (PSD) of the acceleration response per storey under forced excitation in the x-direction, configuration 1, 2 and 3 179
Figure 160: Time history of acceleration response per storey for forced translational vibration in y-direction, configuration 1, 2 and 3..... 180
Figure 161: Power Spectral Density (PSD) of the acceleration response per storey under forced excitation in the y-direction n, configuration 1, 2 and 3 181
Figure 162: Time history of acceleration response per storey for free translational vibration in x-direction, connection height 15cm and height 9cm..... 184
Figure 163: Magnified Power Spectral Density (PSD) storey 3 of the acceleration of the model under free translational vibration in the x-direction , connection height 15cm and height 9cm 185
Figure 164: Magnified Power Spectral Density (PSD) storey 2 of the acceleration of the model under free translational vibration in the x-direction, connection height 15cm and height 9cm 185
Figure 165: Magnified Power Spectral Density (PSD) storey 1 of the acceleration of the model under free translational vibration in the x-direction, connection height 15cm and height 9cm 186
Figure 166: Time history of acceleration response per storey for free translational vibration in y-direction, connection height 15cm and height 9cm..... 187
Figure 167: Magnified Power Spectral Density (PSD) storey 3 of the acceleration of the model under free translational vibration in the y-direction connection height 15cm and height 9cm 188
Figure 168: Magnified Power Spectral Density (PSD) storey 2 of the acceleration of the model under free translational vibration in the y-direction, connection height 15cm and height 9cm 188
Figure 169: Magnified Power Spectral Density (PSD) storey 1 of the acceleration of the model under free translational vibration in the y-direction, connection height 15cm and height 9cm 189
Figure 170: Time history of acceleration response in x-direction per storey for free torsional vibration, height 15cm and height 9cm..... 190
Figure 171: Magnified Power Spectral Density (PSD) storey 3 of the acceleration in the x-direction of the model under free torsional vibration, height 15cm and height 9cm..... 191
Figure 172: Magnified Power Spectral Density (PSD) storey 2 of the acceleration in the x-direction of the model under free torsional vibration, height 15cm and height 9cm..... 191
Figure 173: Magnified Power Spectral Density (PSD) storey 1 of the acceleration in the x-direction of the model under free torsional vibration, height 15cm and height 9cm..... 192
Figure 174: Time history of acceleration response in y-direction per storey for free torsional vibration, height 15cm and height 9cm..... 193

Figure 175: Magnified Power Spectral Density (PSD) storey 3 of the acceleration in the y-direction of the model under free torsional vibration , height 15cm and height 9cm 194
Figure 176: Magnified Power Spectral Density (PSD) storey 2 of the acceleration in the y-direction of the model under free torsional vibration , height 15cm and height 9cm 194
Figure 177: Magnified Power Spectral Density (PSD) storey 1 of the acceleration in the y-direction of the model under free torsional vibration , height 15cm and height 9cm 195
Figure 178: Time history of acceleration response in x-direction per storey for free coupled vibration, height 15cm and height 9cm 196
Figure 179: Magnified Power Spectral Density (PSD) storey 3 of the acceleration in the x-direction of the model under free coupled vibration, height 15cm and height 9cm 197
Figure 180: Magnified Power Spectral Density (PSD) storey 2 of the acceleration in the x-direction of the model under free coupled vibration, height 15cm and height 9cm 197
Figure 181: Magnified Power Spectral Density (PSD) storey 1 of the acceleration in the y-direction of the model under free coupled vibration, height 15cm and height 9cm 198
Figure 182: Time history of acceleration response in y-direction per storey for free coupled vibration, height 15cm and height 9cm 199
Figure 183: Magnified Power Spectral Density (PSD) storey 3 of the acceleration in the y-direction of the model under free coupled vibration, height 15cm and height 9cm 200
Figure 184: Magnified Power Spectral Density (PSD) storey 2 of the acceleration in the y-direction of the model under free coupled vibration, height 15cm and height 9cm 200
Figure 185: Magnified Power Spectral Density (PSD) storey 1 of the acceleration in the y-direction of the model under free coupled vibration, height 15cm and height 9cm 201
Figure 186: Time history of acceleration response per storey for forced translational vibration in x-direction, height 15cm and height 9cm 202
Figure 187: Power Spectral Density (PSD) of the acceleration response per storey under forced excitation in the x-direction, height 15cm and height 9cm 203
Figure 188: Time history of acceleration response per storey for forced translational vibration in y-direction, height 15cm and height 9cm 204
Figure 189: Power Spectral Density (PSD) of the acceleration response per storey under forced excitation in the y-direction, height 15cm and height 9cm 205
Figure 190: Time history of acceleration response per storey for free translational vibration in the x-direction, model mass 52.09kg 208
Figure 191: Time history of acceleration response per storey for free translational vibration in the x-direction, model mass 66.09kg 209
Figure 192: Power Spectral Density (PSD) per storey of the acceleration response for free translational vibration in the x-direction, model mass 54.09kg 210
Figure 193: Power Spectral Density (PSD) per storey of the acceleration response for free translational vibration in the x-direction, model mass 66.09kg 211
Figure 194: Magnified Power Spectral Density (PSD) of the acceleration response for free translational vibration in the x-direction, model mass 54.09kg 211
Figure 195: Magnified Power Spectral Density (PSD) of the acceleration response for free translational vibration in the x-direction, model mass 66.09kg 212

Figure 196: Time history of acceleration response per storey for free translational vibration in the y-direction, model mass 52.09kg 213
Figure 197: Time history of acceleration response per storey for free translational vibration in the y-direction, model mass 66.09kg 214
Figure 198: Power Spectral Density (PSD) per storey of the acceleration response for free translational vibration in the y-direction, model mass 54.09kg 215
Figure 199: Power Spectral Density (PSD) per storey of the acceleration response for free translational vibration in the y-direction, model mass 66.09kg 216
Figure 200: Magnified Power Spectral Density (PSD) of the acceleration response for free translational vibration in the y-direction, model mass 54.09kg 216
Figure 201: Magnified Power Spectral Density (PSD) of the acceleration response for free translational vibration in the y-direction, model mass 66.09kg 217
Figure 202: Time history of acceleration response per storey for free torsional vibration in the x-direction, model mass 52.09kg 218
Figure 203: Time history of acceleration response per storey for free torsional vibration in the x-direction, model mass 66.09kg 219
Figure 204: Power Spectral Density (PSD) per storey of the acceleration response for free torsional vibration in the x-direction, model mass 54.09kg 220
Figure 205: Power Spectral Density (PSD) per storey of the acceleration response for free torsional vibration in the x-direction, model mass 66.09kg 221
Figure 206: Magnified Power Spectral Density (PSD) of the acceleration response for free torsional vibration in the x-direction, model mass 54.09kg 221
Figure 207: Magnified Power Spectral Density (PSD) of the acceleration response for free torsional vibration in the x-direction, model mass 66.09kg 222
Figure 208: Time history of acceleration response per storey for free torsional vibration in the y-direction, model mass 52.09kg 223
Figure 209: Time history of acceleration response per storey for free torsional vibration in the y-direction, model mass 66.09kg 224
Figure 210: Power Spectral Density (PSD) per storey of the acceleration response for free torsional vibration in the y-direction, model mass 54.09kg 225
Figure 211: Power Spectral Density (PSD) per storey of the acceleration response for free torsional vibration in the y-direction, model mass 66.09kg 226
Figure 212: Magnified Power Spectral Density (PSD) of the acceleration response for free torsional vibration in the y-direction, model mass 54.09kg 226
Figure 213: Magnified Power Spectral Density (PSD) of the acceleration response for free torsional vibration in the y-direction, model mass 66.09kg 227
Figure 214: Time history of acceleration response per storey for free coupled vibration (translation in x-direction and torsion), model mass 52.09kg 228
Figure 215: Time history of acceleration response per storey for free coupled vibration (translation in x-direction and torsion), model mass 66.09kg 229
Figure 216: Power Spectral Density (PSD) per storey of the acceleration response for free coupled vibration (translation in x-direction and torsion), model mass 54.09kg 230

Figure 217: Power Spectral Density (PSD) per storey of the acceleration response for free coupled vibration (translation in x-direction and torsion), model mass 66.09kg 231
Figure 218: Magnified Power Spectral Density (PSD) of the acceleration response for free coupled vibration (translation in x-direction and torsion), model mass 54.09kg 231
Figure 219: Magnified Power Spectral Density (PSD) of the acceleration response for free coupled vibration (translation in x-direction and torsion), model mass 66.09kg 232
Figure 220: Time history of acceleration response per storey for free coupled vibration (translation in y-direction and torsion), model mass 52.09kg 234
Figure 221: Time history of acceleration response per storey for free coupled vibration (translation in y-direction and torsion), model mass 66.09kg 234
Figure 222: Power Spectral Density (PSD) per storey of the acceleration response for free coupled vibration (translation in y-direction and torsion), model mass 54.09kg 235
Figure 223: Power Spectral Density (PSD) per storey of the acceleration response for free coupled vibration (translation in y-direction and torsion), model mass 66.09kg 236
Figure 224: Magnified Power Spectral Density (PSD) of the acceleration response for free coupled vibration (translation in y-direction and torsion), model mass 54.09kg 236
Figure 225: Magnified Power Spectral Density (PSD) of the acceleration response for free coupled vibration (translation in y-direction and torsion), model mass 66.09kg 237
Figure 226: Time history of acceleration response per storey for forced translational vibration in x-direction, model mass 54.09kg 239
Figure 227: Power Spectral Density (PSD) of the acceleration response per storey under forced excitation in the x-direction, model mass 66.09kg 240
Figure 228: Time history of acceleration response per storey for forced translational vibration in y-direction, model mass 54.09kg 241
Figure 229: Power Spectral Density (PSD) of the acceleration response per storey under forced excitation in the y-direction, model mass 66.09kg 242
Figure 230: Time history of acceleration response per storey for free translational vibration in the x-direction, model height 27cm 245
Figure 231: Time history of acceleration response per storey for free translational vibration in the x-direction, model height 32cm 246
Figure 232: Power Spectral Density (PSD) per storey of the acceleration response for free translational vibration in the x-direction, model height 27cm 247
Figure 233: Power Spectral Density (PSD) per storey of the acceleration response for free translational vibration in the x-direction, model height 32cm 248
Figure 234: Magnified Power Spectral Density (PSD) of the acceleration response for free translational vibration in the x-direction, model height 27cm 248
Figure 235: Magnified Power Spectral Density (PSD) of the acceleration response for free translational vibration in the x-direction, model height 32 249
Figure 236: Time history of acceleration response per storey for free translational vibration in the y-direction, model height 27cm 250
Figure 237: Time history of acceleration response per storey for free translational vibration in the y-direction, model height 32cm 251

Figure 238: Power Spectral Density (PSD) per storey of the acceleration response for free translational vibration in the y-direction, model height 27cm 252
Figure 239: Power Spectral Density (PSD) per storey of the acceleration response for free translational vibration in the y-direction, model height 32cm 253
Figure 240: Magnified Power Spectral Density (PSD) of the acceleration response for free translational vibration in the y-direction, model height 27cm 253
Figure 241: Magnified Power Spectral Density (PSD) of the acceleration response for free translational vibration in the y-direction, model height 32cm 254
Figure 242: Time history of acceleration response per storey for free torsional vibration in the x-direction, model height 27cm 255
Figure 243: Time history of acceleration response per storey for free torsional vibration in the x-direction, model height 32cm 256
Figure 244: Power Spectral Density (PSD) per storey of the acceleration response for free torsional vibration in the x-direction, model height 27cm 257
Figure 245: Power Spectral Density (PSD) per storey of the acceleration response for free torsional vibration in the x-direction, model height 32cm 258
Figure 246: Magnified Power Spectral Density (PSD) of the acceleration response for free torsional vibration in the x-direction, model height 27cm 258
Figure 247: Magnified Power Spectral Density (PSD) of the acceleration response for free torsional vibration in the x-direction, model height 32cm 259
Figure 248: Time history of acceleration response per storey for free torsional vibration in the y-direction, model height 27cm 260
Figure 249: Time history of acceleration response per storey for free torsional vibration in the y-direction, model height 32cm 261
Figure 250: Power Spectral Density (PSD) per storey of the acceleration response for free torsional vibration in the y-direction, model height 27cm 262
Figure 251: Power Spectral Density (PSD) per storey of the acceleration response for free torsional vibration in the y-direction, model height 32cm 263
Figure 252: Magnified Power Spectral Density (PSD) of the acceleration response for free torsional vibration in the y-direction, model height 27cm 263
Figure 253: Magnified Power Spectral Density (PSD) of the acceleration response for free torsional vibration in the y-direction, model height 32cm 264
Figure 254: Time history of acceleration response per storey for free coupled vibration (translation in x-direction and torsion), model height 27cm 266
Figure 255: Time history of acceleration response per storey for free coupled vibration (translation in x-direction and torsion), model height 32cm 266
Figure 256: Power Spectral Density (PSD) per storey of the acceleration response for free coupled vibration (translation in x-direction and torsion), model height 27cm 267
Figure 257: Power Spectral Density (PSD) per storey of the acceleration response for free coupled vibration (translation in x-direction and torsion), model height 32cm 268
Figure 258: Magnified Power Spectral Density (PSD) of the acceleration response for free coupled vibration (translation in x-direction and torsion), model height 27cm 268

Figure 259: Magnified Power Spectral Density (PSD) of the acceleration response for free coupled vibration (translation in x-direction and torsion), model height 32cm 269
Figure 260: Time history of acceleration response per storey for free coupled vibration (translation in y-direction and torsion), model height 27cm..... 270
Figure 261: Time history of acceleration response per storey for free coupled vibration (translation in y-direction and torsion), model height 32cm..... 271
Figure 262: Power Spectral Density (PSD) per storey of the acceleration response for free coupled vibration (translation in y-direction and torsion), model height 27cm 272
Figure 263: Power Spectral Density (PSD) per storey of the acceleration response for free coupled vibration (translation in y-direction and torsion), model height 32cm 273
Figure 264: Magnified Power Spectral Density (PSD) of the acceleration response for free coupled vibration (translation in x-direction and torsion), model height 27cm 273
Figure 265: Magnified Power Spectral Density (PSD) of the acceleration response for free coupled vibration (translation in y-direction and torsion), model height 32cm 274
Figure 266: Time history of acceleration response per storey for forced translational vibration in x-direction, model height 27cm..... 276
Figure 267: Power Spectral Density (PSD) of the acceleration response per storey under forced excitation in the x-direction, model height 32cm..... 277
Figure 268: Time history of acceleration response per storey for forced translational vibration in y-direction, model height 27cm..... 278
Figure 269: Power Spectral Density (PSD) of the acceleration response per storey under forced excitation in the y-direction, model height 32cm..... 279
Figure 270: Power Spectral Density (PSD) of the acceleration response of the primary model with mass 42.09kg and storey height 37cm under forced excitation in the x-direction 283
Figure 271: Power Spectral Density (PSD) of the acceleration response of the test model with mass 42.09kg and storey height 27cm under forced excitation in the x-direction 283
Figure 272: Power Spectral Density (PSD) of the acceleration response of the test model with mass 66.09kg and storey height 37cm under forced excitation in the x-direction 283
Figure 273: Time history of acceleration response per storey for forced translational vibration in x-direction..... 285
Figure 274: Power Spectral Density (PSD) of the acceleration response per storey under forced excitation in the x-direction..... 286
Figure 275: Time history of acceleration response per storey for forced translational vibration in x-direction..... 287
Figure 276: Power Spectral Density (PSD) of the acceleration response per storey under forced excitation in the x-direction..... 288
Figure 277: Time history of acceleration response per storey for forced translational vibration in x-direction..... 289
Figure 278: Power Spectral Density (PSD) of the acceleration response per storey under forced excitation in the x-direction..... 290
Figure 279: PATPD SUPPORT 304
Figure 280: SIDE VIEW PATPD..... 304
Figure 281: PATPD PULLEYS 304

Figure 282: STRAIN GAUGE USED IN TESTS 305
Figure 283: STRAIN GAUGE CONNECTION AND SET UP 305
Figure 284: Translation Mode 1 306
Figure 285: Translation Mode 2 307
Figure 286: Translation Mode 3 308

LIST OF TABLES

Table 1: Comparison of percentage change of PSD peak for the first natural frequency with and without PATPD for free vibration, for the 42.09kg (primary model), 54.09kg and 66.09kg model mass 243
Table 2: Comparison of percentage change of PSD peak for the first natural frequency with and without PATPD for free vibration, for the 37cm (primary model), 32cm and 27cm model height 280

CHAPTER 1

Introduction

1.1 General

As a result of pressing global issues, such as urbanization and increased population growth, multi-storey (high rise) buildings are the favoured construction choice of late. This shift necessitates improved vibration control making research and application within the field vitally important. The basic aims of structural dynamics are (a) to create systems that ensure the safety of occupants within a structure during vibrational excitation and seismic activity, (b) to improve the habitability of the structure by minimizing said vibrations and (c) for structures under dynamic loading, control or reduction of structural vibration can improve the working conditions of operators.

Structural control refers to the installation of a mechanical system to a structure, which facilitates energy dissipation, such that structural vibrations during loading (e.g. human use, wind and earthquake loads) are reduced. Many structures have recently benefited from the use of these ever improving structural control systems. The focus of this paper is primarily on damping systems[1] which can be differentiated under the general classification of: active, passive or semi-active control systems. The active control system requires electrical power to function and possesses feedback capability. However, active control systems are not always reliable. Reliability is a must, especially during disastrous events such as earthquakes. Thus, this research is focused on a Passive control system.

[1] A brief explanation of other techniques can be found under Literature Review

One of the most commonly used and an extensively studied passive control system is The Tuned Mass Damper (TMD). The greatest drawback with the TMD is that it requires tuning to a specific frequency which limits its efficiency to a narrow band control; furthermore it is inadequate in response to torsional vibration.

This report proposes a Passive Auto-tuning control system - which does not require tuning to any specific frequency. This system works over a wide band of frequencies and is reliable as it is a passive system.

The Passive Auto-Tuning Mass Damper (PATMD) was proposed by Carlisle (2013) for a single-degree-of-freedom system. "The results of the 'PATMD efficiency tests' demonstrate its capability of providing significant control to translational, torsional and coupled vibrations of the structure without being tuned in any way." (Carlisle, 2013) In an effort to further the research of PATMDs, an optimized damper is proposed for use in a multi-degree-of-freedom system.

1.2 Objectives of Study

According to Carlisle (2013) the PATMD improves upon the shortcomings of the TMD in that it does not require tuning to a specific frequency, provides effective control to torsional and coupled vibrations of the structure and is simple to implement. However, as mentioned previously, the investigation was limited to a single-degree-of-freedom system and further research would be required to investigate the PATMDs effect on multi-degree-of-freedom system.

Thus the objective of this research is to investigate the effect of a Passive Auto-Tuning Mass Damper on a multi-storey structure. The PATMD provides control by using inertial force to oppose movement of the structure. The mass damper investigated incorporates pulley connections, hence termed the Passive Auto-Tuning Pulley Damper (PATPD), which transfers a driving force caused by movement of structure to the damper thus increasing the damper control. The PATPD is similar to the PATMD in that it requires no tuning in any way.

The research will focus on the following goal: investigating the control effect of the PATPD on a multi-degree-of-freedom system subject to translational vibration, coupled vibration (translation and torsion) and torsional vibration.

1.3 Scope of investigation

In general the focus of this study was to investigate the control effect that a novel damper, PATPD, would have on a MDOF system. The damper was designed and constructed in the lab using readily available materials namely rope, sand and perspex-attesting to its simplicity. The MDOF system was modelled as a three storey rectangular steel structure.

Laboratory tests were performed both with and without the damper under different excitations. For free vibration tests the structure was fixed to a concrete base, and for forced vibration tests the structure was fixed to a shake table. In each test the structure is subjected to both free and forced excitation with and without the damper, which was placed on the third storey for all tests. The tests were solely to determine the efficacy of the damper in its control response and auto-tuning capability. This was determined by a comparison of both the time history of response and power spectral density (PSD) graphs with and without the damper.

The optimization of damper mechanics, the optimization of sand particle size used as the mass and the optimization of the location of the damper were not included in this investigation.

1.4 Outline of contents herein

Chapter 2 contains the 'Literature Review'; this is a comprehensive summary of the currently available literature on various types of vibration control devices in use. 'Background' gives a brief history of significant events that necessitated vibration control. 'Vibration control in Buildings' discusses building trends in modern society and documents the different damping systems used in buildings. 'Brief History of dampers' explains the origins of the first damper. 'Dampers types and Application'

discusses the various types of auxiliary damping systems and corresponding real life applications of said systems within structures.

Chapter 3 contains the 'Experimental Set-up', and 'Experimental Procedure', which describes the way the primary model (and any other test model) was set up as well as the procedure followed for all tests.

Chapter 4 contains the graphical representation, summary and discussion of results for the efficiency tests on the primary test model.

Chapter 5 contains the graphical representation, summary and discussion of results for the parameter tests on the primary test model.

Chapter 6 contains the graphical representation, summary and discussion of results for the test model when dynamic properties have changed.

Chapter 7 contains the 'Conclusion' summarises the findings and observations from the experimental test results, and 'Further Research' which suggests areas of the study that would require further investigation.

CHAPTER 2

Literature Review

2.1 Background

On September 1st 1923, Japan was struck by what was to be its most significant earthquake to date. **Figure 1** shows the aftermath of the magnitude 8.2 (on the Richter scale) earthquake. Due to a simultaneous typhoon, the fires induced by the earthquake escalated and increased with the disaster claiming the lives of approximately 130 000 people, destroying the port metropolis Yokohama with ninety percent of all homes being destroyed, and destroying an additional 350 000 homes in Tokyo leaving sixty percent of the population homeless (Denawa, 2005) .

Figure 1: Aftermath of the earthquake in Kanto, Japan, 1923 (Anon., n.d.)

As a result of this particular earthquake, the 1924 Revision of Law Enforcement Regulations was introduced. This was the first introduction of the consideration of seismic design forces used in the design and construction of structures (Douglas, 2013).

Main Street, Compton, California, Long Beach Earthquake of 1933
photo credit: Los Angeles Public Library

Figure 2: (CUREE, 1998)

Certain parts of the United States have also been seismically active. This too necessitated legislation to ensure safety. The Field and Riley Acts were signed into law by the Governor in 1933 after the Long Beach Earthquake (**Figure 2**).

The Riley Act stipulated that structures, other than houses, be designed taking into account lateral forces. All seismic codes written thereafter have descended from these two fundamental acts (CUREE, 1998).

2.2 Vibration control in buildings

The continuing economic prosperity and population increase in the urban areas point toward a future with increased activity in high-rise construction of residential and office buildings (Khan, 1965).

Money has been and still is a strong driver within society. Individual lifestyle is often, if not always, governed by money and how much of it one possesses or has the ability and or opportunity to obtain. Access to jobs and opportunities often increases with increasing proximity to a city as they are usually the country's economic hubs. Thus these become pull factors drawing people in from outer surrounding areas. The continuous increase in population is a serious problem within cities- especially those with land scarcity e.g. Tokyo, Dubai and New York City. Progress in engineering and technology has equipped engineers and contractors with more efficient materials, equipment and methods for the construction of these tall buildings. Thus the tendency in modern society within modern cities is towards constructing taller buildings- an observation made by Khan (1965) still trending today.

Figure 3 shows the actual figures of the number of tall buildings (tall buildings are classified as any structure 200m or higher) on the vertical axis against the years from 1960 to 2016 on the horizontal axis. From 1960 to 2014 there is a 98.0% increase in the number of tall buildings completed each year. And a 99.6% increase in the total number of tall buildings in existence per decade from 1920 to 2014.[2]

Tall buildings, or skyscrapers as they have become known, need be designed with consideration of the dynamic response of the structure. If this response is not accounted for, the building can be extremely dangerous to the inhabitants, bystanders and adjacent structures.

[2] The numbers for 2015 and 2016 are predictions only and thus ignored.

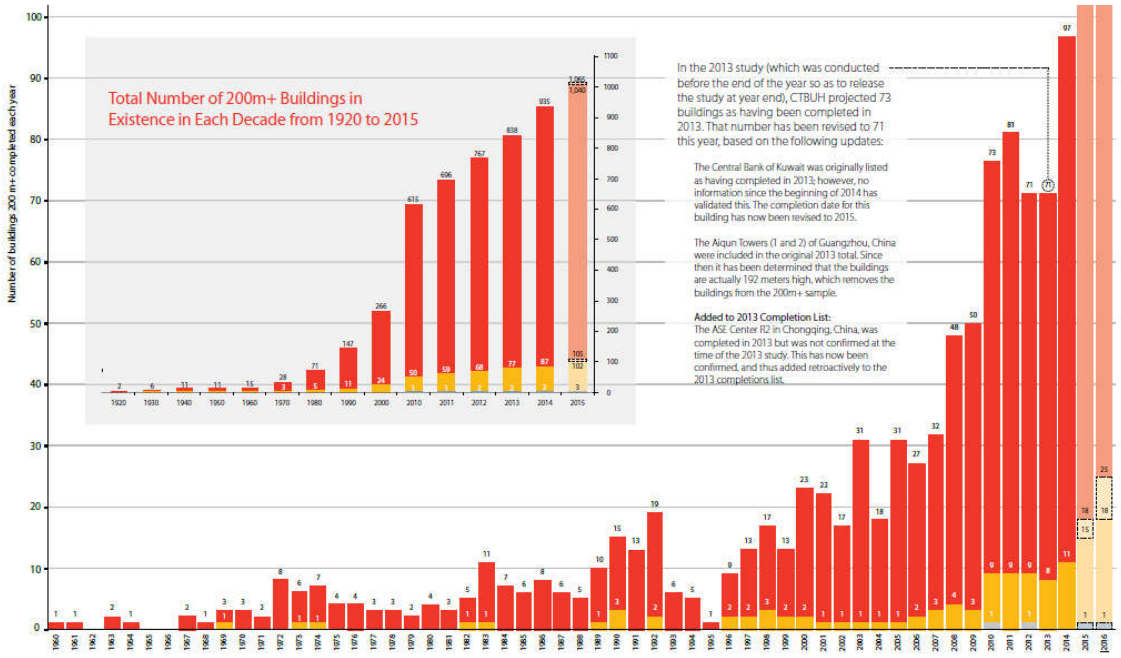

Figure 3: Number of 200m+ buildings completed each year from 1960 to 2016 (CTBUH, 2014)

A structural engineer's ultimate design goal is to produce an efficient and optimized design such that the structure is able to carry design loads throughout its lifetime, and such that it fulfils its function. The serviceability element of design deals directly with the comfort and aesthetics of the structure as it relates to its inhabitants or users.

Tall buildings, or skyscrapers, being high-rise in their nature possess high flexibility and low damping. This makes them much more susceptible to wind action. Especially for tall buildings, the wind force and seismic force are the dominant external design forces, except in some special cases (Tamura, 2009).

Wind loads at high altitudes are less predictable and are more complex. They can place extremely large lateral forces on tall structures, causing it to sway and twist (Mendis, et al., 2007).

Serviceability requirements are vitally important in high rise structures since the sway of the structure due to the wind action can cause much discomfort.

Table 1. Means to suppress wind-induced responses of buildings

Means	Type	Method & Aim	Remarks
Aerodynamic Design	Passive	Improving aerodynamic properties to reduce wind force coefficient	chamfered corners, openings
Structural Design	Passive	Increasing building mass to reduce air/building mass ratio	Increased Material Costs
		Increasing stiffness or natural frequency to reduce non-dimensional windspeed	Bracing Walls, Thick Members
Auxiliary Damping Device	Passive	Addition of materials with energy dissipative properties, increasing building damping ratio	SD, SJD, LD, FD, VED, VD, OD
		Adding auxiliary mass system to increase level of damping	TMD, TLD
	Active	Generating control force using inertia effects to minimize response	AMD, HMD, AGS
		Generating aerodynamic control force to reduce wind force coefficient or minimize response	Rotor, Jet, Aerodynamic Appendages
		Changing stiffness to avoid resonance	AVS

SD: *Steel Damper;* SJD: *Steel Joint Damper;* LD: *Lead Damper;* FD: *Friction Damper;* VED: *Visco-Elastic Damper;* VD: *Viscous Damper;* OD: *Oil Damper;* TMD: *Tuned Mass Damper;* TLD: *Tuned Liquid Damper;* AMD: *Active Mass Damper;* HMD: *Hybrid Mass Damper;* AGS: *Active Gyro Stablilizer;* AVS: *Active Variable Stiffness*

Figure 4: (Kareem, et al., 1999)

Figure 4 shows the systems commonly used to address wind action on the structure. Better still these systems can also assist in controlling the seismic response of a structure.

This research focusses on the third method of vibration suppression 'Auxiliary Damping Device'. Not only is this method applied for reduction of wind induced vibration, it is also vital in controlling the seismic response of a structure i.e. earthquake induced vibration. Hence, the first two methods will be explained briefly followed by an in-depth description of the third method.

Aerodynamic design

Research into the relationship between the aerodynamic characteristics of a structure and the resultant wind excitation has revealed useful results. This leads to the first method of motion/vibration mitigation (see Figure 4) namely aerodynamic modifications. This can be achieved via changes of a building's cross-sectional shape, the variation of its cross-section with height, or even its size, can reduce building motion (Kwok and Isyumov, 1998).

1. Changes in building geometry and cross section

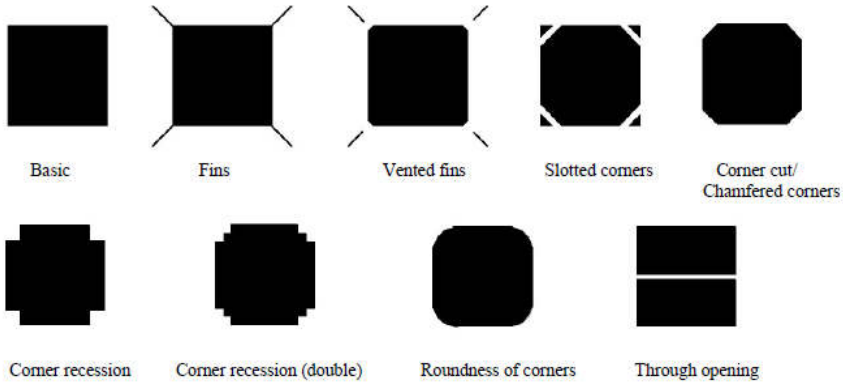

Figure 5: Aerodynamic modifications to Square building shape (Amin & Ahuja, 2010)

The Jin Mao building in China (Figure 6 (a)), the Petronas Towers in Malaysia (Figure 6 (b)) and the Burj Khalifa (Figure 6 (c)) have all benefited from the use of tapering effects, cutting corners, or dropping off corners, along the vertical axis, as height increases.

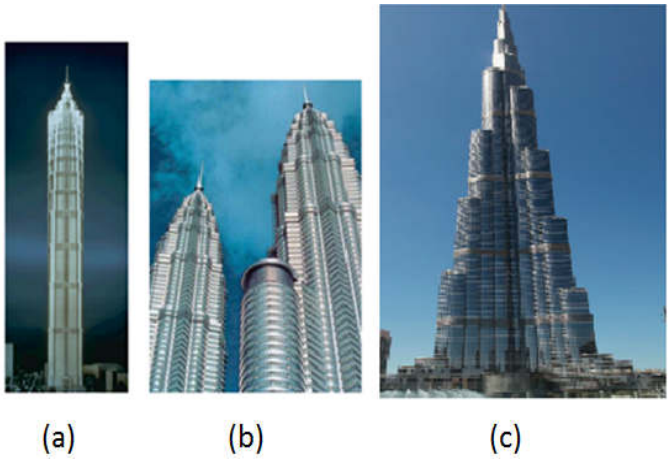

Figure 6: (a) Jan Mao Building China, (b) Petronas Towers Malaysia (Kareem, et al., 1999)**, (c) Burj Khalifa** (World, n.d.)

2. Openings

Another way to improve a buildings aerodynamic response is by the way of adding openings to the structure. These openings need to be located as close to the top of the building as possible and should be completely through the structure in order to be

effective. Reduced effects are felt if the openings are located at lower levels of the building.

It is imperative that these openings be tested thoroughly via wind tunnel testing to ascertain other effects on the building (Kwok and Isyumov, 1998).

Opening is not commonly used in design practice due to potential impact on useable spaces. However in some cases the corner slot can not only significantly reduce the across-wind excitation, but also make internal space design more logical (Xie, 2012).

The Shangai World Financial Center is a building that has effectively benefitted from such an opening Figure 7

Seeking to improve the quality of office spaces located on each of the four orthogonal faces, the new structural system decreased perimeter framing... depending on the breadth of the two sloping faces there is at most only one narrow column along its width. Hence, building occupants will be provided an extraordinary sense of openness and unparalleled views of the surrounding city of Shanghai (Katz, et al., 2008).

Figure 7: Building elevation plan of Shangai World Financial Center (Katz, et al., 2008)

Structural Systems

The second technique of vibration control employed is in the form of altering the structures mass or stiffness. Reduction of vibration/motion can be achieved by (a) increasing the building mass, or (b) increasing the building stiffness. It is not realistic or easy to increase the mass of a building significantly enough such that a reduction in motion is achieved. Since the primary goal is to improve habitability of the structure by reducing unwanted vibration that cause discomfort to users, increasing the stiffness could increase the "jerk response" of the structure which would be counterproductive. Hence an efficient and apt system should be chosen such that the resulting effects are desirable and positive. Some systems that are commonly used are: space frames, mega

frame systems, vierendeel frames, belt trusses, super columns, vierendeel-type bandages and outrigger trusses. Two of the most commonly used systems are elaborated on below.

1. Outrigger systems

These are rigid horizontal structures which are designed to improve the buildings overall stiffness and strength by connecting the buildings core or spine to distant columns. These systems are efficient and cost-effective. The outrigger system acts as arms engaging these distant or outer columns. When the core tried to tilt, its rotation at the outrigger level induces an opposition movement in the form of a tension-compression couple.

The benefits of an outrigger system lies in the fact that building deformations resulting from the overturning moments get reduced, on the other hand greater efficiency is achieved in resisting forces (Rana & Rana, 2014).

2. Belt/Bandage Systems

These are trusses or walls encircling the building which add further complexity to the above system. They improve lateral system efficiency. If used in conjunction with mega columns they assist in directing a greater gravity load to the mega column which aids in minimizing uplift.

In conjunction with external tube systems they reduce shear lag effects, engage axial stiffness and evenly distribute axial loads amoungst columns. For both mega columns and tubes they increase overall stiffness and torsional stiffness.

Auxiliary Damping Systems

These represent the third technique used in vibration control.

Structural damping is a measure of energy dissipation in a vibrating structure that results in bringing the structure to a quiescent state. The damping capacity is defined as the ratio of the energy dissipated in one oscillation cycle to the maximum amount of energy accumulated in the structure in that cycle. There are as many structural damping mechanisms as there are modes of converting mechanical energy into heat. The most important mechanisms are material damping and interfacial damping (Kijewski and Kareem, 2000).

The accuracy of the structural damping in a building is very low, and there is a significant uncertainty in the predicted wind-induced responses; thus the reliability of structural design is also very low. However, a certain amount of damping is guaranteed by using damping devices, and the reliability of structural damping can thus be improved significantly (Tamura, 2009).

Damping cannot be related to a single unique phenomenon. In addition, it is difficult to estimate how much damping a structure inherently possesses- thus the auxiliary damping concept. This is an external or auxiliary source that allows a specific amount of damping to be introduced or added to a structure. This can be achieved via the use of Passive, Active or Hybrid damping systems.

2.3 Brief history of Dampers Background

The British Army was the first to use hydraulic recoil dampers on gun carriages, in 1862. The first mass-produced hydraulic recoil damper was used on the 75 mm French field gun, Model M1897. The carriage of the weapon included a slide to support the gun itself, and a 1.2 m stroke fluid damper combined with a light spring to attenuate recoil energy and return the gun to battery. Towards the end of WWI, another advantage of fluid dampers was discovered - reduced recoil allowed weapons to easily fire larger projectiles. Thus the Paris Gun was created which had a 40 m long barrel, fired a 210 mm diameter shell at a range up to 135 km and weighed over 120 tons (Taylor, 2003).

Then in 1925 Ralph Peo of the Houdaille Company in Buffalo, New York, invented the first automotive fluid damper. This damper ensured – if only for a short while- that the automobile had a smooth ride over all possible road surfaces. The Houdaille rotary damper was actuated by crank arms attached to the moving components of the suspension.

Existing military fluid dampers were installed onto small models of buildings which were placed on a shaking table and subjected to a dynamic load. It was found that the dampers were highly effective in increasing the structure's earthquake resistance. In 1993, 186 of these dampers were used on the five buildings of the Arrowhead Regional

Medical Center in California which is located 3.2 kilometres away from the San Jacinto and 15 kilometres from the San Andreas active fault lines (Carlisle & Li, 2013).

Viscoelastic dampers were first used in 1973 in the famous World Trade Centre buildings in New York. The Tuned Mass Damper was first investigated in 1909 by Frahm, to reduce rolling motion and hull vibration of ships, which in 1928 was improved by Hartzog. This is to date one of the most commonly used passive dampers and gained its fame in 1973 when it was used in the John Hancock building in Boston (Taylor, 2003).

The above-mentioned dampers form the foundation upon which all current dampers and damping systems today are based. Research and analysis are on-going to ensure constant improvement and innovation such that better systems and methods are developed. This ensures that the field of structural dynamics and auxiliary damping systems is constantly growing and expanding to optimize design, safety, economy and comfort.

2.4.0 Dampers types and Application

Active and semi-active control is described first. Passive control is then explored in depth as this research pertains solely to passive control.

2.4.1 Active structural vibration control

Passive dampers are safe, reliable and require no power input. However these devices were incapable of adjusting to a variation in any parameters of the system. For this cause active control was born (Kareem, et al., 1999). The active mode has the ability to control a comparatively wide range of frequencies (Obata, et al., 1996). Active systems are systems that require power input but possess the ability to adjust to changes. A number of issues have come about whilst trying to implement this type of control device in real life structures, which has prevented their wide application. Firstly, AMDs require substantial power to operate. Secondly the time delay which occurs between the sensor picking up a motion of the structure and applying the control forces. This may cause the structure's motion and the control force to be unsynchronised, causing instability of the

structure and exacerbating the response. Furthermore, it is difficult to accurately model the primary structure in order to ascertain its natural frequencies. The control algorithm is created based on the modelling, however if the model is inaccurate, it will not be able to effectively control the structure (Datta, 2003).

One of the most common active damping devices is the active mass damper (AMD). Conventional AMDs generate control forces by accelerating and decelerating auxiliary masses. An actuator, frequently an electric motor, provides the necessary acceleration of such a control mass. The driving power depends on this acceleration and its maximum is generally larger for larger required control forces. Thus, the performance of a conventional active mass damper is limited by the capacity of the installed actuator. The acceleration of the control mass is associated with an increase of the mechanical energy of the control mass. Mechanical breaking power is needed to decelerate the control mass, thereby decreasing its mechanical energy. Consequently, during the continuous process of accelerating and decelerating the control mass, energy is cyclically input into the system and extracted again from the system. The effect of damping the structure results from the fact that the extracted energy is larger than the energy input into the system. By utilizing a force generation mechanism based on the motion of a control mass with constant velocity, an active mass damper can be created that requires significantly less actuator power compared to conventional active mass dampers. The "twin rotor damper" was proposed by (Scheller & Starossek, 2011) where the basic idea was to utilize centrifugal forces generated by pairs of eccentrically rotating masses (unbalances) in such a way that undesired force components cancel. It was shown that the twin rotor damper effectively reduced vibrations requiring only low mass ratios. The rotor damper is highly efficient. Contrary to conventional active mass dampers, the presented damper utilizes a motion with constant velocity leading to a low actuator power demand (Scheller & Starossek, 2011).

A novel AMD design method was proposed by (Ikeda, 2016) based on auto-regressive exogenous models of a building structure. The proposed method uses the results of system identification in the field of active structural control. The uncontrolled structure is identified as auto-regressive exogenous models via measurements under earthquake

excitation and forced vibration. These models are linked with an equation of motion for the AMD to introduce a state equation and output equation for the AMD– structure interaction system in the discrete-time space; the equations apply modern control theories to the AMD design. In the numerical applications of a 10-degree-of-freedom building structure, linear quadratic regulator control is used to understand the fundamental characteristics of the proposed design procedure. The feedback control law requires the AMD's acceleration, velocity and stroke; the structure's acceleration; and the ground acceleration as vibration measurements. The numerical examples confirm the high applicability and control effectiveness of the proposed method. One remarkable advantage of the proposed method is that an equation of motion for the structure becomes unnecessary for designing controllers (Ikeda, 2016).

For active systems energy recovery and vibration absorption has been widely studied [(Adhikari & Ali, 2012); (Tang & Zuo, 2012)]. Another such device was proposed by (Gonzalez-Buelga, et al., 2015) in the form of an electromagnetic vibration absorber (EVA) with energy recovery and frequency tuning control capabilities. The essential component of the EVA is an electromagnetic transducer. This interfaces between electrical and mechanical domains and is connected to an external electrical circuit. Currently the main use for electromagnetic devices in vibration-control is to harvest energy. The electromagnetic transducer acts as a damper in the mechanical domain by connecting a resistance across the terminals of the device. By emulating the resistive components, some of the power that would have been dissipated in the resistor can be converted into usable power. The experimental results are very promising: the presented EVA device can reduce the maximum displacement of the host structure, when compared with a passive device, and the amount of power needed to compensate for the losses in the coil is lower than the power available to harvest.

(Landau, et al., 2015) reviewed developments for adaptive feedback compensation of multiple unknown and time-varying narrow band disturbances and for adaptive feedforward compensation of broad band disturbances in the presence of the inherent internal positive feedback caused by the coupling between the compensator system and the measurement of the image of the disturbance; (Thao & Uchida, 2015) proposed two

techniques based on the feedback linearization (FBL) method to control the active and reactive output powers of three-phase grid-connected photovoltaic (PV) inverters. This is due to PV inverters being widely used to inject energy into the grid, addressing the control goal in PV inverters on how to deliver the active and reactive powers to the utility grid effectively. Piezoelectric materials are also important when using actuators which are what most active systems use as well as piezoelectric energy harvesting. Lead-free ceramics are considered suitable in piezoelectric use. KNN based materials were evaluated for the use of for active vibration control. These materials demonstrated better vibration control behaviour than that of conventional lead-based compounds (Sharma, et al., 2015). As mentioned before in order for an active control system to be efficient it is dependent on the control algorithm. (Ghaffarzadeh & Younespour, 2014) proposed a novel method using block pulse functions (which have been studied and applied frequently in recent years as a basic set of functions for signal characterizations in systems science and control). Their method evolves minimizing computational expenses of analytical approaches by a novel method to suppress the responses of the structure based on block pulse functions. Active base isolation, consisting of a passive isolation system combined with control actuators, has been proposed as an alternative means to address the drawbacks of passive isolation systems. The efficiency offered by the base isolation system in reducing interstory drifts and floor accelerations can be combined with the adaptive nature of the active control system to provide improved performance for a wide range of earthquakes [(Chang & Spencer Jr, 2010); (Yang, et al., 1996); (Nagarajaiah, et al., 1993); (Inaudi & Kelly, 1990)].

Extensive research has been dedicated to active control systems and their optimization the literature reviewed above is a brief summary of some of the research, as this paper pertains to passive control systems that will be the bulk of the review.

2.4.2 Passive structural vibration control

The passive strategy of vibration control utilizing tuned mass dampers (TMDs), tuned liquid dampers (TLDs), and other supplemental damping devices, such as those involving viscous or hysteretic energy dissipation, is the most widely applied. This is due to the systems simplicity and lack of external power supply reliance which in

essence makes them more reliable than other systems (Lu, et al., 2016). This section contains a detailed description of passive damping systems.

The concept of the TMD was created by Frahm, who received a patent for the idea in 1909. The first analysis of the TMD was performed by Den Hartog and Ormondroyd in 1929 (Verdirame, 2003). Vibration control of civil engineering structures using TMDs, which has been through numerous analytical and experimental verifications, is a widely accepted control strategy. Notably, TMDs can be incorporated into any structure with less interference than other energy-dissipation devices. The TMDs have been used in high-rise buildings, observatory towers, building floors, railway bridges, and pedestrian bridges against natural and man-made loadings since 1970 (Lin, et al., 2015).

A tuned mass damper (TMD) is a large, massive block, which is usually mounted on the top or near the top of a tall building. The system consists of a mass, springs and damping devices. Its frequency can be tuned to match the predominant vibration frequency (usually the first modal frequency) of the main structure, so that the structural dynamic responses caused by environmental excitations, such as strong winds and earthquakes, can be significantly reduced (Tuan & Shang, 2014). Energy is dissipated by the damper inertia force acting on the structure (Purdue University, 2002). (Den Hartog, 1956) derived classic results for the optimum TMD parameters for harmonic external forces for displacement minimization of a single-degree-of-freedom (SDOF) main structure (Tuan & Shang, 2014). There are studies which have focused on finding the optimum parameters for TMDs and on evaluating its efficiency under various types of dynamic excitations [(Chang, 1999); (Sgobba & Marano, 2010); (Patil & Jangid, 2011)]. Famous and successful applications of the TMD include the John Hancock Tower, The Citicorp Center, The Canadian National Tower and most recently the Taipei 101.

One of the greatest drawbacks with the TMD is that it requires tuning to a specific frequency which limits its efficiency to a narrow band control and its inadequate response to torsional vibration. A novel damper was proposed by (Carlisle & Li, 2013) to address these disadvantages: the passive auto-tuning mass damper (PATMD)

consists of a mass suspended in the top region of a structure which is forced into motion, due to inertia, when the structure is excited. The PATMD connects to the structure to be controlled by use of rope and is free to move in any translational direction. It moves relative to the structure, utilising and dissipating large amounts of energy as it swings from side to side, and in this way, the vibrational energy of the structure is absorbed and consequently the vibrations of the structure controlled. The PATMD provided significant control to translational, torsional and coupled vibrations of the structure without being tuned in any way; is effective under different system conditions, without having undergone any tuning or specific adjustment and is robust, uncomplicated and versatile. Further investigation is required to implement and optimize the system.

Multiple TMD systems have also been developed and use multiple TMDs to reduce structural vibrations. Instead of using a single large mass tuned to the structures natural frequency, a multiple TMD uses several smaller TMD systems. Multiple TMD systems are innately passive systems; however their design allows them to be more robust to detuning conditions than traditional passive TMD designs (Chen & Wu, 2001).

Initially the idea started with using two TMDs. To guarantee robust seismic performance of structures against detuning, the idea of using two small TMDs, termed a bi-TMD, was explored. The frequencies and damping ratios of the two TMDs are set to values close to the target value, which is the primary structure's fundamental frequency, rather than tuning them exactly. The performance of the bi-TMD is measured using two performance indices which evaluate its effectiveness – the 'nominal' index and the 'robust' index. The nominal index measures the bi-TMD's ability to reduce the building's motion response whilst the robust index measures the robustness of the bi-TMD under variations in the natural frequency of the structure. It was found that the 'nominal' performance of the bi-TMD was not a significant improvement over the single TMD; however, the robustness was greatly improved (Ok, et al., 2008). The tuned viscous mass damper (TVMD) [(Saito, et al., 2007); (Saito & Inoue, 2007); (Ikago, et al., 2009)] consists of a variable mass damper (VMD) with a rotational inertial mass, whose apparent effect is amplified by the ball screw mechanism, and a

spring that connects it to the structure. The additional TVMD vibration system is tuned to have a fundamental period close to that of the primary system. Substantial energy dissipation is achieved by the amplified relative displacement of the viscous material in the device. A single-degree-of-freedom (SDOF) system was used incorporating a TVMD to elucidate the characteristics of the device. A closed-form optimum design for the TVMD system was derived. An effectiveness comparison of viscous damper (VD), VMD, and TVMD was performed by examining the amplitudes of the primary system subjected to harmonic excitation. The TVMD system was found to be the most effective than the two conventional damper systems with the same additional damping coefficient for the two historical ground motions (Ikago, et al., 2012).

MTMDs – having more than two TMDs- have been researched hence: (a) A MTMD system which consists of a number of TMDs which have distributed natural frequencies close to the structure's fundamental frequency (Xu & Igusa, 1992), (b) from a given number of single TMDs, there exists an optimum MTMD having the optimum frequency range and the optimum damping ratio. Furthermore, the optimum MTMD is more effective than the optimum single TMD. MTMD can be more robust than a single TMD (Yamaguchi & Harnpornchai , 1993) and (c) MTMDs can be placed in one position or distributed around a building and can be designed in series or parallel configuration (Bergman, et al., 1991)

If the separate dampers composing the MTMD have the same natural frequencies then they behave as if a single TMD. In addition, the distributed frequency band should not be very wide as this would result in an inefficient system and interfere with the higher vibration modes of primary system. The effect of different variables such as number of dampers; the mass ratio of the individual dampers and the frequency range of the individual dampers on vibration control in the building which is subjected to wind loading showed: (a) adding more dampers to the system flattened the frequency response function (b) MTMD systems with variable damper masses and constant damper masses are similar, (c) frequency range of the dampers has the largest effect on efficiency and robustness and is thus a critical parameter., (d) mass and damping ratios, and the number of individual dampers play a secondary role in its performance, (e)

MTMD has better portability and constructability than TMD and (f) the system will not be compromised if one of the dampers in the MTMD fails or becomes detuned (Kareem & Kline, 1995).

In numerical study of a wind excited benchmark building with TMD/MTMD, the optimum parameters of TMD are obtained by numerical procedure; and the robustness of MTMD is investigated. The effects of design parameters such as mass ratio, damping ratio, number of dampers, tuning frequency and frequency band width is investigated. From the trends of the numerical results of the study, the following conclusions were drawn (a) the optimal value of tuning frequency ratio was close to 1, and the value becomes closer to 1 as the mass ratio decreases in cases of both TMD and MTMD (b) the sensitivity of performance to the tuning frequency ratio is reduced with increasing mass ratio in cases of both TMD and MTMD (c) the optimum value of damping ratio increases with mass ratio for TMD (d) in general the optimum damping ratio of MTMD system is found to be less than that of TMD (e) There exists an optimum damping ratio of MTMD for the performance criteria (f) the sensitivity of the performance to the damping ratio of TMD decreases with increase in mass ratio (g) increasing number of dampers in MTMD beyond 5 does not provide significant response (h) the performance of an MTMD is almost equivalent to that of a single TMD when there exists no uncertainty in stiffness, whereas an MTMD shows superior performance to a single TMD when stiffness uncertainty exists (Patil & Jangid, 2011). The 322m high Burj Al Arab, Dubai, is equipped with a MTMD to control wind induced vibration. It contains 11 four-ton TMDs which are attached to its exoskeleton. The TMDs are located in the columns on various storeys of the structure (Carlisle & Li, 2013).

Another passive control device is the tuned liquid damper (TLD) also known as the tuned sloshing damper (TSD). A TLD is similar to a TMD in principle except that a TLD uses liquid (usually water) as a secondary mass body (Cho, et al., 2012). A TLD is water confined in a container, usually placed on top of a building that uses the sloshing energy of the water to reduce the dynamic response of the system when it is subjected to excitation. The movement of water, which is usually problematic in static engineering regarding water tanks, is seen to be advantageous in dynamics. TLD has also been

found to be very effective in cancelling vibrations caused due to wind. Tuned Sloshing Dampers can be broadly classified into two categories, shallow-water and deep-water dampers based on the ratio of the water depth to the tank length in the direction of motion (Bhattacharyya, 2016). TMDs are the origin of TLDs. The more recent technology TLD is a superior choice to the TMD. The TLD is more effective for absorbing low frequency vibrations produced due to wind, it can substantially damp vibrations in a building, it is cost effective, requires less maintenance and easily implementable (Mondal, et al., 2014). Applications of TLDs include Gold Tower in Kagawa, Japan, Tokyo International Airport Tower (Kareem, et al., 1999) and the Sea Hawk Hotel & Resort (Nagase, 2000).

The tuned liquid column damper (TLCD) was also proposed and tested for vibration mitigating under both wind and earthquake-induced effects on structures. The TLCD was introduced by (Sakai, et al., 1989) and subsequently attracted attention of the vibration control community because of its appealing features, such as ease of installation and consistent performance under a wide range of exciting frequencies. The TLCD consists of a U-shaped tube filled with liquid (preferably water) with an orifice at the middle of the horizontal portion. During the course of motion, the liquid in the tube flows from one arm of the tube to another to trigger actuation of the control force. Very recently, the tuned liquid column ball damper (TLCBD) was been introduced by (Al Saif, et al., 2011) by replacing the fixed orifice with a rolling steel ball in the horizontal portion of the TLCD. The ball essentially acts as a movable orifice modulating the flow in the liquid column to improve the response reduction capability of the damper. The type of excitations adopted for demonstration is also confined to harmonic excitations with the view that the TLCD systems are primarily suitable for narrow-band excitation typically encountered in wind loading (Sourav, et al., 2015). More recently a new bidirectional tuned liquid column damper (BTLCD) was investigated by (Rozas, et al., 2016) for controlling the seismic response of structures. The device acts as two independent and orthogonal TLCDs, but due to its configuration, it requires less liquid than two equivalent independent TLCDs. The results show that the device performs well, and the reduction of the structure displacement and the rapid response decay obtained revealed that the device increases the damping of the controlled structure.

The passive impact vibration damper is also attractive as add on damping for slender structures. They are relatively inexpensive and generally do not require tuning as opposed to TMDs. An example of an impact damper is the ball impact damper where a steady state sinusoidal force acts on a mass and creates a resonant condition. The ball moves between the two walls due to the motion of the structural mass, M, and during a cycle of vibration the ball can impact either wall, both walls, or not impact the walls at all. Optimum damping exists when two impacts per cycle of vibration occur. Many variables are taken into consideration for the design of an impact vibration damper for a given structure; these variables include the amount of space required to locate an absorber on the structure and direction of motion of the structure. Further investigation is suggested to optimize the damper and the important variables that were identified after experimentation (Koss & Melbourne, 2014). The pounding tuned mass damper (PTMD) consists of an L-shaped beam and a specially designed damping element that utilizes viscoelastic material. This damper was found to be a promising method to mitigate the wind-induced vibrations of a cantilevered traffic pole. The displacement control effect was more promising than the acceleration with control. Further research was suggested to develop the design of the proposed system (Li, et al., 2013).

Viscoelastic dampers (VEDs) consisting of viscoelastic material (VEM) bonded to steel plates have been tested and installed in several large buildings structures to reduce seismic and wind responses (Lai, et al., 1996). Fluid viscous dampers (FVD) or Oil Pressure Dampers are forms of viscous damping devices. VEDs dissipate energy by applying a resisting force over a finite displacement through the action of a piston forced through a fluid-filled chamber for a completely viscous, linear behaviour, or in damping walls which use a full-story steel plate traveling in a wall filled with viscous material to provide added damping. Through careful design, the devices are capable of providing viscous damping to the fundamental mode and additional damping and stiffness to higher modes, and may, in effect, completely suppress their contributions, raising the structural damping to 20-50% of critical (Kareem, et al., 1999). These types of dampers are known as velocity-dependent dampers. More recently a comparison between the viscous damper, oil damper and viscoelastic damper was carried out to

determine the realistic seismic behaviour of passively controlled structures. A five-story steel frame, representative of commonly used office building constructions in Japan, was selected as the test specimen. In the test specimen, the velocity-dependent dampers were incorporated with steel bracing members to form 'damper braces'. The viscous dampers were tested first and the oil damper last because they were supposedly able to offer more supplemental damping than viscoelastic dampers. The study showed that (a) damping ratios of the specimen equipped with the velocity-dependent dampers decreased with the increasing order of modes, exhibiting obvious frequency dependency, (b) damping ratios of the specimen equipped with viscous dampers increased significantly along with an increase in vibration amplitudes, because of the viscosity nonlinearity of viscous dampers and (4) in small-amplitude vibrations, viscous and oil dampers provided much lower supplemental damping than their standards, whereas viscoelastic dampers could be very efficient (Ji, et al., 2013).

Unlike viscous and viscoelastic dampers, friction dampers (FDs) are nearly unaffected by amplitude, frequency, temperature or the loading cycles of excitation (Reinhorn & Valles, 1995). A typical friction damper device (FDD) consists of two parts: a mechanism to develop normal force and an interface which provides the dry solid friction to develop a frictional force resulting in desired energy dissipation. The damper consists of a series of wedges, which acting against each other under the load from a compressed spring; apply a normal force to the friction pads. The friction pads slide directly on the inner surface of the steel casing of the device. The friction pads are copper alloy with graphite plug inserts which provide dry lubrication to the unit ensuring a stable friction force and reducing noise during movement (Raut & Jangid, 2013). More recently a study performed on a second generation benchmark building by (Raut & Jangid, 2013) revealed: (a) friction dampers are found to be very effective in reducing performance criteria of the benchmark building for both pre- and post-earthquake evaluation models, (b) there exists an optimum slip force of the friction damper for minimum earthquake response of the benchmark building, (c) a slight variation in the optimum slip force of friction damper does not have much effect on the responses, (d) optimum number of dampers at appropriate locations can significantly reduce the earthquake response almost as much as they are installed on all the floors -

the floors having maximum displacements and high velocities should be selected for effective damper locations, (e) the responses with friction damper of constant slip force installed on all floors are as much as with friction damper of different slip force installed on optimised locations, (f) there is significant reduction in normed responses which depicts that the friction dampers are able to dampen out the responses quickly and (g) the maximum inter-story drift is reduced substantially at every floor of the structure for every earthquake test.

Base isolation is an anti-seismic design strategy that can reduce the effect of earthquake ground motion by decoupling the superstructure from the foundation. The structure can be decoupled from the horizontal components of the ground motion by interposing structural elements with low horizontal stiffness between the foundation and superstructure (Wu, 2001).

Base isolation can be employed to minimize inter-story drifts and floor accelerations via specially designed interfaces at the structural base, or at higher levels of the superstructure. The concept of base isolation is increasingly being adopted in order to minimize inter-story drift and floor accelerations. In this instance the control of structural forces and motion is exercised through specially designed interfaces at the structural base — or potentially at a higher level of the superstructure — thus filtering out the actions transmitted from the ground. The effect of base isolation is to essentially uncouple the building from the ground. There are two common categories of isolation hardware namely sliding bearings and elastomeric bearings. The friction pendulum system (FPS) is of the former category and is comprised of a stainless steel concave surface, an articulated sliding element, and cover plate.

The slider is finished with a self-lubricating composite liner. During an earthquake, the articulated slider within the bearing travels along the concave surface, causing the supported structure to move with gentle pendulum motions. Movement of the slider generates a dynamic frictional force that provides the required damping to absorb the earthquake energy. The lead-plug bearing (LPB) is of the latter category and consists of two steel fixing plates located at the top and bottom of the bearing, several alternating layers of rubber and steel shims, and a central lead core. The elastomeric material provides the isolation component with lateral flexibility; the lead core provides energy

dissipation, while the internal steel shims enhance the vertical load capacity whilst minimizing bulging. All elements contribute to the lateral stiffness. The steel shims, together with the top and bottom steel fixing plates, also confine plastic deformation of the central lead core. The rubber layers deform laterally during seismic excitation of the structure, allowing the structure to translate horizontally, and the bearing to absorb energy when the lead core yields. Lead-Plug and Friction-Pendulum isolator systems effectively reduce elastic base shears and inter-storey drifts, reduce structural and non-structural damage, protect building contents and reduce roof level accelerations (Andrade & Tuxworth, 2015).

2.4.3 Semi-Active structural vibration control

Semi-active control devices are a combination of the passive and active control systems. They respond quickly and require very low power input. They can operate on battery power in event of power loss during extreme excitation for example during an earthquake.

The Semi-active tuned mass damper (STMD) is a combination of a passive tuned mass damper (TMD) and an active control actuator. The ability of this device to reduce structural responses relies mainly on the natural motion of the TMD. The forces from the control actuator are employed to increase the efficiency of the STMD and to increase its robustness to changes in the dynamic characteristics of the structure (Spencer & Soong , 1999).

Numerical studies show that the STMD can reduce the structural responses similar to an active-tuned mass damper (ATMD), but with a significant reduction in power consumption. It also showed that the STMD with a 50kN capacity magnetorheological damper (MR), which is elaborated on below, can effectively control a full-scale tall building subjected to wind excitation (Kang, et al., 2011). Another study investigated the performance of a multi-storey passive and semi-active tuned mass damper (PTMD and STMD) for a 12-storey structure. Segments of the upper stories of structure were isolated to form the tuned mass. A semi-active resettable device is used for energy

dissipation. The time history of analysis shows a response reduction for all seismic disturbances tested. The large STMD was found to effectively manage seismic response for MDOF systems across a wider range of tested ground acceleration than passive solutions (Chey, et al., 2010). Another novel idea investigated the use of an adaptive pendulum tuned mass damper (APTMD). Pendulum tuned mass dampers (PTMDs) replace the translational spring and damper system of the TMD system with a pendulum, which consists of a mass supported by a cable which pivots about a point. An important advantage in using a PTMD as opposed to the TMD system is that it requires no bearings to support the TMD mass. The APTMD was found to provide the capability to autonomously tune to the structural frequency while providing control of the external damping to the PTMD mass. These capabilities allow the APTMD to adapt to changes in structural characteristics which could occur in real structures due to structural modification or deterioration (Lourenco, 2011).

One of the serious problems in the field of building seismic stability provision is the restriction of dangerous displacements occurring due to low-frequency seismic impact. Restriction of these displacements would be possible by means of application of special damping elements placed at the levels of floors (Belash, 2015). Viscous dampers work by using viscous fluid inside a cylinder, thus dissipating. Due to ease of installation, adaptability and coordination with other members also diversity in their sizes, viscous dampers have many applications in designing and retrofitting. This type of dampers is connected to the structure in three ways: (a) damper installation in the floor or foundation, (b) connecting dampers in stern pericardial braces and (c) damper installation in diagonal braces (Heysami, 2015). With friction dampers (FDs) seismic energy is spent in overcoming friction in the contact surfaces (Heysami, 2015). Dry friction dampers can be used as damping components. They are a reliable means for quakeproofing of the building. The most efficient variant of dry friction dampers placing is an even distribution of damping intensity over all floors. The efficiency of dry friction dampers work is achieved in case of intense propagation of relative shears at the level of mass-floors, propagation of which can be provided not only by flexion of building structures, but also by additional application of seismic isolation principle. At high frequency influence the effect is very insignificant, so, in case of certain forecast of

such earthquakes the level of swinging reduction can be provided directly by building structures themselves due to their flexibility and structural damping (Belash, 2015). A variable friction damper (VFD) was proposed by (Ribakov, et al., 2006). The unique feature of this damper is the use of a wedge-form part which changes the frictional force as a function of the displacement transferred to the damper.

Addition of the VFD to a viscous damped structure creates a hybrid system. The hybrid system compared to the viscous damped system yielded significant reduction in structural response; reduced peak displacements and peak accelerations - thus rendering the hybrid system an effective and attractive solution for practical use in buildings (Ribakov, 2011) .

Smart damping technology forms part of semi-active control which uses variable dampers such as: variable orifice, magneto-rheological (MR) fluid and electro-rheological fluid dampers. The MR damper is a type of viscous damper of which the viscous force generated within can be controlled. They are used in buildings to reduce its response in lateral directions, the damper should be placed between 2 points where a significant displacement is expected (Aly, et al., 2011). The “smart” fluids as they are called provide the energy dissipative mechanism for these devices and develop resistive forces under the application of an electrical or magnetic field. As a result, the degree of polarization of the fluid, and thus its dissipative capacity, may be modified by the regulation of the voltage source which controls the fields (Kareem, et al., 1999). Cyclic and hybrid tests performed on a tuned-mass magnetorheological damper (TM-MR) prototype damper found that the MR damper effectively controlled the TM displacements, as well as the simulated building response for different ground motions and harmonic excitation (Zemp, et al., 2011). A more recent development is a novel approach with MR dampers is a ‘Linear Matrix Inequality-based’ feedback version of the input shaping control theory. With this method the structures displacement is used to control the passive part, while the proposed input shaping scheme is used to produce the active damper response. The input shaping response, originally derived for second order systems, was expanded to account for the case of higher-order structures in the area of structural control. The required control force using the TM-MR was much less than

when using other controllers. The input shape comptroller results are less than comparable results with less control force required. Thus, the input shaping theory is highly recommended for more investigation (Alqado, et al., 2016).

More recently, a new application for eddy current damping was created by incorporating eddy current damping into a large scale pendulum based TMD in a super high building. A magnet is attached to the bottom of the TMD's mass. As the mass and magnet move in one direction eddy currents are induced creating a magnetic field which induces a counter-clockwise current hence producing a retarding force, thus retarding the movement of the TMD and dissipating energy. This system was implemented in the Shanghai Center Tower with a performance that was judged to be good as of 17 April 2016 (Lu, et al., 2016).

Other dampers recently in development and in use include dampers such as the semiactive distributed mass damper (DMD) (Fu & Johnson, 2016); semi-active shape memory alloy systems (SMAs) (Dhar, et al., 2015) and semi-active tuned liquid dampers (TLDs) (Soliman, et al., 2016).

2.5 Conclusions

The literature on vibration control is extensive with continual research into the improvement of the current damping systems and development of new systems. What is evident is the main disadvantage of each control system: (a) for the active system it is unreliability due to its reliance on power input, and (b) for the passive system its efficiency is limited to a narrow band control. This report proposes a Passive Auto-Tuning Mass Damper which eliminates both the above-mentioned disadvantages, rendering a control system that is not only reliable, robust and simple to implement but also effectively providing wide band control.

CHAPTER 3

Experimental Method

3.1 Introduction

The experimental approach was twofold (1) firstly a primary test model was subject to translational vibration, coupled vibration (translation and torsion) and torsional vibration such that its effectiveness could be established and (2) parameter tests (such as changing mass and stiffness of structure, changing mass of damper and changing configurations) were performed to investigate the range within which the PATPD remained effective. These tests were performed under free and forced vibration.

3.2.0 Experimental set-up and details

3.2.1 PATPD Efficiency Tests

The experimental tests were carried out on a flexible three storey test model. The primary model, as can be seen in Figure 8, consists of four 1.5m high, 8mm threaded rod columns with each storey being represented by a 300mm x 600mm x 10mm thick

S355J mild steel plate[3]. They are secured with nuts to the columns at a constant distance of 0.37m between each storey. Four more threaded rods are connected to the plate and are used for the sole purpose of connecting the PATPD to the model.

The columns are bolted to a base plate which in turn is fixed to a unidirectional shake table. The column base connection is fixed-fixed as are the column- plate connections.

Figure 8: Left - Primary model set-up, Top right - Data Logger and Bottom right - computer used

A model with the first natural frequency between 1.5 Hz - 2.0Hz was deemed an acceptable representation of a three storey structure [(Cha, et al., 2016); (Clinton, et al., 2005); (Lord & Ventura, 2016)]. Manual calculations and trial and error set-ups were conducted until an ideal set-up heights, as well as ideal column diameter, were obtained.

Via measurement, the primary test model's first three translational (along the length of structure or y-direction) natural frequencies, corresponding to the first three mode shapes are fn1 = 1.747Hz, fn2 = 5.095Hz and fn3 = 7.569Hz. The program SAP2000 was used to check that the measured and experimental frequencies were within close range. The corresponding natural frequencies[4], are fn1 = 2.033Hz, fn2 = 5.707Hz and

[3] The aspect ratio of the model was not considered a critical property in this experiment. It is the principle of the PATPD that is being investigated.
[4] The SAP2000 simulations and mode shapes can be found in the Appendix B.

fn3 = 8.270Hz. The difference is acceptable and attributed to the simulation being based on an 'ideal' test structure.

The PATPD, as can be seen in Figure 9, is made up of a Perspex[5] box with the same 2:1 aspect ratio of the model. The box is glued to a larger Perspex plate with the same aspect ratio, but which in addition has 8 holes punched into it. These eight holes form the connection mechanism for the rope that is used to secure the damper to the 8 pulleys. The pulleys are fixed diagonally to each of the 4 support columns of the structure with cable ties, and also transversely to each of the other 4 rods. The pulleys and rope transfer a driving force to the damper, caused by the movement of the structure. This movement is in an opposing direction to the structures movement. The box is then filled with 1.263kg of silica sand which represents 3% of the primary model's total mass of 42.09kg. The silica sand provides the mass of the damper. The mass provides an inertial force which in addition to the driving force of pulleys provides the vibration control of the structure. This box then sits on a roller support such that the damper has a 360 degree freedom of movement along the horizontal plane. The roller support is provided by use of 26 marbles of diameter 20mm which are enclosed within a ring that is fixed to the top storey of the model.

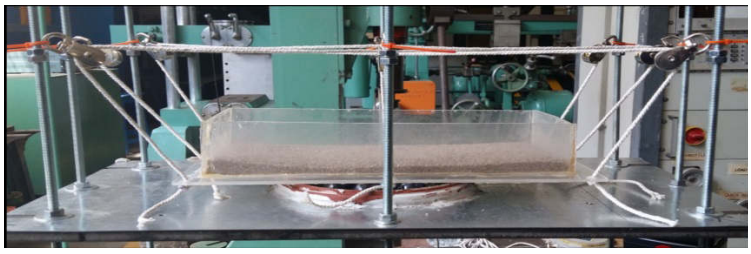

Figure 9: PATPD configuration

The test set-up including equipment used can be seen in Figure 8. Three accelerometers are securely fixed with a rubber-like temporary adhesive (Prestik) to each of the primary model's three storeys (in either the transverse or longitudinal directions depending on the direction of acceleration being measured). They are then connected – via a cable- to a data logger which records the accelerations within a user specified period. The data logger is also connected to a computer via a communications cable. The software

[5] Poly(methyl methacrylate) (PMMA) is a transparent thermoplastic also known as Plexiglas, Acrylite and Lucite

program TCE Build v21.0 is used as an interface such that tests can be run and test data from the logger saved.

Data processing is done via software programs Infield, Notepad and Matlab.

3.2.2 Parameter Study

A parameter study on the damper was performed by changing only one variable at a time with all else being constant. The selected variables were: Damper mass ratio, friction and connection configurations. They are explained in detail as follows.

3.2.2.1 Changing the PATPD Mass Ratio

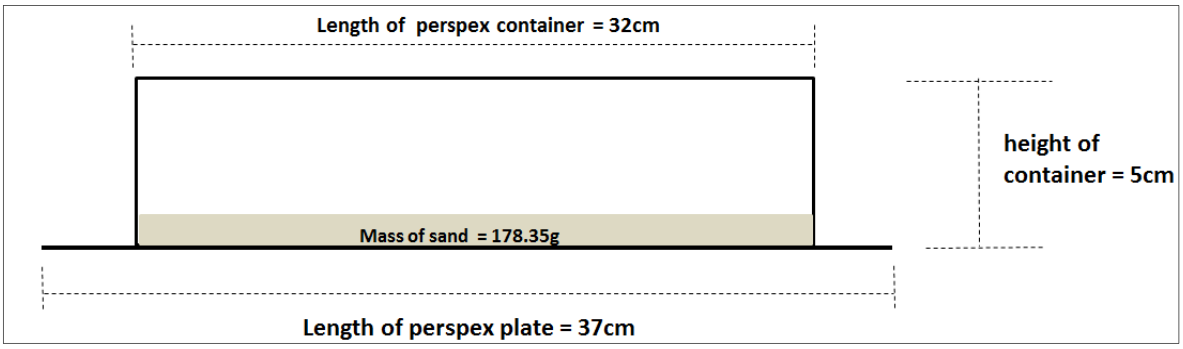

Figure 10: Schematic of 1.5% mass ratio (N.T.S)

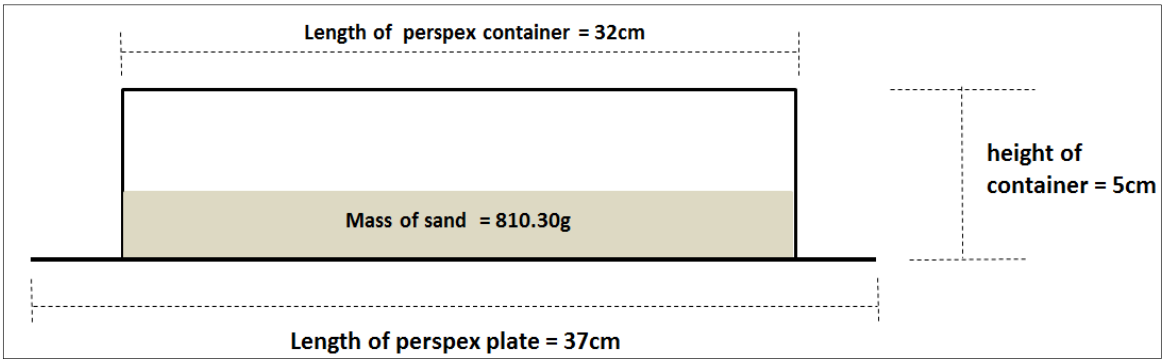

Figure 11: Schematic of 3% mass ratio (N.T.S), primary model mass ratio

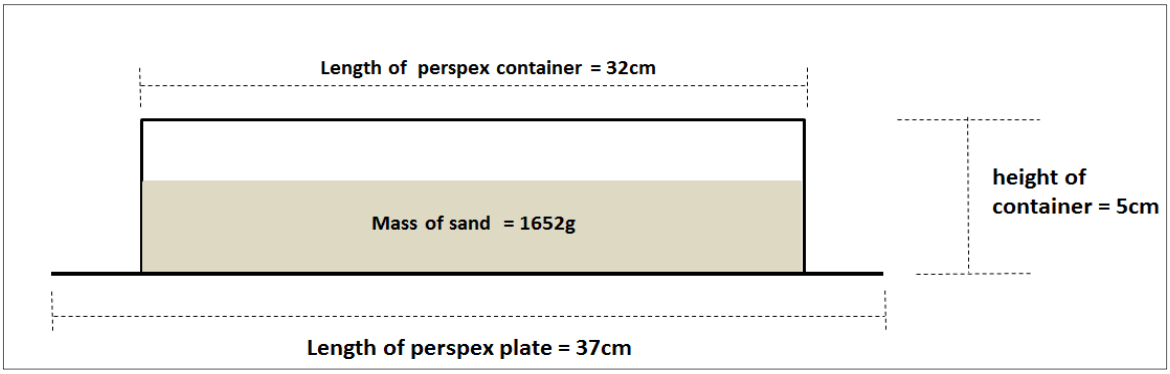

Figure 12: Schematic of 5% mass ratio (N.T.S)

The mass ratio of the damper was varied by changing the mass of the soil contained within the container: $mass_{soil} = \frac{mass\ ratio\ (\%) * mass_{total\ model}}{100} - mass_{container}$

, where $mass_{container} = 453g$

, and $mass_{total\ model} = 42\ 090g$

Figure 10, **Figure 11**, and **Figure 12** shows the mass ratios considered in the tests: 1.5%, 3% and 5%.

3.2.2.2 Changing the friction of PATPD support

Figure 13: Steel rolling surface, primary model

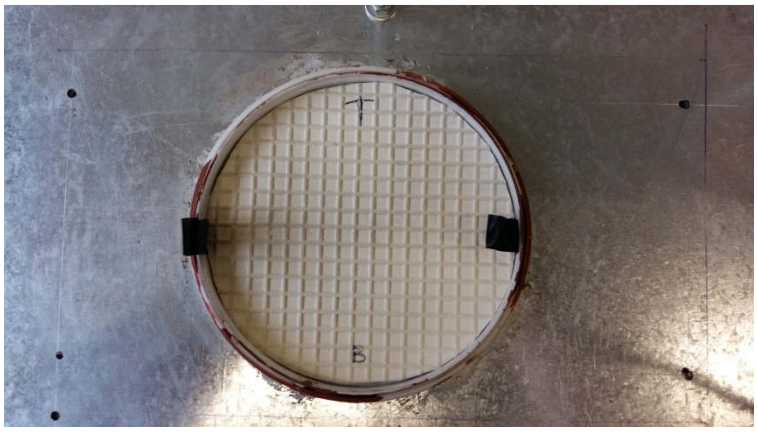

Figure 14: Rubber rolling surface

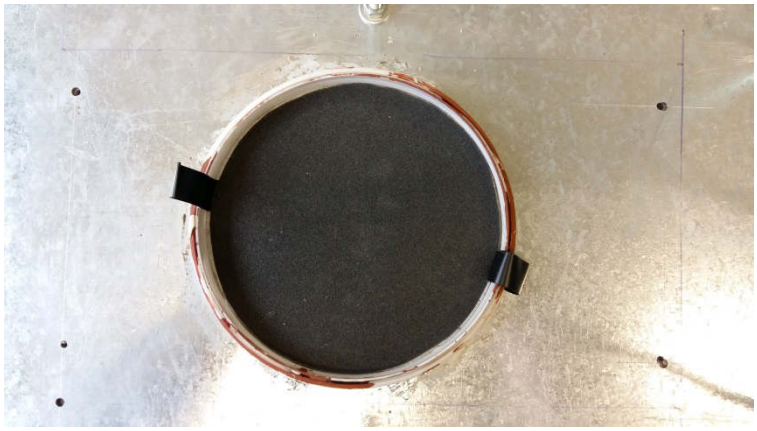

Figure 15: Sandpaper rolling surface

Figure 13, **Figure 14** and **Figure 15** shows the various rolling surfaces used. The primary model used least friction in the form of a steel plate (figure 34). The friction was then increased by using a rubber surface (figure 35) and by using sandpaper (figure 36).

3.2.2.3 Changing the PATPD connection configuration

(a) Configuration 1

Figure 16 shows the primary model with normal rope:

- height of 9cm to pulleys
- 8 pulley connections.

Figure 16: Primary configuration

(b) Configuration 2

Figure 17 shows 4 pulley diagonal connections only with normal rope.

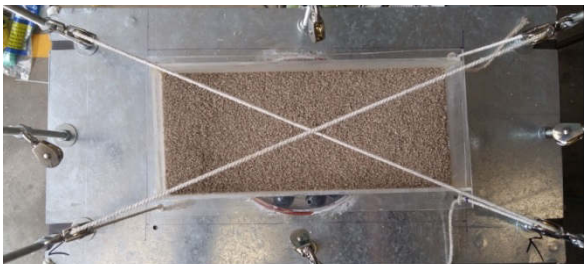

Figure 17: only diagonal connection

(c) Configuration 3

Figure 18 shows 2 pulley transverse connections only with normal rope.

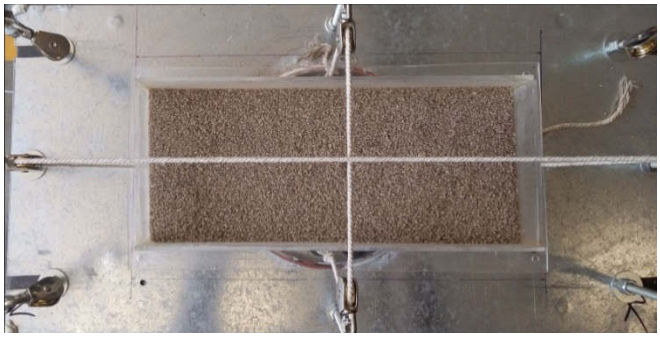

Figure 18: transverse connection only

(d) Configuration 4

Figure 19 shows the change height model with normal rope:

- height of 15cm to pulleys
- 8 pulley connections.

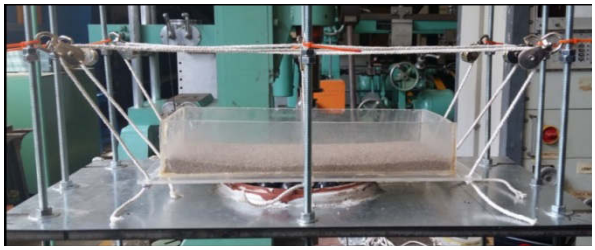

Figure 19: The height to connection 15cm

(e) Configuration 5

Figure 20 shows the model with nylon rope:

- height of 9cm to pulleys
- 8 pulley connections.

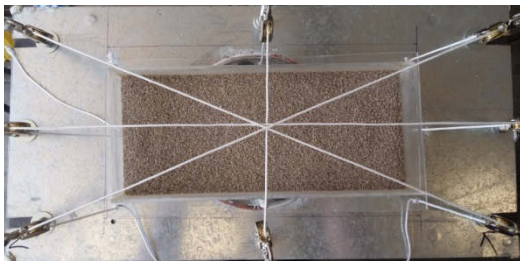

Figure 20: Nylon rope

(f) Configuration 6

Figure 21 shows the model with ski rope:

- height of 9cm to pulleys
- 8 pulley connections.

Figure 21: Ski rope

3.2.3.0 Changing Dynamic Properties

3.2.3.1 Changing model mass

Figure 22, **Figure 23** and **Figure 24** show changing of model mass. To increase overall structural mass only storey 1 and 2 are loaded with weights (figures 44-45). 1kg weights are used.

Figure 22: Primary model with mass 42.09kg

Figure 23: Model with mass 54.09kg

Figure 24: Model with mass 66.09kg

3.2.3.2 Changing model stiffness

Figure 25 shows a schematic representation of the variation of stiffness. **Figure 25** (a) shows primary model height which is the maximum possible height achievable without columns buckling (b) shows the first decrease in height and (c) shows a further decrease.

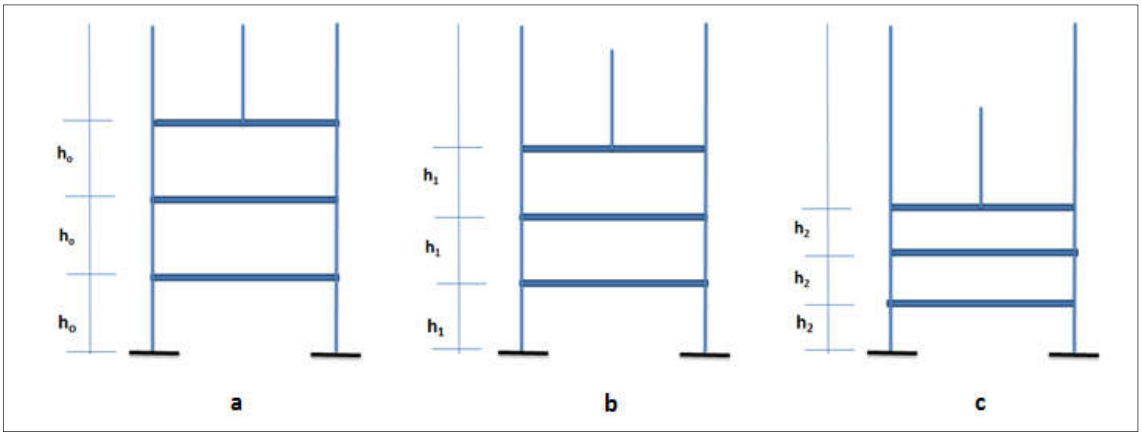

Figure 25: (a) primary model original height ho = 37.00cm, (b) height change 1 h1 = 32.00cm, (c) height change 2 h2 = 27.75cm

3.3.0 Experimental procedure

3.3.1 Free Vibration tests

Free Vibration tests were executed as follows:

1. Efficiency tests performed on:
    - Primary undamped model
    - Primary damped model as shown in configuration 1 as shown in Figure 37.

2. Parameter tests performed on:
    - Damped model using configurations 2-6 as shown in Figures 38-42.

3. Tests after dynamic property changes:
    - Undamped model.
    - Damped model as shown in Figures 43-46

Figure 26: Direction definition used for testing

The tests were performed as 3 sets of excitation on both damped and undamped models, with directions used shown in **Figure 26**:

a) **Translational:** the model is given an initial displacement of 35mm (measured using a dial gauge) in the x direction. Accelerometers are placed on each storey in the x direction to measure accelerations. This process is then repeated for the y direction.

b) **Torsional:** the model is subject to an initial twist and then released. Accelerometers are set up in x direction to measure accelerations. This process is then repeated with accelerometers set up in y direction to measure accelerations.

c) **Coupled:** the model is then subject to two coupled excitations achieved by applying translational and torsional displacements simultaneously. This is performed for both x and y directions with accelerations measured respectively.

A sampling frequency of 500Hz is used i.e. 500 acceleration readings taken per second. Time-history of acceleration graphs and Power Spectral Density (PSD) graphs are used to show the PATPD's damping effects.

3.3.1 Forced Vibration tests

These tests were also carried out on both damped and undamped model. In order to produce a sinusoidal base excitation, the test model was fixed to a unidirectional shake table. A sampling frequency of 500Hz was still used for measuring acceleration of structure. Forced vibration tests were restricted to translational in the x and y directions only, since forced torsional excitation could not be produced. A frequency sweep from 0.2Hz to 8Hz in 120 seconds was used.

Power Spectral Density (PSD) graphs are used to show the PATPD's damping effects.

CHAPTER 4

Experimental results: Primary Model PATPD Efficiency tests

4.1 Damper optimization

Carlisle (2013) investigated the Passive Auto-tuning Mass Damper (PATMD) which used a solid steel weight to provide the required mass to the damper. Due to the initial high acceleration peak incurred when the damper is engaged, an alternative form of mass was used. Silica sand was found to be most suitable; the grains used allowed the sand mass within the damper to move gradually, unlike the solid weight which has a sudden jerk when it is engaged, thus reducing the initial high acceleration peak.

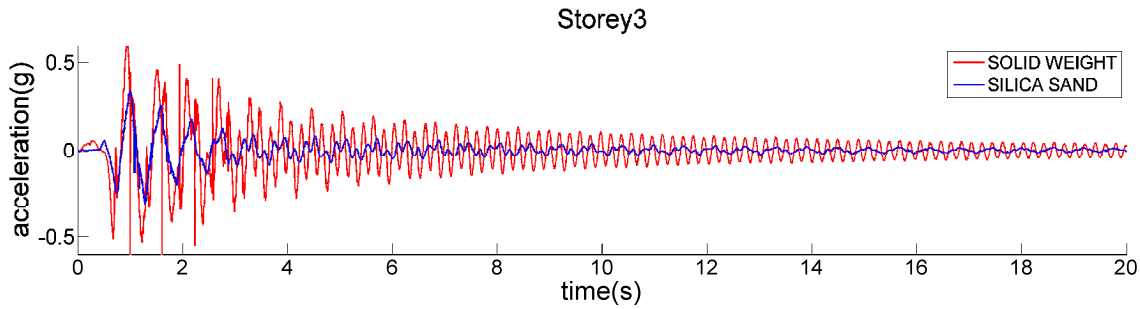

Figure 27: Time history of acceleration response for free translational vibration in the x-direction

Figure 27 shows the time-history of acceleration graph for the x-direction. Storey 3 is used for comparison since it is the storey with the highest acceleration and is used as worst case. As can be seen the initial acceleration peak is significantly reduced with the use of silica sand instead of a solid weight. Thus the PATPD used silica sand to provide the damper mass instead of a solid steel weight.

The PATMD was suspended from the structures columns using rope. The damping control was provided by the inertial force induced by the mass of the damper. The PATPD used pulleys and rope which provided an additional driving force to the damper. When the structure started moving under excitation the ropes transferred a force (termed the driving force) to the damper which caused it to move in the opposite direction. Since the damper rested on a roller support it was free to move in all horizontal directions limited, only, by the length of the rope. The opposition of movement provided additional driving force which improved the PATPDs' control effect.

4.2 Free Vibration

4.2.1 Translation in the X-direction

The undamped primary test model was manually displaced by 35mm and then released in the x-direction and the corresponding accelerations measured. The PATPD was then connected and the process was repeated. The comparison of results is in the form of acceleration-time and power spectral density graphs.

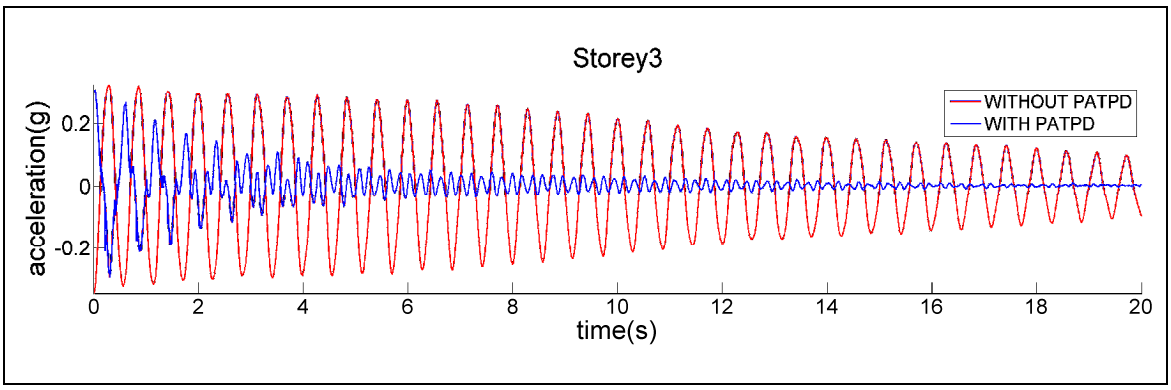

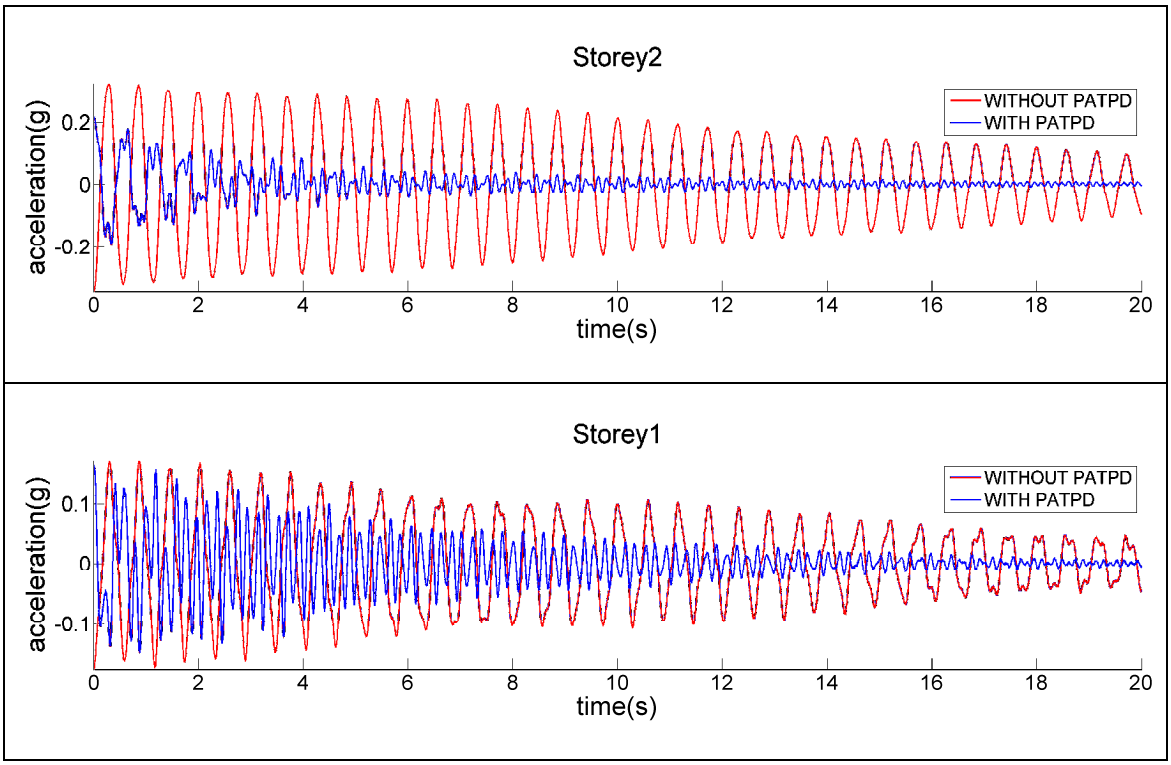

Figure 28: Time history of acceleration response per storey for free translational vibration in the x-direction, primary model

Figure 28 shows that at the beginning of the test for all 3 storeys, as the PATPD started moving, the acceleration peaks generated in the damped model were as high as those generated in the undamped model. However, in less than a second the high accelerations subsided and the accelerations rapidly decrease compared to that of the undamped model. As is expected, the accelerations experienced in storey 3 were highest but the positive damping effect of the PATPD was still significant.

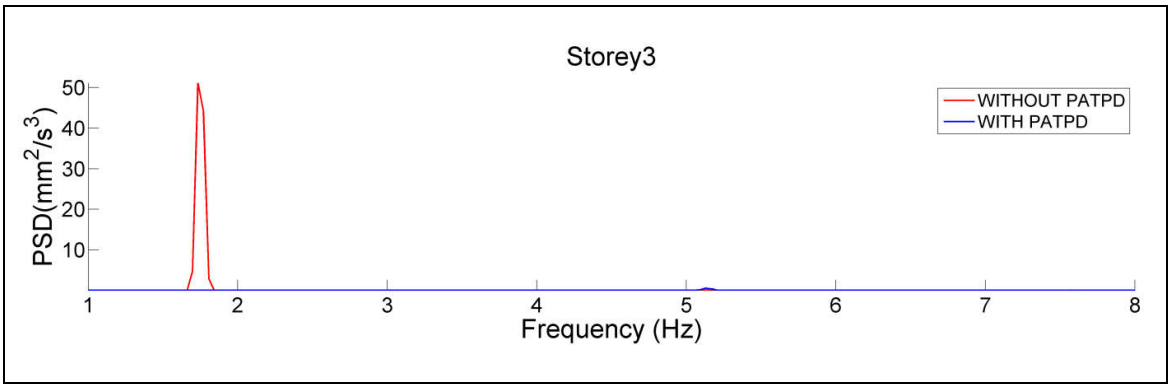

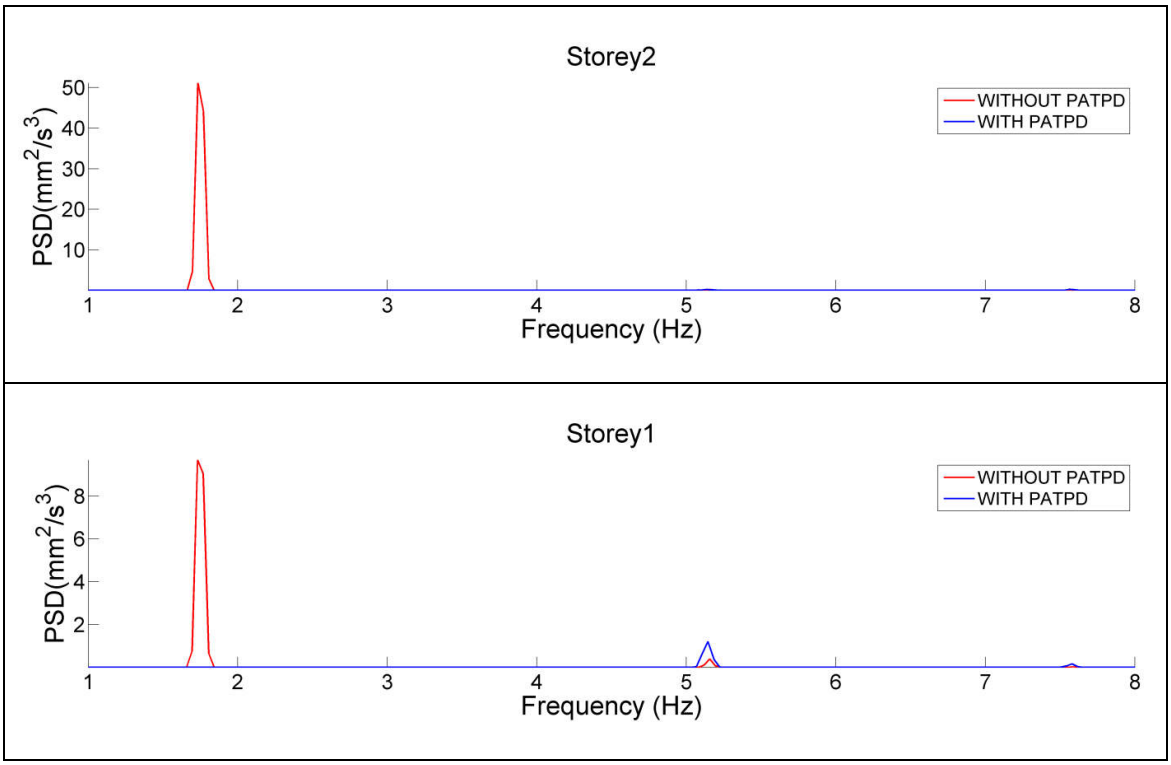

Figure 29: Power Spectral Density (PSD) per storey of the acceleration response for free translational vibration in the x-direction, primary model

Figure 29 shows the PSD for storeys 3-1: there is high peak at 1.733Hz, 5.164Hz and 7.584Hz. This represents the model's first, second and third natural frequency for translation in the x-direction.

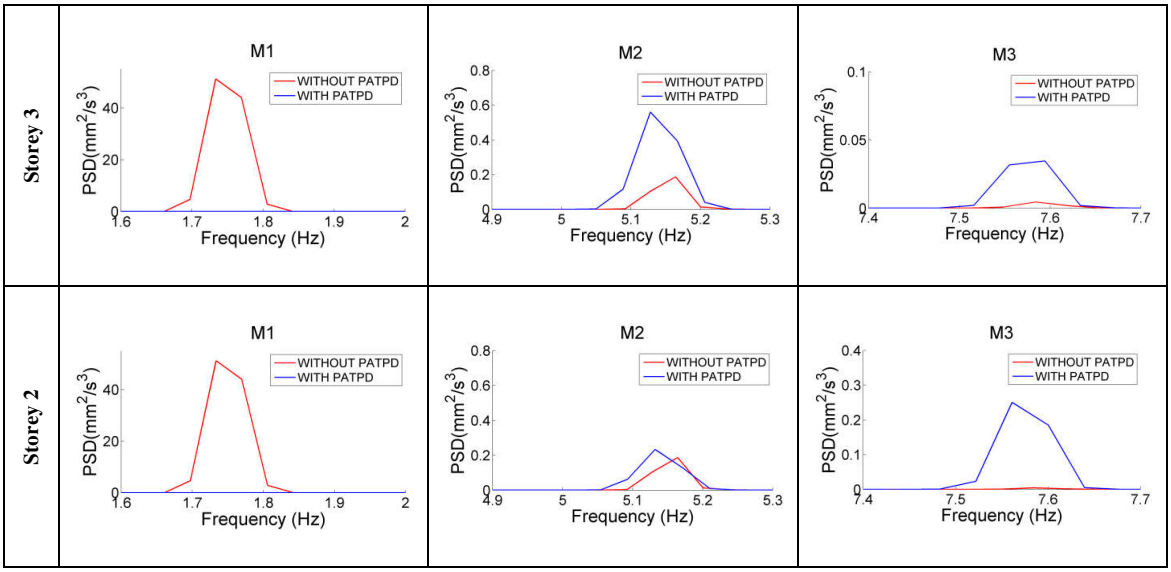

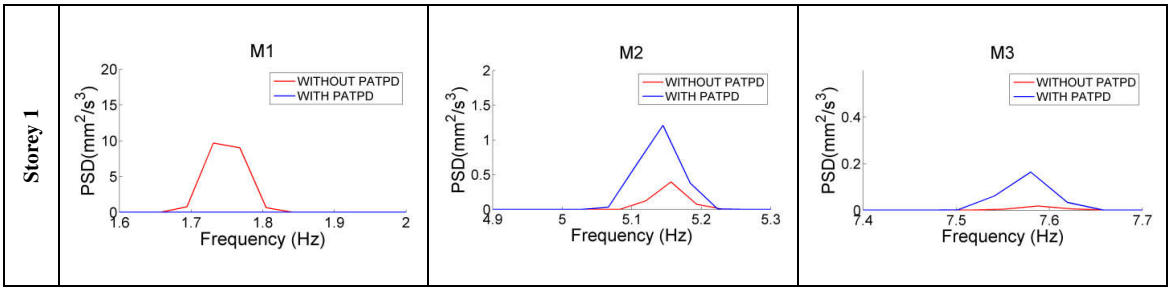

Figure 30: Magnified Power Spectral Density (PSD) per storey of the acceleration response for free translational vibration in the x-direction, primary model

As can be seen in Figure 30, the PATPD provided a high level of attenuation for all 3 storeys to the first natural frequency. The peak under consideration, at 1.733Hz was reduced by at least 99.9%. The PSD peaks at 5.164Hz and 7.584Hz, corresponding to the second and third natural frequency shows an increase with the addition of PATPD. However, this increase is minimal in comparison to the reduction gained in PSD peak for the first natural frequency.

4.2.2 Translation in the Y-direction

The primary test model was manually displaced by 35mm and then released in the y-direction and the corresponding accelerations measured. The PATPD was then connected and the process was repeated. The comparison of results is in the form of acceleration-time and power spectral density graphs.

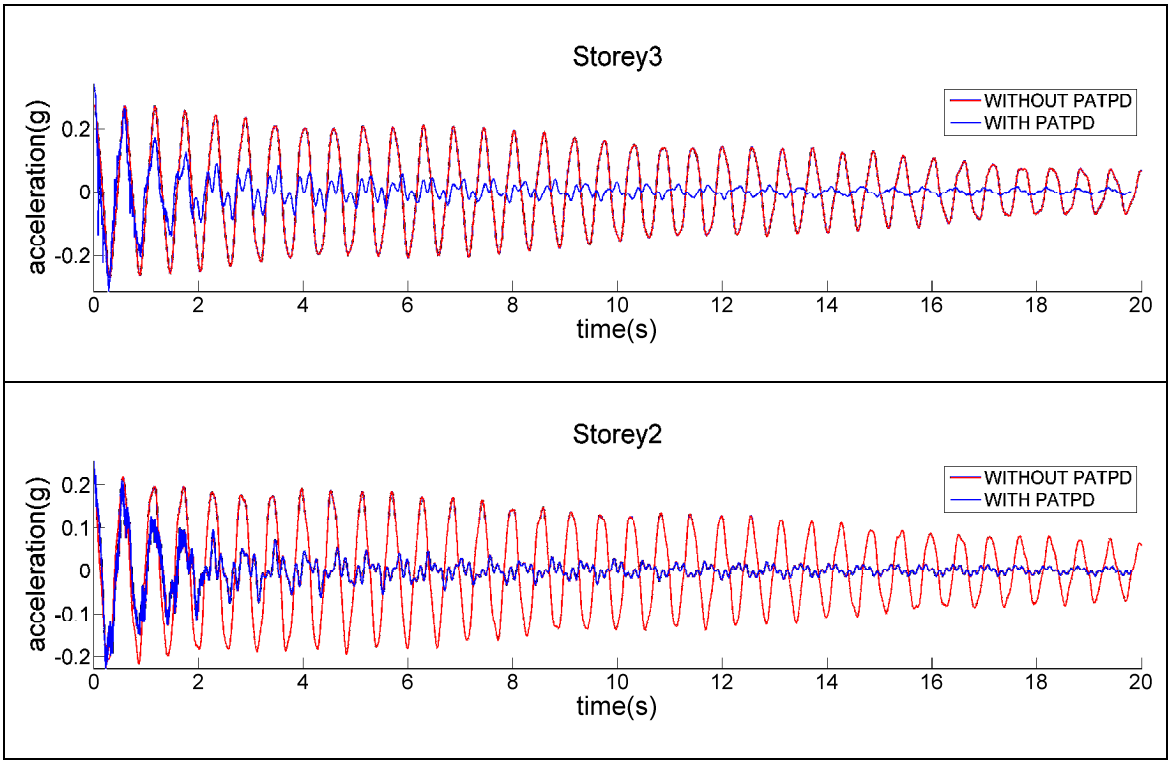

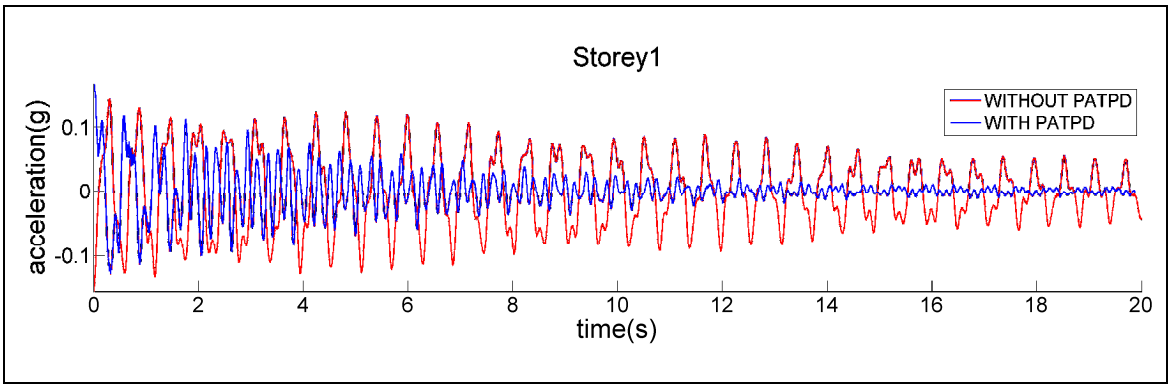

Figure 31: Time history of acceleration response per storey for free translational vibration in the y-direction, primary model

Figure 31 shows similar results to y-direction, at the beginning of the test for all 3 storeys, as the PATPD started moving, the acceleration peaks generated in the damped model were as high as those generated in the undamped model. However, in less than a second these high accelerations subside and the accelerations rapidly decrease compared to that of the undamped model. As is expected, the accelerations experienced in storey 3 were highest but the positive damping effect of the PATPD was still significant.

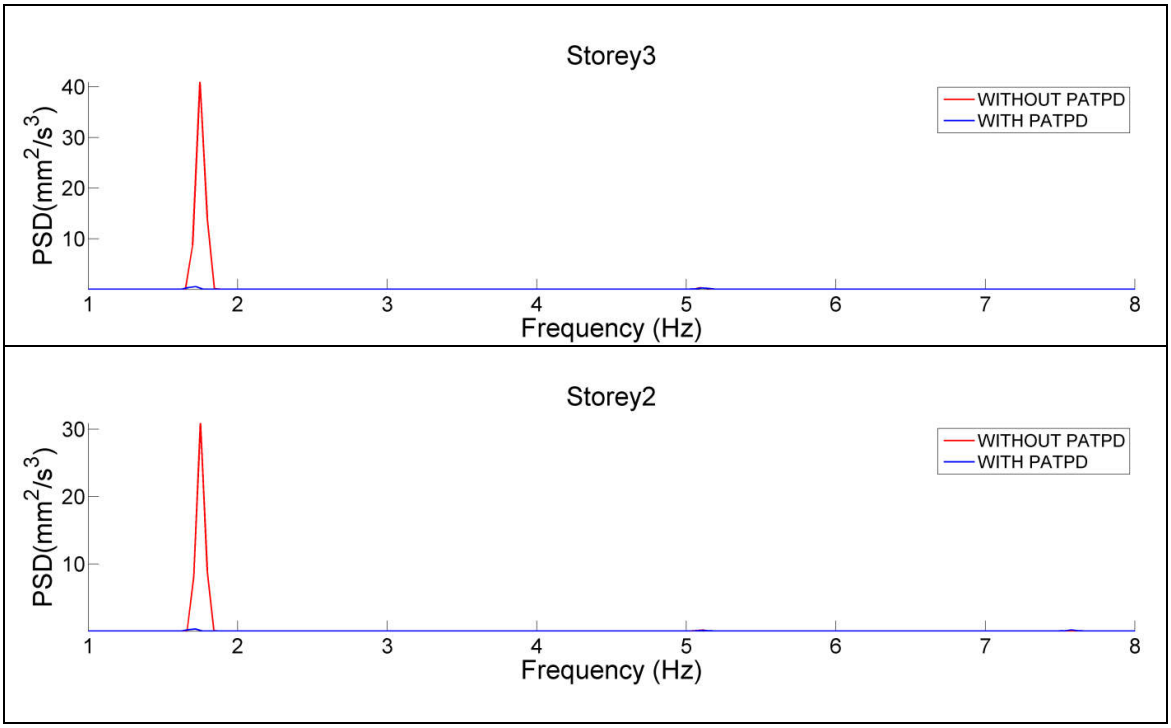

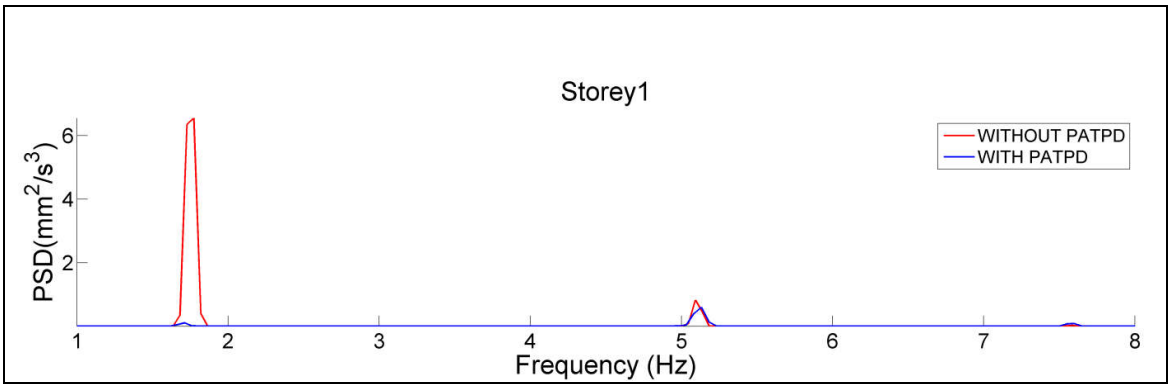

Figure 32: Power Spectral Density (PSD) per storey of the acceleration response for free translational vibration in the y-direction, primary model

Figure 32 shows the PSD for storeys 3-1: there is high peak at 1.747Hz, 5.095Hz and 7.569Hz. This represents the model's first, second and third natural frequency for translation in the y-direction.

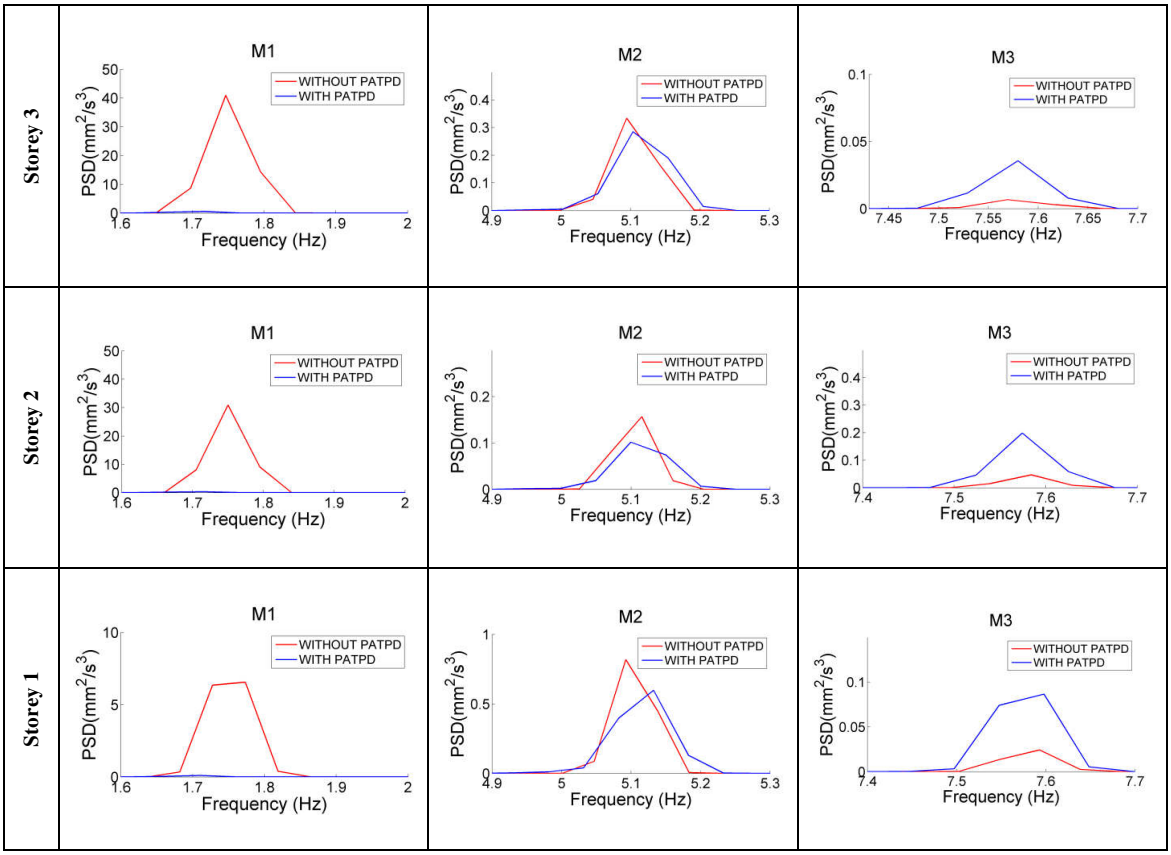

Figure 33: Magnified Power Spectral Density (PSD) of the acceleration response for free translational vibration in the y-direction, primary model

As can be seen in Figure 33, the PATPD provided a high level of attenuation for all 3 storeys to the first natural frequency. The peak under consideration, at 1.747Hz was reduced by 98.7%. The PSD peak at 5.095Hz, corresponding to the second natural

frequency also shows slight attenuation for storeys 3-1 respectively. The PSD peak at 7.569Hz, corresponding to the third natural frequency shows an increase with the addition of PATPD. However, this increase is minimal in comparison to the reduction gained in PSD peak for the first natural frequency. The PATPD has achieved control for translational vibration in the y-direction.

As can be seen from the set of results from both directions the PATPD provided better control in the x-direction than in the y-direction.

4.2.3 Torsional Vibration

The primary model was displaced torsionally before releasing it and the corresponding accelerations measured for both the x and y directions. The PATPD was then connected and the process was repeated. The comparison of results is in the form of acceleration-time and power spectral density graphs.

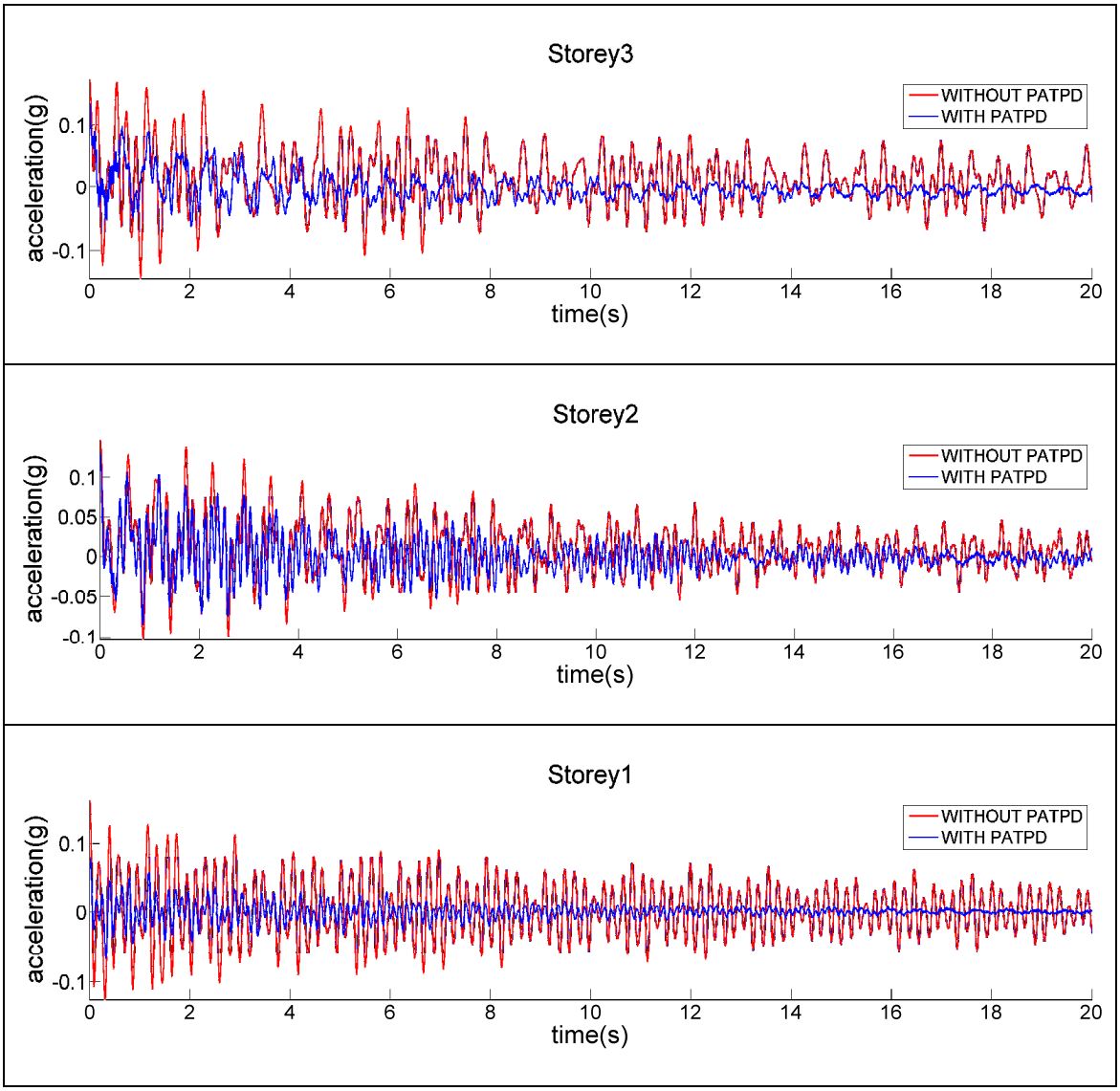

Figure 34: Time history of acceleration response per storey for free torsional vibration in the x-direction, primary model

According to Figure 34 time history of acceleration response for the model containing the PATPD shows a more gradual decrease in accelerations as opposed to the translational time history graphs. However, the effect of the PATPD is still obvious as time passes for all 3 storeys.

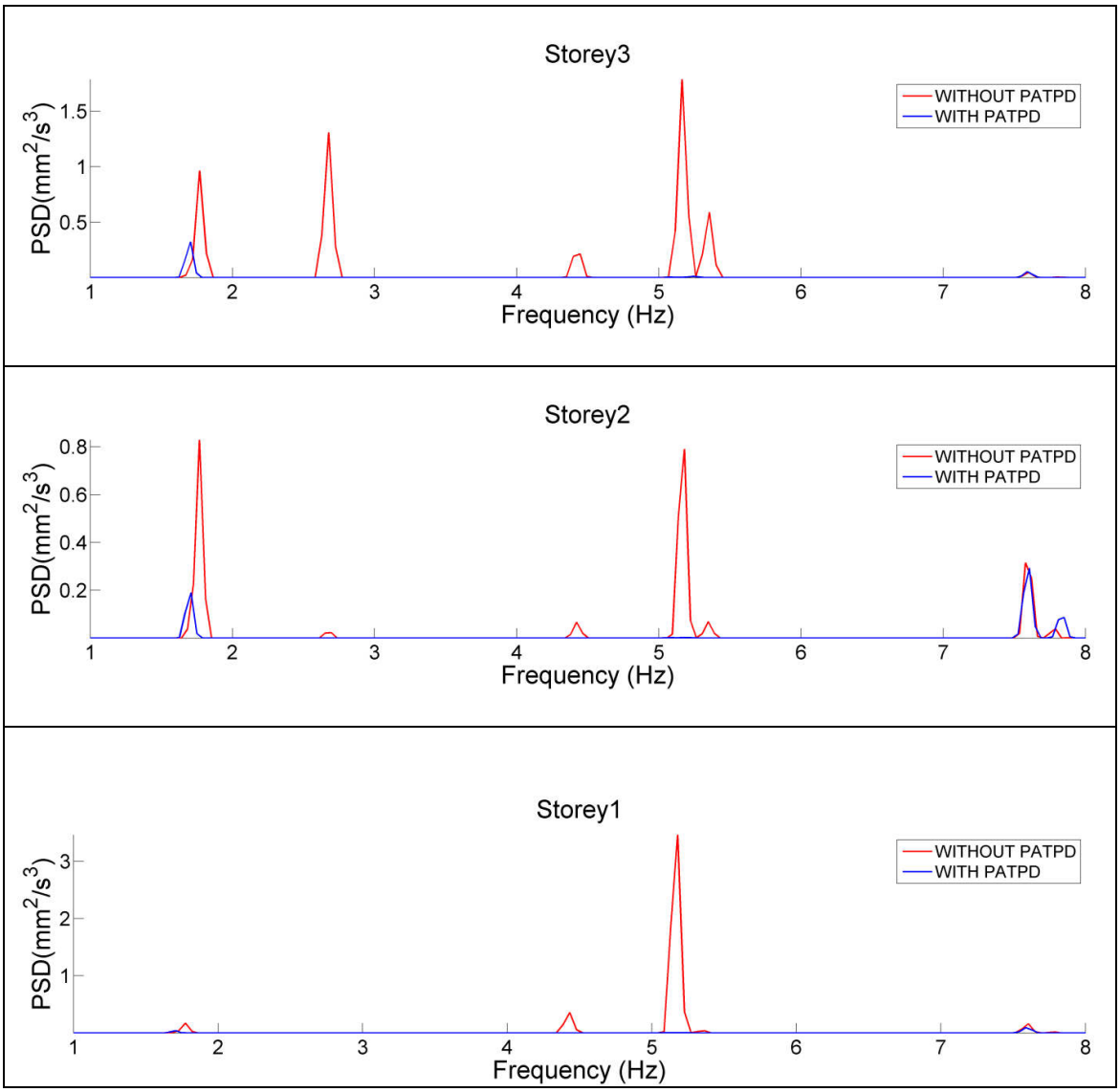

Figure 35: Power Spectral Density (PSD) per storey of the acceleration response for free torsional vibration in the x-direction, primary model

Figure 35 shows the PSD for storeys 3-1: there is a high peak at 2.677Hz, 4.446Hz and 7.792Hz. This represents the model's first, second and third natural frequency for torsion in the x-direction.

Peaks at 1.733Hz, 5.164 Hz and 7.584Hz indicate that although the model was excited in torsion, it had some movement in the x-direction as well. All translational peaks are significantly attenuated as well demonstrating the positive control effect of the PATPD.

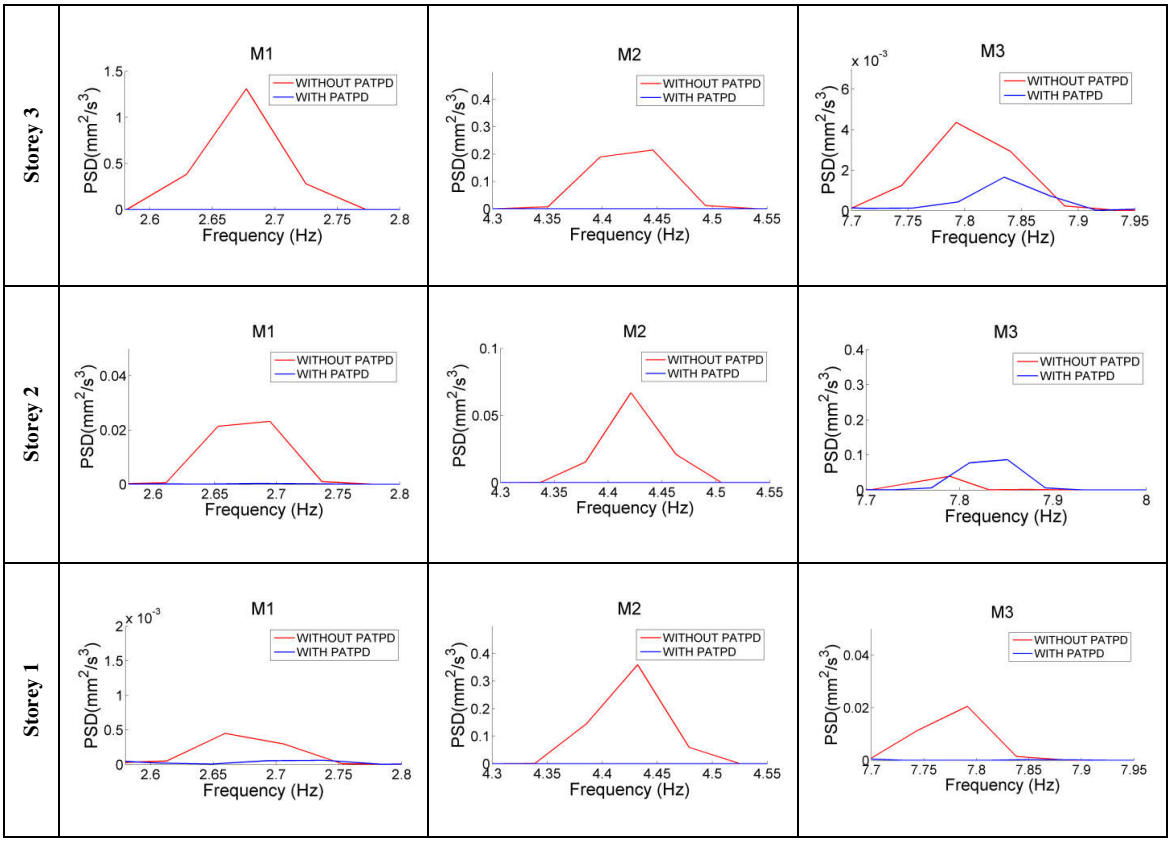

Figure 36: Magnified Power Spectral Density (PSD) per storey of the acceleration response for free torsional vibration in the x-direction, primary model

As can be seen in Figure 36, the PATPD provided a high level of attenuation for all 3 storeys to the first and second natural frequency. The peaks under consideration, at 2.677Hz and 4.446Hz were reduced by at least 99%. The PSD peak at 7.792Hz, corresponding to the third natural frequency for storey 3 attenuated by at least 50%, storey 2 showing a minimal increase in PSD peak and storey 1 attenuated by at least 99%. The PATPD achieved positive effect overall in the x-direction for free torsional vibration.

The comparison of results is in the form of acceleration-time and power spectral density graphs for torsional vibration in the y direction are as follows:

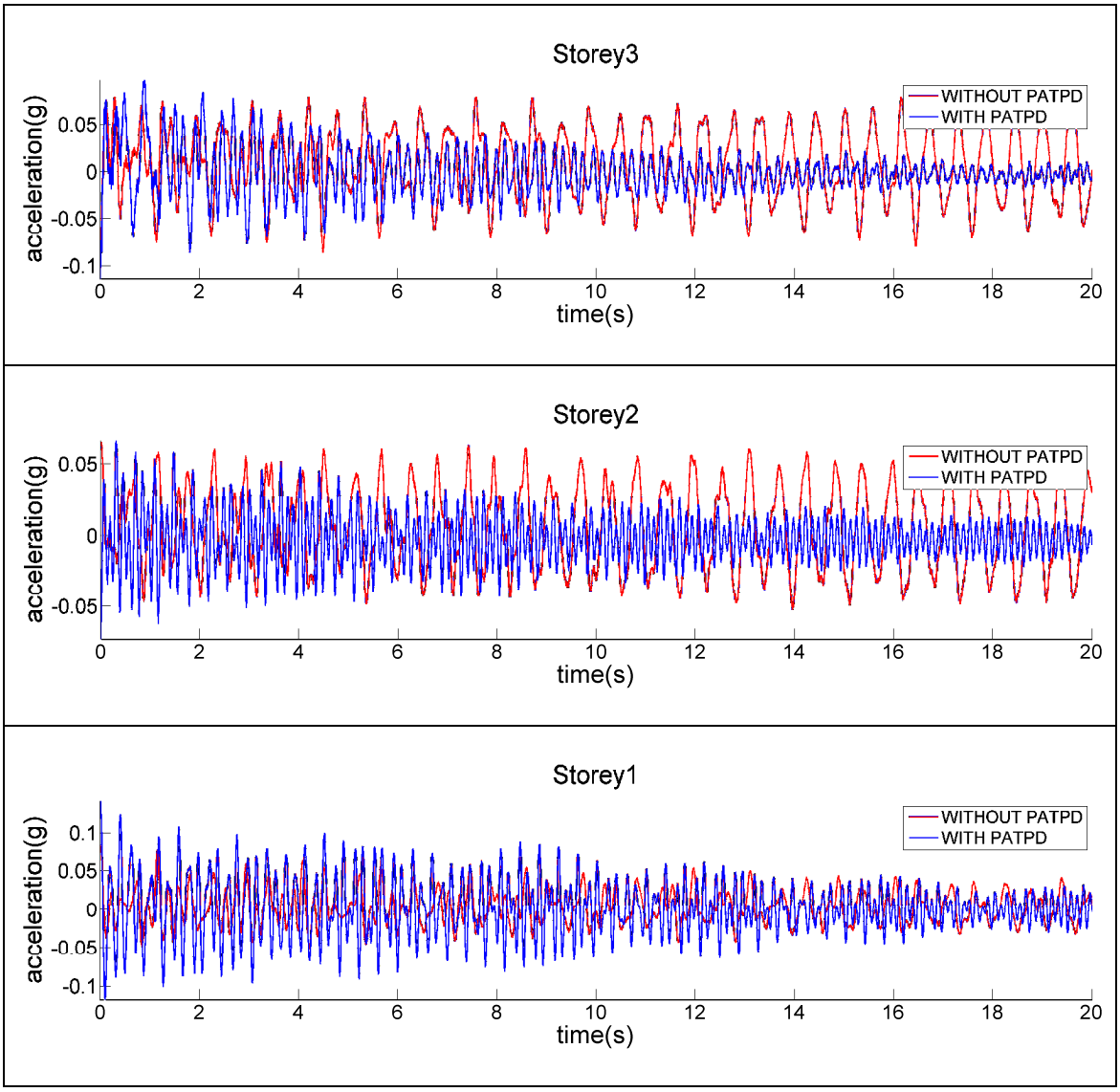

Figure 37: Time history of acceleration response per storey for free torsional vibration in the y-direction, primary model

According to Figure 37 the time history of acceleration response for the model containing the PATPD shows a more gradual decrease in accelerations as opposed to the translational time history graphs. However, the effect of the PATPD is still obvious as time passes for storey 2 and 3. The acceleration for storey 1 seems to increase slightly with the addition of the PATPD.

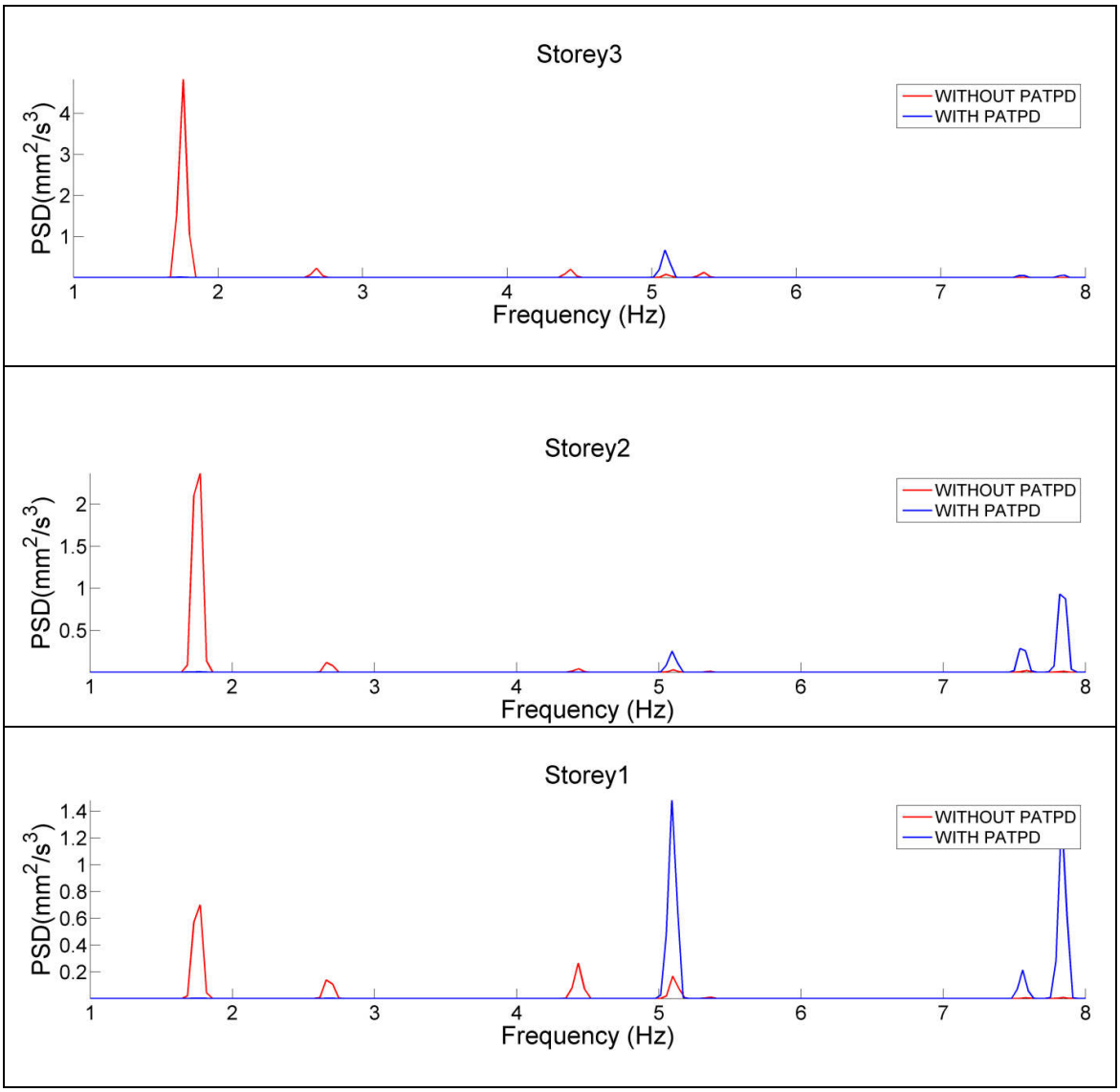

Figure 38: Power Spectral Density (PSD) per storey of the acceleration response for free torsional vibration in the y-direction, primary model

Figure 38 shows the PSD for storeys 3-1: there is a high peak at 2.680Hz, 4.438Hz and 7.842Hz. This represents the model's first, second and third natural frequency for torsion in the y-direction.

Peaks at 1.747Hz, 5.095 Hz and 7.569Hz indicate that although the model was excited in torsion, it had some movement in the x-direction as well. In the case of the y-direction not all translational peaks are attenuated this demonstrates that the PATPD had better control effect in x-direction than in the y-direction for free torsional vibration. Further investigation is required, where fine tuning of the PATPD could improve or eradicate this problem.

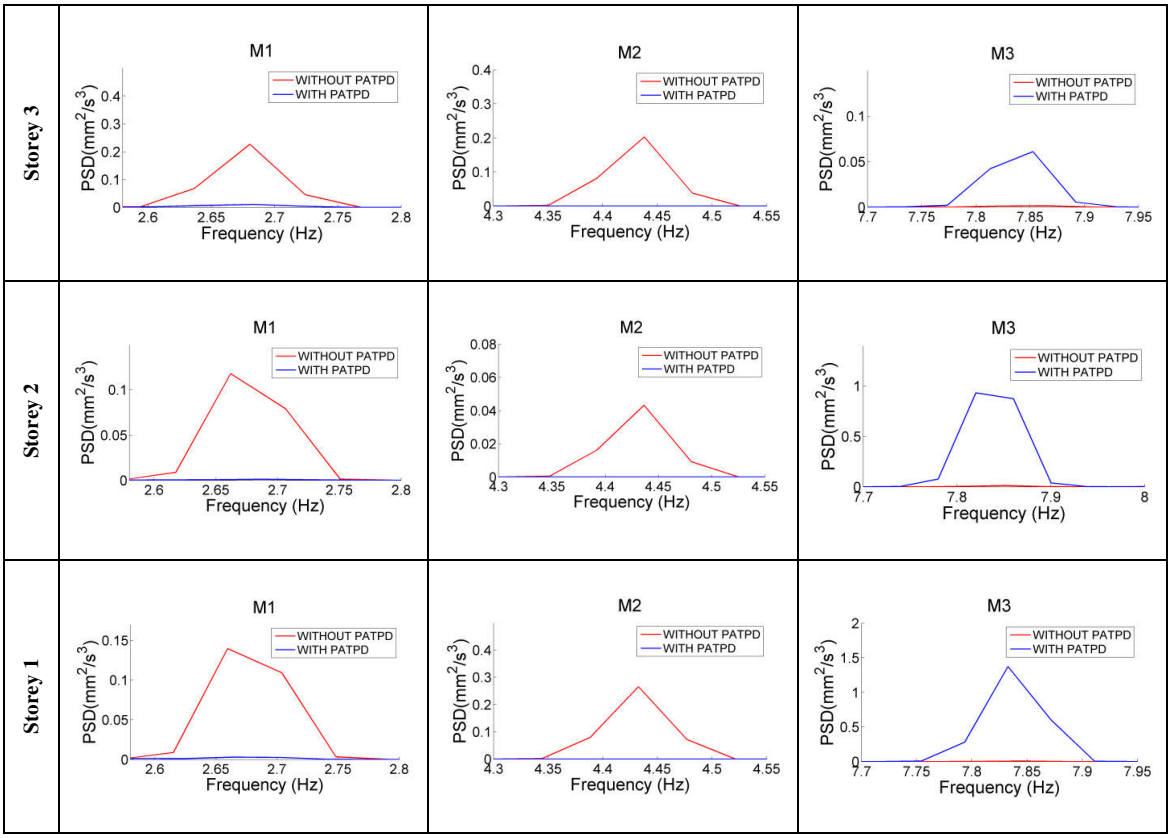

Figure 39: Magnified Power Spectral Density (PSD) per storey of the acceleration response for free torsional vibration in the y-direction, primary model

As can be seen in Figure 39 the PATPD provided a high level of attenuation for all 3 storeys to the first and second natural frequency. The peaks under consideration, at 2.680Hz and 4.438Hz are reduced by at least 99%. The PSD peak for the third natural frequency, 7.842Hz, shows an increase which is minimal in comparison to the positive effect on the first natural frequency. Thus the PATPD achieved positive effect overall in the y-direction for free torsional vibration.

As can be seen from the set of results from both directions the PATPD provided better control in the x-direction than in the y-direction.

4.2.4 Coupled Vibration

The primary model was displaced simultaneously in the x-direction (translation) and torsionally by 35mm before releasing it and the corresponding accelerations measured in the x-direction. The procedure was then repeated for the y direction. The PATPD was then connected and the entire process was repeated. The comparison of results is in the

form of acceleration-time and power spectral density graphs for measurements for the x-direction.

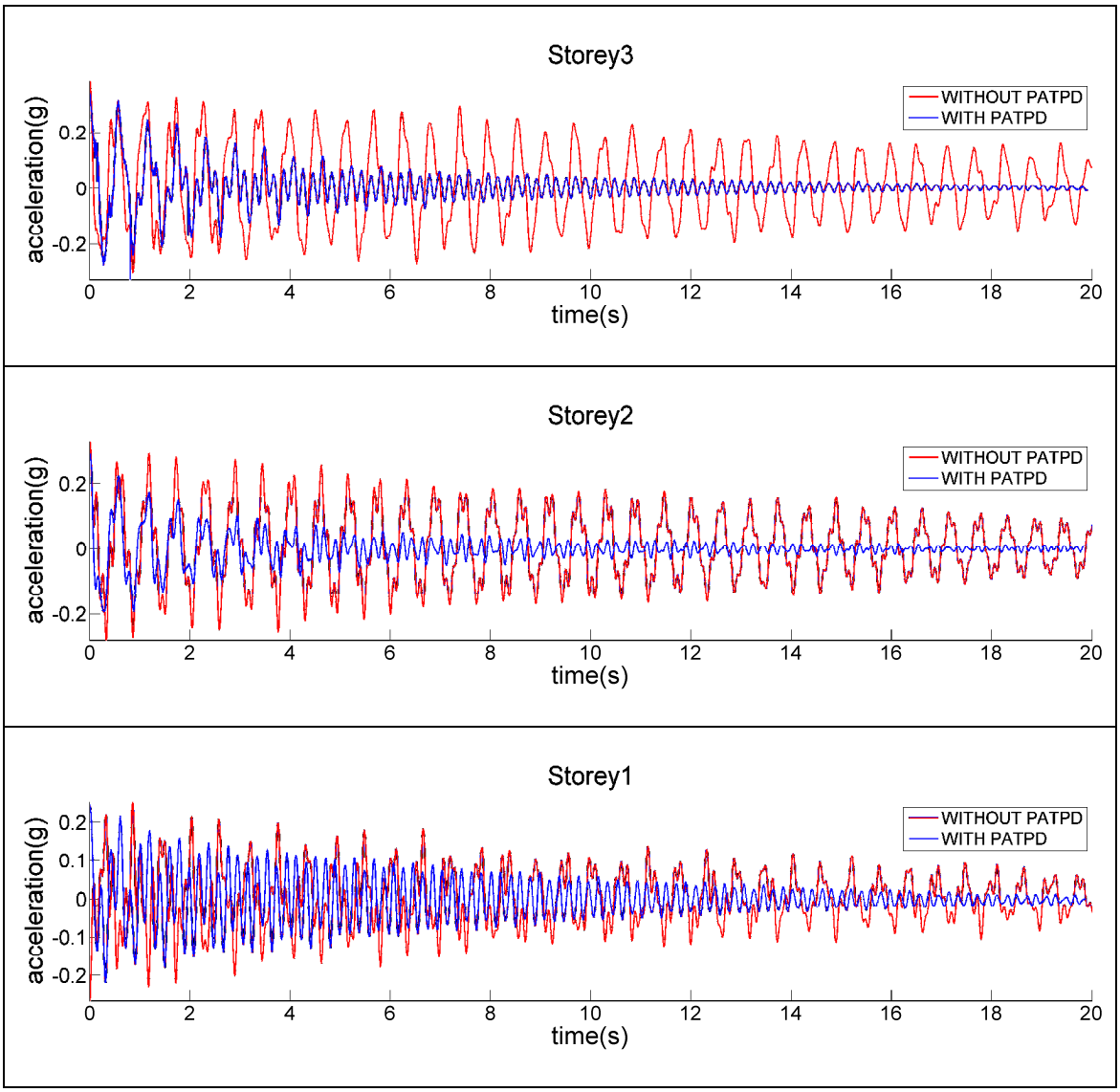

Figure 40: Time history of acceleration response per storey for free coupled vibration (translation in the x-direction and torsion), primary model

Figure 40 shows that at the beginning of the test for all 3 storeys, as the PATPD started moving, the acceleration peaks generated in the damped model were as high as those generated in the undamped model. However, in less than a second these high accelerations subside and the accelerations rapidly decrease compared to that of the undamped model. As is expected, the accelerations experienced in storey 3 are highest and the positive damping effect of the PATPD was still significant.

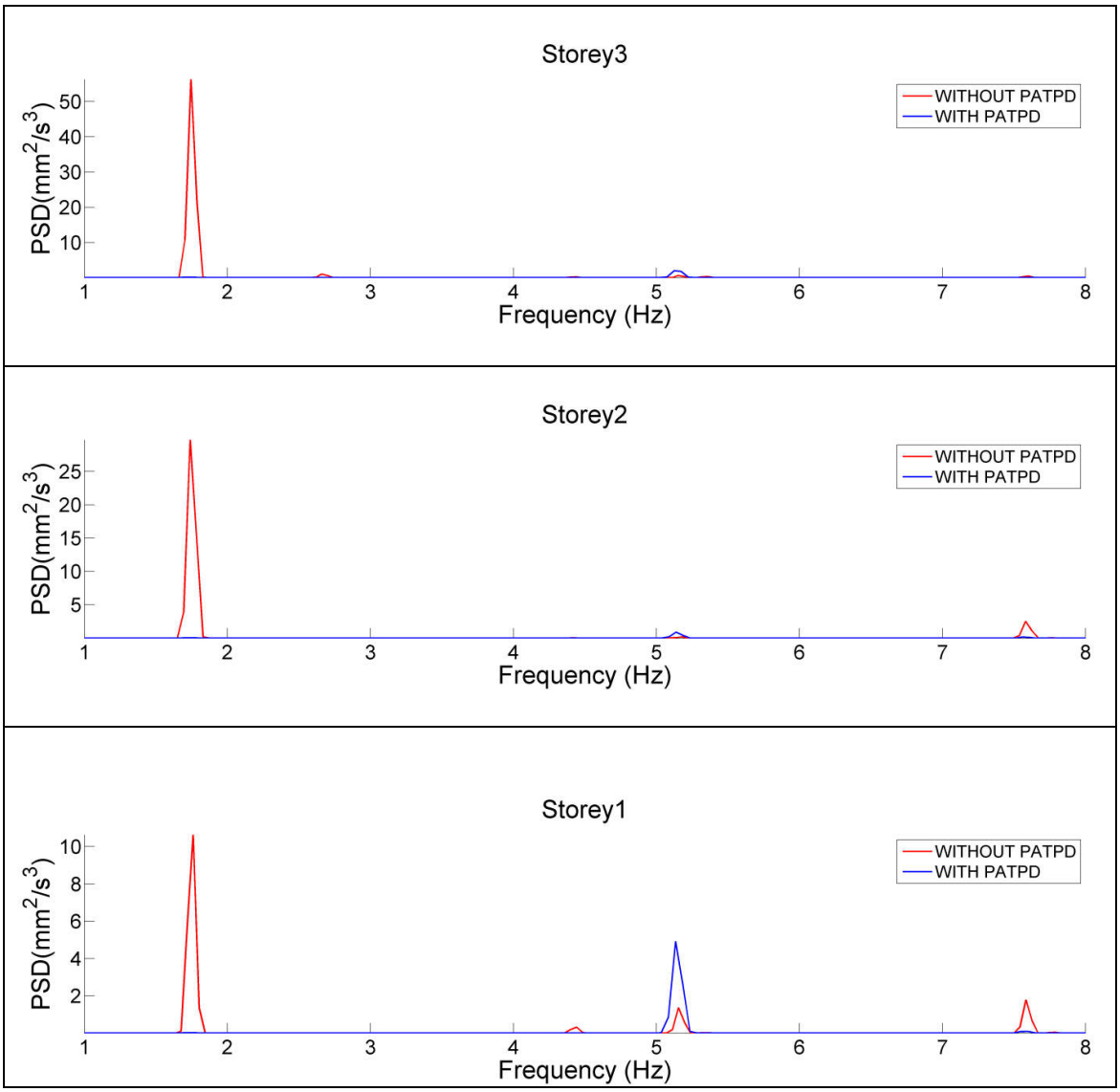

Figure 41: Power Spectral Density (PSD) per storey of the acceleration response for free coupled vibration (translation in the x-direction and torsion) , primary model

Figure 41 shows the PSD for storeys 3-1: there is a high peak at 1.733Hz, 5.164 Hz and 7.584Hz. This represents the model's first, second and third natural frequency for translation in the x-direction. There are also peaks at: 2.677Hz, 4.446Hz and at 7.792Hz. This represents the model's first, second and third natural frequency for torsion in the x-direction. Together these represent the models natural frequencies under coupled vibration in x-direction.

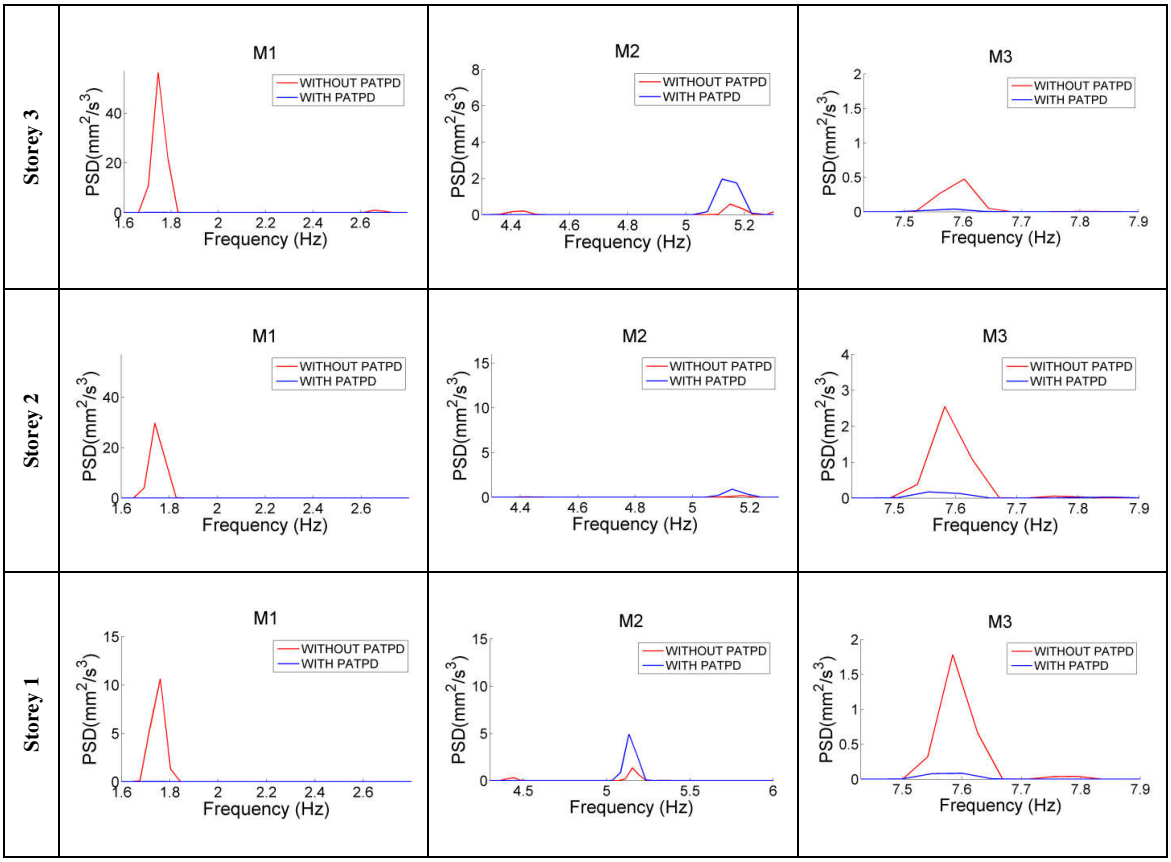

Figure 42: Magnified Power Spectral Density (PSD) per storey of the acceleration response for free coupled vibration (translation in the x-direction and torsion), primary model

As can be seen in Figure 42, the PATPD provided a high level of attenuation for all 3 storeys to the first and third natural frequency for both translation and torsion. The PSD peaks corresponding to first natural frequency under consideration, at 1.733Hz and 2.677Hz are reduced by at least 99%. The PSD peaks corresponding to third natural frequency under consideration, at 7.584Hz and 7.792Hz are also reduced by at least 99%. The PSD peak, 4.446Hz, corresponding to the second natural frequency for torsion is controlled significantly by at least 99%. The PSD peak, 5.164Hz, corresponding to the second natural frequency for translation shows a slight increase. However, this increase is minimal in comparison to the reduction gained in PSD peak for the first natural frequency. The PATPD has achieved control for free coupled vibration in the x-direction.

The comparison of results is in the form of acceleration-time and power spectral density graphs for coupled vibration in the y direction.

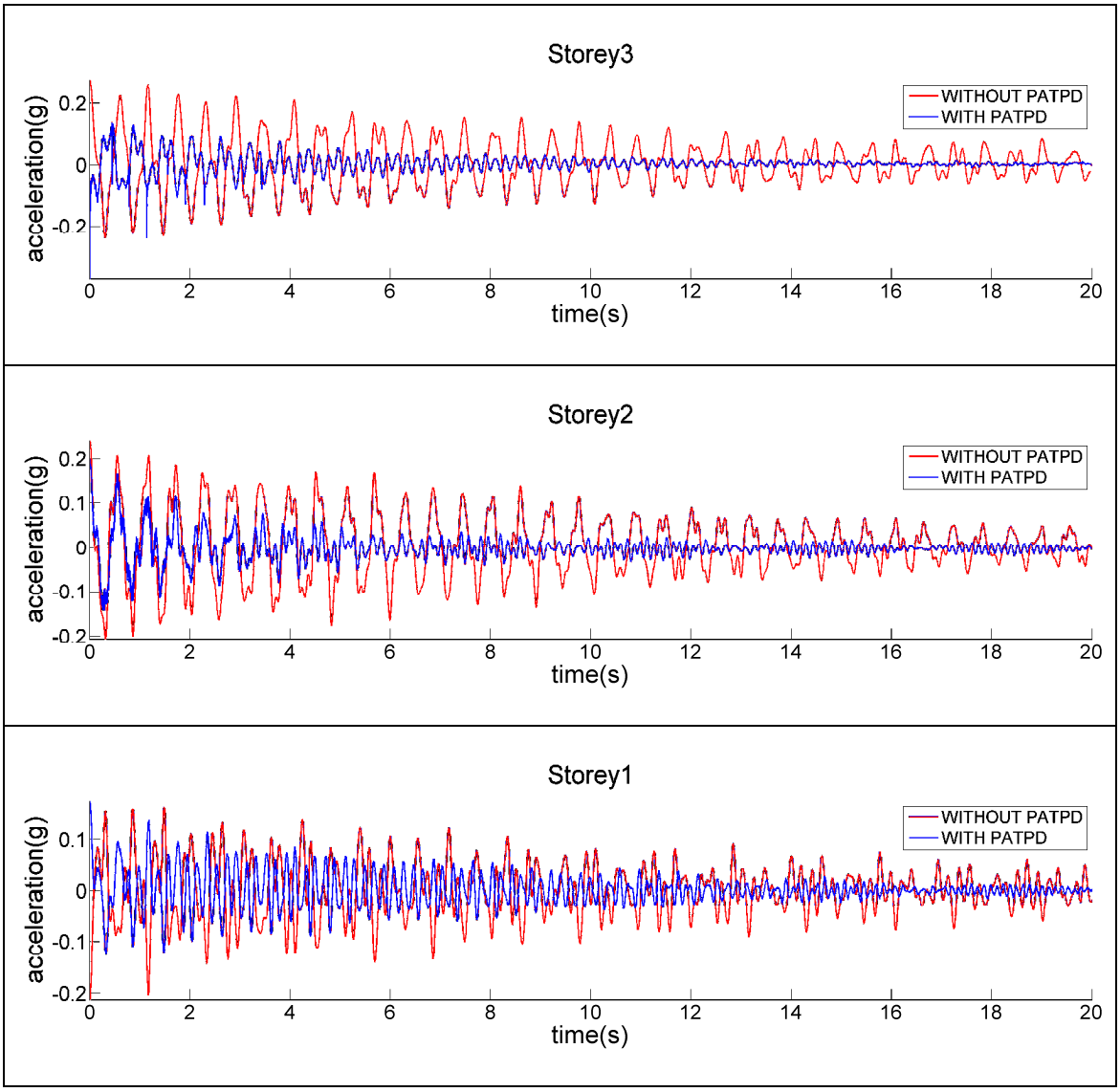

Figure 43: Time history of acceleration response per storey for free coupled vibration (translation in the y-direction and torsion), primary model

Figure 43 shows that at the beginning of the test for all 3 storeys, as the PATPD started moving, the acceleration peaks generated in the damped model are as high as those generated in the undamped model. However, in less than a second these high accelerations subside and the accelerations rapidly decrease compared to that of the undamped model. As is expected, the accelerations experienced in storey 3 are highest and the positive damping effect of the PATPD was still significant.

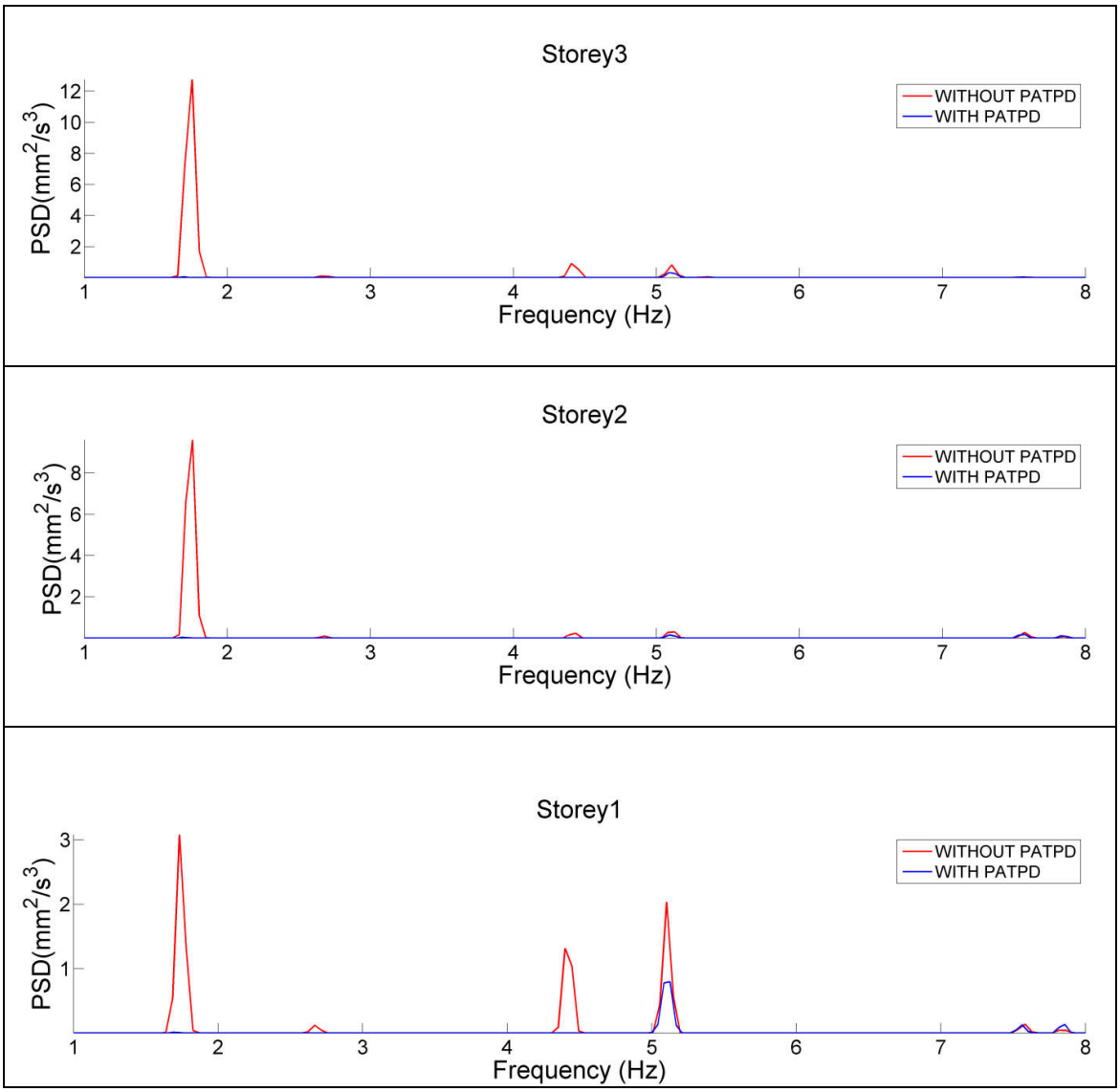

Figure 44: Power Spectral Density (PSD) per storey of the acceleration response for free coupled vibration (translation in the y-direction and torsion), primary model

Figure 44 shows the PSD for storeys 3-1: there is a high peak at 1.747Hz, 5.095Hz and 7.569Hz. This represents the model's first, second and third natural frequency for translation in the y-direction. There are also peaks at: 2.680Hz, 4.438Hz and at 7.842Hz. This represents the model's first, second and third natural frequency for torsion in the x-direction. Together these represent the models natural frequencies under coupled vibration in y-direction.

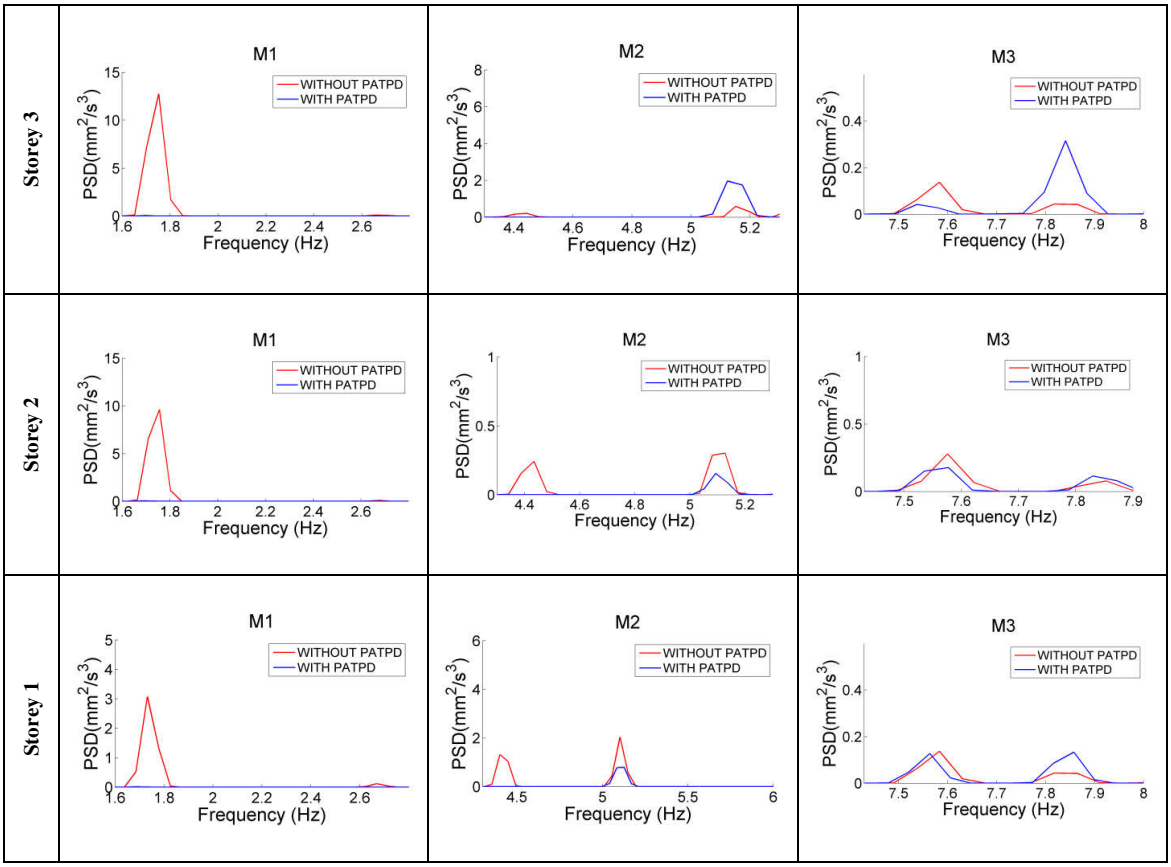

Figure 45: Magnified Power Spectral Density (PSD) per storey of the acceleration response for free coupled vibration (translation in the y-direction and torsion), primary model

As can be seen in Figure 45, the PATPD provided a high level of attenuation for all 3 storeys to the first and second natural frequency for both translation and torsion. The PSD peaks corresponding to first natural frequency under consideration, at 1.747Hz and 2.680Hz were reduced by at least 99%. The PSD peaks corresponding to second natural frequency under consideration, at 5.095Hz and 4.438Hz were also reduced. The PSD peaks at, 7.569Hz and 7.842Hz, shows a slight increase in some cases. However, this increase is minimal in comparison to the reduction gained in PSD peak for the first natural frequency. The PATPD has achieved control for free coupled vibration in the y-direction.

As can be seen from the set of results from both directions the PATPD provided better control in the x-direction than in the y-direction.

4.3.0 Forced Vibration

4.3.1 Translational Vibration in the X-Direction

The test model was orientated on the shake table so as to generate forced vibrations in the x-direction on the model. A frequency sweep was performed from 0.2Hz to 10Hz with and without the damper. The test duration was 150 seconds.

The comparison of results is in the form of acceleration-time and power spectral density graphs.

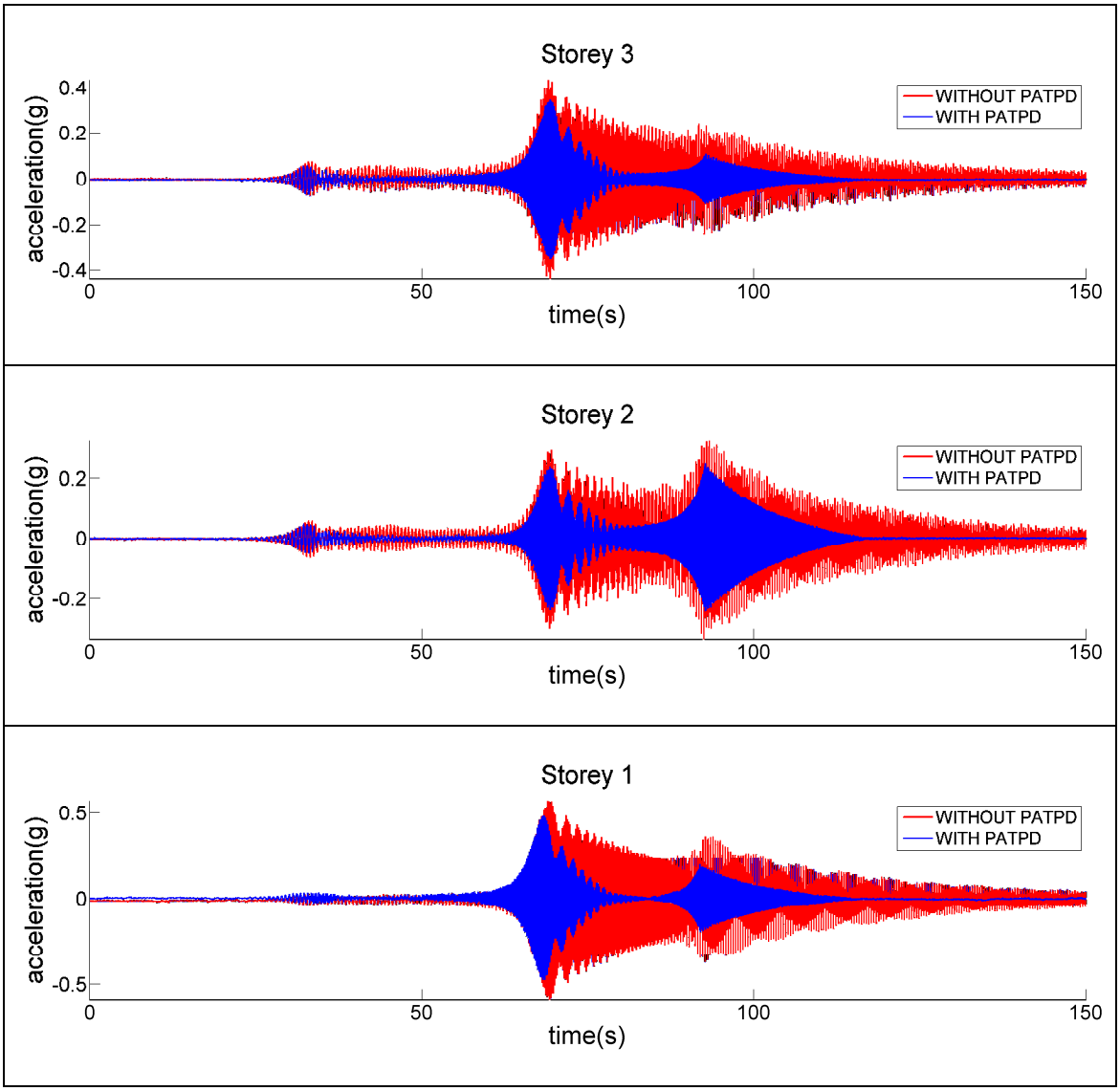

Figure 46: Time history of acceleration response per storey for forced translational excitation in the x-direction, primary model

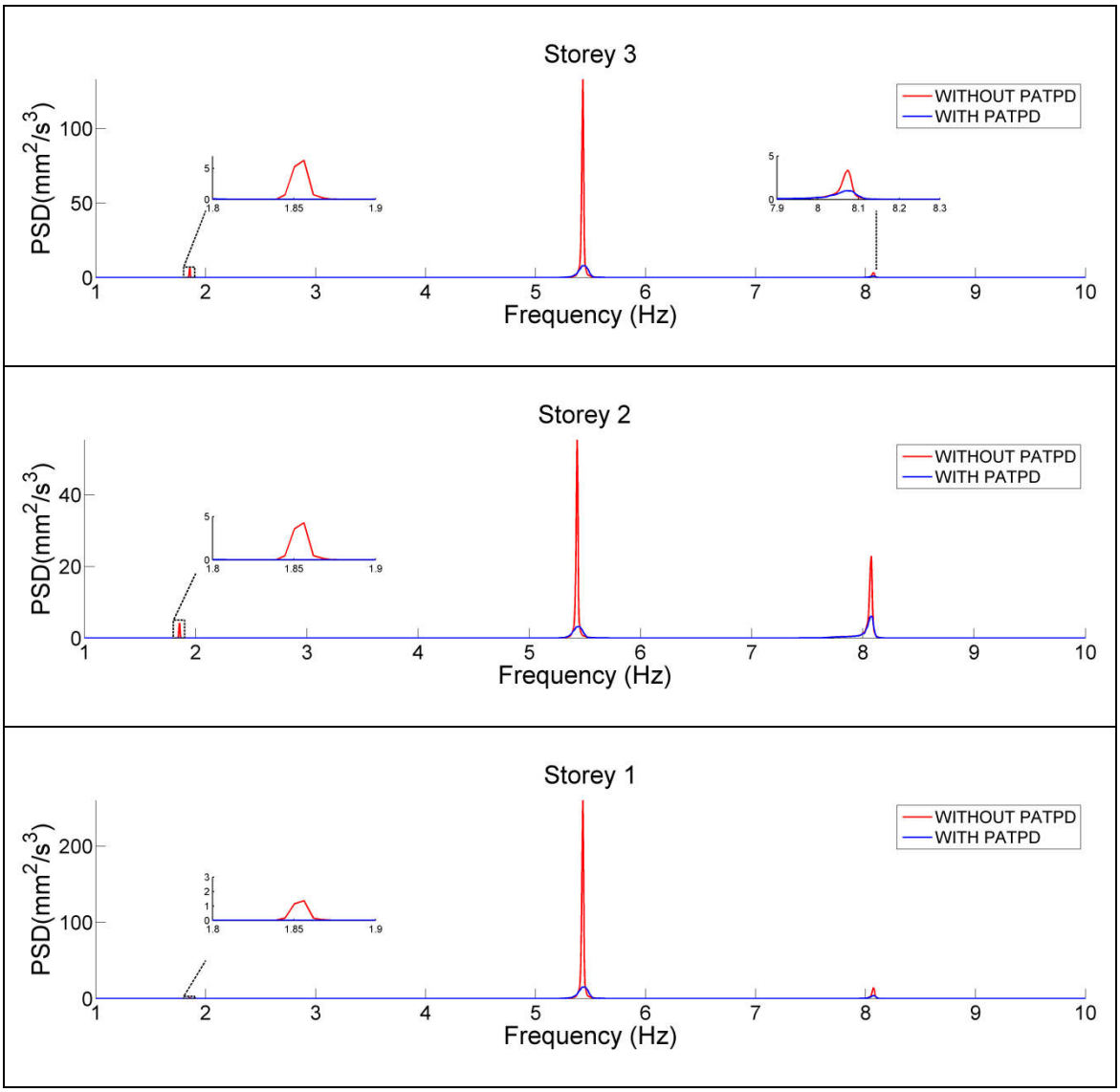

Figure 47: Power Spectral Density (PSD) of the acceleration response per storey under forced excitation in the x-direction, primary model

Figure 46 shows for all 3 storeys that by adding the damper onto the model the acceleration experience was significantly decreased.

Figure 47 shows PSD peaks at 1.856Hz, 5.429Hz and 8.047Hz. This corresponds to the models first, second and third frequencies. The positive control effect is evident as PSD peaks for all 3 frequencies are significantly reduced.

4.3.2 Translational Vibration in the Y-Direction

The test model is orientated on the shake table so as to generate forced vibrations in the y-direction on the model. The test duration was 150 seconds.

The comparison of results is in the form of acceleration-time and power spectral density graphs.

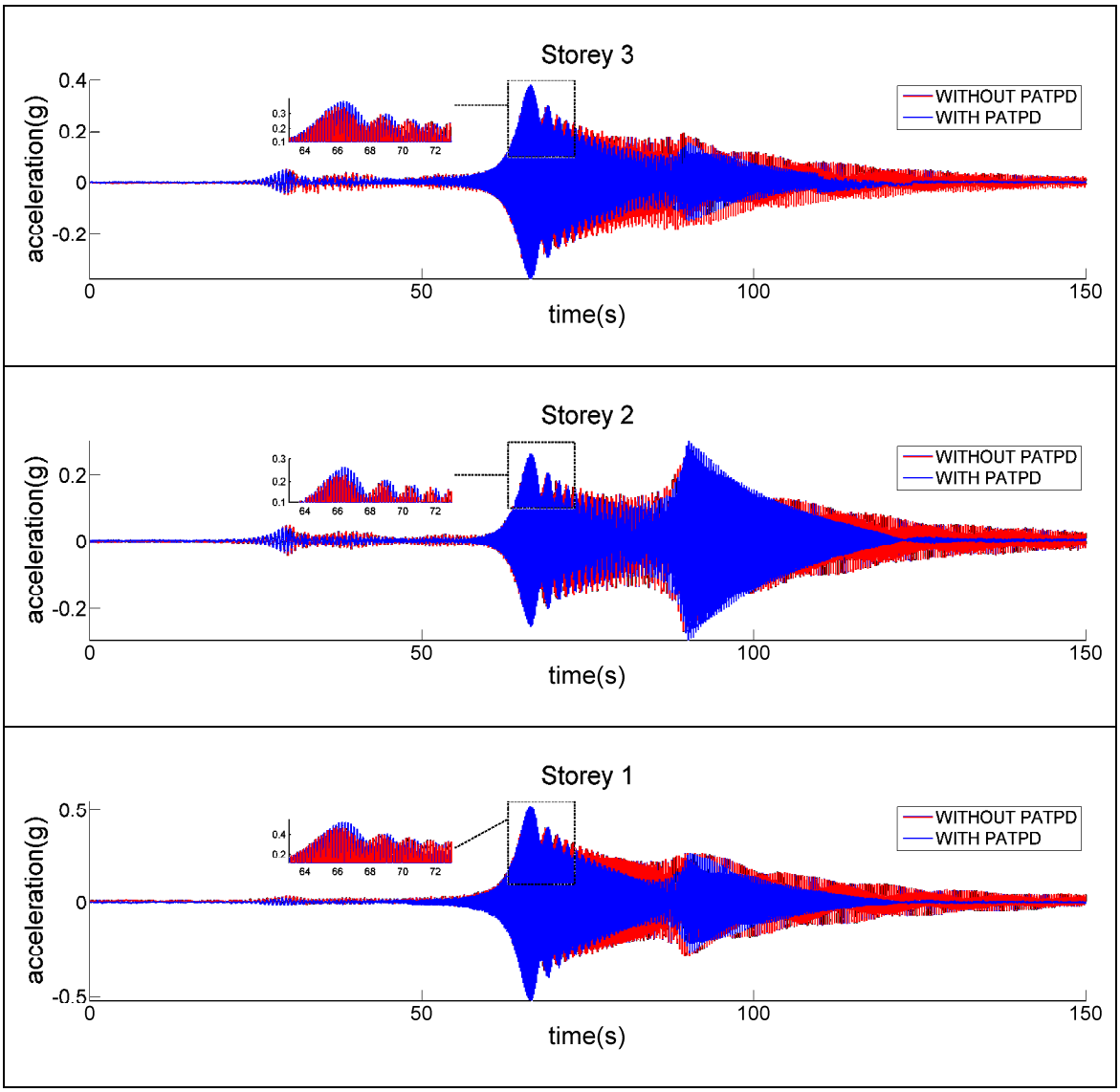

Figure 48: Time history of acceleration response per storey for forced translational excitation in the y-direction, primary model

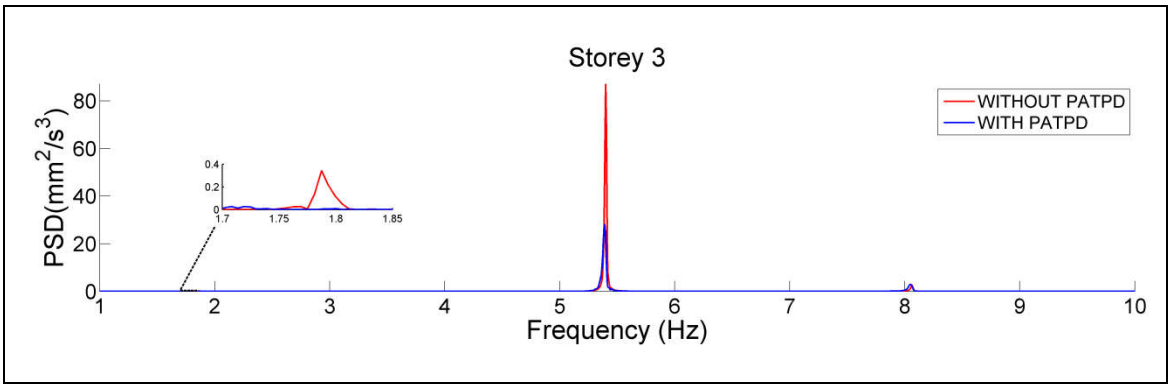

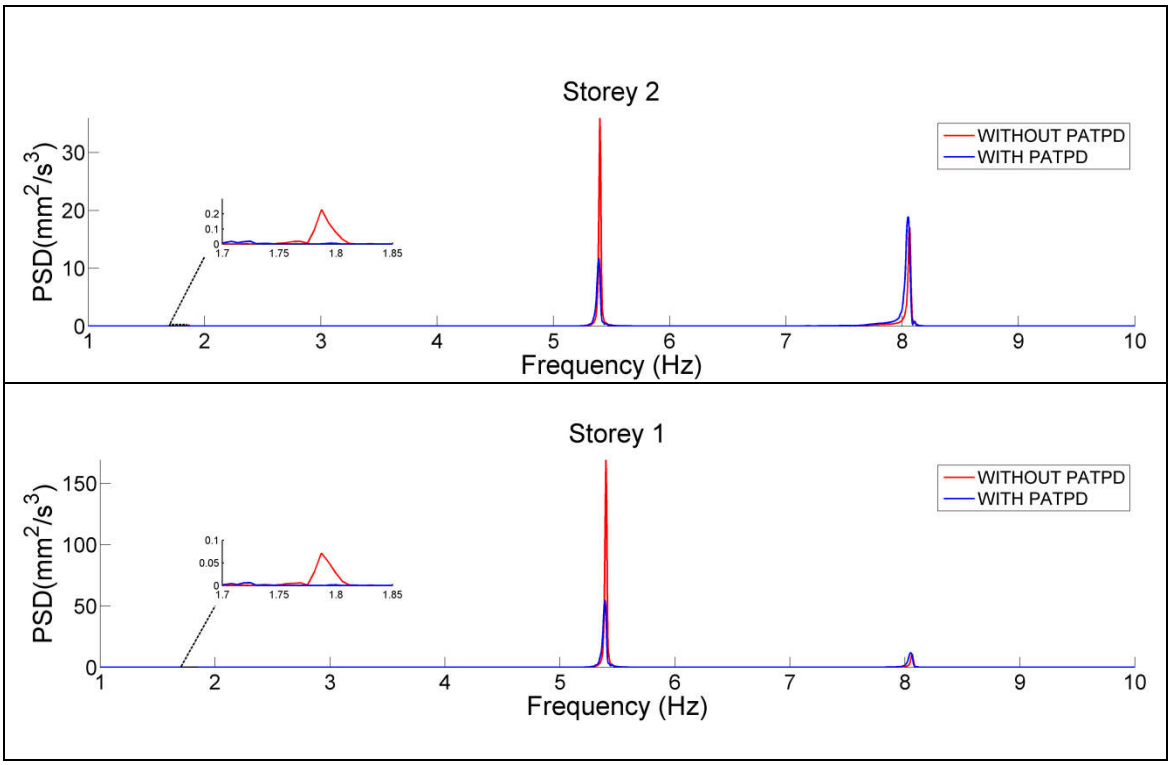

Figure 49: Power Spectral Density (PSD) of the acceleration response per storey under forced excitation in the y-direction, primary model

Figure 48 shows for all 3 storeys that by adding the damper onto model the initial accelerations experienced were slightly higher than without damper, but then the accelerations decrease.

Figure 49 shows PSD peaks at 1.787Hz, 5.399Hz and 8.065Hz. This corresponds to the models first, second and third frequencies. The positive control effect is evident as PSD peaks for the first and second frequencies are significantly reduced, with the third PSD frequency peak having same value as with no damper.

As can be seen from the set of results from both directions the PATPD provided better control in the x-direction than in the y-direction.

4.4.0 Summary and Conclusions

Free Vibration

As the PATPD started moving, the acceleration peaks generated in the damped model are as high as those generated in the undamped model. However, in less than a second these high accelerations subside and the accelerations rapidly decrease compared to that of the undamped model. This is so for all tests except torsion where storey 1

experienced increased accelerations. As is expected the accelerations experienced in storey 3 were highest, still yet the positive damping effect of the PATPD was still significant.

For all tests carried out – translation, torsion and coupled vibrations - the first natural frequency was significantly controlled with least control being 95%. The second and third natural frequencies were controlled in some cases and not in others – where there were slight increases in PSD peaks. However, these increases were minimal in comparison with the control effect provided to the first natural frequency. There is room for improvement with torsional control which would require further investigation.

All PATPD tests performed indicated better overall control effect in x-direction than y-direction.

Forced Vibration

For Forced Vibration the PATPD provides significant control to all 3 frequencies.

The results reveal that the PATPD performed better in translation the x –direction than the y-direction.

CHAPTER 5

Experimental results: Parameter Study

5.1 Parameter Test 1: Effect of changing damper mass ratio

Tests were carried out using three different damper mass ratios, a 1.5% (0.632kg) mass, a 3% (1.263kg) mass and a 5% (2.105kg) mass. All other parameters during these tests remained constant, with the test model having a mass of 42.09kg and a height of 37cm per storey. The mass ratio was changed by changing the mass of the sand within the PATPD. As with the previous tests the model was given an initial displacement, in the according directions, and the acceleration with and without the damper measured.

The data for each mass ratio is processed and they are plotted together on graphs such that extrapolations and comparisons can be made.

5.1.1 Free Vibration

5.1.1.1 Translational Vibration in the X-direction

The model was given an initial displacement in the x-direction and respective acceleration measured. The damping effect of each of the PATPD masses can be seen in the graphs to follow.

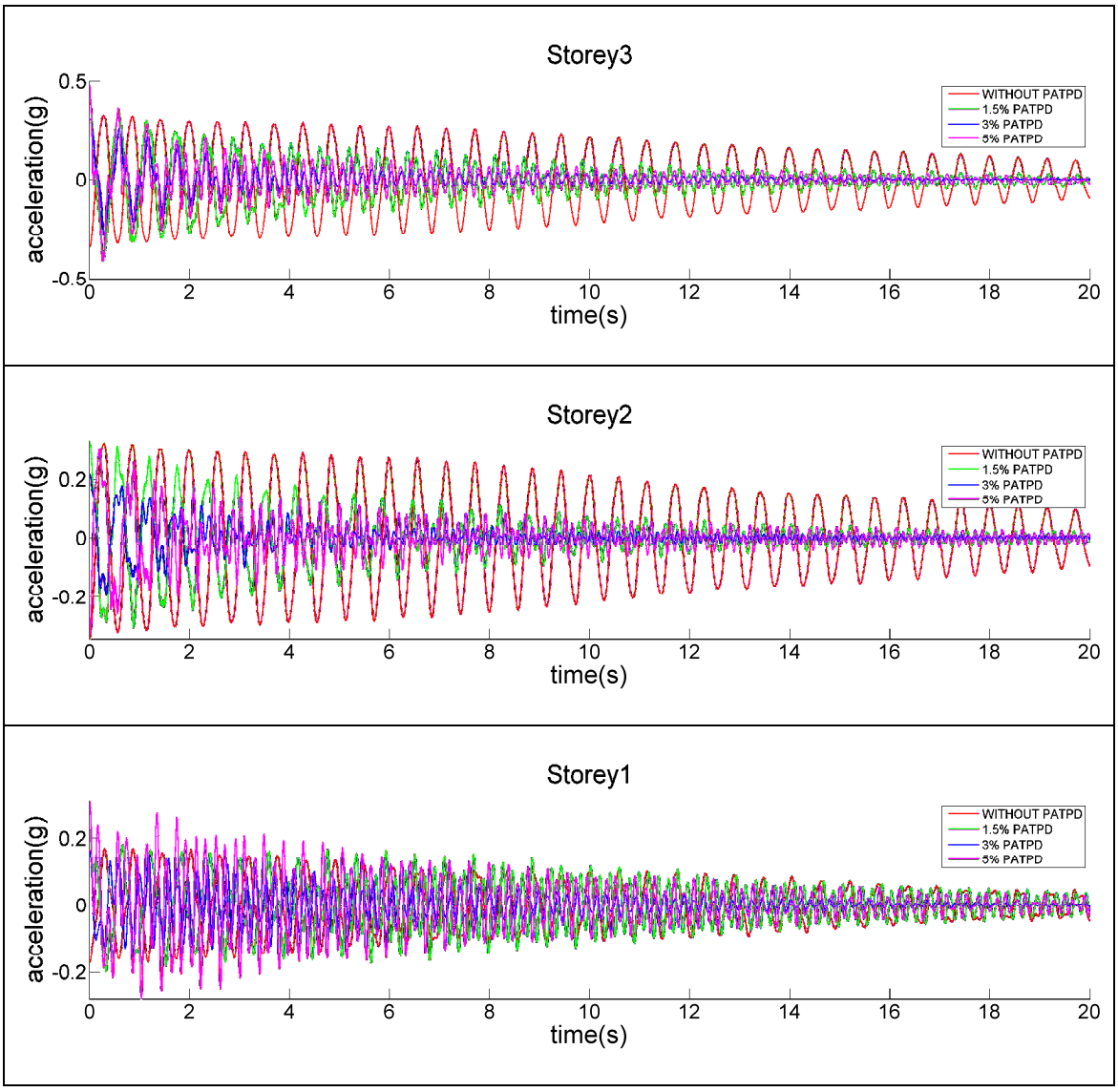

Figure 50: Time history of acceleration response per storey for free translational vibration in x-direction, mass ratios 1.5%, 3% and 5%

Figure 50 shows that for all masses tested as the PATPD started moving; the acceleration peaks generated in the damped model are as high as those generated in the undamped model. However, these high accelerations subside and the accelerations rapidly decrease compared to that of the undamped model. As is expected the accelerations experienced in storey 3 are highest and the positive damping effect of the

PATPD was still significant for all mass ratios. The best control effect was seen in storey 3, since the damper was installed on this storey.

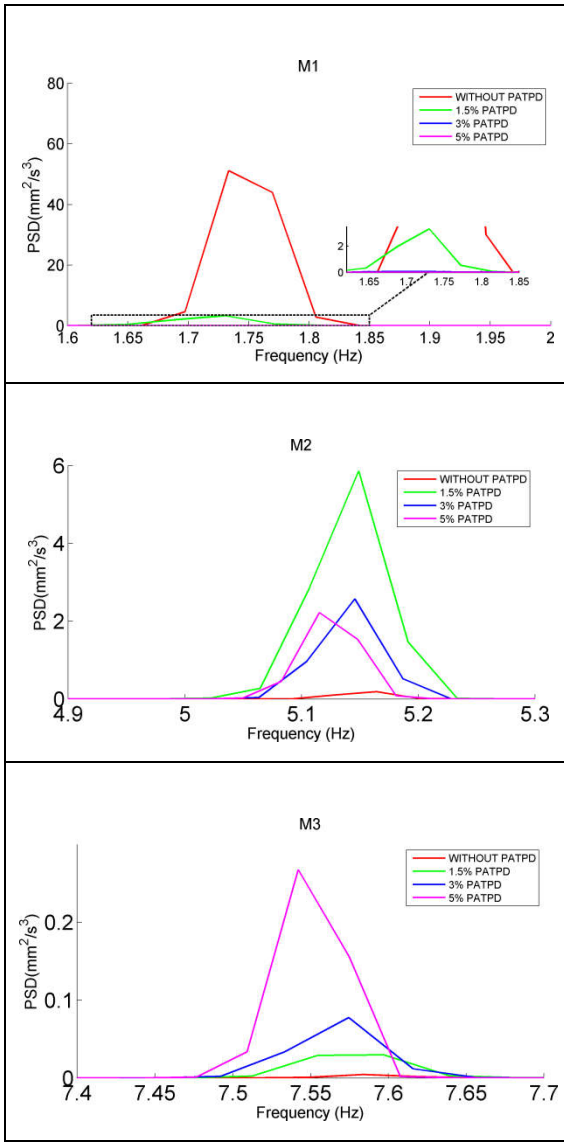

Figure 51: Magnified Power Spectral Density (PSD) storey 3 of the acceleration of the model under free translational vibration in the x-direction, mass ratios 1.5%, 3% and 5%

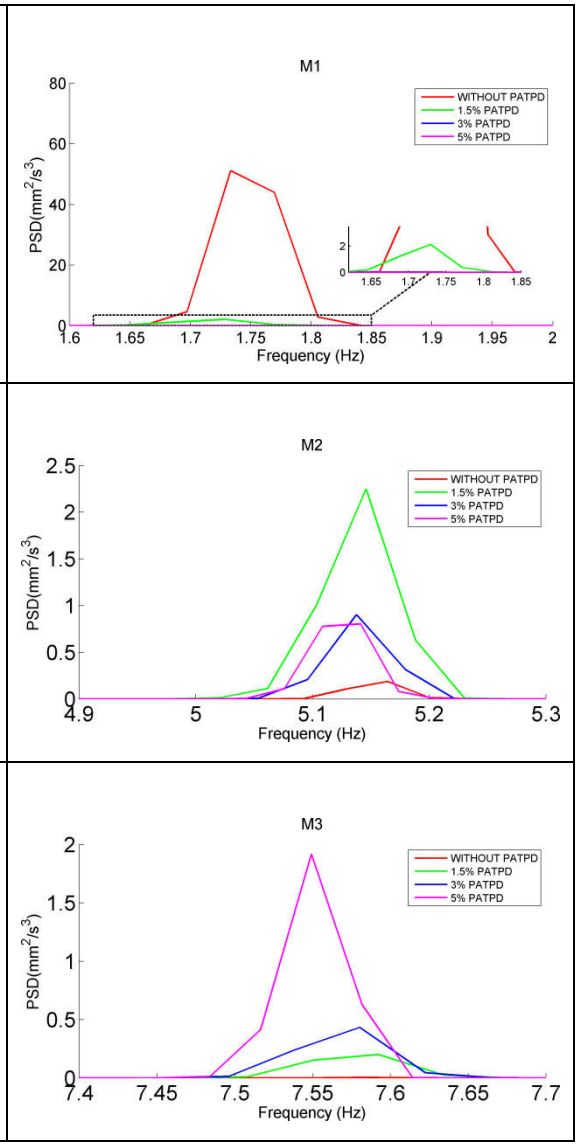

Figure 52: Magnified Power Spectral Density (PSD) storey 2 of the acceleration of the model under free translational vibration in the x-direction, mass ratios 1.5%, 3% and 5%

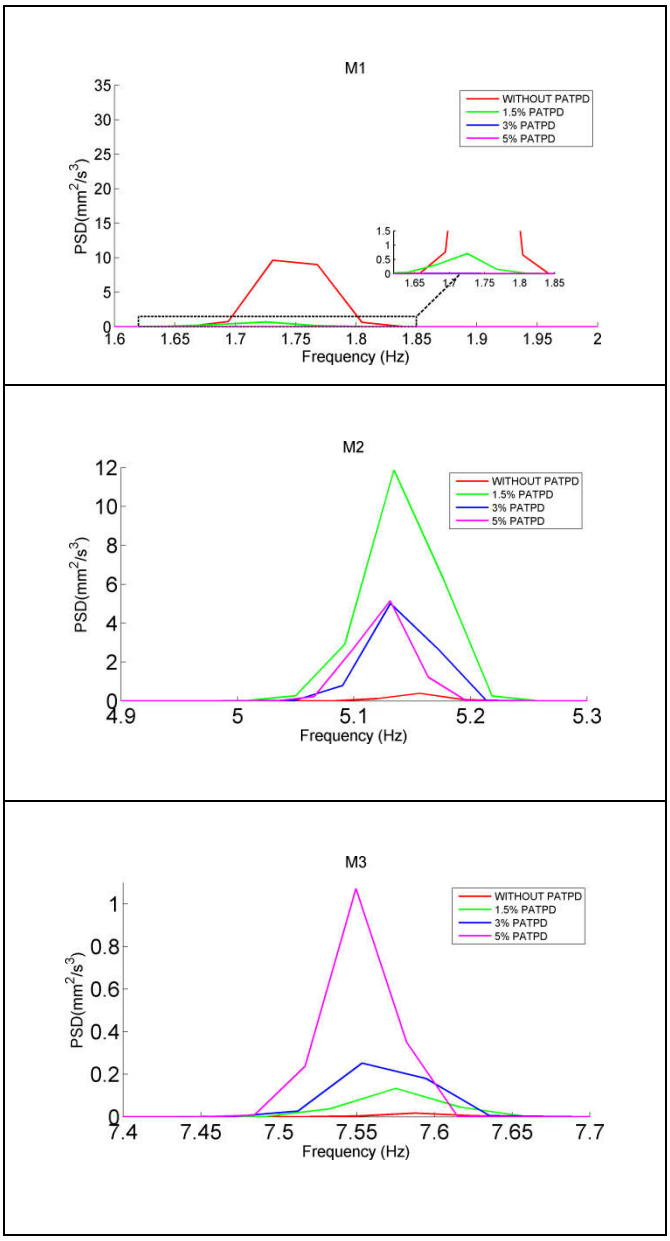

Figure 53: Magnified Power Spectral Density (PSD) storey 1 of the acceleration of the model under free translational vibration in the x-direction, mass ratios 1.5%, 3% and 5%

Figure 51, Figure 52 and Figure 53 shows for first natural frequency with PSD peak, 1.733Hz, all three of the masses of the PATPD produced significant damping of the model's vibrations, reducing the PSD peak by at least 90%. Both the 3% (primary model) and 5% PATPD demonstrates best control effect and the 1.5% PATPD the least. For the second natural frequency, 5.164Hz, the 3% (primary model) and 5% PATPD shows a similar increase in density, with the 1.5% increase almost twice that. For the third natural frequency, 7.584Hz, the 1.5% and 3% (primary model) PATPD show a similar increase in density, with the 5% increase almost twice that. Overall PSD peak increases were minimal in comparison to the reduction gained in PSD peak for the first natural frequency.

5.1.1.2 Translational Vibration in the Y-direction

The model was given an initial displacement in the y-direction and respective acceleration measured. The damping effect of each of the PATPD masses can be seen in the graphs to follow.

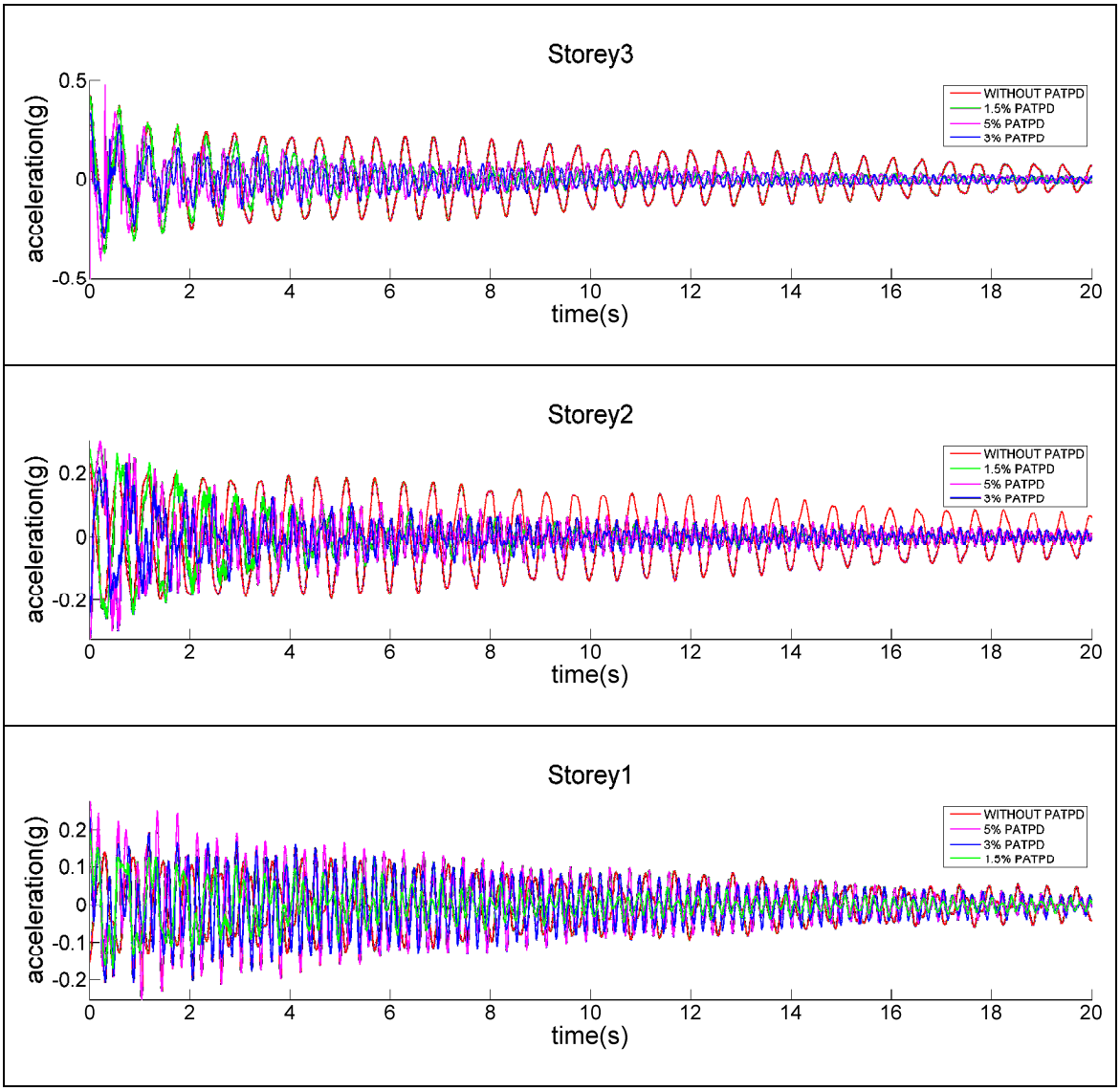

Figure 54: Time history of acceleration response per storey for free translational vibration in y-direction, mass ratios 1.5%, 3% and 5%

Figure 54 shows that for all masses tested as the PATPD started moving; the acceleration peaks generated in the damped model are as high as those generated in the undamped model. However, these high accelerations subside and the accelerations rapidly decrease compared to that of the undamped model. As is expected, the accelerations experienced in storey 3 were highest and the positive damping effect of the PATPD is still significant for all mass ratios. The 1.5% and 3% dampers have a

similar effect. The best control effect was seen in storey 3, since the damper was installed on this storey.

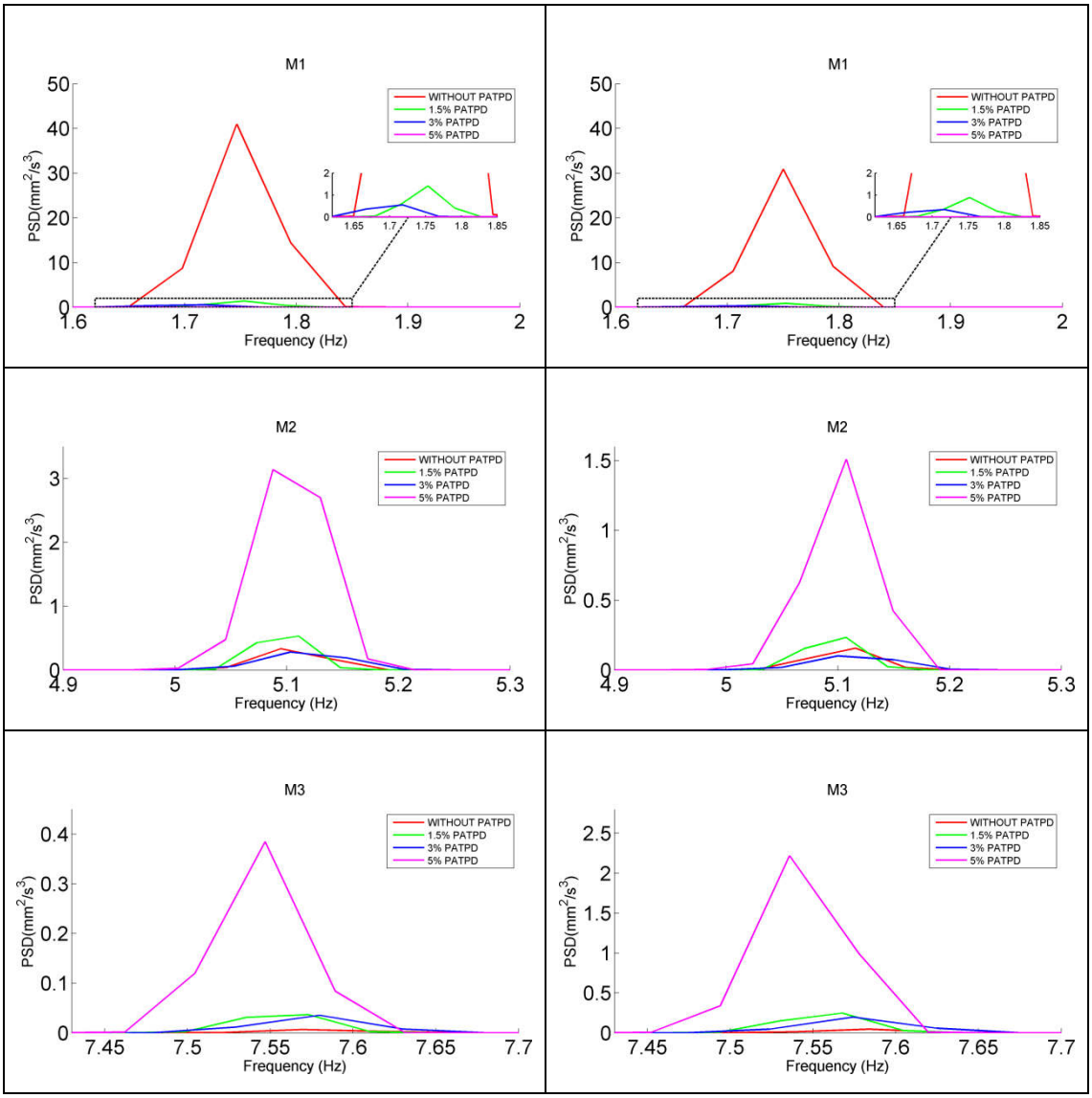

Figure 55: Magnified Power Spectral Density (PSD) storey 3 of the acceleration of the model under free translational vibration in the y-direction, mass ratios 1.5%, 3% and 5%

Figure 56: Magnified Power Spectral Density (PSD) storey 2 of the acceleration of the model under free translational vibration in the y-direction, mass ratios 1.5%, 3% and 5%

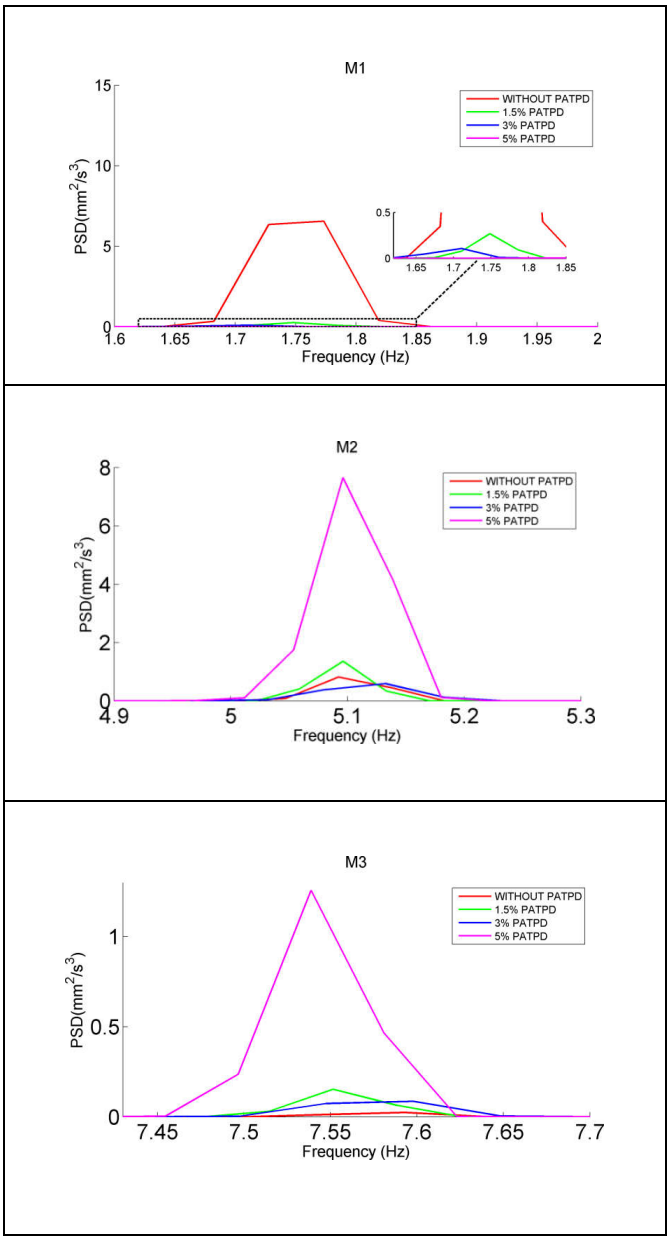

Figure 57: Magnified Power Spectral Density (PSD) storey 1 of the acceleration of the model under free translational vibration in the y-direction, mass ratios 1.5%, 3% and 5%

Figure 55, Figure 56 and Figure 57 shows for first natural frequency with PSD peak, 1.747Hz, all three of the masses of the PATPD produced significant damping of the model's vibrations, reducing the PSD peak by at least 90%. For the second and third natural frequency with PSD peaks, 5.164Hz and 7.584Hz, the 5% PATPD demonstrates best control effect and the 1.5% PATPD the least. The 3% PATPD (primary model) demonstrates best control effect, showing a slight decrease. The 5% PATPD, however, shows an increase in PSD peak of the second and third natural frequency.

Overall PSD peak increases were minimal in comparison to the reduction gained in PSD peak for the first natural frequency.

5.1.1.3 Torsional Vibration (acceleration measured in the X-direction)

The model was given an initial torsional displacement and respective acceleration measured in the x-direction. The damping effect of each of the PATPD masses can be seen in the graphs to follow.

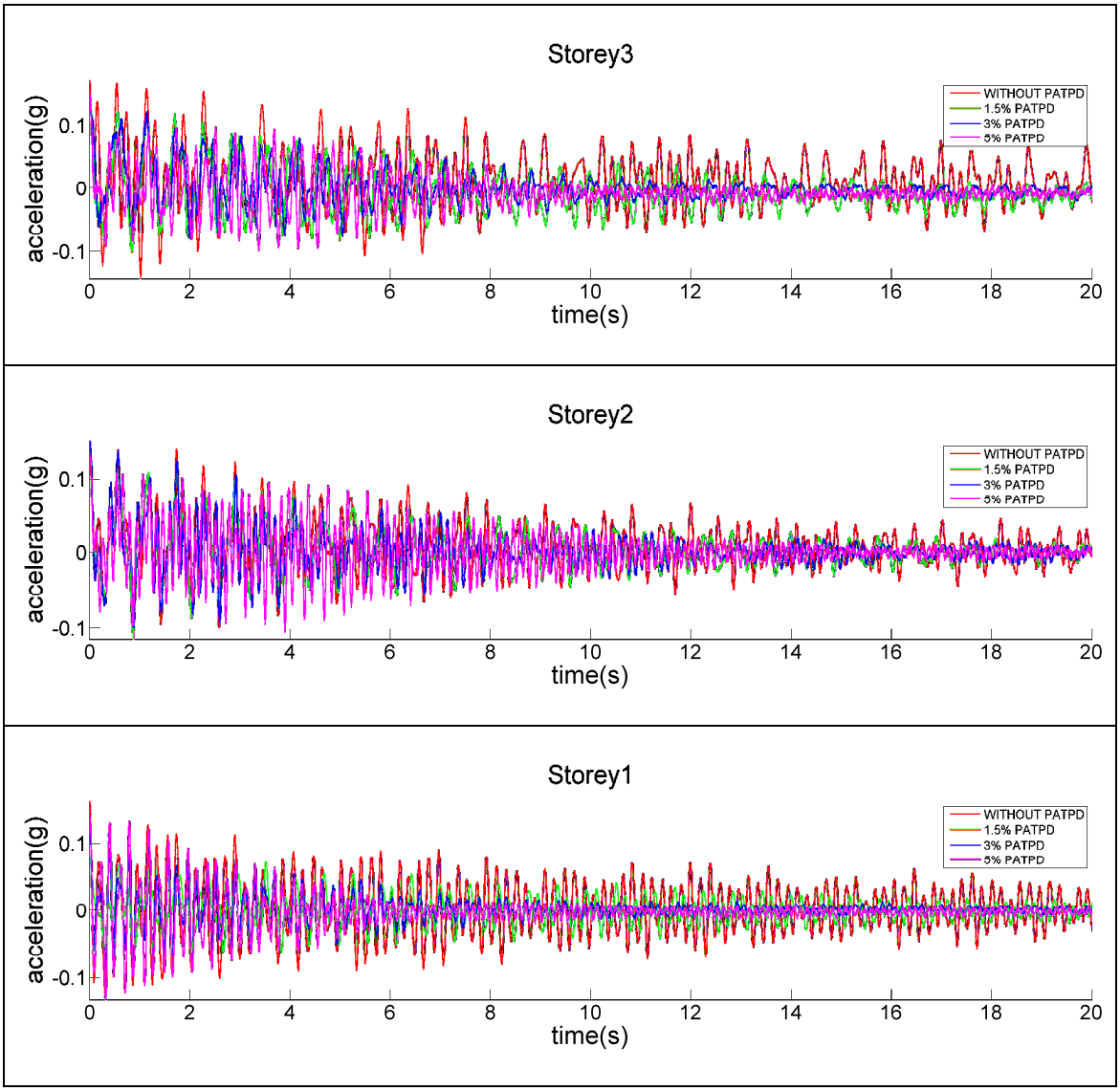

Figure 58: Time history of acceleration response in x-direction per storey for free torsional vibration, mass ratios 1.5%, 3% and 5%

Figure 58 shows that for all masses tested as the PATPD started moving; the acceleration peaks generated in the damped model are as high as those generated in the undamped model. However, these high accelerations subside and the accelerations rapidly decrease compared to that of the undamped model. As is expected the accelerations experienced in storey 3 are highest and the positive damping effect of the

PATPD was still significant for all mass ratios. The best control effect is seen in storey 3, since the damper was installed on this storey.

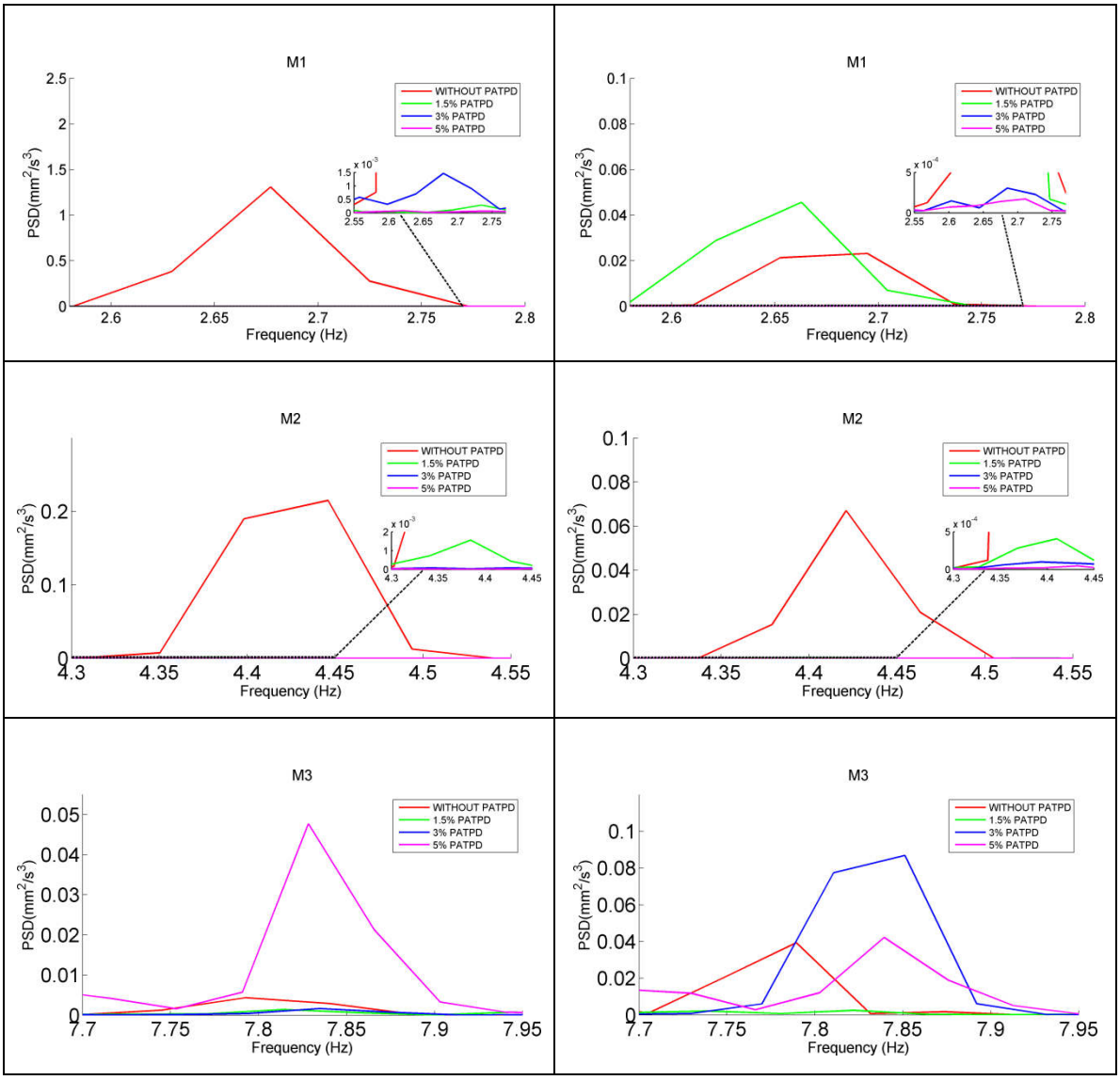

Figure 59: Magnified Power Spectral Density (PSD) storey 3 of the acceleration in the x-direction of the model under free torsional vibration, mass ratios 1.5%, 3% and 5%

Figure 60: Magnified Power Spectral Density (PSD) storey 2 of the acceleration in the x-direction of the model under free torsional vibration, mass ratios 1.5%, 3% and 5%

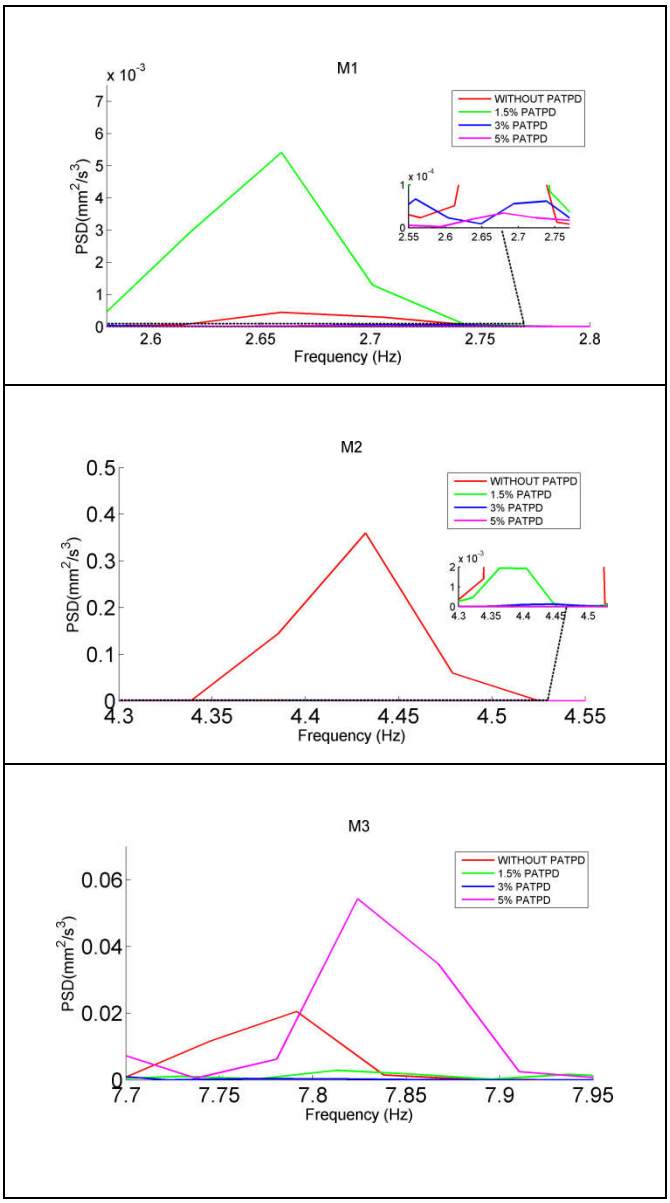

Figure 61: Magnified Power Spectral Density (PSD) storey 1 of the acceleration in the x-direction of the model under free torsional vibration, mass ratios 1.5%, 3% and 5%

Figure 59 Figure 60 and Figure 61 shows that both the 3% and 5% mass PATPD for first natural frequency with PSD peak, 2.677Hz, produce significant damping of the model's vibrations, the 1.5% proves effective in storey 3 but not so in the other storeys. For second natural frequency with PSD peak, 4.446Hz, all masses of PATPD provide significant control, with the 5% demonstrating best control effect and the 1.5% PATPD the least. For third natural frequency with PSD peak, 7.792Hz, for both storeys 1 and 3, the 1.5% and 3% PATPD provides best control effect. However, for storey 2 the 1.5% provides best control effect with the 3% being worst. Overall PSD peak increases were minimal in comparison to the reduction gained in PSD peak for the first natural frequency.

5.1.1.4 Torsional Vibration (acceleration measured in the Y-direction)

The model was given an initial torsional displacement and respective acceleration measured in the y-direction. The damping effect of each of the PATPD masses can be seen in the graphs to follow.

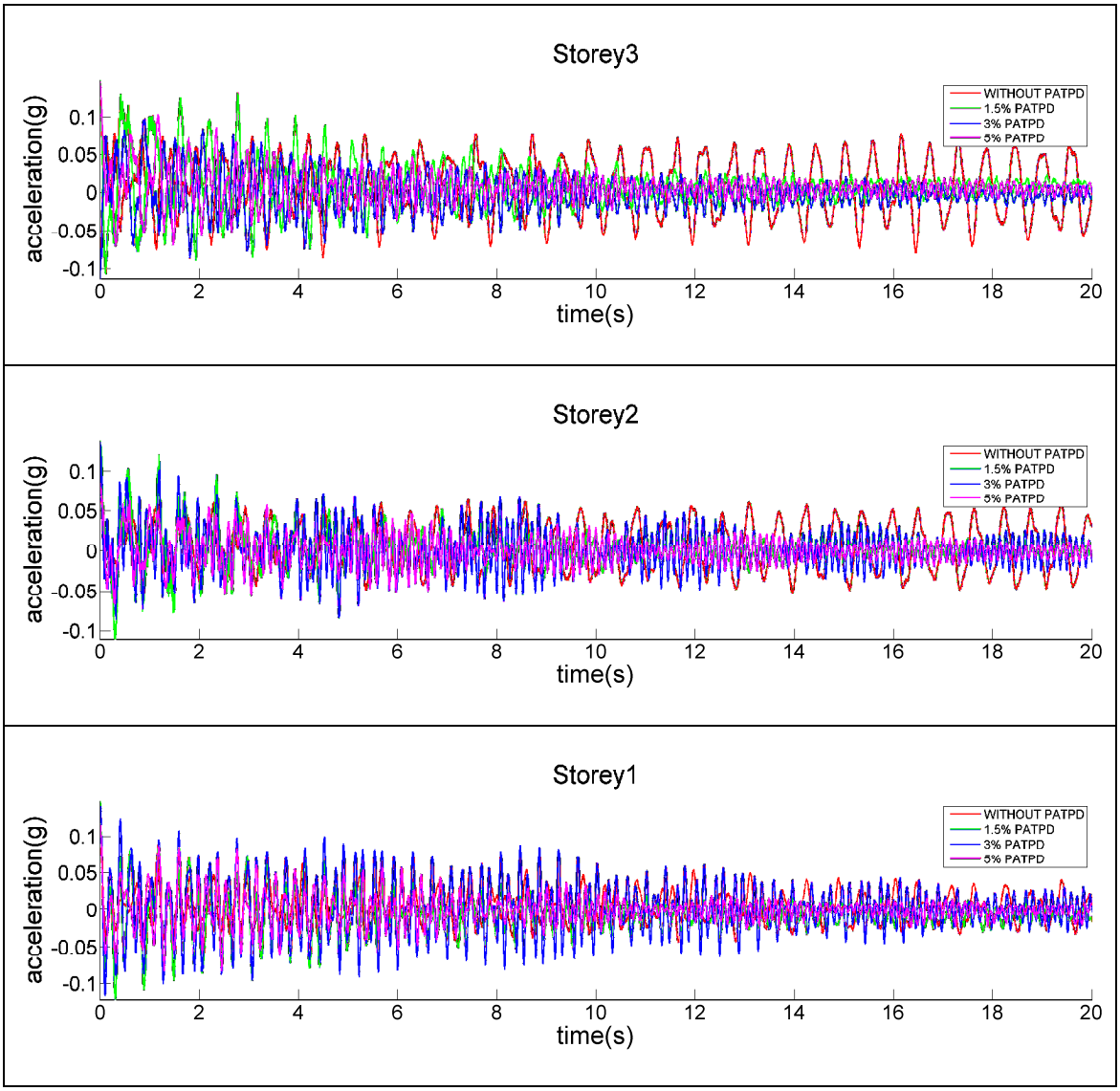

Figure 62: Time history of acceleration response in y-direction per storey for free torsional vibration, mass ratios 1.5%, 3% and 5%

Figure 62 shows that for all masses tested as the PATPD started moving; the acceleration peaks generated in the damped model are as high as those generated in the undamped model. However, these high accelerations subside and the accelerations rapidly decrease compared to that of the undamped model. As is expected the accelerations experienced in storey 3 are highest and the positive damping effect of the

PATPD was still significant for all mass ratios. The best control effect is seen in storey 3, since the damper was installed on this storey.

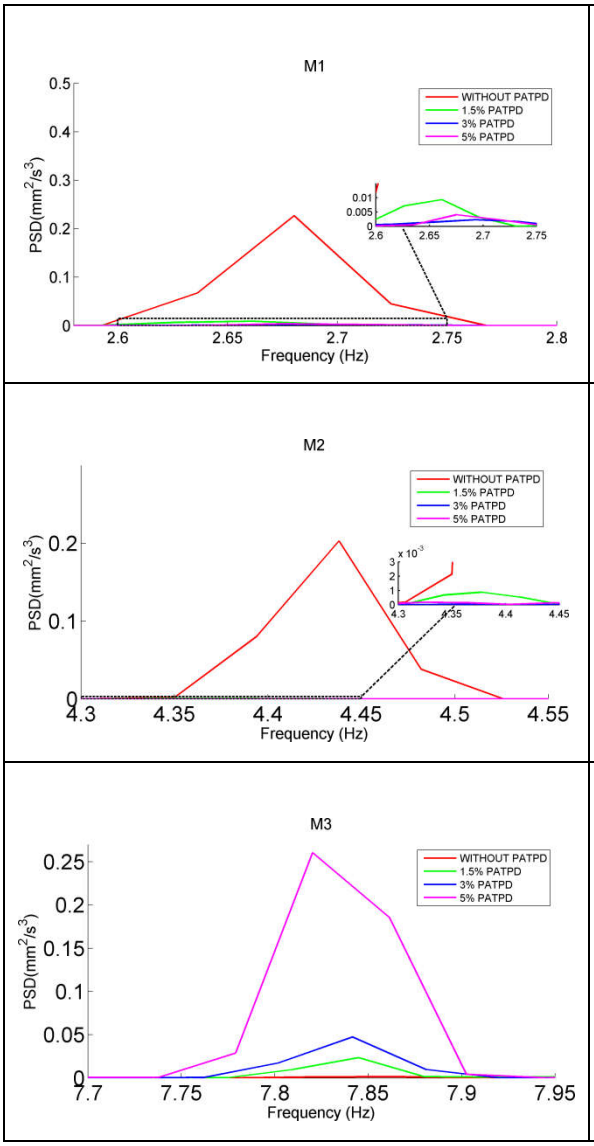

Figure 63: Magnified Power Spectral Density (PSD) storey 3 of the acceleration in the y-direction of the model under free torsional vibration, mass ratios 1.5%, 3% and 5%

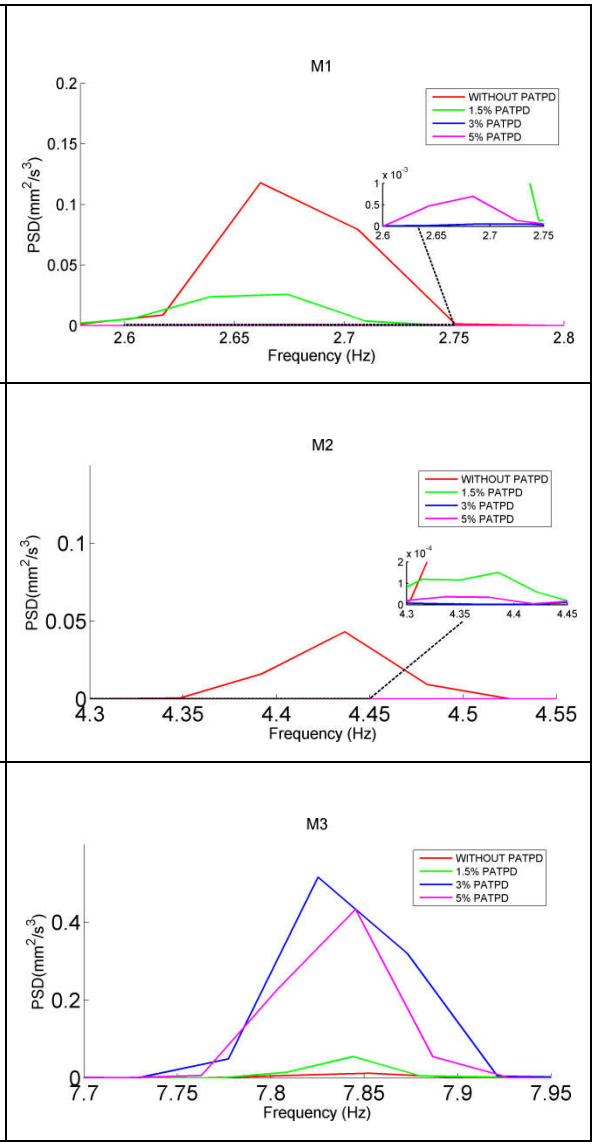

Figure 64: Magnified Power Spectral Density (PSD) storey 2 of the acceleration in the y-direction of the model under free torsional vibration, mass ratios 1.5%, 3% and 5%

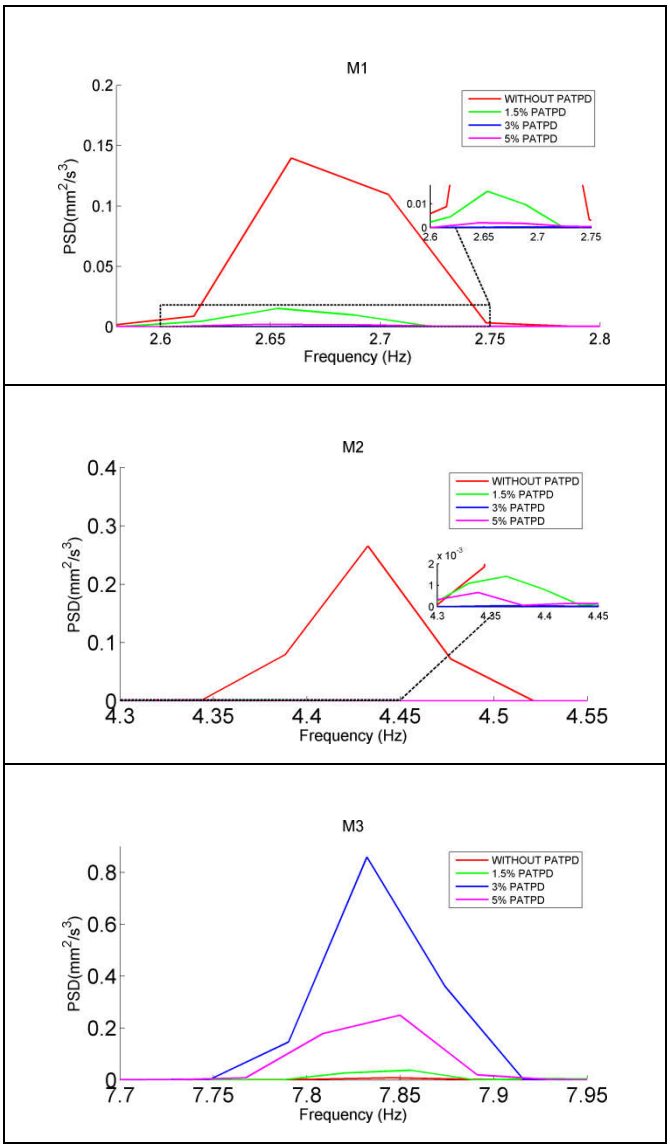

Figure 65: Magnified Power Spectral Density (PSD) storey 1 of the acceleration in the y-direction of the model under free torsional vibration, mass ratios 1.5%, 3% and 5%

Figure 63, Figure 64 and Figure 65 shows for first natural frequency with PSD peak, 2.680Hz, all three of the masses of the PATPD produced significant damping of the model's vibrations, reducing the PSD peak by at least 90%. Both the 3% (primary model) and 5% PATPD demonstrates best control effect and the 1.5% PATPD the least. For second natural frequency with PSD peak, 4.438 Hz, all of the masses of the PATPD produce damping of the model's vibrations. The 3% (primary model) demonstrates best control effect and the 1.5% PATPD the least. For third natural frequency with PSD peak, 7.842 Hz, all masses show an increase in density, with the 1.5% being the least.

Overall PSD peak increases were minimal in comparison to the reduction gained in PSD peak for the first natural frequency.

5.1.1.5 Coupled Vibration (Translation in X-direction and torsion)

The model was given an initial torsional displacement and displacement in x-direction simultaneously, respective acceleration measured in the x-direction. The damping effect of each of the PATPD masses can be seen in the graphs to follow.

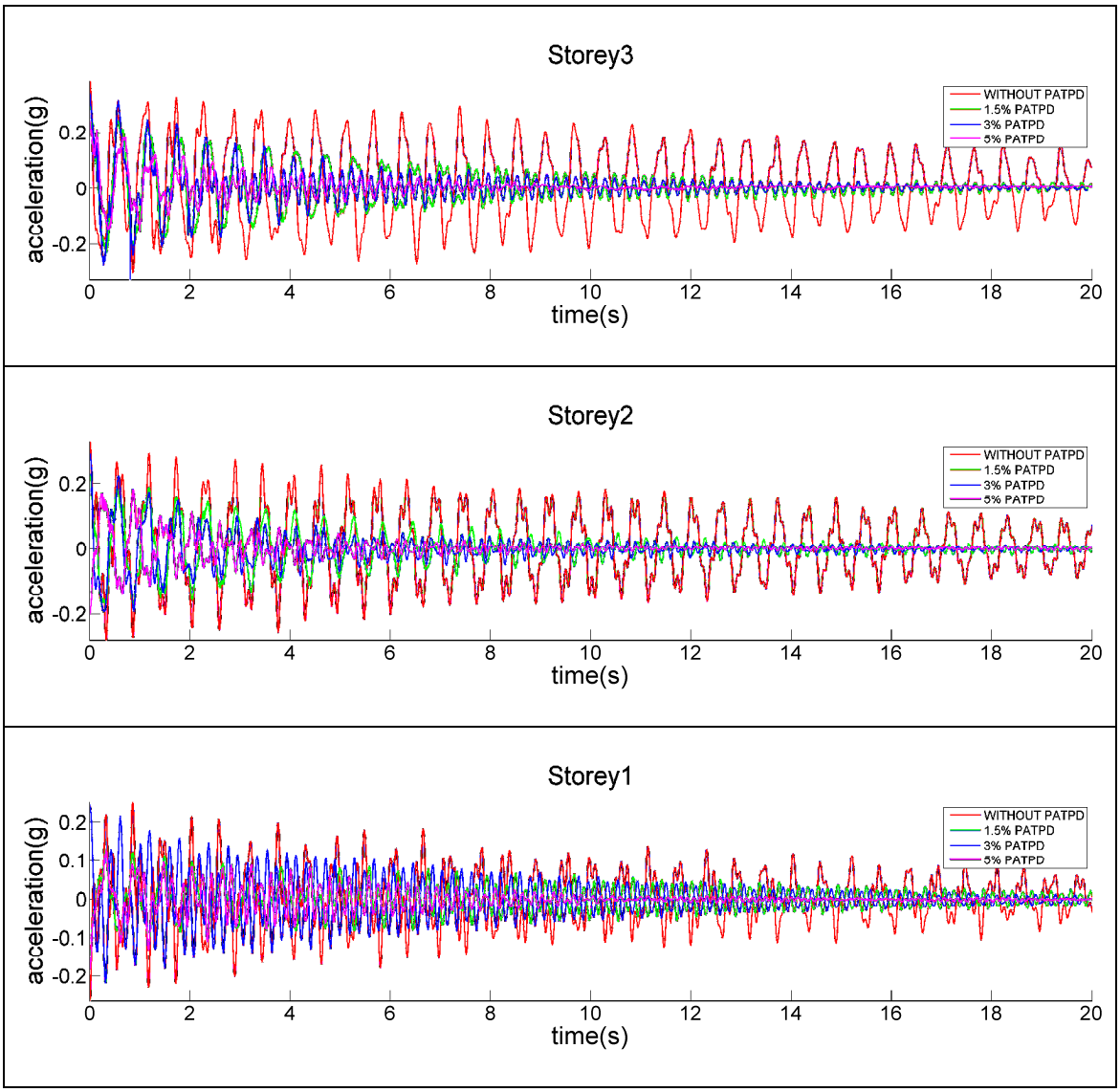

Figure 66: Time history of acceleration response in x-direction per storey for free coupled vibration, mass ratios 1.5%, 3% and 5%

Figure 66 shows that for all masses tested as the PATPD started moving; the acceleration peaks generated in the damped model are as high as those generated in the undamped model. However, these high accelerations subside and the accelerations rapidly decrease compared to that of the undamped model. As is expected the accelerations experienced in storey 3 are highest and the positive damping effect of the

PATPD was still significant for all mass ratios. The best control effect is seen in storey 3, since the damper was installed on this storey.

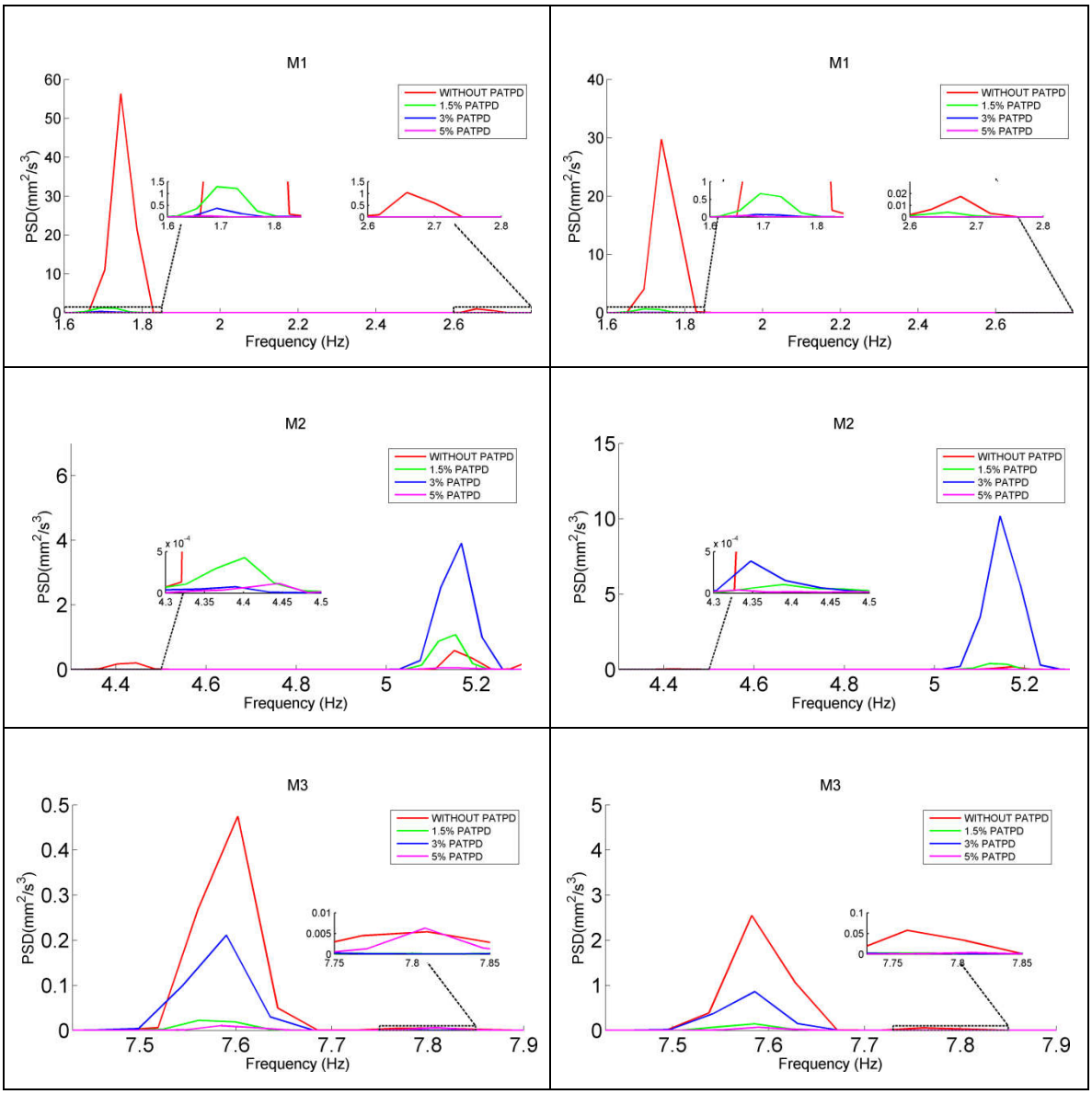

Figure 67: Magnified Power Spectral Density (PSD) storey 3 of the acceleration in the x-direction of the model under free coupled vibration, mass ratios 1.5%, 3% and 5%

Figure 68: Magnified Power Spectral Density (PSD) storey 2 of the acceleration in the x-direction of the model under free coupled vibration, mass ratios 1.5%, 3% and 5%

Figure 67, Figure 68 and Figure 69 show for first natural frequency with PSD peak, 1.733Hz and 2.677Hz, for both translation and torsion, all 3 PATPD masses provided significant damping of the model's vibrations across all 3 storeys, with the 5% demonstrating best control effect and the 1.5% PATPD the least.

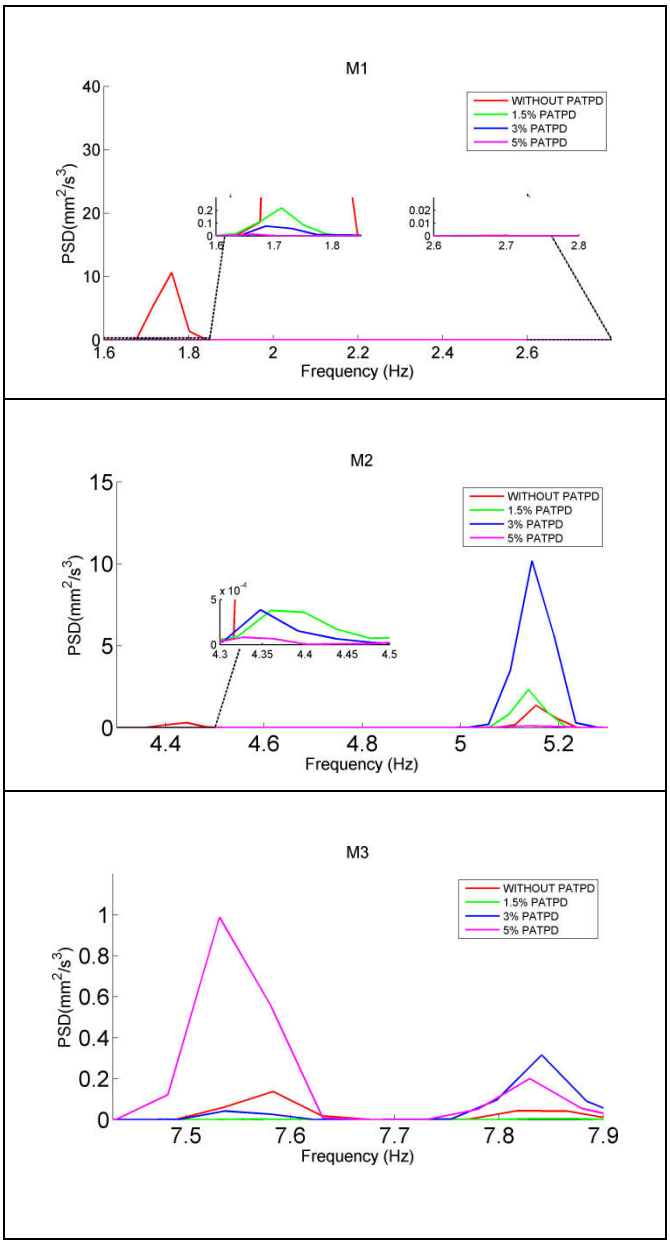

Figure 69: Magnified Power Spectral Density (PSD) storey 1 of the acceleration in the x-direction of the model under free coupled vibration, mass ratios 1.5%, 3% and 5%

For second natural frequency with PSD peak, 5.164Hz and 4.446Hz, for torsion across all 3 storeys, all PATPD masses provide significant damping of the model's vibrations across all 3 storeys, with the 5% demonstrating best control effect and the 1.5% and 3% PATPD similar effect. For translation across all 3 storeys, the 3% and 5% provides best control effect. For third natural frequency with PSD peak, 7.584Hz, for translation, all PATPD masses provide significant damping of the model's vibrations across storey 2-3, with the 5% demonstrating best control effect. For storey 1, however, 5% PATPD significantly increases PSD peak. For third natural frequency with PSD peak 7.792Hz, for torsion, overall 1.5% PATPD behaves best and the others do not provide much difference to undamped model.

Overall PSD peak increases were minimal in comparison to the reduction gained in PSD peak for the first natural frequency.

5.1.1.6 Coupled Vibration (Translation in Y-direction and torsion)

The model was given an initial torsional displacement and displacement in y-direction simultaneously, respective acceleration measured in the y-direction. The damping effect of each of the PATPD masses can be seen in the graphs to follow.

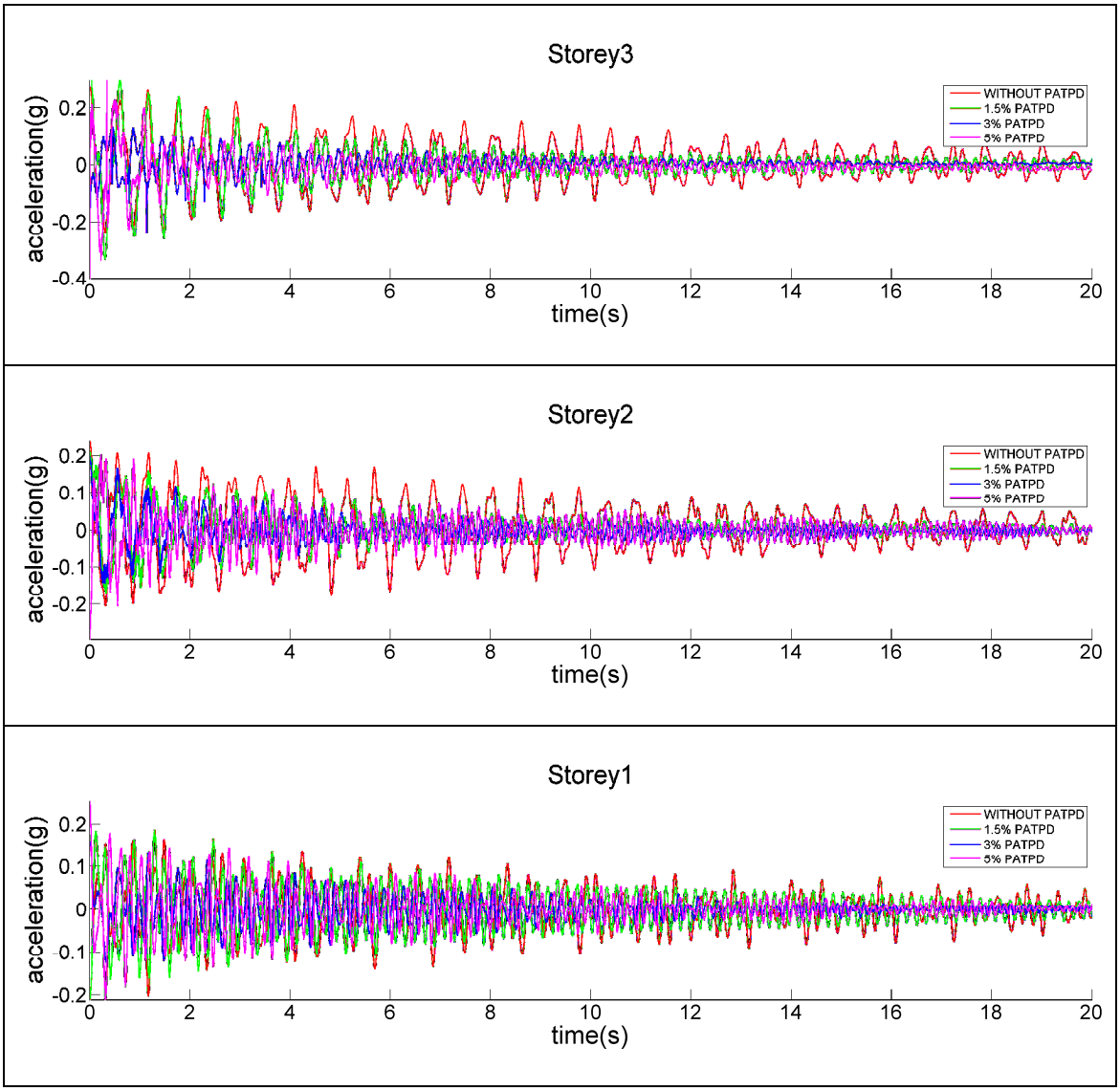

Figure 70: Time history of acceleration response in y-direction per storey for free coupled vibration, mass ratios 1.5%, 3% and 5%

Figure 70 shows that for all masses tested as the PATPD started moving; the acceleration peaks generated in the damped model are as high as those generated in the undamped model. However, these high accelerations subside and the accelerations rapidly decrease compared to that of the undamped model. As is expected the accelerations experienced in storey 3 are highest and the positive damping effect of the

PATPD was still significant for all mass ratios. The best control effect is seen in storey 3, since the damper was installed on this storey.

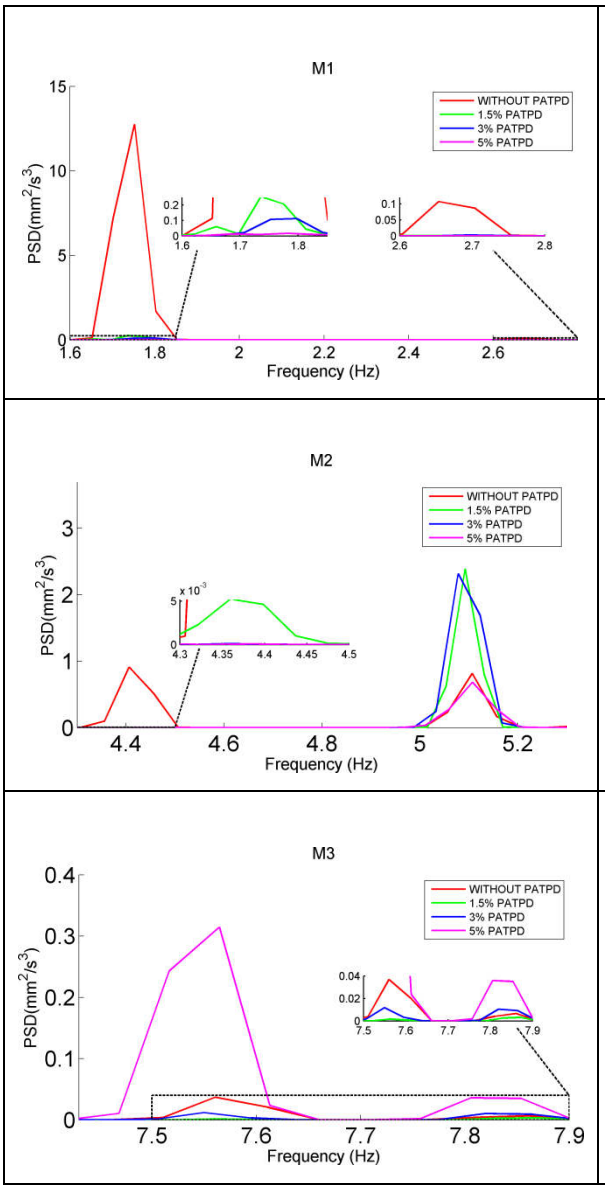

Figure 71: Magnified Power Spectral Density (PSD) storey 3 of the acceleration in the y-direction of the model under free coupled vibration, mass ratios 1.5%, 3% and 5%

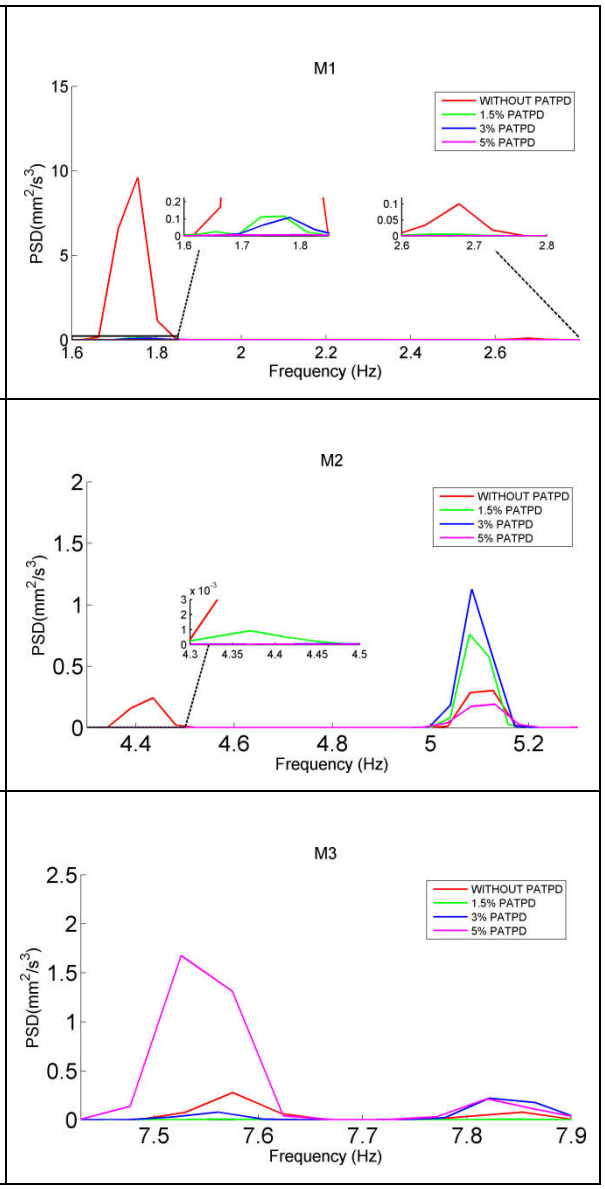

Figure 72: Magnified Power Spectral Density (PSD) storey 2 of the acceleration in the y-direction of the model under free coupled vibration, mass ratios 1.5%, 3% and 5%

Figure 71, Figure 72 and Figure 73 show for first natural frequency with PSD peak, 1.747Hz and 2.680Hz, for both translation and torsion, all 3 PATPD masses provide significant damping of the model's vibrations across all 3 storeys, with the 5% demonstrating best control effect and the 1.5% PATPD the least.

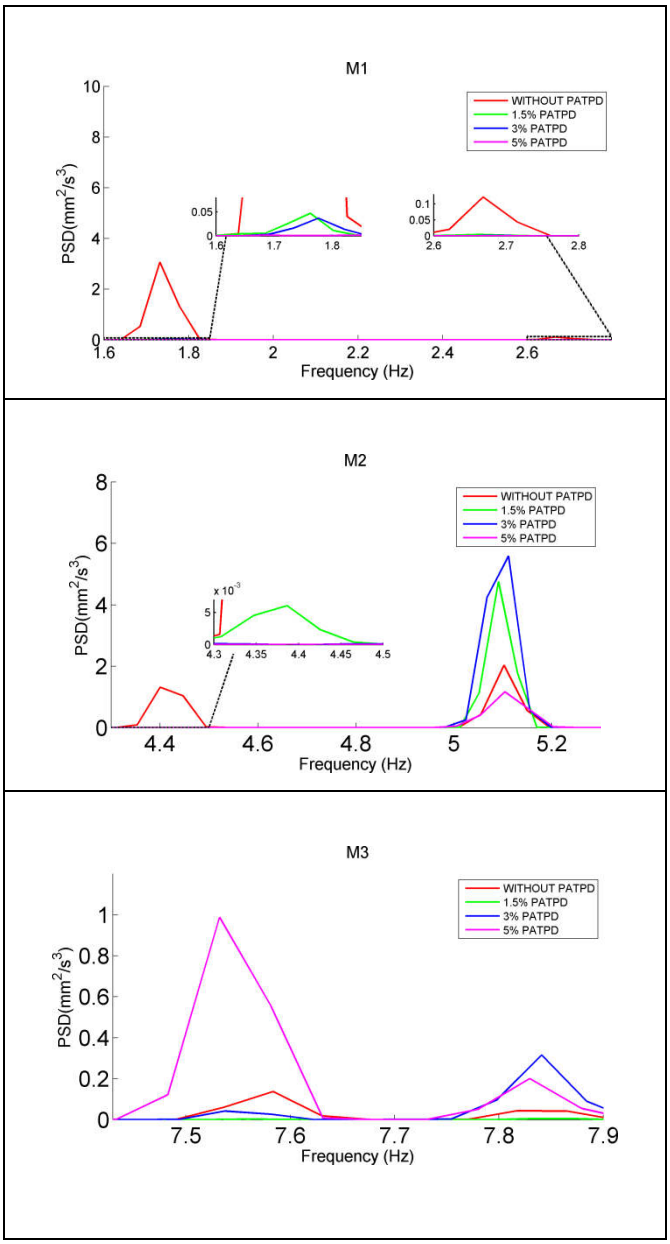

Figure 73: Magnified Power Spectral Density (PSD) storey 1 of the acceleration in the y-direction of the model under free coupled vibration, mass ratios 1.5%, 3% and 5%

For second natural frequency with PSD peak, 4.438 Hz, for torsion across all 3 storeys, all PATPD masses provide significant damping of the model's vibrations across all 3 storeys, with the 3% and 5% demonstrating best control effect and the 1.5% PATPD the least. For translation across all 3 storeys , the 5% provides best control effect, even if slightly so, with the 1.5% and 3% PATPD having the similar effect of increasing the density of the frequency. For third natural frequency with PSD peak, 7.569Hz and 7.842 Hz, for both translation and torsion, both the 1.5% and 3% PATPD masses provide slight damping of the model's vibrations across all 3 storeys, with the 5% demonstrating least control effect by way of increasing the density of both frequencies.

Overall PSD peak increases were minimal in comparison to the reduction gained in PSD peak for the first natural frequency.

5.1.2.0 Forced Vibration

5.1.2.1 Translational Vibration in the X-direction

The model was placed on the shake table in order to carry out the forced vibration tests. The PATPD's were connected one-by-one and the respective accelerations measured. The damping effect of each of the PATPD masses can be seen in the graphs to follow.

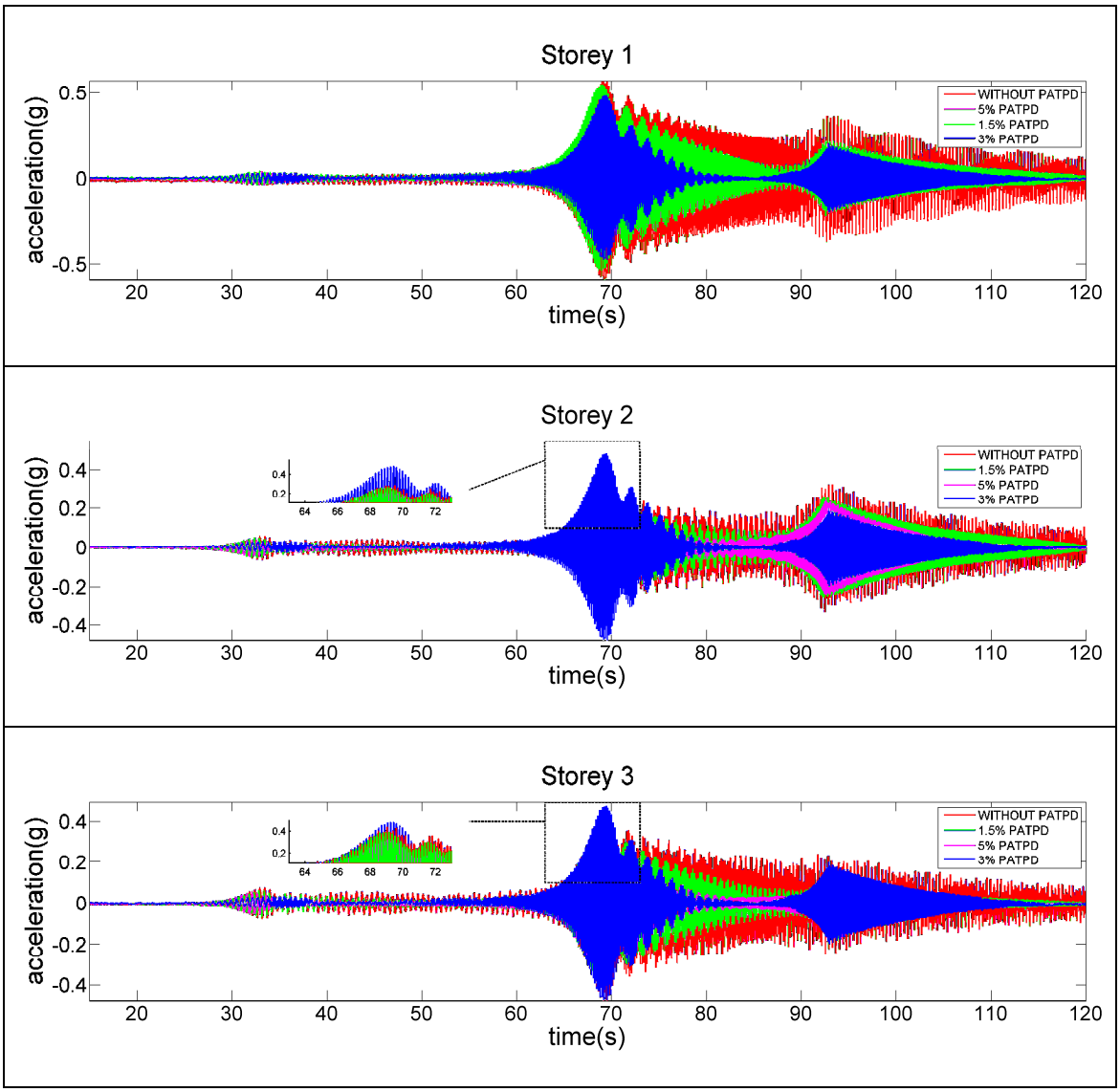

Figure 74: Time history of acceleration response per storey for forced translational vibration in x-direction, mass ratios 1.5%, 3% and 5%

Figure 74 shows for all 3 storeys, and all mass ratios, that by adding the damper onto model the initial accelerations experienced were slightly higher than without damper, but then the accelerations decrease.

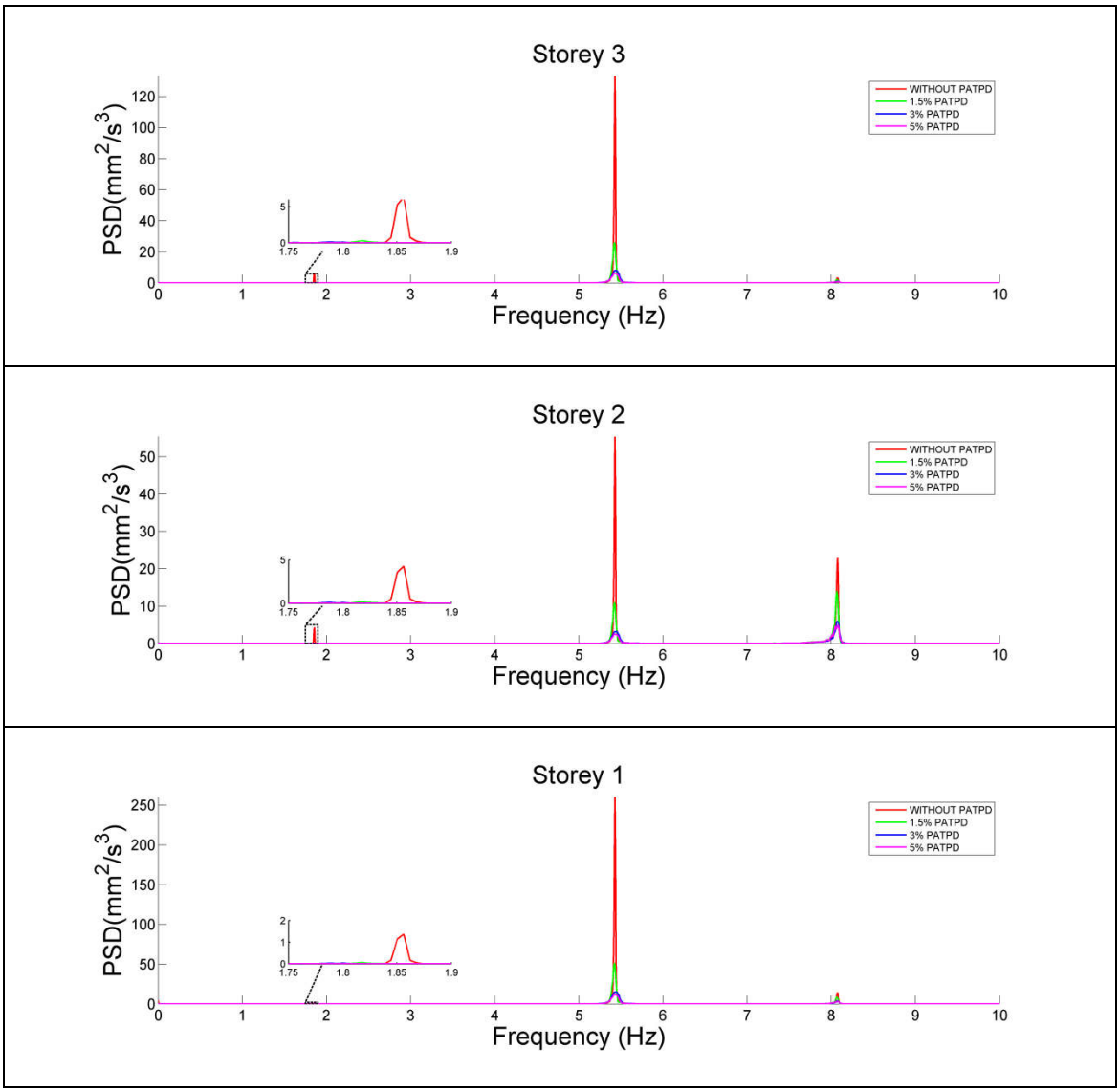

Figure 75: Power Spectral Density (PSD) of the acceleration response per storey under forced excitation in the x-direction, mass ratios 1.5%, 3% and 5%

Figure 75 shows PSD peaks at 1.856Hz, 5.429Hz and 8.047Hz. This corresponds to the models first, second and third frequencies. The positive control effect is evident as PSD peaks for all 3 frequencies are significantly reduced. This is true for all mass ratios.

5.1.2.2 Translational Vibration in the Y-direction

The model was placed on the shake table in order to carry out the forced vibration tests. The PATPD's were connected one-by-one and the respective accelerations measured. The damping effect of each of the PATPD masses can be seen in the graphs to follow.

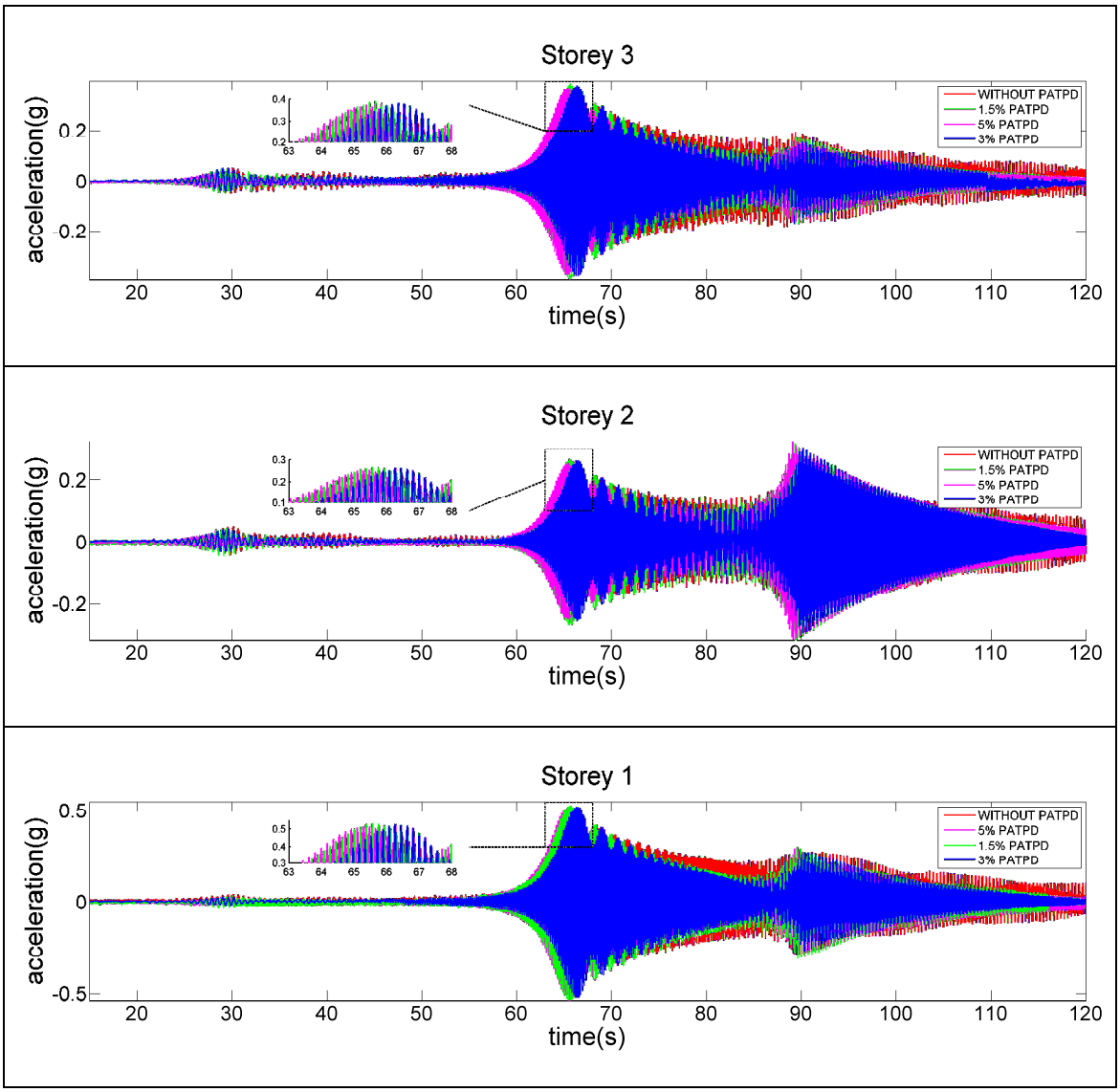

Figure 76: Time history of acceleration response per storey for forced translational vibration in y-direction, mass ratios 1.5%, 3% and 5%

Figure 76 shows for all 3 storeys, and all mass ratios, that by adding the damper onto model the initial accelerations experienced are slightly higher than without damper, but then the accelerations decrease.

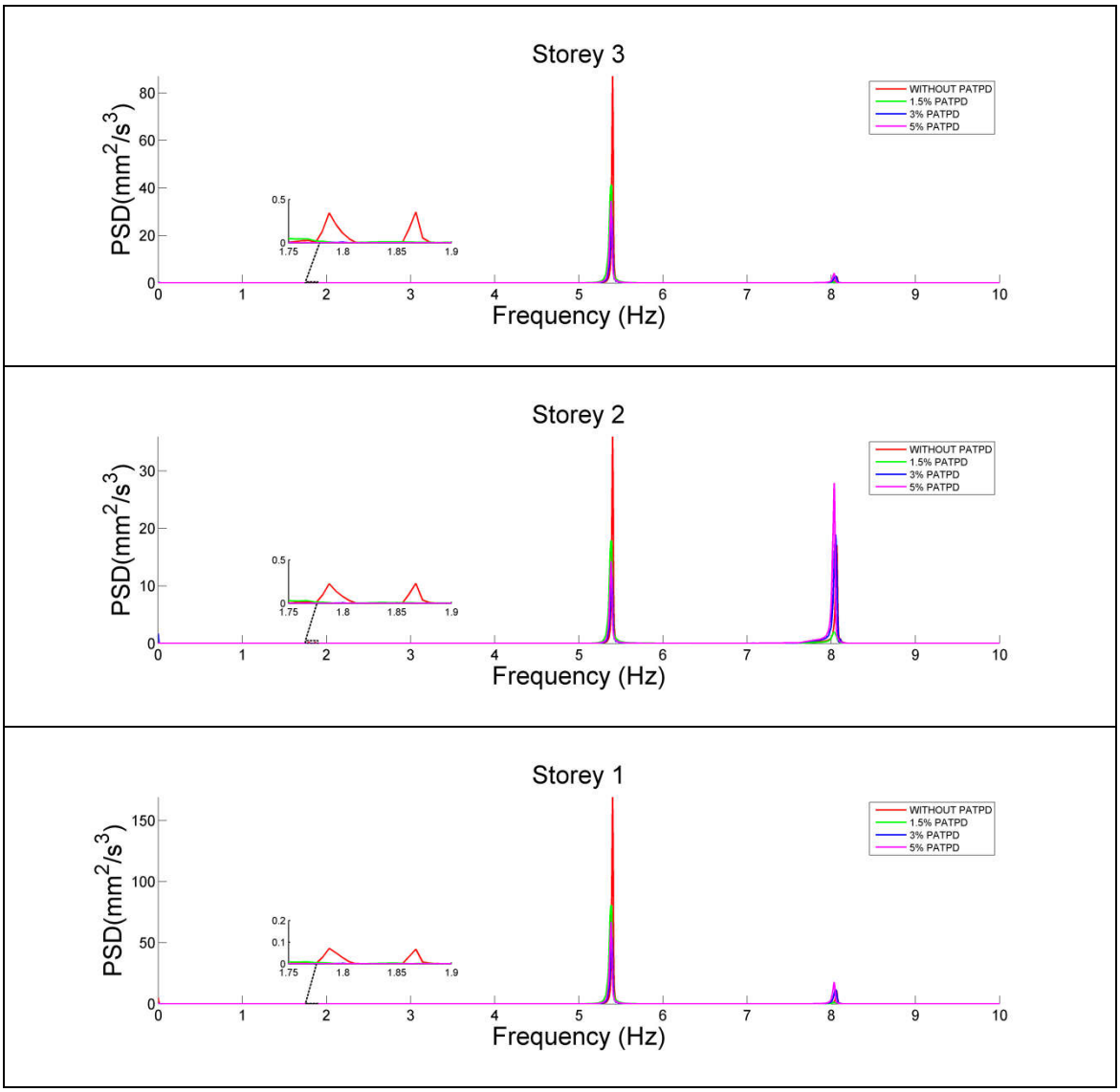

Figure 77: Power Spectral Density (PSD) of the acceleration response per storey under forced excitation in the y-direction, mass ratios 1.5%, 3% and 5%

Figure 77 shows PSD peaks at 1.787Hz, 5.399Hz and 8.065Hz. This corresponds to the models first, second and third frequencies. The positive control effect is evident as PSD peaks for all 3 frequencies are significantly reduced. This is true for all mass ratios.

As can be seen from the set of results from both directions the PATPD provides better control in the x-direction than in the y-direction.

5.1.3.0 Summary

Free Vibration

This set of parameter tests indicates better control in x than in y direction.

Even though a higher mass ratio is expected to perform better, these tests indicate otherwise. The higher mass ratio means that the sand has less ability to 'move' and thus does not perform as well, overall, as the 3% wherein the sand can do so.

The 1.5% ratio did not perform as well, even though it had greatest sand mobility, since it was too light.

All mass ratios provided control effect to the first natural frequency for all free vibration tests for all storeys.

Forced Vibration

For Forced Vibration the PATPD provides significant control to all 3 frequencies for all mass ratios.

The results reveal that the PATPD performs better in translation the x –direction than the y-direction.

5.2 Parameter Test 2: Effect of changing friction

The pulleys transfer the driving force from the structure's movement to the damper pulling it in an opposing direction thus dissipating energy and reducing vibration. The more reactive the damper, the quicker it responds and moves depends on the friction of the roller support, the better the reduction. Tests were carried out using three different damper support surfaces to effect a frictional change, a steel surface, a rubber surface and a sandpaper surface[6]. All other parameters during these tests remained constant, with the test model having a mass of 42.09kg and a height of 37cm per storey. As with the previous tests the model was given an initial displacement, in the according directions, and the acceleration with and without the damper measured.

The data for each case is processed and they are plotted together on graphs such that extrapolations and comparisons can be made.

5.2.1 Free Vibration

5.2.1.1 Translational Vibration in the X-direction

The model was given an initial displacement in the x-direction and respective acceleration measured. The damping effect of each can be seen in the graphs to follow.

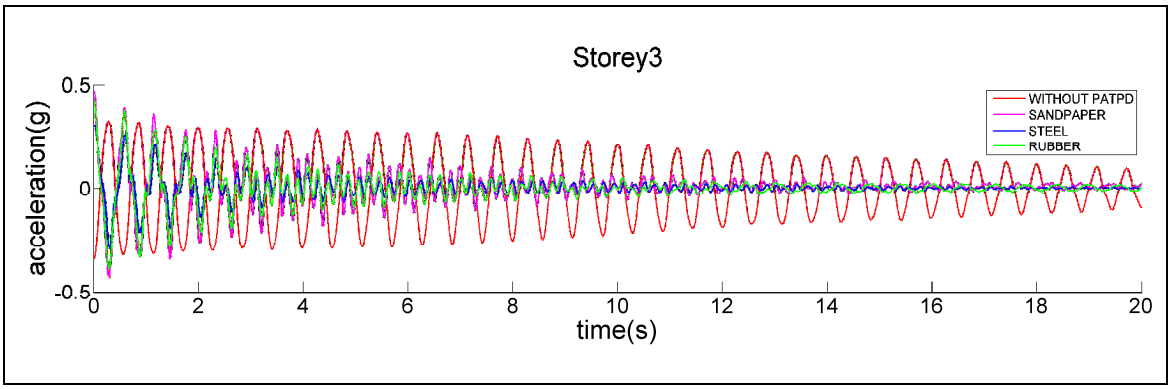

[6] These configurations can be found on page 55-56

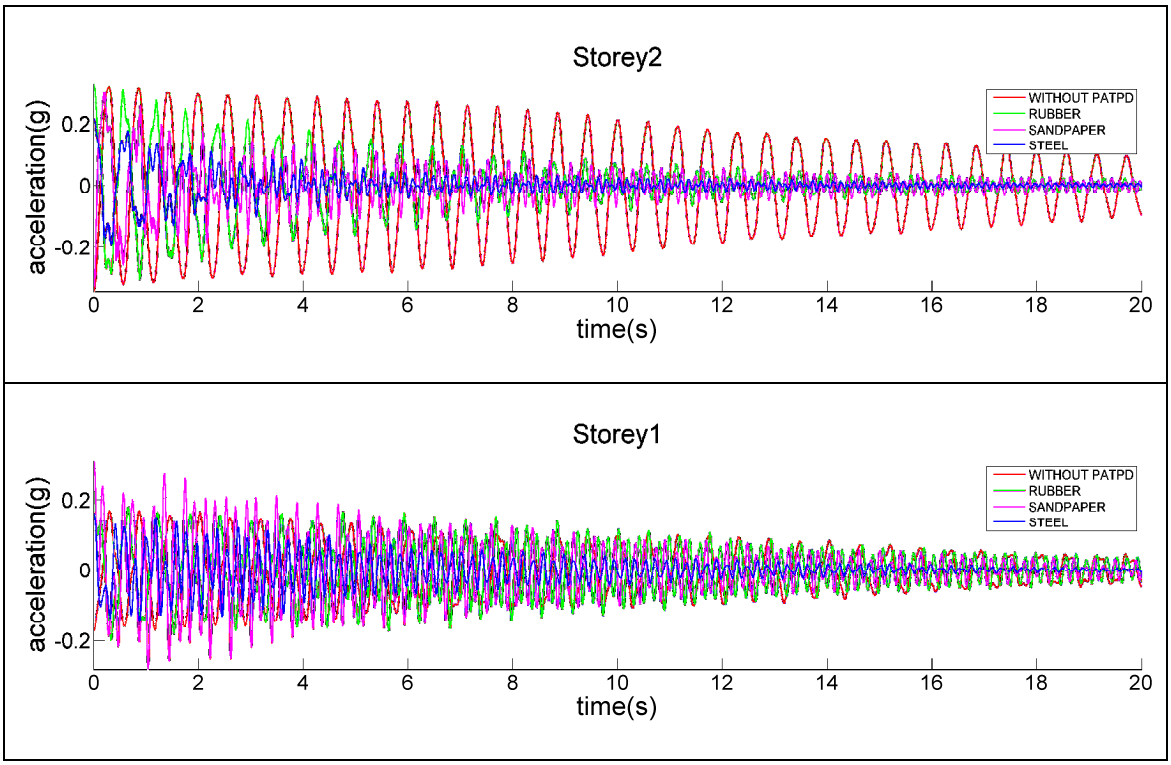

Figure 78: Time history of acceleration response per storey for free translational vibration in x-direction, steel, rubber and sandpaper surfaces

Figure 78 shows that for all masses tested as the PATPD started moving; the acceleration peaks generated in the damped model are as high as those generated in the undamped model. However, these high accelerations subside and the accelerations rapidly decrease compared to that of the undamped model. As is expected the accelerations experienced in storey 3 are highest and the positive damping effect of the PATPD is still significant for all mass ratios. The best control effect is seen in storey 3, since the damper was installed on this storey.

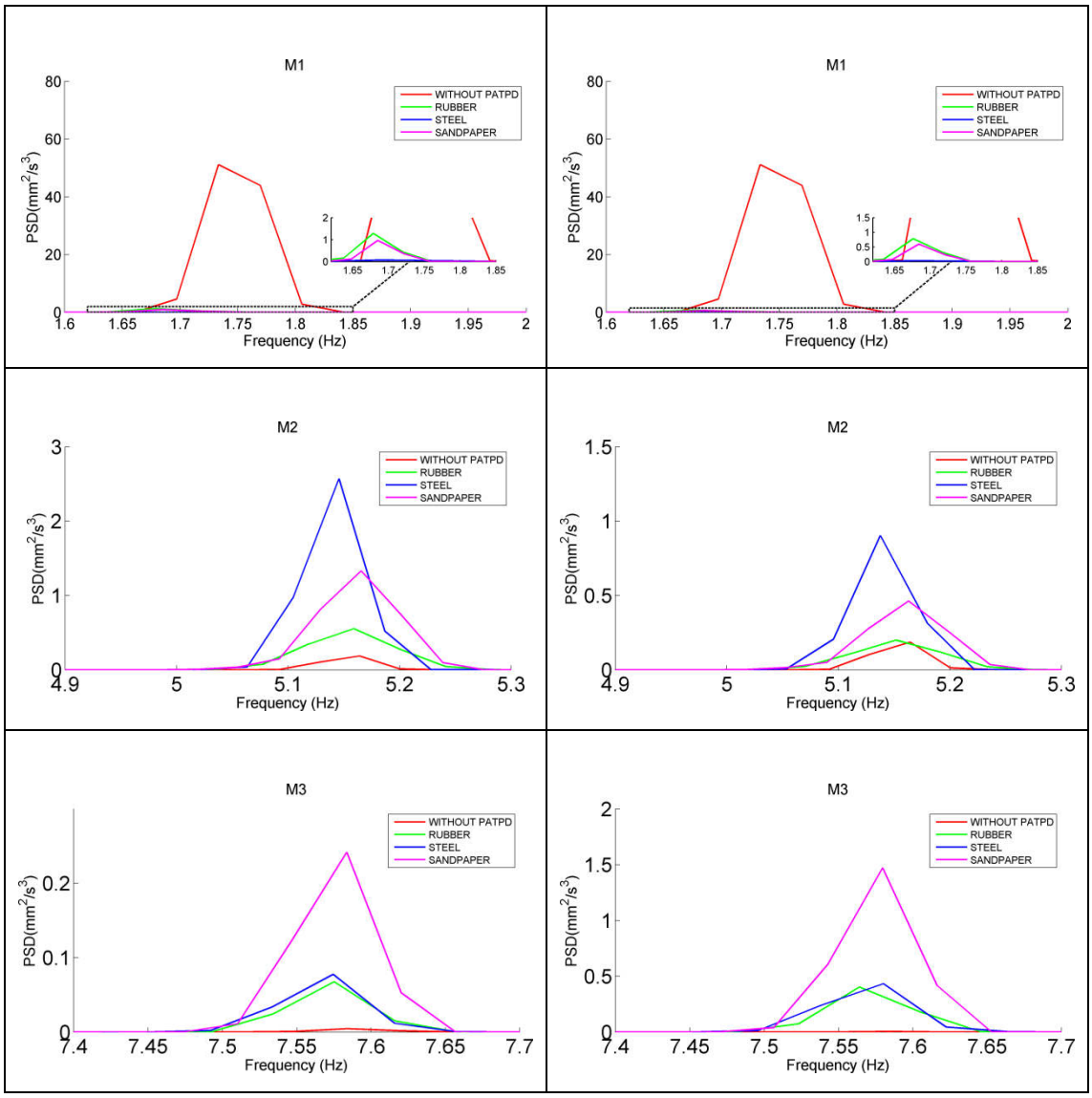

Figure 79: Magnified Power Spectral Density (PSD) storey 3 of the acceleration of the model under free translational vibration in the x-direction , steel, rubber and sandpaper surfaces

Figure 80: Magnified Power Spectral Density (PSD) storey 2 of the acceleration of the model under free translational vibration in the x-direction, steel, rubber and sandpaper surfaces

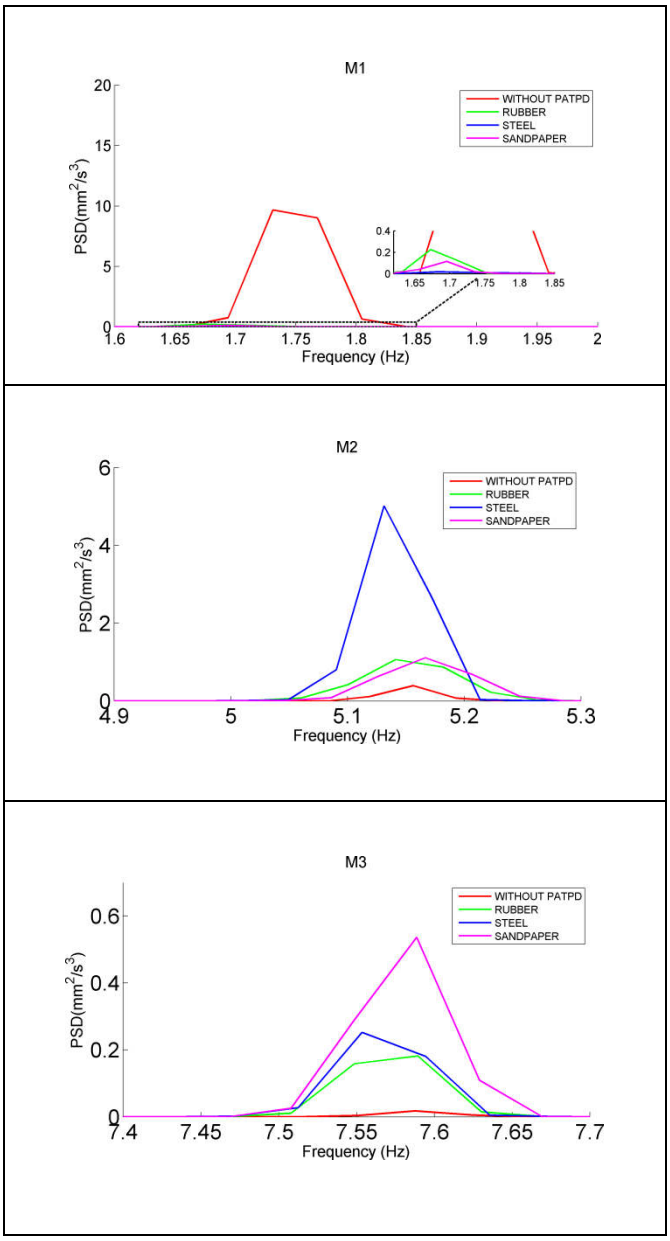

Figure 81: Magnified Power Spectral Density (PSD) storey 1 of the acceleration of the model under free translational vibration in the x-direction, steel, rubber and sandpaper surfaces

Figure 79, Figure 80 and Figure 81 shows for first natural frequency with PSD peak, 1.733Hz, across all storeys, all three surfaces produced significant damping of the model's vibrations, reducing the PSD peak by at least 90%. Steel demonstrates best control effect.

For both second and third natural frequency with PSD peaks, 5.164Hz and 7.584Hz across all storeys, however, none produce damping of the model's vibrations they actually increase frequency density. For second natural frequency rubber behaves best and steel worst. For third natural frequency rubber and steel behave best and sandpaper worst.

Overall PSD peak increases were minimal in comparison to the reduction gained in PSD peak for the first natural frequency.

5.2.1.2 Translational Vibration in the Y-direction

The model was given an initial displacement in the y-direction and respective acceleration measured. The damping effect of each of the PATPD can be seen in the graphs to follow.

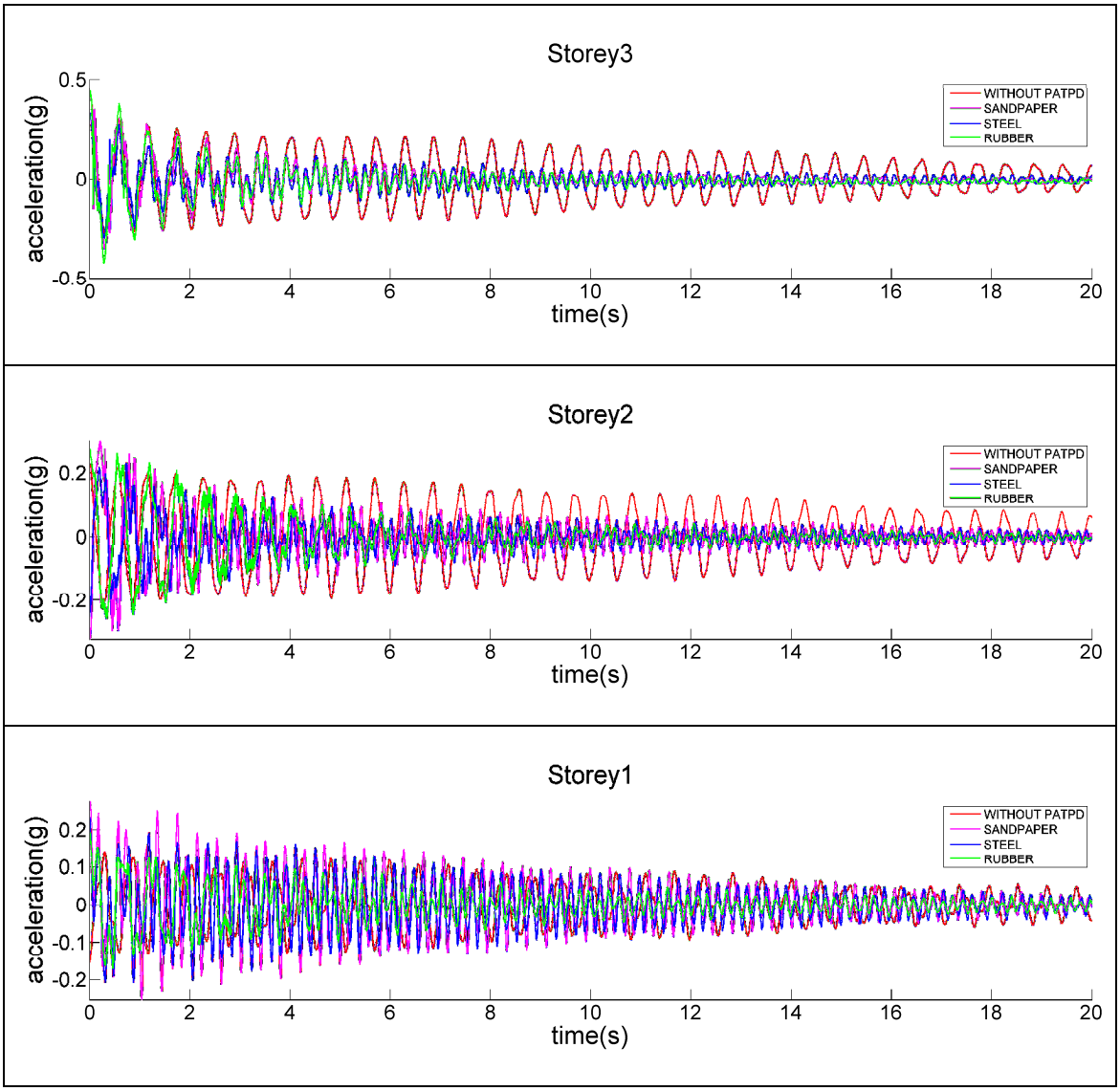

Figure 82: Time history of acceleration response per storey for free translational vibration in y-direction, steel, rubber and sandpaper surfaces

Figure 82 shows that for all surfaces as the PATPD started moving; the acceleration peaks generated in the damped model are as high as those generated in the undamped model. However, these high accelerations subside and the accelerations rapidly decrease compared to that of the undamped model. As is expected the accelerations experienced in storey 3 are highest and the positive damping effect of the PATPD was still

significant for all surfaces. The best control effect is seen in storey 3, since the damper was installed on this storey.

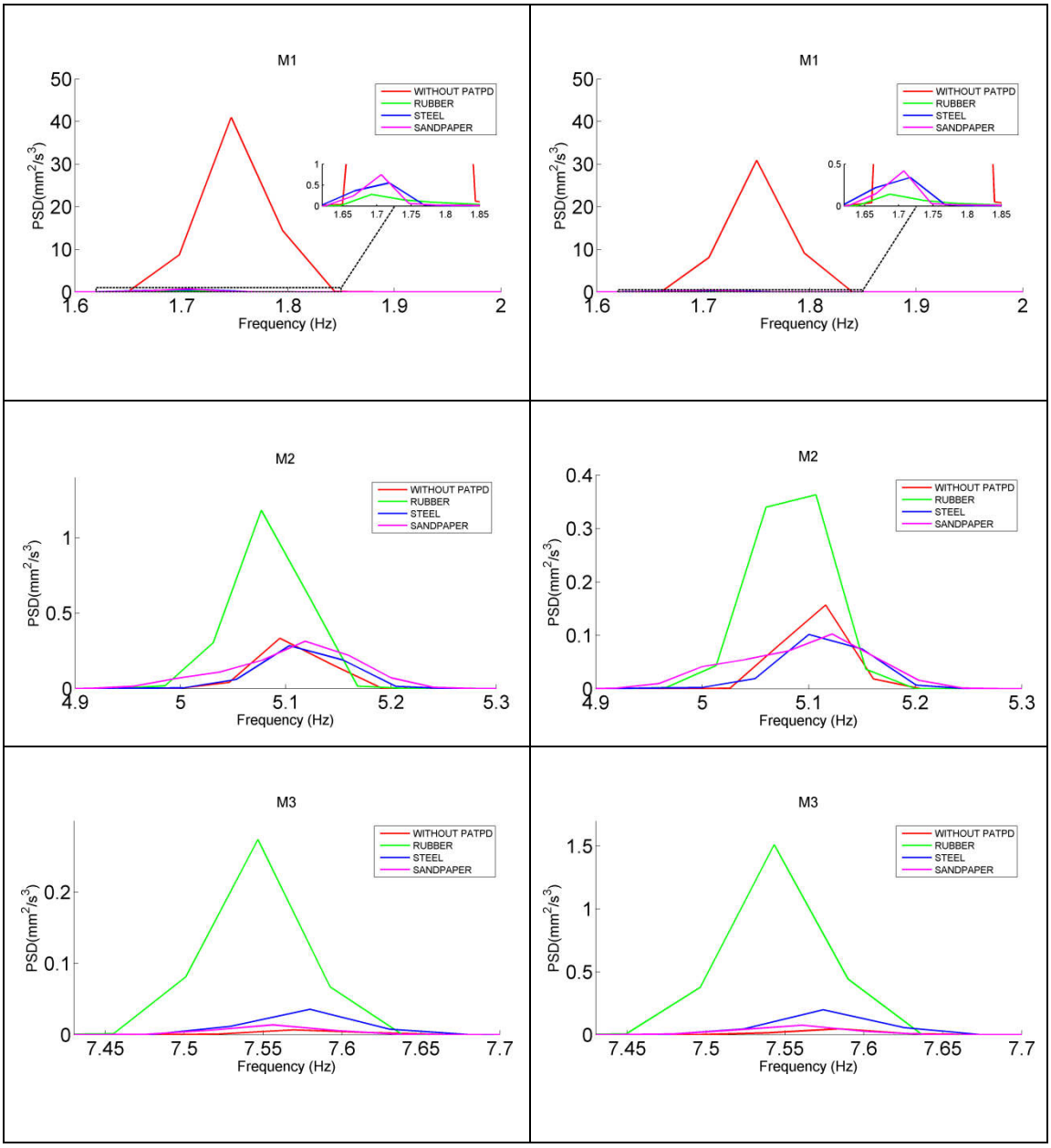

Figure 83: Magnified Power Spectral Density (PSD) storey 3 of the acceleration of the model under free translational vibration in the y-direction, steel, rubber and sandpaper surfaces

Figure 84: Magnified Power Spectral Density (PSD) storey 2 of the acceleration of the model under free translational vibration in the y-direction, steel, rubber and sandpaper surfaces

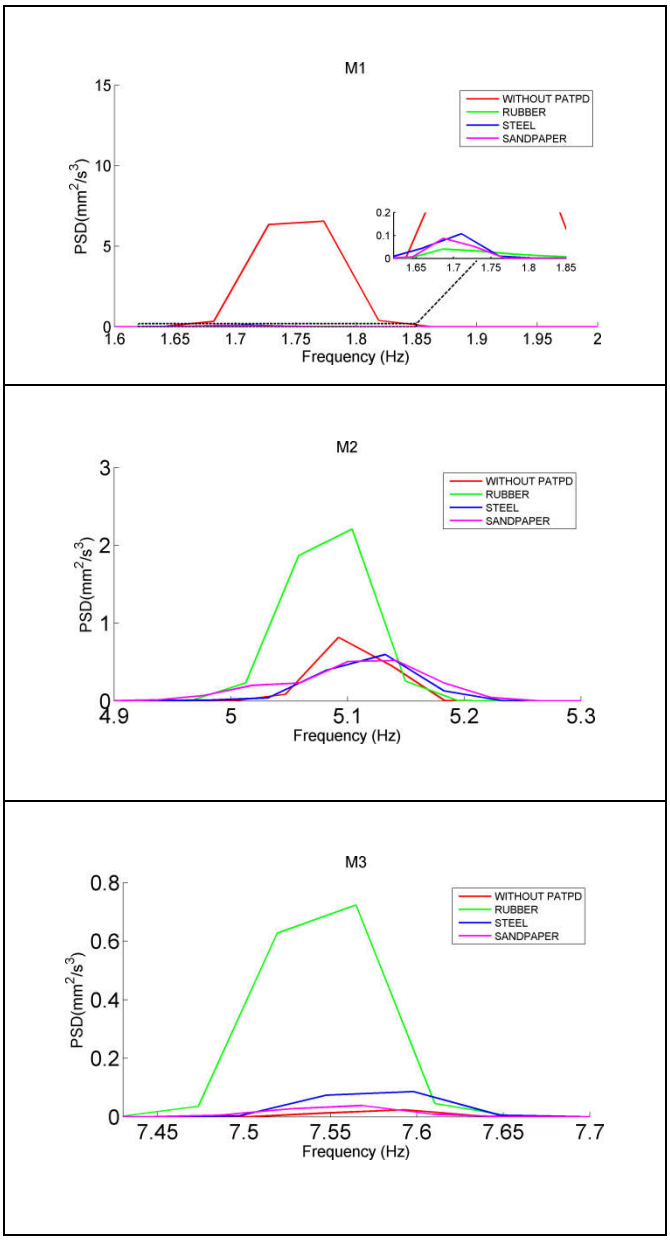

Figure 85: Magnified Power Spectral Density (PSD) storey 1 of the acceleration of the model under free translational vibration in the y-direction, steel, rubber and sandpaper surfaces

Figure 83, Figure 84 and Figure 85 shows for first natural frequency with PSD peak, 1.747Hz, surfaces used produced significant damping of the model's vibrations across all storeys, reducing the PSD peak by at least 90%. Sandpaper demonstrates best control effect.

Both second and third natural frequency with PSD peaks, 5.095Hz and 7.569Hz show a slight increase with sandpaper and steel across all storeys, but it is minimal. Rubber, however, provides a significant increase in the model's vibrations across all storeys.

Overall PSD peak increases were minimal in comparison to the reduction gained in PSD peak for the first natural frequency.

5.2.1.3 Torsional Vibration (acceleration measured in the X-direction)

The model was given an initial torsional displacement and respective acceleration measured in the x-direction. The damping effect of each can be seen in the graphs to follow.

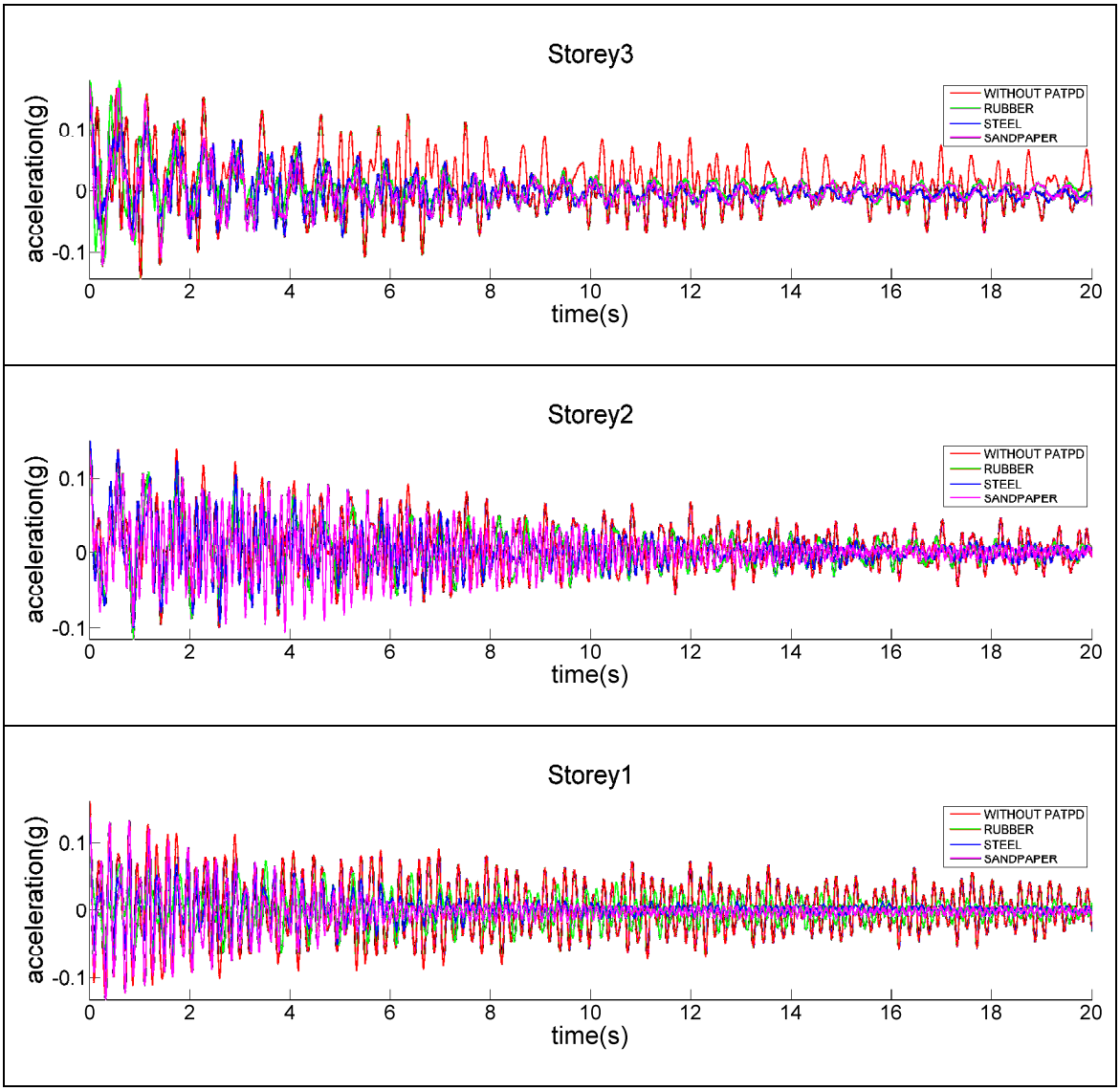

Figure 86: Time history of acceleration response in x-direction per storey for free torsional vibration, steel, rubber and sandpaper surfaces

Figure 86 shows that for all surfaces as the PATPD started moving; the acceleration peaks generated in the damped model are as high as those generated in the undamped model. However, these high accelerations subside and the accelerations rapidly decrease compared to that of the undamped model. As is expected the accelerations experienced in storey 3 are highest and the positive damping effect of the PATPD was still

significant for all surfaces. The best control effect is seen in storey 3, since the damper was installed on this storey.

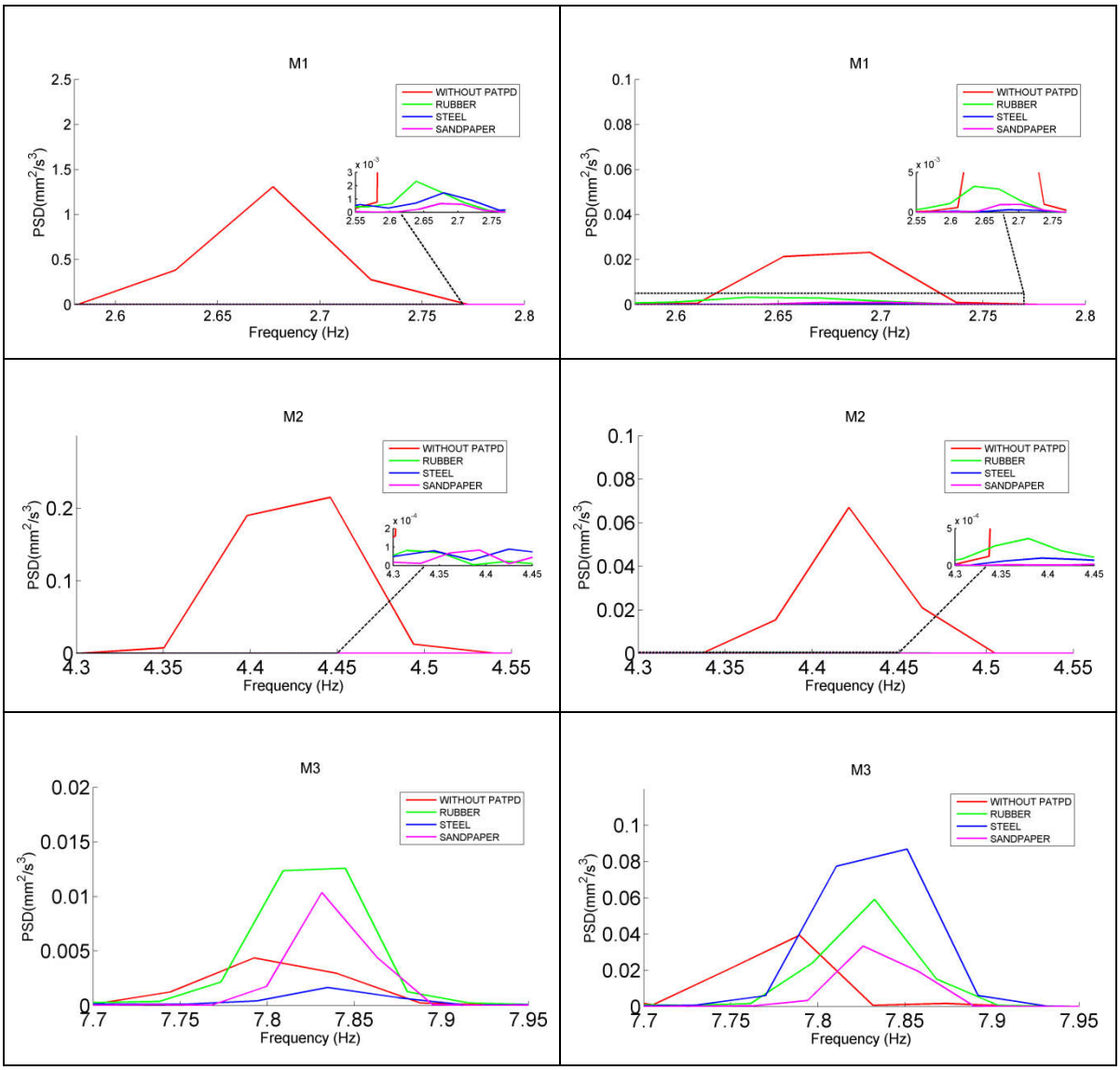

Figure 87: Magnified Power Spectral Density (PSD) storey 3 of the acceleration in the x-direction of the model under free torsional vibration, steel, rubber and sandpaper surfaces

Figure 88: Magnified Power Spectral Density (PSD) storey 2 of the acceleration in the x-direction of the model under free torsional vibration, steel, rubber and sandpaper surfaces

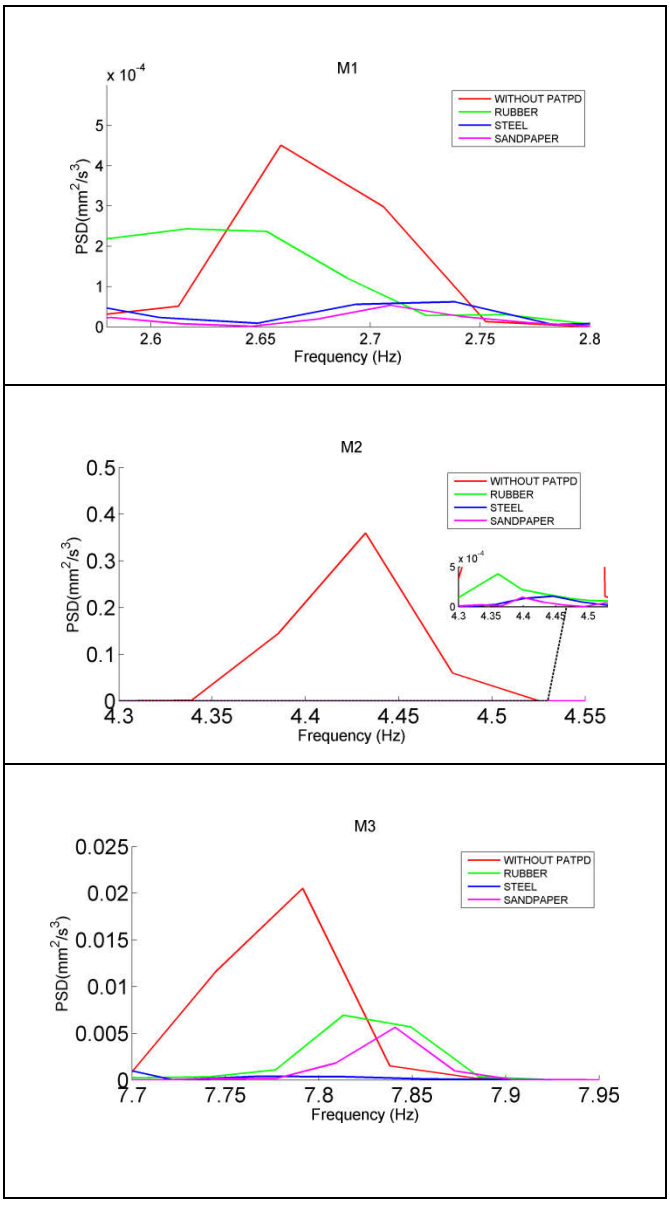

Figure 89: Magnified Power Spectral Density (PSD) storey 1 of the acceleration in the x-direction of the model under free torsional vibration, steel, rubber and sandpaper surfaces

Figure 87, Figure 88 and Figure 89 shows for first and second natural frequency with PSD peaks, 2.677Hz and 4.446Hz, across all storeys, all three surfaces produced significant damping of the model's vibrations. Rubber demonstrates least control effect. For third natural frequency with PSD peak, 7.792Hz, storey 1, all surfaces provides significant control – with steel demonstrating best control effect. Storey 2 shows no significant control effect – with steel demonstrating worst control and rubber and sandpaper showing almost no difference to undamped model. Storey 3 shows steel with as only surface that manages to provide control effect, with the other two actually increasing frequency densities.

Overall PSD peak increases were minimal in comparison to the reduction gained in PSD peak for the first natural frequency.

5.2.1.4 Torsional Vibration (acceleration measured in the Y-direction)

The model was given an initial torsional displacement and respective acceleration measured in the y-direction. The damping effect of each can be seen in the graphs to follow.

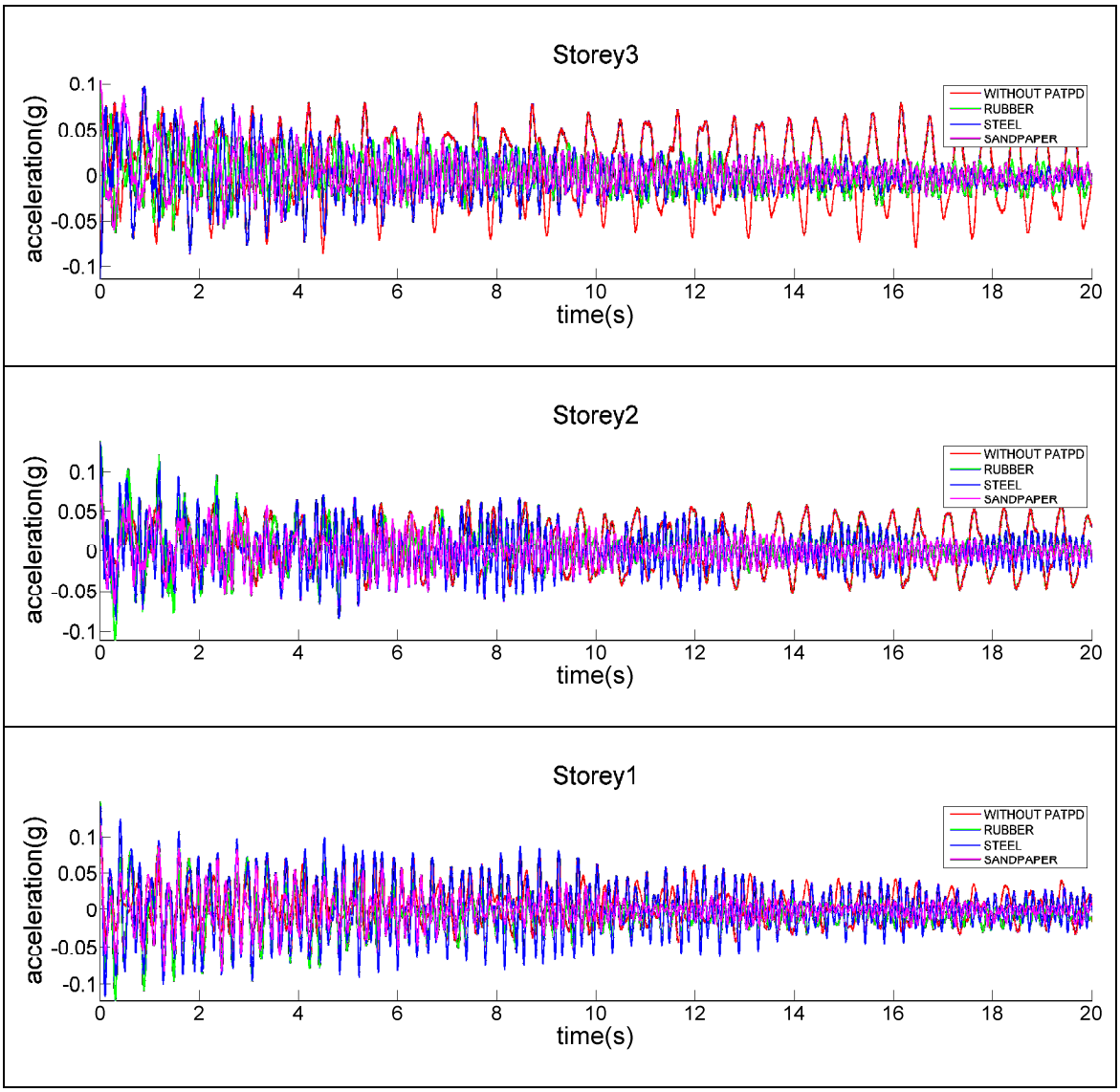

Figure 90: Time history of acceleration response in y-direction per storey for free torsional vibration, steel, rubber and sandpaper surfaces

Figure 90 shows that for all surfaces as the PATPD started moving; the acceleration peaks generated in the damped model are as high as those generated in the undamped model. However, these high accelerations subside and the accelerations rapidly decrease compared to that of the undamped model. As is expected the accelerations experienced in storey 3 are highest and the positive damping effect of the PATPD was still significant for all surfaces. The best control effect is seen in storey 3, since the damper was installed on this storey.

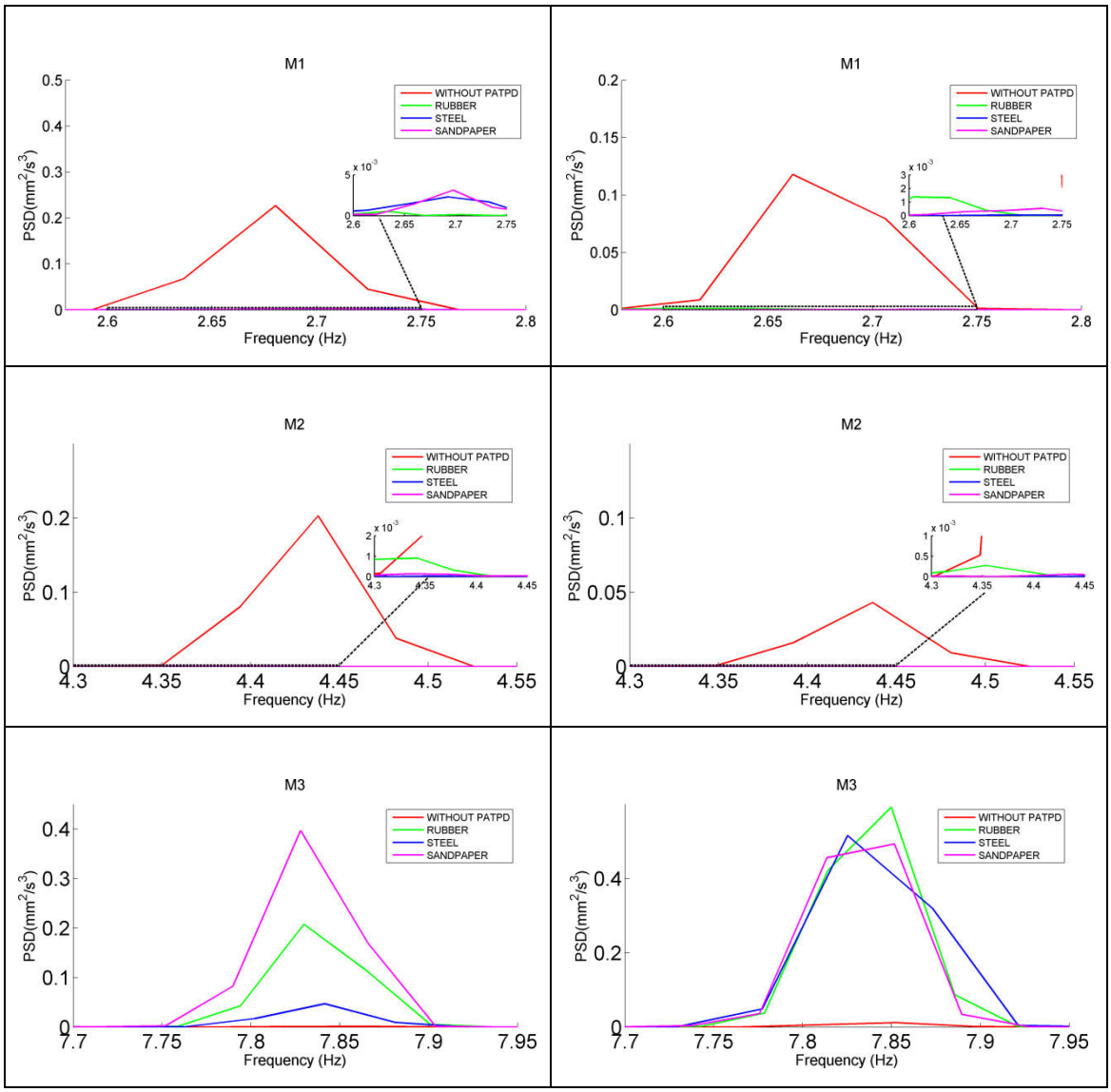

Figure 91: Magnified Power Spectral Density (PSD) storey 3 of the acceleration in the y-direction of the model under free torsional vibration, steel, rubber and sandpaper surfaces

Figure 92: Magnified Power Spectral Density (PSD) storey 2 of the acceleration in the y-direction of the model under free torsional vibration, steel, rubber and sandpaper surfaces

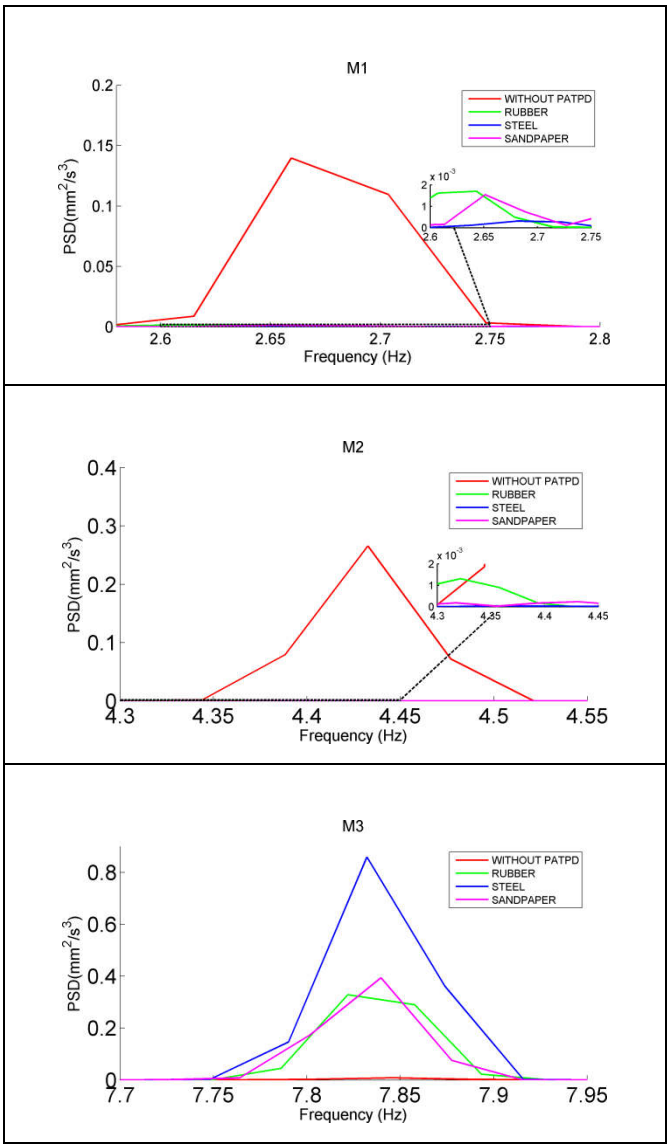

Figure 93: Magnified Power Spectral Density (PSD) storey 1 of the acceleration in the y-direction of the model under free torsional vibration, steel, rubber and sandpaper surfaces

Figure 91, Figure 92 and Figure 93 shows first and second natural frequency with PSD peaks, 2.680Hz and 4.438 Hz, across all storeys; all three surfaces produced significant damping of the model's vibrations, reducing the PSD peak by at least 90%. Steel demonstrates best control effect.

For third natural frequency with PSD peak, 7.842 Hz, across all storeys, however, none produce damping of the model's vibrations they actually increase frequency density. For storey 2 they behave similarly, storey 1 shows similar values for rubber and sandpaper – with steel being worst. For storey 3 steel shows least increase with sandpaper being highest.

Overall PSD peak increases were minimal in comparison to the reduction gained in PSD peak for the first natural frequency.

5.2.1.5 Coupled Vibration (Translation in X-direction and torsion)

The model was given an initial torsional displacement and displacement in x-direction simultaneously, respective acceleration measured in the x-direction. The damping effect of each can be seen in the graphs to follow.

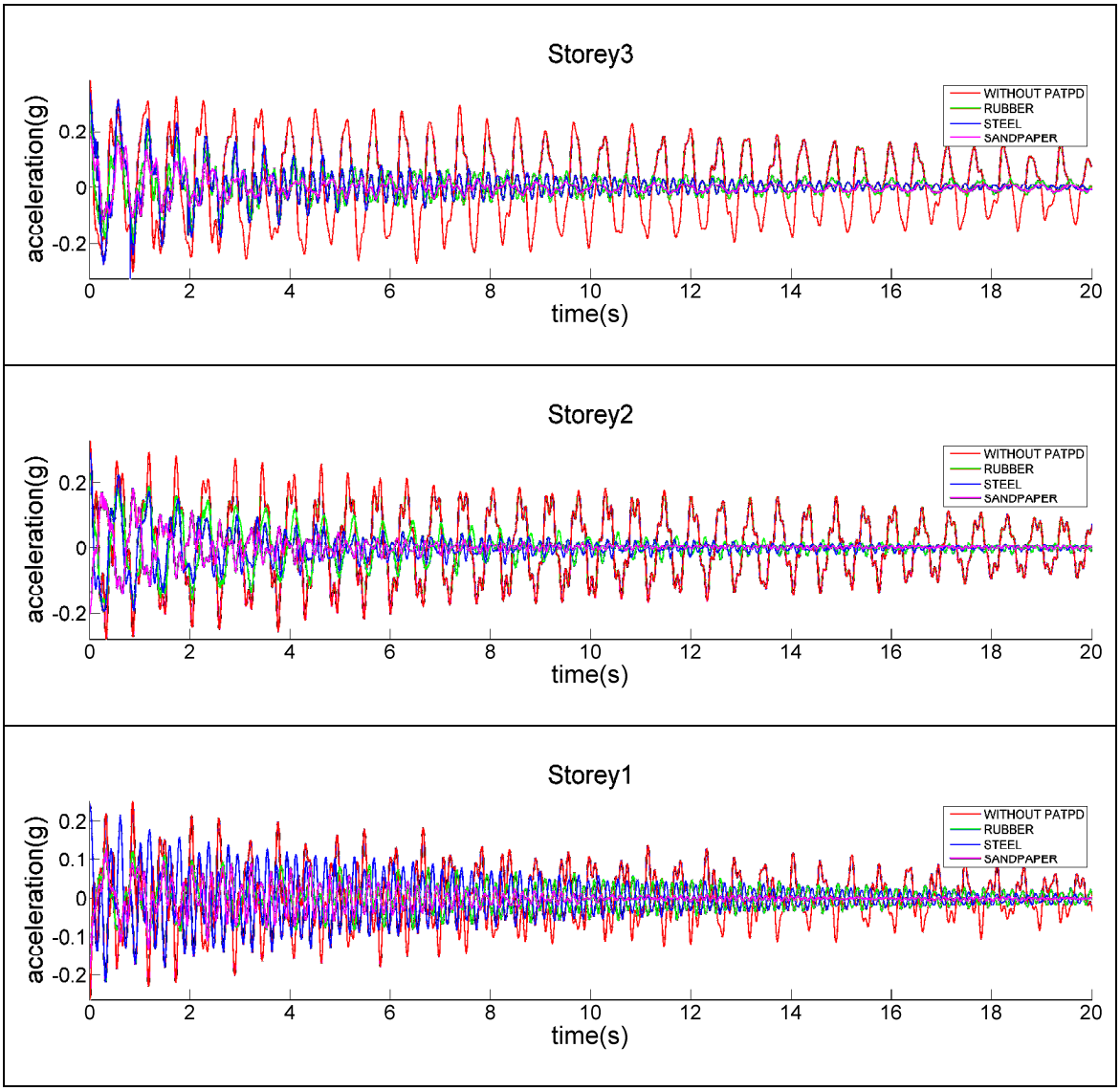

Figure 94: Time history of acceleration response in x-direction per storey for free coupled vibration, steel, rubber and sandpaper surfaces

Figure 94 shows that for all surfaces as the PATPD started moving; the acceleration peaks generated in the damped model are as high as those generated in the undamped model. However, these high accelerations subside and the accelerations rapidly decrease compared to that of the undamped model. As is expected the accelerations experienced in storey 3 are highest and the positive damping effect of the PATPD was still

significant for all surfaces. The best control effect is seen in storey 3, since the damper was installed on this storey.

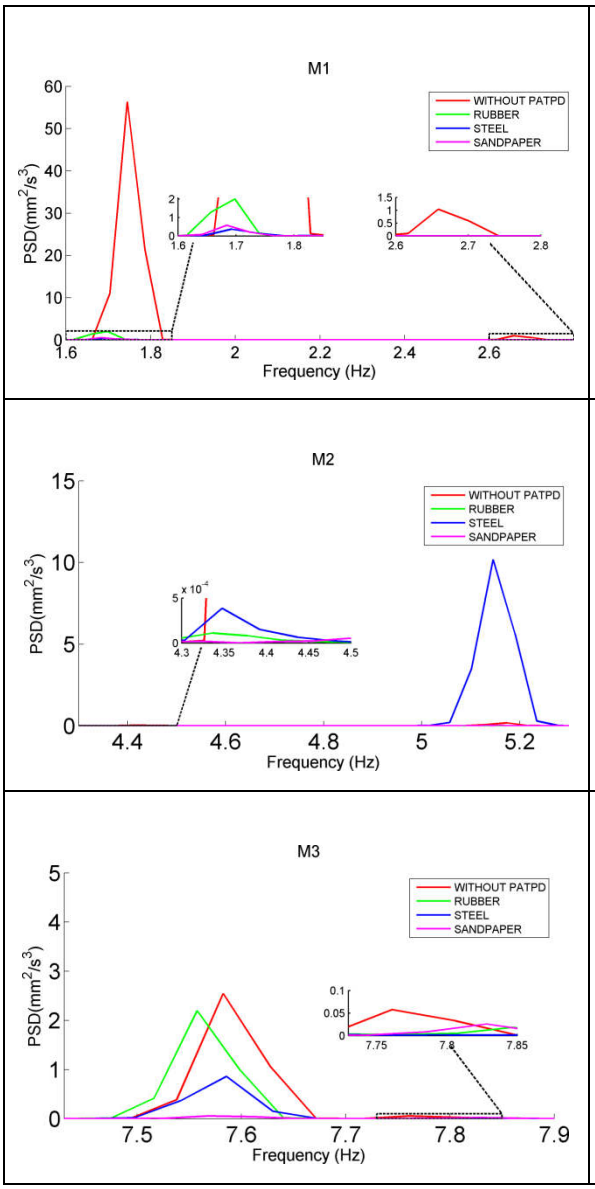

Figure 95: Magnified Power Spectral Density (PSD) storey 3 of the acceleration in the x-direction of the model under free coupled vibration, steel, rubber and sandpaper surfaces

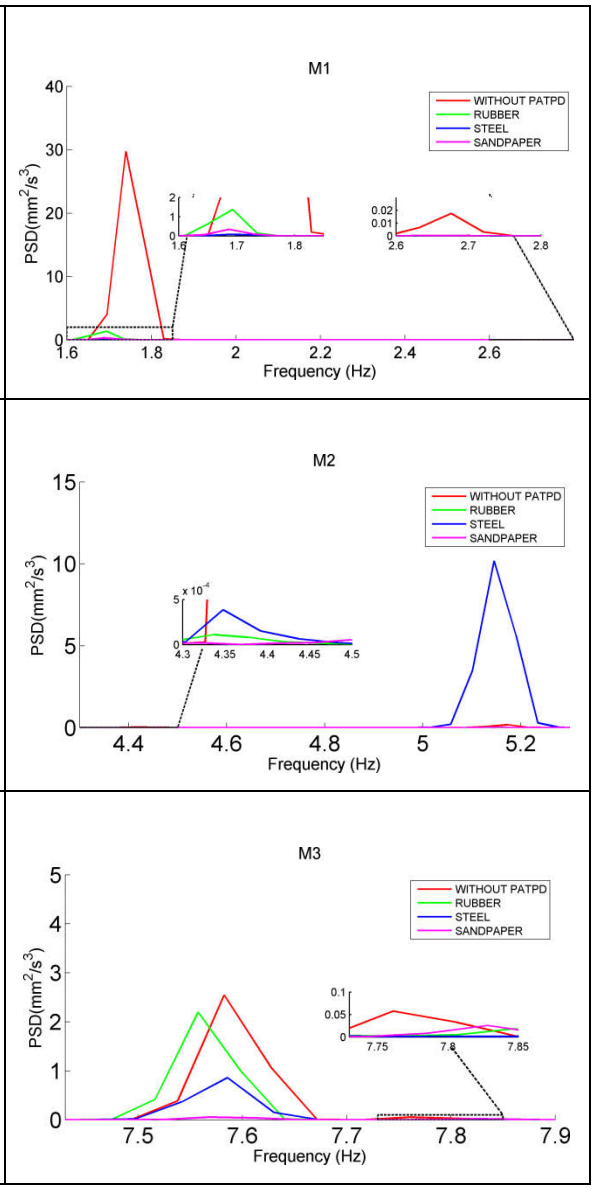

Figure 96: Magnified Power Spectral Density (PSD) storey 2 of the acceleration in the x-direction of the model under free coupled vibration, steel, rubber and sandpaper surfaces

Figure 95, Figure 96 and Figure 97 show for first natural frequency with PSD peak, 1.733Hz and 2.677Hz, for translation and torsion, all 3 PATPD masses provided significant damping of the model's vibrations across all 3 storeys, with the steel and sandpaper demonstrating best control effect and rubber the least.

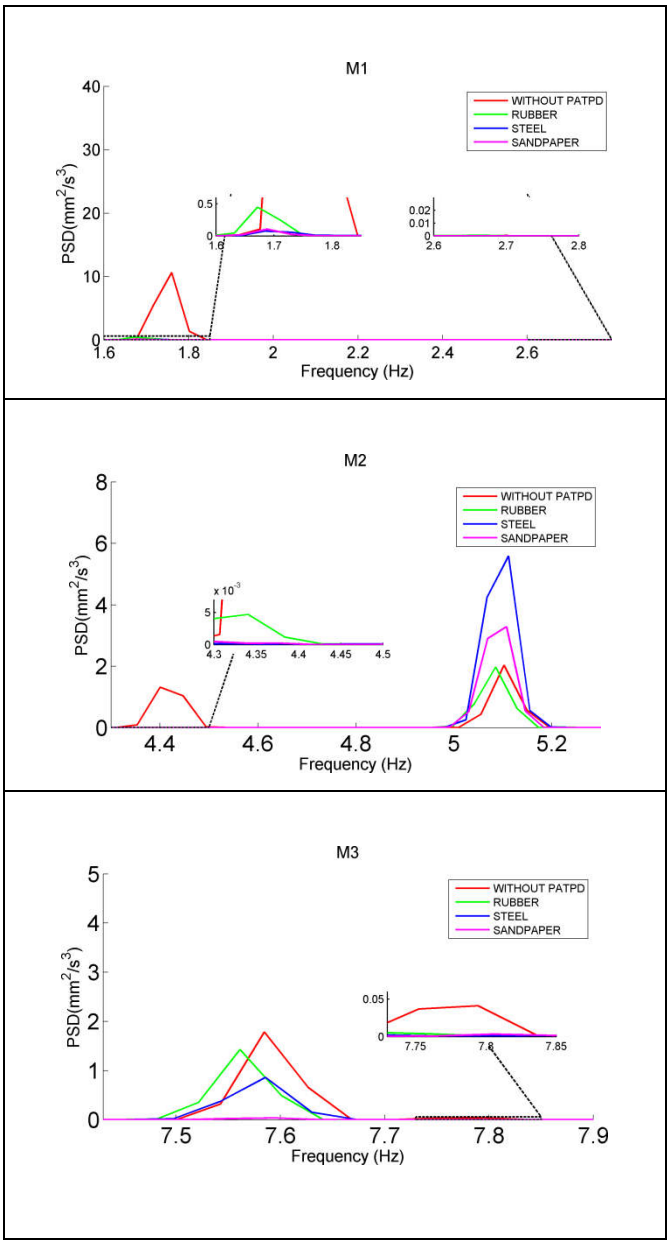

Figure 97: Magnified Power Spectral Density (PSD) storey 1 of the acceleration in the x-direction of the model under free coupled vibration, steel, rubber and sandpaper surfaces

For second natural frequency with PSD peak, 4.446Hz, for torsion across all 3 storeys, all PATPD surfaces provide damping of the model's vibrations across all 3 storeys, with the steel and sandpaper demonstrating best control effect and the rubber the least. For translation, with PSD peak, 5.164Hz, across all 3 storeys, rubber and sandpaper provides best control effect, even if slightly so– steel being the worst. For third natural frequency with PSD peak, 7.584Hz, for translation all surfaces provide control with sandpaper being best. For torsion with PSD peak, 7.792Hz, they all provide control effect, even if slightly.

Overall PSD peak increases were minimal in comparison to the reduction gained in PSD peak for the first natural frequency.

5.2.1.6 Coupled Vibration (Translation in Y-direction and torsion)

The model was given an initial torsional displacement and displacement in y-direction simultaneously, respective acceleration measured in the y-direction. The damping effect of each can be seen in the graphs to follow.

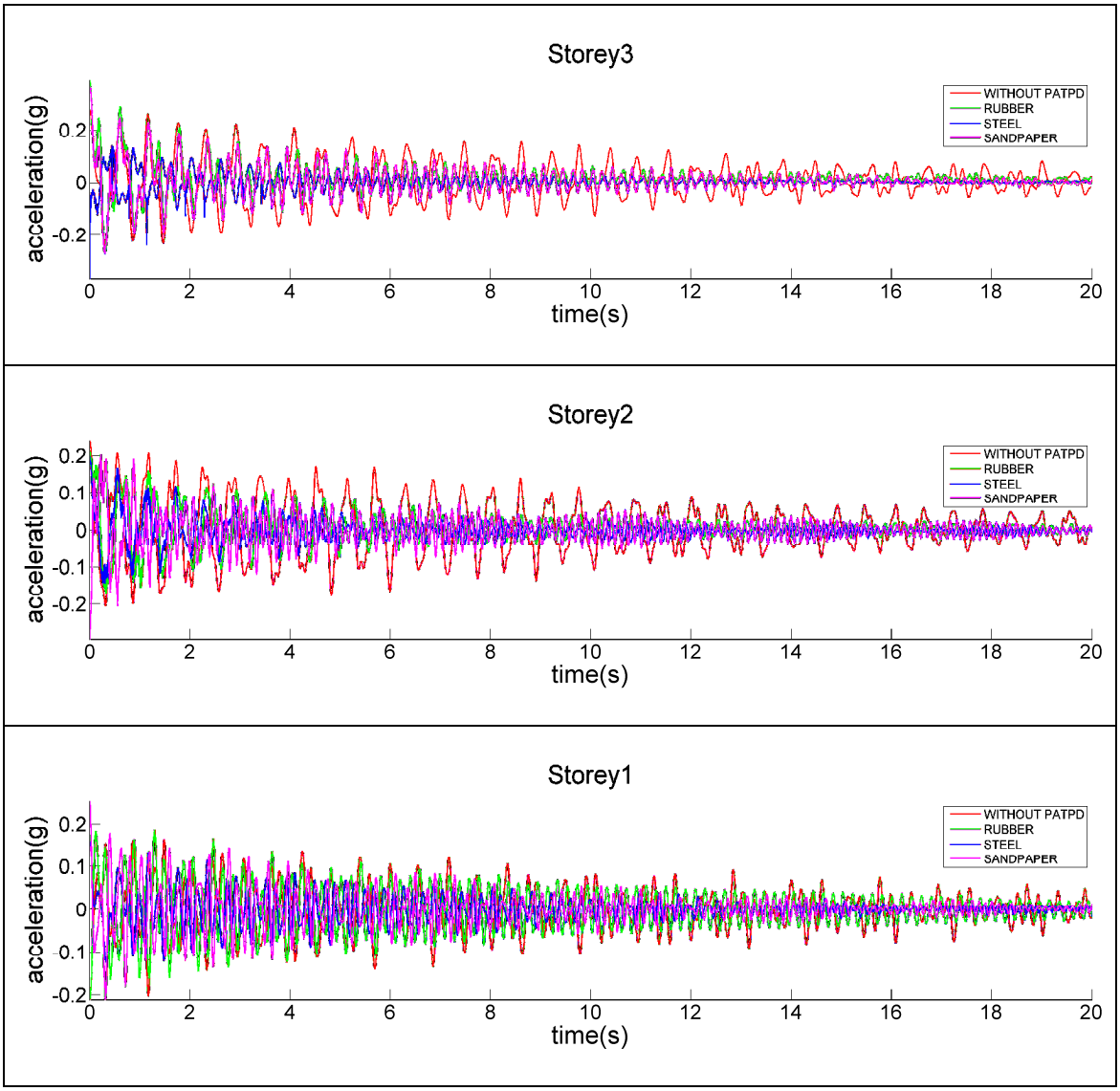

Figure 98: Time history of acceleration response in y-direction per storey for free coupled vibration, steel, rubber and sandpaper surfaces

Figure 98 shows that for all surfaces as the PATPD started moving; the acceleration peaks generated in the damped model are as high as those generated in the undamped model. However, these high accelerations subside and the accelerations rapidly decrease compared to that of the undamped model. As is expected the accelerations experienced in storey 3 are highest and the positive damping effect of the PATPD was still

significant for all surfaces. The best control effect is seen in storey 3, since the damper was installed on this storey.

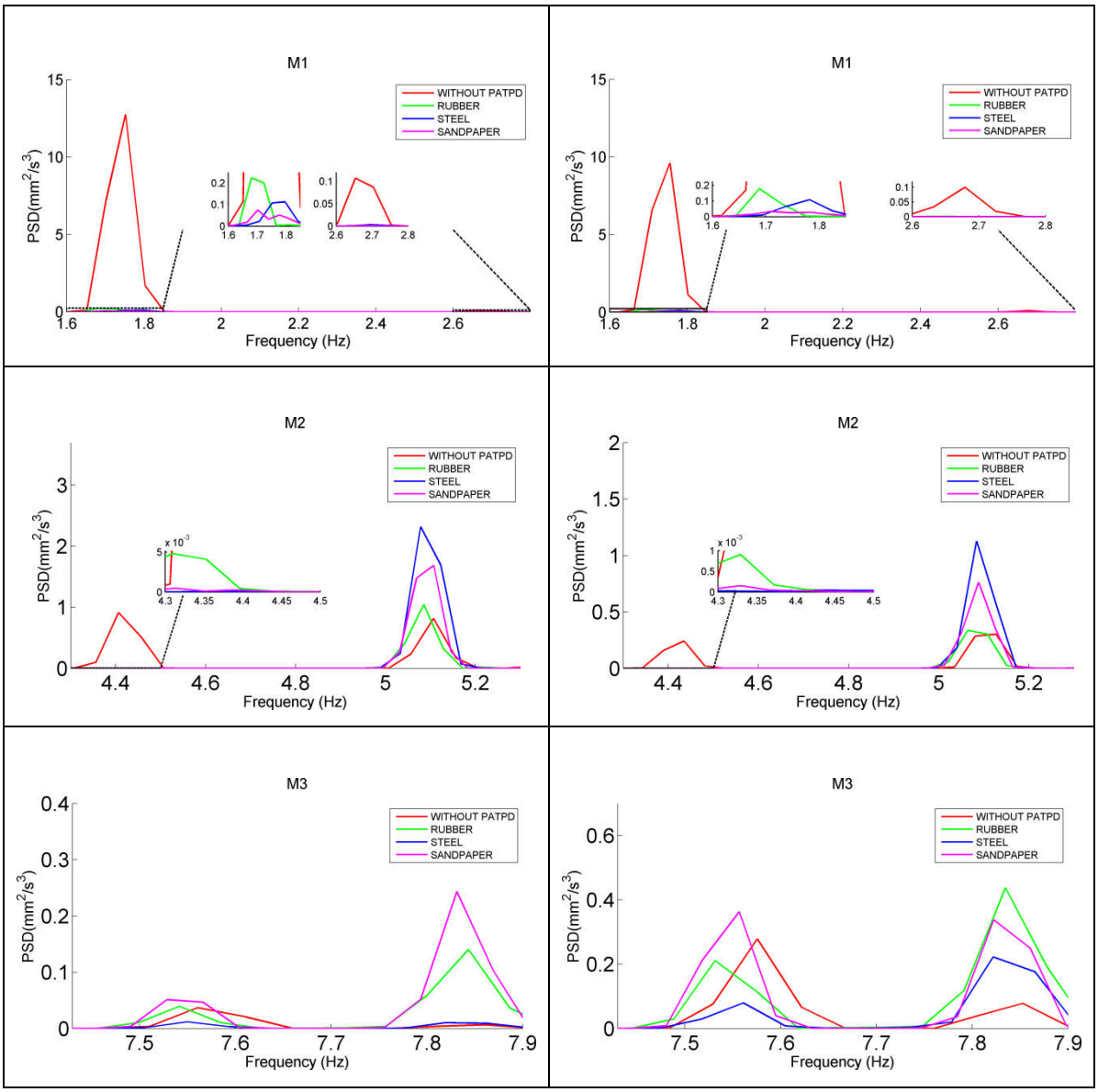

Figure 99: Magnified Power Spectral Density (PSD) storey 3 of the acceleration in the y-direction of the model under free coupled vibration, steel, rubber and sandpaper surfaces

Figure 100: Magnified Power Spectral Density (PSD) storey 2 of the acceleration in the y-direction of the model under free coupled vibration, steel, rubber and sandpaper surfaces

Figure 99, Figure 100 and Figure 101 show for first natural frequency with PSD peak, 1.747Hz and 2.680Hz, for both translation and torsion, all 3 PATPD masses provided significant damping of the model's vibrations across all 3 storeys, with the sandpaper demonstrating best control effect and rubber the least.

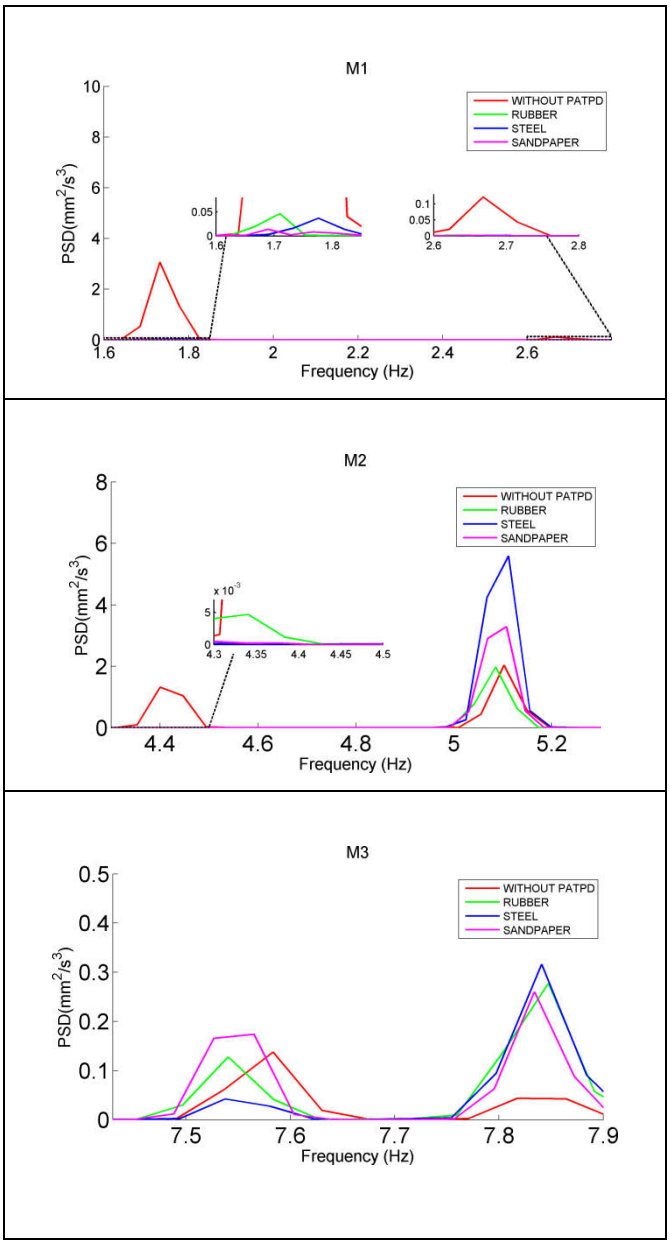

Figure 101: Magnified Power Spectral Density (PSD) storey 1 of the acceleration in the y-direction of the model under coupled vibration, , steel, rubber and sandpaper surfaces

For second natural frequency with PSD peak, 4.438 Hz, for torsion across all 3 storeys, all PATPD surfaces provide significant damping of the model's vibrations across all 3 storeys, with the steel and sandpaper demonstrating best control effect and the rubber the least. For translation, with PSD peak, 5.095Hz , across all 3 storeys, rubber provides best control effect, even if slightly so, with the others increasing the density of the frequency – steel being the worst. For third natural frequency with PSD peak, 7.569Hz, for translation only steel provides control with the others increasing the density of the frequency. For torsion with PSD peak, 7.842 Hz, they all show increased frequency density, but storey 3 shows control effect with steel.

Overall PSD peak increases were minimal in comparison to the reduction gained in PSD peak for the first natural frequency.

5.2.2.0 Forced Vibration

5.2.2.1 Translational Vibration in the X-direction

The model was placed on the shake table in order to carry out the forced vibration tests. The PATPD's were connected one-by-one and the respective accelerations measured. The damping effect of each friction change of the PATPD can be seen in the graphs to follow.

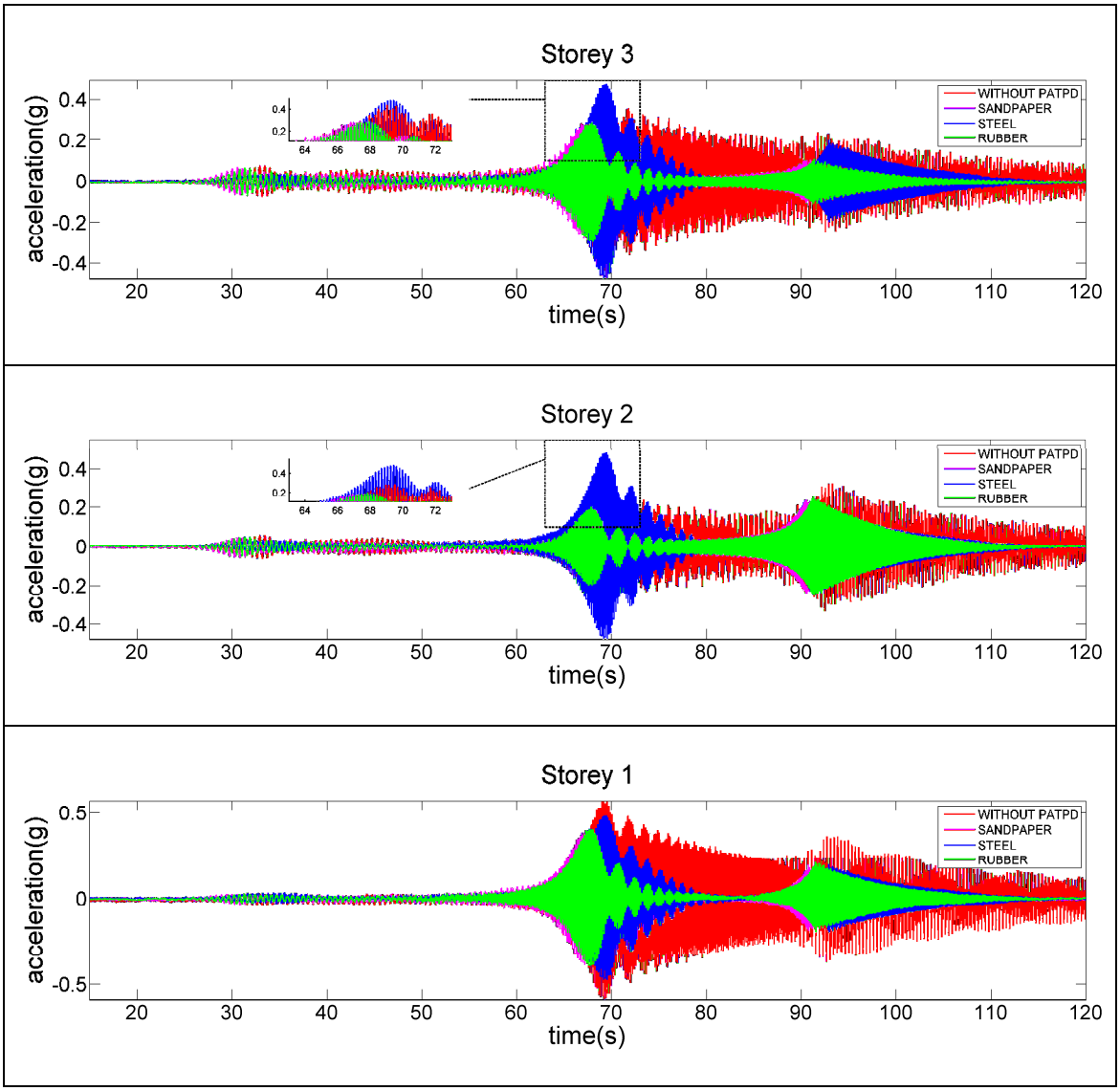

Figure 102: Time history of acceleration response per storey for forced translational vibration in x-direction, steel, rubber and sandpaper surfaces

Figure 102 shows for all 3 storeys that by adding the damper onto model the acceleration experience was significantly decreased for all surfaces.

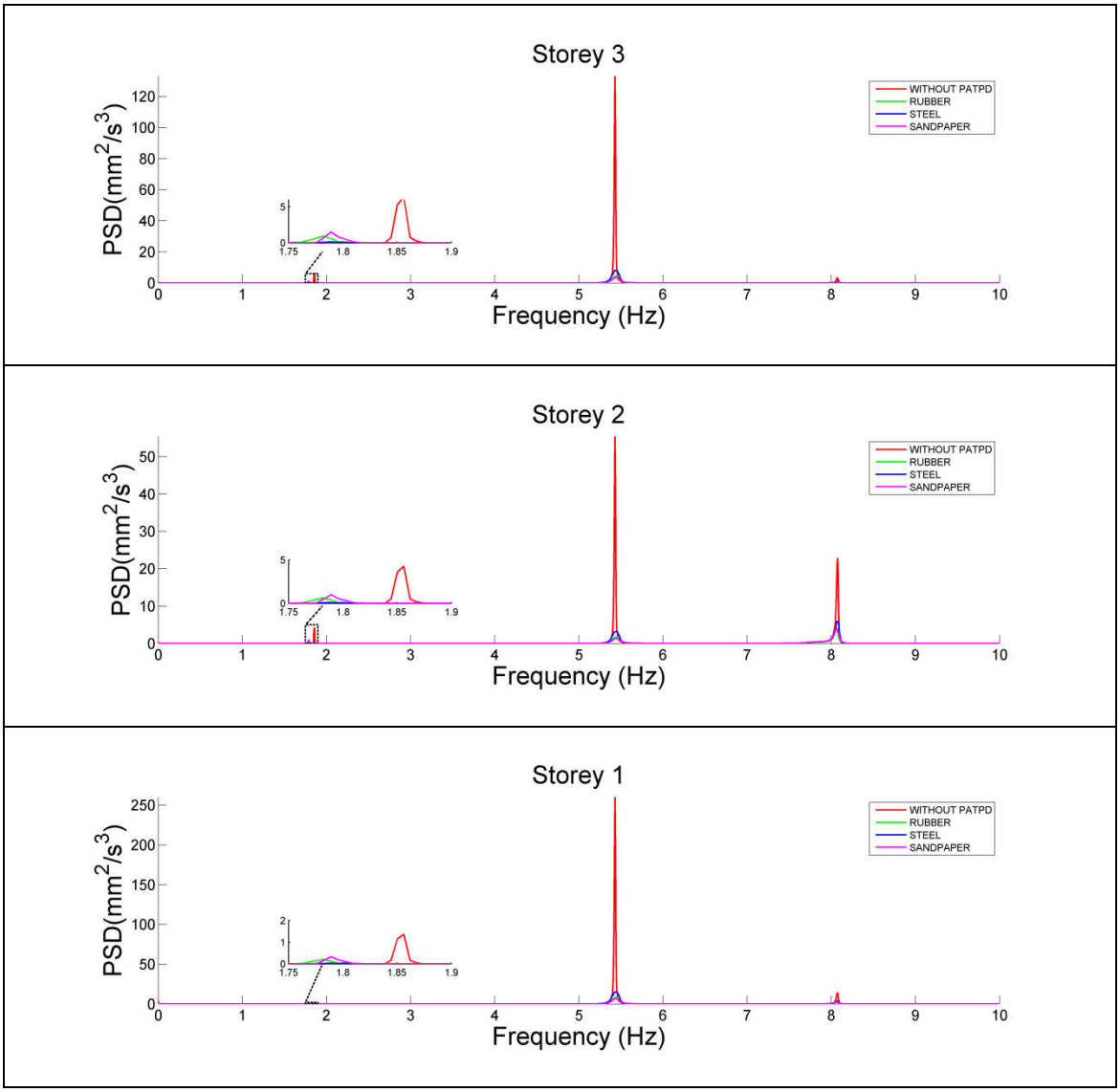

Figure 103: Power Spectral Density (PSD) of the acceleration response per storey under forced excitation in the x-direction, steel, rubber and sandpaper surfaces

Figure 103 shows PSD peaks at 1.856Hz, 5.429Hz and 8.047Hz. This corresponds to the models first, second and third frequencies. The positive control effect is evident as PSD peaks for all 3 frequencies are significantly reduced by surfaces used.

5.2.2.2 Translational Vibration in the Y-direction

The model was placed on the shake table in order to carry out the forced vibration tests. The PATPD's were connected one-by-one and the respective accelerations measured. The damping effect of each of the PATPD masses can be seen in the graphs to follow.

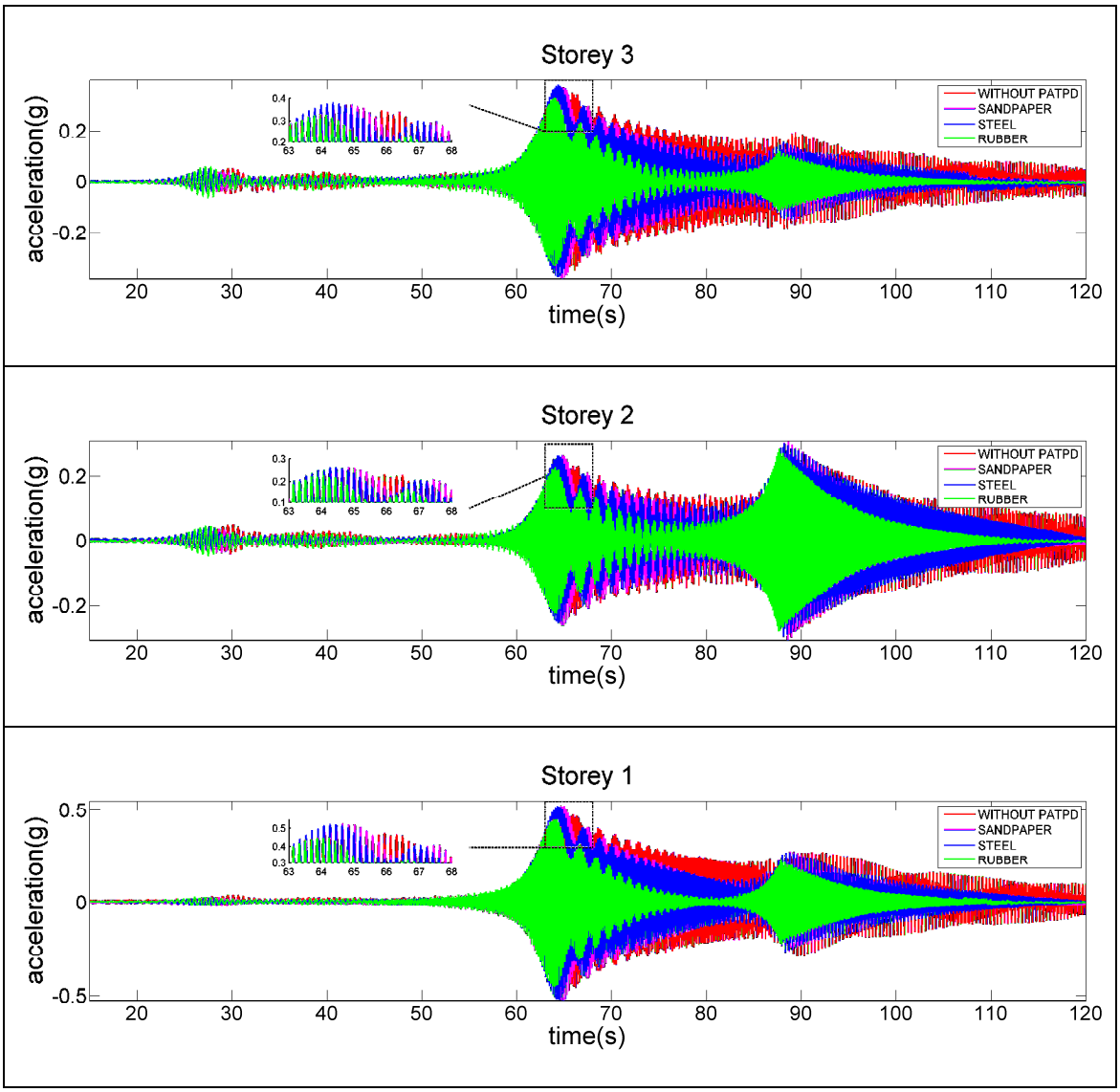

Figure 104: Time history of acceleration response per storey for forced translational vibration in y-direction, steel, rubber and sandpaper surfaces

Figure 104 shows for all 3 storeys that by adding the damper onto model the acceleration experience was significantly decreased for all surfaces.

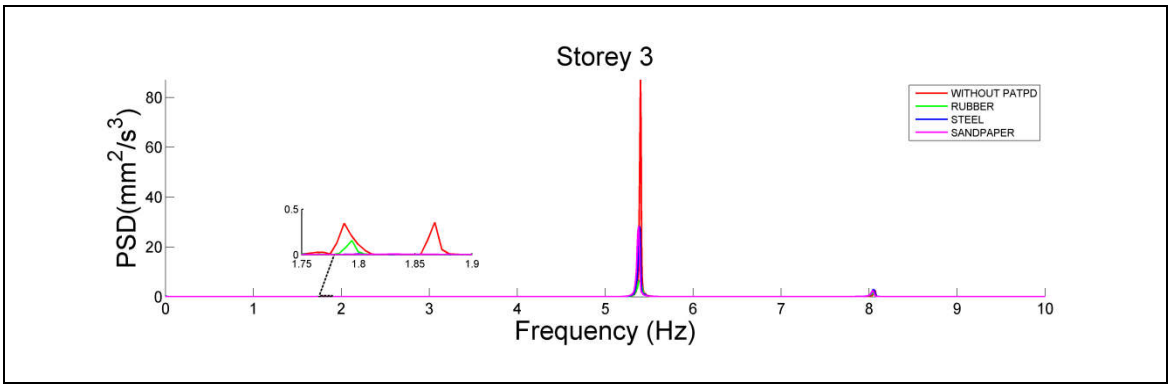

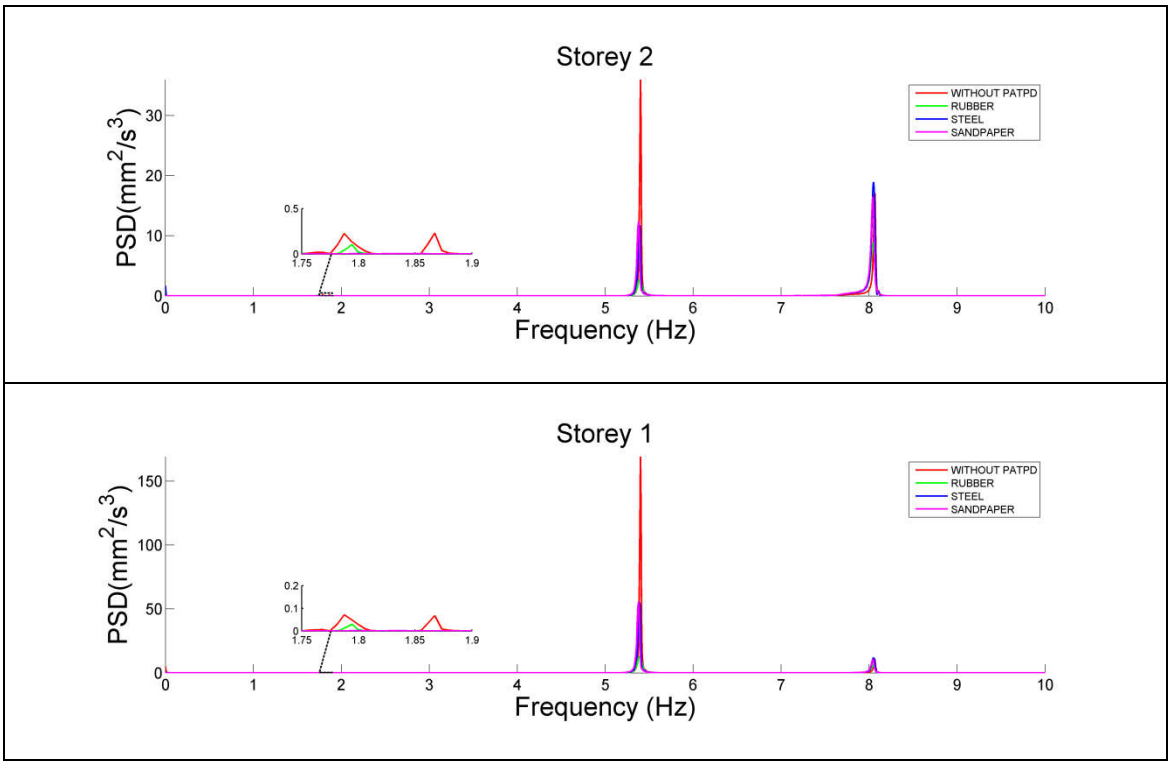

Figure 105: Power Spectral Density (PSD) of the acceleration response per storey under forced excitation in the y-direction, steel, rubber and sandpaper surfaces

Figure 105 shows PSD peaks at 1.787Hz, 5.399Hz and 8.065Hz. This corresponds to the models first, second and third frequencies. The positive control effect is evident as PSD peaks for all 3 frequencies are significantly reduced. This is true for all surfaces. Control effect of PATPD was better in x-direction than in y-direction.

5.2.3.0 Summary

Free Vibration

This set of parameter tests indicate better control in y than in x direction. Steel and sandpaper demonstrates best control effect for first natural frequency. Rubber is worst under translational vibration. They all behave similarly under coupled vibrations. All friction surfaces provided control effect to the first natural frequency for all free vibration tests for all storeys.

Forced Vibration

For Forced Vibration the PATPD provides significant control to all 3 frequencies for all friction surfaces tested.

The results reveal that the PATPD performs better in translation the x –direction than the y-direction.

5.3 Parameter Test 3: Effect of changing rope type

Tests were carried out using three different types of rope, a cotton rope (primary model), a nylon rope and ski-rope[7]. All other parameters during these tests remained constant, with the test model having a mass of 42.09kg and a height of 37cm per storey. As with the previous tests the model was given an initial displacement, in the according directions, and the acceleration with and without the damper measured.

The data for each case is processed and they are plotted together on graphs such that extrapolations and comparisons can be made.

5.3.1 Free Vibration

5.3.1.1 Translational Vibration in the X-direction

The model was given an initial displacement in the x-direction and respective acceleration measured. The damping effect of each can be seen in the graphs to follow.

[7] These configurations can be found on page 58

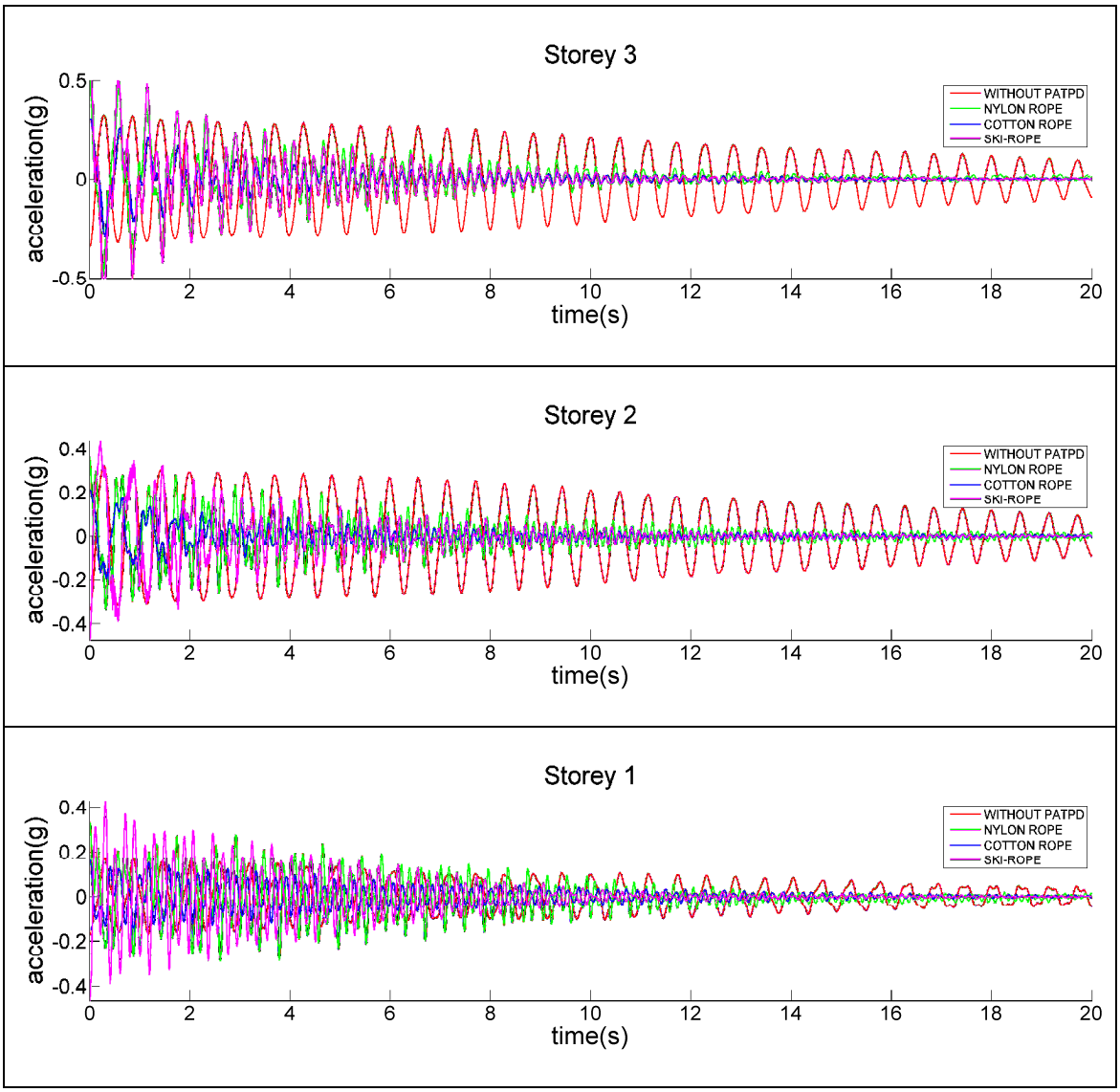

Figure 106: Time history of acceleration response per storey for free translational vibration in x-direction, cotton rope, nylon rope and ski-rope

Figure 106 shows that for all rope types tested as the PATPD started moving; the acceleration peaks generated in the damped model are as high as those generated in the undamped model. However, these high accelerations subside and the accelerations rapidly decrease compared to that of the undamped model. As is expected the accelerations experienced in storey 3 are highest and the positive damping effect of the PATPD was still significant for all rope types tested. The best control effect is seen in storey 3, since the damper was installed on this storey.

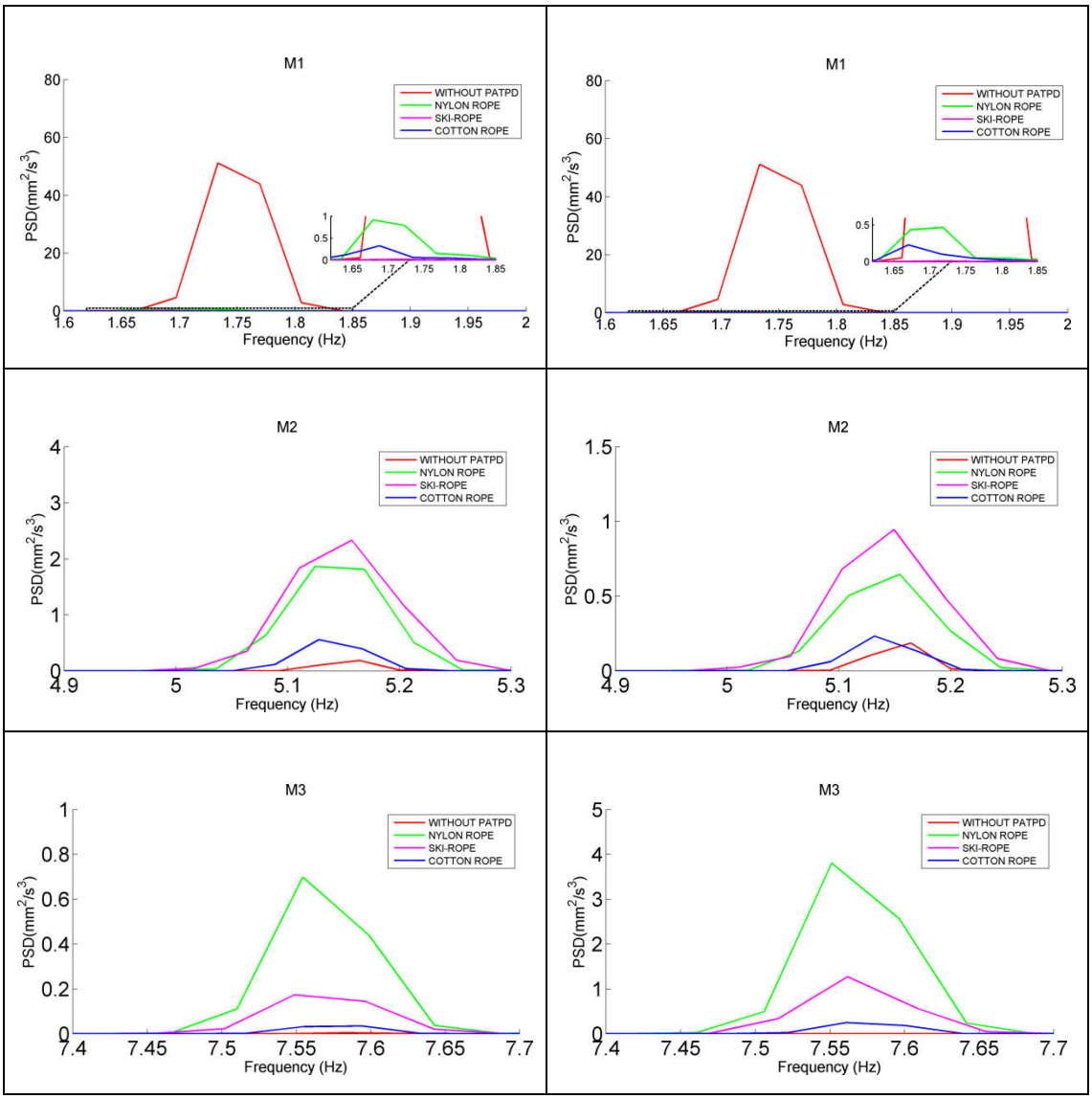

Figure 107: Magnified Power Spectral Density (PSD) storey 3 of the acceleration of the model under free translational vibration in the x-direction , cotton rope, nylon rope and ski-rope

Figure 108: Magnified Power Spectral Density (PSD) storey 2 of the acceleration of the model under free translational vibration in the x-direction, cotton rope, nylon rope and ski-rope

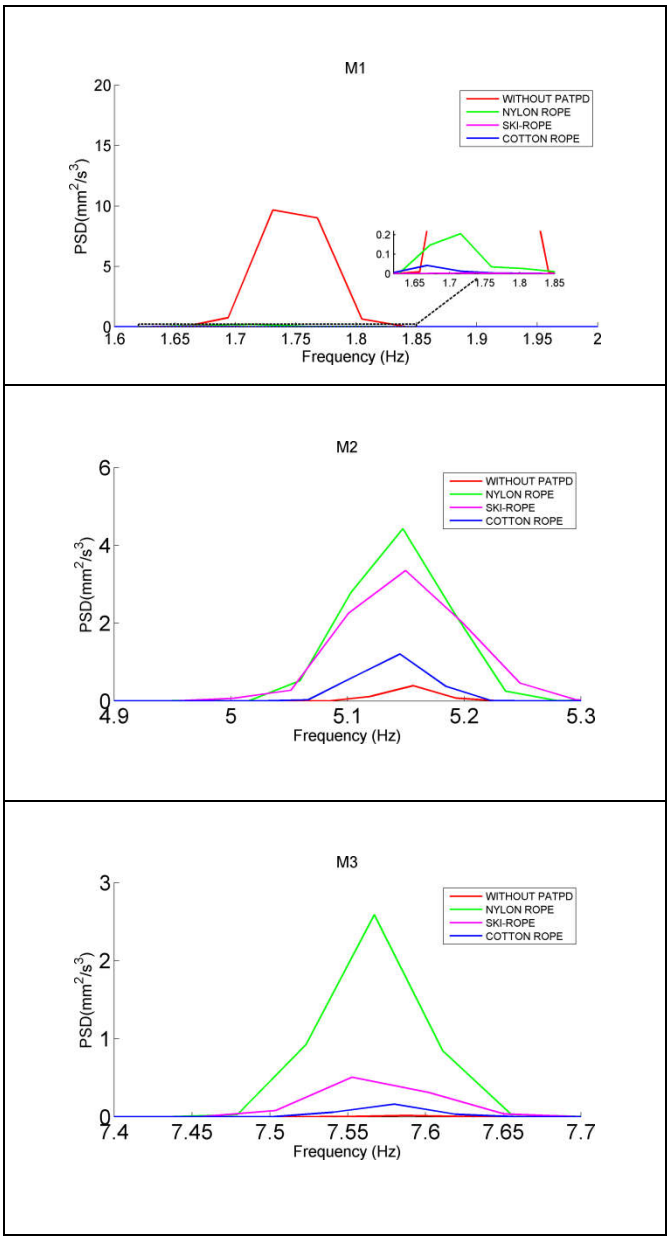

Figure 109: Magnified Power Spectral Density (PSD) storey 1 of the acceleration of the model under free translational vibration in the x-direction, cotton rope, nylon rope and ski-rope

Figure 107, Figure 108 and Figure 109 shows for first natural frequency with PSD peak, 1.733Hz, all ropes tested produced significant damping of the model's vibrations across all storeys, reducing the PSD peak by at least 90%. Ski-rope demonstrates slightly better control than cotton rope, nylon the least.

For second natural frequency with PSD peak, 5.164Hz, all rope types show significant increase in the model's vibrations across all storeys, ski-rope being worst, cotton the best.

For third natural frequency with PSD peak, 7.584Hz, all rope types show significant increase in the model's vibrations across all storeys, nylon being worst, cotton the best.

Overall PSD peak increases were minimal in comparison to the reduction gained in PSD peak for the first natural frequency.

5.3.1.2 Translational Vibration in the Y-direction

The model was given an initial displacement in the y-direction and respective acceleration measured. The damping effect of each PATPD can be seen in the graphs to follow.

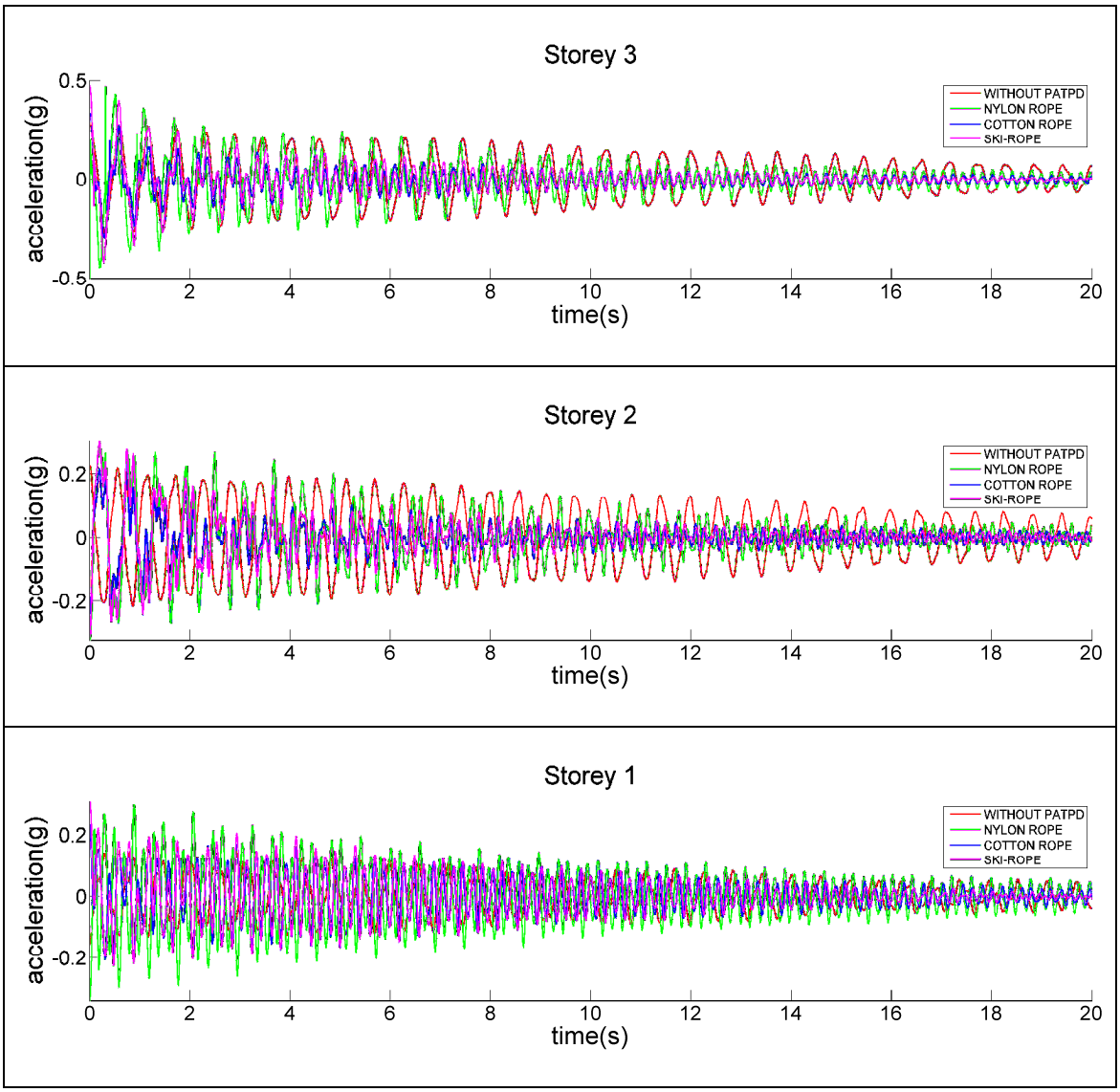

Figure 110: Time history of acceleration response per storey for free translational vibration in y-direction, cotton rope, nylon rope and ski-rope

Figure 110 shows that for all rope types tested as the PATPD started moving; the acceleration peaks generated in the damped model are as high as those generated in the undamped model. However, these high accelerations subside and the accelerations rapidly decrease compared to that of the undamped model. As is expected the accelerations experienced in storey 3 are highest and the positive damping effect of the PATPD was still significant for all rope types tested. The best control effect was seen in storey 3, since the damper was installed on this storey.

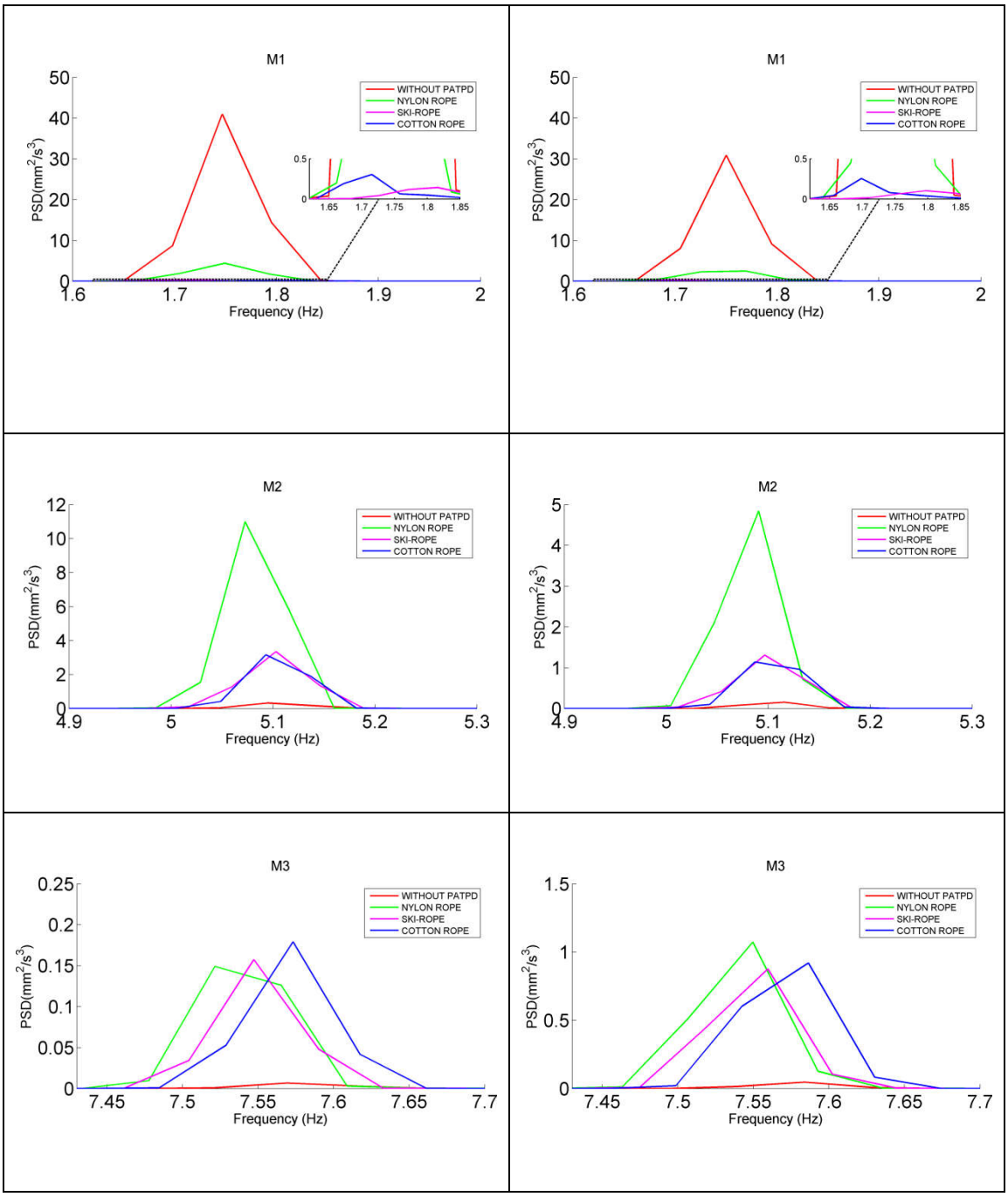

Figure 111: Magnified Power Spectral Density (PSD) storey 3 of the acceleration of the model under free translational vibration in the y-direction, cotton rope, nylon rope and ski-rope s

Figure 112: Magnified Power Spectral Density (PSD) storey 2 of the acceleration of the model under free translational vibration in the y-direction, cotton rope, nylon rope and ski-rope

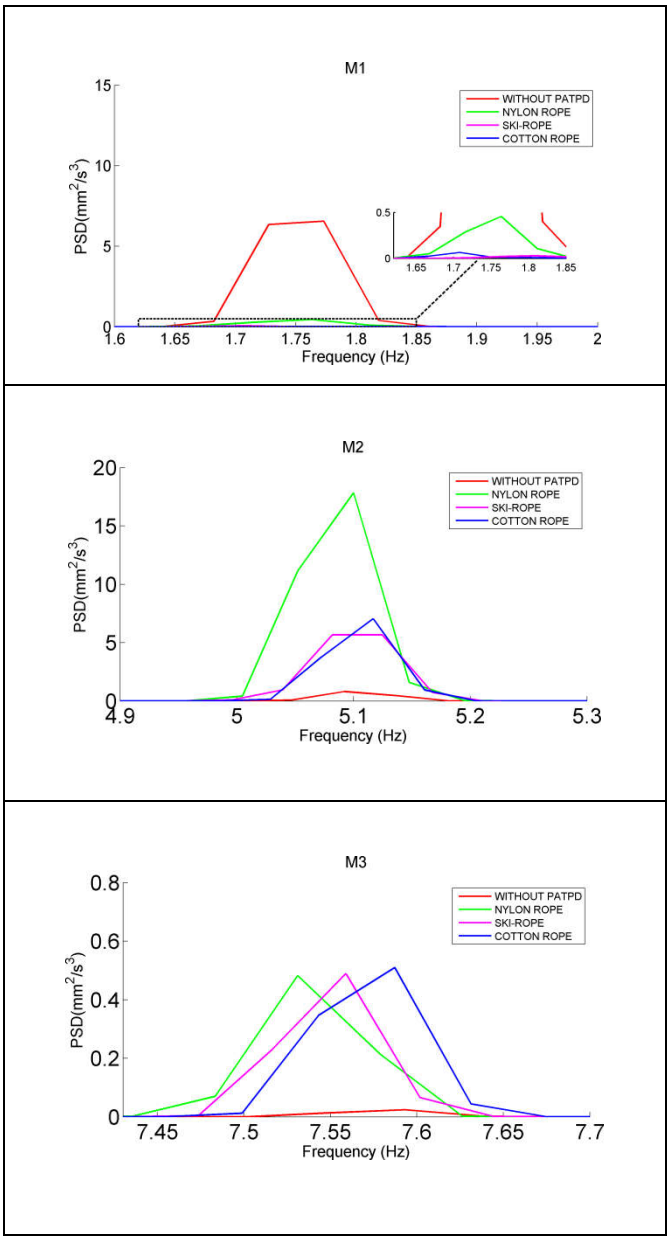

Figure 113: Magnified Power Spectral Density (PSD) storey 1 of the acceleration of the model under free translational vibration in the y-direction, cotton rope, nylon rope and ski-rope

Figure 111, Figure 112 and Figure 113 shows for first natural frequency with PSD peak, 1.747Hz, ropes tested produced significant damping of the model's vibrations across all storeys, reducing the PSD peak by at least 90%. Ski-rope demonstrates slightly better control than cotton rope, nylon the least.

Both second and third natural frequency with PSD peaks, 5.095Hz and 7.569Hz show significant increase in the model's vibrations across all storeys for all rope types, nylon being worst for second natural frequency PSD peak.

Overall PSD peak increases were minimal in comparison to the reduction gained in PSD peak for the first natural frequency.

5.3.1.3 Torsional Vibration (acceleration measured in the X-direction)

The model was given an initial torsional displacement and respective acceleration measured in the x-direction. The damping effect of each can be seen in the graphs to follow.

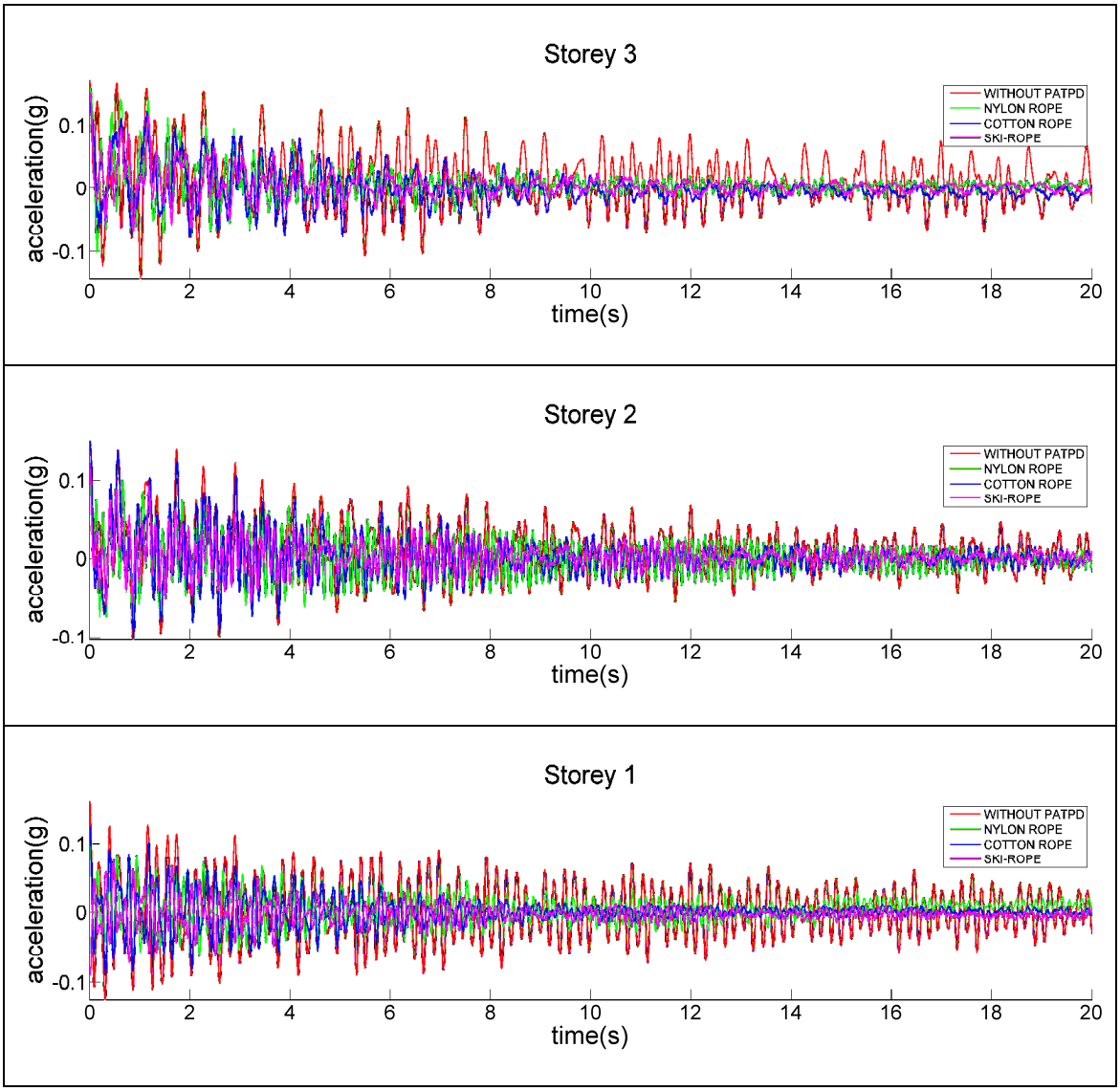

Figure 114: Time history of acceleration response in y-direction per storey for free torsional vibration, cotton rope, nylon rope and ski-rope

Figure 114 shows that for all rope types tested as the PATPD started moving; the acceleration peaks generated in the damped model are as high as those generated in the undamped model. However, these high accelerations subside and the accelerations rapidly decrease compared to that of the undamped model. As is expected the accelerations experienced in storey 3 are highest and the positive damping effect of the

PATPD was still significant for all rope types tested. The best control effect is seen in storey 3, since the damper was installed on this storey.

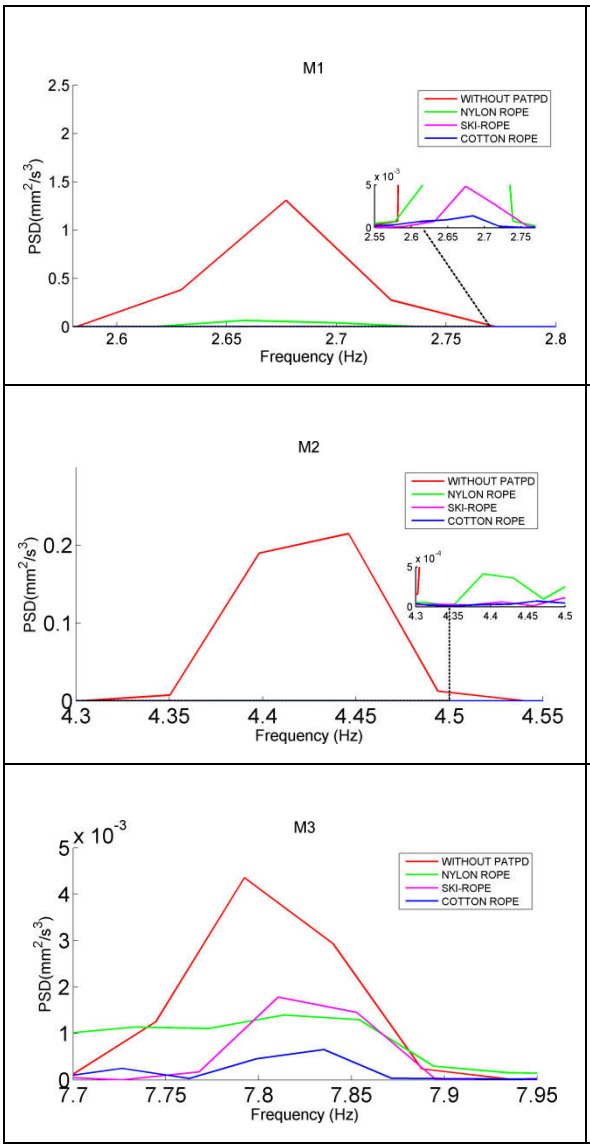

Figure 115: Magnified Power Spectral Density (PSD) storey 3 of the acceleration in the x-direction of the model under free torsional vibration, cotton rope, nylon rope and ski-rope

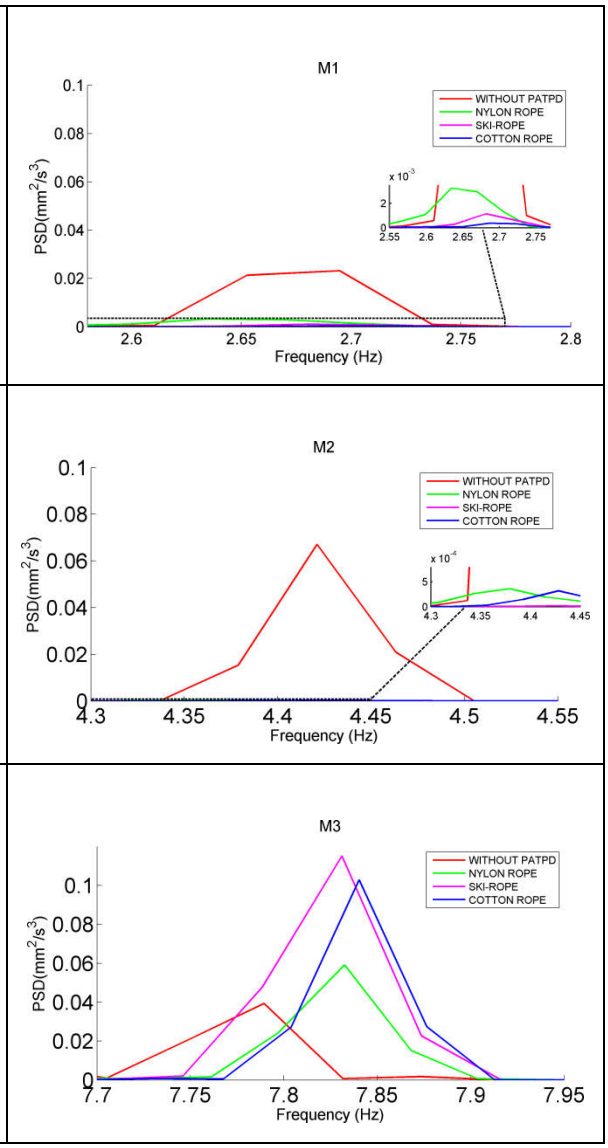

Figure 116: Magnified Power Spectral Density (PSD) storey 2 of the acceleration in the x-direction of the model under free torsional vibration, cotton rope, nylon rope and ski-rope

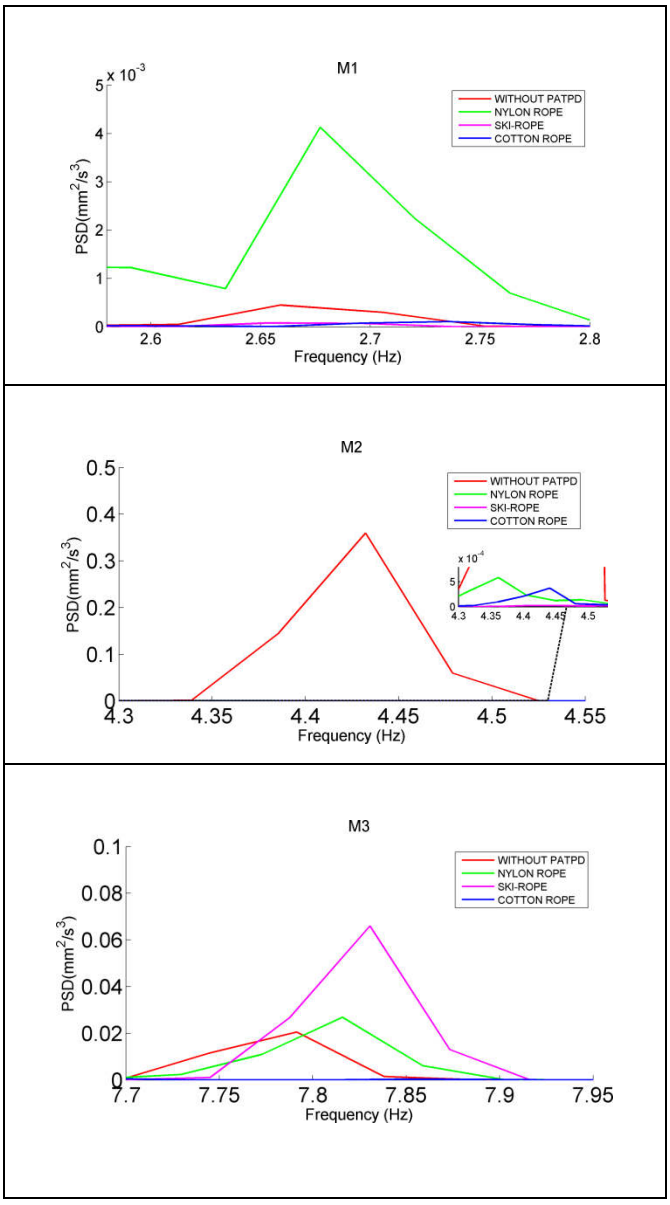

Figure 117: Magnified Power Spectral Density (PSD) storey 1 of the acceleration in the x-direction of the model under free torsional vibration, cotton rope, nylon rope and ski-rope

Figure 115, Figure 116 and Figure 117 shows for first and second natural frequency with PSD peaks, 2.677Hz and 4.446Hz, all ropes tested produced damping of the model's vibrations across all storeys. The PSD peak is reduced by at least 90%, except for first natural frequency PSD peak for storey 1 where nylon increases frequency.

For third natural frequency with PSD peak, 7.792Hz, storey 1 cotton provides 100% attenuation, with others increasing slightly. Storey 2 shows all rope types with slight increase in the model's vibrations, ski-rope being worst for. Storey 3 all ropes tested produced damping of the model's vibrations, cotton being best.

Overall PSD peak increases were minimal in comparison to the reduction gained in PSD peak for the first natural frequency.

5.3.1.4 Torsional Vibration (acceleration measured in the Y-direction)

The model was given an initial torsional displacement and respective acceleration measured in the y-direction. The damping effect of each can be seen in the graphs to follow.

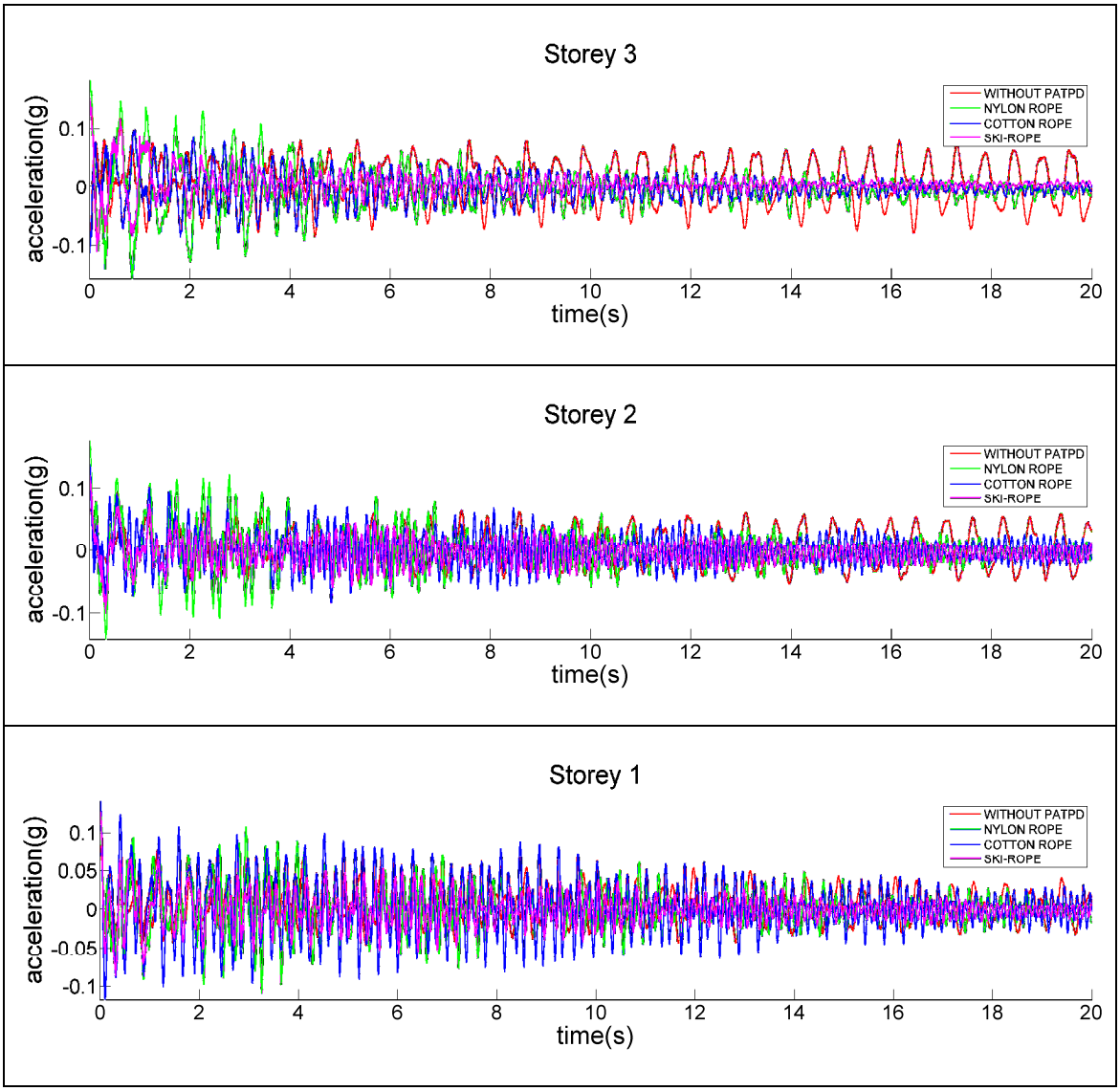

Figure 118: Time history of acceleration response in y-direction per storey for free torsional vibration, cotton rope, nylon rope and ski-rope

Figure 118 shows that for all rope types tested as the PATPD started moving; the acceleration peaks generated in the damped model are as high as those generated in the undamped model. However, these high accelerations subside and the accelerations rapidly decrease compared to that of the undamped model. As is expected the accelerations experienced in storey 3 are highest and the positive damping effect of the

PATPD was still significant for all rope types tested. The best control effect is seen in storey 3, since the damper was installed on this storey.

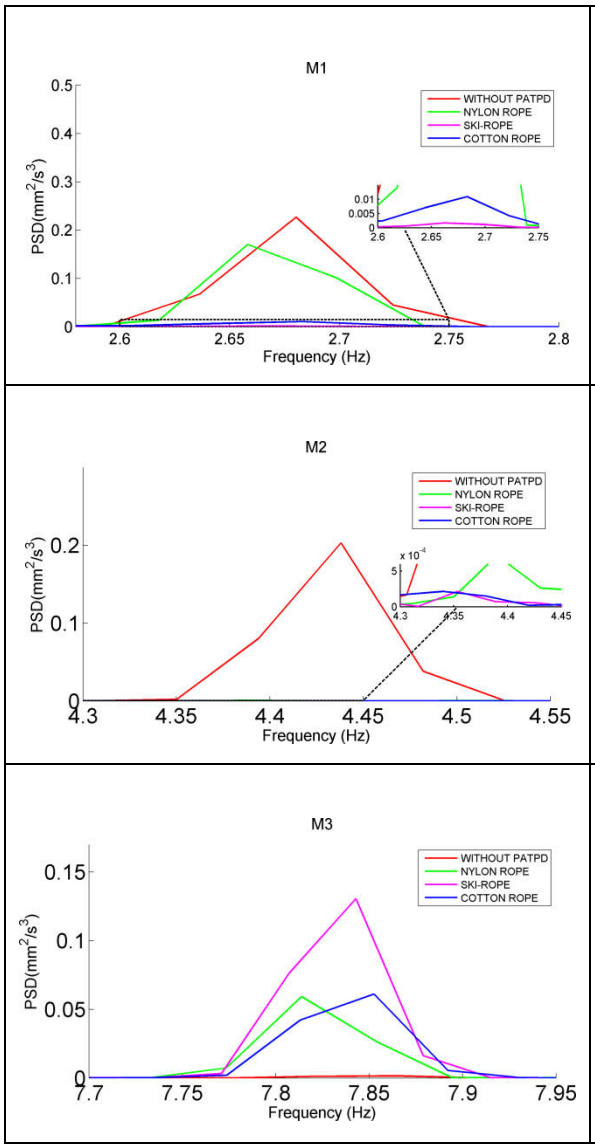

Figure 119: Magnified Power Spectral Density (PSD) storey 3 of the acceleration in the y-direction of the model under free torsional vibration, cotton rope, nylon rope and ski-rope

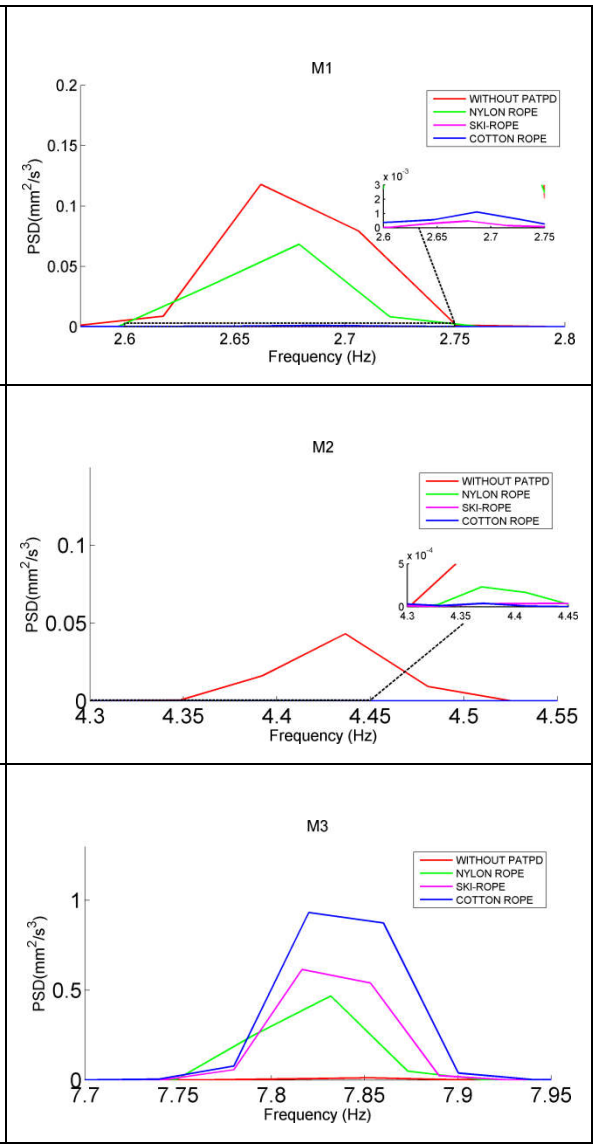

Figure 120: Magnified Power Spectral Density (PSD) storey 2 of the acceleration in the y-direction of the model under free torsional vibration, cotton rope, nylon rope and ski-rope

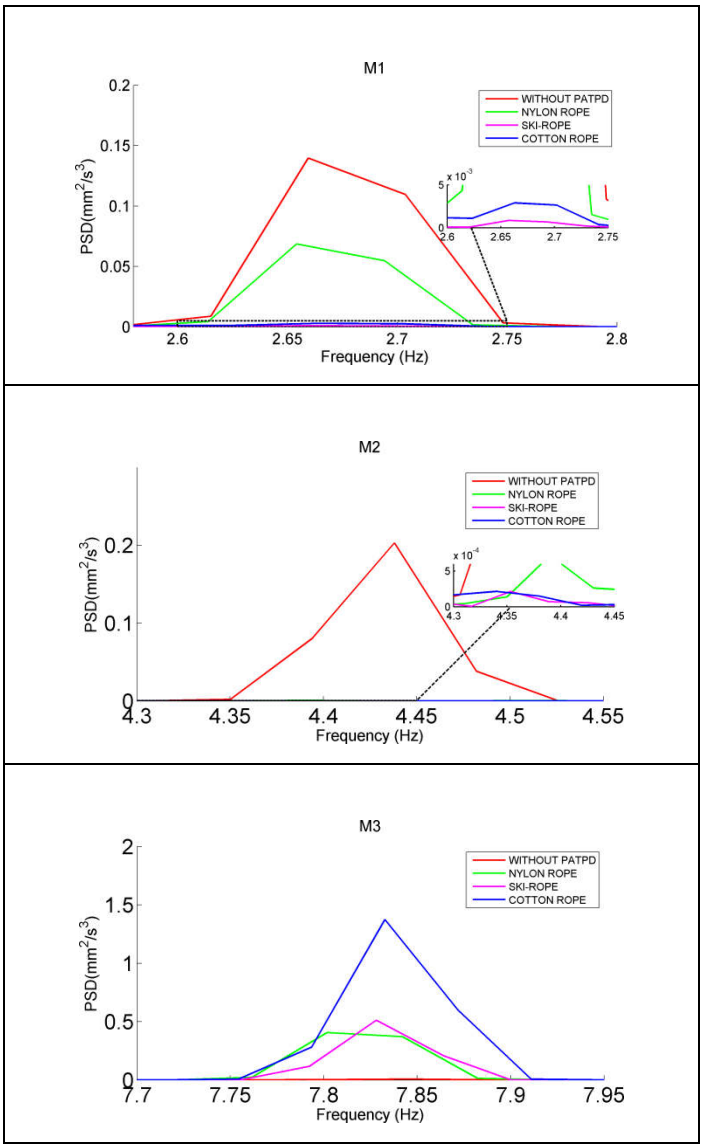

Figure 121: Magnified Power Spectral Density (PSD) storey 1 of the acceleration in the y-direction of the model under free torsional vibration , cotton rope, nylon rope and ski-rope

Figure 119, Figure 120 and Figure 121 shows for first and second natural frequency with PSD peak, 2.680Hz and 4.438 Hz, all ropes tested produced damping of the model's vibrations across all storeys. Ski-rope and cotton reduce the PSD peak by at least 90%. Nylon demonstrates least control. The damping is more significant for PSD peak of second frequency than the first.

For third natural frequency with PSD peak, 7.842 Hz, all rope types show significant increase in the model's vibrations across all storeys, cotton being worst for storey 1-2, and best for storey 3.

Overall PSD peak increases were minimal in comparison to the reduction gained in PSD peak for the first natural frequency.

5.3.1.5 Coupled Vibration (Translation in X-direction and torsion)

The model was given an initial torsional displacement and displacement in x-direction simultaneously, respective acceleration measured in the x-direction. The damping effect of each can be seen in the graphs to follow.

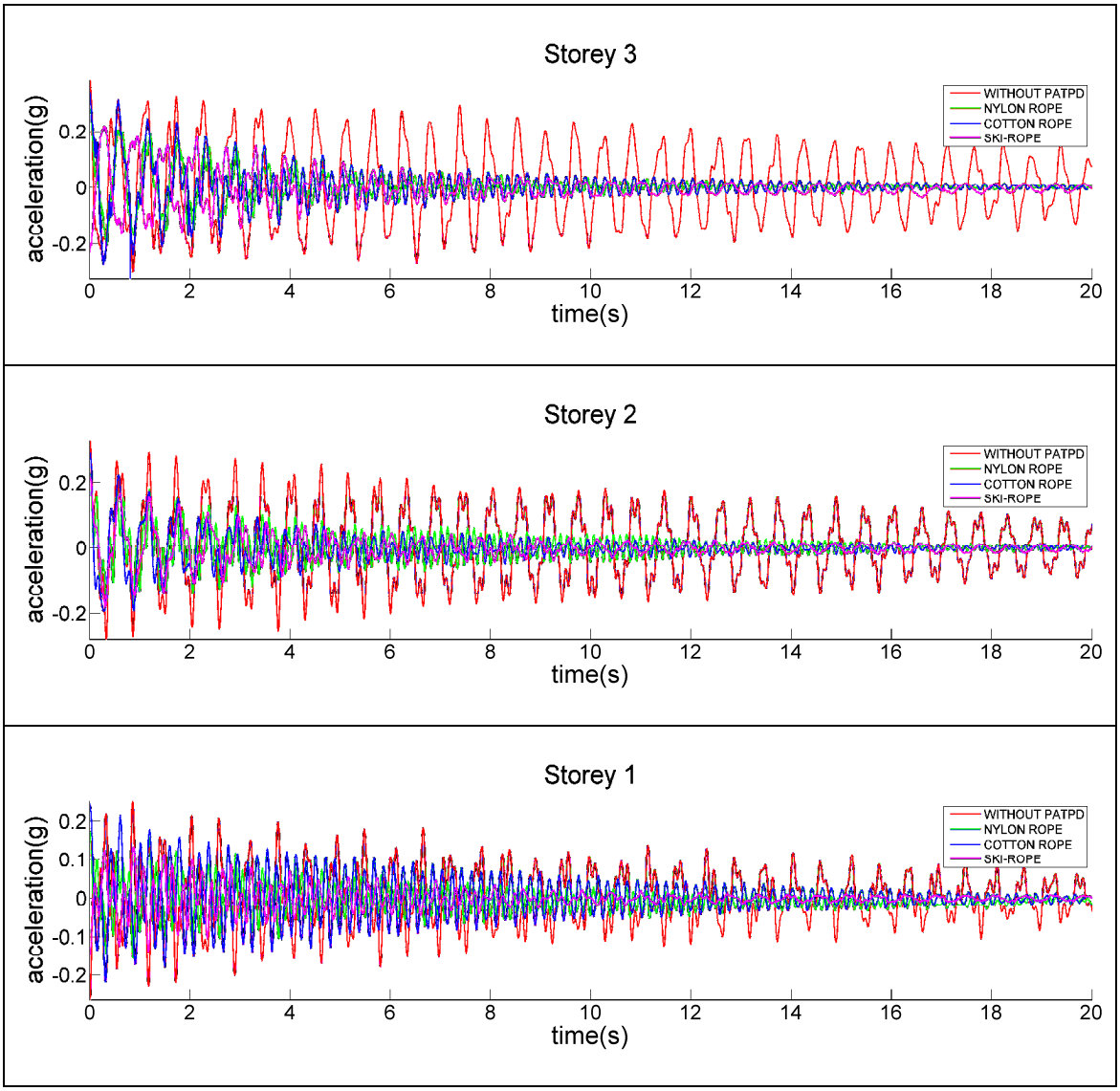

Figure 122: Time history of acceleration response in x-direction per storey for free coupled vibration, cotton rope, nylon rope and ski-rope

Figure 122 shows that for all rope types tested as the PATPD started moving; the acceleration peaks generated in the damped model are as high as those generated in the undamped model. However, these high accelerations subside and the accelerations rapidly decrease compared to that of the undamped model. As is expected the accelerations experienced in storey 3 are highest and the positive damping effect of the

PATPD was still significant for all rope types tested. The best control effect is seen in storey 3, since the damper was installed on this storey.

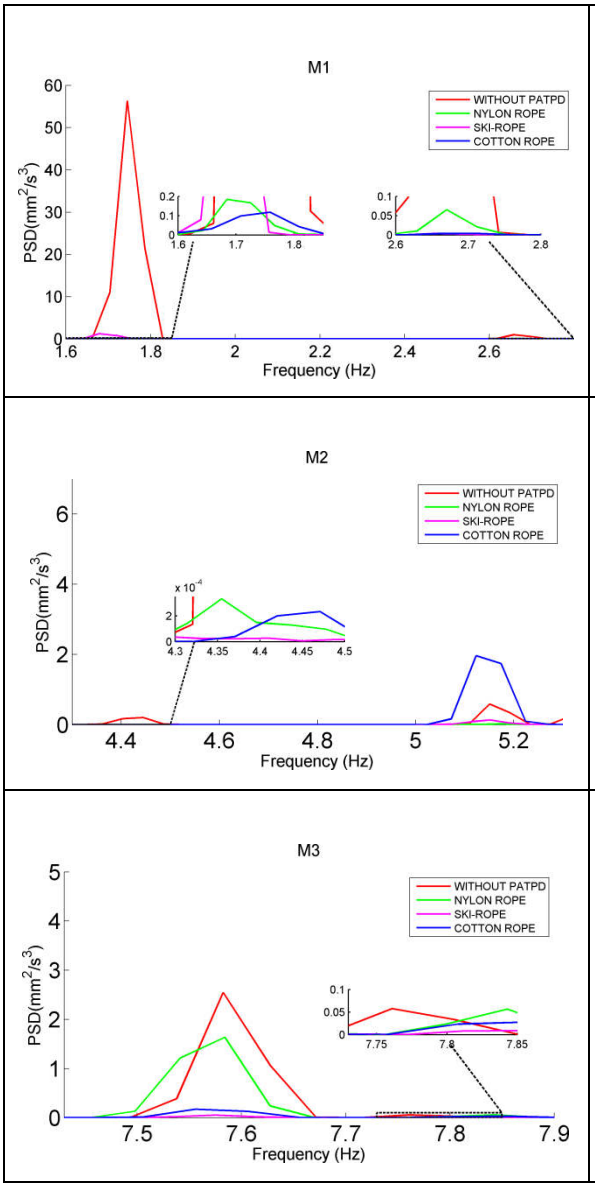

Figure 123: Magnified Power Spectral Density (PSD) storey 3 of the acceleration in the x-direction of the model under free coupled vibration, cotton rope, nylon rope and ski-rope

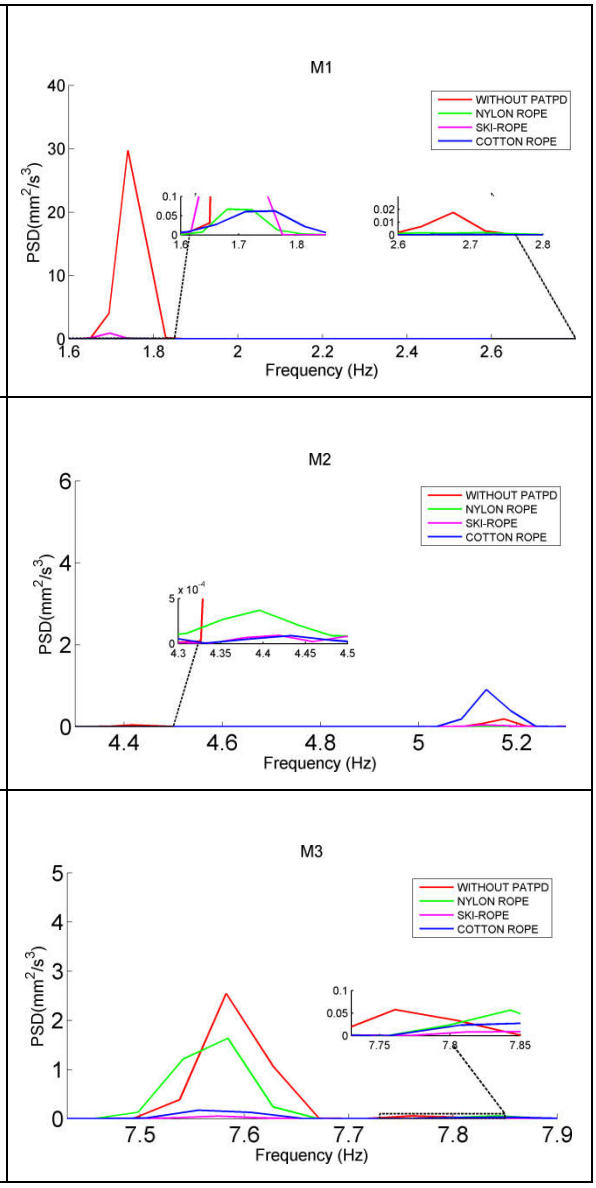

Figure 124: Magnified Power Spectral Density (PSD) storey 2 of the acceleration in the x-direction of the model under free coupled vibration, cotton rope, nylon rope and ski-rope

Figure 123, Figure 124 and Figure 125 show for first natural frequency with PSD peak, 1.733Hz and 2.677Hz, for both translation and torsion, all 3 PATPD masses provide significant damping of the model's vibrations across all 3 storeys, with the cotton demonstrating best control effect overall.

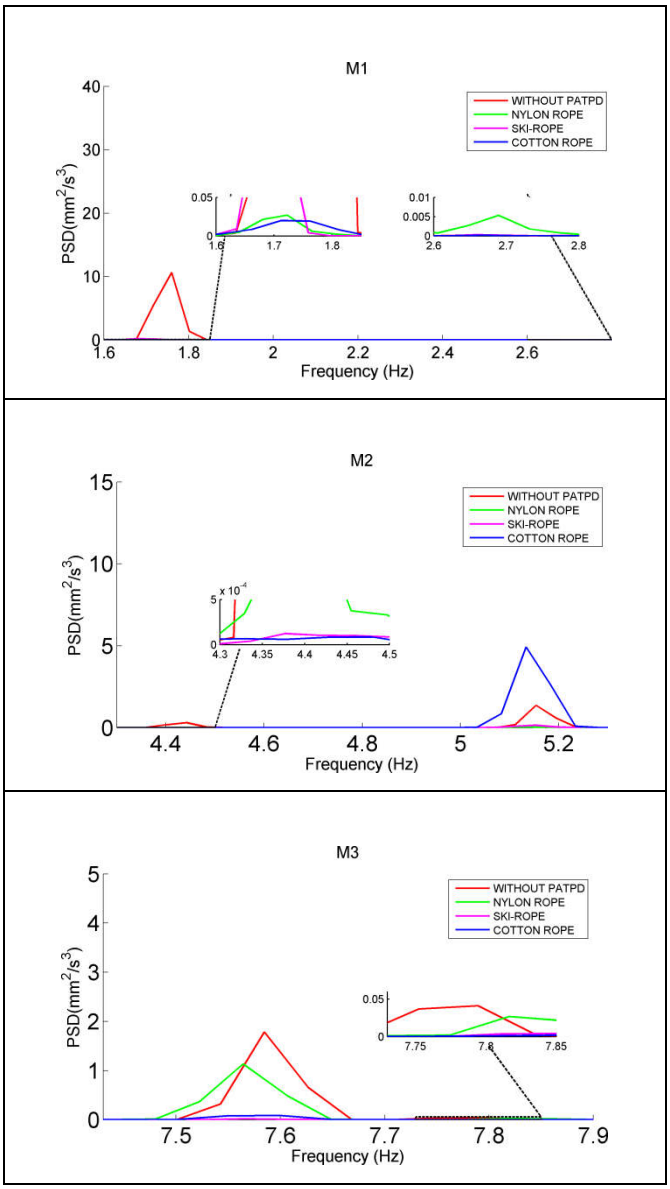

Figure 125: Magnified Power Spectral Density (PSD) storey 1 of the acceleration in the x-direction of the model under free coupled vibration, cotton rope, nylon rope and ski-rope

For second natural frequency with PSD peak, 4.446Hz, for torsion across all 3 storeys, all rope types tested provide significant damping of the model's vibrations across all 3 storeys, with the nylon the least. For translation with PSD peak, 5.164Hz, across all 3 storeys, nylon and ski-rope provide slight control effect, with the cotton increasing the density of the frequency.

For third natural frequency with PSD peak, 7.584Hz and 7.792Hz, for translation and torsion all provide control with nylon providing least.

Overall PSD peak increases were minimal in comparison to the reduction gained in PSD peak for the first natural frequency.

5.3.1.6 Coupled Vibration (Translation in Y-direction and torsion)

The model was given an initial torsional displacement and displacement in y-direction simultaneously, respective acceleration measured in the y-direction. The damping effect of each can be seen in the graphs to follow.

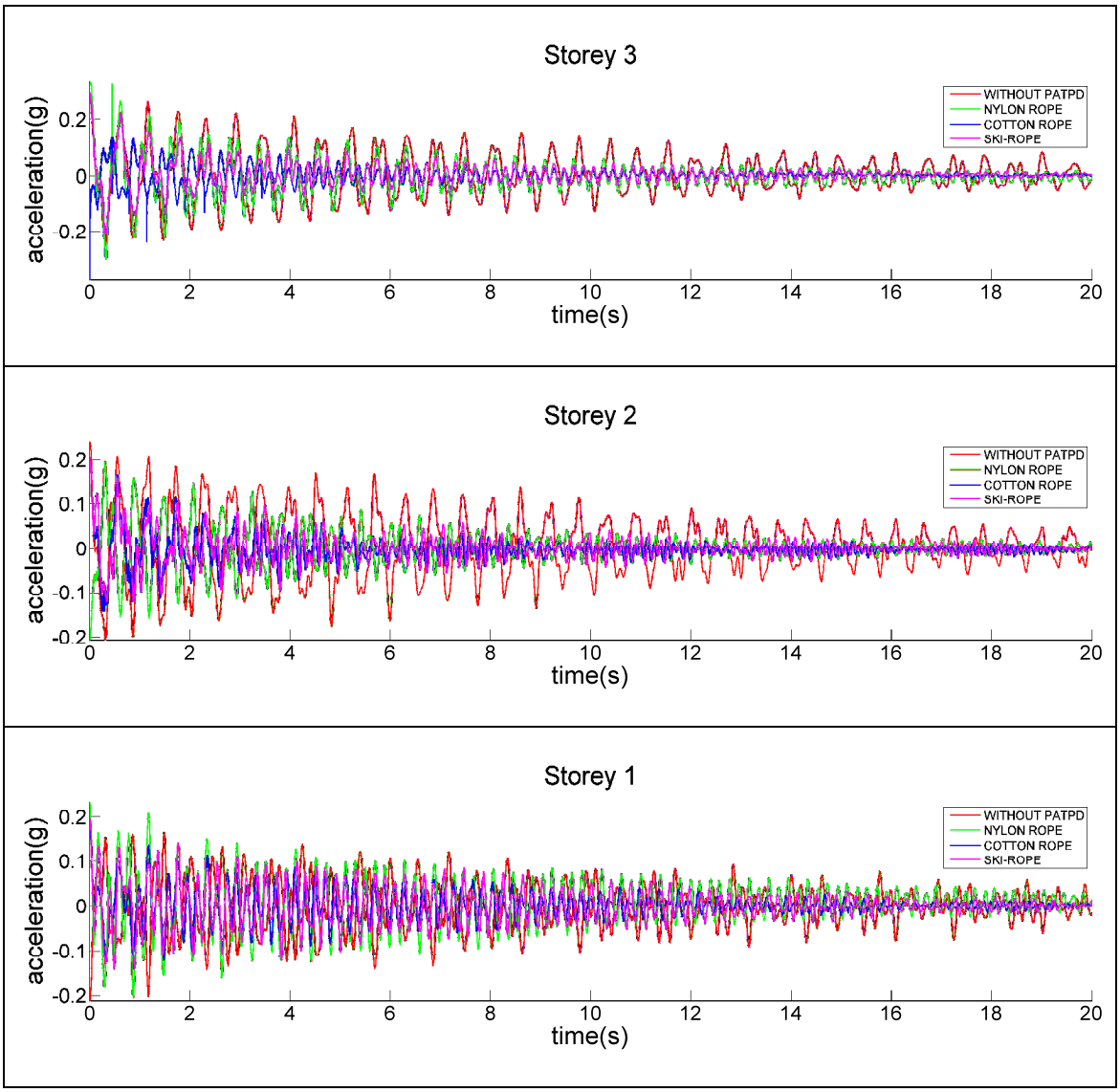

Figure 126: Time history of acceleration response in y-direction per storey for free coupled vibration, cotton rope, nylon rope and ski-rope

Figure 126 shows that for all rope types tested as the PATPD started moving; the acceleration peaks generated in the damped model are as high as those generated in the undamped model. However, these high accelerations subside and the accelerations rapidly decrease compared to that of the undamped model. As is expected the accelerations experienced in storey 3 are highest and the positive damping effect of the

PATPD was still significant for all rope types tested. The best control effect is seen in storey 3, since the damper was installed on this storey.

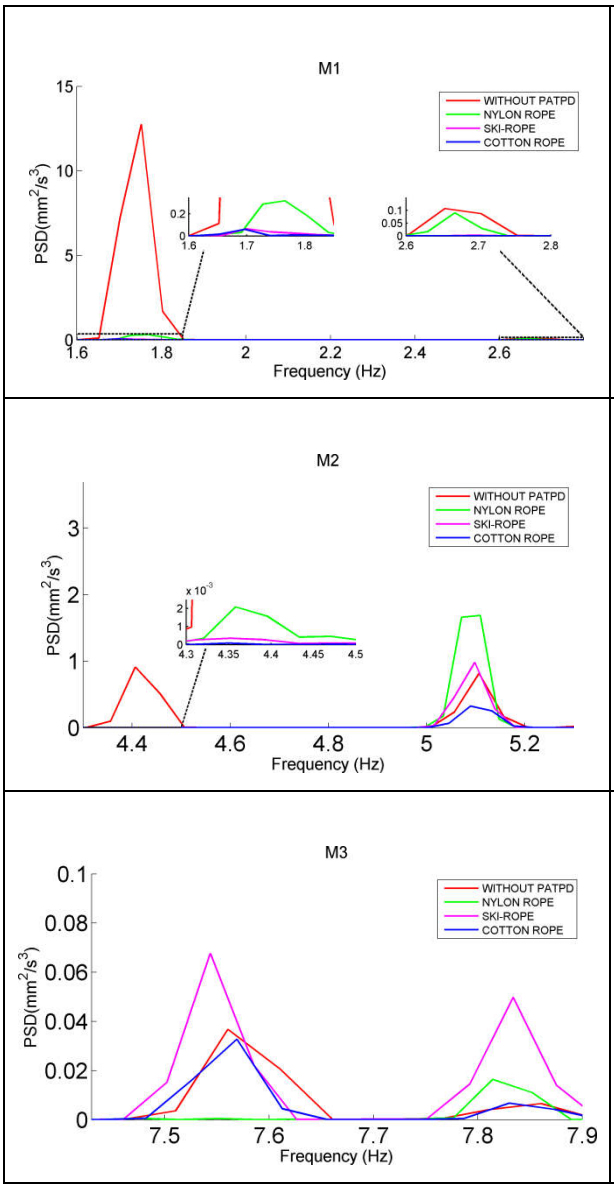

Figure 127: Magnified Power Spectral Density (PSD) storey 3 of the acceleration in the y-direction of the model under free coupled vibration, cotton rope, nylon rope and ski-rope

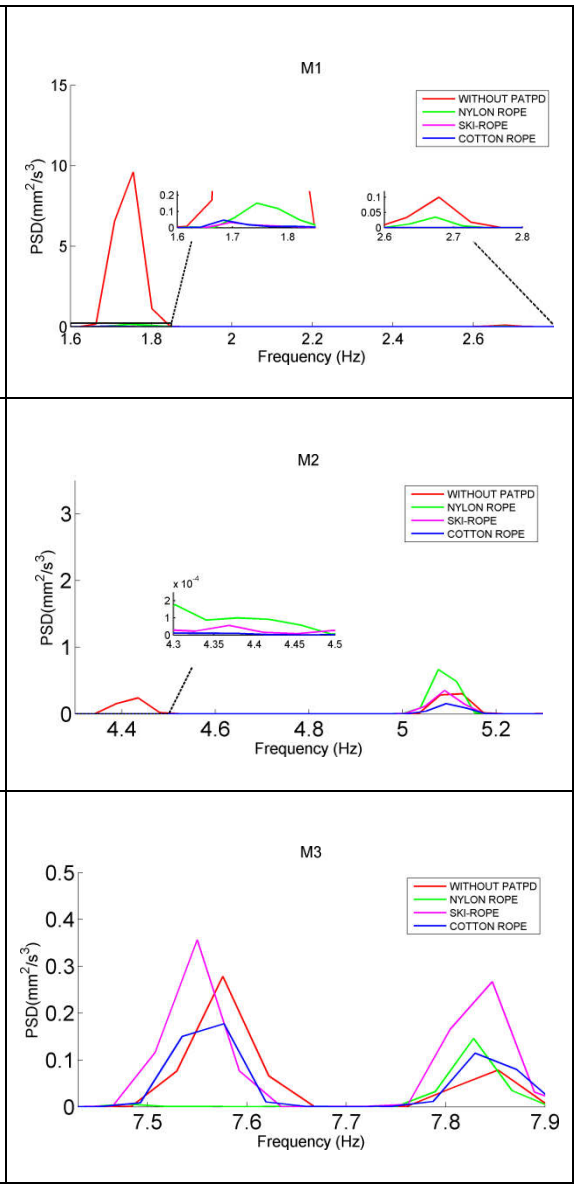

Figure 128: Magnified Power Spectral Density (PSD) storey 2 of the acceleration in the y-direction of the model under free coupled vibration, cotton rope, nylon rope and ski-rope

Figure 127, Figure 128 and Figure 129 show for first natural frequency with PSD peak, 1.747Hz and 2.680Hz, for both translation and torsion, all 3 ropes tested provide significant damping of the model's vibrations across all 3 storeys, with the ski-rope and cotton demonstrating best control effect and nylon the least.

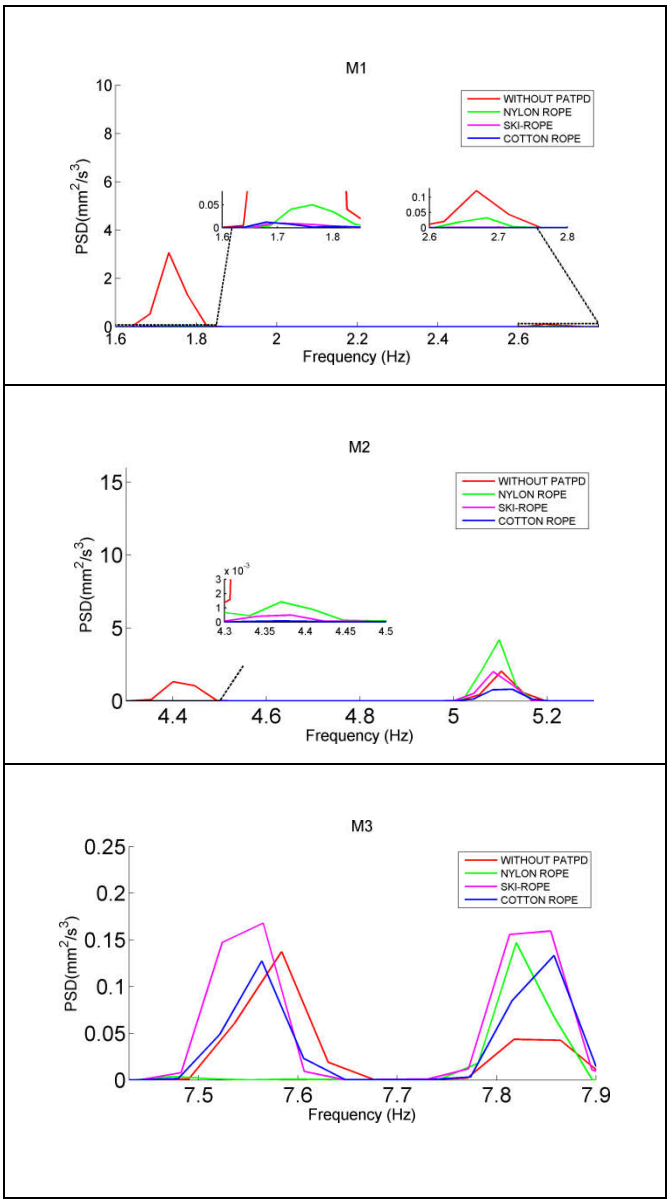

Figure 129: Magnified Power Spectral Density (PSD) storey 1 of the acceleration in the y-direction of the model under free coupled vibration, cotton rope, nylon rope and ski-rope

For second natural frequency with PSD peak, 4.438 Hz, for torsion across all 3 storeys, all rope types tested provide significant damping of the model's vibrations across all 3 storeys, with the nylon the least. For translation, with PSD peak, 5.095Hz, across all 3 storeys, cotton provides only control effect, even if slightly so, with the others increasing the density of the frequency – nylon being the worst. For third natural frequency with PSD peak, 7.569Hz, for translation only nylon provides control with ski-rope increasing the density of the frequency and cotton similar to undamped. For torsion, with PSD peak, 7.842 Hz, cotton is still similar to undamped for storey 2-3, and increases like the others for storey 1.

Overall PSD peak increases were minimal in comparison to the reduction gained in PSD peak for the first natural frequency.

5.3.2.0 Forced Vibration

5.3.2.1 Translational Vibration in the X-direction

The model was placed on the shake table in order to carry out the forced vibration tests. The PATPD's were connected one-by-one and the respective accelerations measured. The damping effect of each rope change of the PATPD can be seen in the graphs to follow.

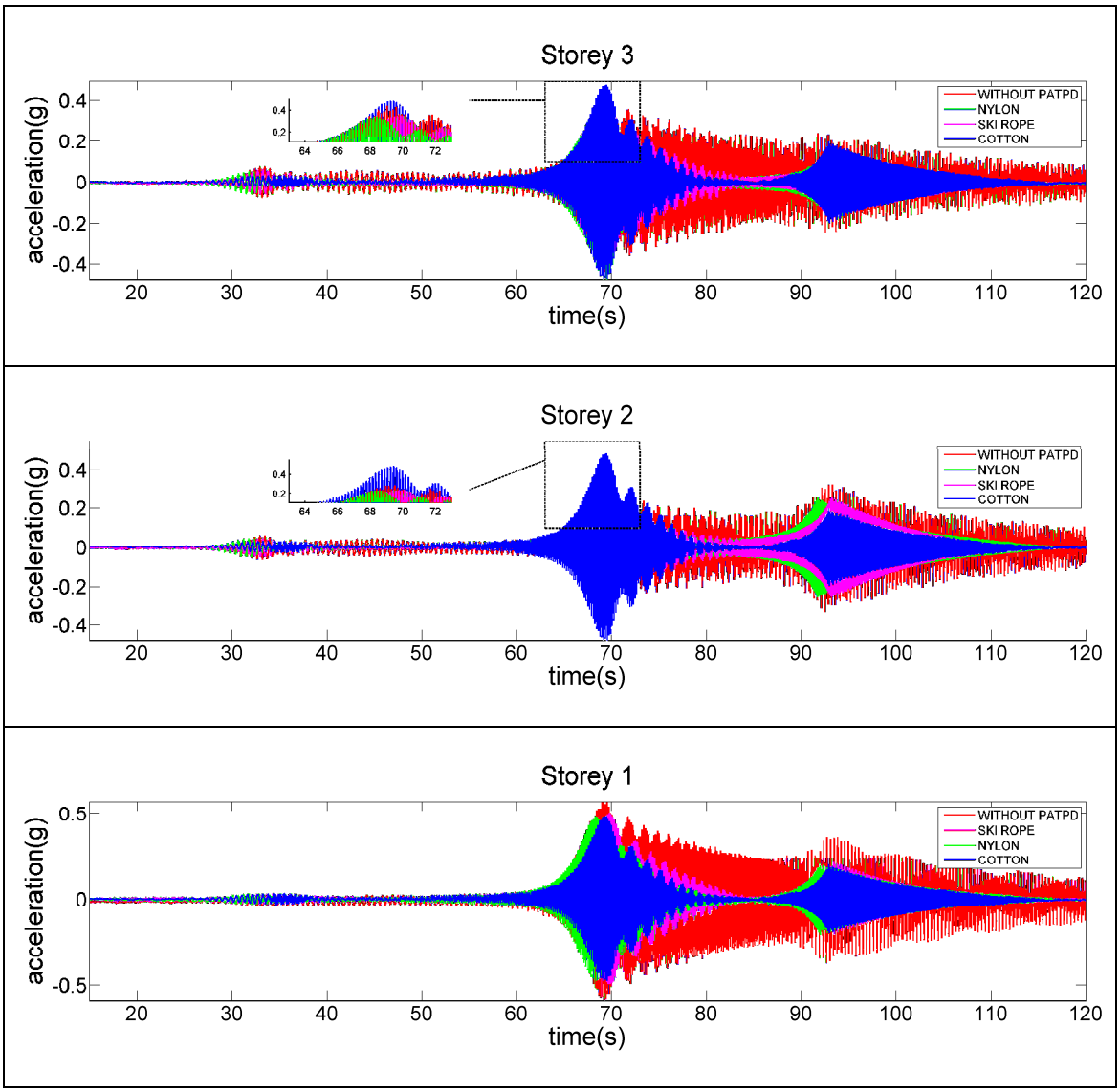

Figure 130: Time history of acceleration response per storey for forced translational vibration in x-direction, steel, cotton rope, nylon rope and ski-rope

Figure 130 shows for all 3 storeys that by adding the damper onto model the acceleration experience is significantly decreased for all rope types.

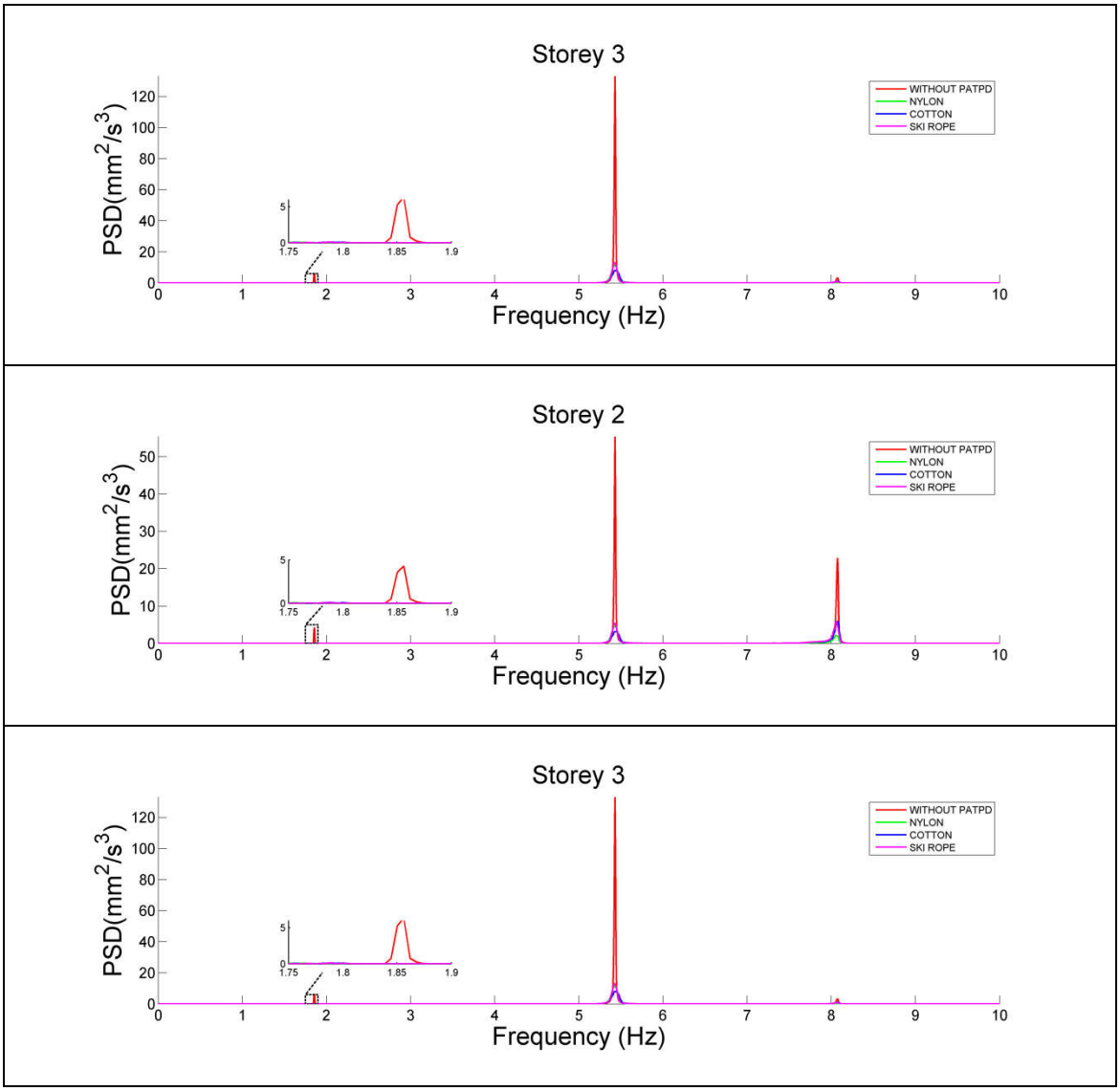

Figure 131: Power Spectral Density (PSD) of the acceleration response per storey under forced excitation in the x-direction, cotton rope, nylon rope and ski-rope

Figure 131 shows PSD peaks at 1.856Hz, 5.429Hz and 8.047Hz. This corresponds to the models first, second and third frequencies. The positive control effect is evident as PSD peaks for all 3 frequencies are significantly reduced by ropes used.

5.3.2.2 Translational Vibration in the Y-direction

The model was placed on the shake table in order to carry out the forced vibration tests. The PATPD's were connected one-by-one and the respective accelerations measured. The damping effect of each of the PATPD masses can be seen in the graphs to follow.

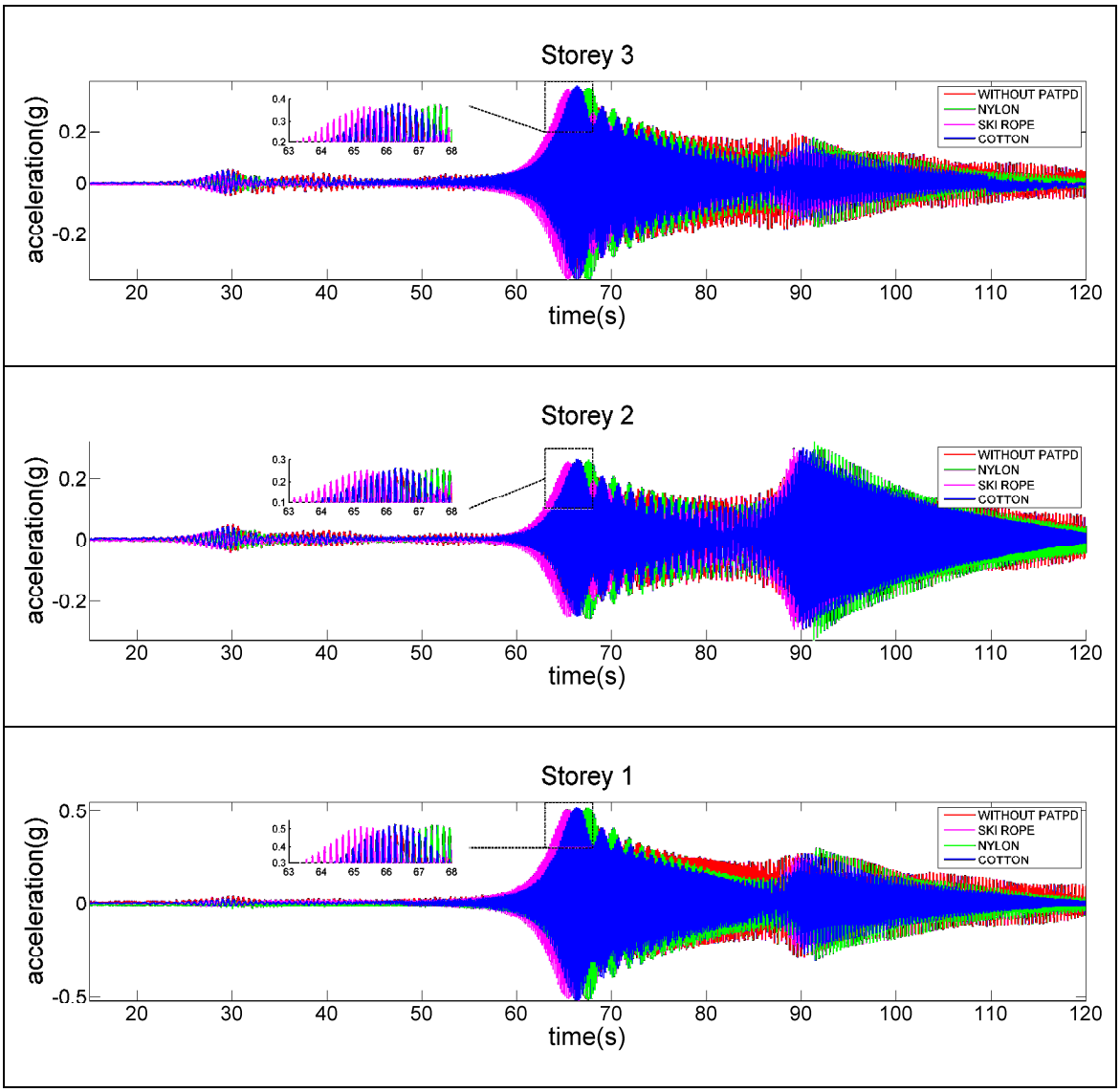

Figure 132: Time history of acceleration response per storey for forced translational vibration in y-direction, cotton rope, nylon rope and ski-rope

Figure 132 shows for all 3 storeys that by adding the damper onto model the acceleration experience is significantly decreased for all rope types used.

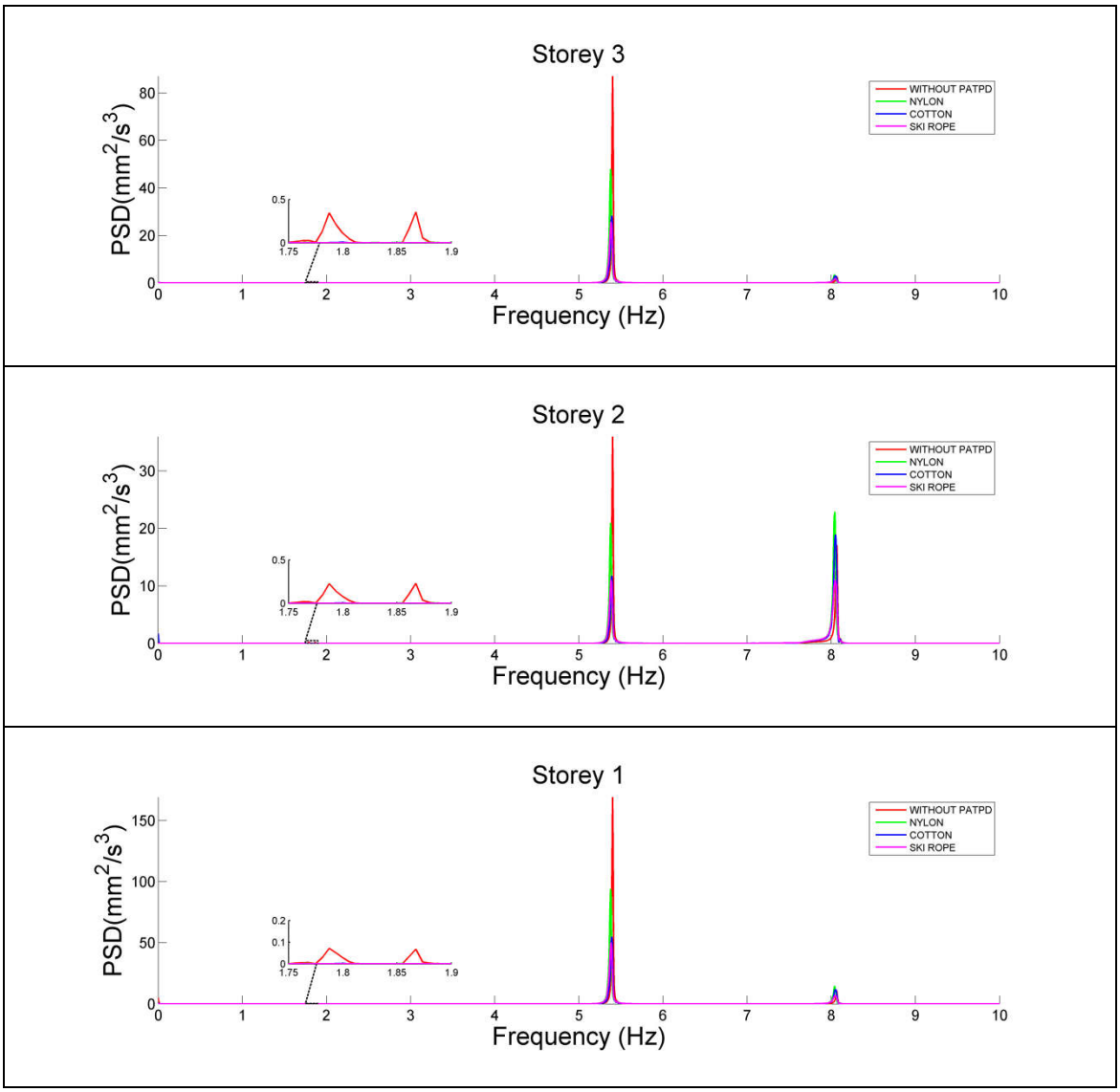

Figure 133: Power Spectral Density (PSD) of the acceleration response per storey under forced excitation in the y-direction, cotton rope, nylon rope and ski-rope

Figure 133 shows PSD peaks at 1.787Hz, 5.399Hz and 8.065Hz. This corresponds to the models first, second and third frequencies. The positive control effect is evident as PSD peaks for all 3 frequencies are significantly reduced. This is true for all rope types used. Control effect of PATPD is better in x-direction than in y-direction.

5.3.3.0 Summary

Free Vibration

This set of parameter tests indicates better control in x than in y direction. Cotton and ski-rope demonstrates best control effect for first natural frequency. Nylon is poor in translation. All ropes provided control effect to the first natural frequency for all free vibration tests for all storeys, except Nylon which did not control the first natural frequency for storey 1 under torsional vibration (x-direction).

Forced Vibration

For Forced Vibration the PATPD provides significant control to all 3 frequencies for all rope types tested.

The results reveal that the PATPD performs better in translation the x –direction than the y-direction.

5.4 Parameter Test 4: Effect of changing connections

Tests were carried out using three different types of connections[8]: (a) configuration 1 (primary model): 8 connections to pulleys (2 transversely and 2 diagonally), (b) configuration 2: 4 connections to pulleys (2 diagonally), and (c) configuration 3: 4 connections to pulleys (2 transversely).

All other parameters during these tests remained constant, with the test model having a mass of 42.09kg and a height of 37cm per storey. As with the previous tests the model was given an initial displacement, in the according directions, and the acceleration with and without the damper measured.

The data for each case is processed and they are plotted together on graphs such that extrapolations and comparisons can be made.

5.4.1 Free Vibration

5.4.1.1 Translational Vibration in the X-direction

The model was given an initial displacement in the x-direction and respective acceleration measured. The damping effect of each can be seen in the graphs to follow.

[8] These configurations can be found on page 57

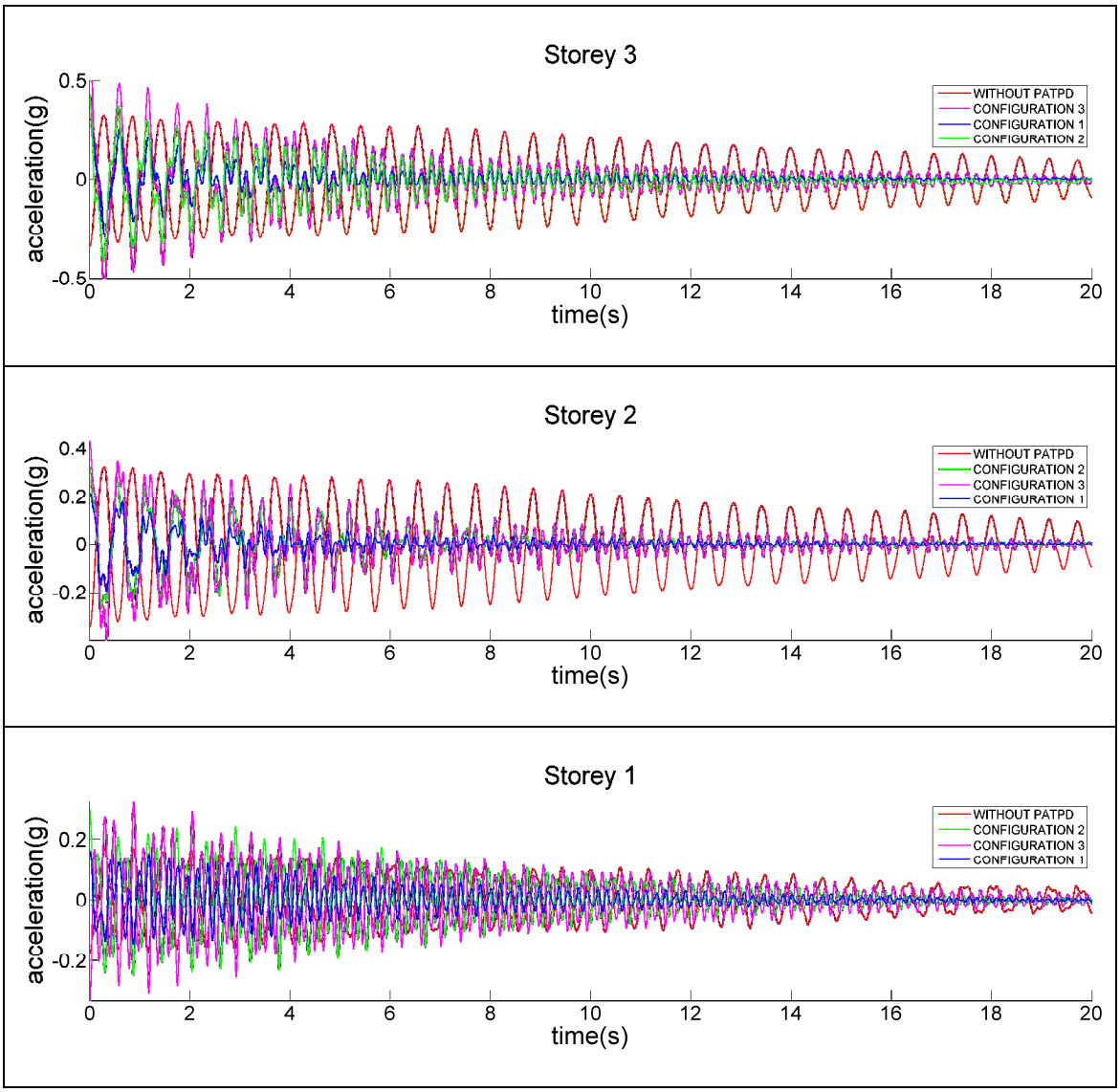

Figure 134: Time history of acceleration response per storey for free translational vibration in x-direction, configuration 1, 2 and 3

Figure 134 shows that for all configurations the PATPD starts moving; the acceleration peaks generated in the damped model are as high as those generated in the undamped model. However, these high accelerations subside and the accelerations rapidly decrease compared to that of the undamped model. As is expected the accelerations experienced in storey 3 are highest and the positive damping effect of the PATPD was still significant for all configurations tested. The best control effect is seen in storey 3, since the damper was installed on this storey.

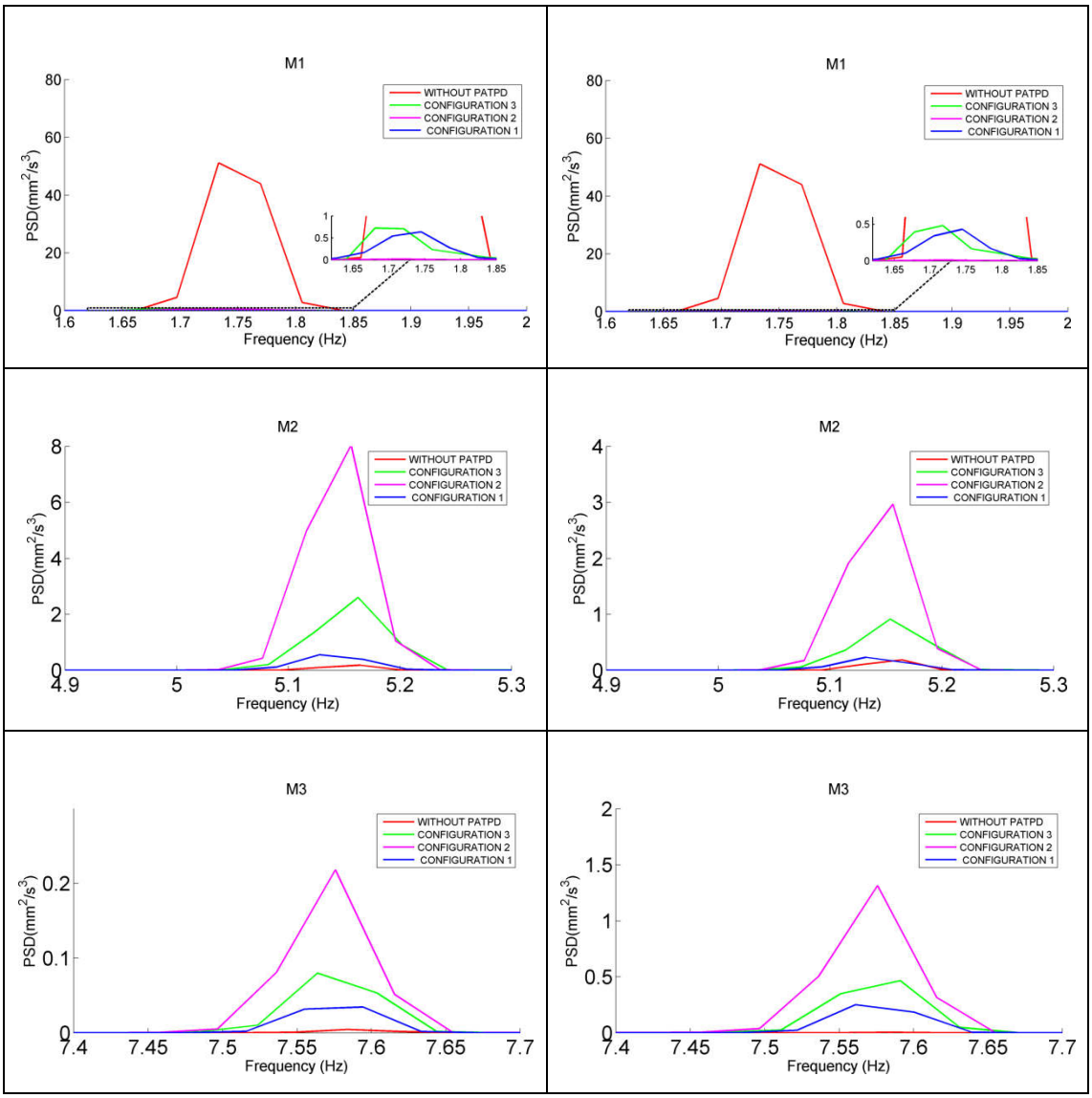

Figure 135: Magnified Power Spectral Density (PSD) storey 3 of the acceleration of the model under free translational vibration in the x-direction , configuration 1,2 and 3

Figure 136: Magnified Power Spectral Density (PSD) storey 2 of the acceleration of the model under free translational vibration in the x-direction, configuration 1, 2 and 3

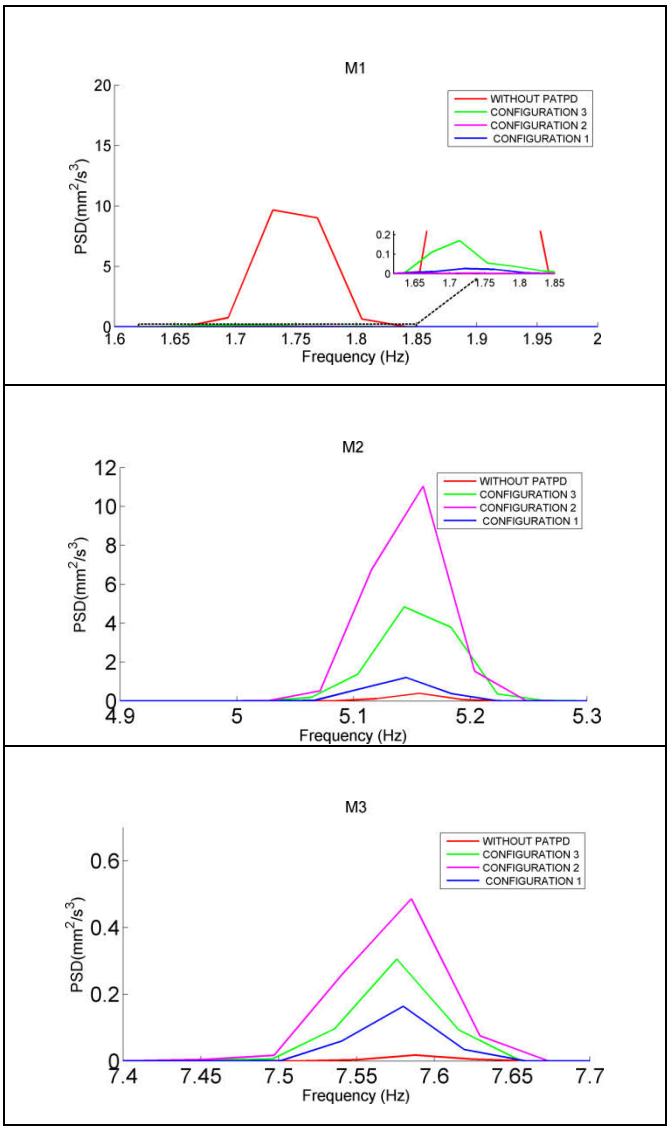

Figure 137: Magnified Power Spectral Density (PSD) storey 1 of the acceleration of the model under free translational vibration in the x-direction, configuration 1,2 and 3

Figure 135, Figure 136 and Figure 137 shows for first natural frequency with PSD peak, 1.733Hz, all configurations produced significant damping of the model's vibrations across all storeys, reducing the PSD peak by at least 90%. Configuration 2 demonstrates best control.

For second and third natural frequency with PSD peaks, 5.164Hz and 7.584Hz all configurations show significant increase in the models' vibrations across all storeys. Configuration 1 behaves best and, configuration 2 worst.

Overall PSD peak increases were minimal in comparison to the reduction gained in PSD peak for the first natural frequency.

.

5.4.1.2 Translational Vibration in the Y-direction

The model was given an initial displacement in the y-direction and respective acceleration measured. The damping effect of each PATPD can be seen in the graphs to follow.

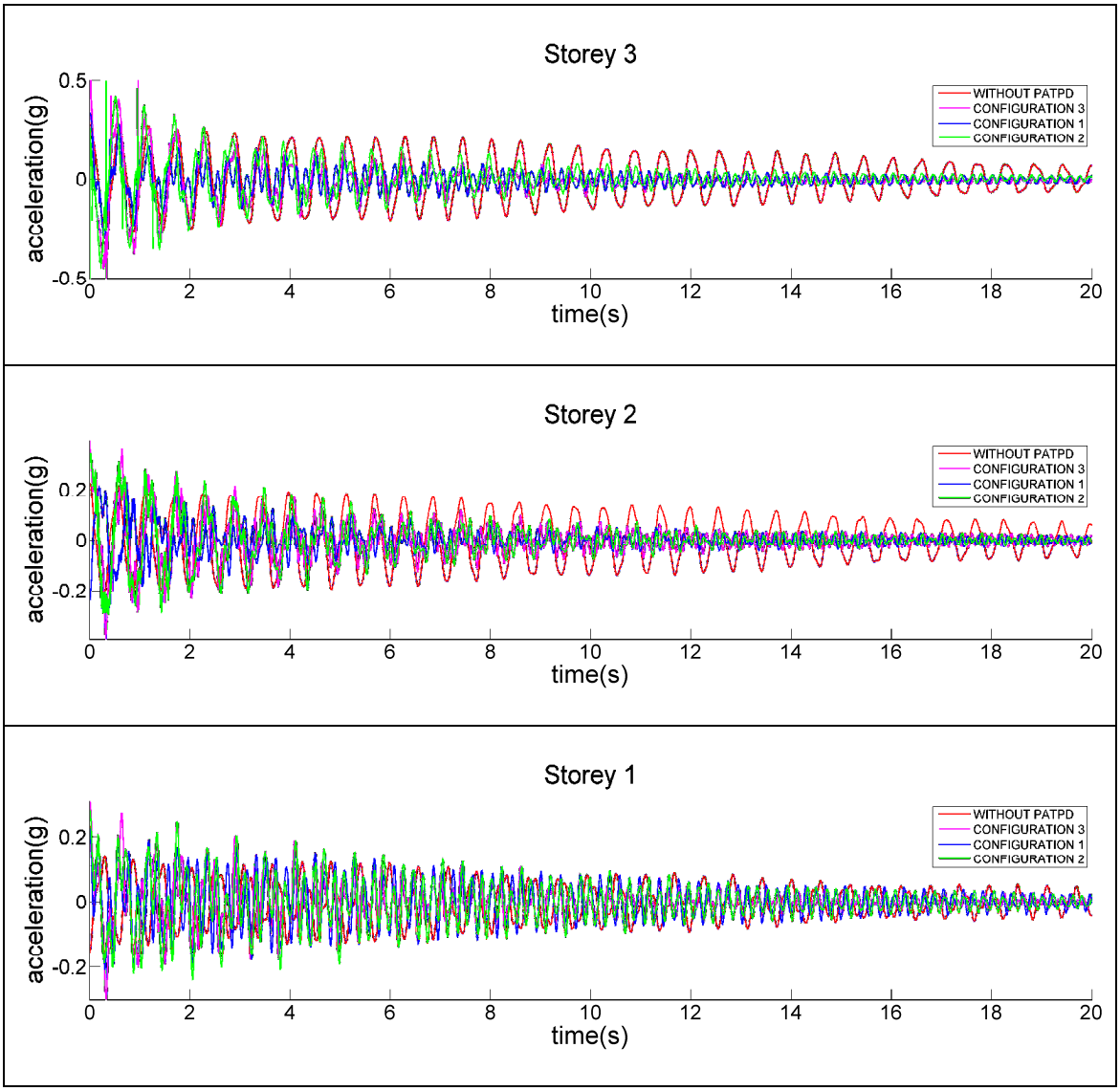

Figure 138: Time history of acceleration response per storey for free translational vibration in y-direction, configuration 1, 2 and 3

Figure 138 shows that for all configurations the PATPD starts moving; the acceleration peaks generated in the damped model are as high as those generated in the undamped model. However, these high accelerations subside and the accelerations rapidly decrease compared to that of the undamped model. As is expected the accelerations experienced in storey 3 are highest and the positive damping effect of the PATPD was still

significant for all configurations tested. The best control effect is seen in storey 3, since the damper was installed on this storey.

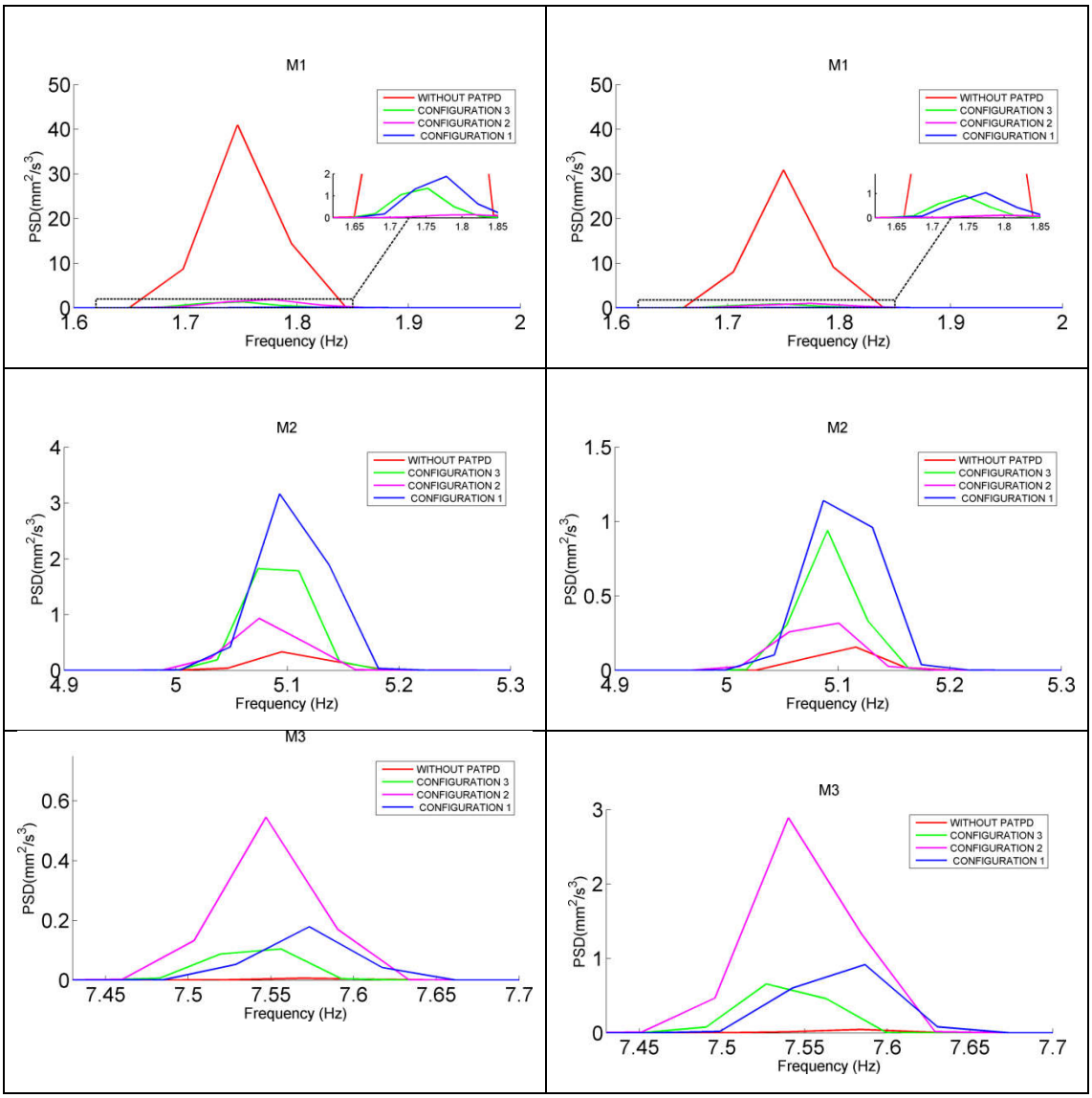

Figure 139: Magnified Power Spectral Density (PSD) storey 3 of the acceleration of the model under free translational vibration in the y-direction, configuration 1, 2 and 3

Figure 140: Magnified Power Spectral Density (PSD) storey 2 of the acceleration of the model under free translational vibration in the y-direction, configuration 1,2 and 3

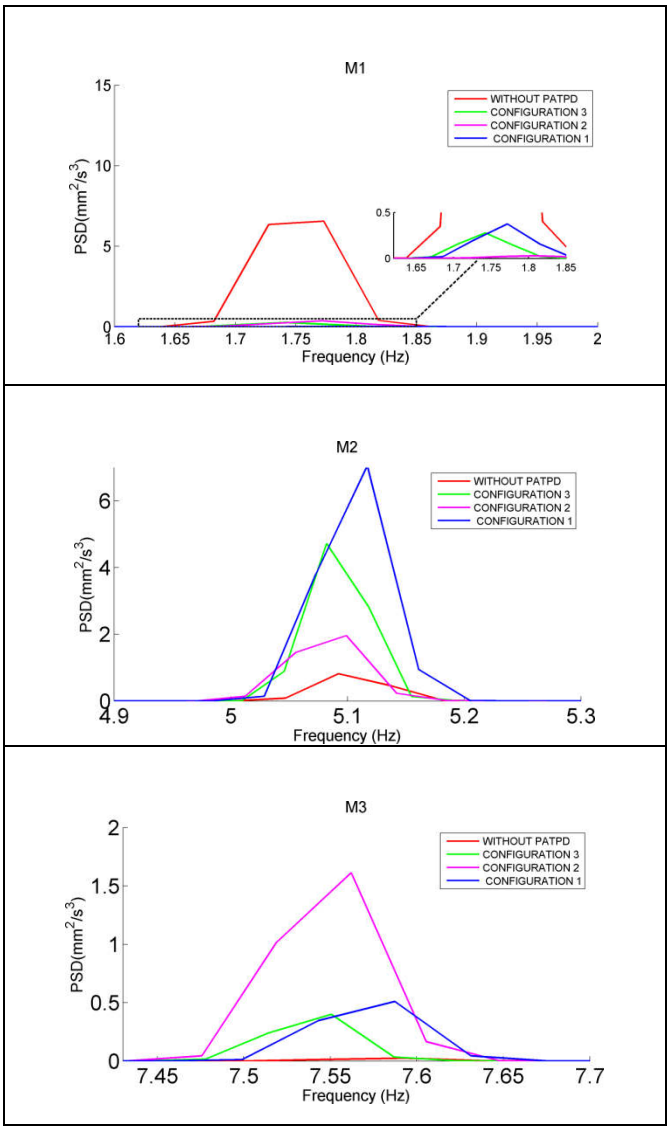

Figure 141: Magnified Power Spectral Density (PSD) storey 1 of the acceleration of the model under free translational vibration in the y-direction, configuration 1, 2 and 3

Figure 139, Figure 140 and Figure 141 shows for first natural frequency with PSD peak, 1.747Hz, all configurations produced significant damping of the model's vibrations across all storeys, reducing the PSD peak by at least 90%. Configuration 2 demonstrates best control.

For second and third natural frequency with PSD peaks, 5.095Hz and 7.569Hz all configurations show significant increase in the model's vibrations across all storeys. M2 shows configuration 1 being highest, M3 shows configuration 2 highest.

Since we are concerned mainly with controlling the first natural frequency, all configurations tested provided significant damping of the model's vibrations.

5.4.1.3 Torsional Vibration (acceleration measured in the X-direction)

The model was given an initial torsional displacement and respective acceleration measured in the x-direction. The damping effect of each can be seen in the graphs to follow.

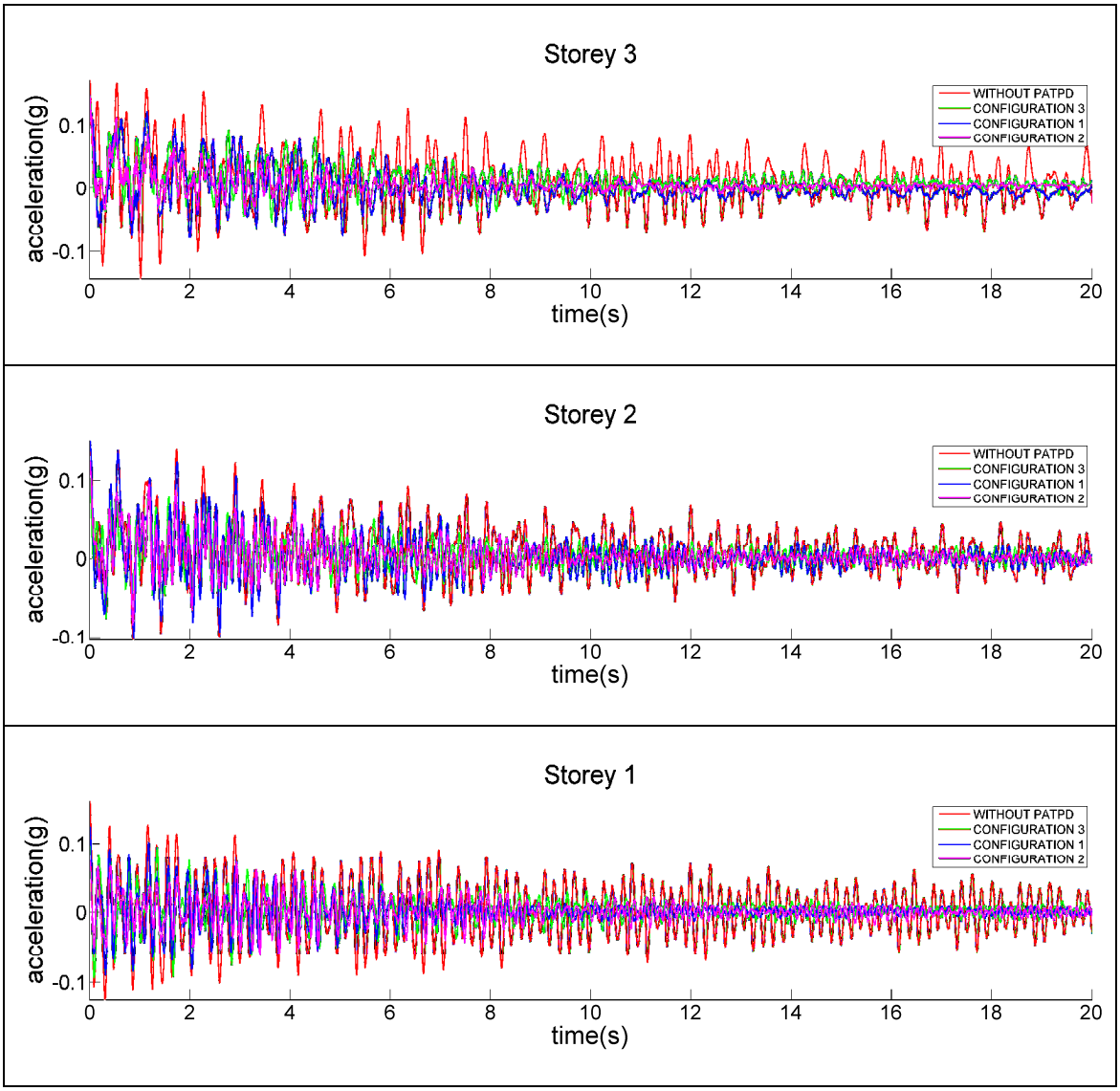

Figure 142: Time history of acceleration response in x-direction per storey for free torsional vibration, configuration 1, 2 and 3

Figure 142 shows that for all configurations the PATPD starts moving; the acceleration peaks generated in the damped model are as high as those generated in the undamped model. However, these high accelerations subside and the accelerations rapidly decrease compared to that of the undamped model. As is expected the accelerations experienced in storey 3 are highest and the positive damping effect of the PATPD was still significant for all configurations tested. The best control effect is seen in storey 3, since the damper was installed on this storey.

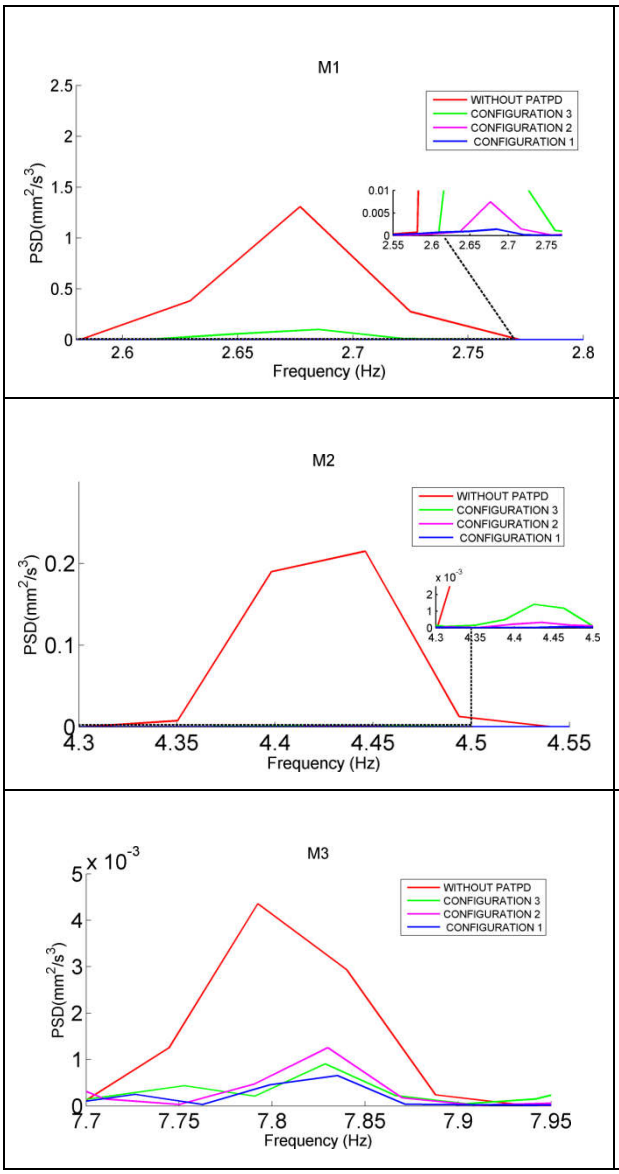

Figure 143: Magnified Power Spectral Density (PSD) storey 3 of the acceleration in the x-direction of the model under free torsional vibration, configuration 1,2 and 3

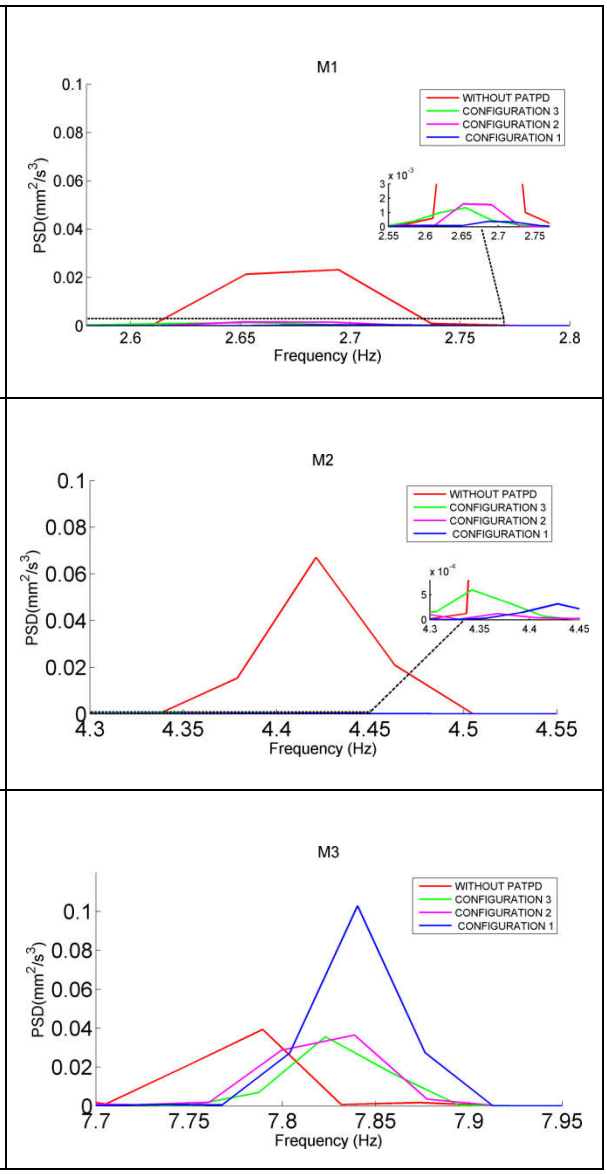

Figure 144: Magnified Power Spectral Density (PSD) storey 2 of the acceleration in the x-direction of the model under free torsional vibration, configuration 1,2 and 3

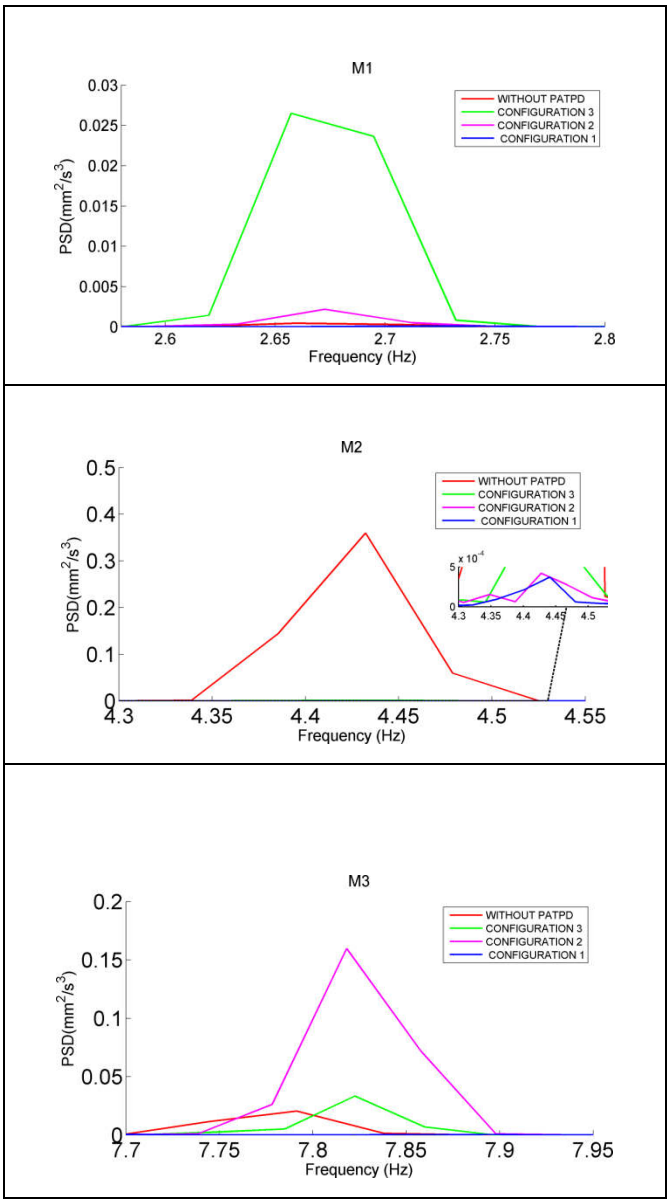

Figure 145: Magnified Power Spectral Density (PSD) storey 1 of the acceleration in the x-direction of the model under free torsional vibration, configuration 1,2 and 3

Figure 143, Figure 144 and Figure 145 shows for first and second natural frequency with PSD peak, 2.677Hz and 4.446Hz, all ropes tested produced damping of the model's vibrations for storey 2 and 3. The PSD peak is reduced by at least 90%. Storey 1 M1 shows a significant increase in frequency for configuration 3.

For third natural frequency with PSD peak, 7.792Hz, storey 3 is controlled by all configurations. Storey 1 and 2 sees an in increase in frequency.

Overall PSD peak increases were minimal in comparison to the reduction gained in PSD peak for the first natural frequency.

5.4.1.4 Torsional Vibration (acceleration measured in the Y-direction)

The model was given an initial torsional displacement and respective acceleration measured in the y-direction. The damping effect of each can be seen in the graphs to follow.

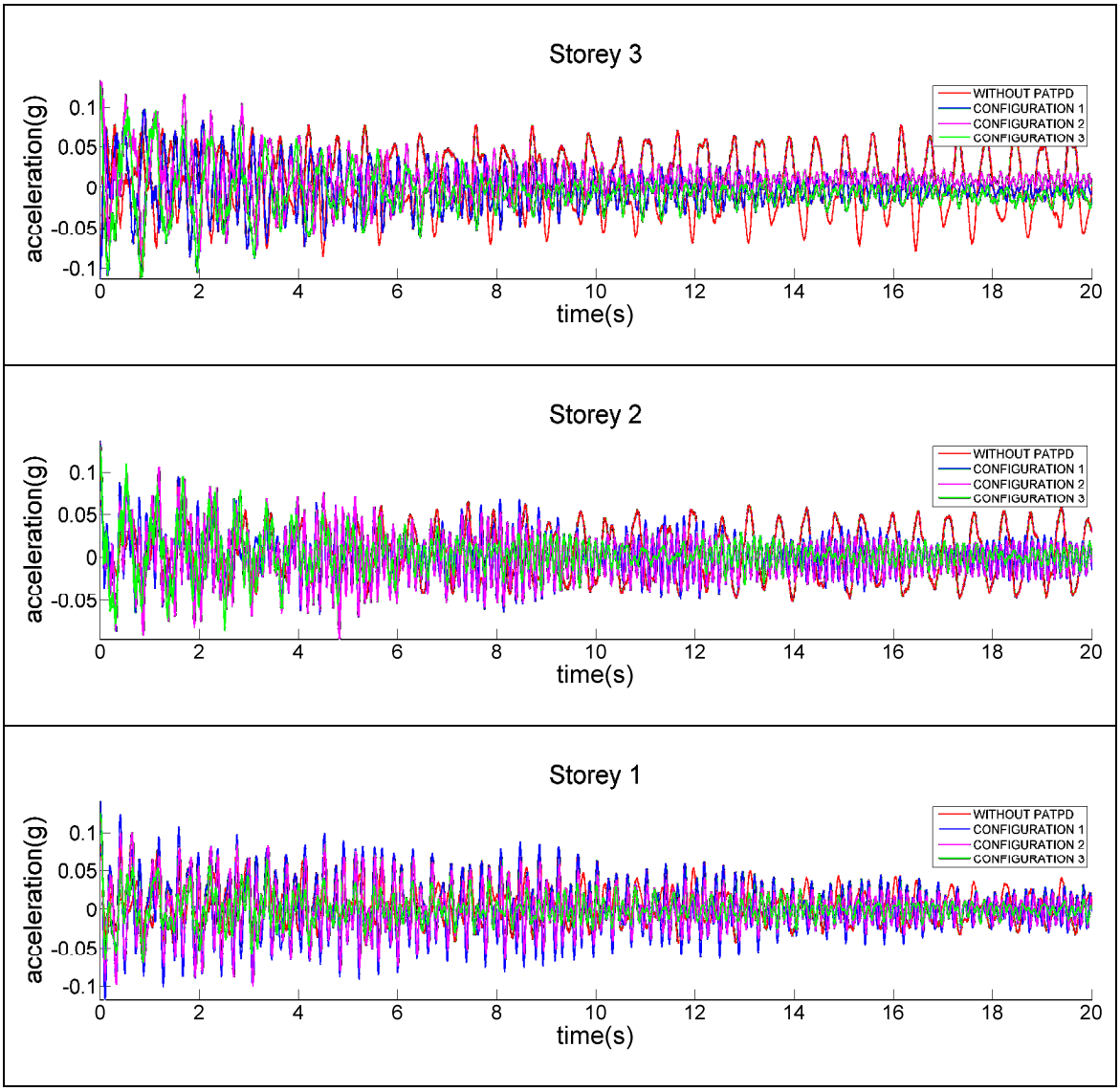

Figure 146: Time history of acceleration response in y-direction per storey for free torsional vibration, configuration 1, 2 and 3

Figure 146 shows that for all configurations the PATPD starts moving; the acceleration peaks generated in the damped model are as high as those generated in the undamped model. However, these high accelerations subside and the accelerations rapidly decrease compared to that of the undamped model. As is expected the accelerations experienced in storey 3 are highest and the positive damping effect of the PATPD was still significant for all configurations tested. The best control effect is seen in storey 3, since the damper was installed on this storey.

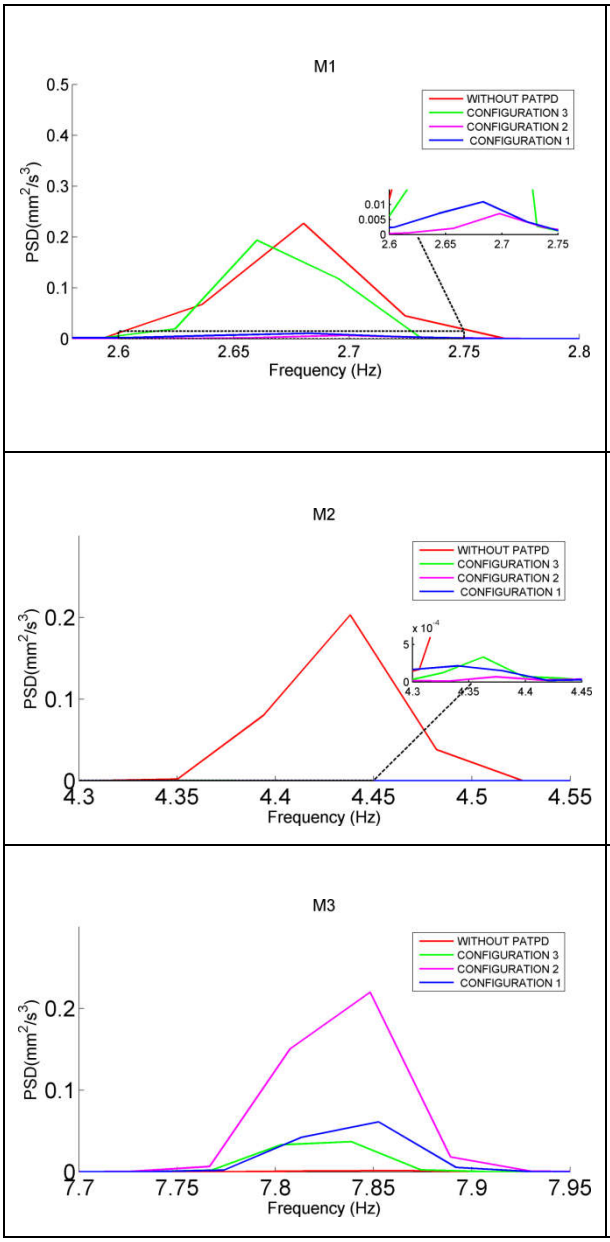

Figure 147: Magnified Power Spectral Density (PSD) storey 3 of the acceleration in the y-direction of the model under free torsional vibration , configuration 1,2 and 3

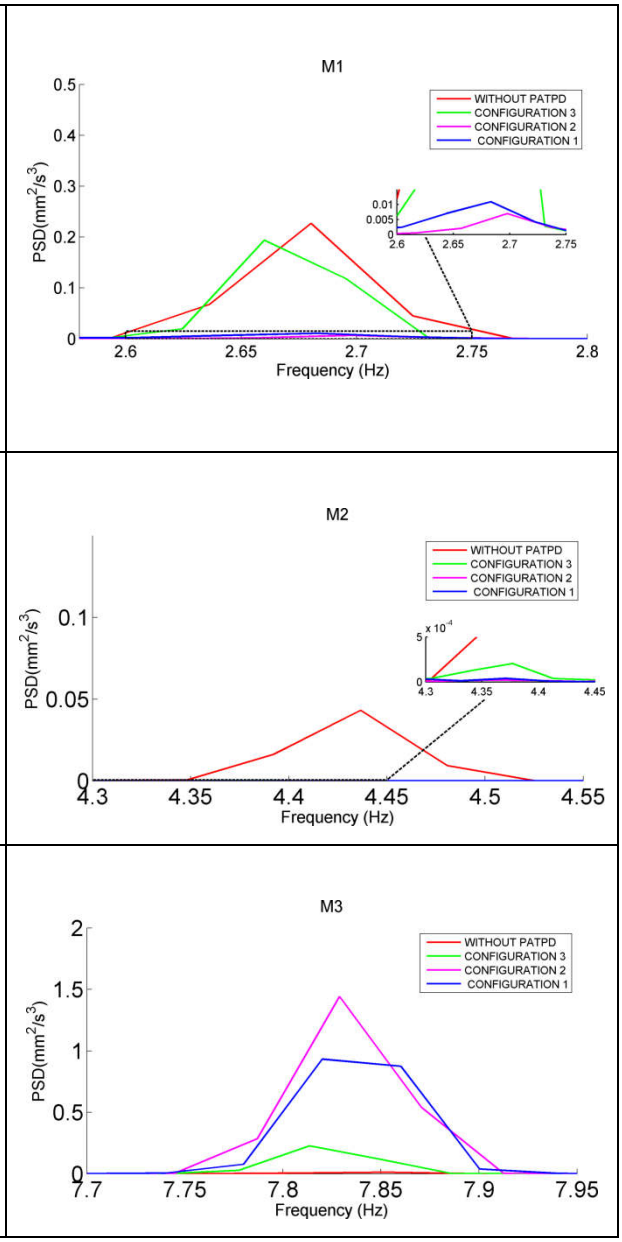

Figure 148: Magnified Power Spectral Density (PSD) storey 2 of the acceleration in the y-direction of the model under free torsional vibration , configuration 1,2 and 3

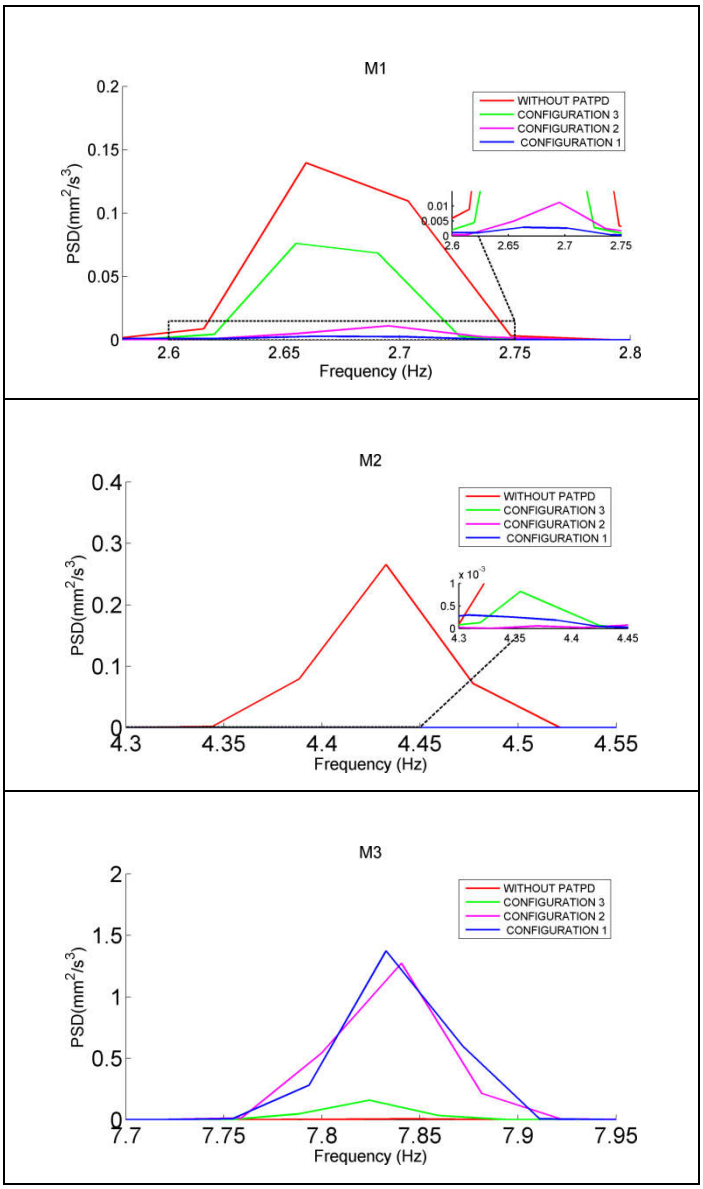

Figure 149: Magnified Power Spectral Density (PSD) storey 1 of the acceleration in the y-direction of the model under free torsional vibration , configuration 1, 2 and 3

Figure 147, Figure 148 and Figure 149 shows for first natural frequency with PSD peak, 2.680Hz, all configurations, except configuration3, produced significant damping of the model's vibrations across all storeys, reducing the PSD peak by at least 90%. Configuration 2 demonstrates best control. For second natural frequency with PSD peak, 4.438 Hz, all configurations produced significant damping of the model's vibrations across all storeys, reducing the PSD peak by at least 90%. For third natural frequency with PSD peak, 7.842 Hz, all configurations show significant increase in the model's vibrations across all storeys. Configuration 3 behaves best and, configuration 2 worst.

Overall PSD peak increases were minimal in comparison to the reduction gained in PSD peak for the first natural frequency.

5.4.1.5 Coupled Vibration (Translation in X-direction and torsion)

The model was given an initial torsional displacement and displacement in x-direction simultaneously, respective acceleration measured in the x-direction. The damping effect of each can be seen in the graphs to follow.

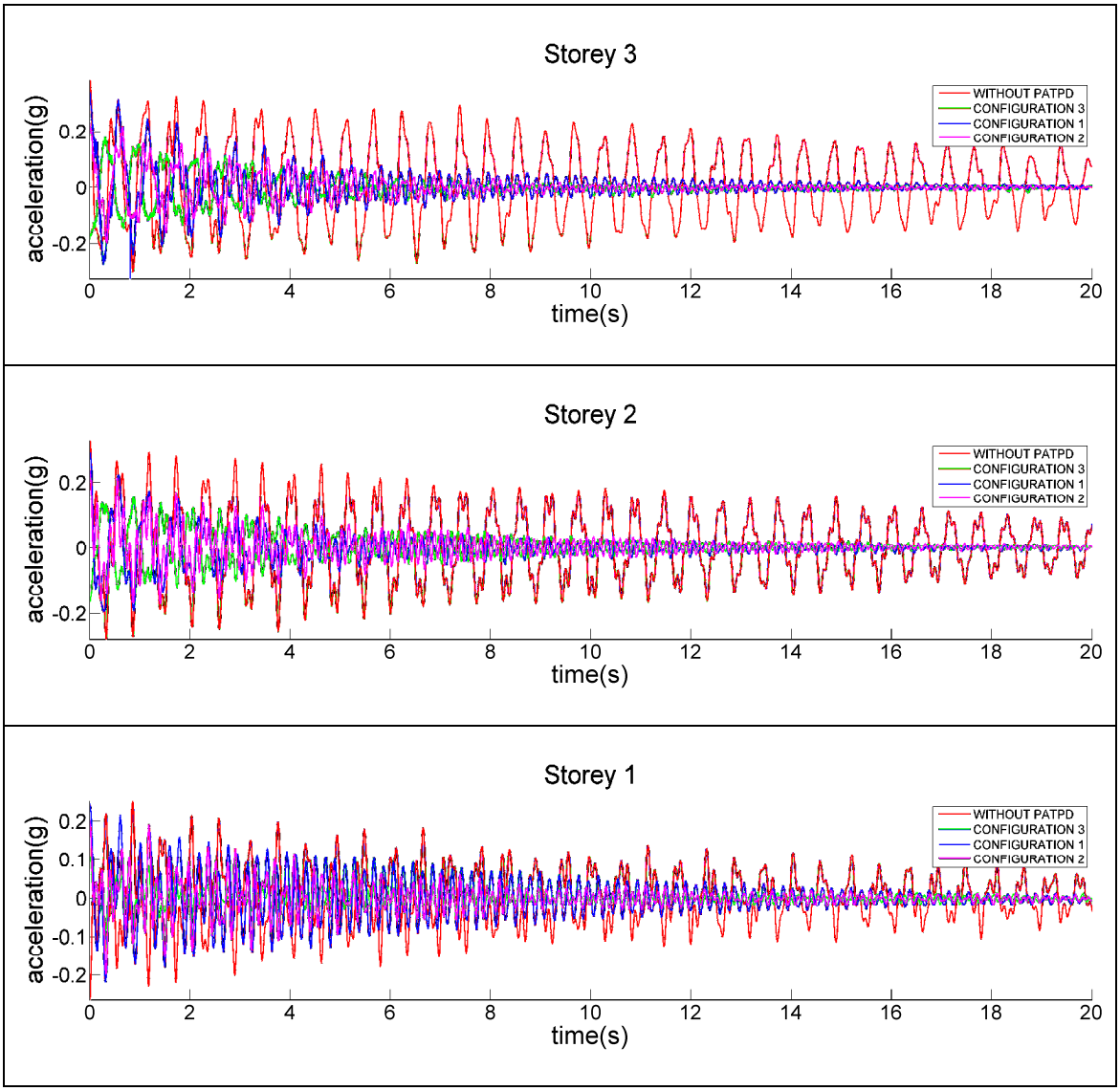

Figure 150: Time history of acceleration response in x-direction per storey for free coupled vibration, configuration 1, 2 and 3

Figure 150 shows that the PATPD starts moving; the acceleration peaks generated in the damped model are as high as those generated in the undamped model. However, these high accelerations subside and the accelerations rapidly decrease compared to that of the undamped model. As is expected the accelerations experienced in storey 3 are highest and the positive damping effect of the PATPD is still significant. The best control effect is seen in storey 3, since the damper was installed on this storey.

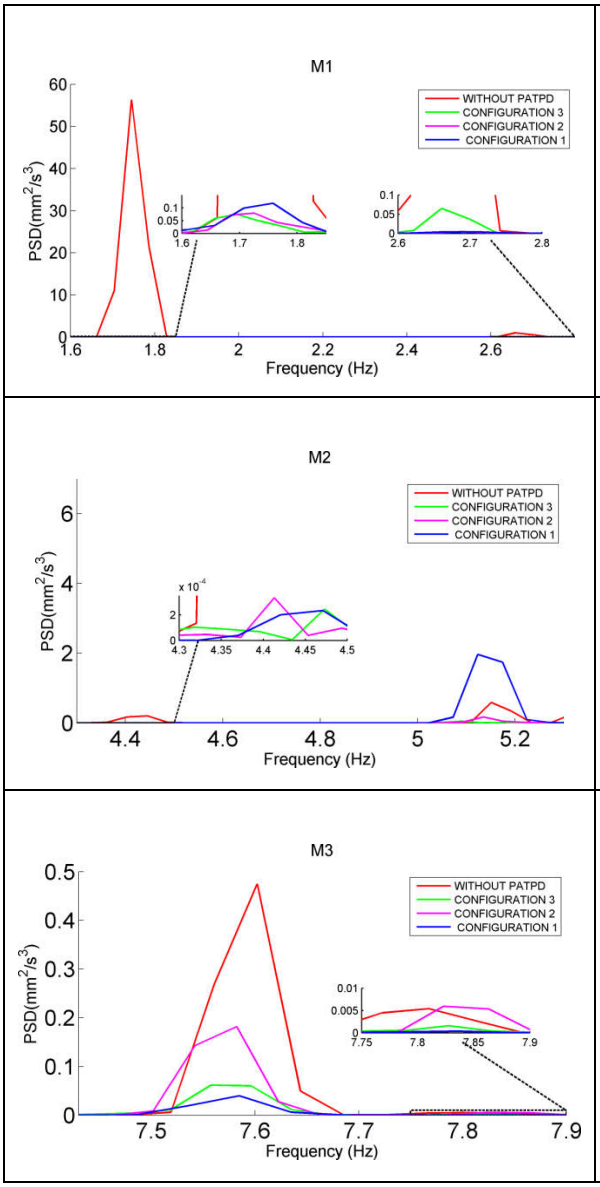

Figure 151: Magnified Power Spectral Density (PSD) storey 3 of the acceleration in the x-direction of the model under free coupled vibration, configuration 1,2 and 3

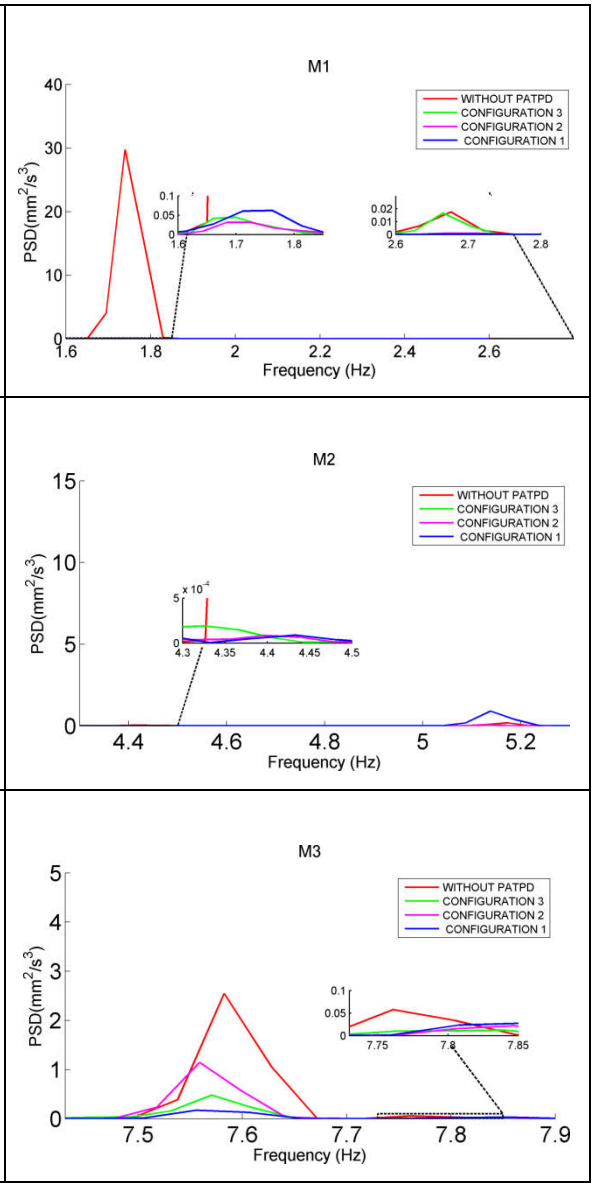

Figure 152: Magnified Power Spectral Density (PSD) storey 2 of the acceleration in the x-direction of the model under free coupled vibration, configuration 1,2 and 3

Figure 151, Figure 152 and Figure 153 show for first natural frequency with PSD peak, 1.733Hz, translation, all 3 configurations provide significant damping of the model's vibrations across all 3 storeys. Torsion with PSD peak, 2.677Hz, shows a slight increase.

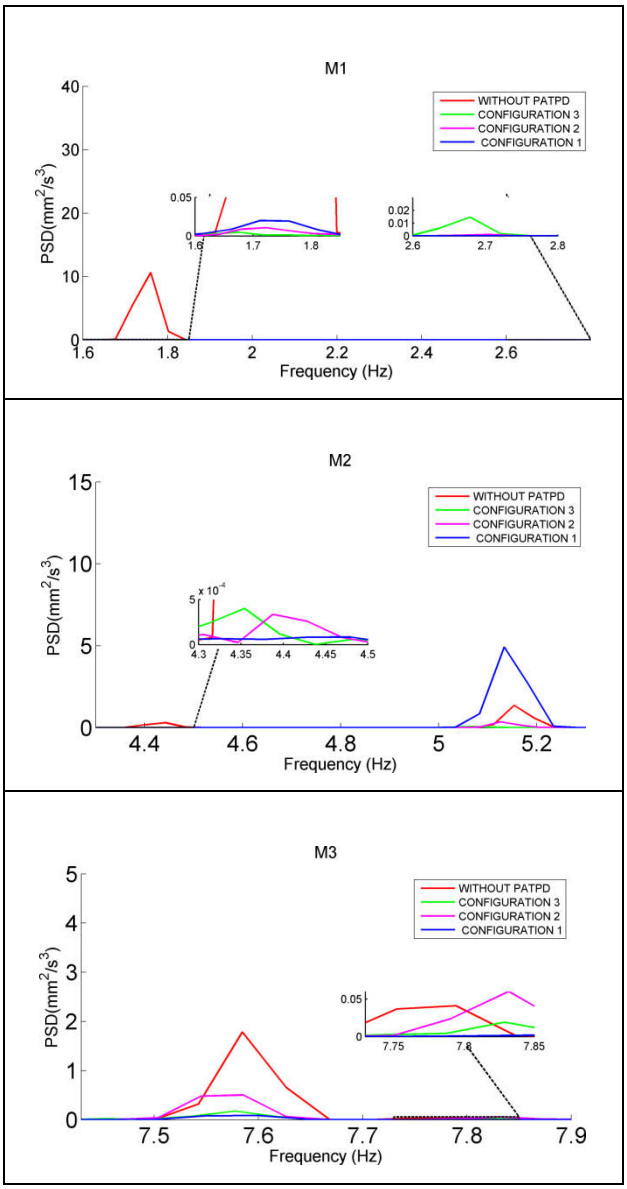

Figure 153: Magnified Power Spectral Density (PSD) storey 1 of the acceleration in the x-direction of the model under free coupled vibration, configuration 1,2 and 3

For second natural frequency with PSD peak, 4.446Hz, for torsion across all 3 storeys, all configurations tested provide significant damping of the model's vibrations across all 3 storeys. For translation with PSD peak, 5.164Hz, across all 3 storeys, configurations 2 and 3 provide slight control effect, with configuration 1 increasing the density of the frequency.

For third natural frequency with PSD peak, 7.584Hz, for translation all provide control with configuration 1 being best. Torsion with PSD peak, 7.792Hz, shows a slight increase.

Overall PSD peak increases were minimal in comparison to the reduction gained in PSD peak for the first natural frequency.

5.4.1.6 Coupled Vibration (Translation in Y-direction and torsion)

The model was given an initial torsional displacement and displacement in y-direction simultaneously, respective acceleration measured in the y-direction. The damping effect of each can be seen in the graphs to follow.

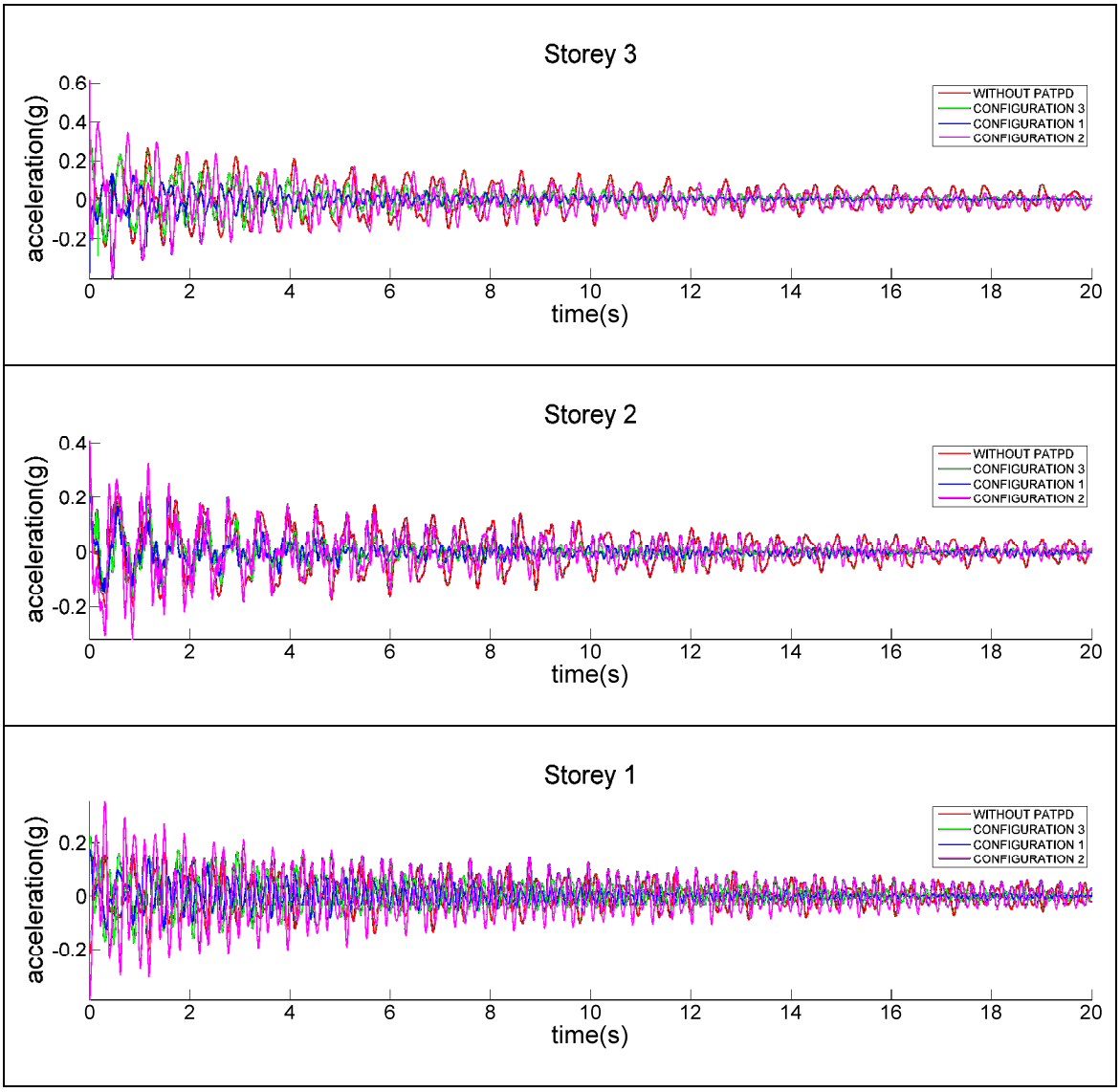

Figure 154: Time history of acceleration response in y-direction per storey for free coupled vibration, configuration 1, 2 and 3

Figure 154 that the PATPD starts moving; the acceleration peaks generated in the damped model are as high as those generated in the undamped model. However, these high accelerations subside and the accelerations rapidly decrease compared to that of the undamped model. As is expected the accelerations experienced in storey 3 are highest and the positive damping effect of the PATPD is still significant. The best control effect

is seen in storey 3, since the damper was installed on this storey. Configuration 2 has similar acceleration to undamped model.

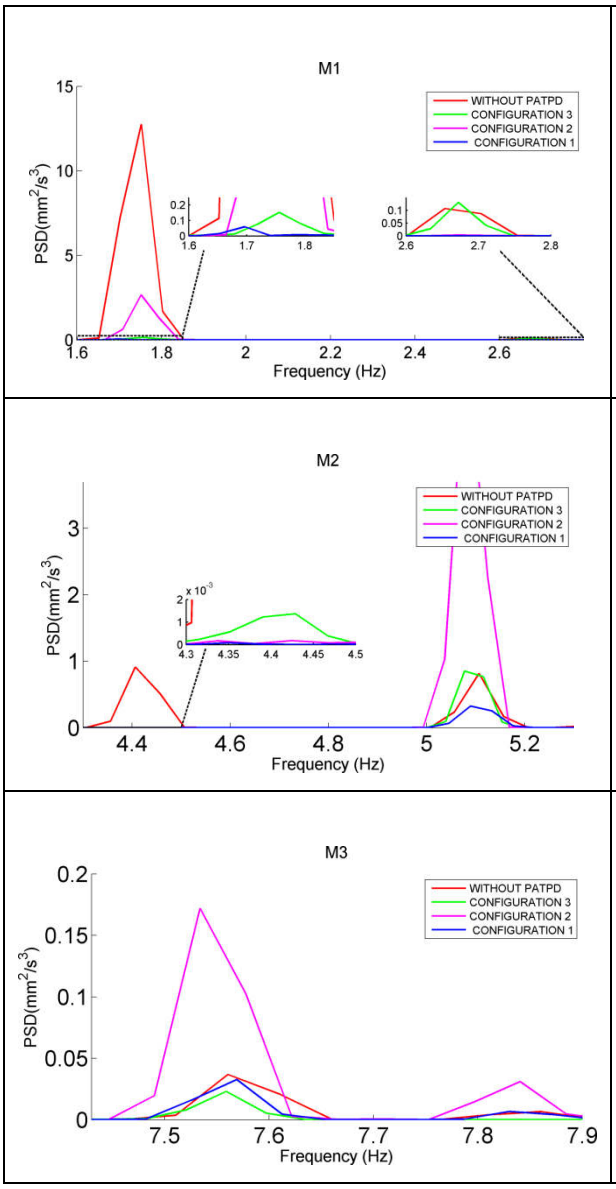

Figure 155: Magnified Power Spectral Density (PSD) storey 3 of the acceleration in the y-direction of the model under free coupled vibration, configuration 1,2 and 3

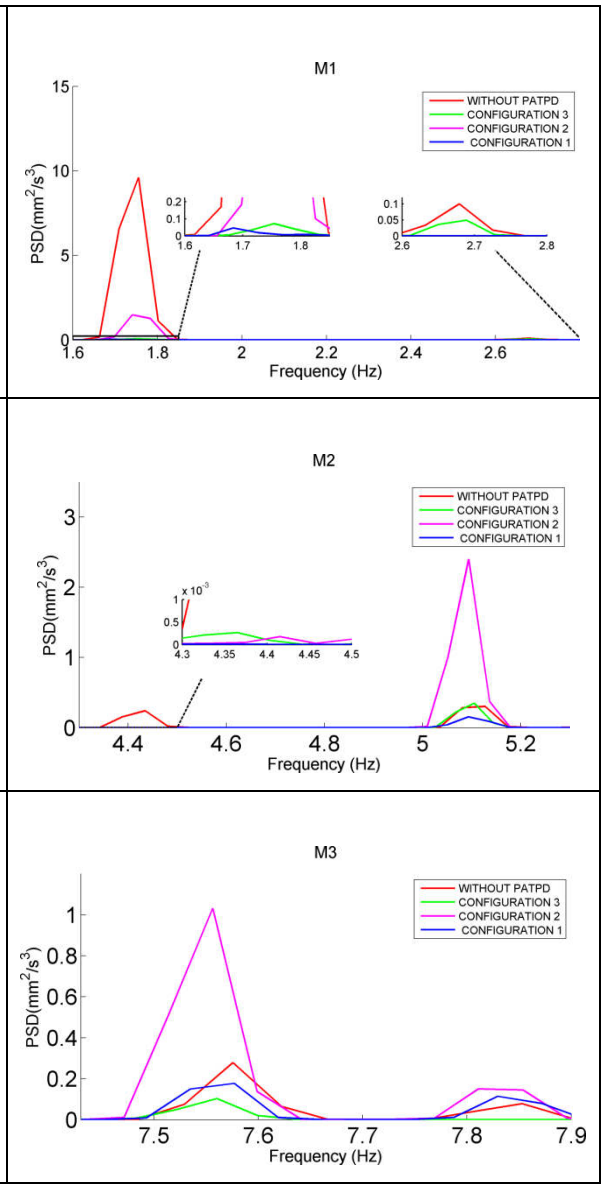

Figure 156: Magnified Power Spectral Density (PSD) storey 2 of the acceleration in the y-direction of the model under free coupled vibration, configuration 1, 2 and 3

Figure 155, Figure 156 and Figure 157 show for first natural frequency with PSD peak, 1.747Hz and 2.680Hz, for both translation and torsion, all 3 configurations tested provide significant damping of the model's vibrations across all 3 storeys, with configurations 1 and 3 demonstrating best control effect, configuration 2 the least.

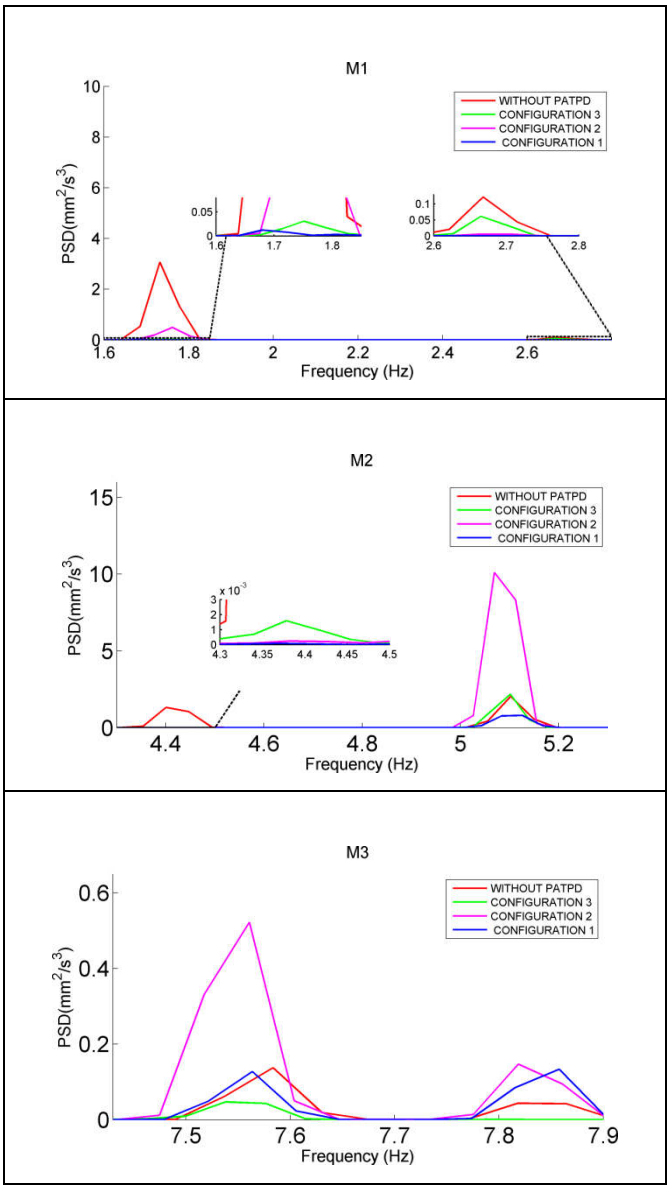

Figure 157: Magnified Power Spectral Density (PSD) storey 1 of the acceleration in the y-direction of the model under free coupled vibration, configuration 1,2 and 3

For second natural frequency with PSD peak, 4.438 Hz, for torsion across all 3 storeys, all configurations tested provide significant damping of the model's vibrations across all 3 storeys, with configuration 3 the least. For translation, with PSD peak, 5.095Hz, across all 3 storeys, configuration 1 and 3 provide slight control effect, with configuration 2 significantly increasing the density of the frequency.

For third natural frequency with PSD peak, 7.569Hz and 7.842 Hz, for translation and torsion across all 3 storeys, configuration 1 and 3 provide slight control effect, with configuration 2 significantly increasing the density of the frequencies.

Overall PSD peak increases were minimal in comparison to the reduction gained in PSD peak for the first natural frequency.

5.4.2.0 Forced Vibration

5.4.2.1 Translational Vibration in the X-direction

The model was placed on the shake table in order to carry out the forced vibration tests. The PATPD's were connected one-by-one and the respective accelerations measured. The damping effect of each rope change of the PATPD can be seen in the graphs to follow.

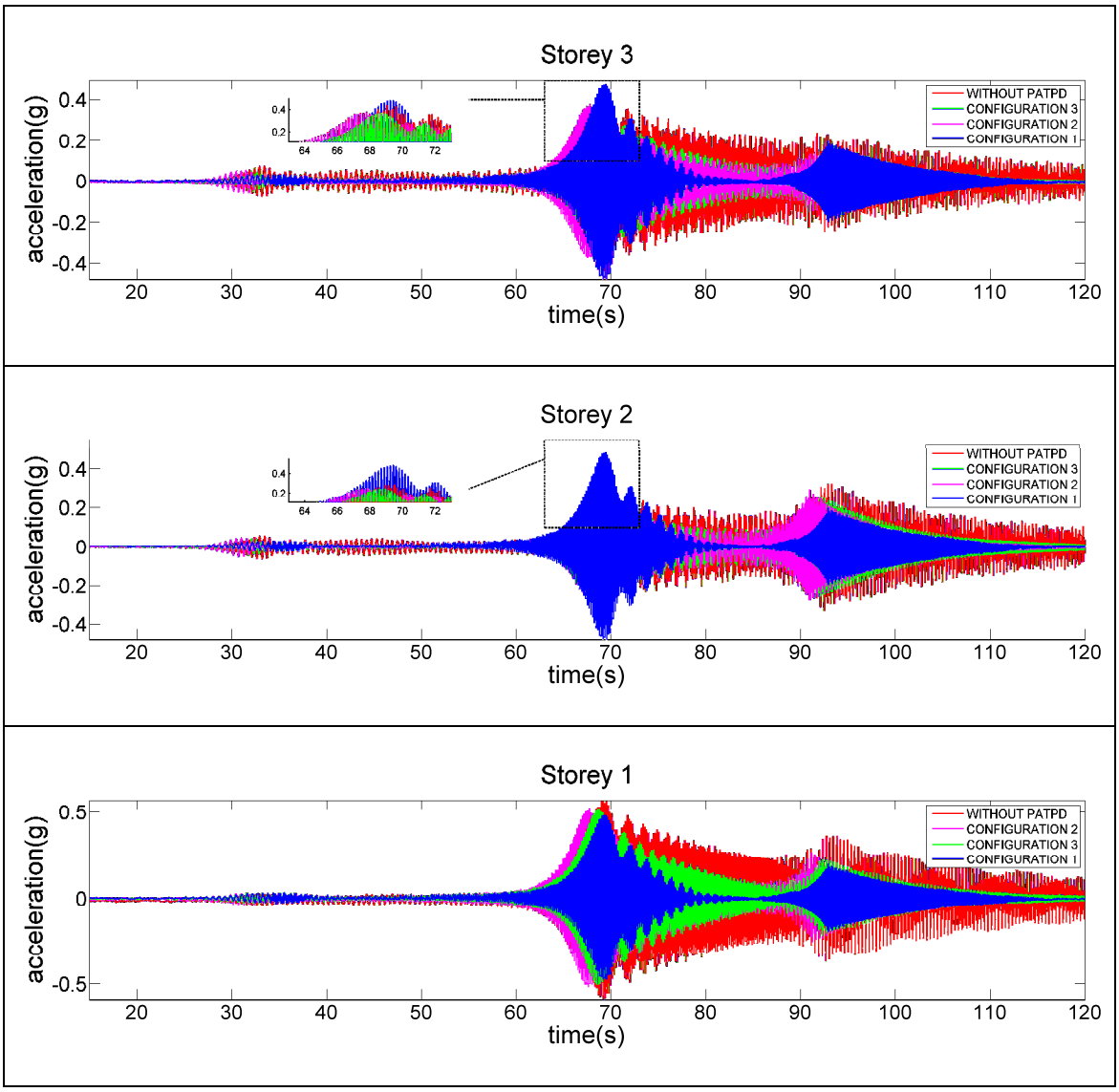

Figure 158: Time history of acceleration response per storey for forced translational vibration in x-direction, configuration 1, 2 and 3

Figure 158 shows for all 3 storeys that by adding the damper onto model the acceleration experience is significantly decreased for all rope types.

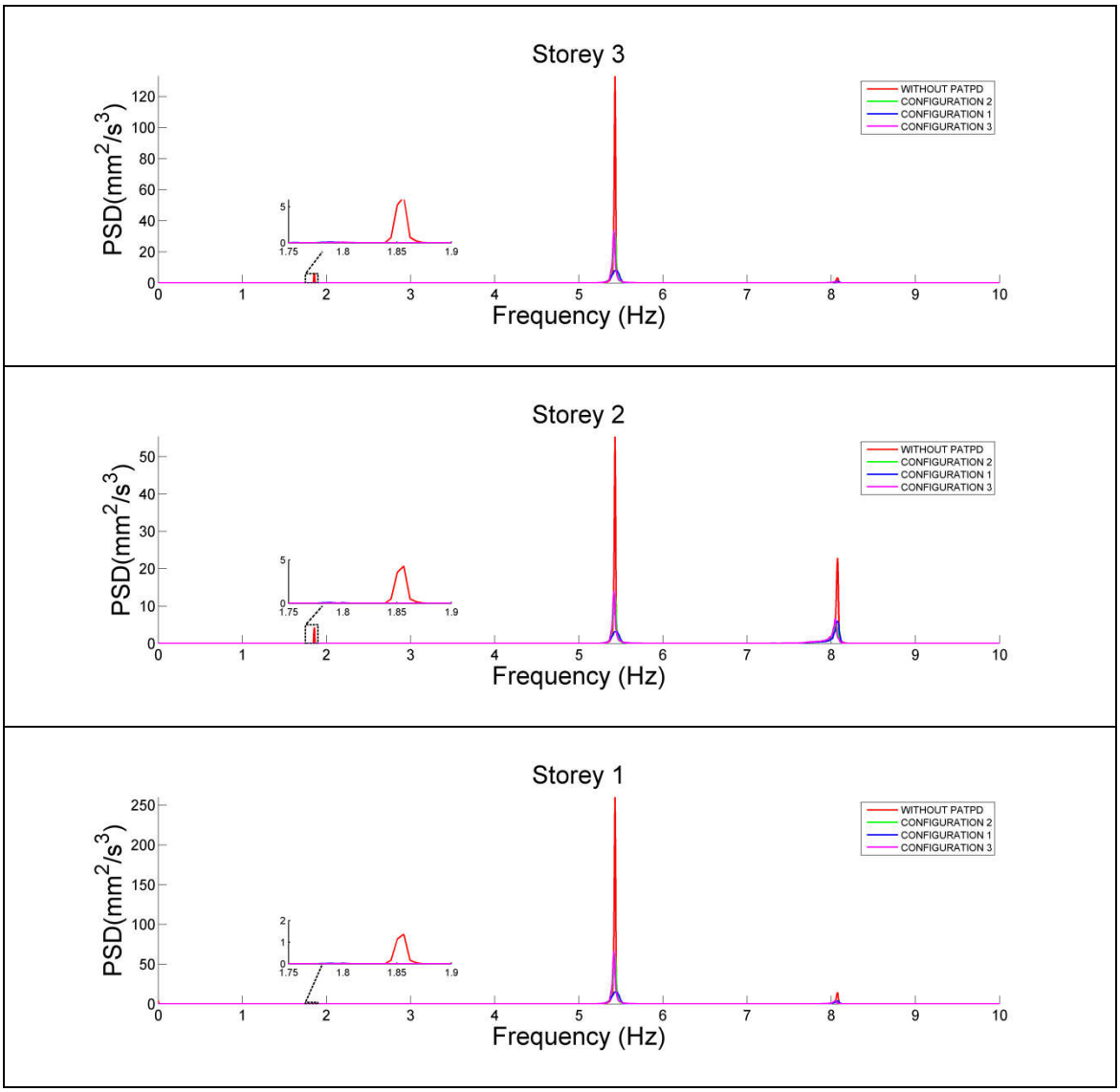

Figure 159: Power Spectral Density (PSD) of the acceleration response per storey under forced excitation in the x-direction, configuration 1, 2 and 3

Figure 159 shows PSD peaks at 1.856Hz, 5.429Hz and 8.047Hz. This corresponds to the models first, second and third frequencies. The positive control effect is evident as PSD peaks for all 3 frequencies are significantly reduced by all connection configurations used.

5.4.2.2 Translational Vibration in the Y-direction

The model was placed on the shake table in order to carry out the forced vibration tests. The PATPD's were connected one-by-one and the respective accelerations measured. The damping effect of each of the PATPD masses can be seen in the graphs to follow.

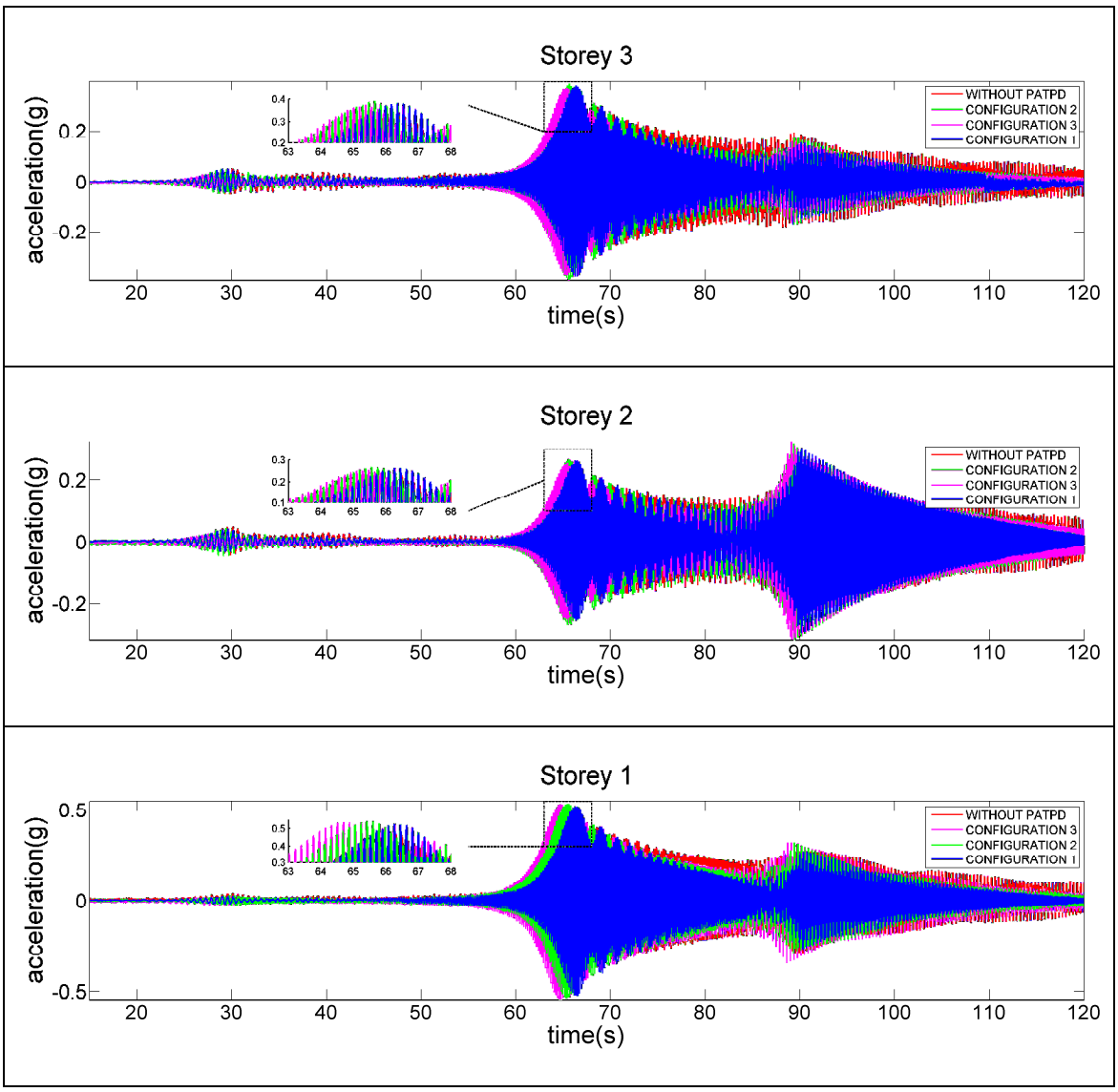

Figure 160: Time history of acceleration response per storey for forced translational vibration in y-direction, configuration 1, 2 and 3

Figure 160 shows for all 3 storeys that by adding the damper onto model the acceleration experience is significantly decreased for all configurations used.

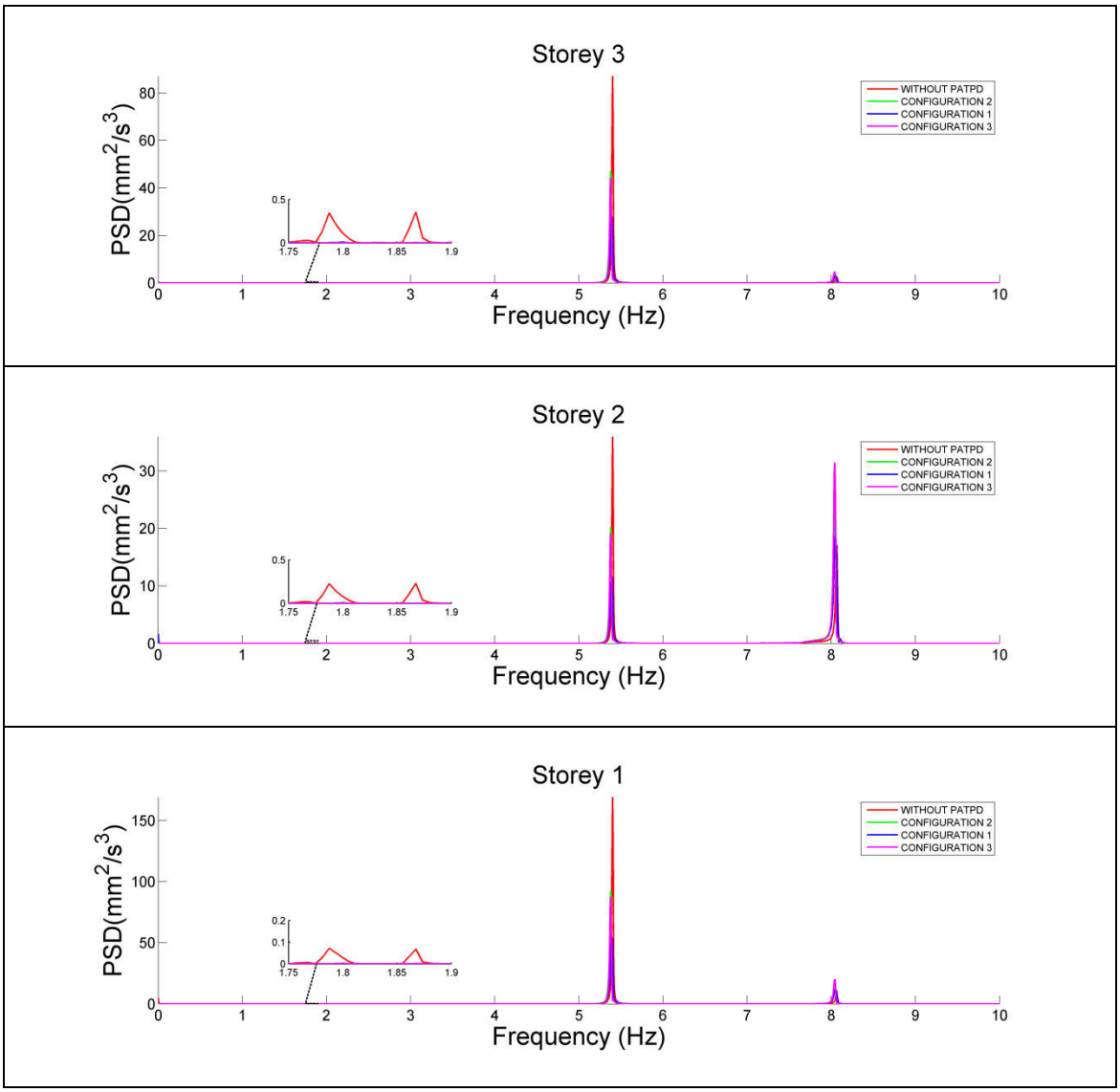

Figure 161: Power Spectral Density (PSD) of the acceleration response per storey under forced excitation in the y-direction n, configuration 1, 2 and 3

Figure 161 shows PSD peaks at 1.787Hz, 5.399Hz and 8.065Hz. This corresponds to the models first, second and third frequencies. The positive control effect is evident as PSD peaks for all 3 frequencies are significantly reduced. This is true for all configurations used.

Control effect of PATPD is better in x-direction than in y-direction.

5.4.3.0 Summary

Free Vibration

This set of parameter tests indicates better control in x than in y direction.

All configurations provided control effect to the first natural frequency for all free vibration tests for all storeys, except Configuration 3 (transverse only) which did not control first natural frequency for storey 1 under torsional vibration (y direction). Configuration 2 behaves best for control of natural frequency 1 and worst for 2 and 3. Configuration 1behaves consistently which is the primary model configuration.

A greater the number of connections improves behaviour. Also, having more connections along the x-axis spaced more closely together would improve imparting of inertia reaction force as well as the drive force from structure which is transferred through pulleys thus improving control.

Forced Vibration

For Forced Vibration the PATPD provides significant control to all 3 frequencies for all connection configurations tested.

The results reveal that the PATPD performs better in translation the x –direction than the y-direction.

5.5 Parameter Test 5: Effect of changing connection height

Tests were carried out using two different pulley heights[9]: (a) height of primary model of 9cm, (b) height of 15cm.

All other parameters during these tests remained constant, with the test model having a mass of 42.09kg and a storey height of 37cm per storey. As with the previous tests the model was given an initial displacement, in the according directions, and the acceleration with and without the damper measured.

The data for each case is processed and they are plotted together on graphs such that extrapolations and comparisons can be made.

5.5.1 Free Vibration

5.5.1.1 Translational Vibration in the X-direction

The model was given an initial displacement in the x-direction and respective acceleration measured. The damping effect of each can be seen in the graphs to follow.

[9] These configurations can be found on page 58

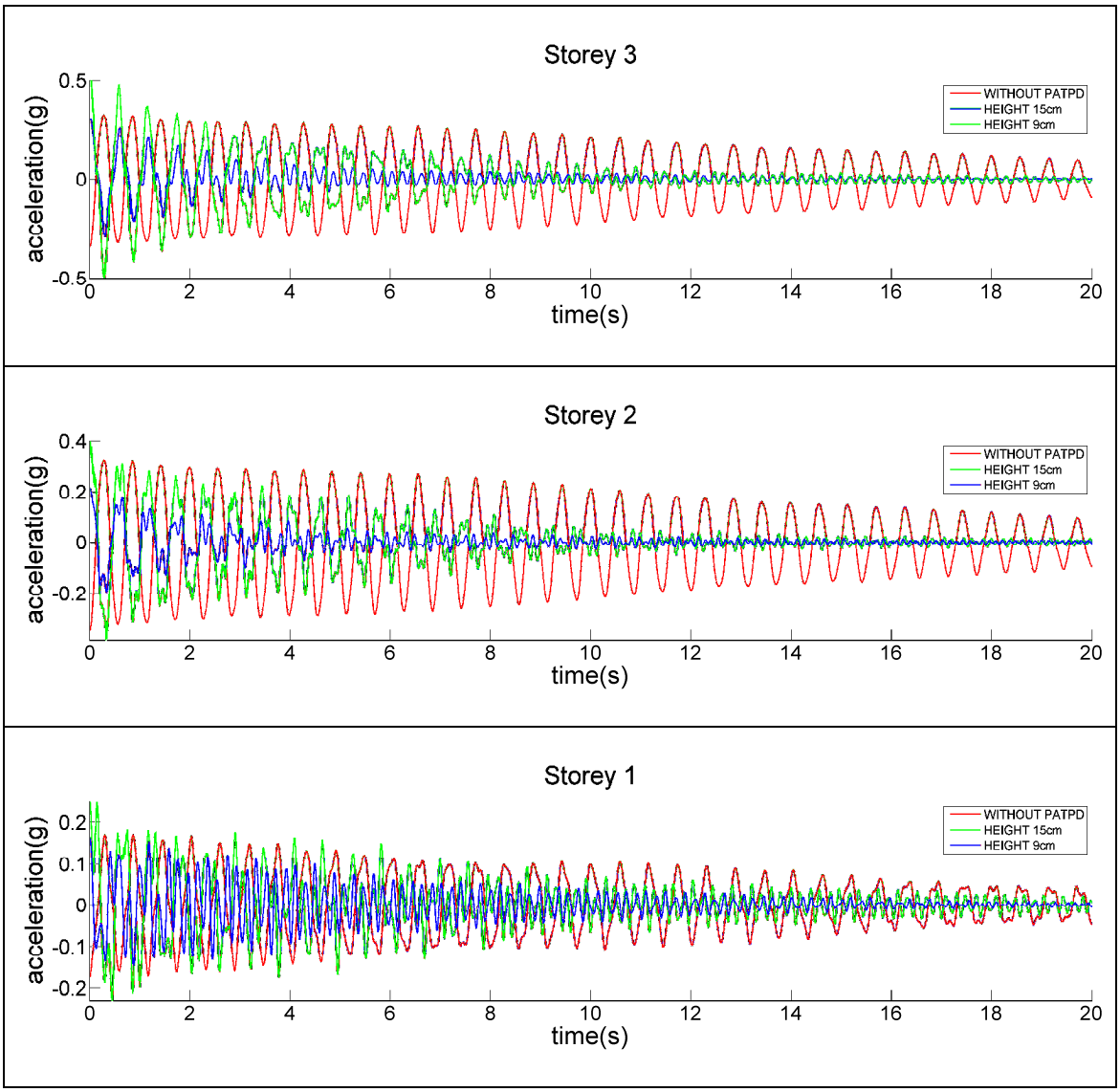

Figure 162: Time history of acceleration response per storey for free translational vibration in x-direction, connection height 15cm and height 9cm

Figure 162 shows that for both heights tested as the PATPD started moving; the acceleration peaks generated in the damped model are as high as those generated in the undamped model. However, these high accelerations subside and the accelerations rapidly decrease compared to that of the undamped model. As is expected the accelerations experienced in storey 3 are highest and the positive damping effect of the PATPD was still significant for both heights tested. The best control effect is seen in storey 3, since the damper was installed on this storey.

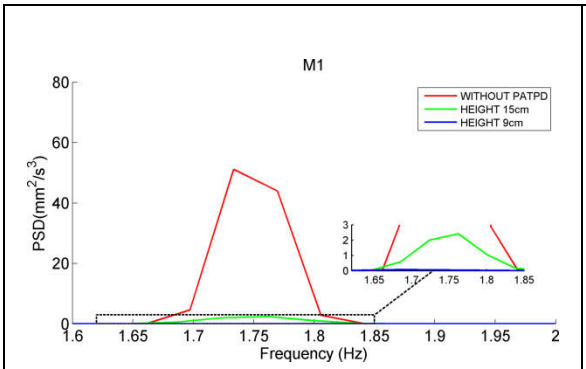

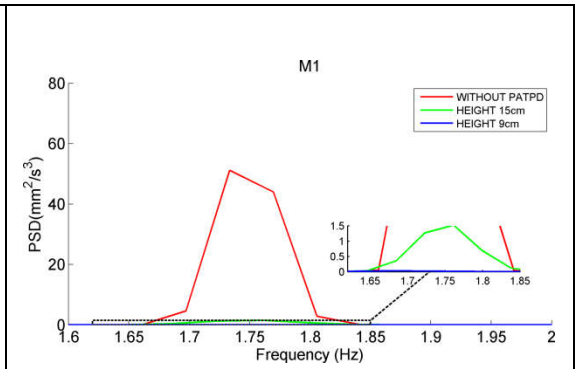

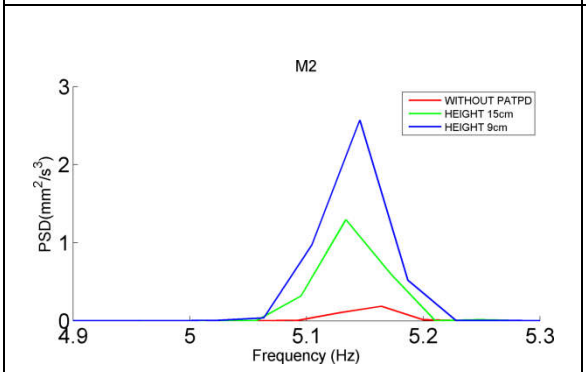

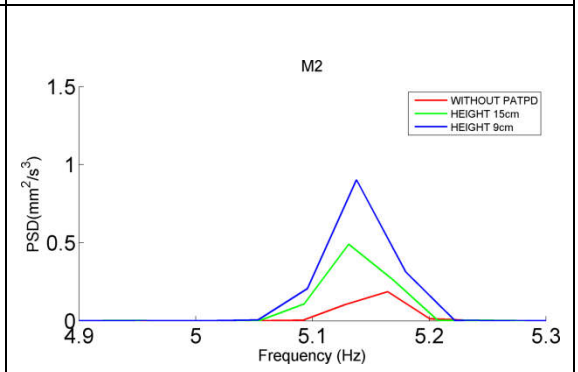

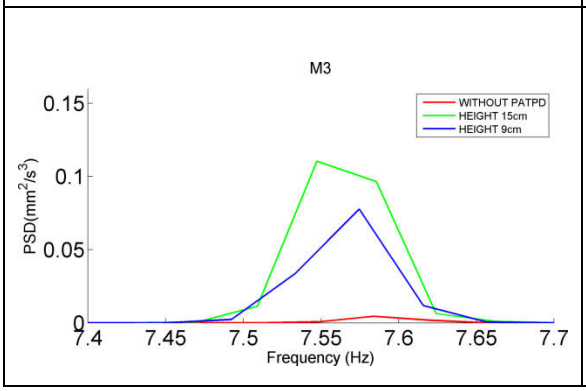

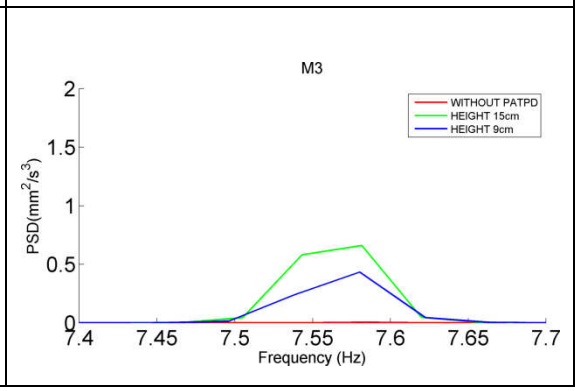

Figure 163: Magnified Power Spectral Density (PSD) storey 3 of the acceleration of the model under free translational vibration in the x-direction , connection height 15cm and height 9cm

Figure 164: Magnified Power Spectral Density (PSD) storey 2 of the acceleration of the model under free translational vibration in the x-direction, connection height 15cm and height 9cm

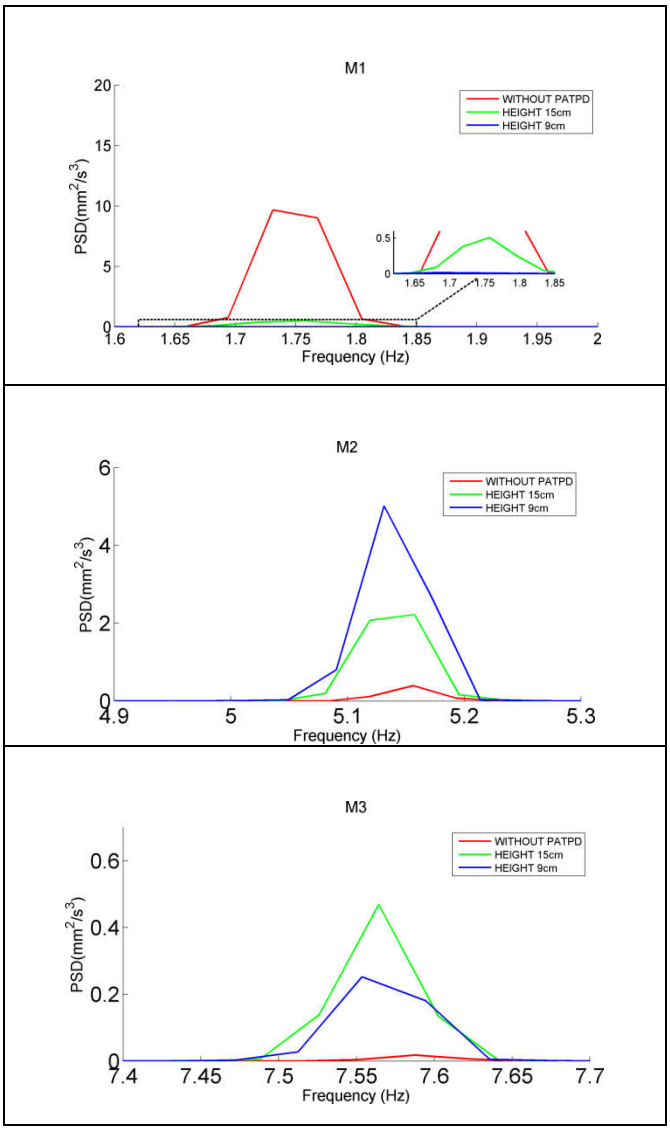

Figure 165: Magnified Power Spectral Density (PSD) storey 1 of the acceleration of the model under free translational vibration in the x-direction, connection height 15cm and height 9cm

Figure 163, Figure 164 and Figure 165 shows for first natural frequency with PSD peak, 1.733Hz, both heights tested produced significant damping of the model's vibrations across all storeys, reducing the PSD peak by at least 90%. The lower height demonstrates slightly better control. Both second and third natural frequency with PSD peaks, 5.164Hz and 7.584Hz across all storeys for both heights, both heights cause significant increase in density of frequency. For M2 the lower height is least effective, and for M3 the higher height is least effective.

Overall PSD peak increases were minimal in comparison to the reduction gained in PSD peak for the first natural frequency.

5.5.1.2 Translational Vibration in the Y-direction

The model was given an initial displacement in the y-direction and respective acceleration measured. The damping effect of each PATPD can be seen in the graphs to follow.

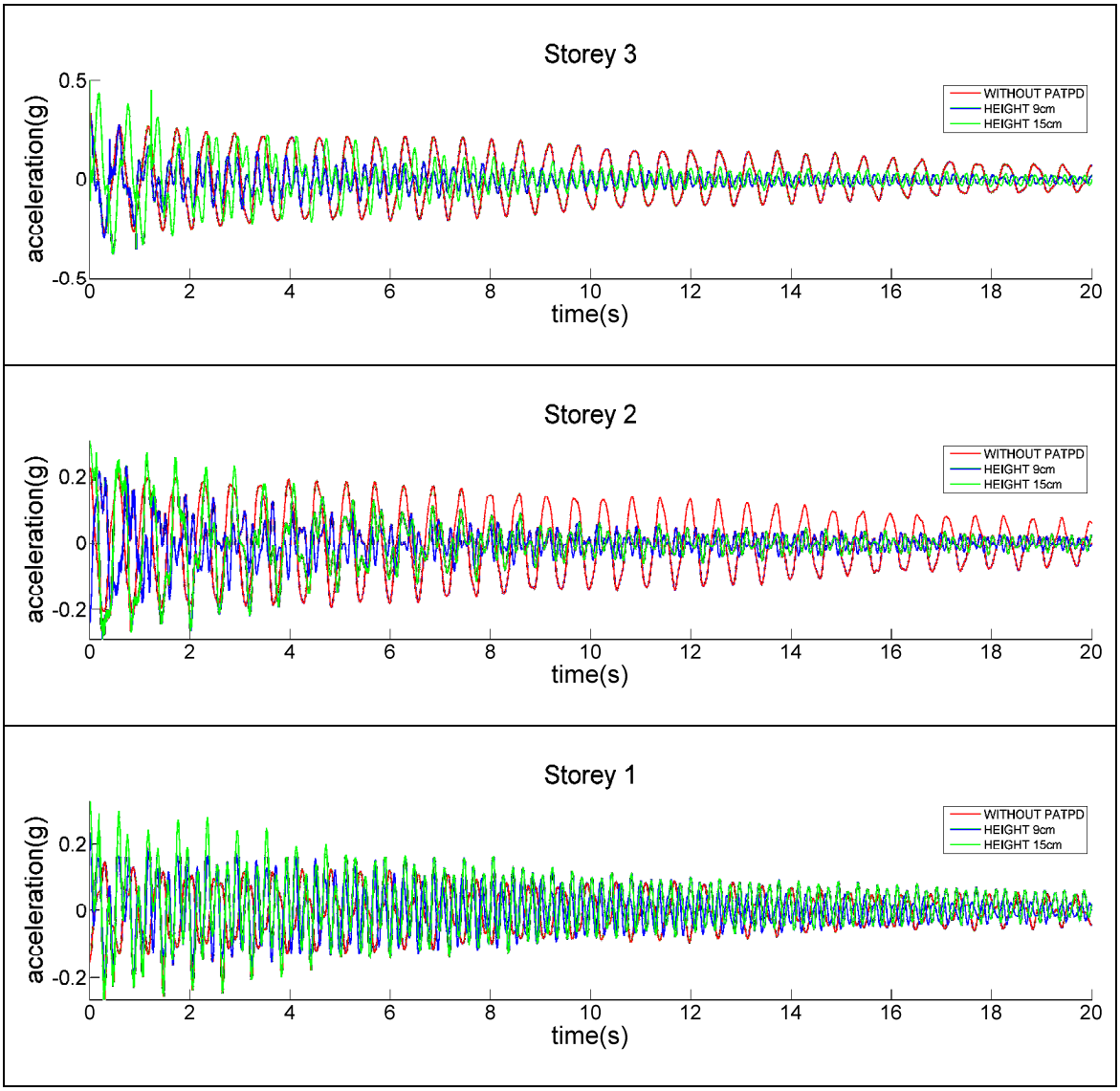

Figure 166: Time history of acceleration response per storey for free translational vibration in y-direction, connection height 15cm and height 9cm

Figure 166 shows that for both heights tested as the PATPD started moving; the acceleration peaks generated in the damped model are as high as those generated in the undamped model. However, these high accelerations subside and the accelerations rapidly decrease compared to that of the undamped model. As is expected the accelerations experienced in storey 3 are highest and the positive damping effect of the

PATPD was still significant for both heights tested. The best control effect is seen in storey 3, since the damper was installed on this storey.

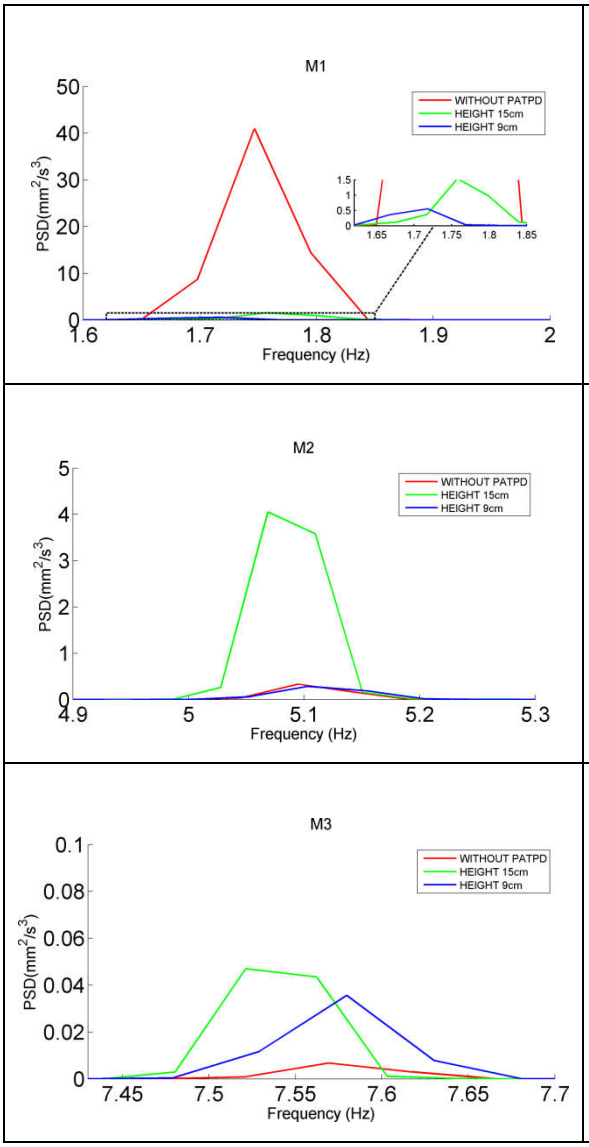

Figure 167: Magnified Power Spectral Density (PSD) storey 3 of the acceleration of the model under free translational vibration in the y-direction connection height 15cm and height 9cm

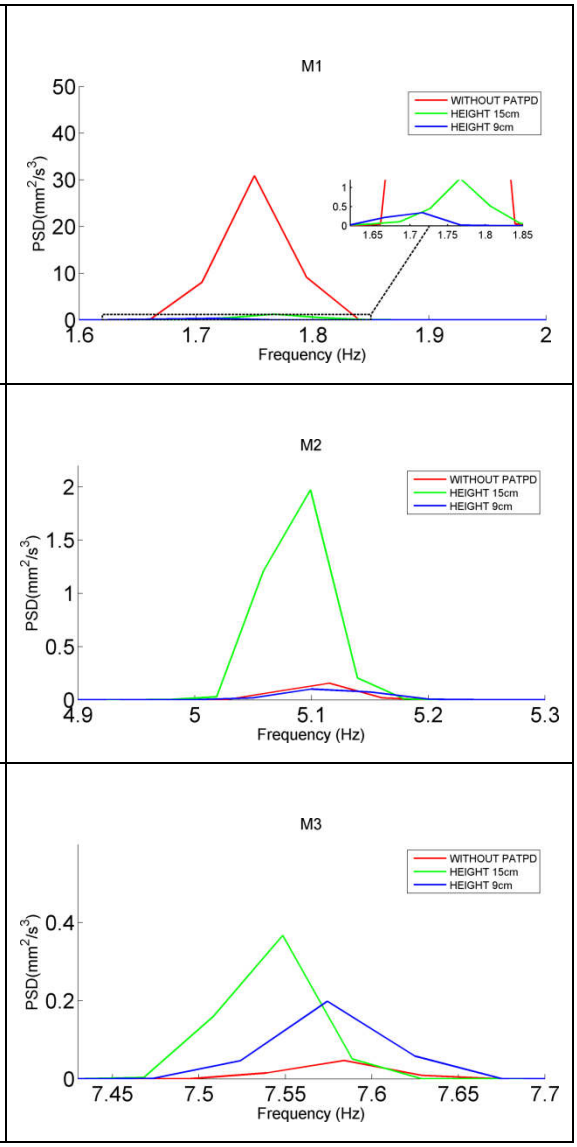

Figure 168: Magnified Power Spectral Density (PSD) storey 2 of the acceleration of the model under free translational vibration in the y-direction, connection height 15cm and height 9cm

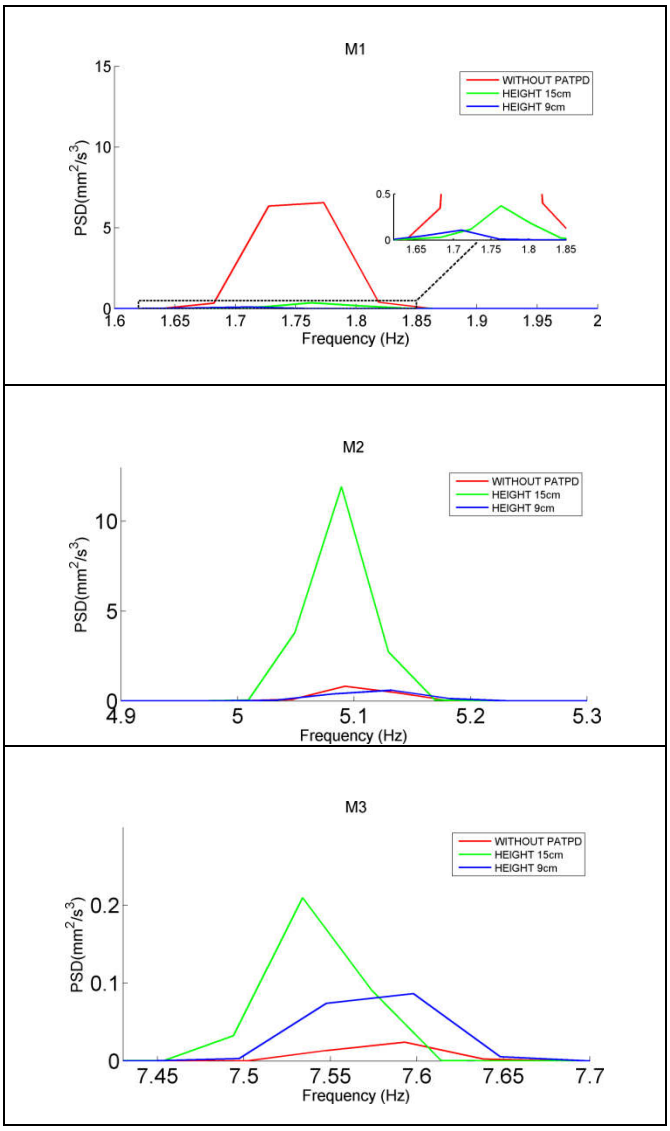

Figure 169: Magnified Power Spectral Density (PSD) storey 1 of the acceleration of the model under free translational vibration in the y-direction, connection height 15cm and height 9cm

Figure 167, Figure 168 and Figure 169 shows for first natural frequency with PSD peak, 1.747Hz, both heights tested produced significant damping of the model's vibrations across all storeys, reducing the PSD peak by at least 90%. The lower height demonstrates slightly better control. The second natural frequency with PSD peak, 5.095Hz, across all storeys for both heights, the lower height provides best control and the other height causes a significant increase in density of frequency.

For third natural frequency with PSD peak, 7.569Hz, both heights cause a slight increase in density.

Overall PSD peak increases were minimal in comparison to the reduction gained in PSD peak for the first natural frequency.

5.5.1.3 Torsional Vibration (acceleration measured in the X-direction)

The model was given an initial torsional displacement and respective acceleration measured in the x-direction. The damping effect of each can be seen in the graphs to follow.

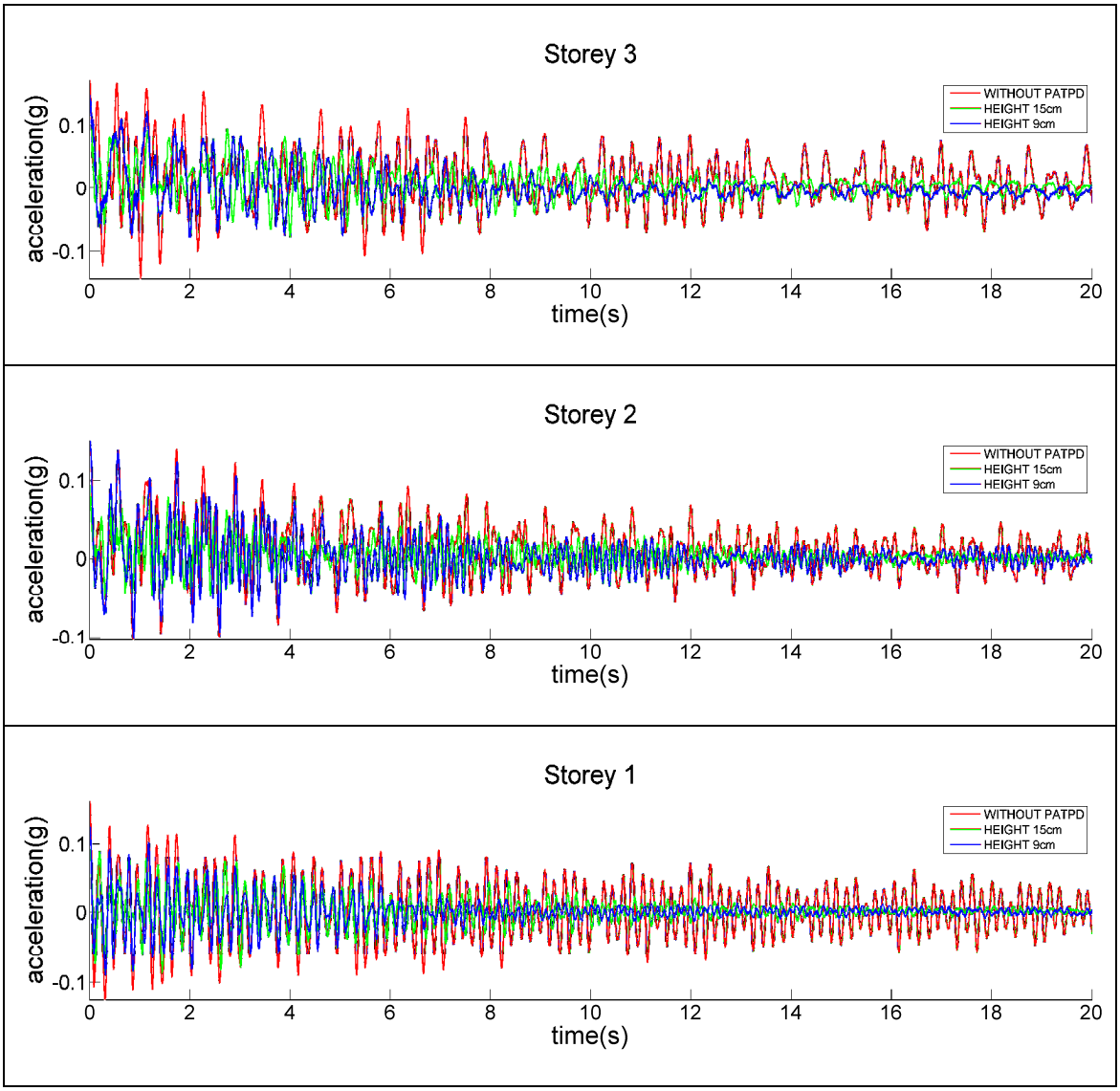

Figure 170: Time history of acceleration response in x-direction per storey for free torsional vibration, height 15cm and height 9cm

Figure 170 shows that for both heights tested as the PATPD started moving; the acceleration peaks generated in the damped model are as high as those generated in the undamped model. However, these high accelerations subside and the accelerations rapidly decrease compared to that of the undamped model. As is expected the accelerations experienced in storey 3 are highest and the positive damping effect of the

PATPD was still significant for both heights tested. The best control effect is seen in storey 3, since the damper was installed on this storey.

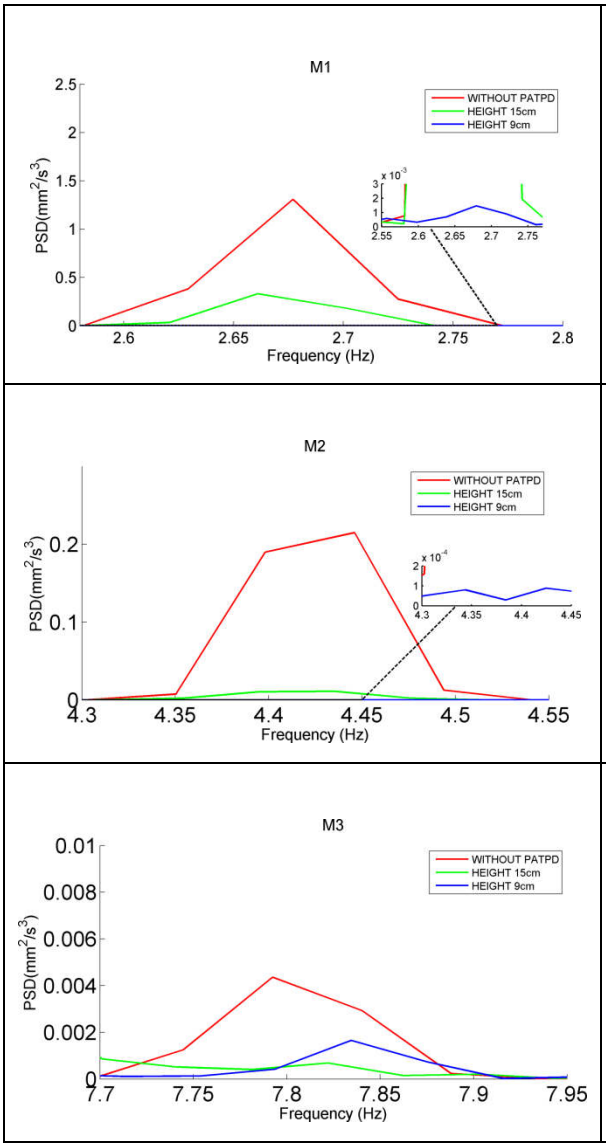

Figure 171: Magnified Power Spectral Density (PSD) storey 3 of the acceleration in the x-direction of the model under free torsional vibration, height 15cm and height 9cm

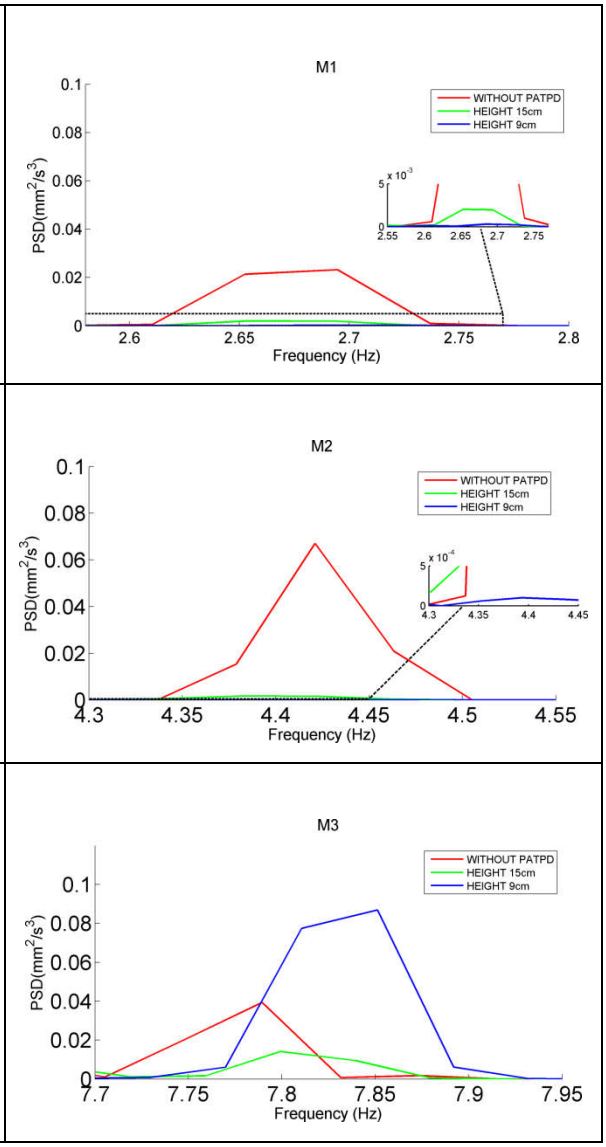

Figure 172: Magnified Power Spectral Density (PSD) storey 2 of the acceleration in the x-direction of the model under free torsional vibration, height 15cm and height 9cm

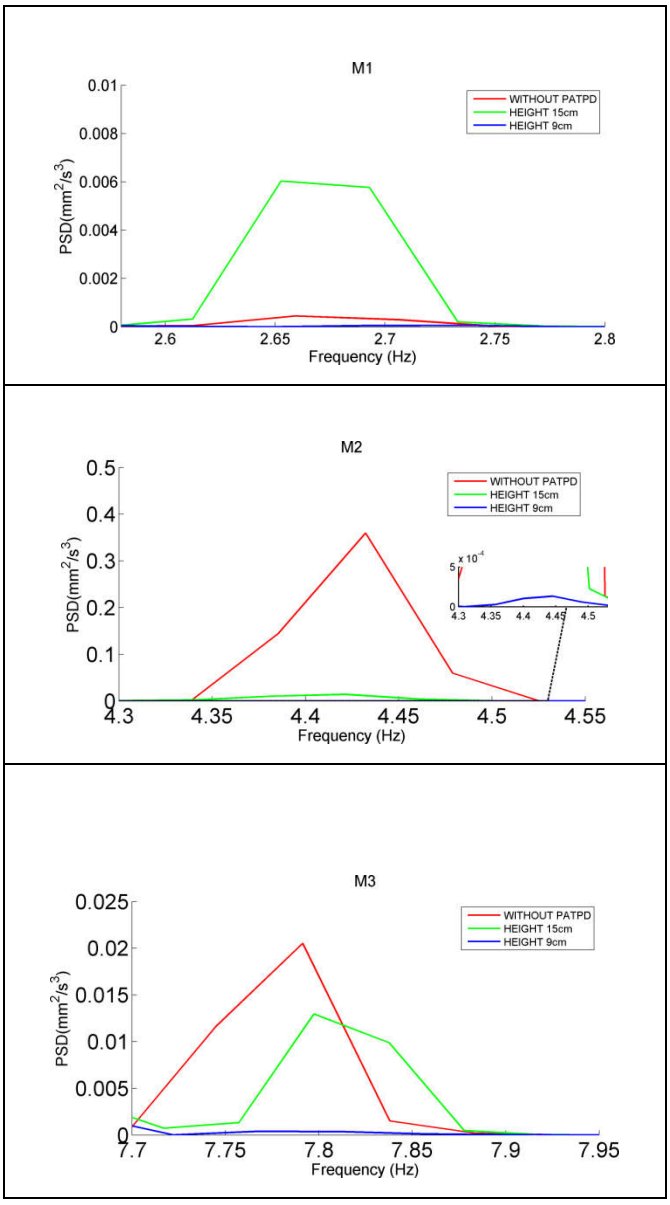

Figure 173: Magnified Power Spectral Density (PSD) storey 1 of the acceleration in the x-direction of the model under free torsional vibration, height 15cm and height 9cm

Figure 171, Figure 172 and Figure 173 shows for first and second natural frequency with PSD peak, 2.677Hz and 4.446Hz, both heights tested produced damping of the model's vibrations across all storeys, except for storey M1 storey 1 where higher height increases frequency.

For third natural frequency with PSD peak, 7.792Hz, storey 1 and 3 are controlled by both heights, storey 2, however, shows an increase in frequency for lower height.

Since we are concerned mainly with controlling the first natural frequency - only the 9cm height (lower one) provided significant damping of the model's vibrations.

5.5.1.4 Torsional Vibration (acceleration measured in the Y-direction)

The model was given an initial torsional displacement and respective acceleration measured in the y-direction. The damping effect of each can be seen in the graphs to follow.

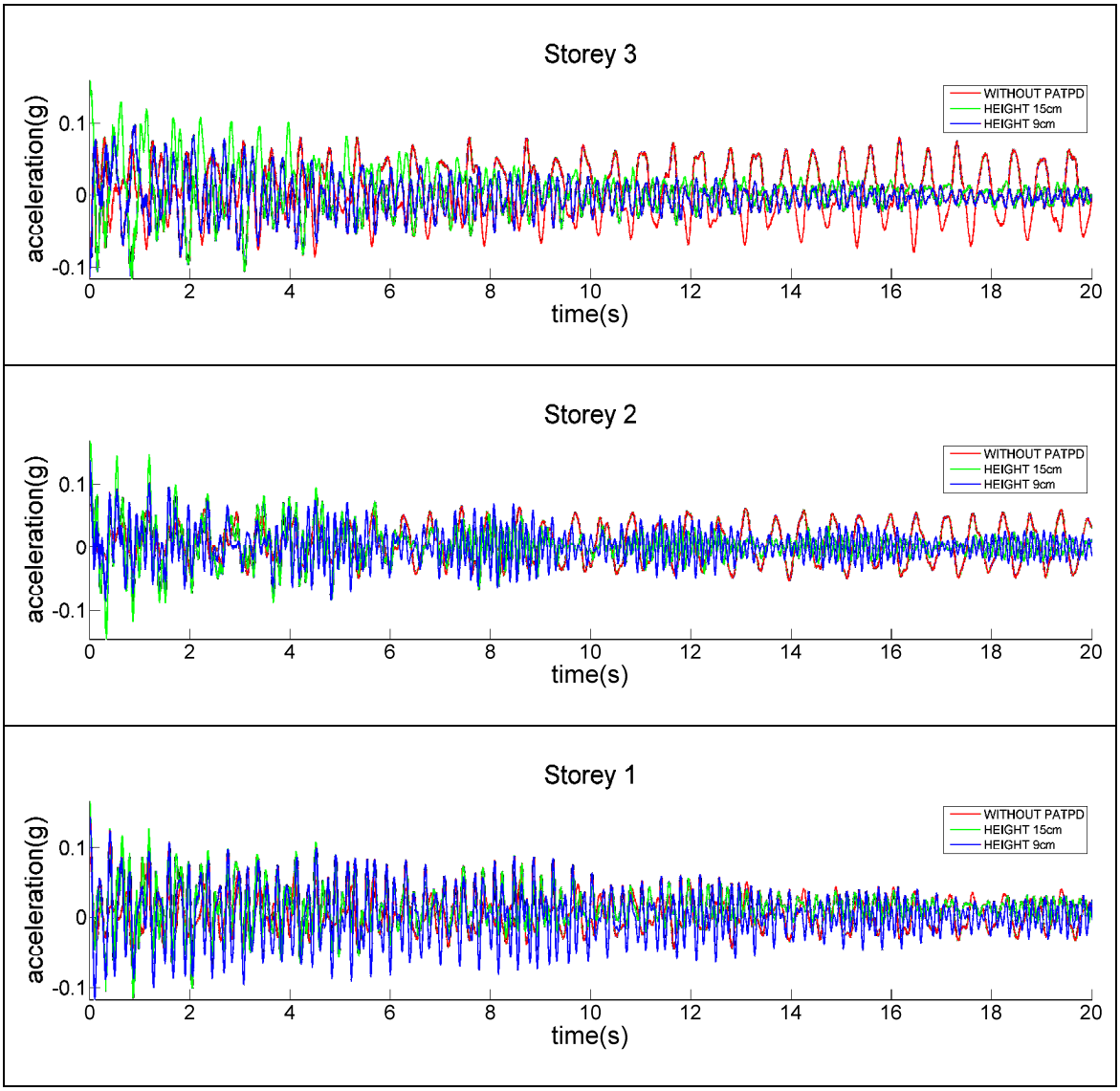

Figure 174: Time history of acceleration response in y-direction per storey for free torsional vibration, height 15cm and height 9cm

Figure 174 shows that for both heights tested as the PATPD started moving; the acceleration peaks generated in the damped model are as high as those generated in the undamped model. However, these high accelerations subside and the accelerations rapidly decrease compared to that of the undamped model. As is expected the accelerations experienced in storey 3 are highest and the positive damping effect of the

PATPD was still significant for both heights tested. The best control effect is seen in storey 3, since the damper was installed on this storey.

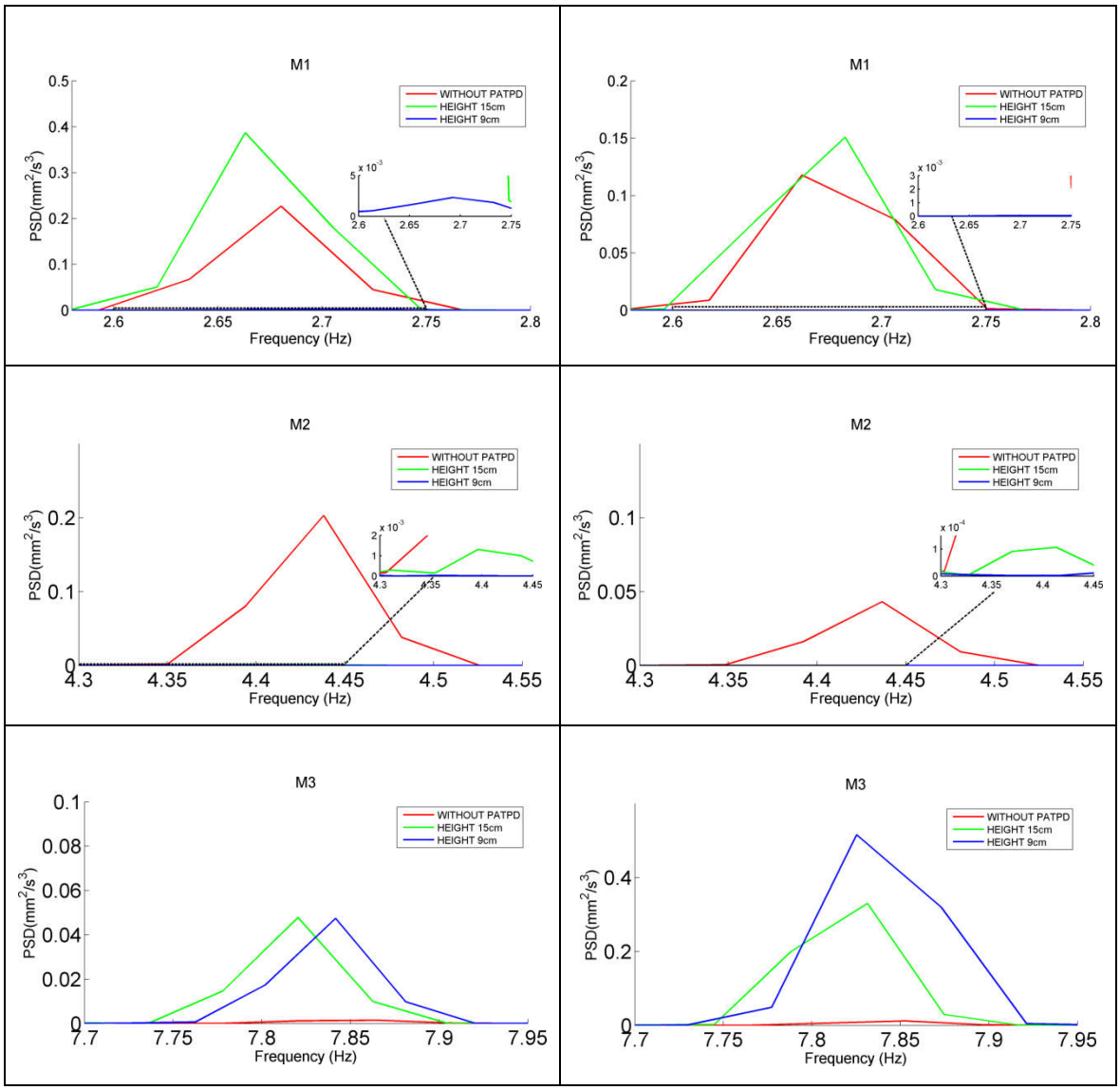

Figure 175: Magnified Power Spectral Density (PSD) storey 3 of the acceleration in the y-direction of the model under free torsional vibration , height 15cm and height 9cm

Figure 176: Magnified Power Spectral Density (PSD) storey 2 of the acceleration in the y-direction of the model under free torsional vibration , height 15cm and height 9cm

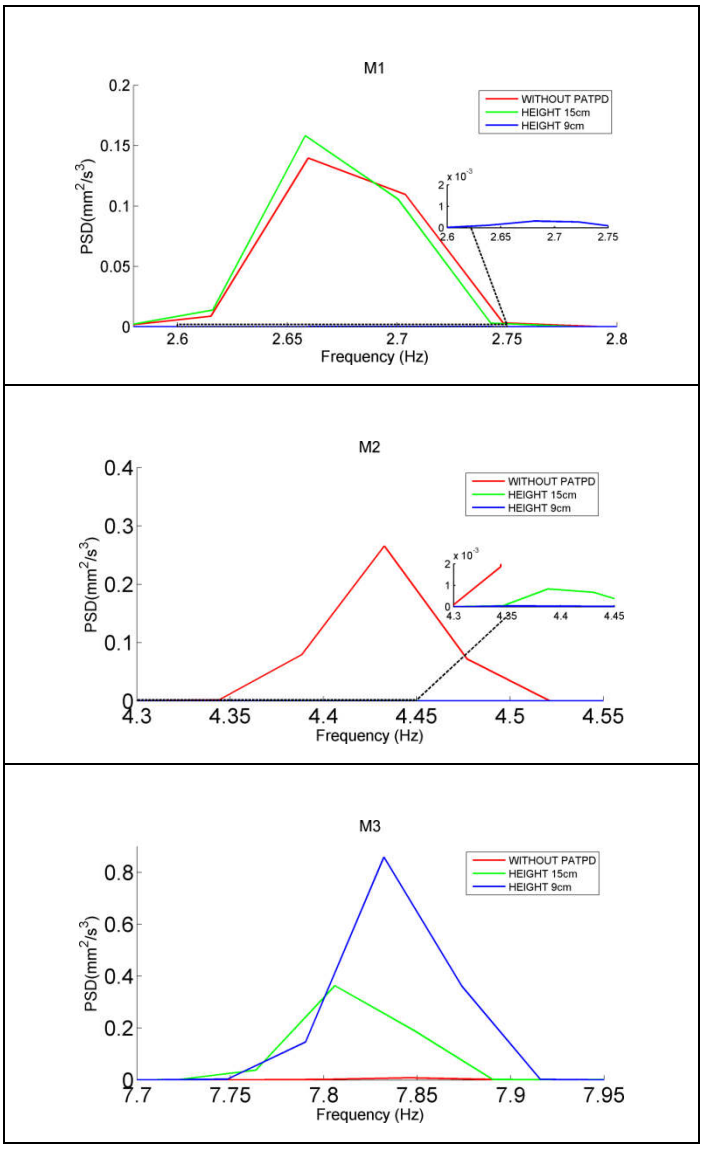

Figure 177: Magnified Power Spectral Density (PSD) storey 1 of the acceleration in the y-direction of the model under free torsional vibration , height 15cm and height 9cm

Figure 175, Figure 176 and Figure 177 shows for first natural frequency with PSD peak, 2.680Hz, only the lower height produced significant damping of the model's vibrations across all storeys, reducing the PSD peak by at least 98%.

For M second natural frequency with PSD peak, 4.438 Hz, across all storeys both heights cause significant control effect.

For third natural frequency with PSD peak, 7.842 Hz, both cause similar increase in frequency density.

Overall PSD peak increases were minimal in comparison to the reduction gained in PSD peak for the first natural frequency.

5.5.1.5 Coupled Vibration (Translation in X-direction and torsion)

The model was given an initial torsional displacement and displacement in x-direction simultaneously, respective acceleration measured in the x-direction. The damping effect of each can be seen in the graphs to follow.

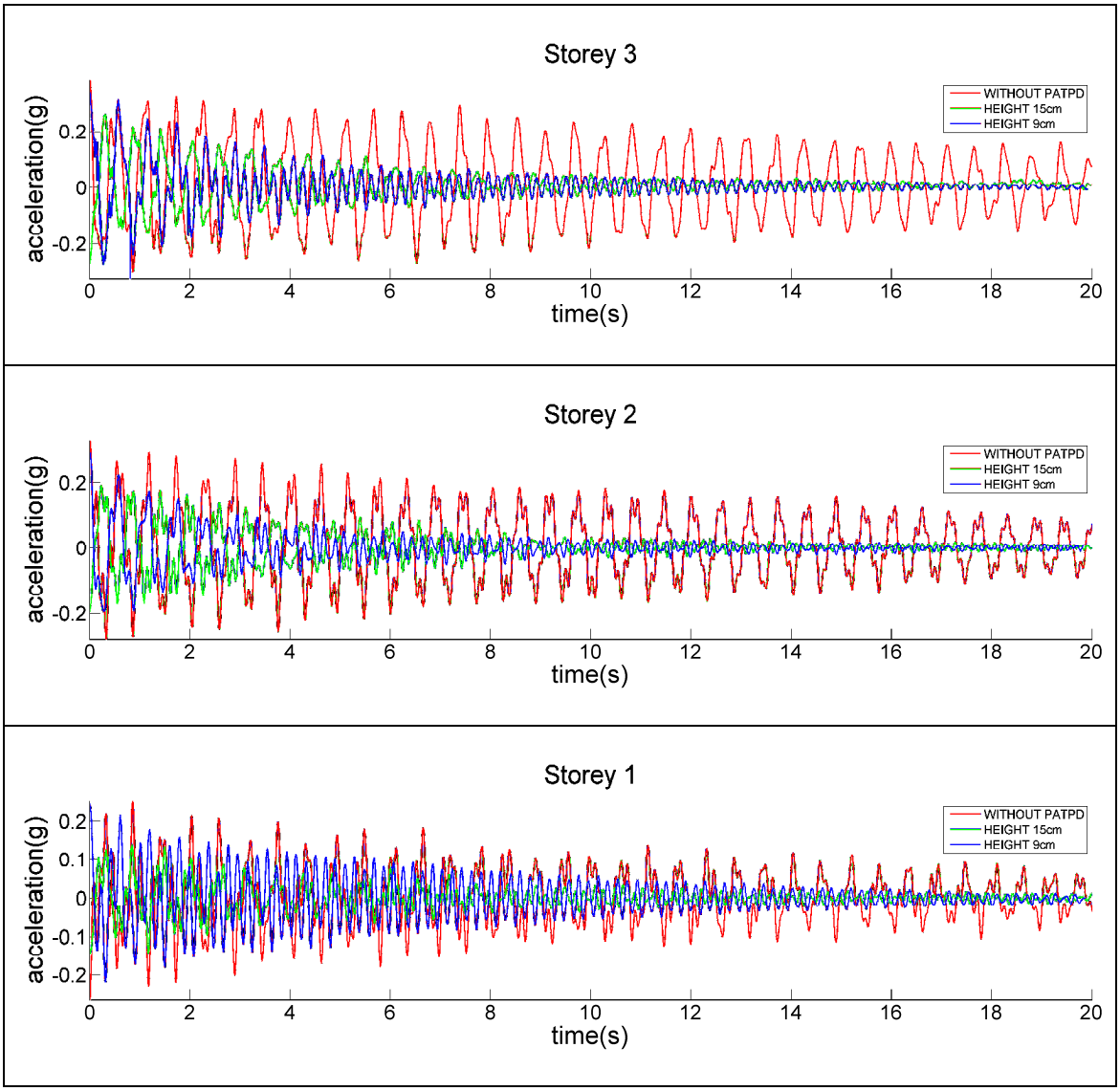

Figure 178: Time history of acceleration response in x-direction per storey for free coupled vibration, height 15cm and height 9cm

Figure 178 shows that for both heights tested as the PATPD started moving; the acceleration peaks generated in the damped model are as high as those generated in the undamped model. However, these high accelerations subside and the accelerations rapidly decrease compared to that of the undamped model. As is expected the accelerations experienced in storey 3 are highest and the positive damping effect of the

PATPD was still significant for both heights tested. The best control effect is seen in storey 3, since the damper was installed on this storey.

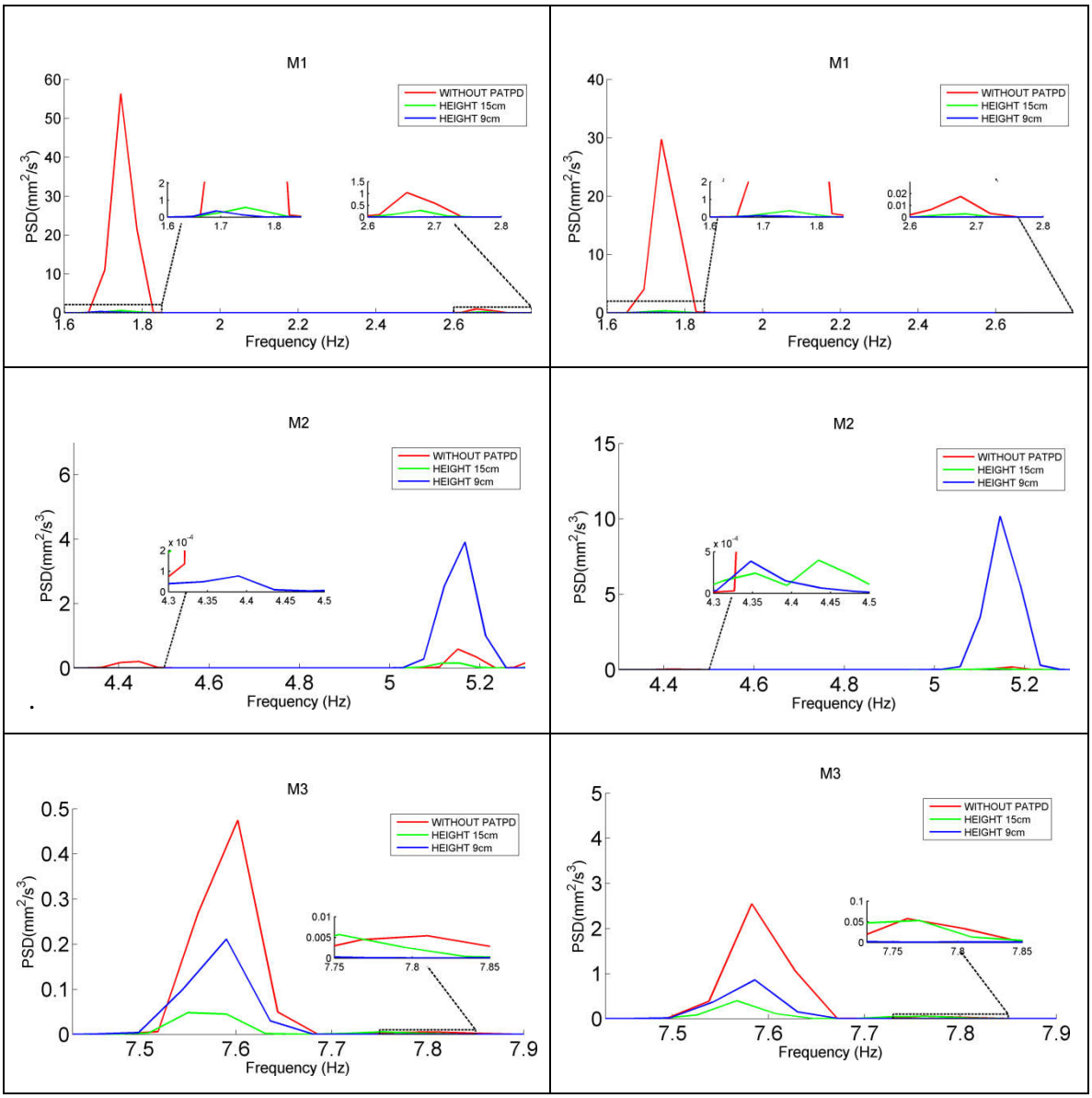

Figure 179: Magnified Power Spectral Density (PSD) storey 3 of the acceleration in the x-direction of the model under free coupled vibration, height 15cm and height 9cm

Figure 180: Magnified Power Spectral Density (PSD) storey 2 of the acceleration in the x-direction of the model under free coupled vibration, height 15cm and height 9cm

Figure 179, Figure 180 and Figure 181 show for first natural frequency with PSD peak, 1.733Hz and 2.677Hz , for both translation and torsion, both heights provide significant damping of the model's vibrations across all 3 storeys, with the lower height demonstrating best control effect overall.

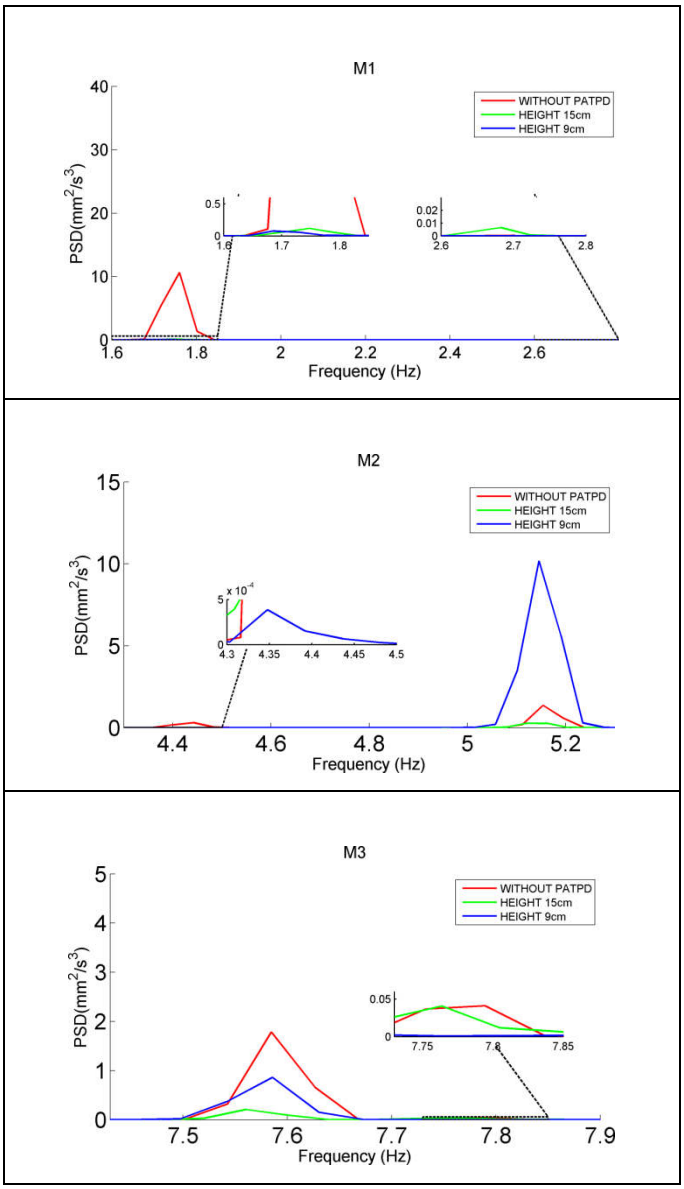

Figure 181: Magnified Power Spectral Density (PSD) storey 1 of the acceleration in the y-direction of the model under free coupled vibration, height 15cm and height 9cm

For second natural frequency with PSD peak, 4.446Hz, for torsion across all 3 storeys, both heights tested provide significant damping of the model's vibrations. For translation with PSD peak, 5.164Hz, across all 3 storeys, the 15cm height provides slight control effect, with the lower height causing significant increase in the density of the frequency.

For third natural frequency with PSD peak, 7.584Hz, for translation both provide control. For torsion, with PSD peak, 7.792Hz, only the lower height controls with higher height having no effect.

Overall PSD peak increases were minimal in comparison to the reduction gained in PSD peak for the first natural frequency.

5.5.1.6 Coupled Vibration (Translation in Y-direction and torsion)

The model was given an initial torsional displacement and displacement in y-direction simultaneously, respective acceleration measured in the y-direction. The damping effect of each can be seen in the graphs to follow.

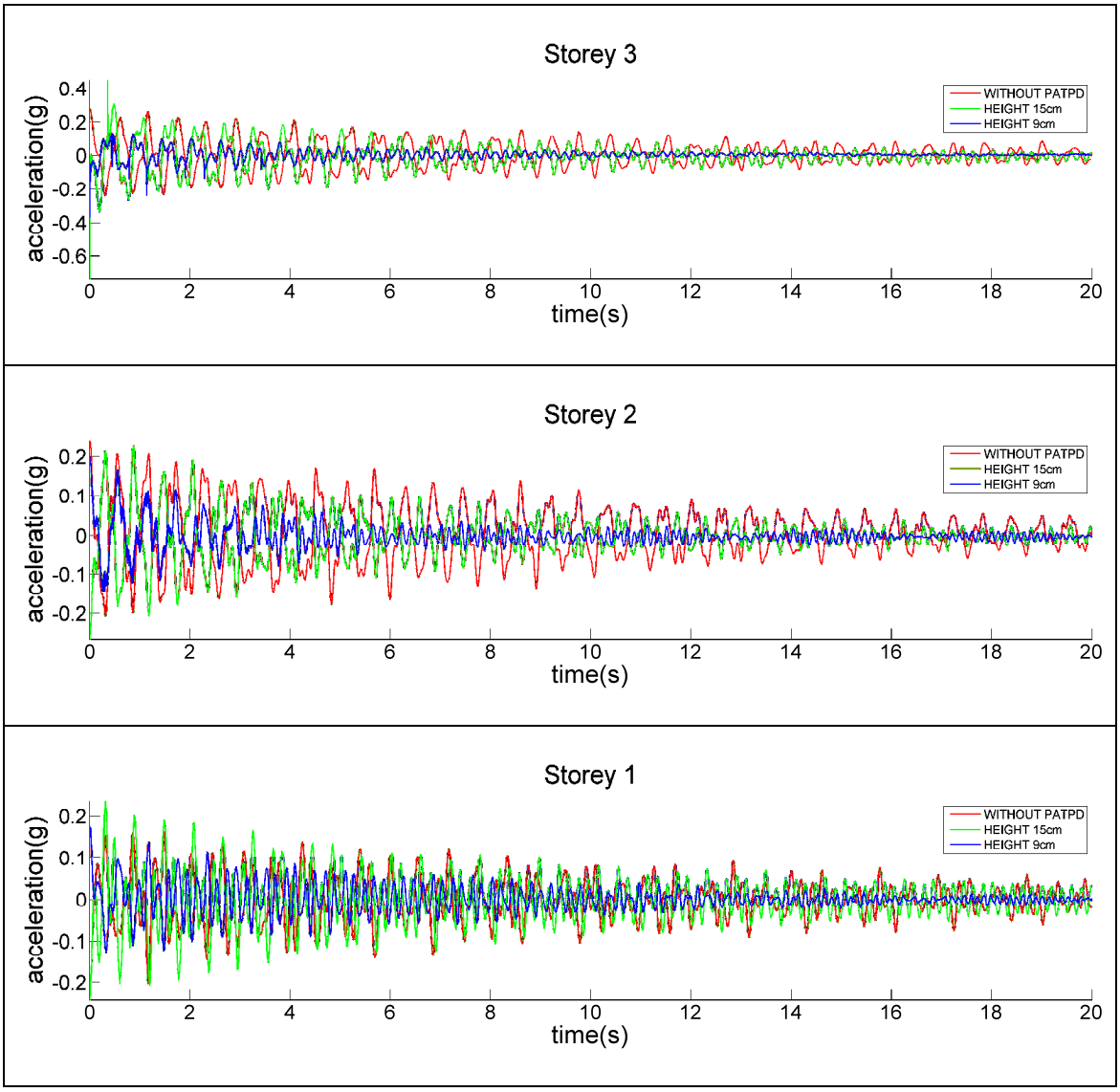

Figure 182: Time history of acceleration response in y-direction per storey for free coupled vibration, height 15cm and height 9cm

Figure 182 shows that for both heights tested as the PATPD started moving; the acceleration peaks generated in the damped model are as high as those generated in the undamped model. However, these high accelerations subside and the accelerations rapidly decrease compared to that of the undamped model. As is expected the accelerations experienced in storey 3 are highest and the positive damping effect of the

PATPD was still significant for both heights tested. The best control effect is seen in storey 3, since the damper was installed on this storey.

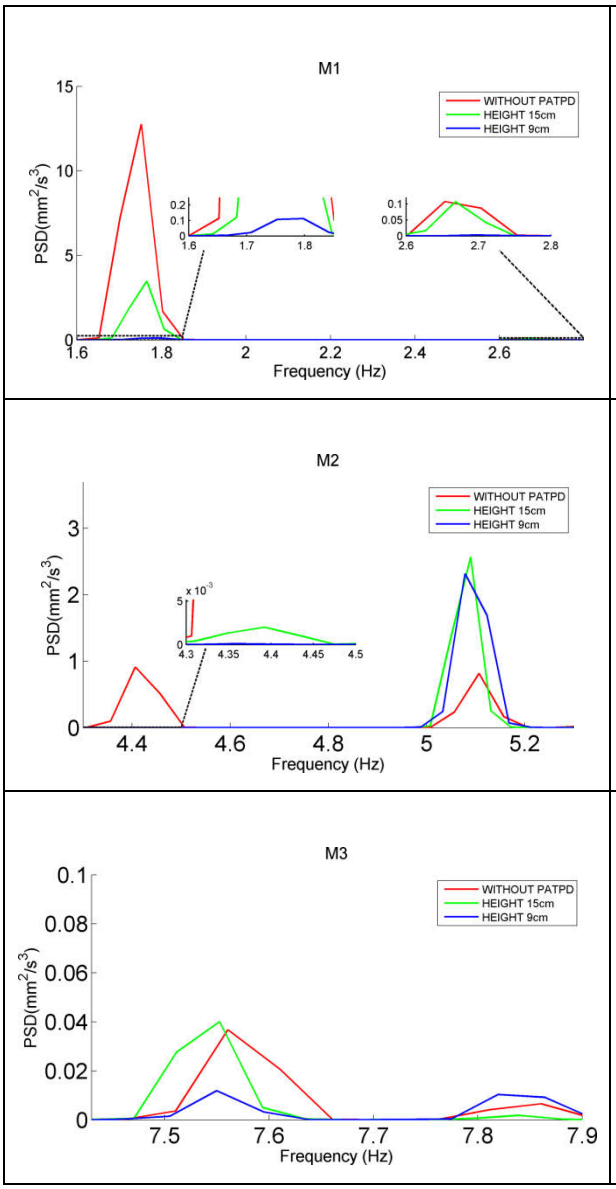

Figure 183: Magnified Power Spectral Density (PSD) storey 3 of the acceleration in the y-direction of the model under free coupled vibration, height 15cm and height 9cm

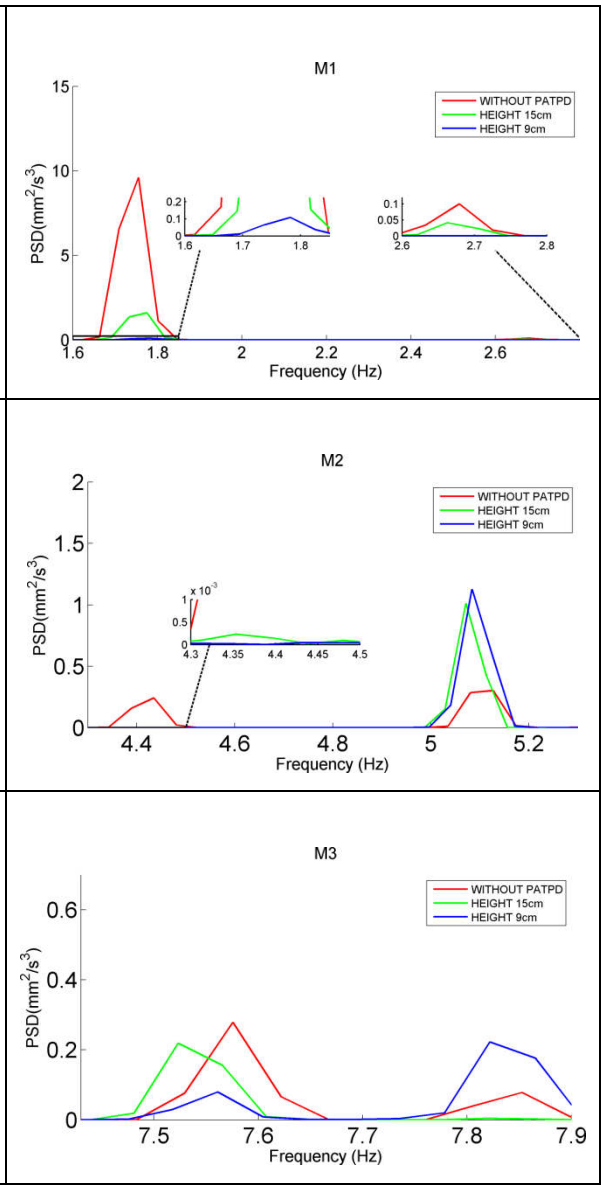

Figure 184: Magnified Power Spectral Density (PSD) storey 2 of the acceleration in the y-direction of the model under free coupled vibration, height 15cm and height 9cm

Figure 183, Figure 184 and Figure 185 show for first natural frequency with PSD peak, 1.747Hz and 2.680Hz, for translation and torsion, both heights provide significant damping of the model's vibrations across all 3 storeys, with the lower height demonstrating best control effect.

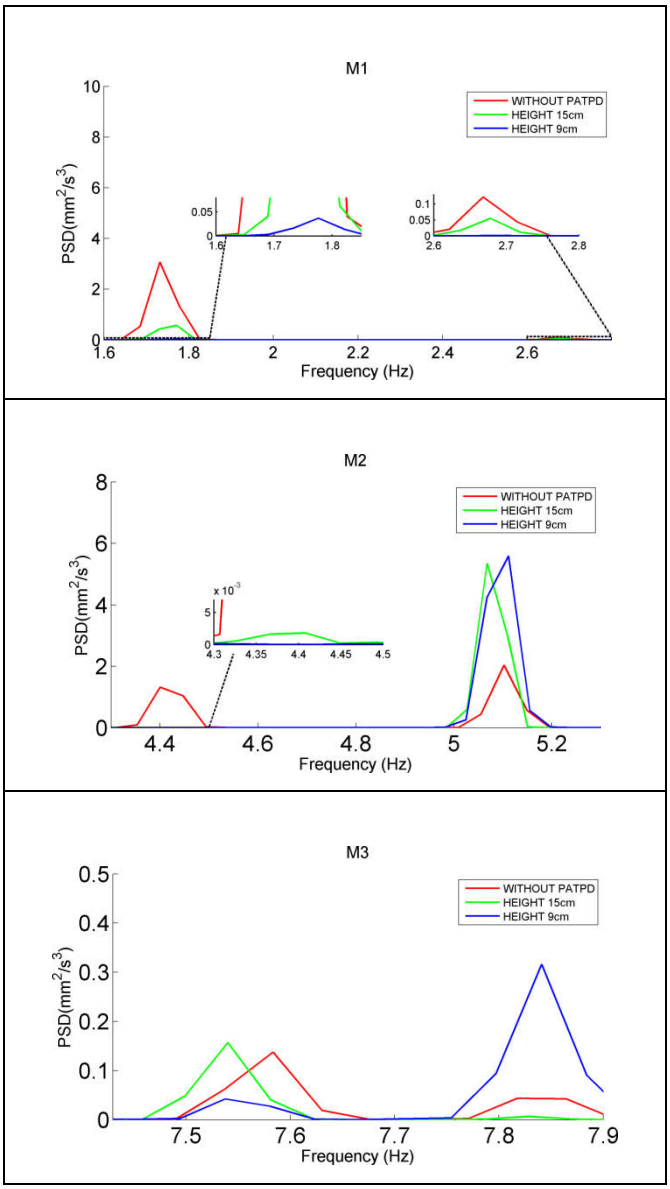

Figure 185: Magnified Power Spectral Density (PSD) storey 1 of the acceleration in the y-direction of the model under free coupled vibration, height 15cm and height 9cm

For second natural frequency with PSD peak, 4.438 Hz, for torsion across all 3 storeys, both heights tested provide significant damping of the model's vibrations across all 3 storeys. For translation with PSD peak, 5.095Hz, across all 3 storeys, both increase the density of the frequency similarly.

For third natural frequency with PSD peak, 7.569Hz, for translation lower height provides control. The other increases frequency. For torsion with PSD peak, 7.842 Hz, the higher height controls and the lower height increase frequency.

Overall PSD peak increases were minimal in comparison to the reduction gained in PSD peak for the first natural frequency.

5.5.2.0 Forced Vibration

5.5.2.1 Translational Vibration in the X-direction

The model was placed on the shake table in order to carry out the forced vibration tests. The PATPD's were connected one-by-one and the respective accelerations measured. The damping effect of each rope change of the PATPD can be seen in the graphs to follow.

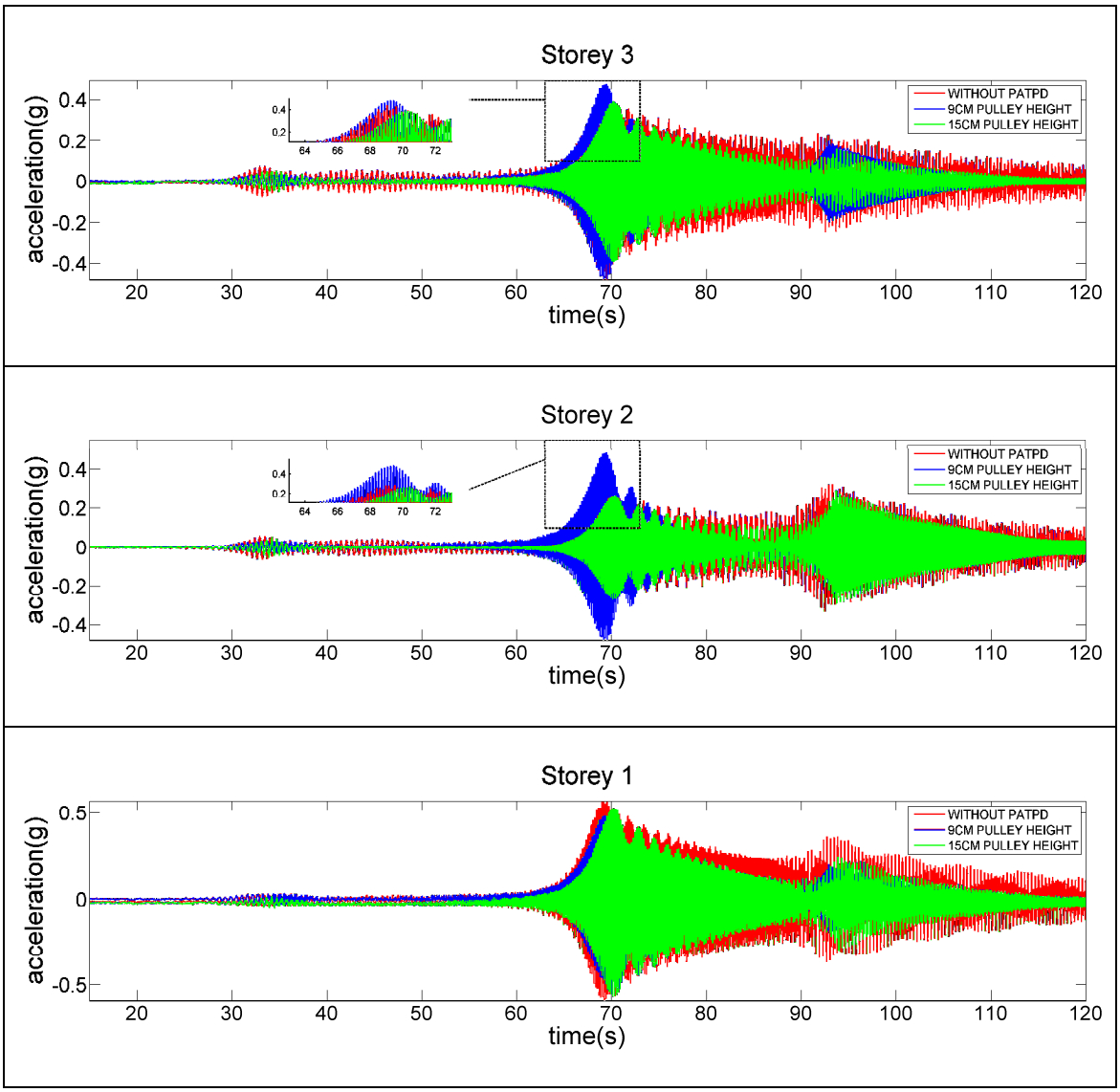

Figure 186: Time history of acceleration response per storey for forced translational vibration in x-direction, height 15cm and height 9cm

Figure 186 shows for all 3 storeys that by adding the damper onto model the acceleration experience is significantly decreased for all rope types.

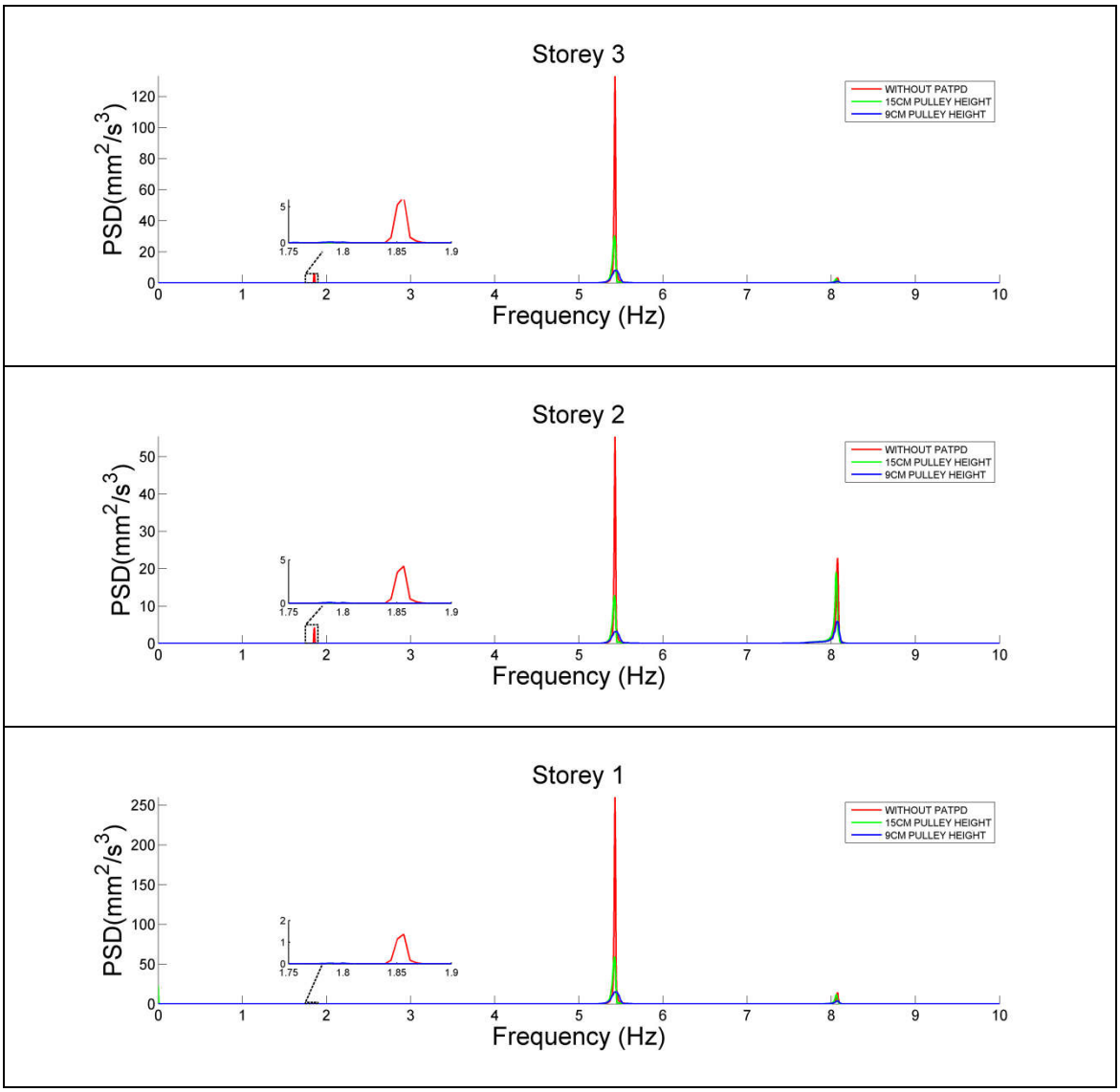

Figure 187: Power Spectral Density (PSD) of the acceleration response per storey under forced excitation in the x-direction, height 15cm and height 9cm

Figure 187 shows PSD peaks at 1.856Hz, 5.429Hz and 8.047Hz. This corresponds to the models first, second and third frequencies. The positive control effect is evident as PSD peaks for all 3 frequencies are significantly reduced by all connection heights used.

5.5.2.2 Translational Vibration in the Y-direction

The model was placed on the shake table in order to carry out the forced vibration tests. The PATPD's were connected one-by-one and the respective accelerations measured. The damping effect of each of the PATPD masses can be seen in the graphs to follow.

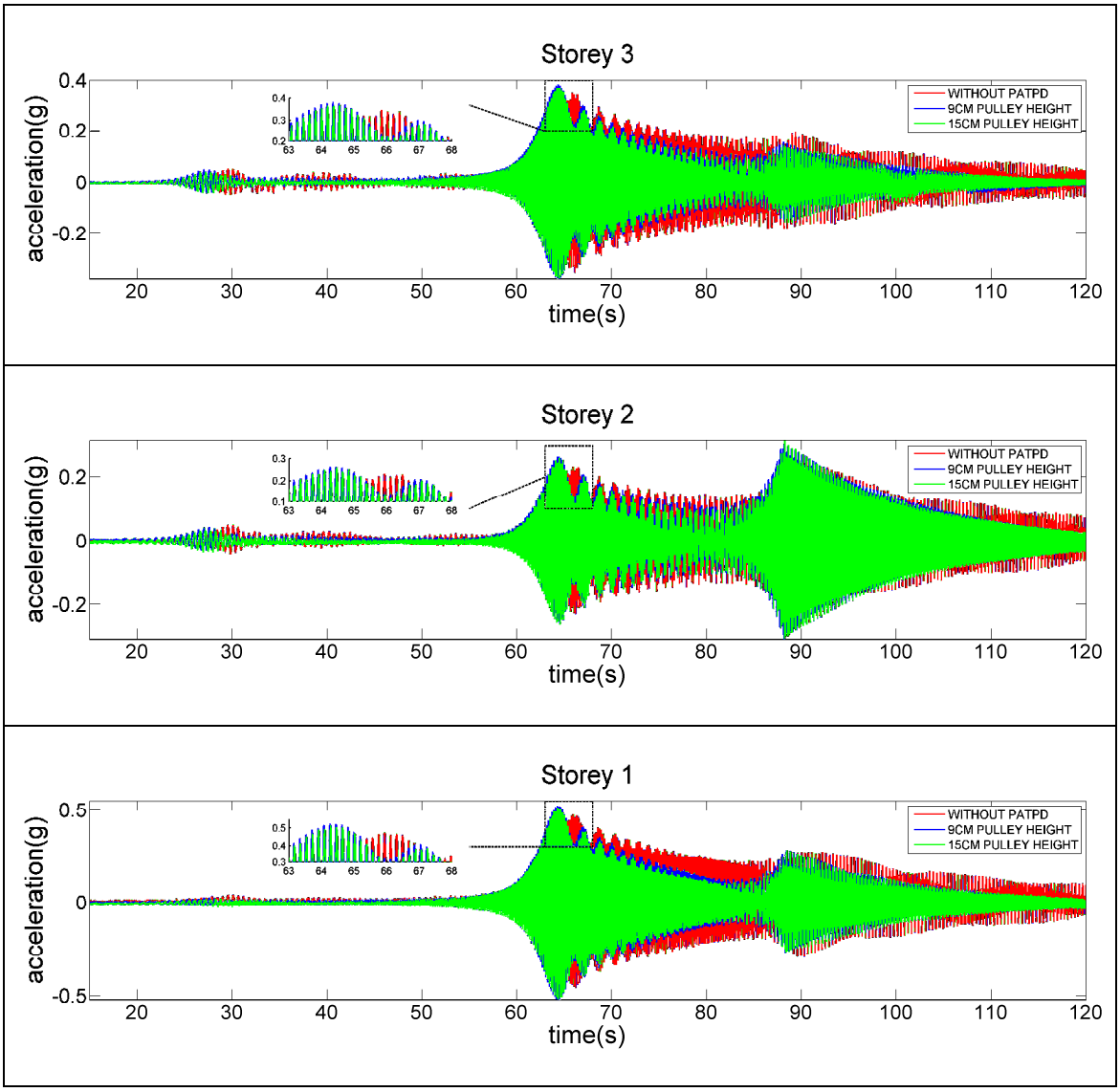

Figure 188: Time history of acceleration response per storey for forced translational vibration in y-direction, height 15cm and height 9cm

Figure 188 shows for all 3 storeys that by adding the damper onto model the acceleration experience is significantly decreased for all heights used.

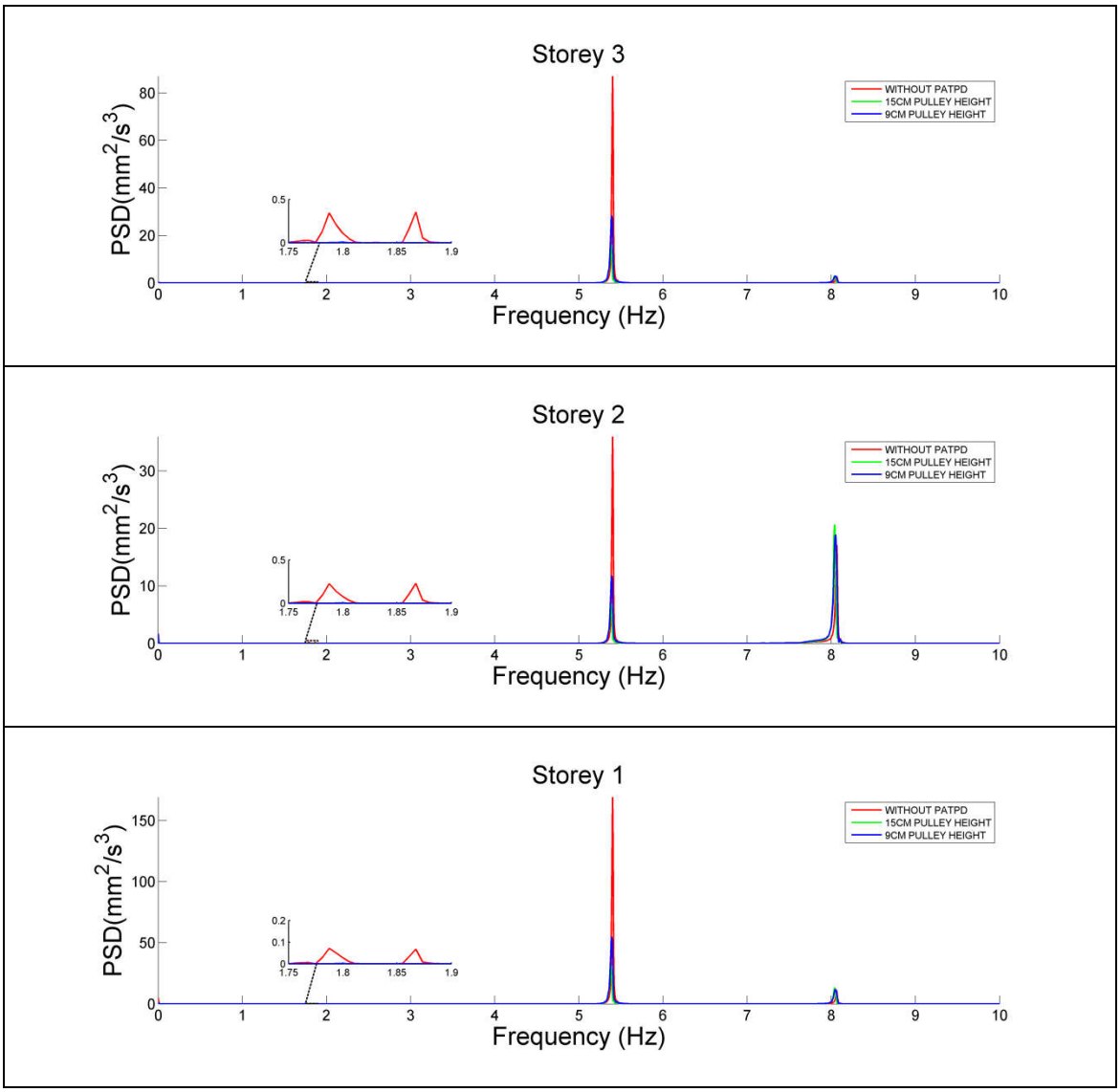

Figure 189: Power Spectral Density (PSD) of the acceleration response per storey under forced excitation in the y-direction, height 15cm and height 9cm

Figure 189 shows PSD peaks at 1.787Hz, 5.399Hz and 8.065Hz. This corresponds to the models first, second and third frequencies. The positive control effect is evident as PSD peaks for all 3 frequencies are significantly reduced. This is true for all heights used.

Control effect of PATPD is better in x-direction than in y-direction.

5.5.3.0 Summary

Free Vibration

This set of parameter tests indicates better control in x than in y direction.

All configurations provided control effect to the first natural frequency for all free vibration tests for all storeys, except height 15cm which did not control M1 storey 1 under torsional vibration (y direction).

The lower height behaves best for control of natural frequency in most cases. The higher height means looser ropes as more slack is required for movement thus reducing the imparting of inertia reaction to the structure. The lower height performs better since it is tighter and has less slack.

Forced Vibration

For Forced Vibration the PATPD provides significant control to all 3 frequencies for all connection heights tested.

The results reveal that the PATPD performs better in translation the x –direction than the y-direction.

CHAPTER 6

Experimental results: Changing Dynamic Properties of model

6.1 Changing Dynamic Properties: Effect of changing model mass

In order to demonstrate that the proposed PATPD is adaptive to any frequency, the primary model's natural frequencies will be changed. This can be achieved by either (a) changing the model mass, or (b) changing the model's stiffness. This chapter encloses results from tests with and without the PATPD as the model mass[10] was changed thus changing its frequencies. The primary model mass is 42.09kg - the test model mass is then increased to 54.09kg and then 66.09kg. This is achieved by adding 12 x 1kg and 24 x 1kg masses to the test structure[11] respectively.

[10] Chapter 6.2 will cover results for changing the model stiffness

[11] A detailed explanation with relevant photographs can be found on page 59

6.1.1 Free Vibration

6.1.1.1Translational Vibration in the X-direction

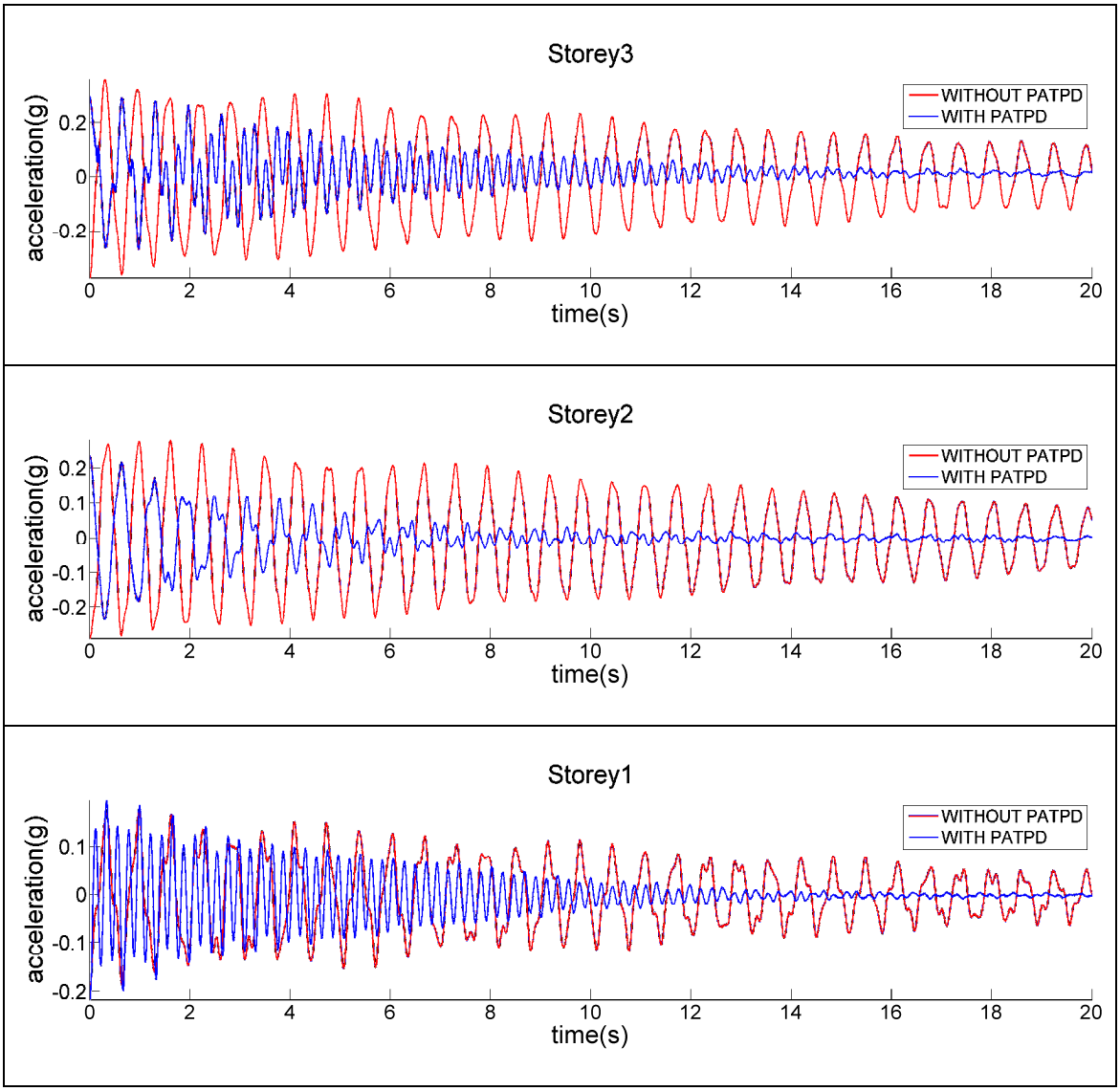

Figure 190: Time history of acceleration response per storey for free translational vibration in the x-direction, model mass 52.09kg

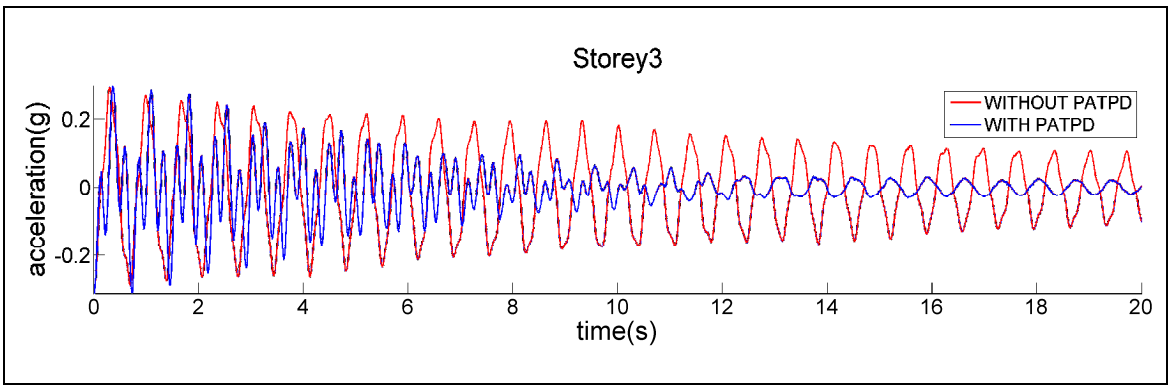

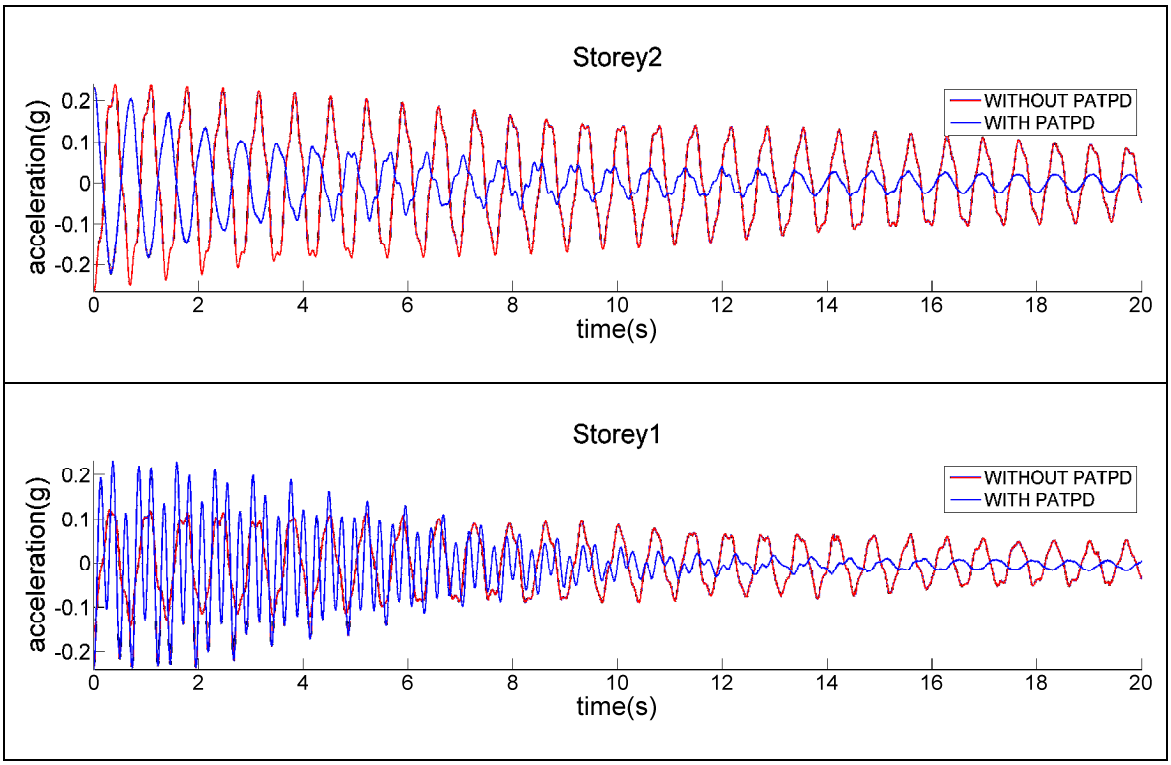

Figure 191: Time history of acceleration response per storey for free translational vibration in the x-direction, model mass 66.09kg

Figure 190 and Figure 191 shows similarity to the results for the primary model[12], of mass 42.09kg, as the PATPD started moving, the acceleration peaks generated in the damped model are as high as those generated in the undamped model. However, these high accelerations subside and the accelerations rapidly decrease compared to that of the undamped model. As is expected the accelerations experienced in storey 3 are highest and the positive damping effect of the PATPD is still significant.

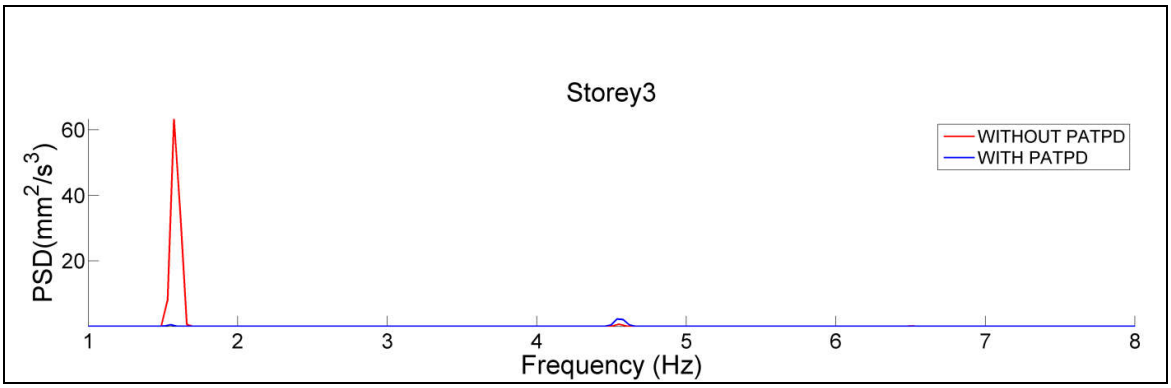

[12] Primary model (mass 42.09kg) figures can be found on page 63 onwards

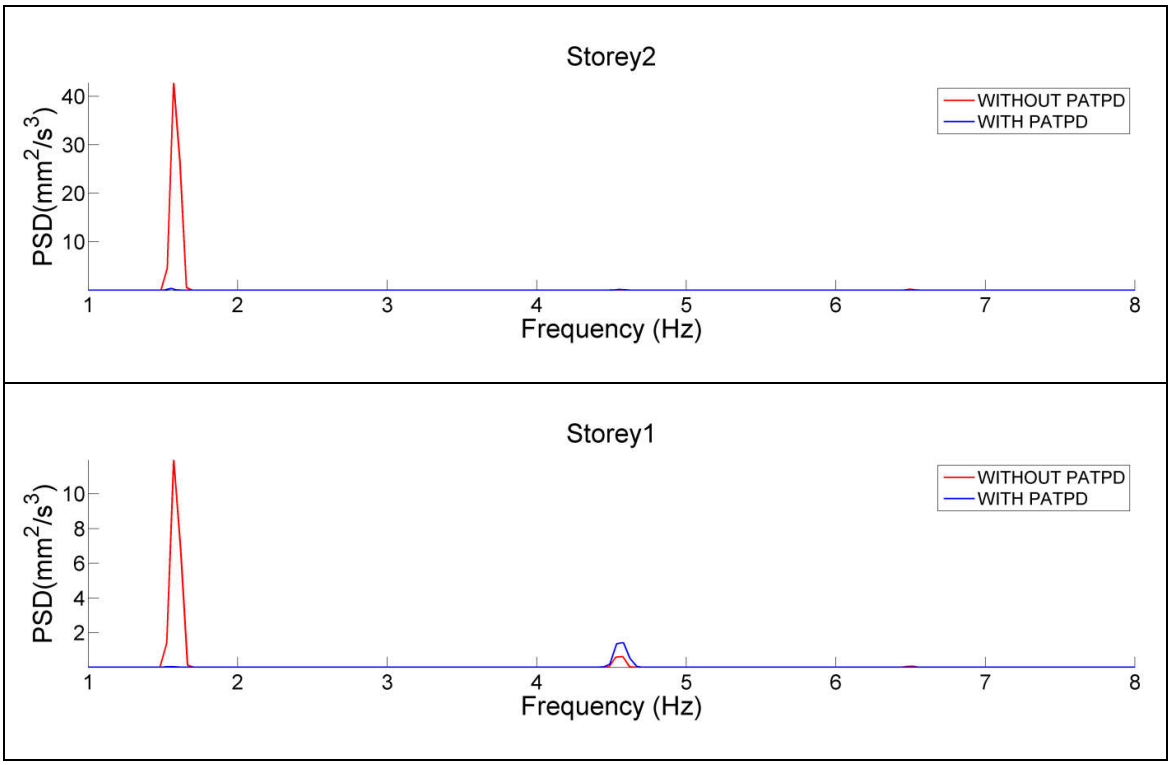

Figure 192: Power Spectral Density (PSD) per storey of the acceleration response for free translational vibration in the x-direction, model mass 54.09kg

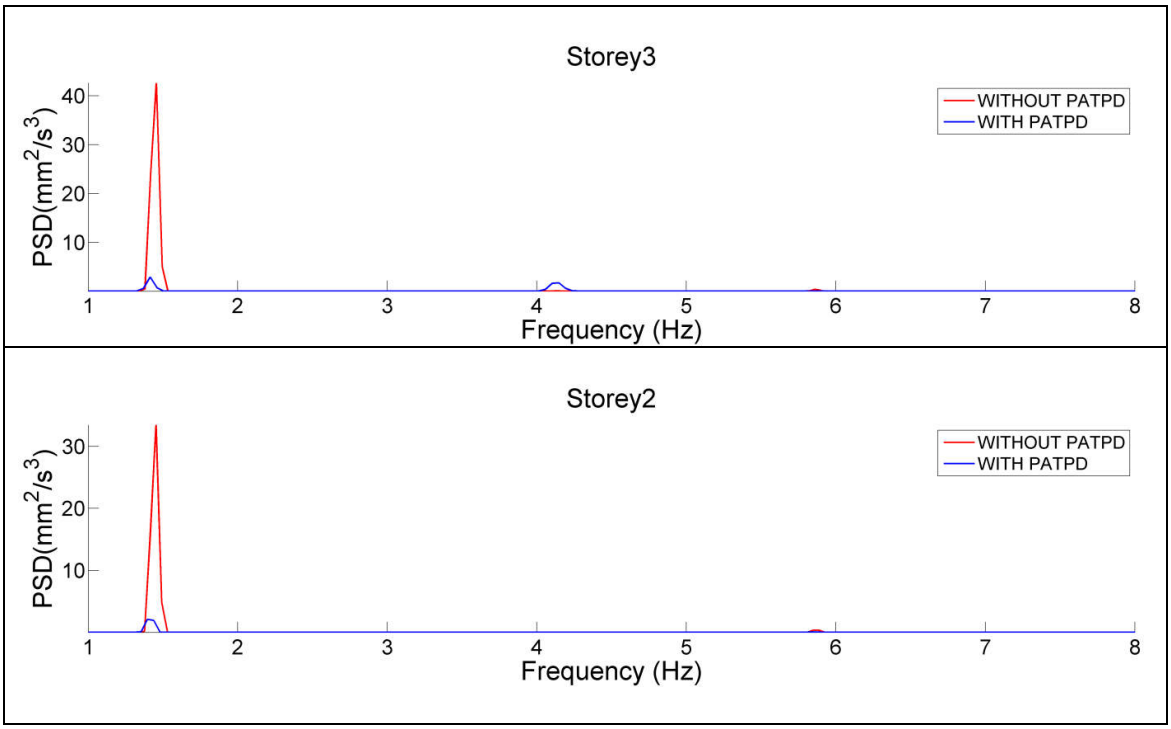

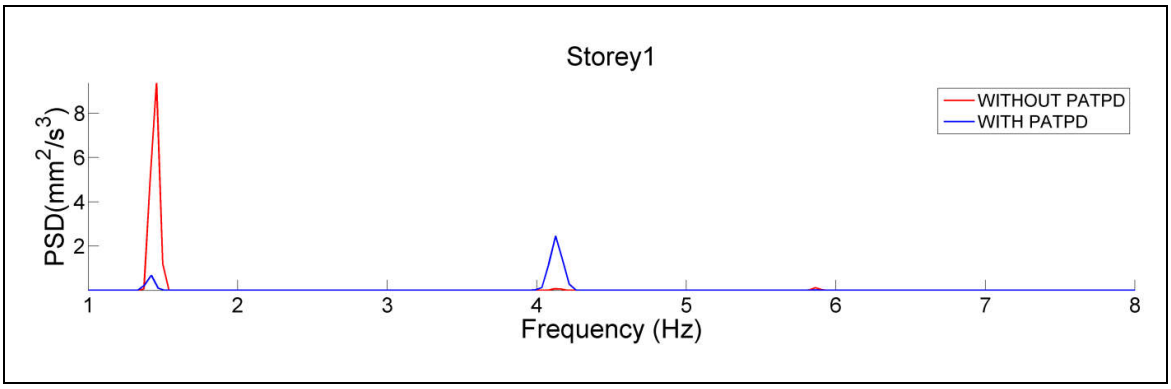

Figure 193: Power Spectral Density (PSD) per storey of the acceleration response for free translational vibration in the x-direction, model mass 66.09kg

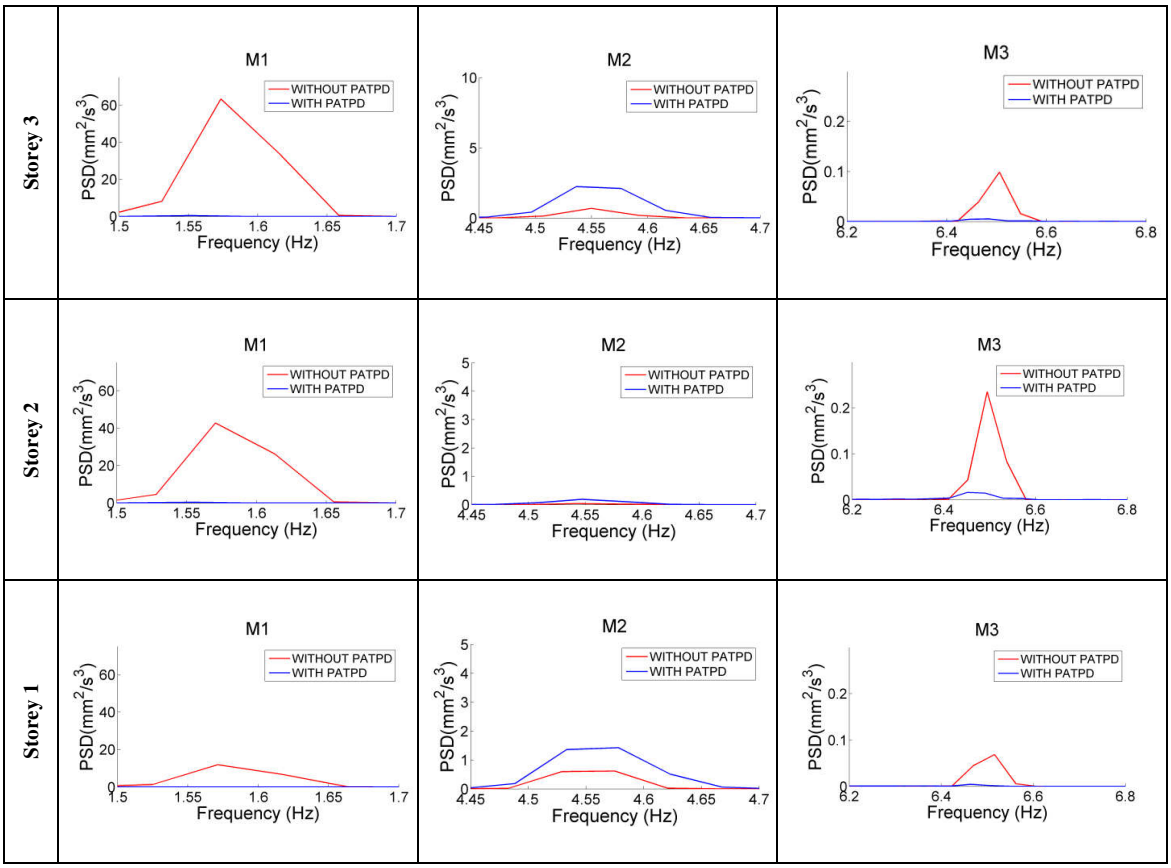

Figure 194: Magnified Power Spectral Density (PSD) of the acceleration response for free translational vibration in the x-direction, model mass 54.09kg

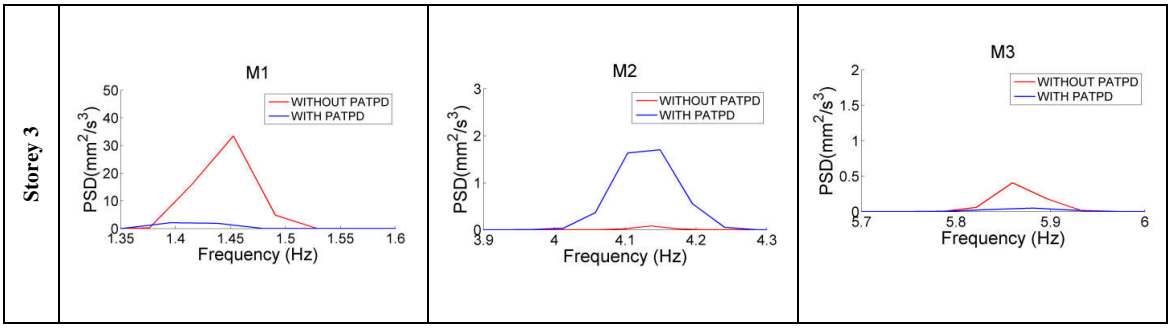

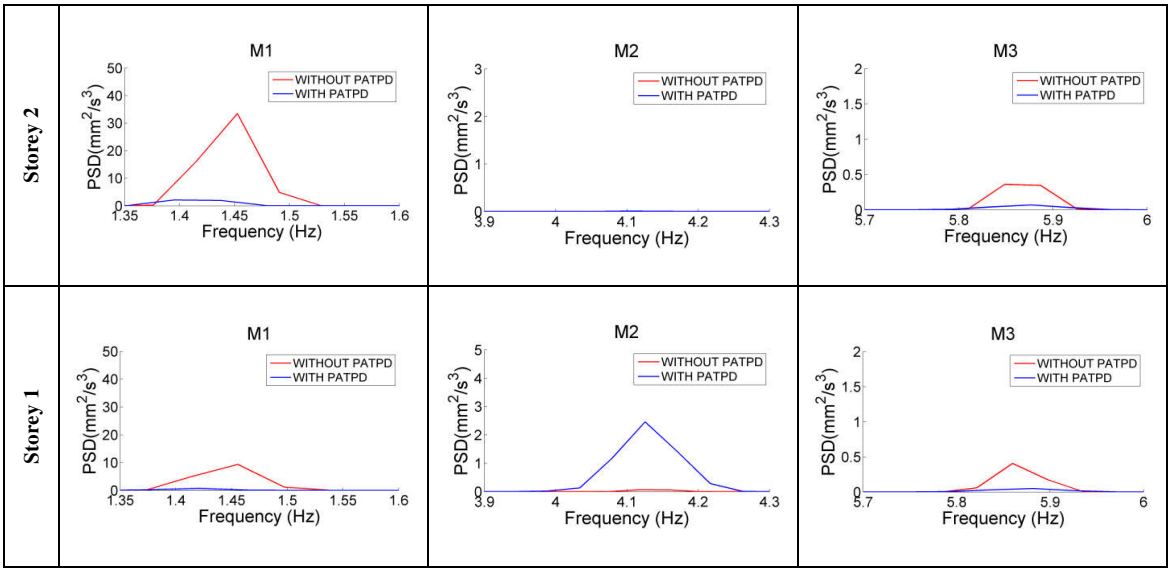

Figure 195: Magnified Power Spectral Density (PSD) of the acceleration response for free translational vibration in the x-direction, model mass 66.09kg

Figure 192 shows the PSD for storeys 3-1 for test model with mass 54.09kg: there is a high peak at 1.573Hz, 4.550Hz and 6.506Hz. This represents the model's first, second and third natural frequency for translation in the x-direction. Figure 193 shows the PSD for storeys 3-1 for test model with mass 66.09kg: there is a high peak at 1.455Hz, 4.136Hz and 5.860Hz. This represents the model's first, second and third natural frequency for translation in the x-direction.

As can be seen from Figure 194 and Figure 195, PATPD provides a high level of attenuation for all 3 storeys to the first natural frequency for both model masses.

The second natural frequency with PSD peak, 4.550Hz and 4.136 Hz, for the 54.09kg and 66.09kg mass respectively overall shows a slight increase in density of frequency, except for storey 2 M2 of the 66.09kg model mass which is attenuated by at least 99%.

The PATPD provides at least 99% attenuation for all 3 storeys to the third natural frequency, 6.506Hz and 5.860Hz, for the 54.09kg and 66.09kg mass respectively.

The PATPD has achieved attenuating the first natural frequency which has the greatest amplitude for translational vibration in the x-direction covering a relatively wide range of frequencies, by adapting to dynamic changes i.e. change in the models mass.

6.1.1.2 Translational Vibration in the Y-direction

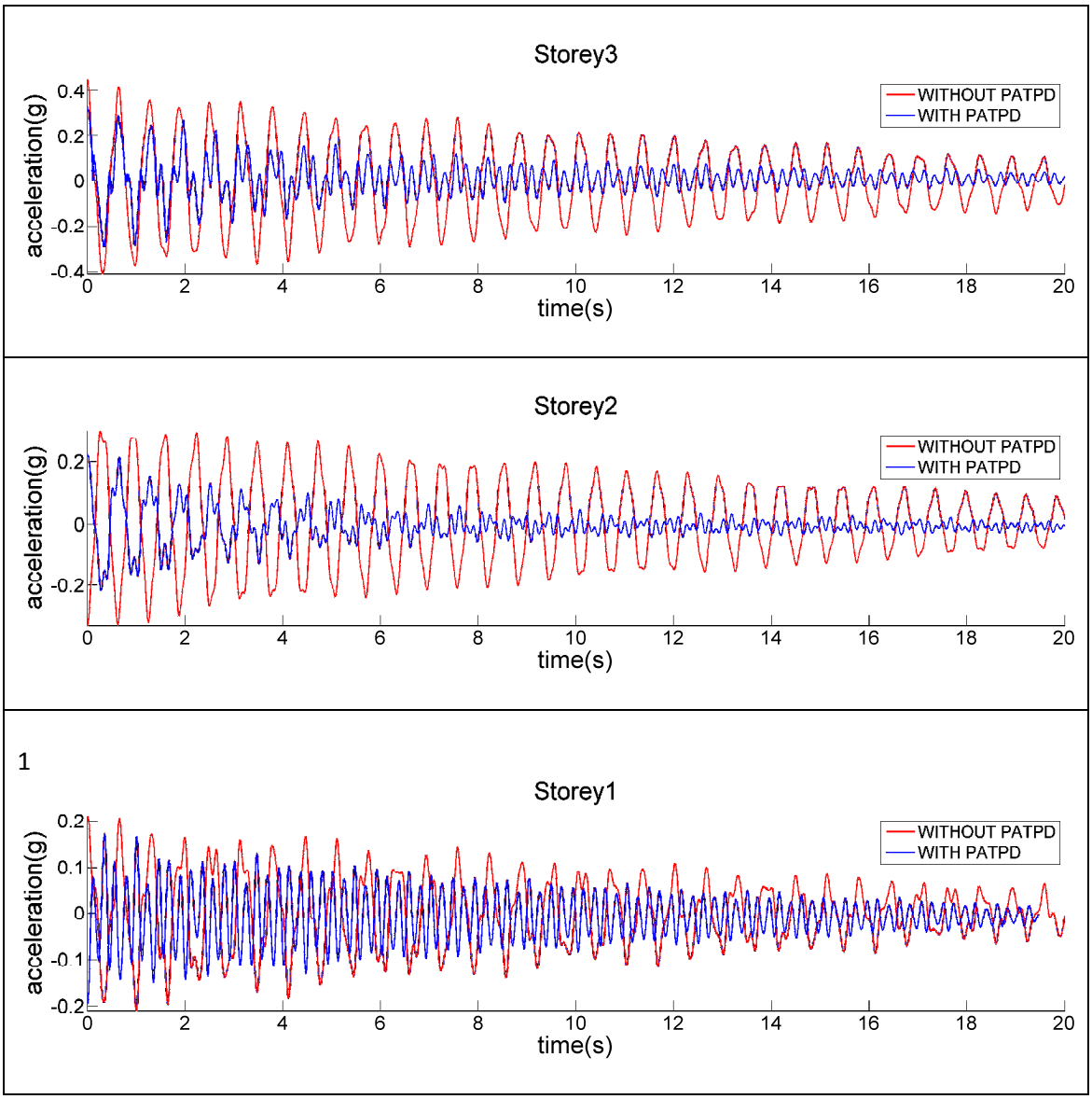

Figure 196: Time history of acceleration response per storey for free translational vibration in the y-direction, model mass 52.09kg

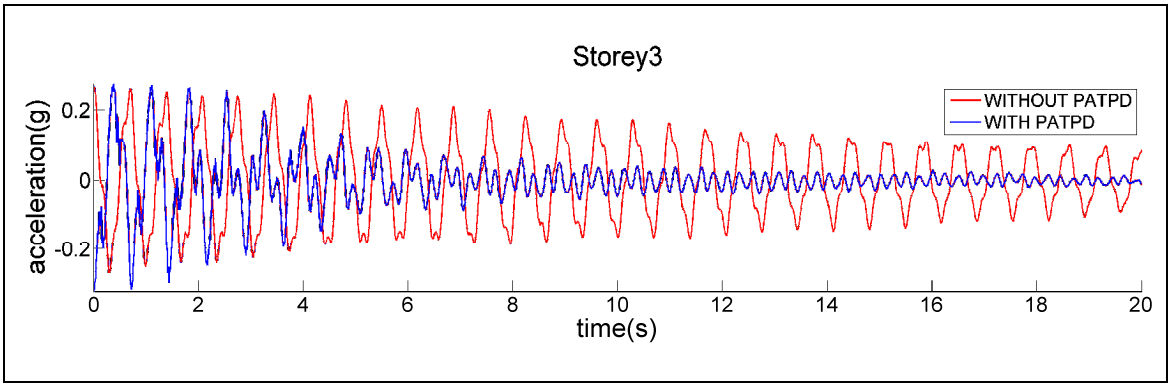

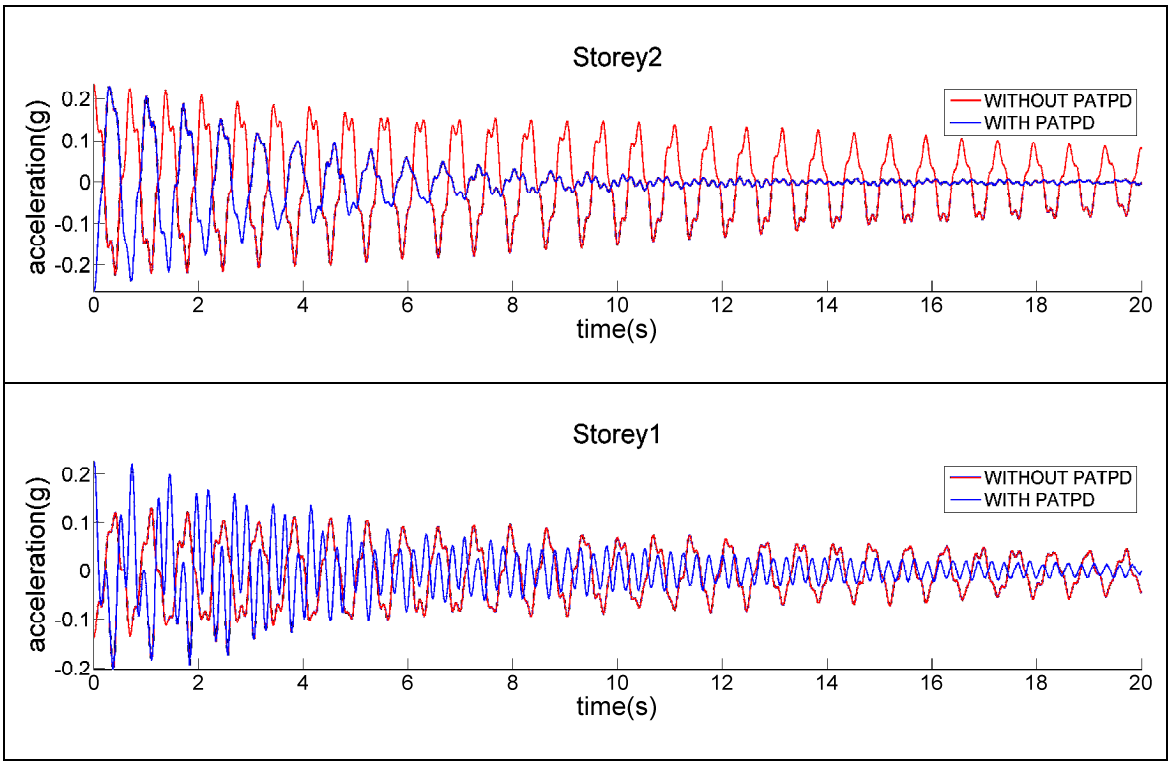

Figure 197: Time history of acceleration response per storey for free translational vibration in the y-direction, model mass 66.09kg

Figure 196 and Figure 197 shows similarity to the results for the primary model[13], of mass 42.09kg, as the PATPD started moving, the acceleration peaks generated in the damped model are as high as those generated in the undamped model. However, these high accelerations subside and the accelerations rapidly decrease compared to that of the undamped model. As is expected the accelerations experienced in storey 3 are highest and the positive damping effect of the PATPD is still significant.

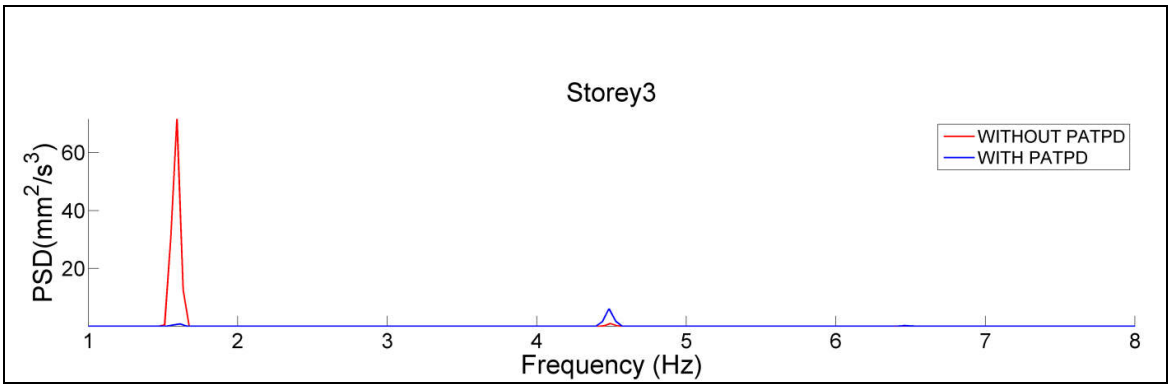

[13] Primary model (mass 42.09kg) figures can be found on pages 43-45

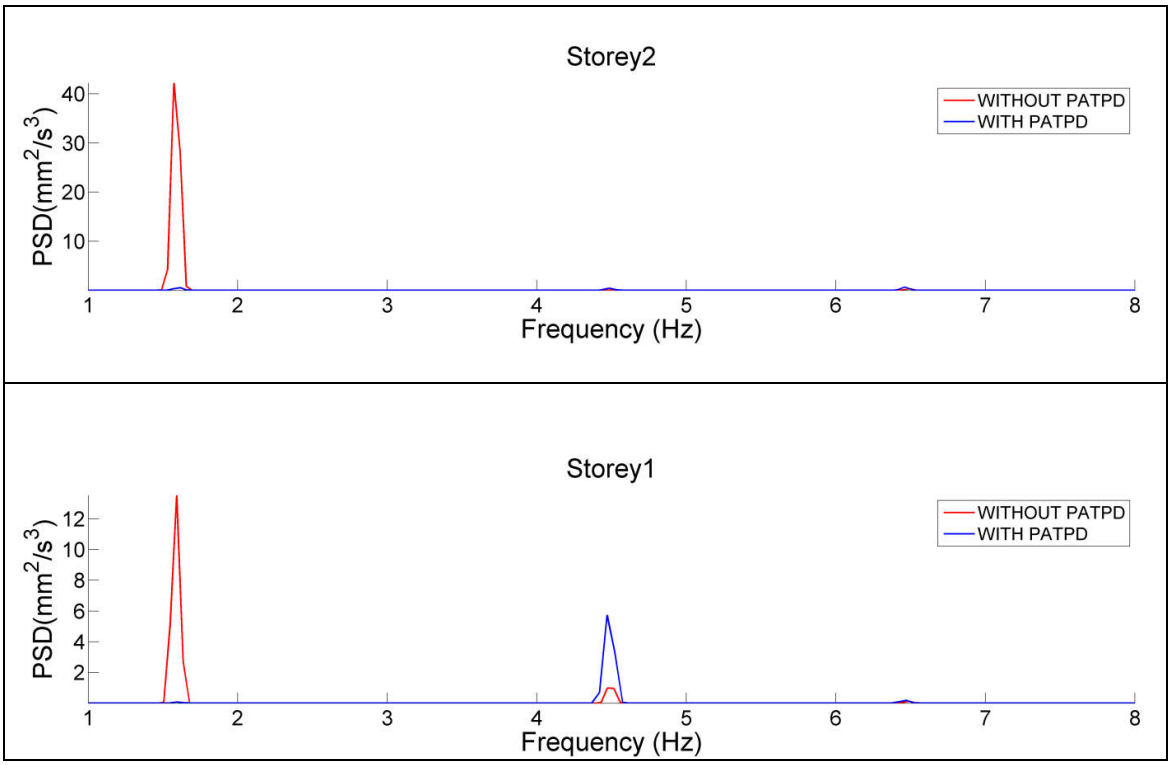

Figure 198: Power Spectral Density (PSD) per storey of the acceleration response for free translational vibration in the y-direction, model mass 54.09kg

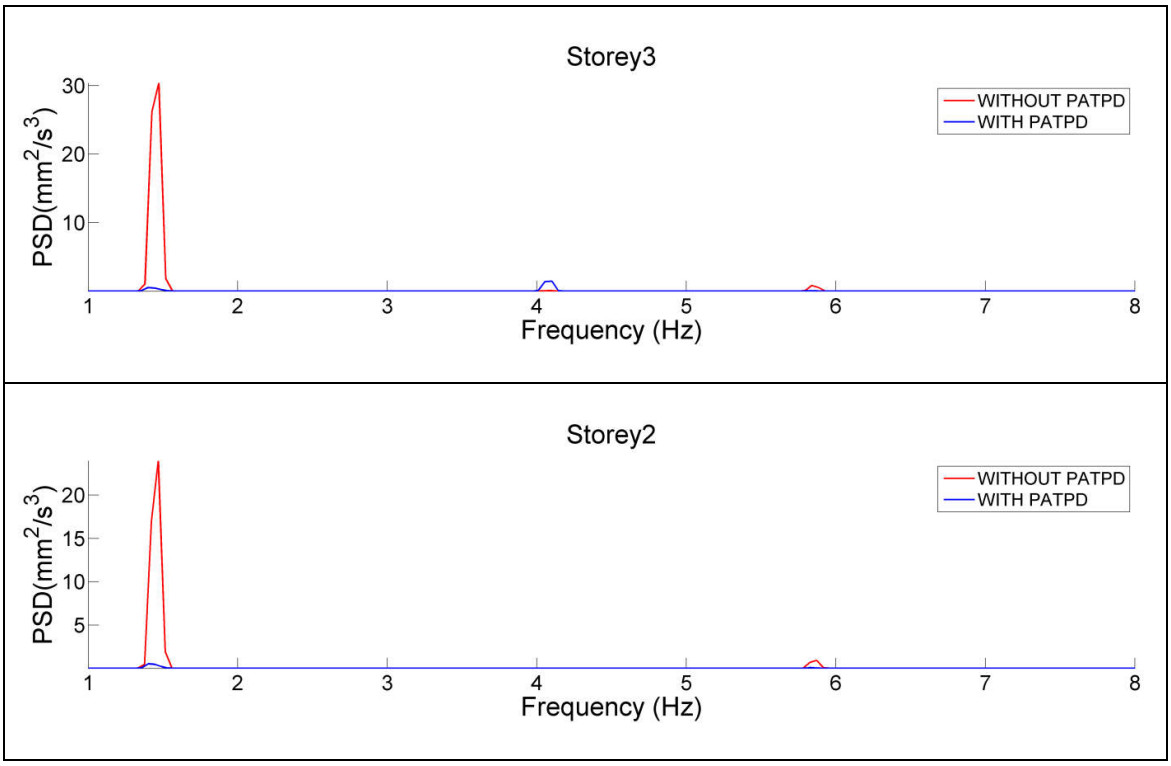

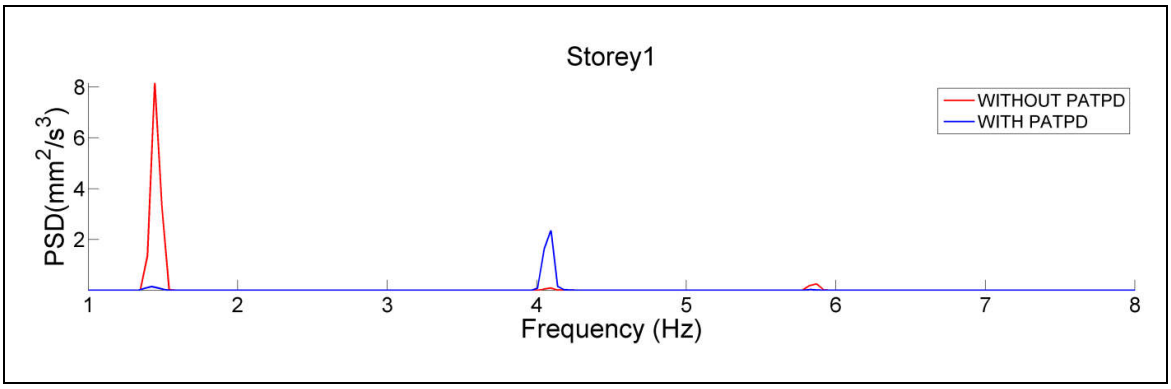

Figure 199: Power Spectral Density (PSD) per storey of the acceleration response for free translational vibration in the y-direction, model mass 66.09kg

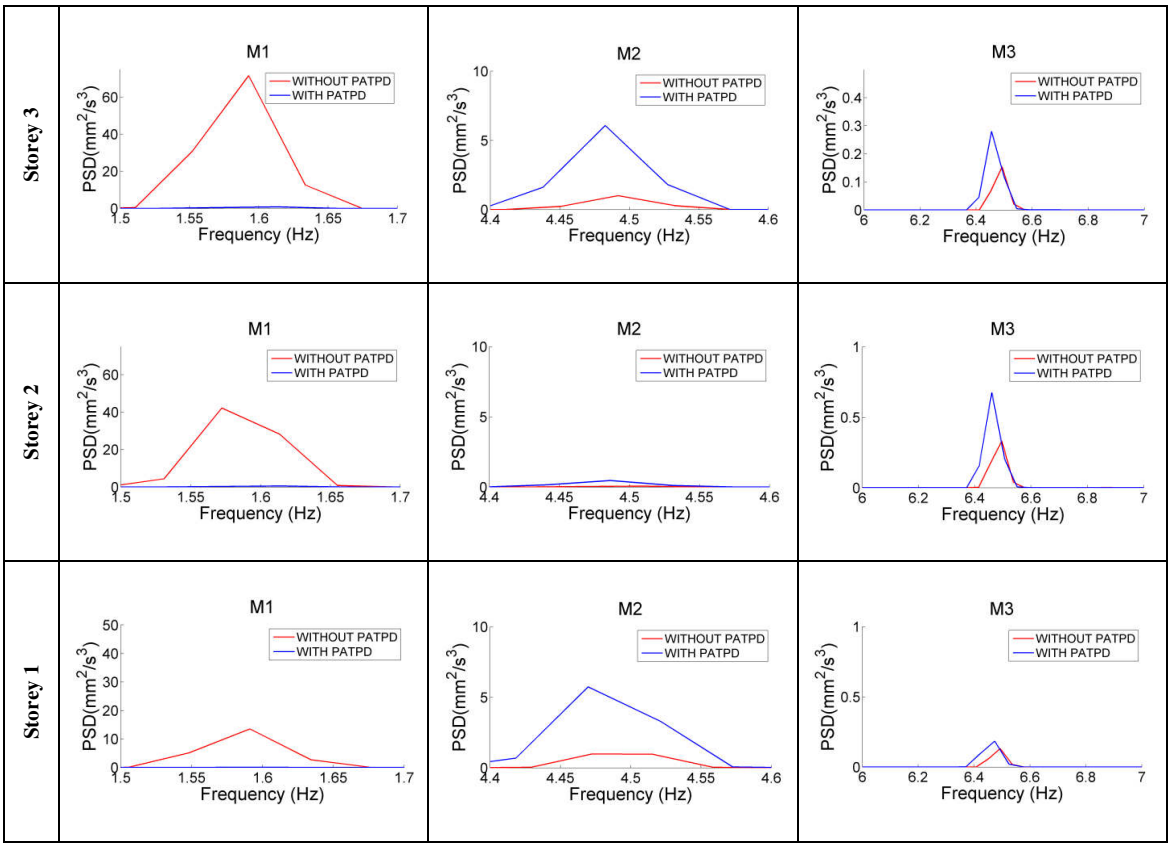

Figure 200: Magnified Power Spectral Density (PSD) of the acceleration response for free translational vibration in the y-direction, model mass 54.09kg

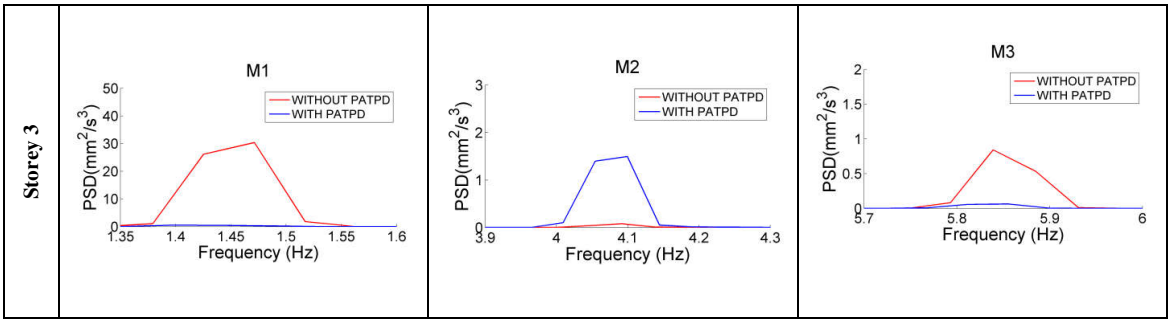

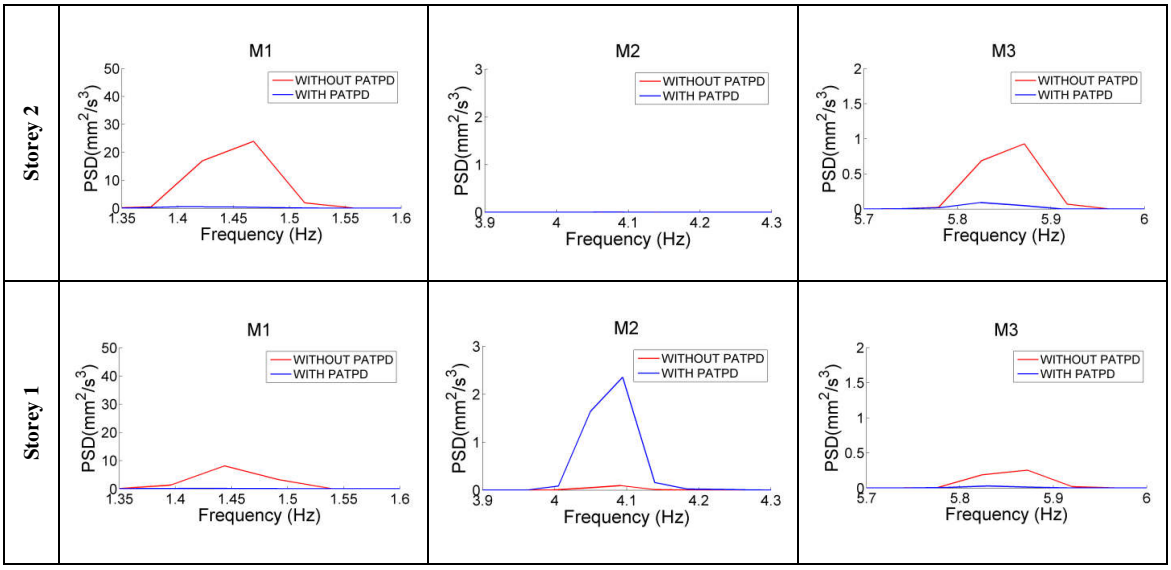

Figure 201: Magnified Power Spectral Density (PSD) of the acceleration response for free translational vibration in the y-direction, model mass 66.09kg

Figure 198 shows the PSD for storeys 3-1 for test model with mass 54.09kg: there is a high peak at 1.593Hz, 4.492Hz and 6.500Hz. This represents the model's first, second and third natural frequency for translation in the y-direction Figure 199 shows the PSD for storeys 3-1 for test model with mass 66.09kg: there is a high peak at 1.471Hz, 4.092Hz and 5.839Hz. For the first, second and third storeys respectively for model mass 66.09kg. This represents the model's first, second and third natural frequency for translation in the y-direction.

As can be seen from Figure 200 and Figure 201, the PATPD provides a high level of attenuation for all 3 storeys to the first natural frequency for both model masses.

.

The second natural frequency with PSD peak, 4.492Hz and 4.092Hz, for the 54.09kg and 66.09kg mass respectively overall shows a slight increase in density of frequency, except for storey 2 M2 of the 66.09kg model mass which is attenuated by at least 99%.

The third natural frequency with PSD peak, 6.500Hz, for the 54.09kg mass shows a slight increase in PSD peak for all 3 storeys. The PATPD provides at least 99% attenuation for all 3 storeys to the third natural frequency, 5.839Hz, for the 66.09kg mass.

The PATPD has achieved attenuating the first natural frequency which has the greatest amplitude for translational vibration in the y-direction covering a relatively wide range of frequencies, by adapting to dynamic changes i.e. change in the models mass.

It is also evident, as with the primary model, that the PATPD control in the x-direction is better than in the y-direction.

6.1.1.3 Torsional Vibration (acceleration measured in X-direction)

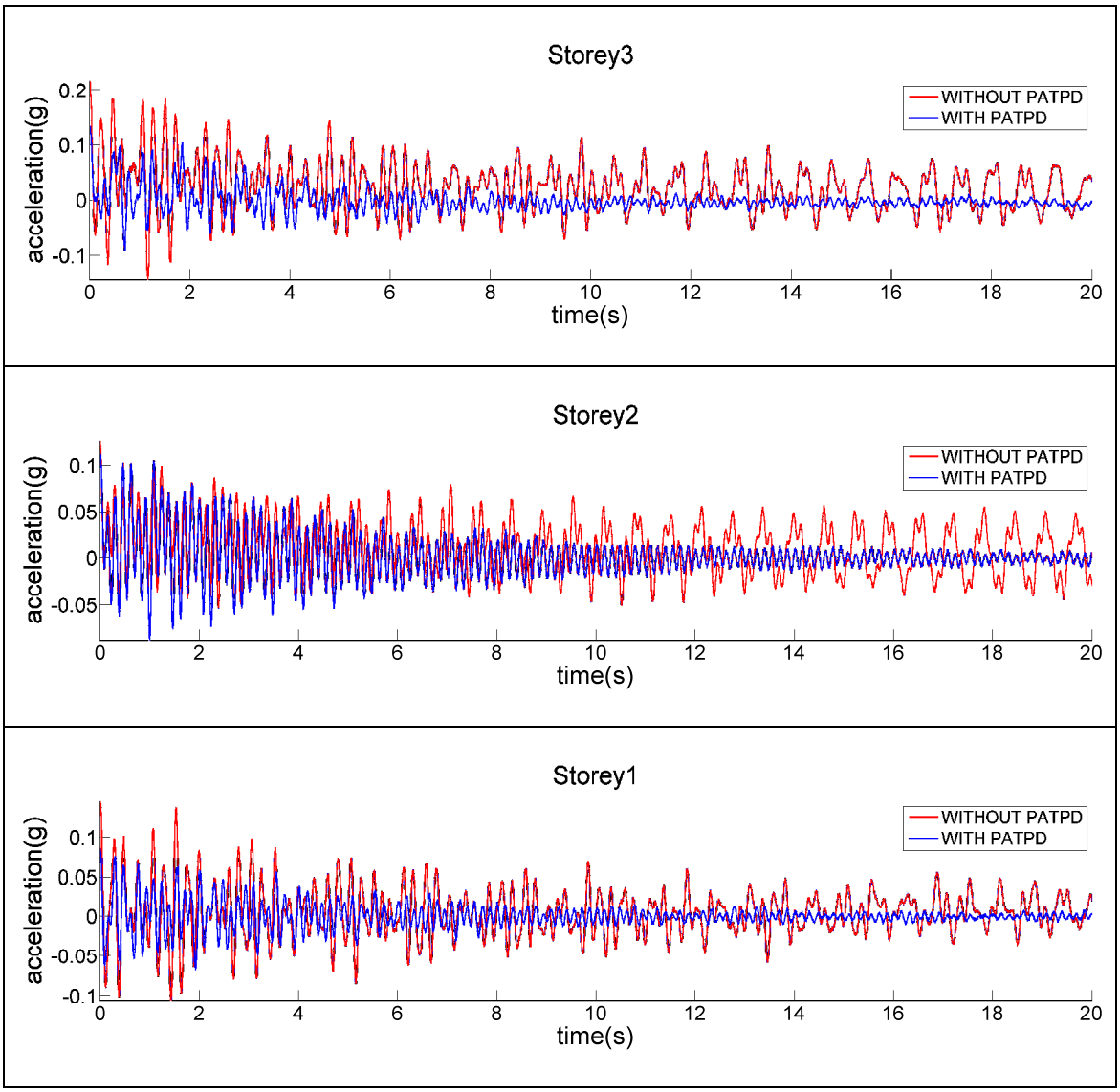

Figure 202: Time history of acceleration response per storey for free torsional vibration in the x-direction, model mass 52.09kg

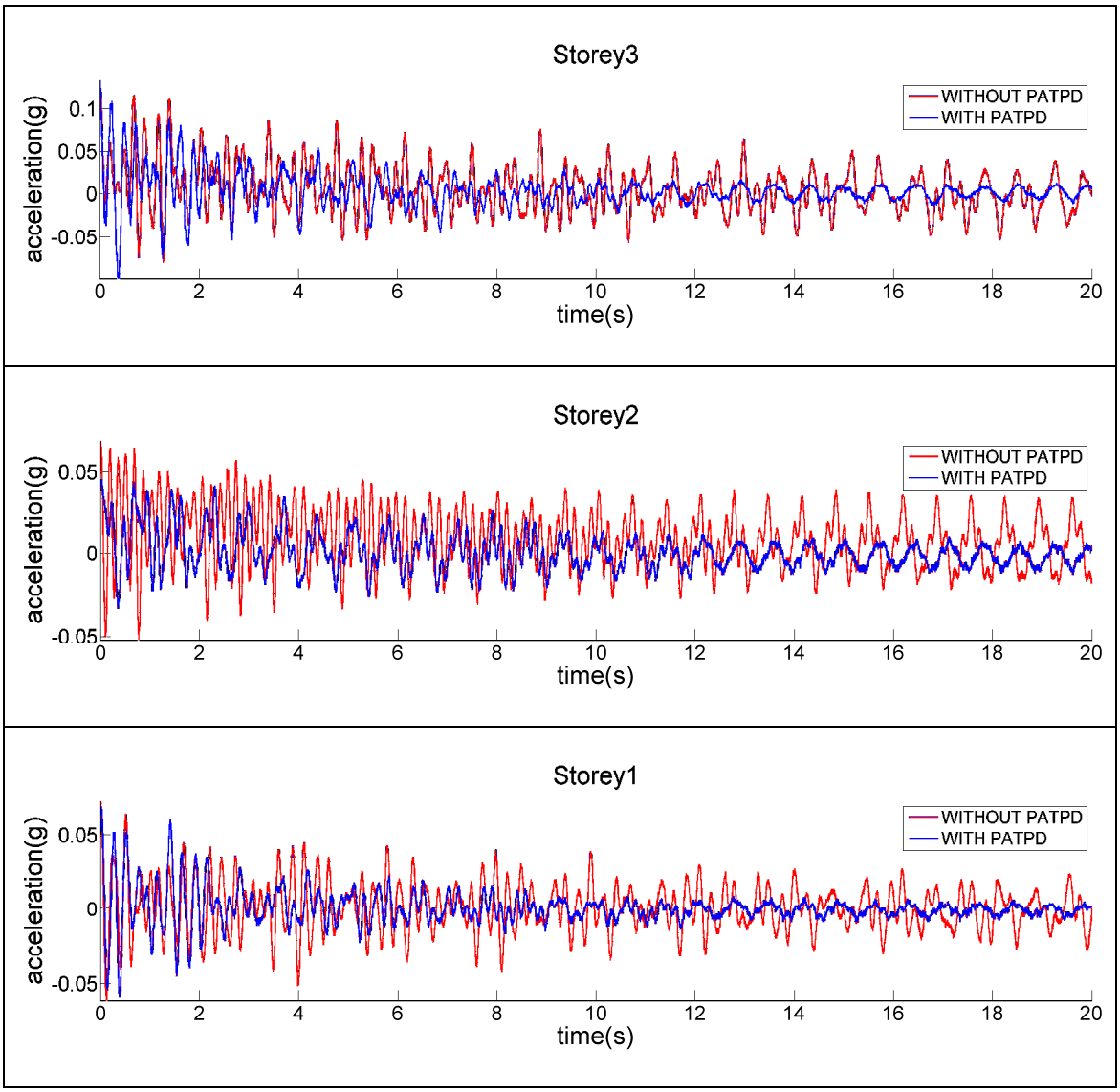

Figure 203: Time history of acceleration response per storey for free torsional vibration in the x-direction, model mass 66.09kg

Figure 202 and Figure 203 shows similarity to the results for the primary model[14], of mass 42.09kg, as the PATPD started moving, the acceleration peaks generated in the damped model are as high as those generated in the undamped model. However, these high accelerations subside and the accelerations rapidly decrease compared to that of the undamped model. As is expected the accelerations experienced in storey 3 are highest and the positive damping effect of the PATPD is still significant.

[14] Primary model (mass 42.09kg) figures can be found in Chapter 4 page 63 onwards

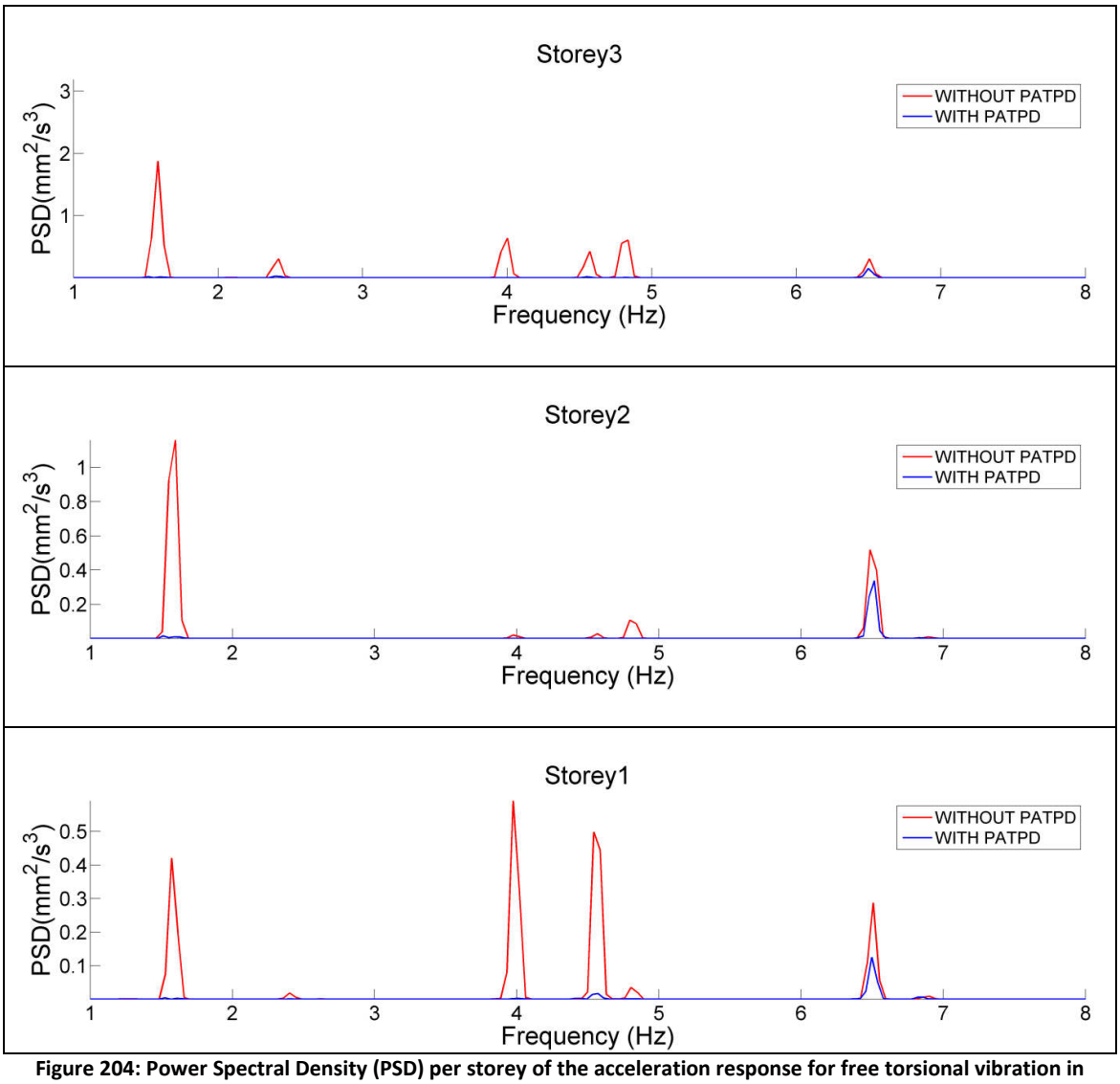

Figure 204: Power Spectral Density (PSD) per storey of the acceleration response for free torsional vibration in the x-direction, model mass 54.09kg

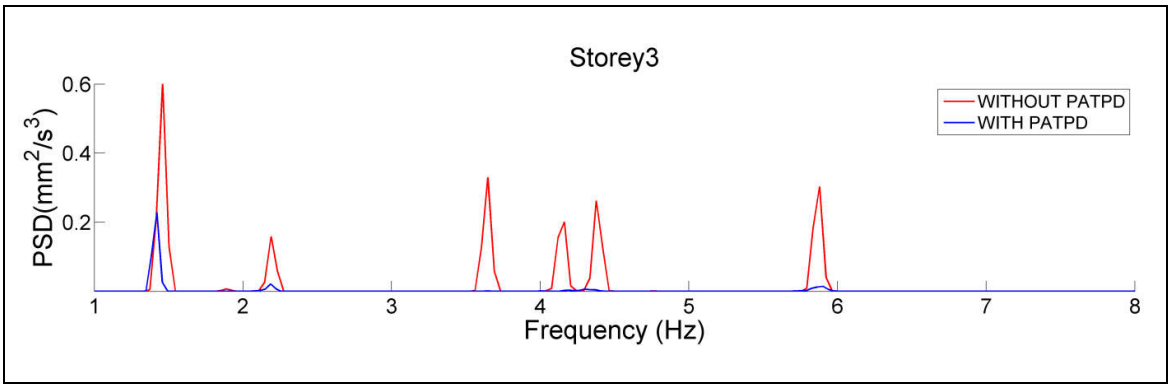

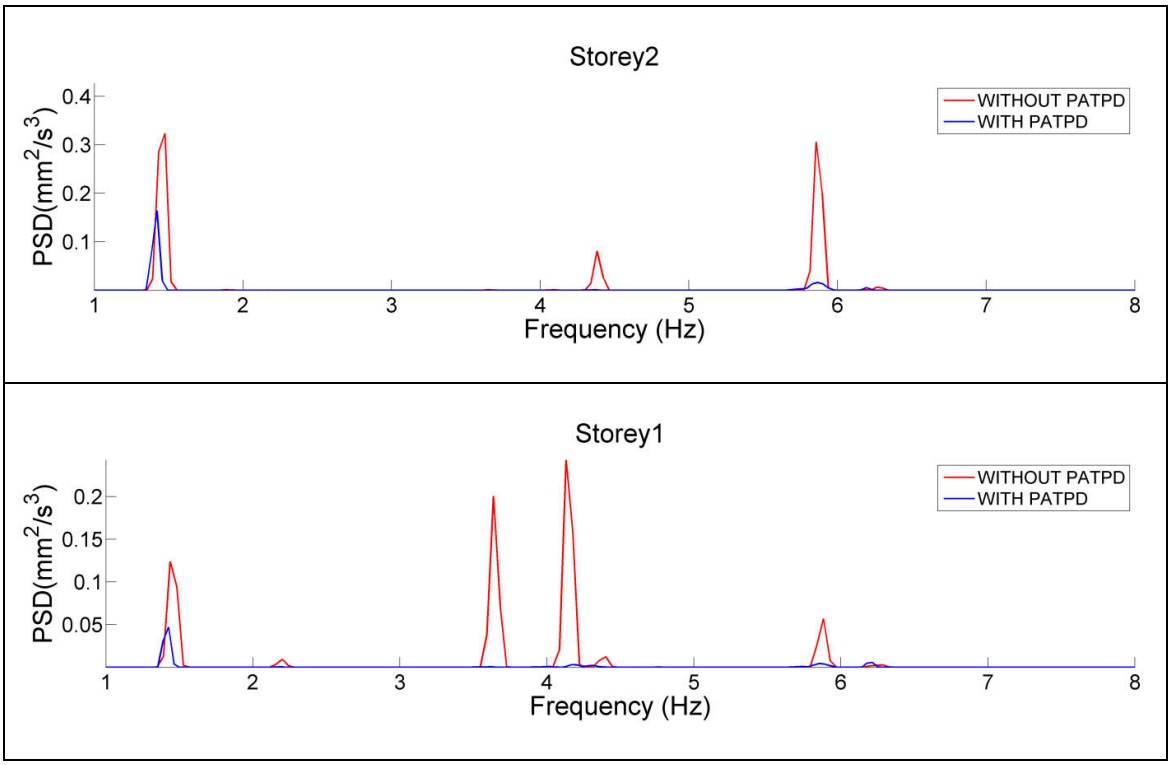

Figure 205: Power Spectral Density (PSD) per storey of the acceleration response for free torsional vibration in the x-direction, model mass 66.09kg

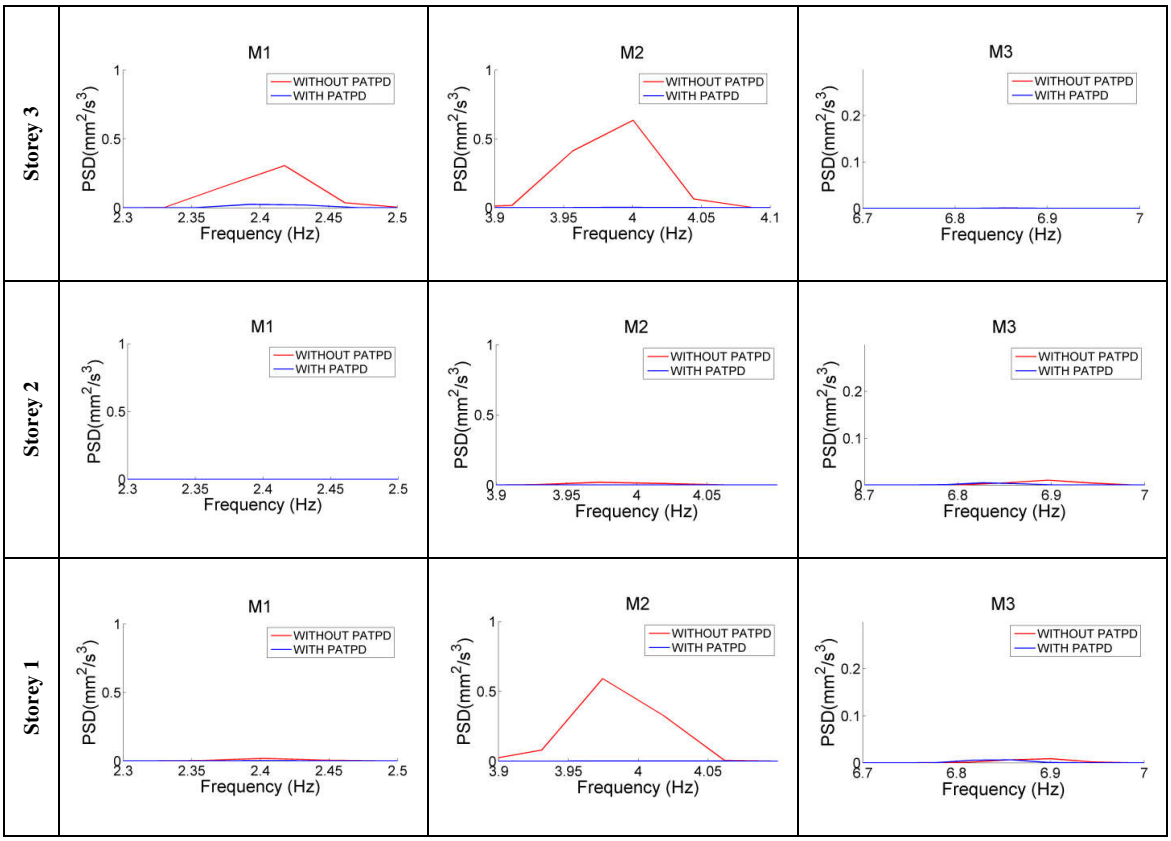

Figure 206: Magnified Power Spectral Density (PSD) of the acceleration response for free torsional vibration in the x-direction, model mass 54.09kg

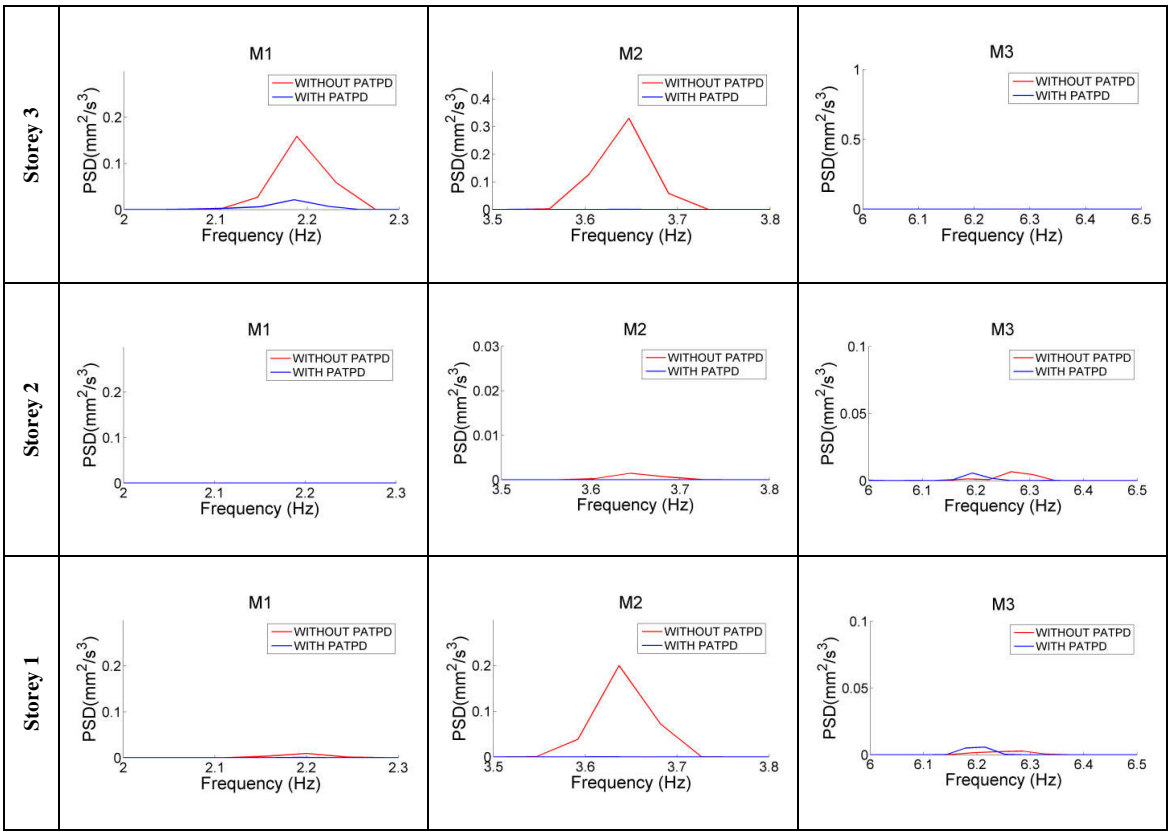

Figure 207: Magnified Power Spectral Density (PSD) of the acceleration response for free torsional vibration in the x-direction, model mass 66.09kg

Figure 204 shows a high peak for storeys 3-1 for mass for model mass 54.09kg at: 2.418Hz, 4.000Hz and 6.858Hz for first, second and third natural frequencies. Figure 205 shows a high peak for storeys 3-1 for mass for model mass 66.09kg at: 2.188Hz, 3.647Hz and 6.625Hz for the first, second and third natural frequencies. This represents the model's natural frequency for torsion in the x-direction.

Peaks are also visible at natural frequencies for translation in the x-direction which is expected as the structure had some movement in the x-direction as well as torsionally. As is also evident all translational frequencies are controlled by at least 99%.

As can be seen from Figure 206 and Figure 207 , the PATPD provides at least 99% attenuation for all 3 storeys to the first and second natural frequency for both model masses.

The third natural frequency PSD peak for both masses storey1-3 overall shows a slight increase in density of frequency, the increase is less than that of the y-direction thus again supporting the PATPDs better control in x-direction than y-direction.

The PATPD has achieved attenuating the first natural frequency which has the greatest amplitude for torsional vibration in the x-direction covering a relatively wide range of frequencies, by adapting to dynamic changes i.e. change in the models mass.

6.1.1.4 Torsional Vibration (acceleration measured in Y-direction)

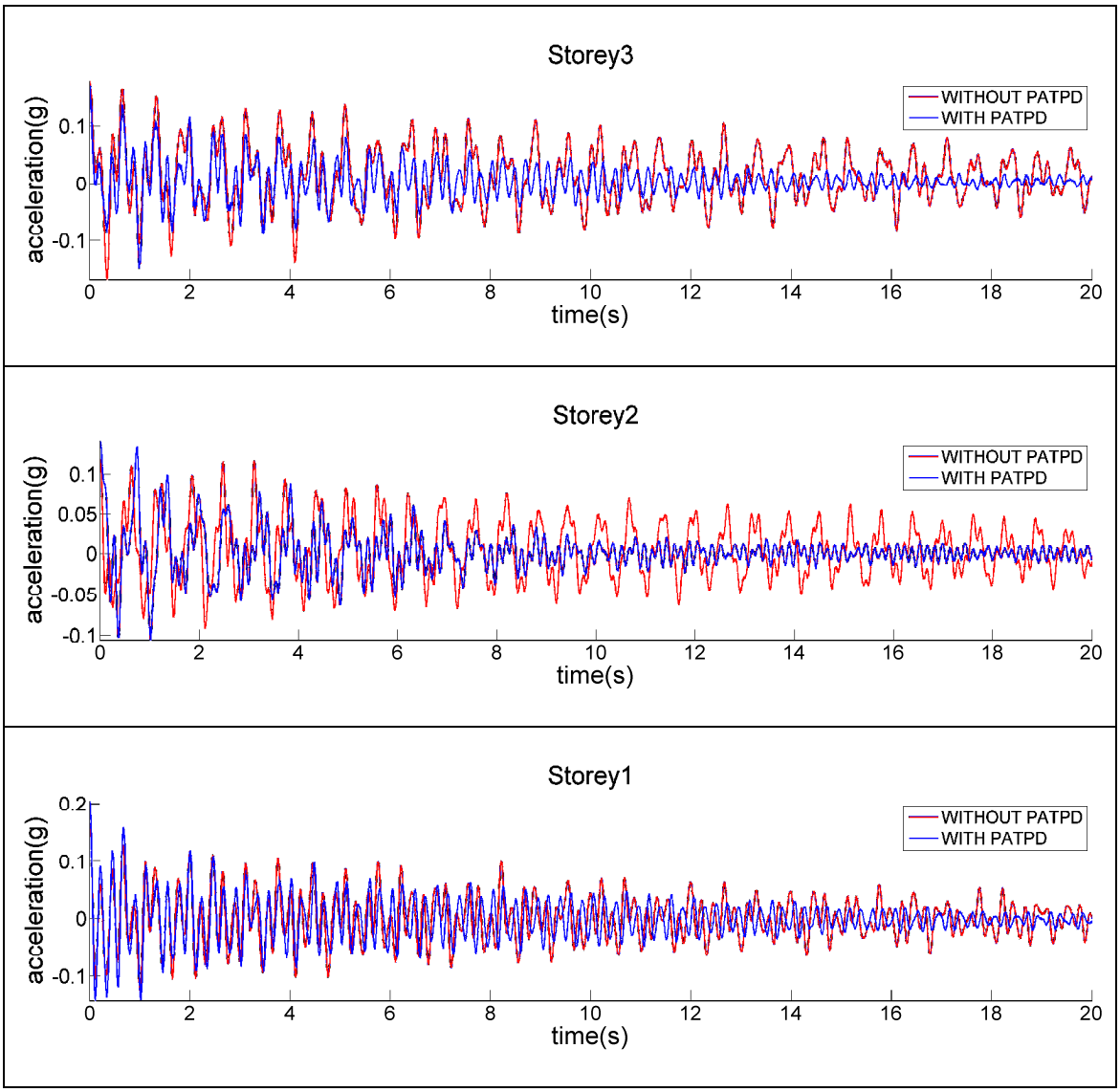

Figure 208: Time history of acceleration response per storey for free torsional vibration in the y-direction, model mass 52.09kg

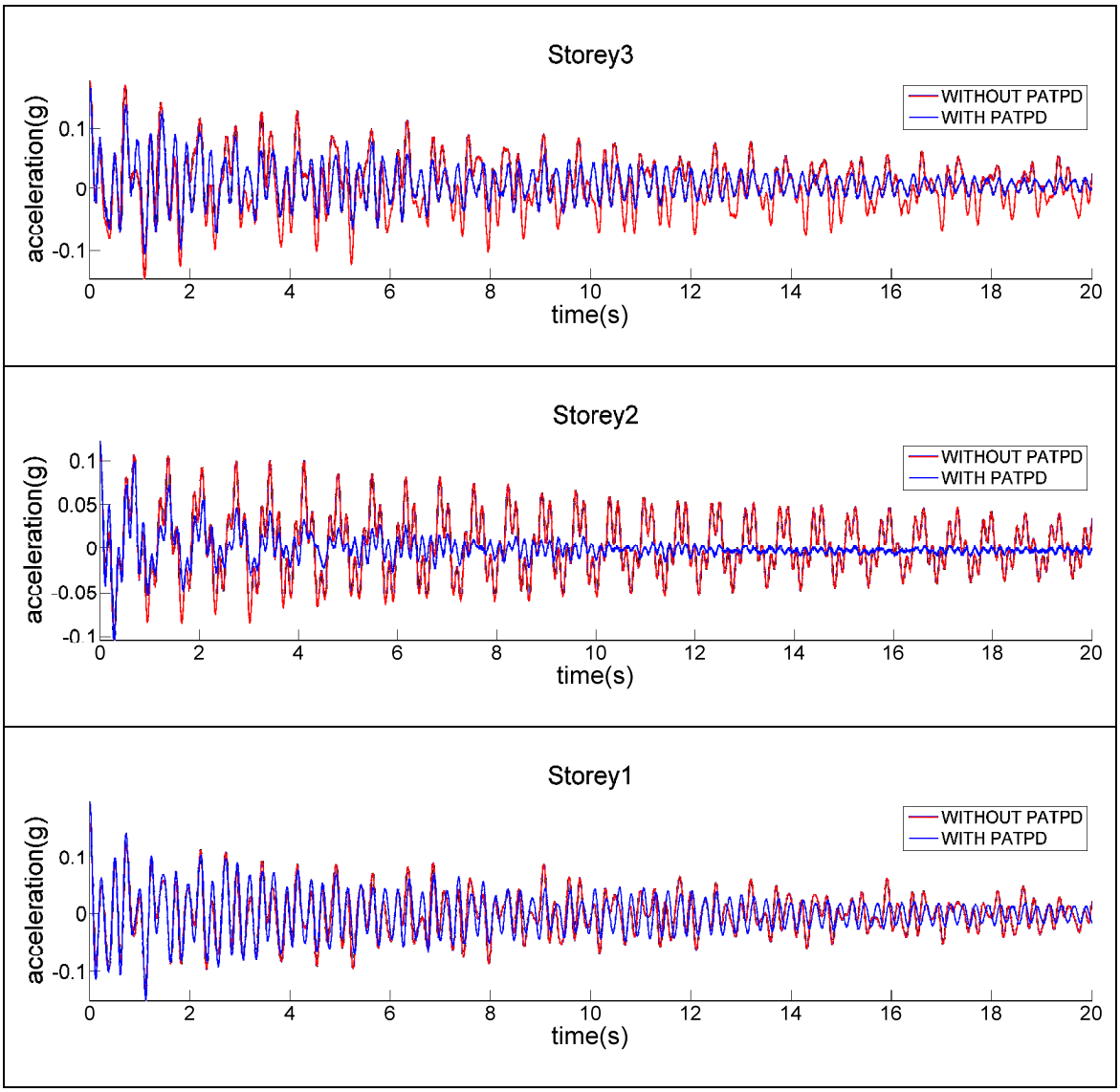

Figure 209: Time history of acceleration response per storey for free torsional vibration in the y-direction, model mass 66.09kg

Figure 208 and Figure 209 shows similarity to the results for the primary model[15], of mass 42.09kg, as the PATPD started moving, the acceleration peaks generated in the damped model are as high as those generated in the undamped model. However, these high accelerations subside and the accelerations rapidly decrease compared to that of the undamped model. As is expected the accelerations experienced in storey 3 are highest and the positive damping effect of the PATPD is still significant.

[15] Primary model (mass 42.09kg) figures can be found in Chapter 4 page 63 onwards

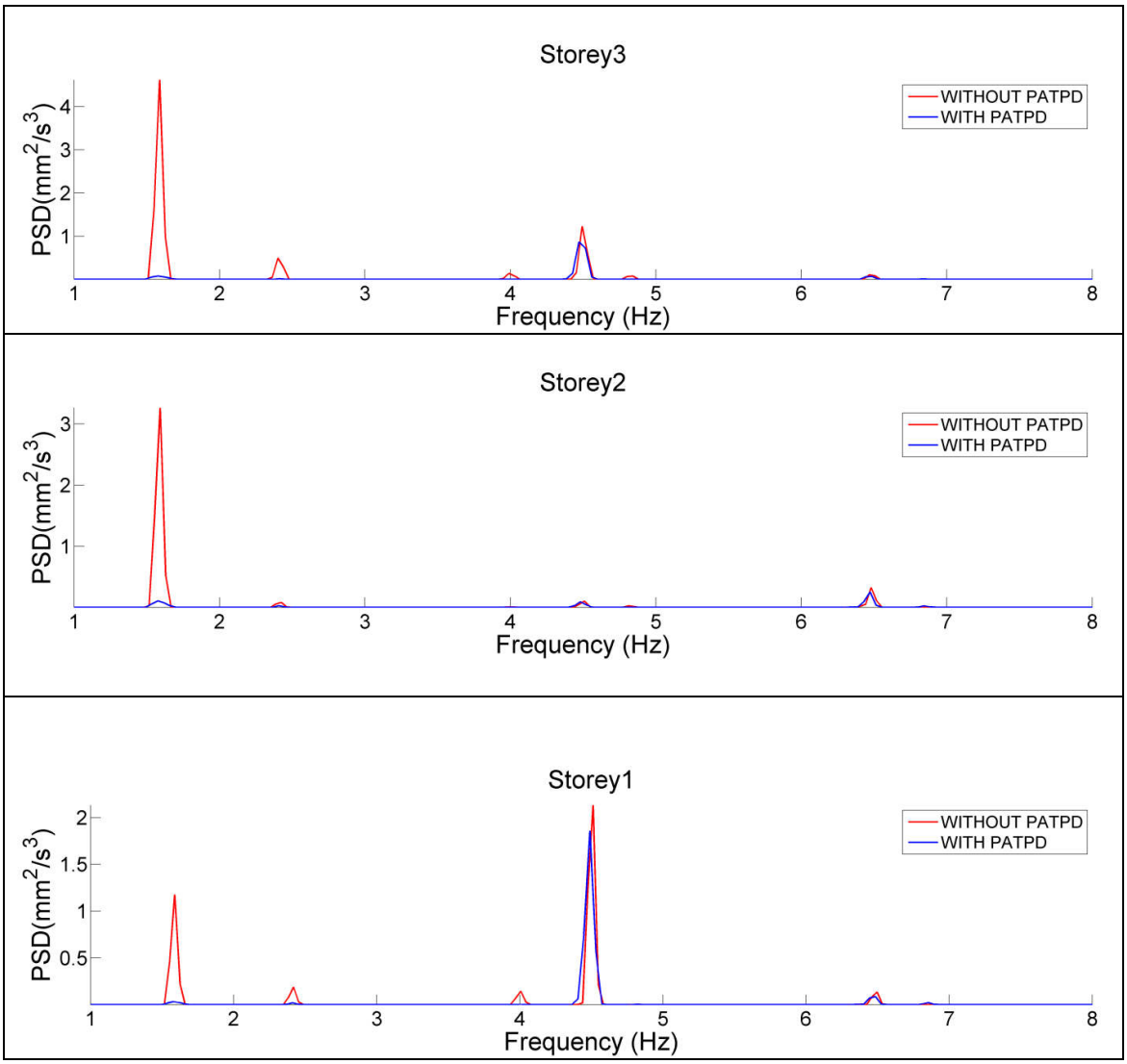

Figure 210: Power Spectral Density (PSD) per storey of the acceleration response for free torsional vibration in the y-direction, model mass 54.09kg

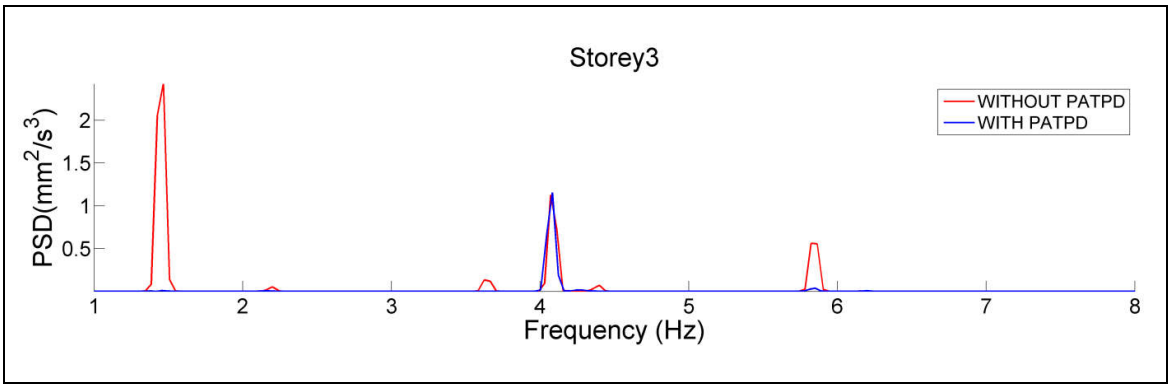

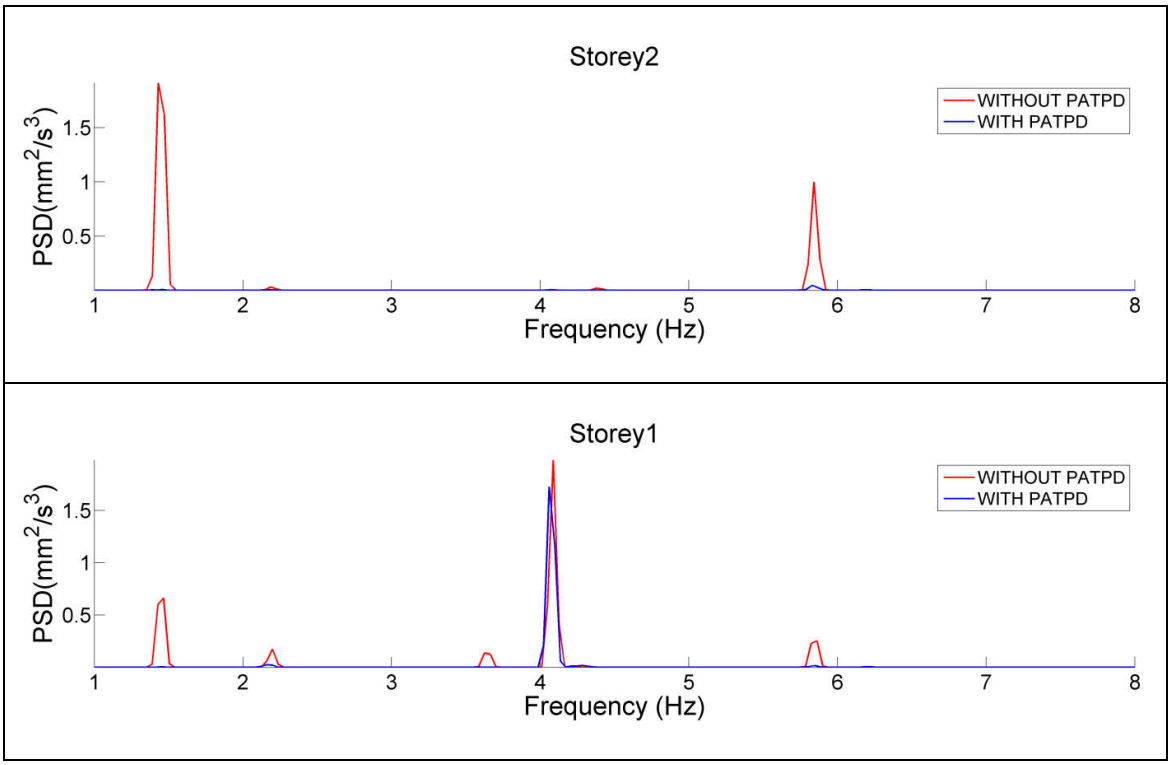

Figure 211: Power Spectral Density (PSD) per storey of the acceleration response for free torsional vibration in the y-direction, model mass 66.09kg

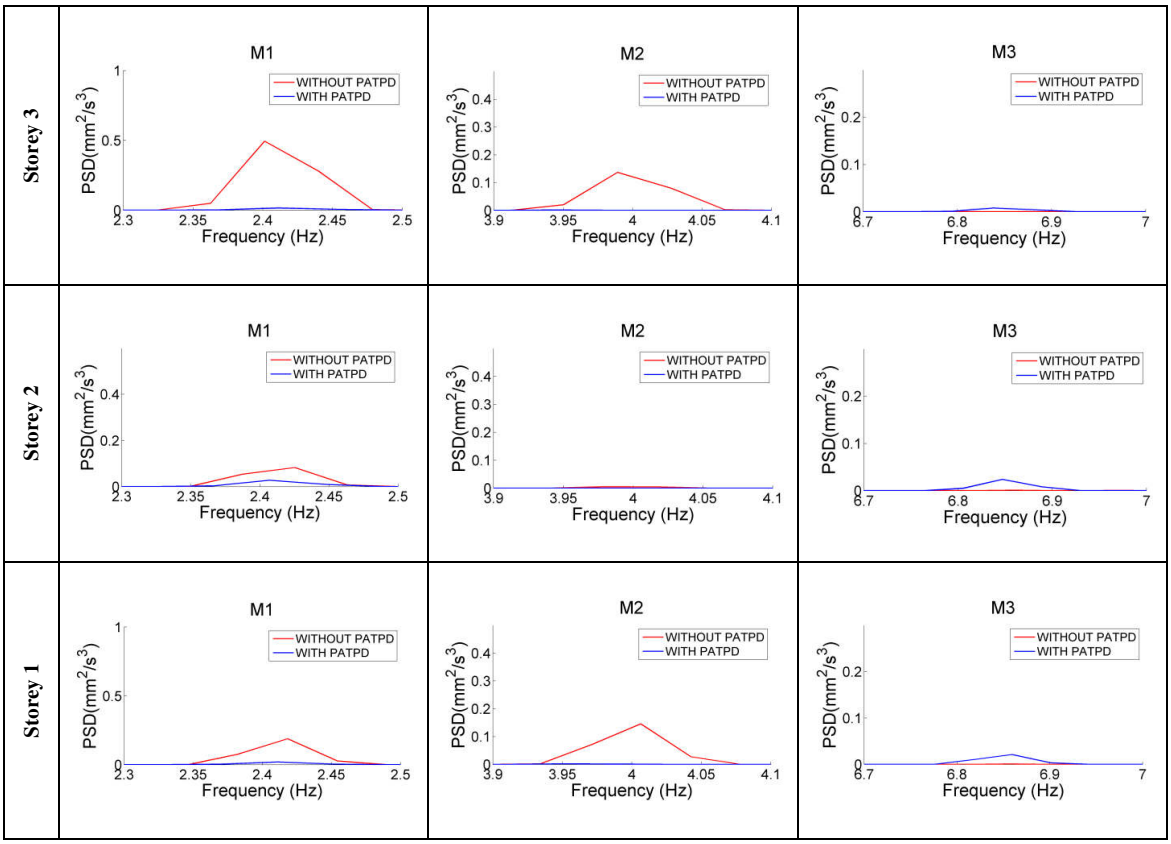

Figure 212: Magnified Power Spectral Density (PSD) of the acceleration response for free torsional vibration in the y-direction, model mass 54.09kg

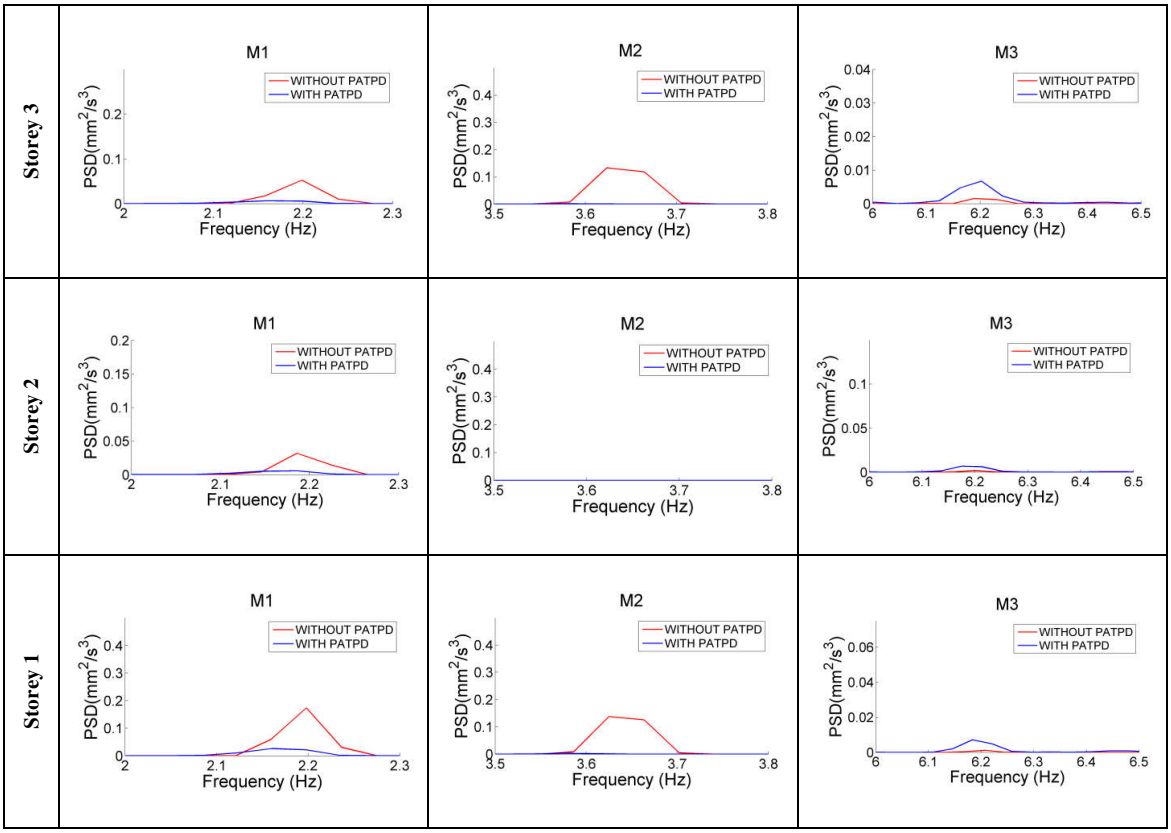

Figure 213: Magnified Power Spectral Density (PSD) of the acceleration response for free torsional vibration in the y-direction, model mass 66.09kg

Figure 210 shows a high peak for storeys 3-1, for model mass 54.09kg, at: 2.401Hz, 3.989Hz and 6.839Hz for the first. Figure 211 shows a high peak for storeys 3-1, for model mass 66.09kg, at: 2.199Hz, 3.624Hz and 6.189Hz. This represents the model's natural frequency for torsion in the y-direction.

Peaks are also visible at natural frequencies for translation in the y-direction which is expected as the structure had some movement in the y-direction as well as torsionally. As is also evident all translational frequencies are controlled by at least 99%, aside from second natural frequency PSD peak which is controlled but slightly.

As can be seen from Figure 212 and Figure 213, the PATPD provides at least 99% attenuation for all 3 storeys to the first and second natural frequency for both model masses. The second natural frequency PSD peak for both masses storey1-3 overall shows a slight increase in density of frequency.

It is also evident, as with the primary model, that the PATPD control in the x-direction is better than in the y-direction.

The PATPD has achieved attenuating the first natural frequency which has the greatest amplitude for translational vibration in the y-direction covering a relatively wide range of frequencies, by adapting to dynamic changes i.e. change in the models mass.

6.1.1.5 Coupled Vibration (translation in X-direction and torsion)

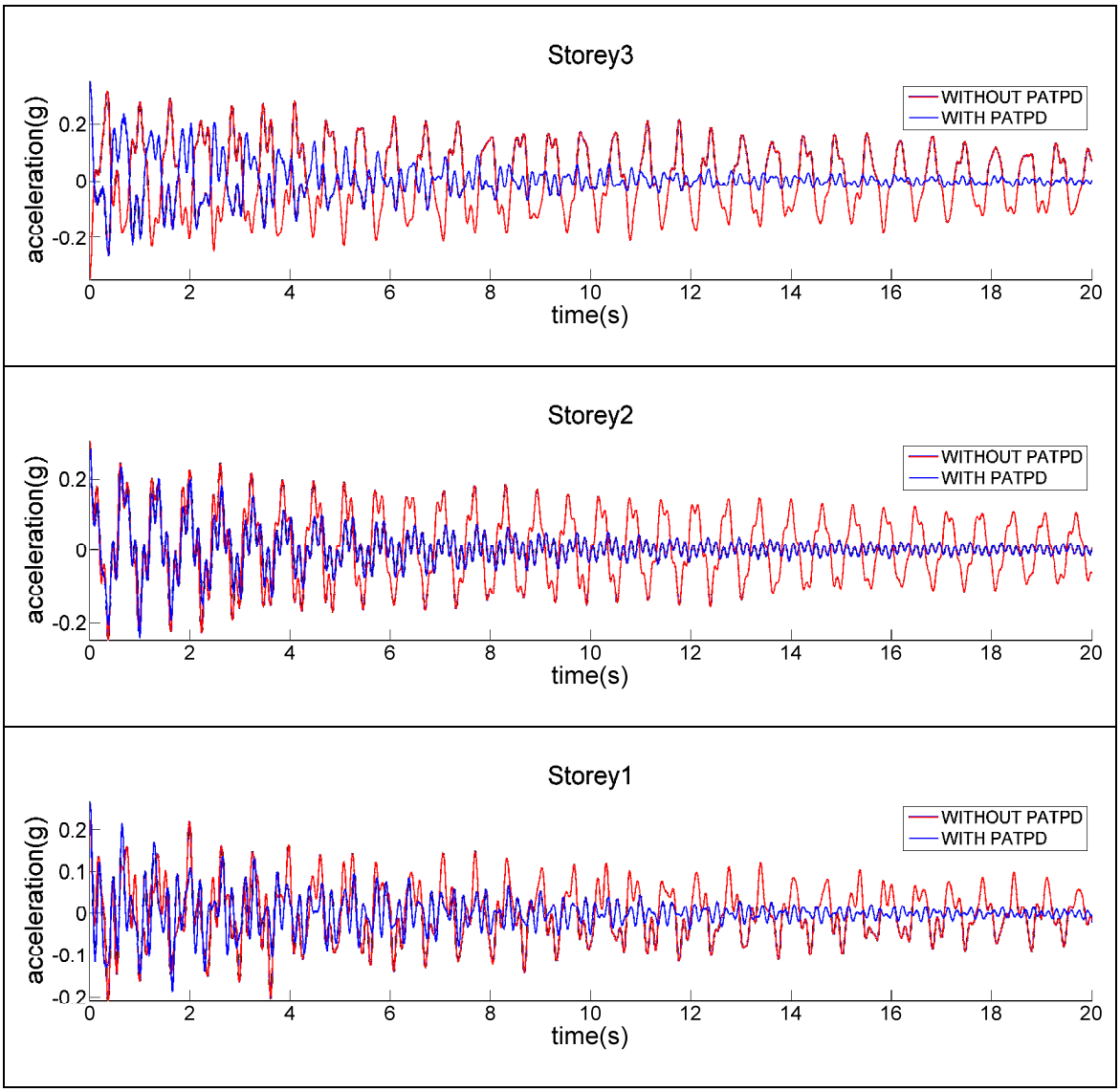

Figure 214: Time history of acceleration response per storey for free coupled vibration (translation in x-direction and torsion), model mass 52.09kg

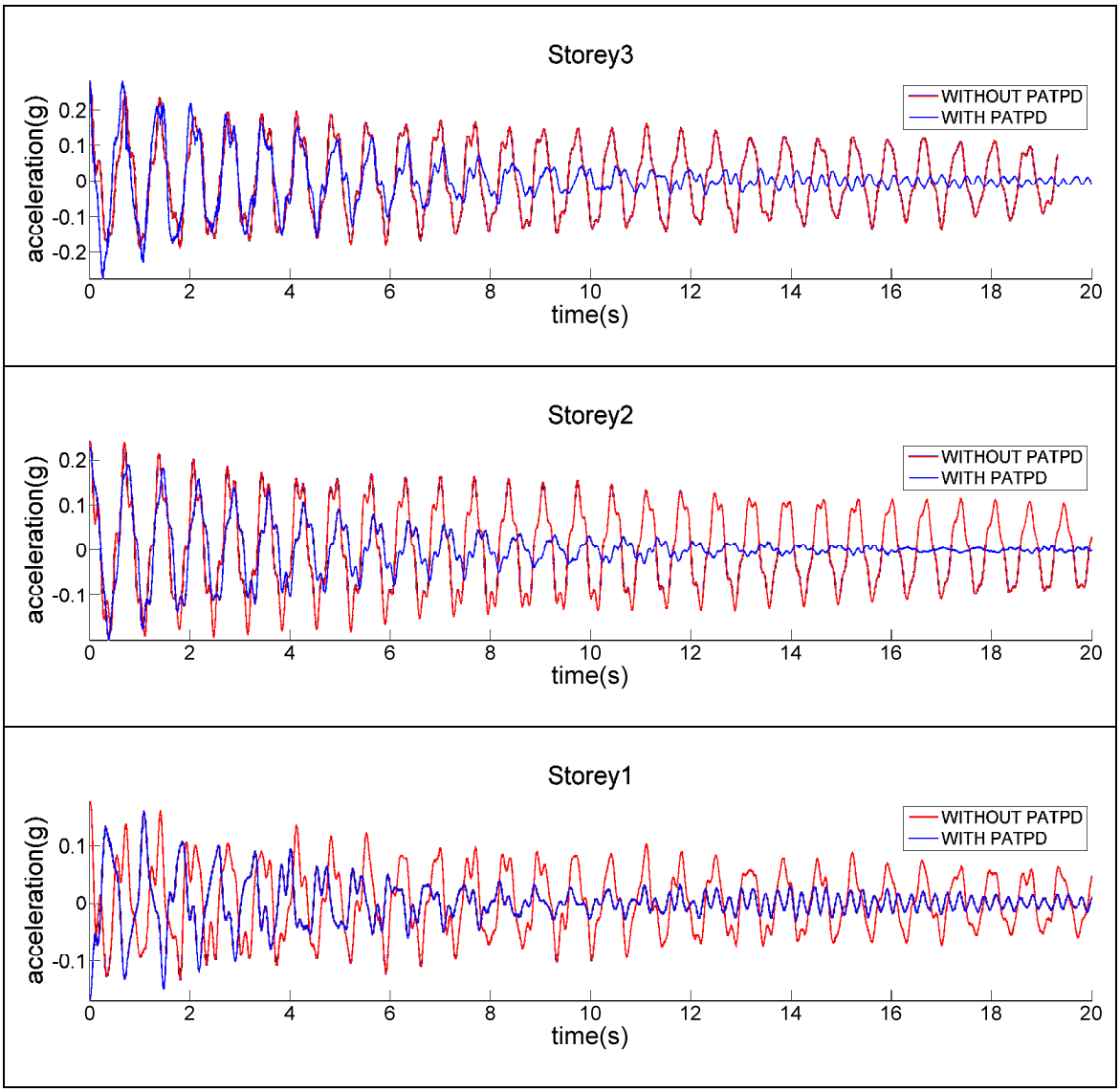

Figure 215: Time history of acceleration response per storey for free coupled vibration (translation in x-direction and torsion), model mass 66.09kg

Figure 214 and Figure 215 shows similarity to the results for the primary model[16], of mass 42.09kg, as the PATPD started moving, the acceleration peaks generated in the damped model are as high as those generated in the undamped model. However, these high accelerations subside and the accelerations rapidly decrease compared to that of the undamped model. As is expected the accelerations experienced in storey 3 are highest and the positive damping effect of the PATPD is still significant.

[16] Primary model (mass 42.09kg) figures can be found in Chapter 4 page 63 onwards

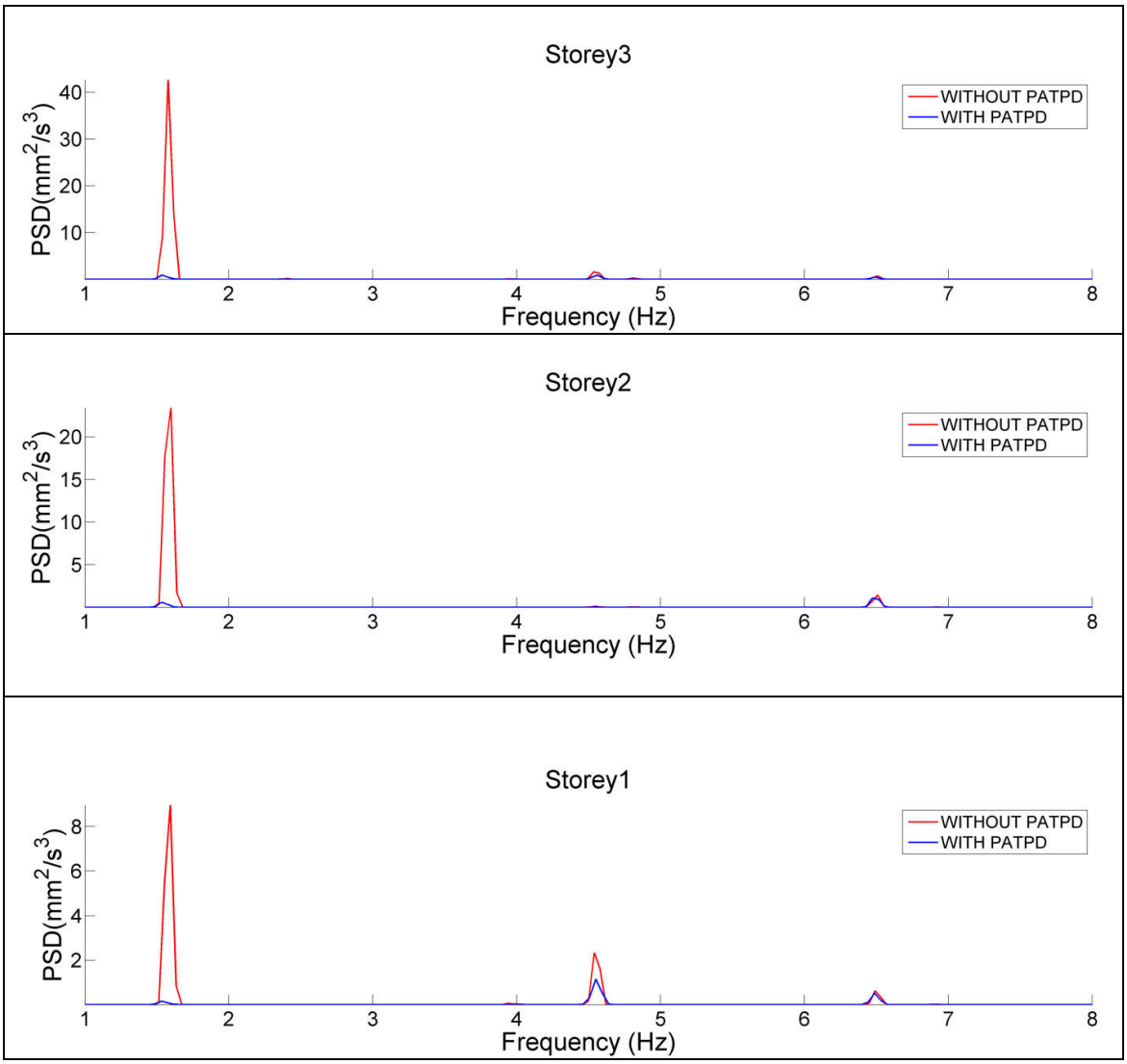

Figure 216: Power Spectral Density (PSD) per storey of the acceleration response for free coupled vibration (translation in x-direction and torsion), model mass 54.09kg

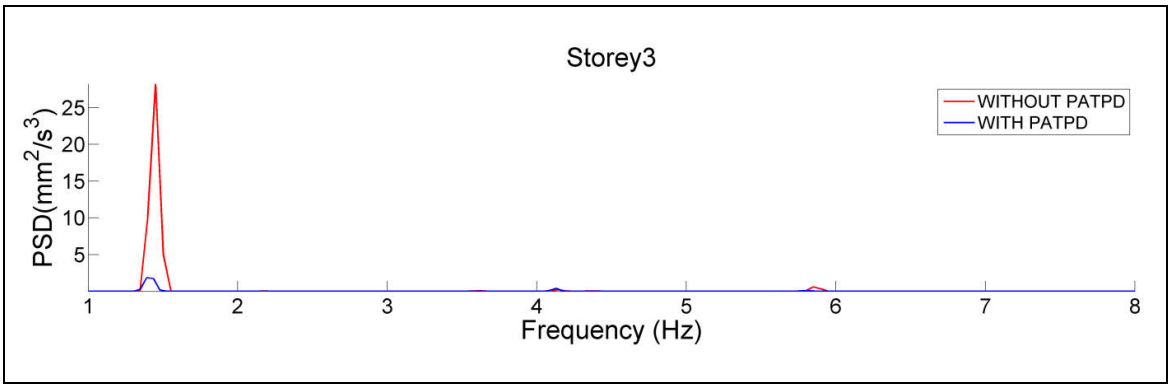

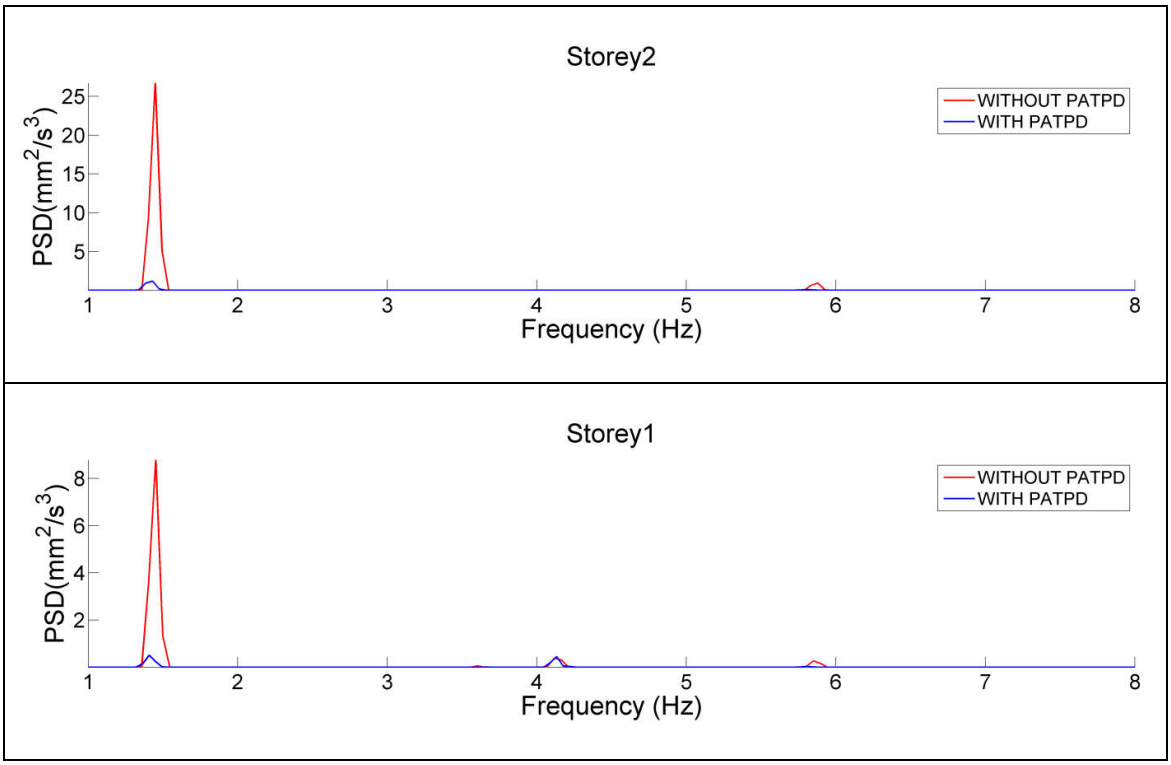

Figure 217: Power Spectral Density (PSD) per storey of the acceleration response for free coupled vibration (translation in x-direction and torsion), model mass 66.09kg

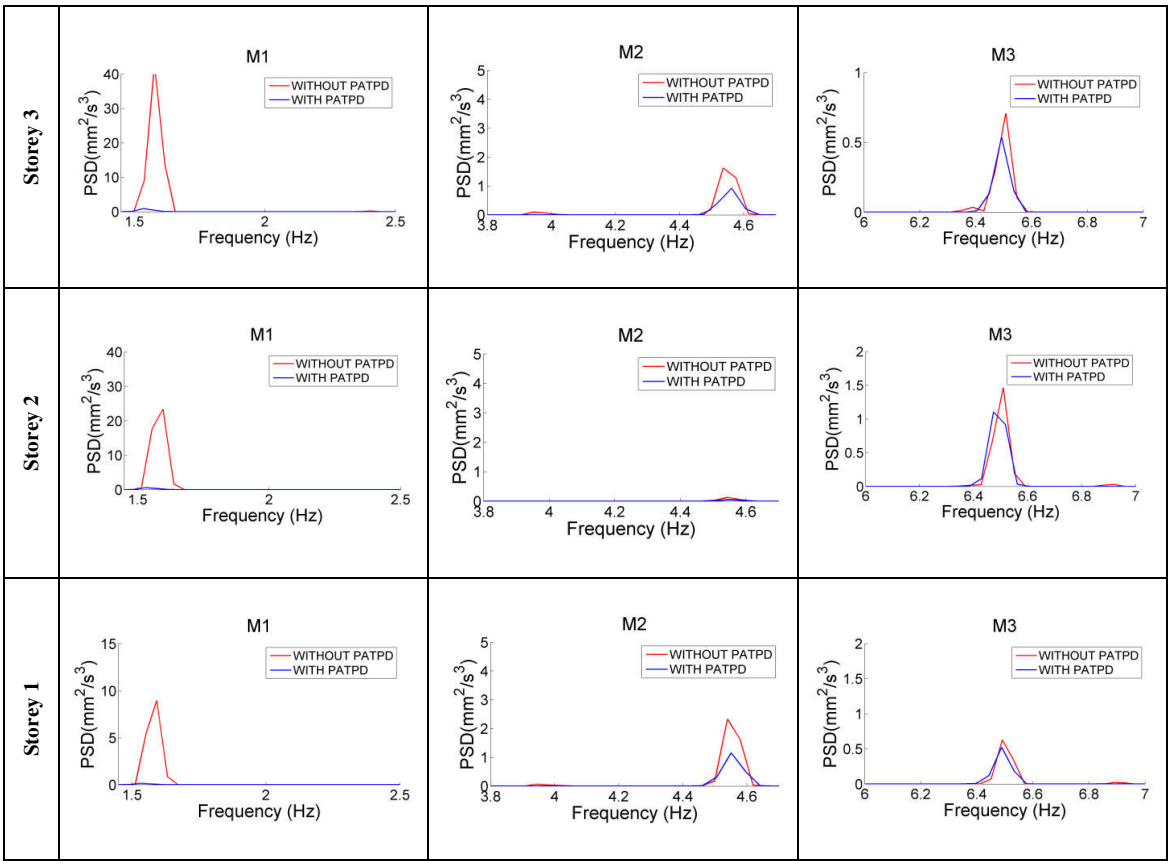

Figure 218: Magnified Power Spectral Density (PSD) of the acceleration response for free coupled vibration (translation in x-direction and torsion), model mass 54.09kg

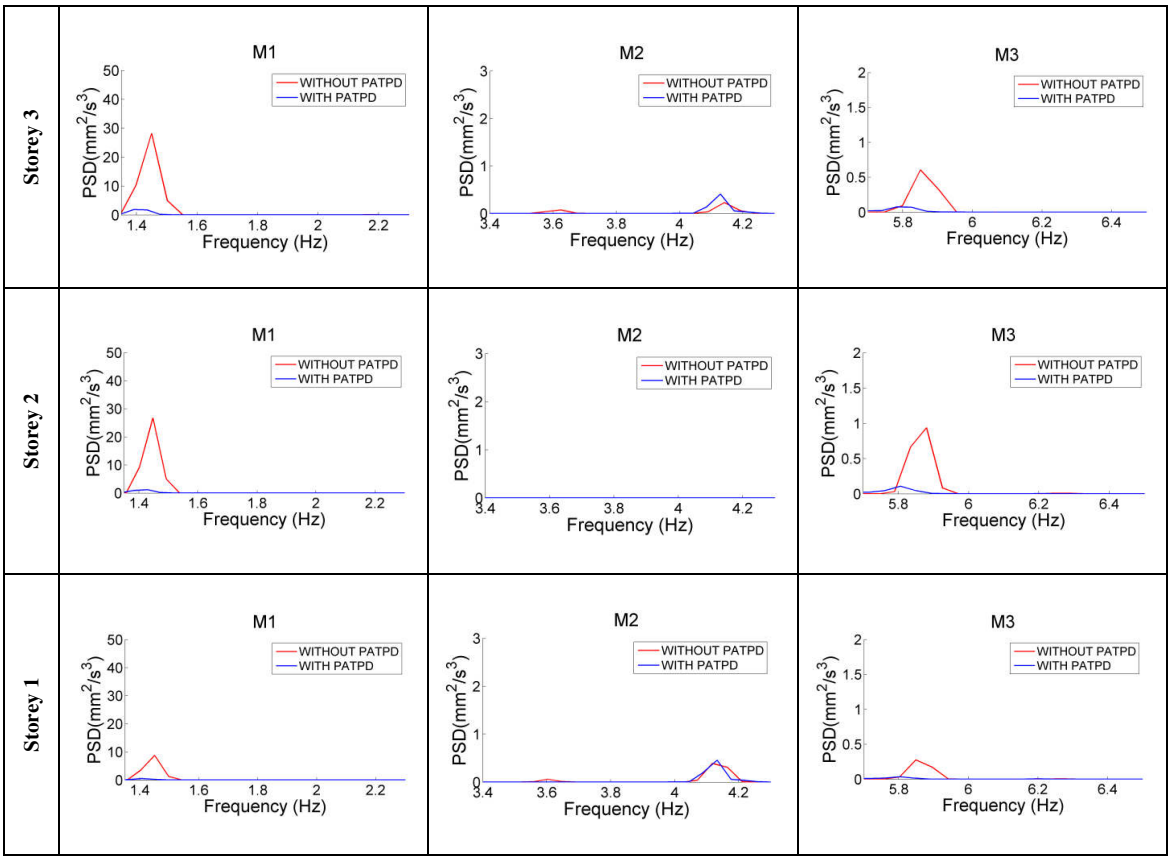

Figure 219: Magnified Power Spectral Density (PSD) of the acceleration response for free coupled vibration (translation in x-direction and torsion), model mass 66.09kg

Figure 216 for storeys 3-1, mass 54.09kg, shows a high peak at: 1.573Hz and 2.418; 4.550Hz and 4.000; and 6.506Hz and 6.858 for the first, second and third natural frequencies for translation and torsion respectively.

Figure 217 for storeys 3-1, mass 66.09kg shows a high peak at: 1.455Hz and 2.188; 4.136Hz and 3.647; and 5.860Hz and 6.625 for the first, second and third natural frequencies for translation and torsion respectively.

As can be seen from Figure 218 and Figure 219, for both translation and torsion the PATPD provides at least 99% attenuation for all 3 storeys to the first natural frequency for both model masses.

For the 54.09kg mass, the second natural torsional frequency is attenuated by at least 99% for all 3 storeys, whilst for translation shows at least 50% attenuation for all 3

storeys. For the 66.09kg mass the second natural torsional frequency is attenuated by at least 99% for the first and third storeys, whilst for translation shows minimal increase.

For both the 54.09kg and 66.09kg model mass the third natural torsional frequency is attenuated by at least 99% for all 3 storeys. For translation there is a slight attenuation for all 3 storeys for mass 54.09kg and at least 98% attenuation for model mass 66.09kg.

The PATPD has achieved attenuating the first natural frequency which has the greatest amplitude for coupled vibration in the x-direction covering a relatively wide range of frequencies, by adapting to dynamic changes i.e. change in the models mass.

6.1.1.6 Coupled Vibration (translation in Y-direction and torsion)

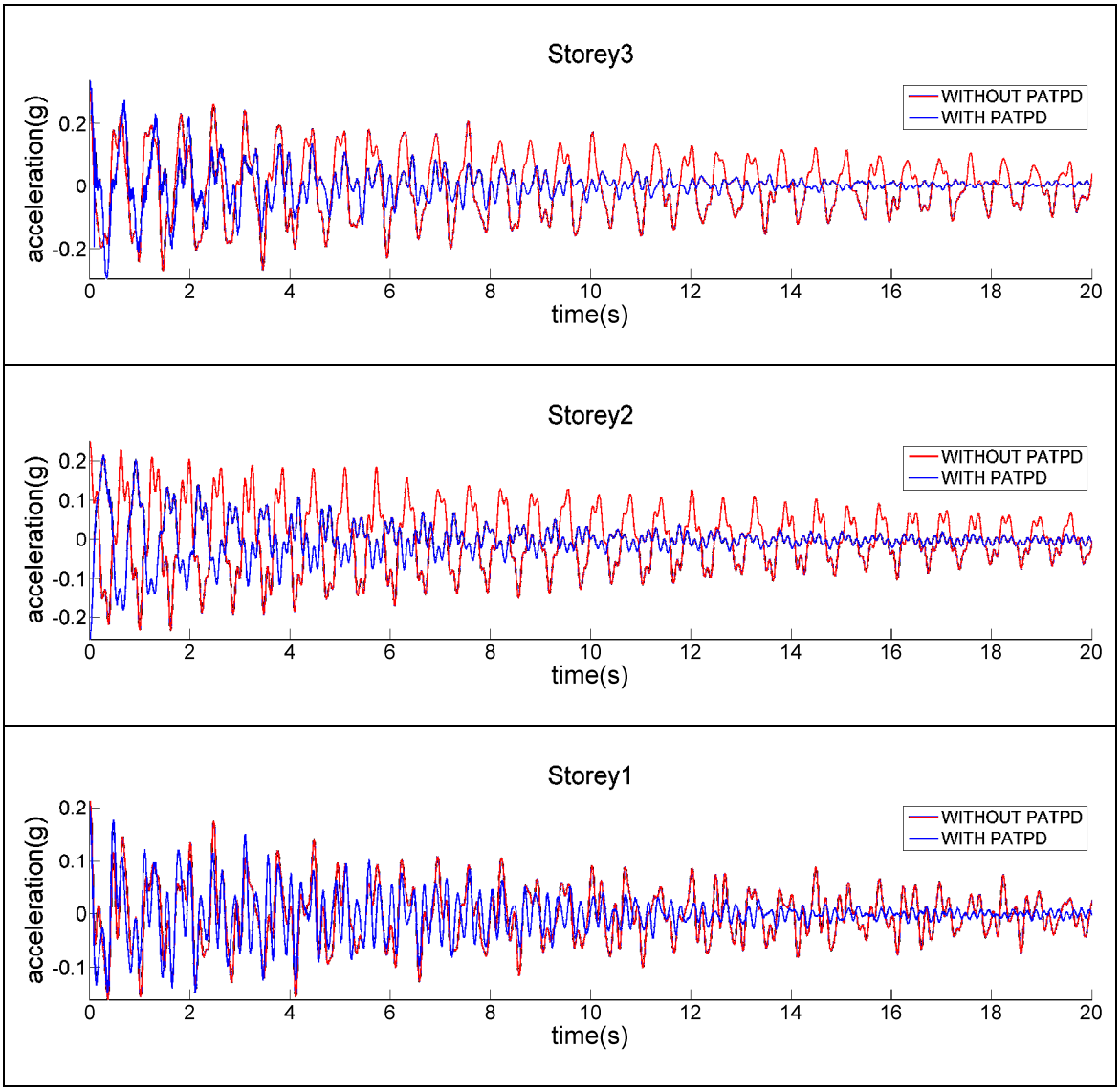

Figure 220: Time history of acceleration response per storey for free coupled vibration (translation in y-direction and torsion), model mass 52.09kg

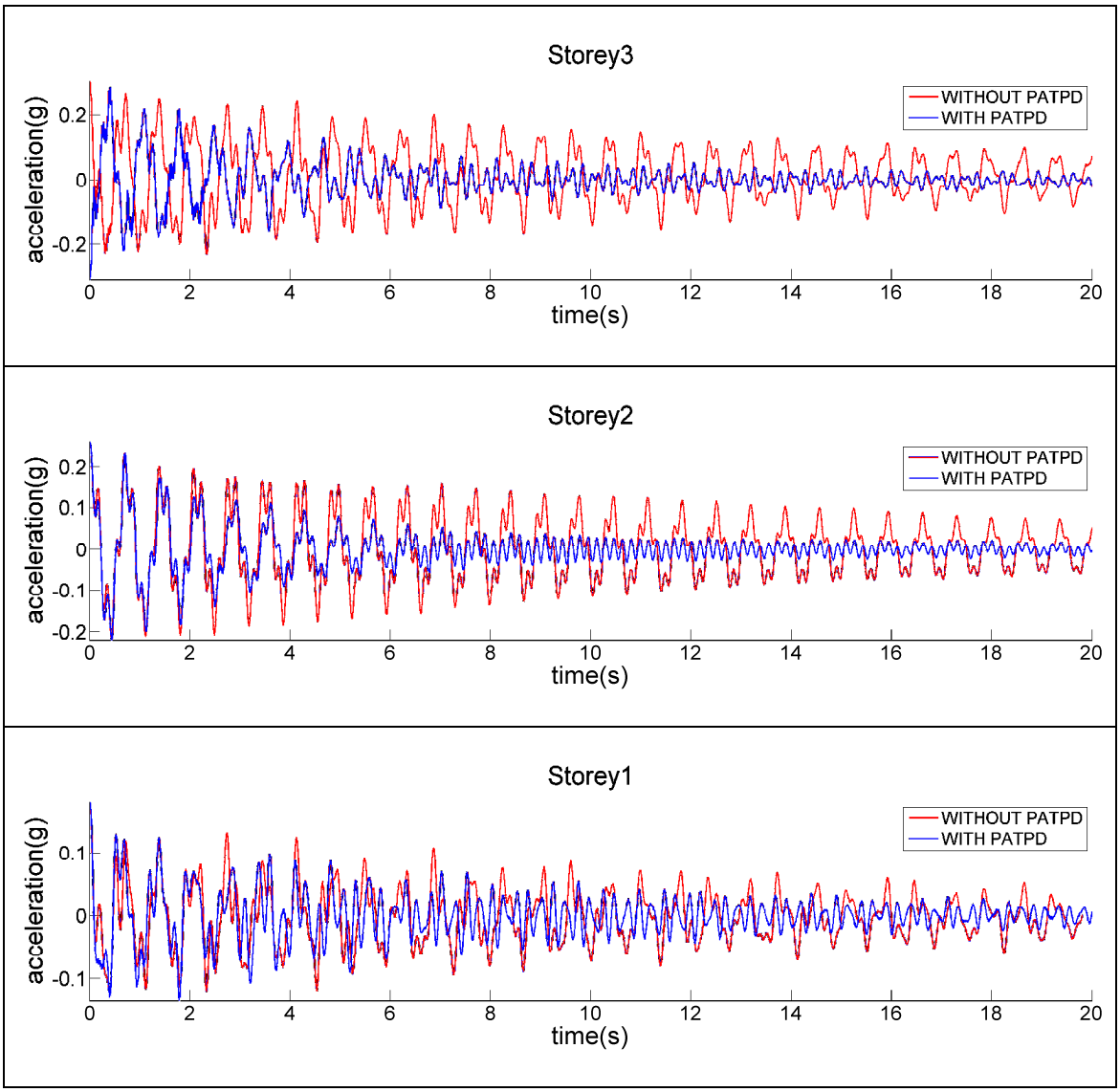

Figure 221: Time history of acceleration response per storey for free coupled vibration (translation in y-direction and torsion), model mass 66.09kg

Figure 220 and Figure 221 shows similarity to the results for the primary model[17], of mass 42.09kg, as the PATPD started moving, the acceleration peaks generated in the damped model are as high as those generated in the undamped model. However, these high accelerations subside and the accelerations rapidly decrease compared to that of the undamped model. As is expected the accelerations experienced in storey 3 are highest and the positive damping effect of the PATPD is still significant.

[17] Primary model (mass 42.09kg) figures can be found in Chapter 4 page 63 onwards

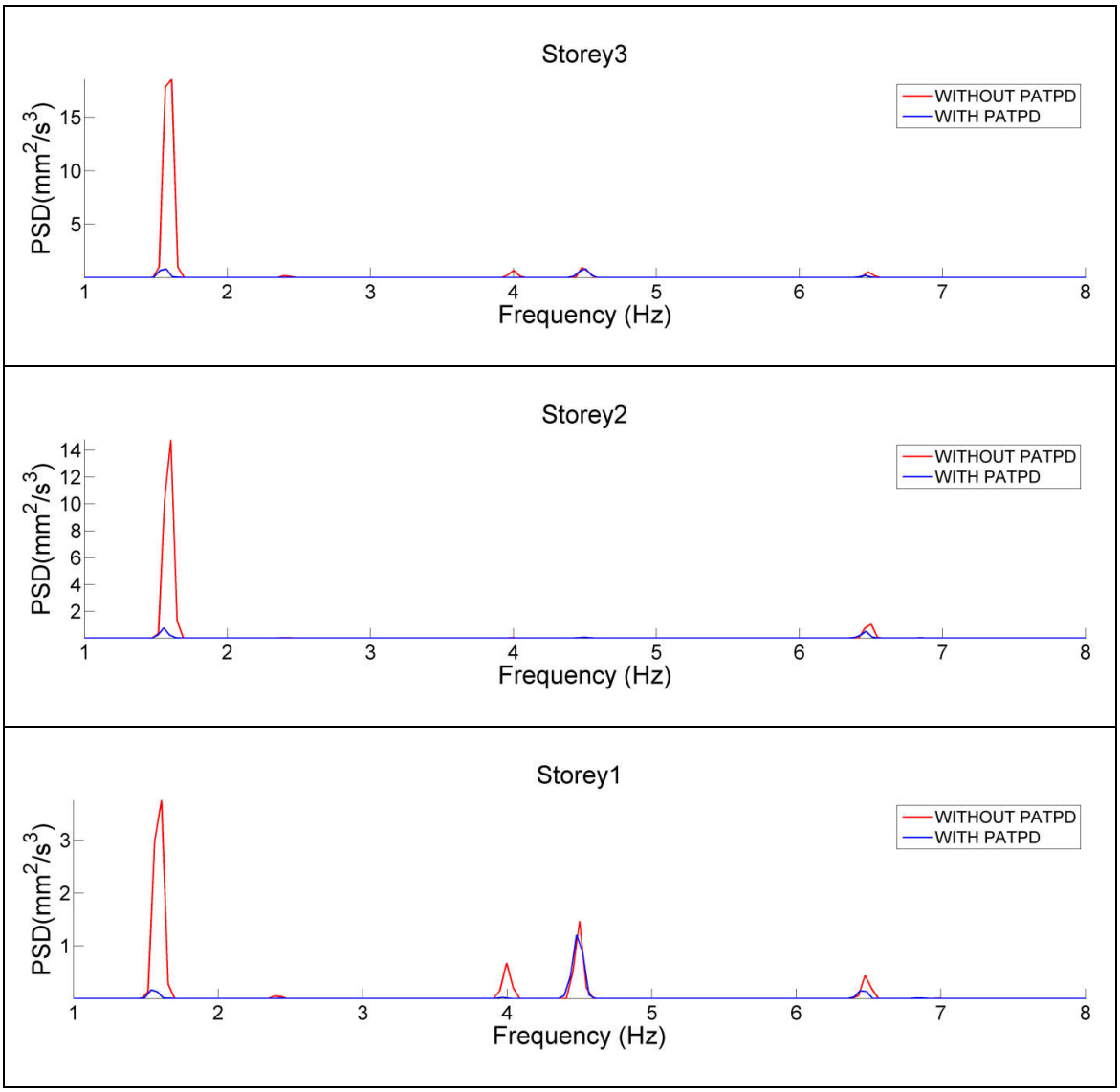

Figure 222: Power Spectral Density (PSD) per storey of the acceleration response for free coupled vibration (translation in y-direction and torsion), model mass 54.09kg

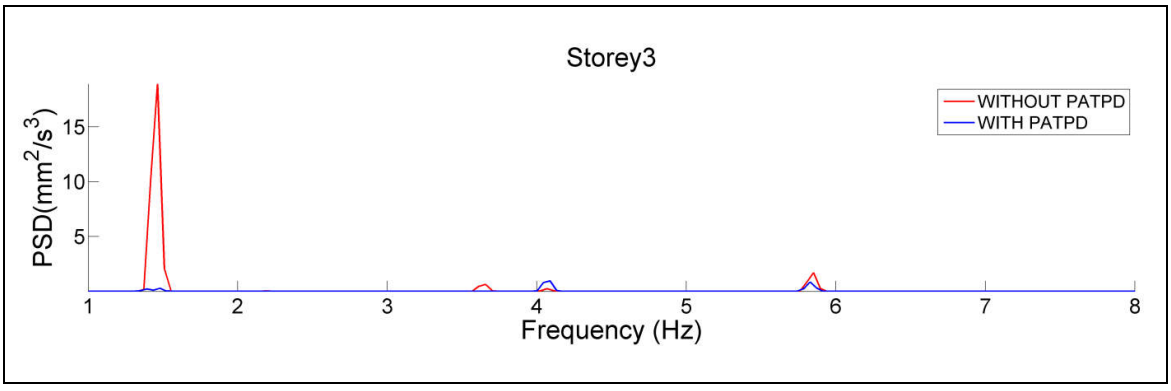

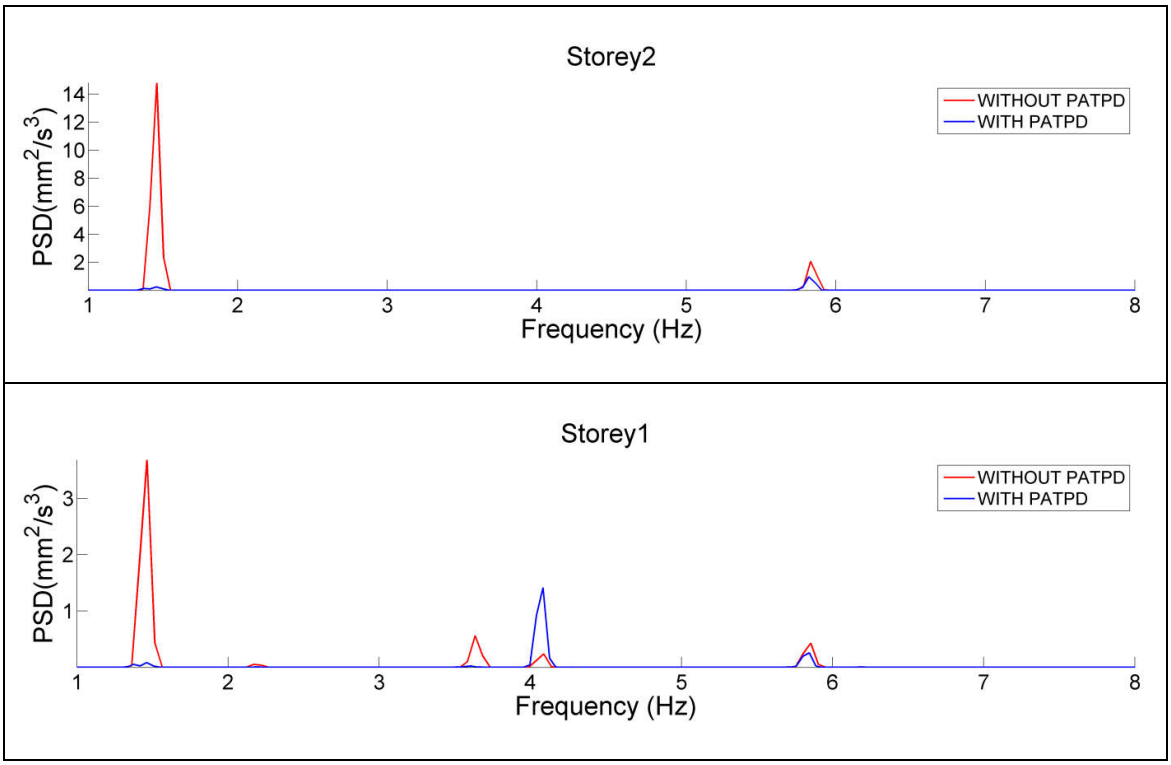

Figure 223: Power Spectral Density (PSD) per storey of the acceleration response for free coupled vibration (translation in y-direction and torsion), model mass 66.09kg

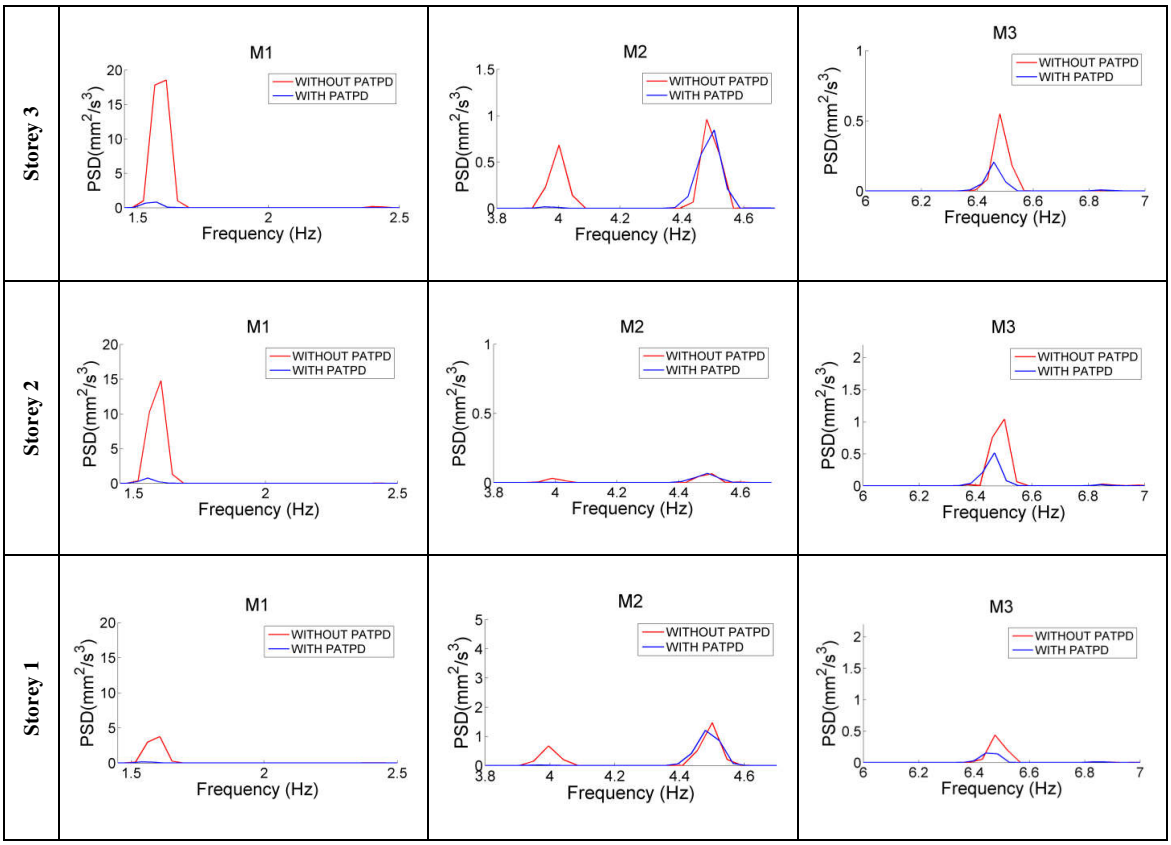

Figure 224: Magnified Power Spectral Density (PSD) of the acceleration response for free coupled vibration (translation in y-direction and torsion), model mass 54.09kg

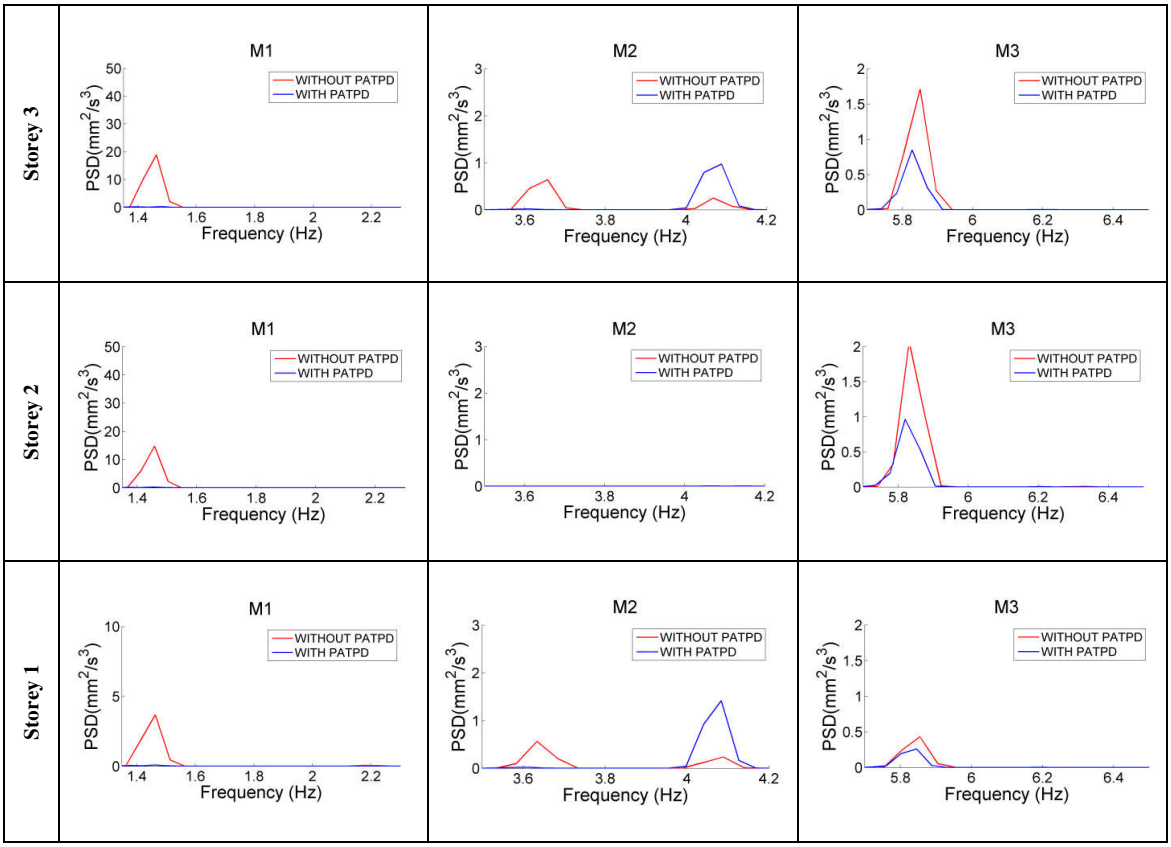

Figure 225: Magnified Power Spectral Density (PSD) of the acceleration response for free coupled vibration (translation in y-direction and torsion), model mass 66.09kg

Figure 222 for storeys 3-1, mass 55.09kg, shows a high peak at: 1.593Hz and 2.401; 4.492Hz and 3.989; and 6.500Hz and 6.839 for the first, second and third translational and torsional natural frequencies.

Figure 223 for storeys 3-1, mass 66.09kg, shows a high peak at: 1.471Hz and 2.199; 4.092Hz and 3.624; and 5.839Hz and 6.189 for the first, second and third translational and torsional natural frequencies.

As can be seen from Figure 224 and Figure 225, for both translation and torsion the PATPD provides at least 99% attenuation for all 3 storeys to the first natural frequency for both model masses.

For the 54.09kg mass the second torsional PSD peak is attenuated by at least 99% for all 3 storeys, whilst for translation shows slight attenuation for all 3 storeys. For the

66.09kg mass the second torsional PSD peak is attenuated by at least 99% for the first and third storeys, whilst for translation shows slight increase.

For both the 54.09kg and 66.09kg model mass the third torsional PSD peak is attenuated by at least 99% for all 3 storeys, whilst for translation shows at least 50% attenuation for all 3 storeys.

The PATPD has achieved attenuating the first natural frequency which has the greatest amplitude for coupled vibration in the y-direction covering a relatively wide range of frequencies, by adapting to dynamic changes i.e. change in the models mass.

It is also evident, as with the primary model, that the PATPD control in the x-direction is better than in the y-direction.

6.1.2.0 Forced Vibration

6.1.2.1 Translational Vibration in the X-Direction

The test model is orientated on the shake table so as to generate forced vibrations in the x-direction. The test model was chosen such that it would have the largest change from the primary model, thus the model with mass of 66.09kgwas used instead of 54.09kg. A frequency sweep was performed from 0Hz to 10Hz with and without the damper. The test duration was 120 seconds.

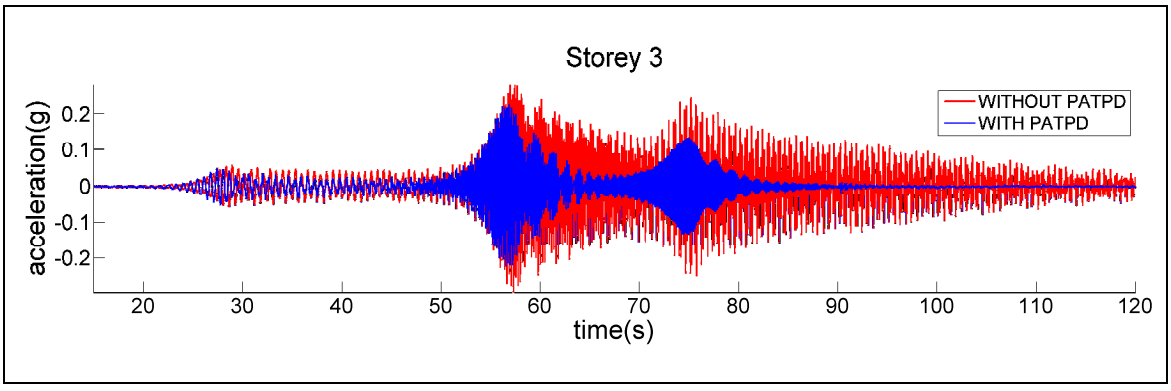

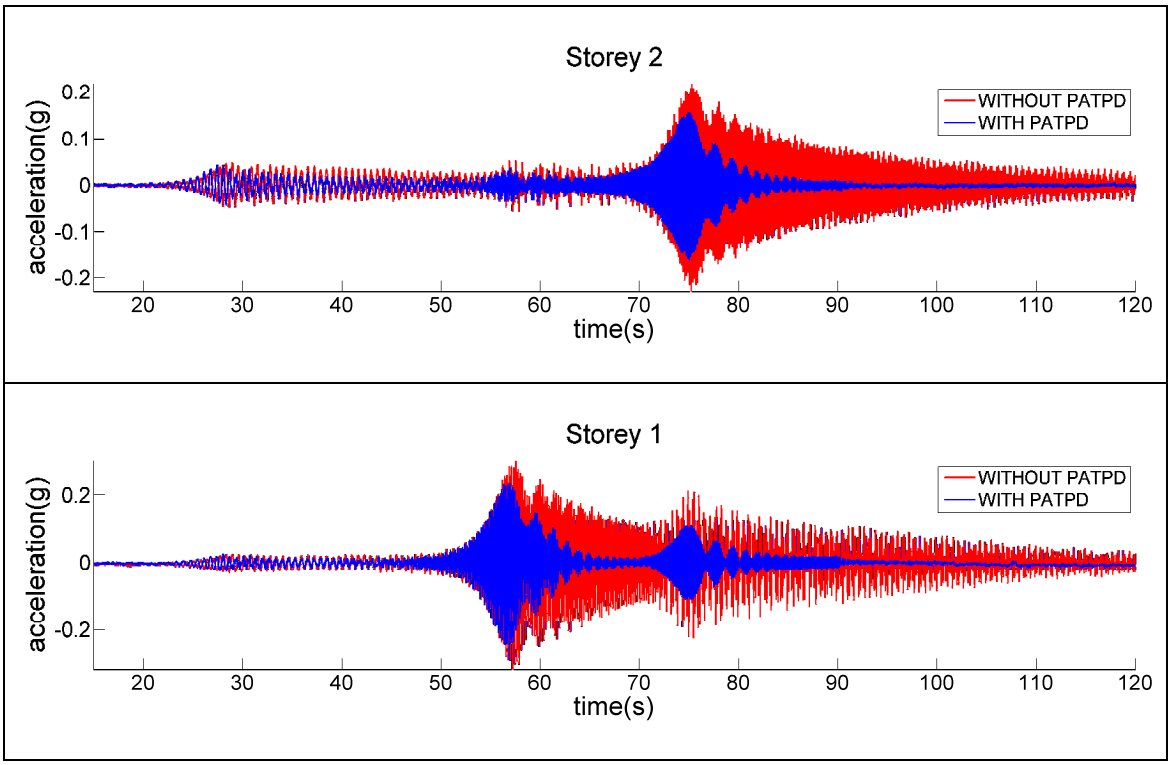

Figure 226: Time history of acceleration response per storey for forced translational vibration in x-direction, model mass 54.09kg

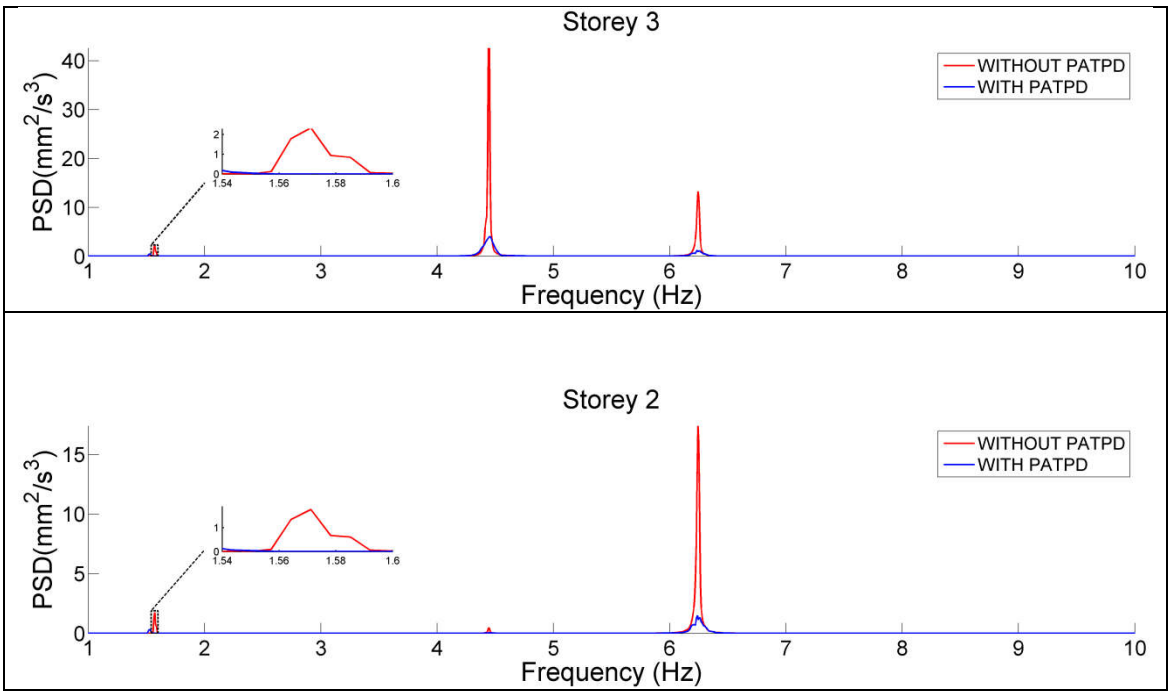

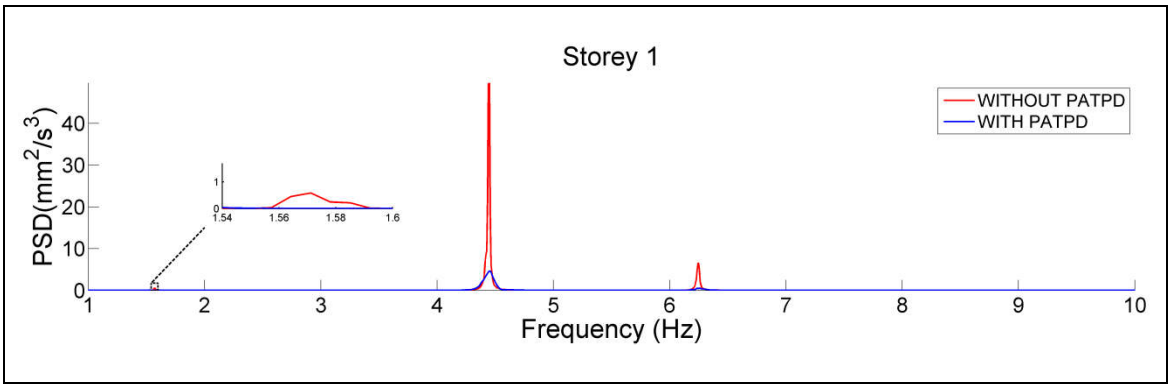

Figure 227: Power Spectral Density (PSD) of the acceleration response per storey under forced excitation in the x-direction, model mass 66.09kg

Figure 226 shows for all 3 storeys that by adding the damper onto model the acceleration experience is significantly decreased.

Figure 227 shows PSD peaks at 1.571Hz, 4.441Hz and 6.243Hz. This corresponds to the models first, second and third frequencies. The positive control effect is evident as PSD peaks for all 3 frequencies are significantly reduced by at least 95%.

6.1.2.2 Translational Vibration in the Y-Direction

The test model is orientated on the shake table so as to generate forced vibrations in the y-direction on the model. The test duration was 120 seconds.

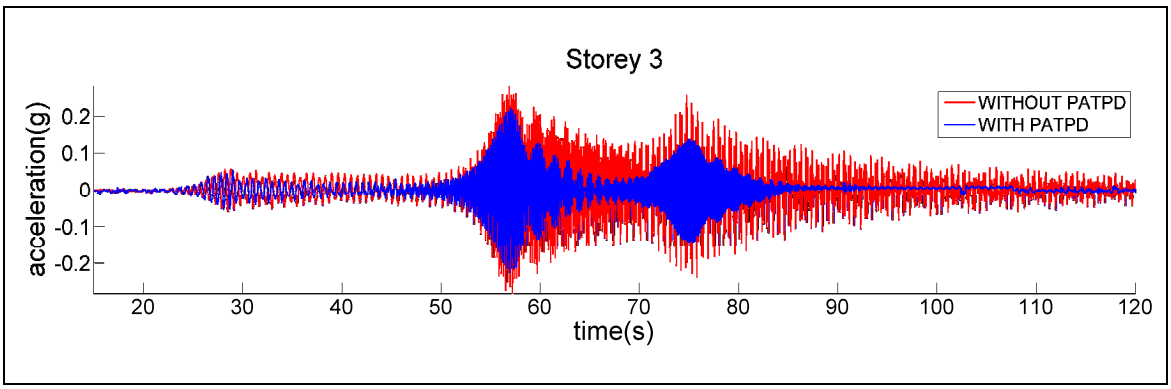

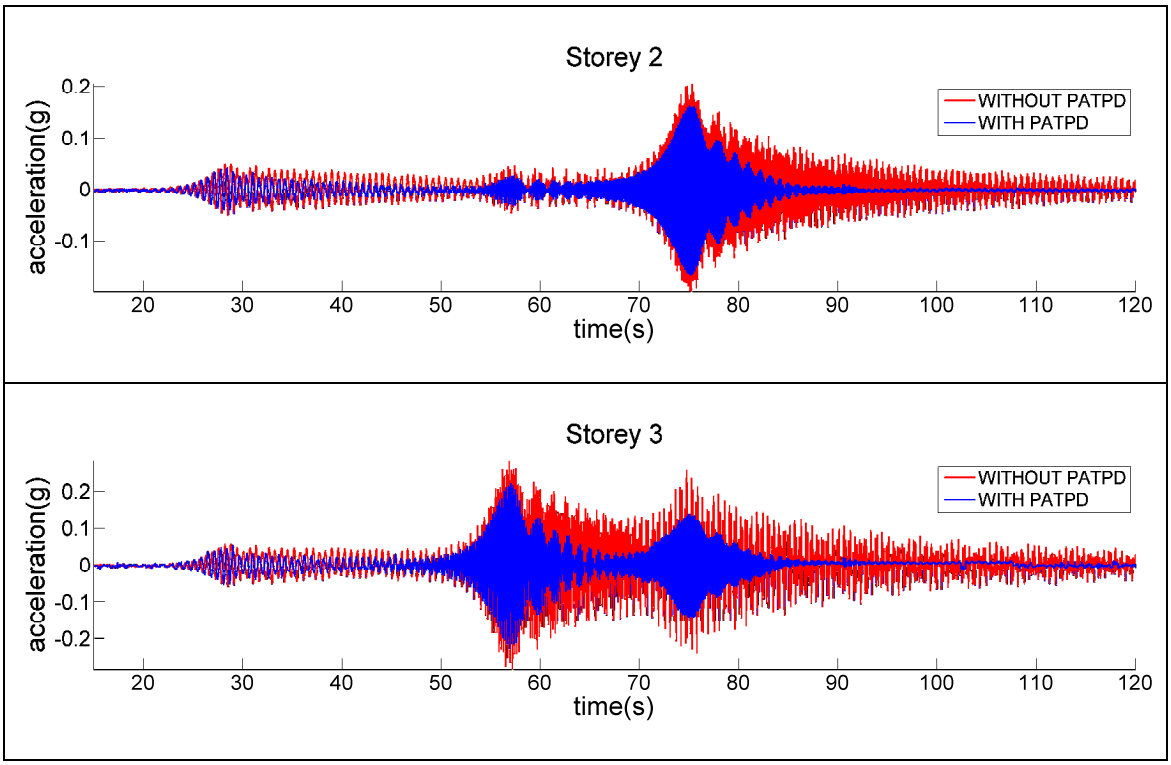

Figure 228: Time history of acceleration response per storey for forced translational vibration in y-direction, model mass 54.09kg

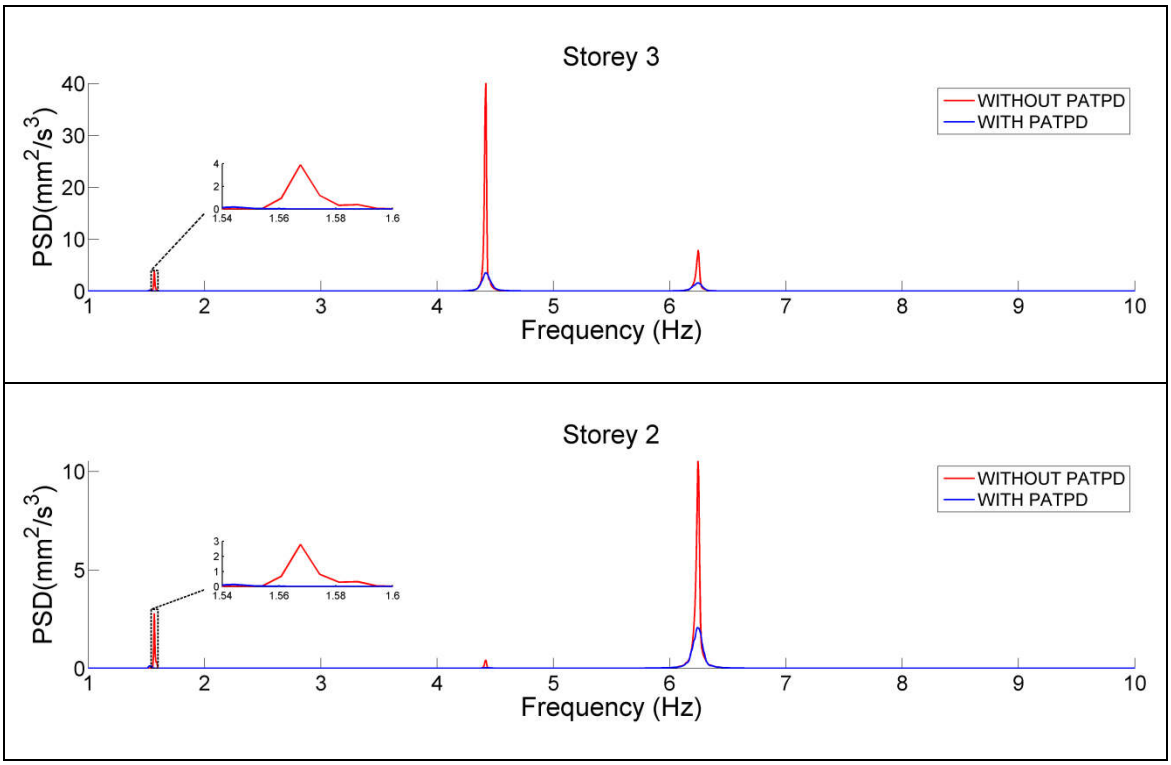

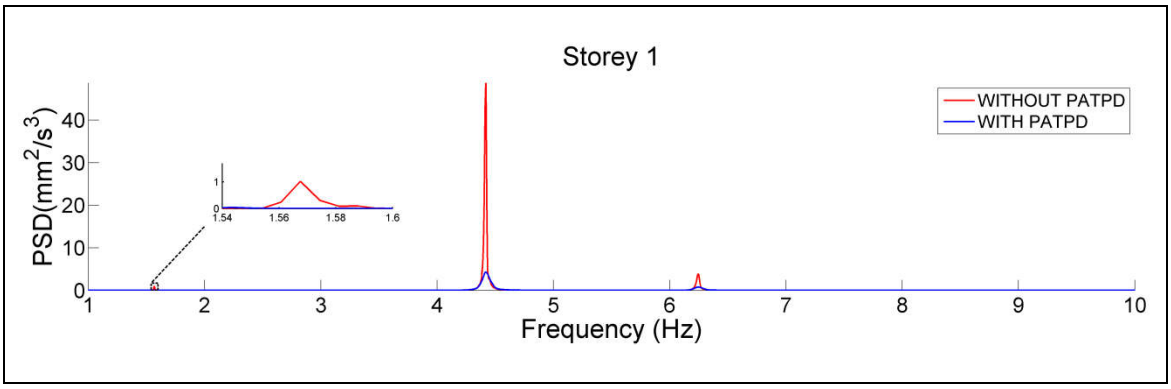

Figure 229: Power Spectral Density (PSD) of the acceleration response per storey under forced excitation in the y-direction, model mass 66.09kg

Figure 228 shows for all 3 storeys that by adding the damper onto model the acceleration experience is significantly decreased.

Figure 229 shows PSD peaks at 1.568Hz, 4.419Hz and 6.243Hz. This corresponds to the models first, second and third frequencies. The positive control effect is evident as PSD peaks for all 3 frequencies are significantly reduced by at least 95%.

6.1.3.0 Summary and Conclusions

Free Vibration

The results for both model masses show similar trend to the primary model. As the PATPD started moving, the acceleration peaks generated in the damped model are as high as those generated in the undamped model. However, these high accelerations subside and the accelerations rapidly decrease compared to that of the undamped model.

For translational vibration in the x directions the PATPD provides at least 93% attenuation to both first and third natural frequency PSD peaks. However, the second natural frequency PSD peak shows an increase in density for both model masses. Results in the y-direction are similar except that in addition to the increase to second natural frequency PSD peak, there is so too an increase in the third natural frequency PSD peak thus indicating better control effect in x-direction than y-direction for translation.

Under Torsional vibration the PATPD provides at least 99% attenuation for all 3 storeys to the first and second natural frequency for both model masses. This applies to both the x and y directions. The third natural frequency PSD peak for both masses storey1-3

overall shows a slight increase in density of frequency, the increase is less than that of the y-direction thus again supporting the PATPDs better control in x-direction than y-direction.

For coupled vibration the torsional frequency measured in y-direction, for all 3 natural frequency PSD peaks, for all storeys is attenuated by at least 99%, with the translational frequencies also being attenuated slightly, albeit not completely. Torsion measured in y-direction shows same trend except that there is a slight increase in density of second translational frequency PSD peak.

Table 1: Comparison of percentage change of PSD peak for the first natural frequency with and without PATPD for free vibration, for the 42.09kg (primary model), 54.09kg and 66.09kg model mass

	Translation vibration		Torsion vibration		Coupled vibration			
					Translation		Torsion	
	x	y	x	y	x	y	x	y
42.09kg - first natural frequency	1.733	1.747	2.677	2.680	1.733	1.747	2.677	2.680
42.09kg - % change in PSD peak	99.9%	98.7%	99.9%	99.9%	99.3%	99.3%	99.9%	99.2%
54.09kg - first natural frequency	1.573	1.593	2.418	2.401	1.573	1.593	2.418	2.401
54.09kg - % change in PSD peak	99.2%	98.8%	91.9%	96.8%	97.8%	95.6%	86.1%	95.5%
66.09kg - first natural frequency	1.455	1.471	2.188	2.199	1.455	1.471	2.188	2.199
66.09kg - % change in PSD peak	93.2%	98.4%	86.5%	88.8%	98.8%	99.2%	93.7%	95.5%

As is evident from Table 1 even though the mass has changed, which resulted in the change of the structures' natural frequency, the control provided by the PATPD was still significant for all tests. Without any tuning or adjustment to the damper it still efficiently controlled vibration.

Forced Vibration

For Forced Vibration the PATPD provides significant control to all 3 frequencies for the dynamic property change of mass. This demonstrates the auto-tuning or adaptivity of the PATPD.

The results reveal that the PATPD performs better in translation the x –direction than the y-direction.

6.2 Changing Dynamic Properties: Effect of changing model stiffness

In order to demonstrate that the proposed PATPD is adaptive to any frequency, the primary model's natural frequencies were changed in Chapter 5. Now the model's stiffness will be changed. This chapter encloses results from tests with and without the PATPD as the model stiffness is changed thus changing its frequencies. This is achieved by changing the storey heights – they are kept constant for all 3 storeys. The primary model storey height is 37.0cm - the test model height is then decreased to 32cm and then to 27cm[18]. The height was changed by decreasing only since the maximum height of 37cm was used in primary model, the height cannot be increased further as the columns would have buckled.

[18] A detailed description of configuration 8 can be found on 60

6.2.1 Free Vibration

6.2.1.1 Translational Vibration in the X-direction

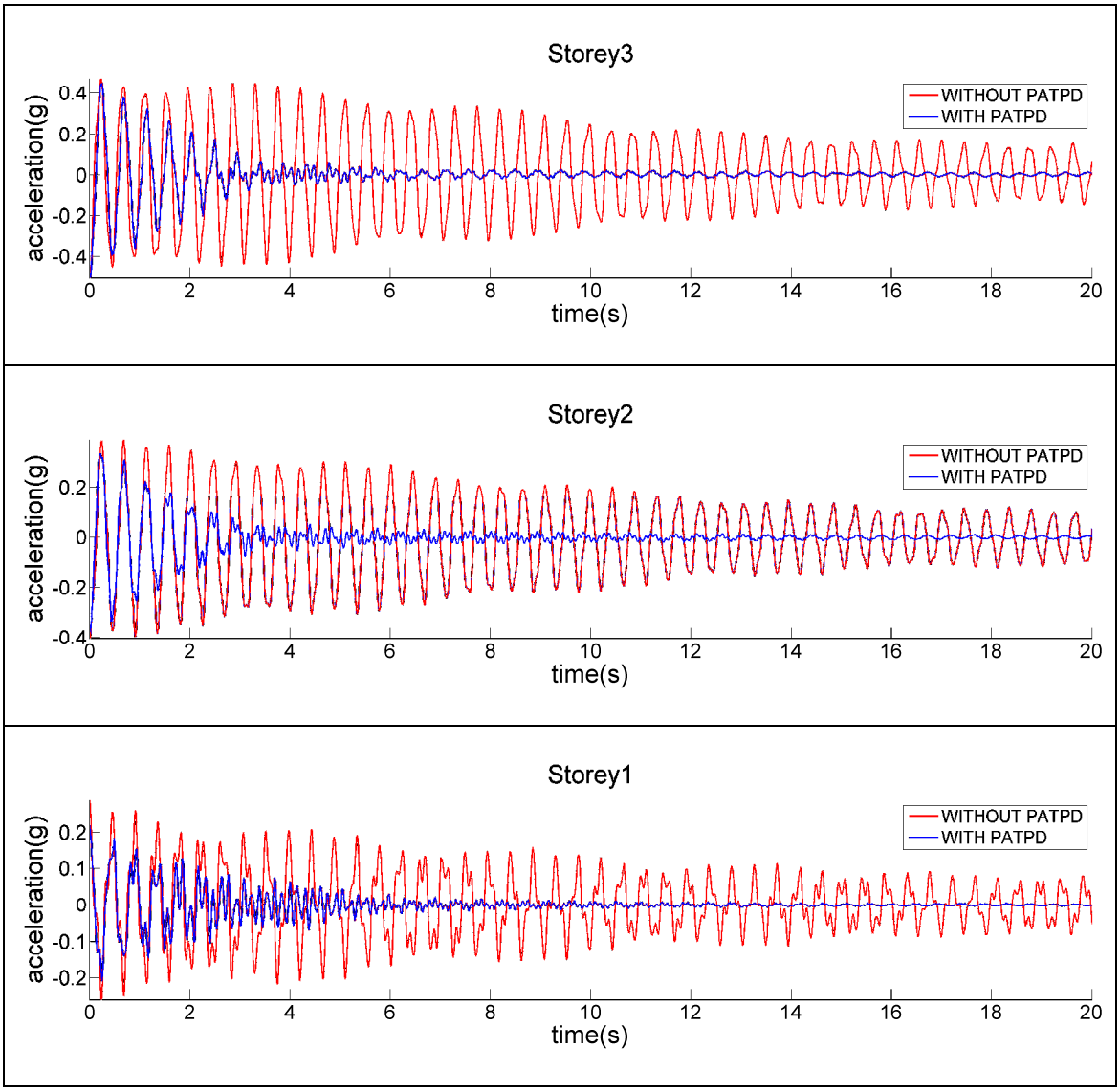

Figure 230: Time history of acceleration response per storey for free translational vibration in the x-direction, model height 27cm

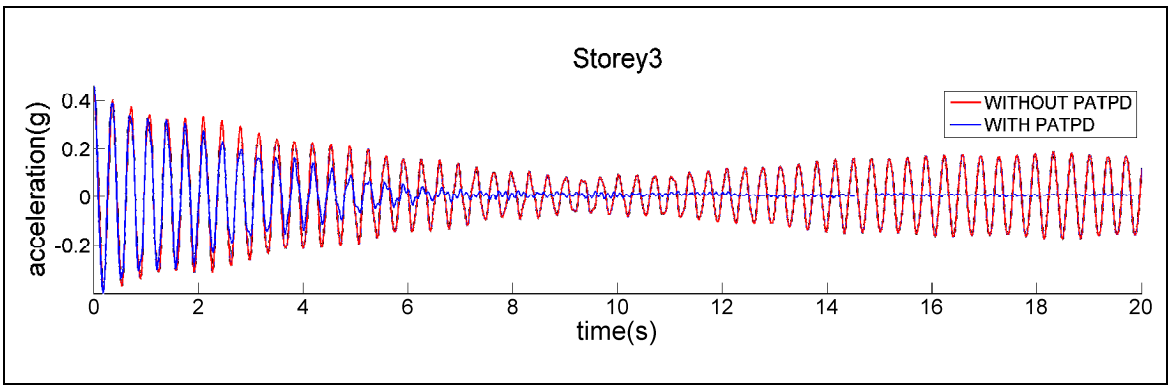

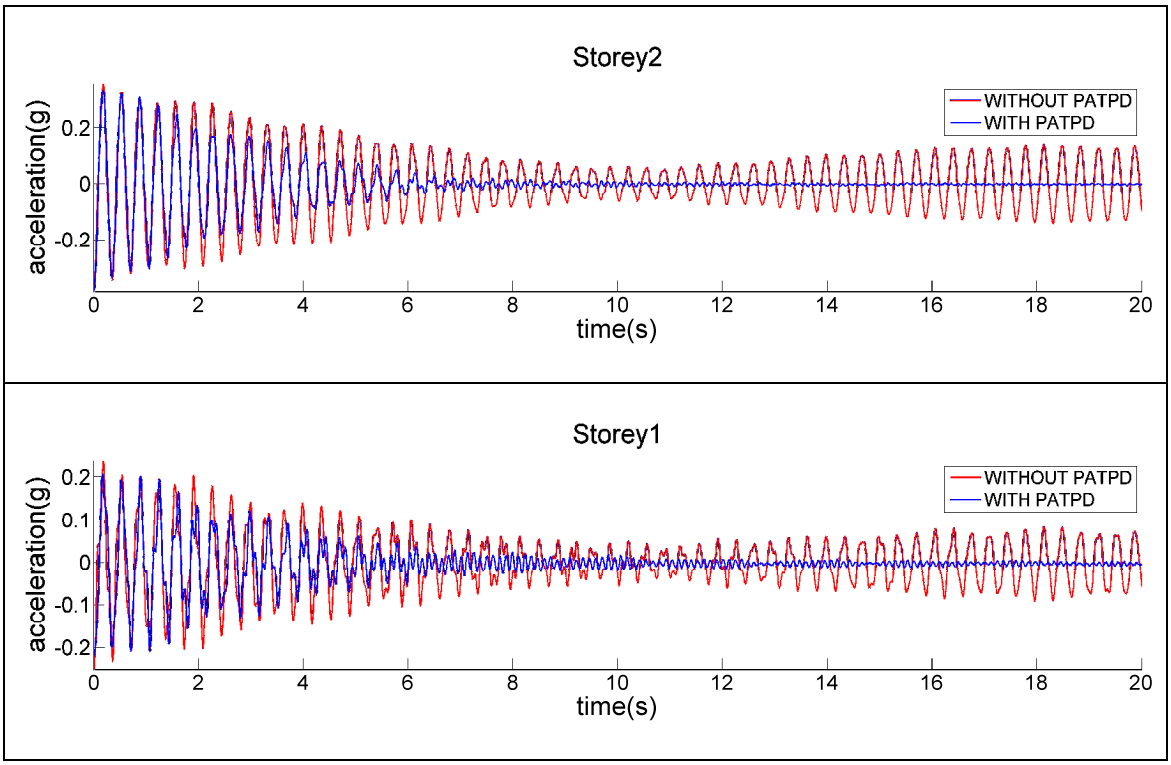

Figure 231: Time history of acceleration response per storey for free translational vibration in the x-direction, model height 32cm

Figure 230 and Figure 231 shows similarity to the results for the primary model[19], of height 37cm, as the PATPD started moving, the acceleration peaks generated in the damped model are as high as those generated in the undamped model. However, these high accelerations subside and the accelerations rapidly decrease compared to that of the undamped model. As is expected the accelerations experienced in storey 3 are highest and the positive damping effect of the PATPD is still significant.

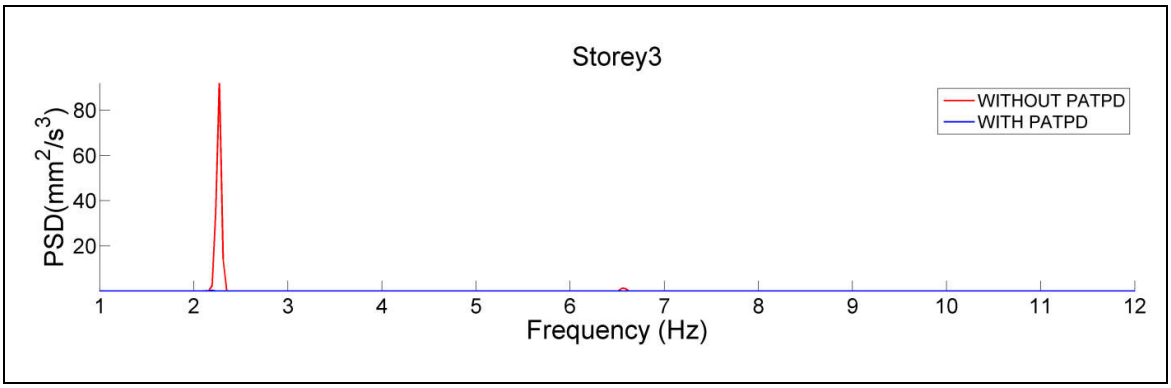

[19] Primary model (height 37.0cm) figures can be found in Chapter 4 page 63 onwards

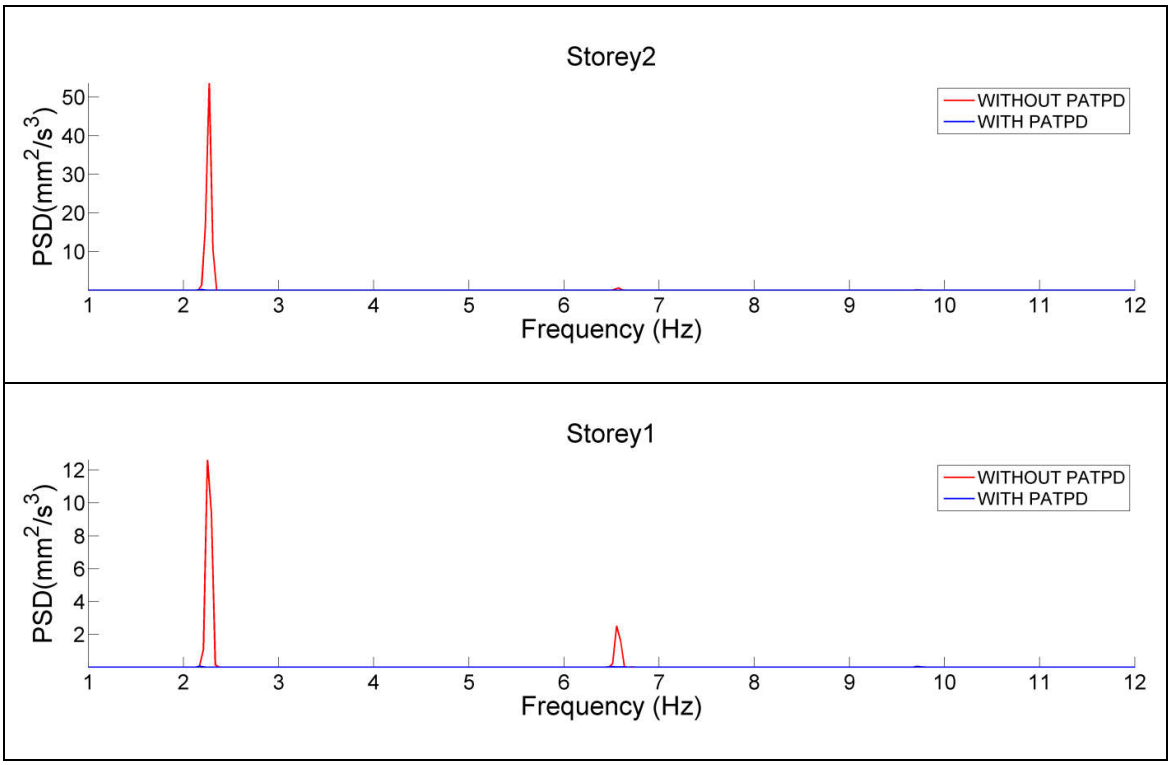

Figure 232: Power Spectral Density (PSD) per storey of the acceleration response for free translational vibration in the x-direction, model height 27cm

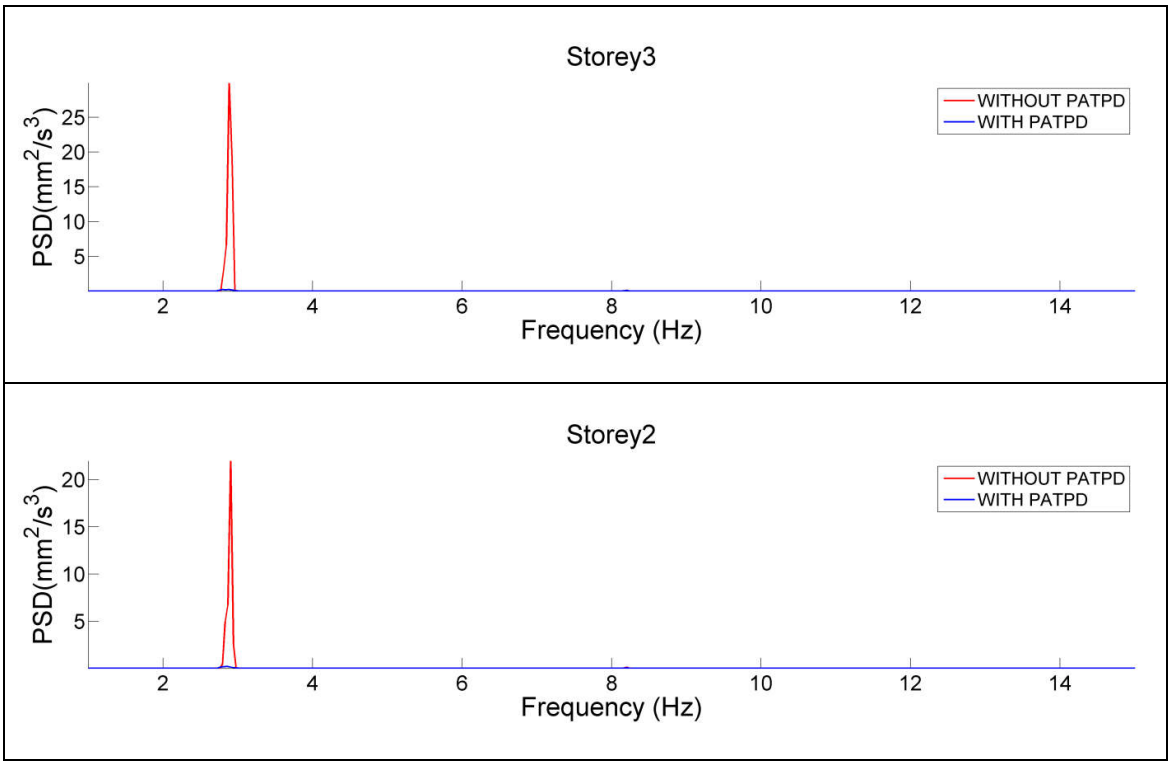

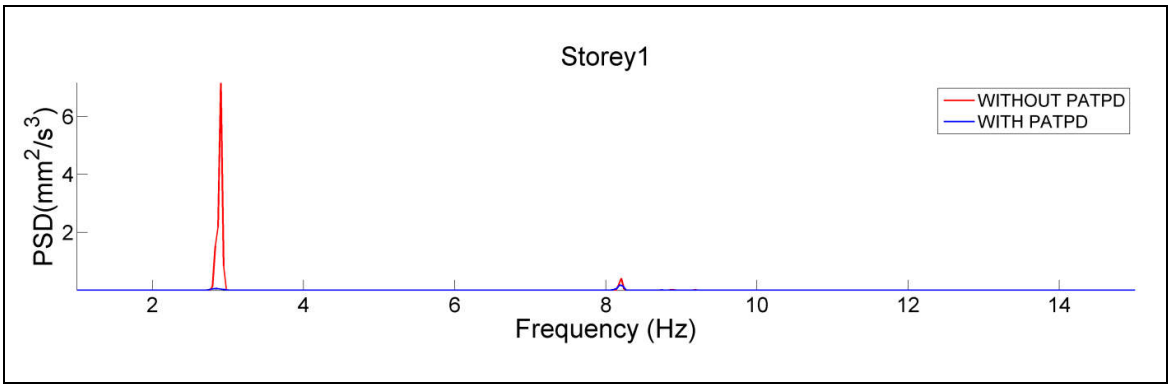

Figure 233: Power Spectral Density (PSD) per storey of the acceleration response for free translational vibration in the x-direction, model height 32cm

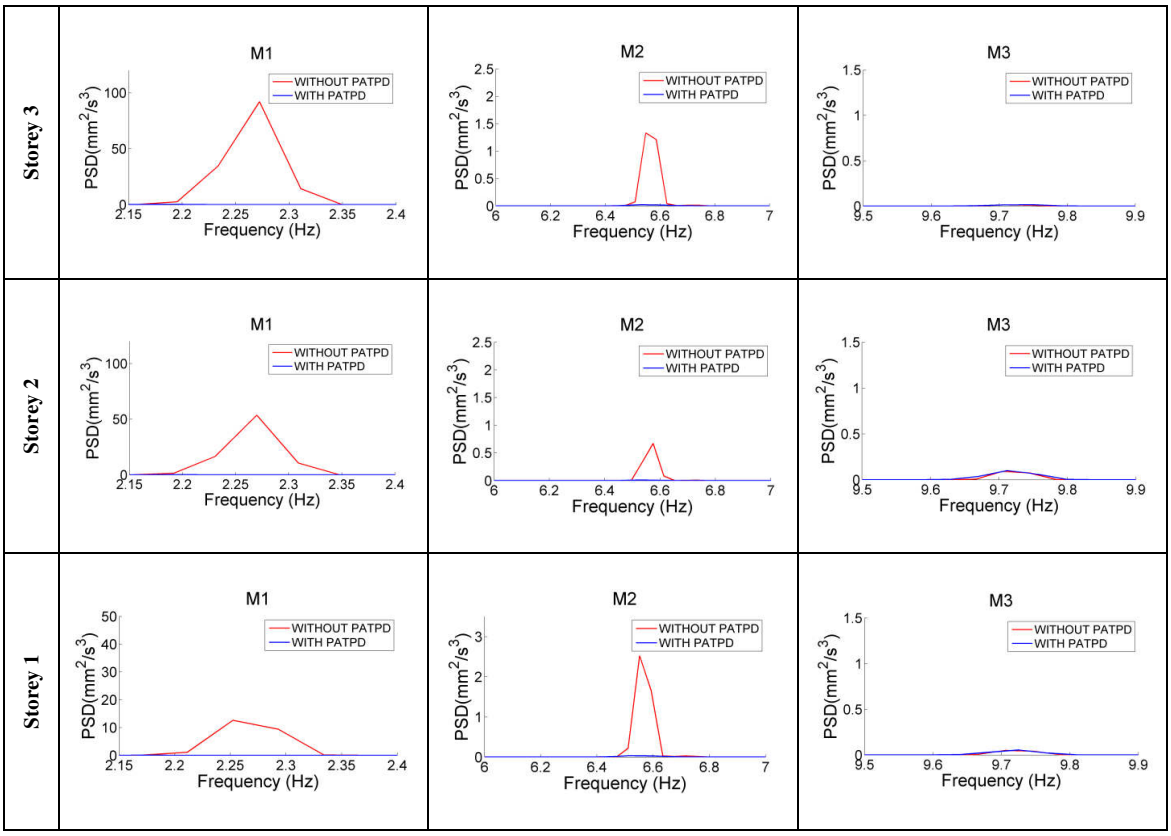

Figure 234: Magnified Power Spectral Density (PSD) of the acceleration response for free translational vibration in the x-direction, model height 27cm

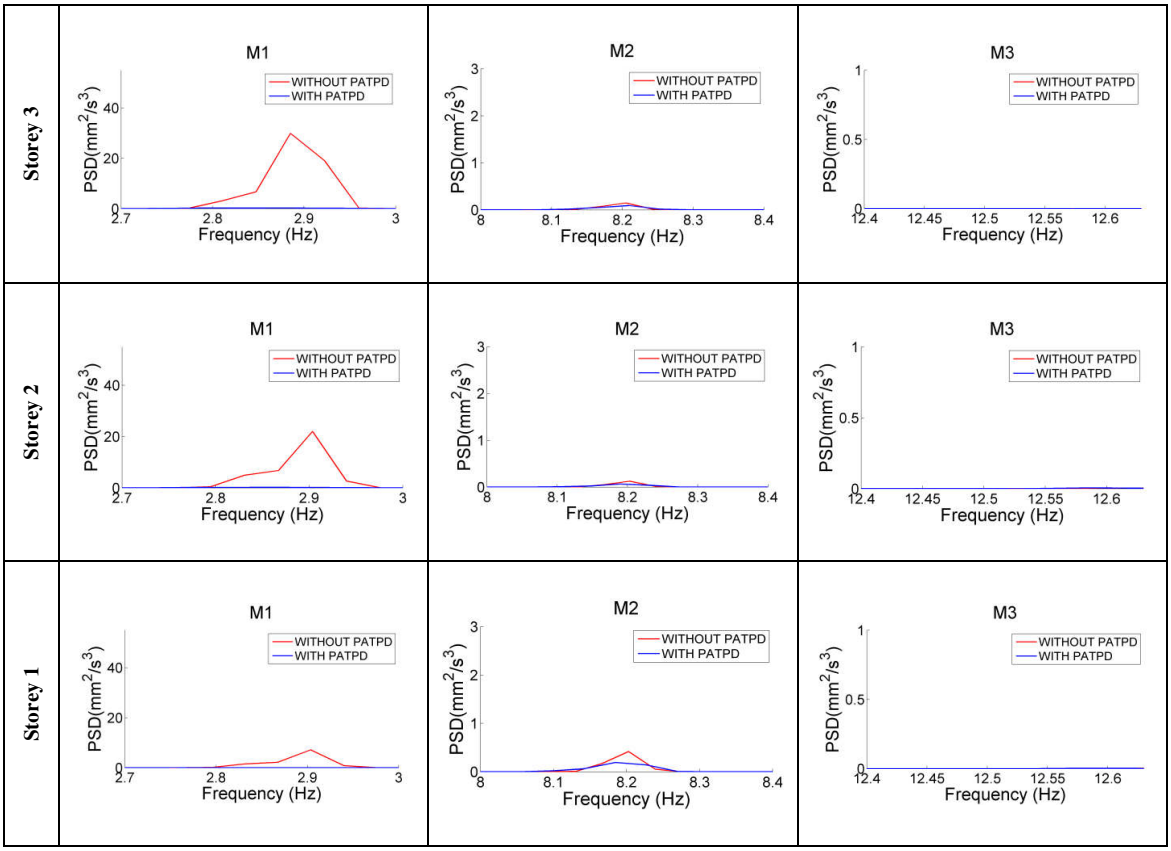

Figure 235: Magnified Power Spectral Density (PSD) of the acceleration response for free translational vibration in the x-direction, model height 32

Figure 232 for storeys 3-1 with height 27cm shows a high peak at: 2.272Hz, 6.548Hz and 9.707Hz for the first, second and third translational frequencies.

Figure 233 for storeys 3-1 with height 32cm shows a high peak at: 2.855Hz, 8.205Hz and 12.590Hz for the first, second and third translational frequencies.

As can be seen from Figure 234 and Figure 235, the PATPD provides at least 99% attenuation for all 3 storeys to all 3 natural frequencies for both model heights.

The PATPD has achieved attenuating the first natural frequency which has the greatest amplitude for translational vibration in the x-direction covering a relatively wide range of frequencies, by adapting to dynamic changes i.e. change in the models stiffness.

6.2.1.2 Translational Vibration in the Y-direction

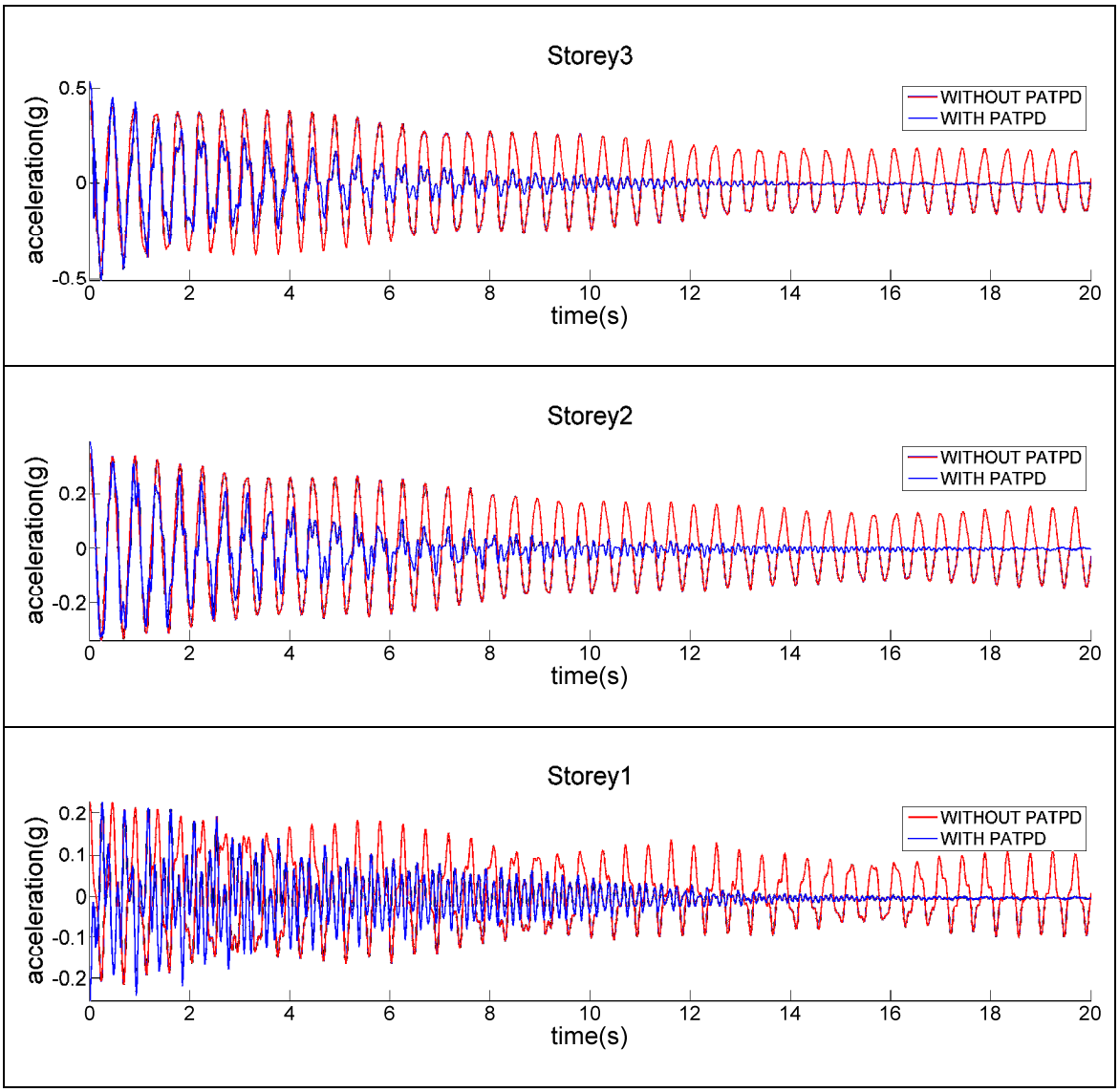

Figure 236: Time history of acceleration response per storey for free translational vibration in the y-direction, model height 27cm

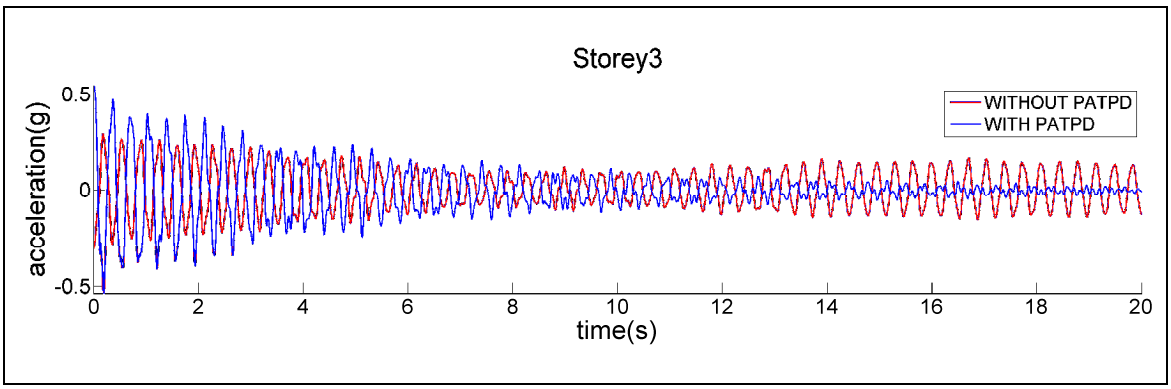

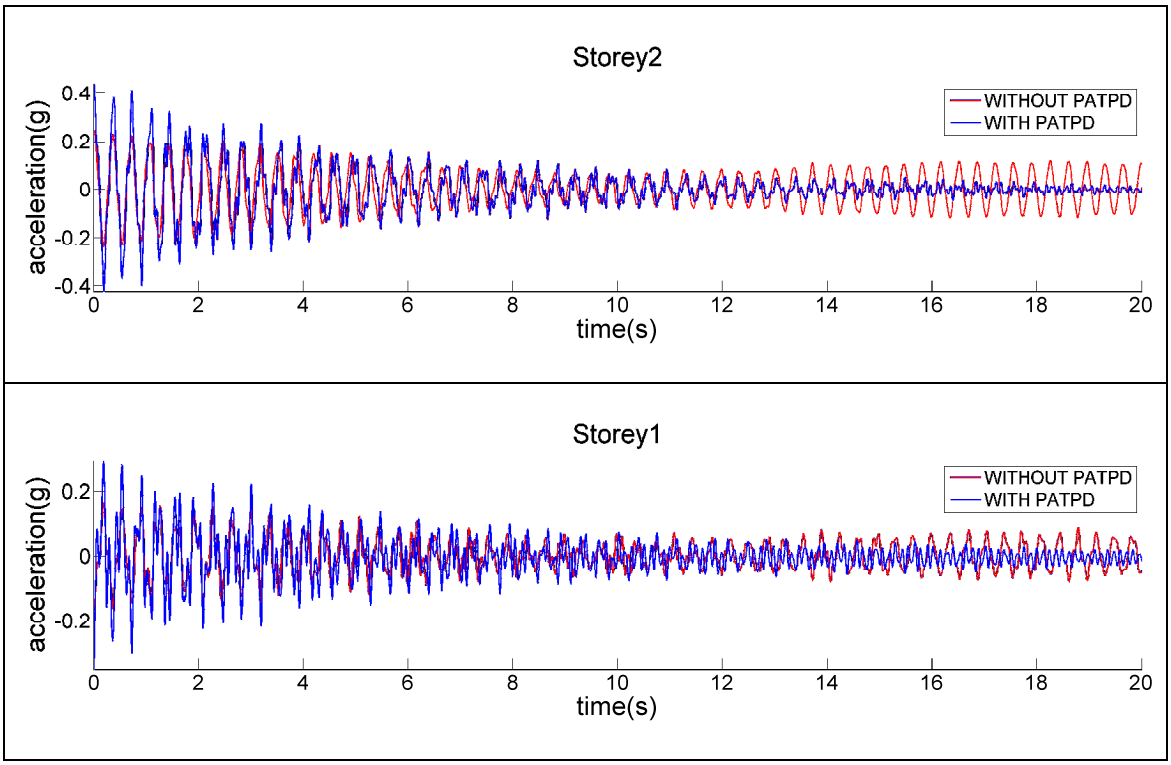

Figure 237: Time history of acceleration response per storey for free translational vibration in the y-direction, model height 32cm

Figure 236 and Figure 237 shows similarity to the results for the primary model[20], of storey height 37cm, as the PATPD started moving, the acceleration peaks generated in the damped model are as high as those generated in the undamped model. However, these high accelerations subside and the accelerations rapidly decrease compared to that of the undamped model. As is expected the accelerations experienced in storey 3 are highest and the positive damping effect of the PATPD is still significant.

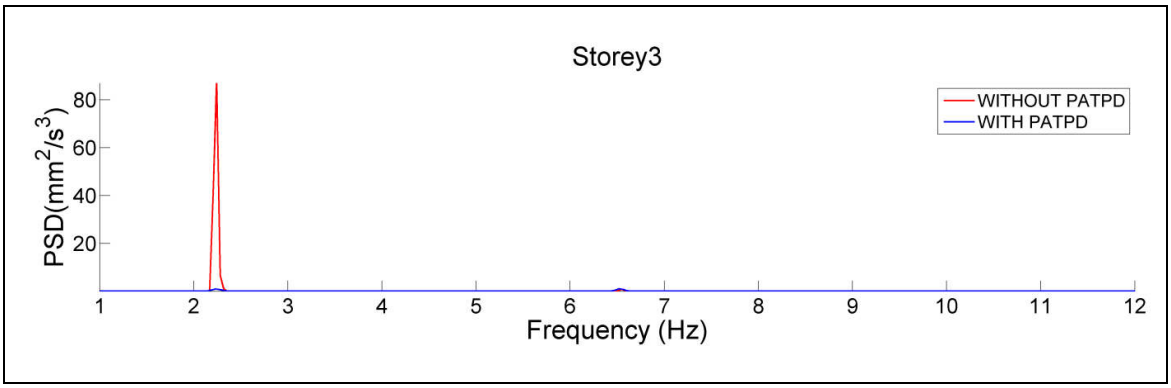

[20] Primary model (mass 42.09kg and height 37.0cm) figures can be found in Chapter 4 page 63 onwards

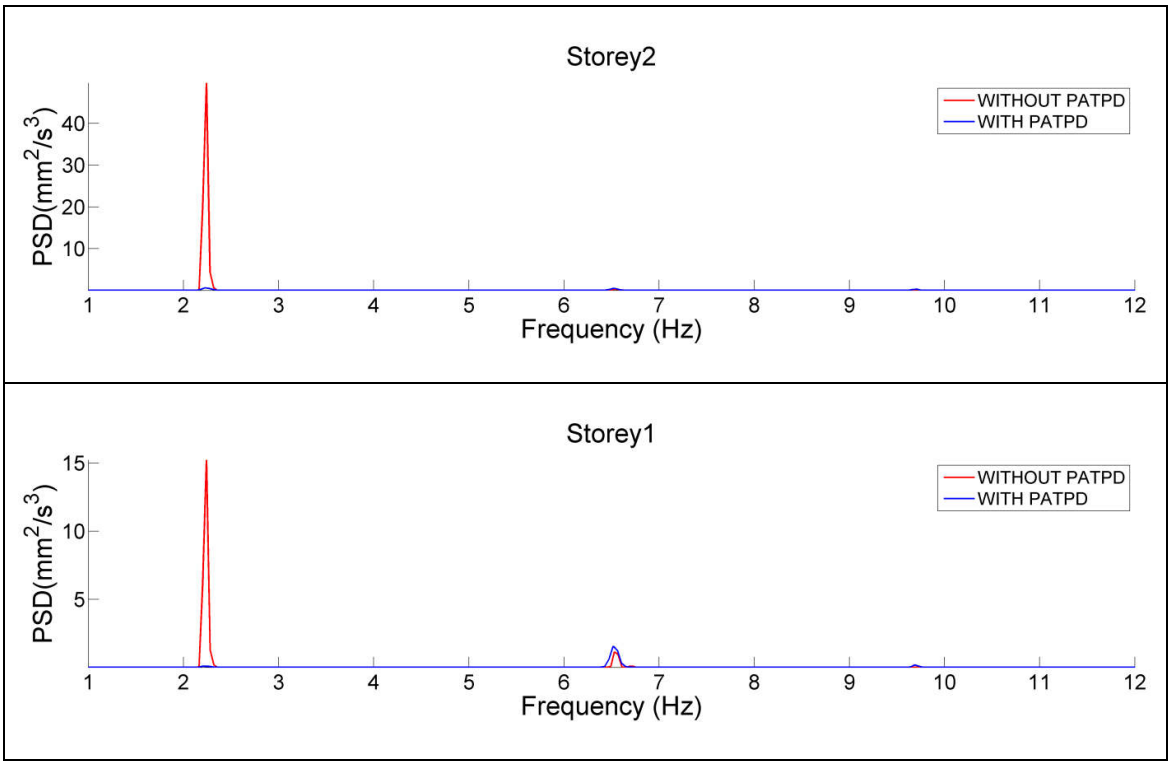

Figure 238: Power Spectral Density (PSD) per storey of the acceleration response for free translational vibration in the y-direction, model height 27cm

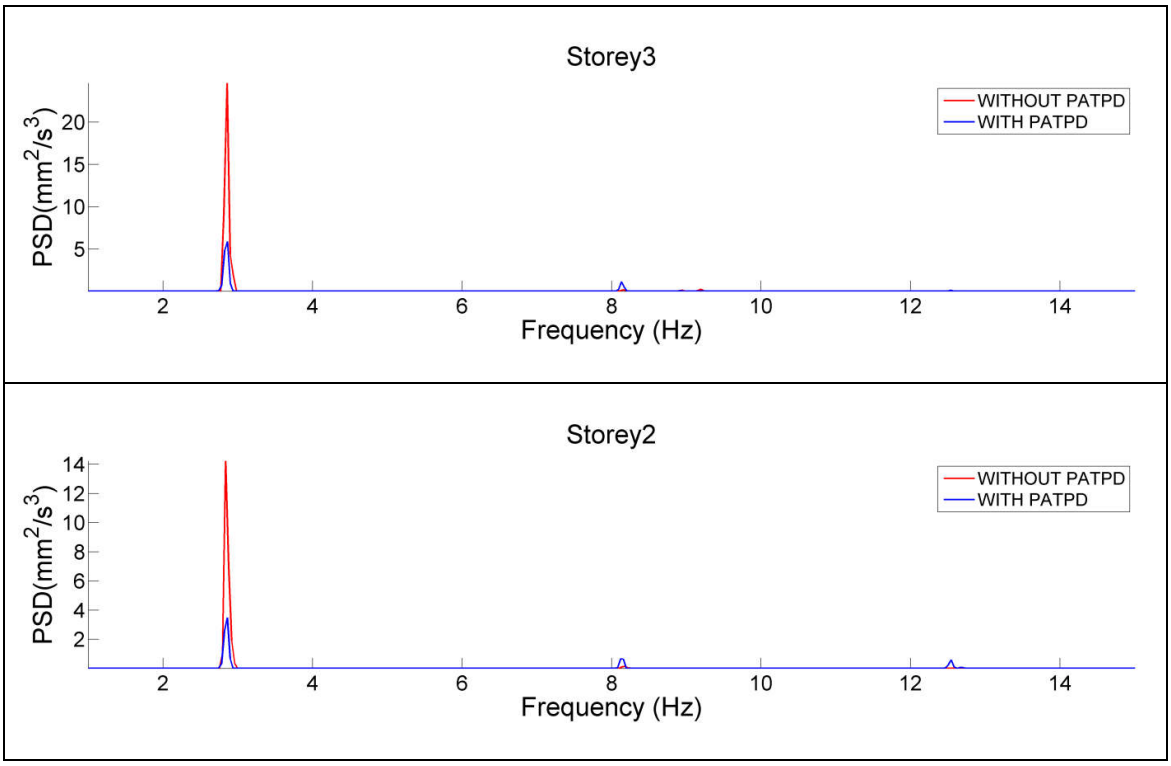

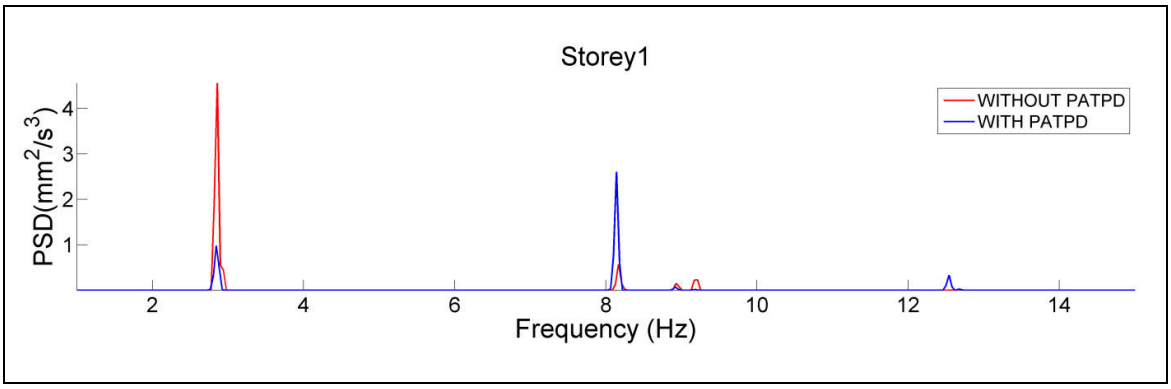

Figure 239: Power Spectral Density (PSD) per storey of the acceleration response for free translational vibration in the y-direction, model height 32cm

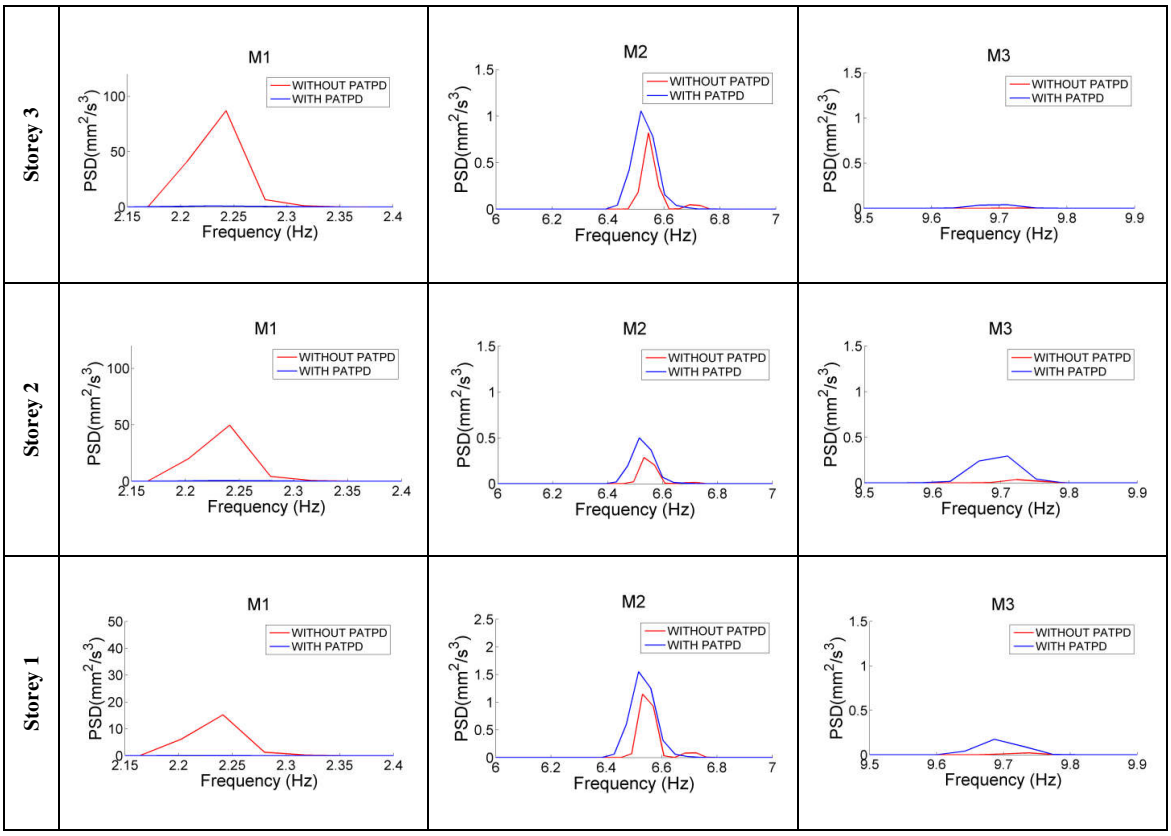

Figure 240: Magnified Power Spectral Density (PSD) of the acceleration response for free translational vibration in the y-direction, model height 27cm

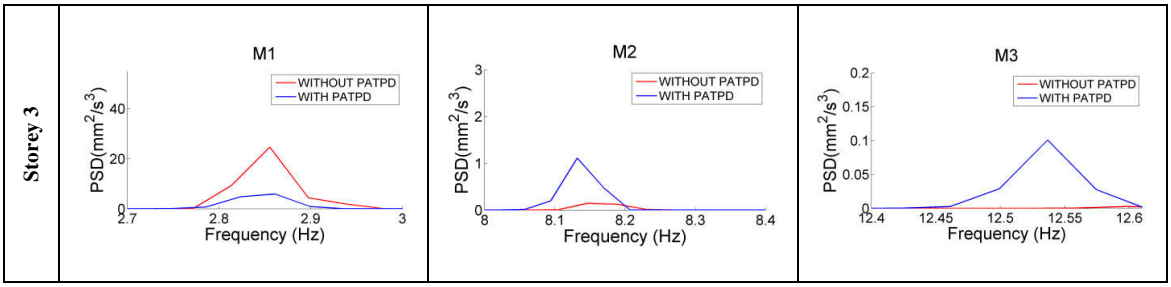

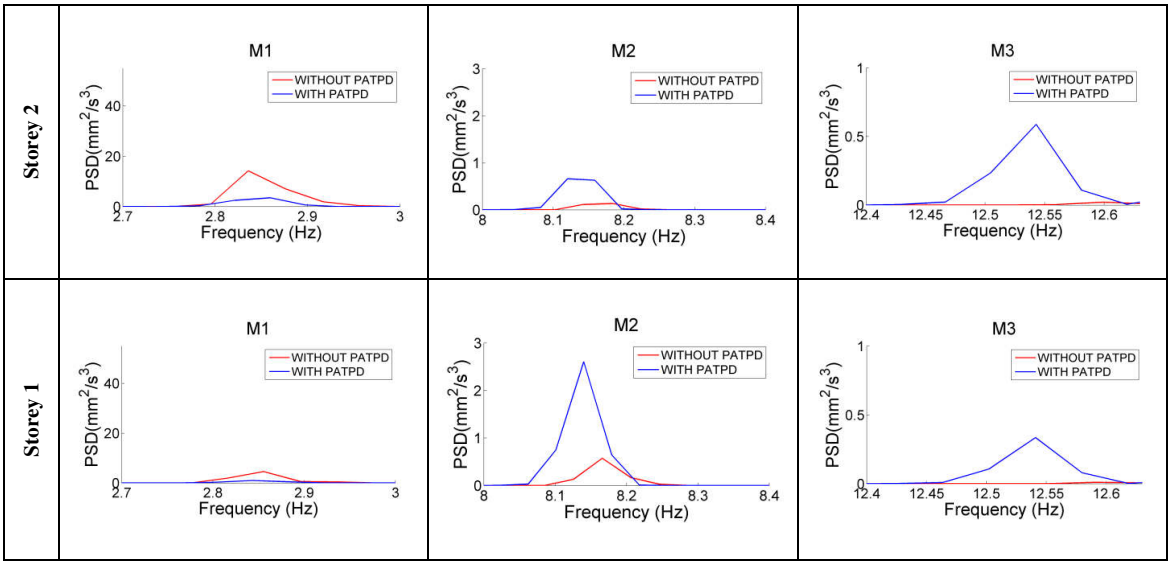

Figure 241: Magnified Power Spectral Density (PSD) of the acceleration response for free translational vibration in the y-direction, model height 32cm

Figure 238 for storey 3-1 with height 27cm shows a high peak at: 2.243Hz, 6.545Hz and 9.703Hz for the first, second and third natural translational frequencies.

Figure 239 for storey 3-1 with height 27cm shows a high peak at: 2.855Hz, 8.132Hz and 12.540Hz for the first, second and third natural translational frequencies.

As can be seen from Figure 240 and Figure 241, the PATPD provides at least 99% attenuation for all 3 storeys to the first natural frequency for model with greatest stiffness i.e. height 27cm, and 70% for the 32cm model height. For the second and third natural frequencies overall, for both heights, storeys 3-1 shows a slight increase in the PSD peaks.

The PATPD has achieved attenuating the first natural frequency which has the greatest amplitude for translational vibration in the y-direction covering a relatively wide range of frequencies, by adapting to dynamic changes i.e. change in the models stiffness.

It is also evident, as with the primary model, that the PATPD control in the x-direction is better than in the y-direction.

6.2.1.3 Torsional Vibration (acceleration measured in X-direction)

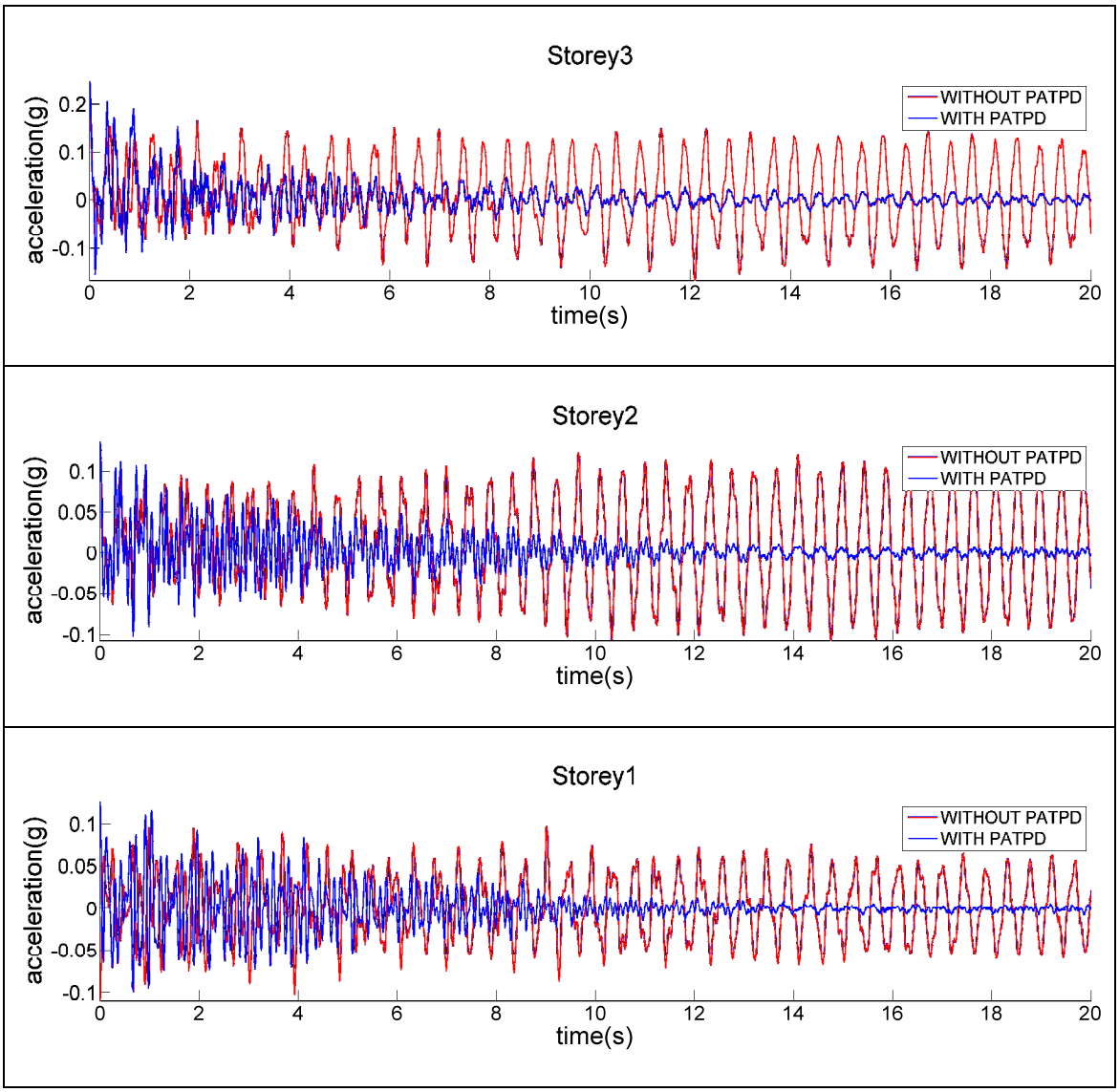

Figure 242: Time history of acceleration response per storey for free torsional vibration in the x-direction, model height 27cm

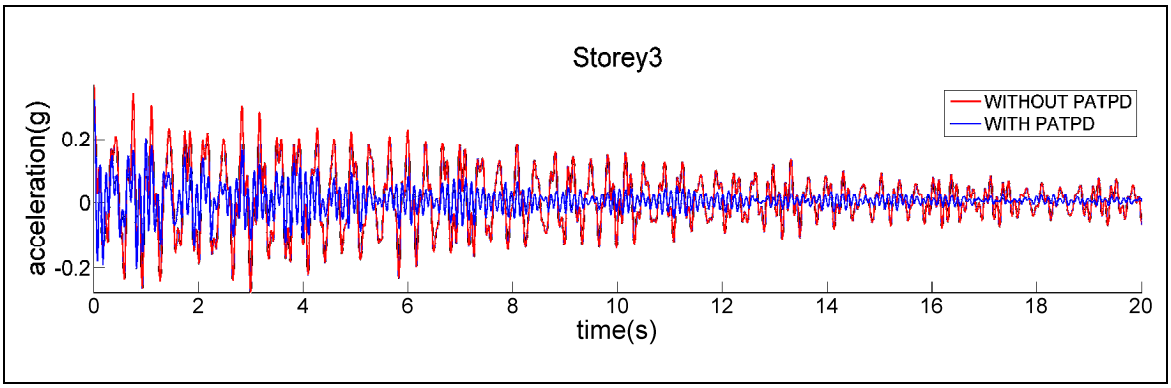

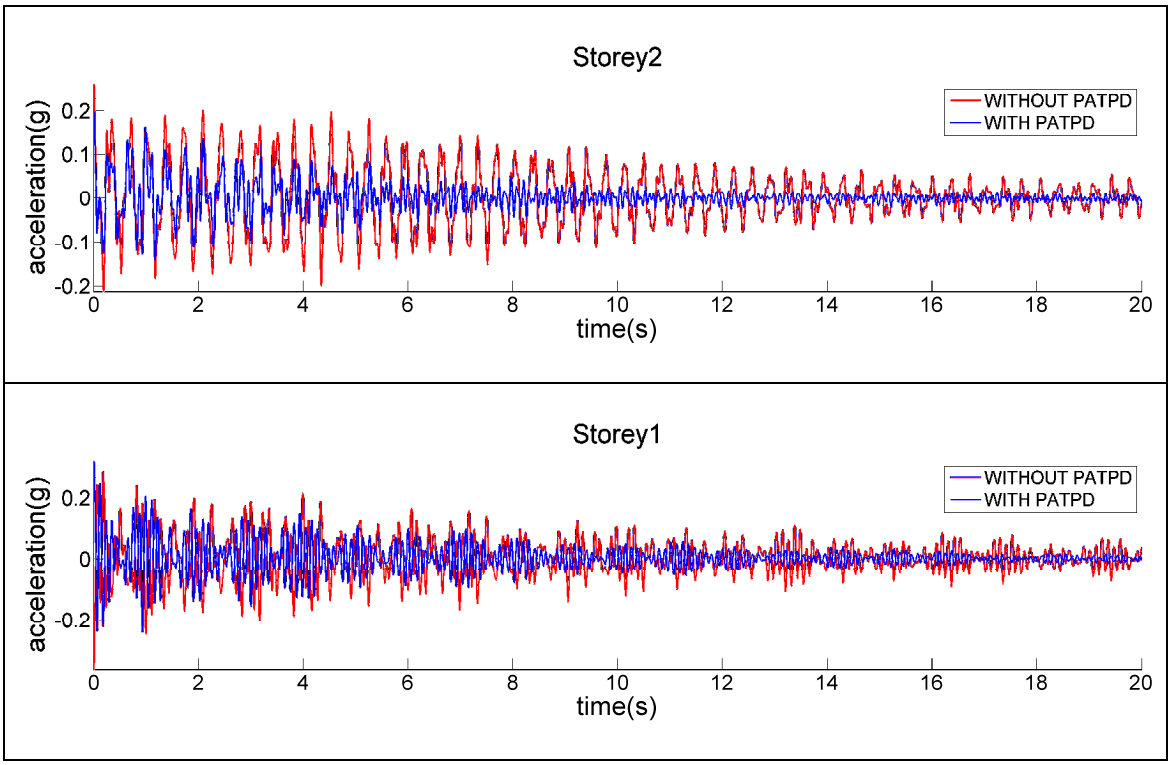

Figure 243: Time history of acceleration response per storey for free torsional vibration in the x-direction, model height 32cm

Figure 242 and Figure 243 shows similarity to the results for the primary model[21], height of 37cm, as the PATPD started moving, the acceleration peaks generated in the damped model are as high as those generated in the undamped model. However, these high accelerations subside and the accelerations rapidly decrease compared to that of the undamped model. As is expected the accelerations experienced in storey 3 are highest and the positive damping effect of the PATPD is still significant. Acceleration in x-direction is controlled better than in the y-direction.

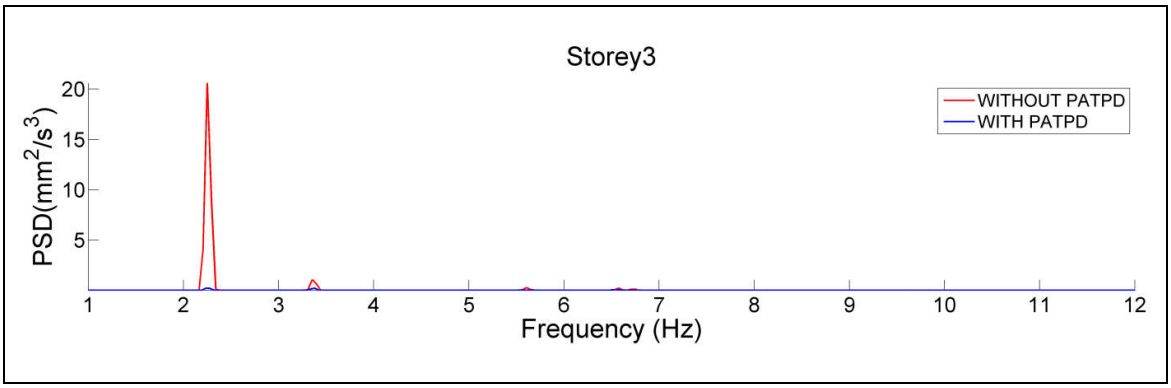

[21] Primary model (height 37cm) figures can be found in Chapter 4 page 63 onwards

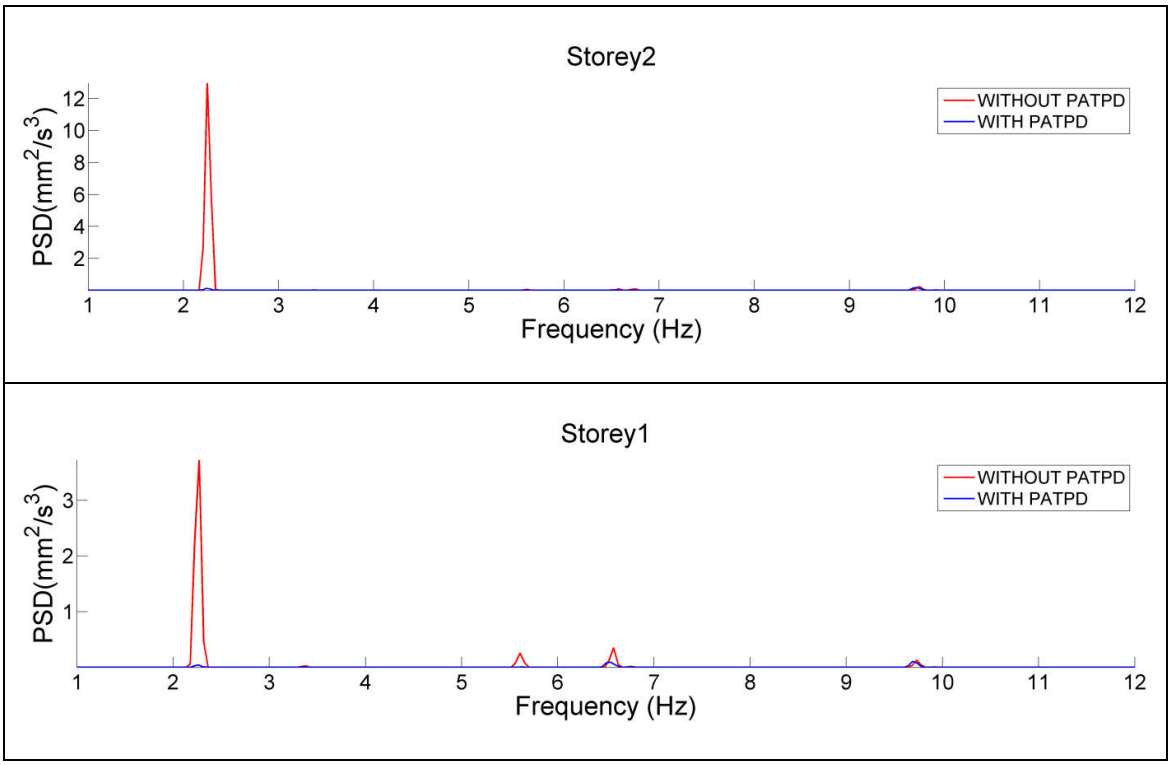

Figure 244: Power Spectral Density (PSD) per storey of the acceleration response for free torsional vibration in the x-direction, model height 27cm

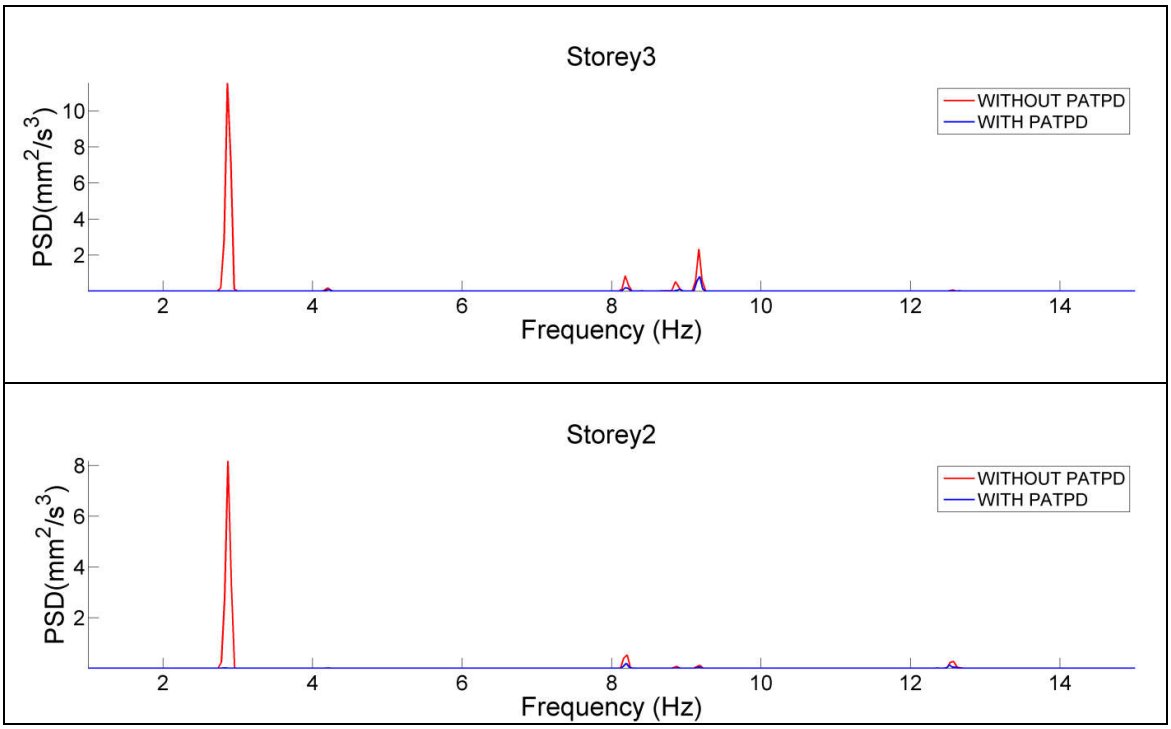

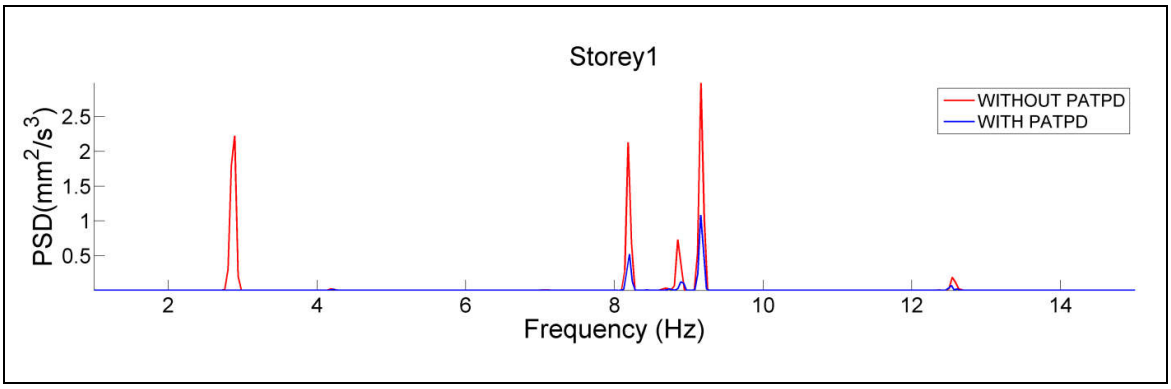

Figure 245: Power Spectral Density (PSD) per storey of the acceleration response for free torsional vibration in the x-direction, model height 32cm

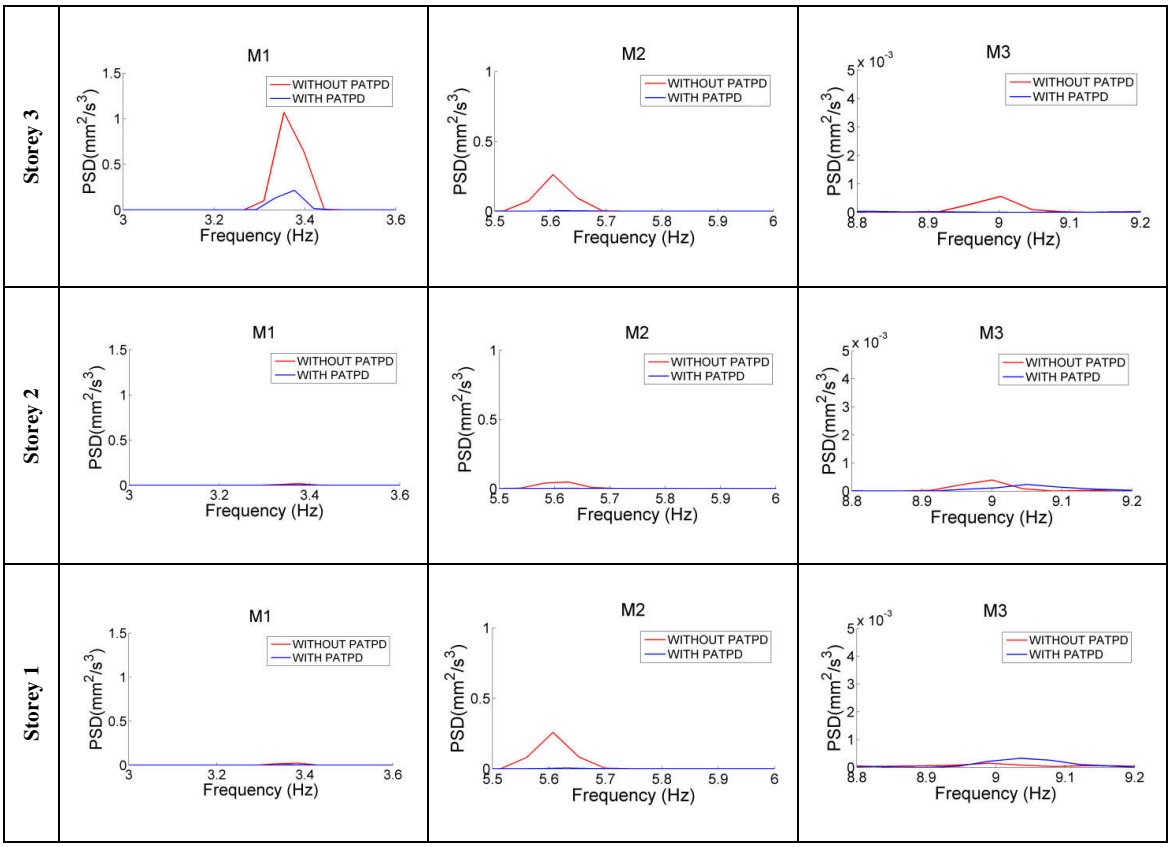

Figure 246: Magnified Power Spectral Density (PSD) of the acceleration response for free torsional vibration in the x-direction, model height 27cm

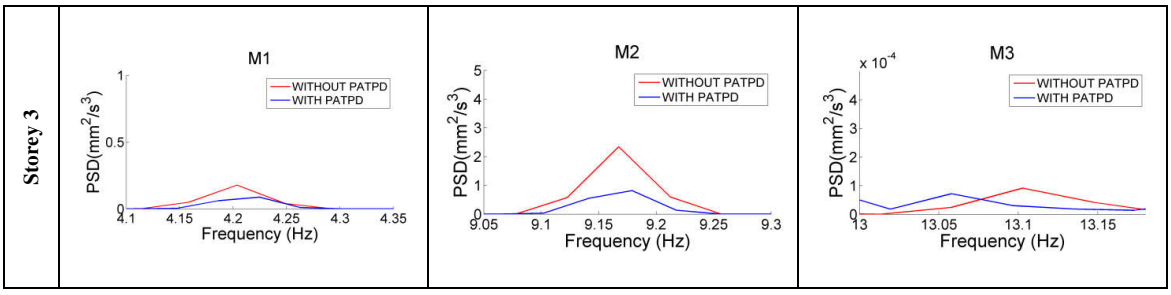

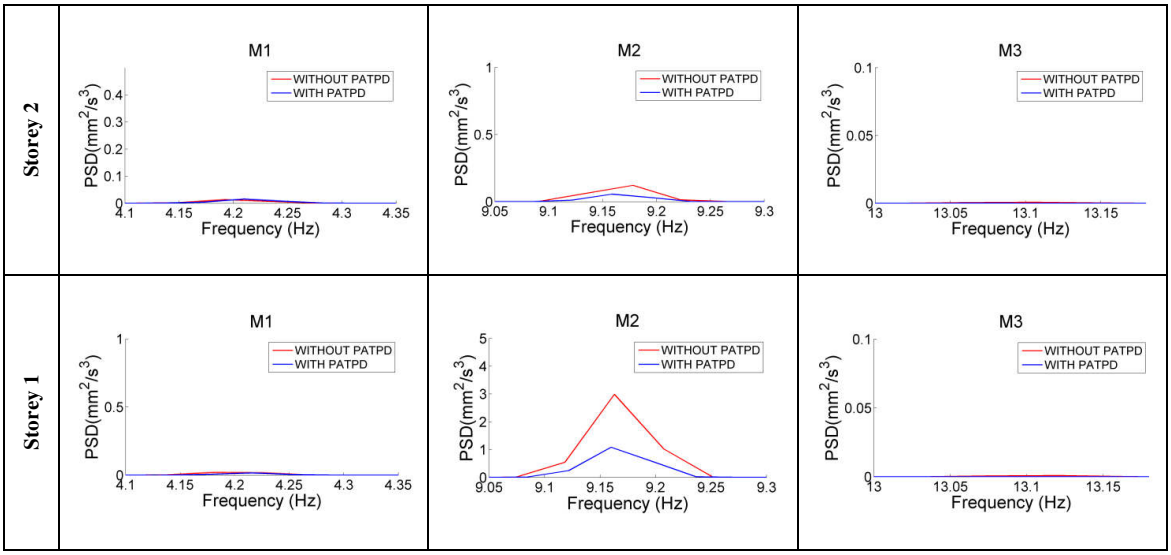

Figure 247: Magnified Power Spectral Density (PSD) of the acceleration response for free torsional vibration in the x-direction, model height 32cm

Figure 244 for storeys 3-1 with height 27cm shows a high peak at: 3.354Hz, 5.605Hz and 9.003Hz for the first, second and third torsional natural frequency.

Figure 245 for storeys 3-1 with height 32cm shows a high peak at: 4.204Hz, 9.167Hz and 13.100Hz for the first, second and third torsional natural frequency.

Peaks are also visible at natural frequencies for translation in the x-direction which is expected as the structure had some movement in the x-direction as well as torsionally. As is also evident all translational frequencies are controlled.

As can be seen from Figure 246 and Figure 247, the PATPD provides at least 99% attenuation for storeys 1-2 to the first natural frequency for both model heights. Storey 3 for both has at least 50% attenuation.

For second natural frequency, PSD peak for height 27cm is attenuated by at least 99% for all 3 storeys, and for the 32cm height by at least 50% for all storeys.

For third natural frequency overall, PSD peak for both heights, storeys 3-1 shows similar frequency for both damped and undamped models.

The PATPD has achieved attenuating the first natural frequency which has the greatest amplitude for torsional vibration in the x-direction covering a relatively wide range of frequencies, by adapting to dynamic changes i.e. change in the models stiffness.

6.2.1.4 Torsional Vibration (acceleration measured in Y-direction)

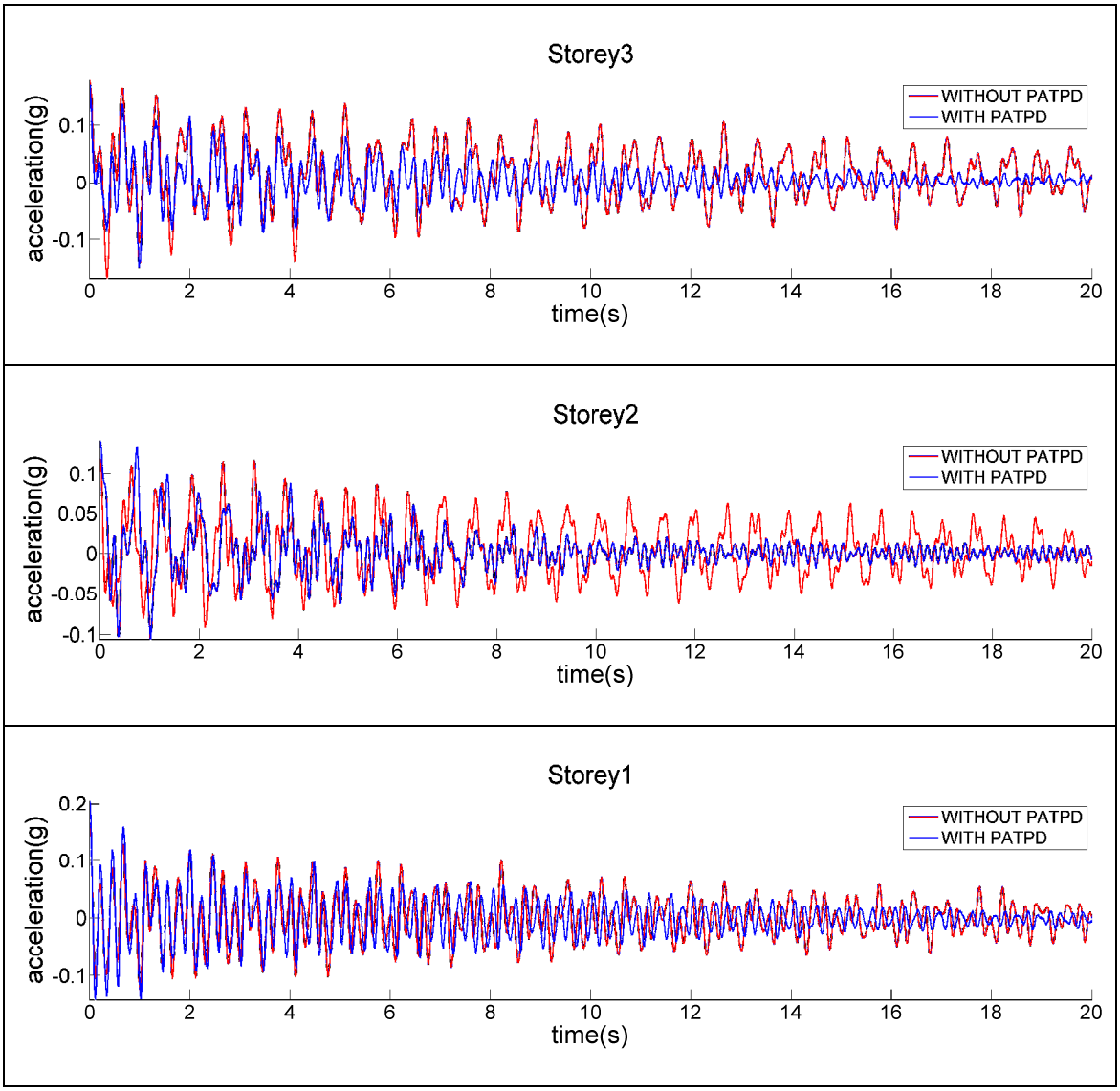

Figure 248: Time history of acceleration response per storey for free torsional vibration in the y-direction, model height 27cm

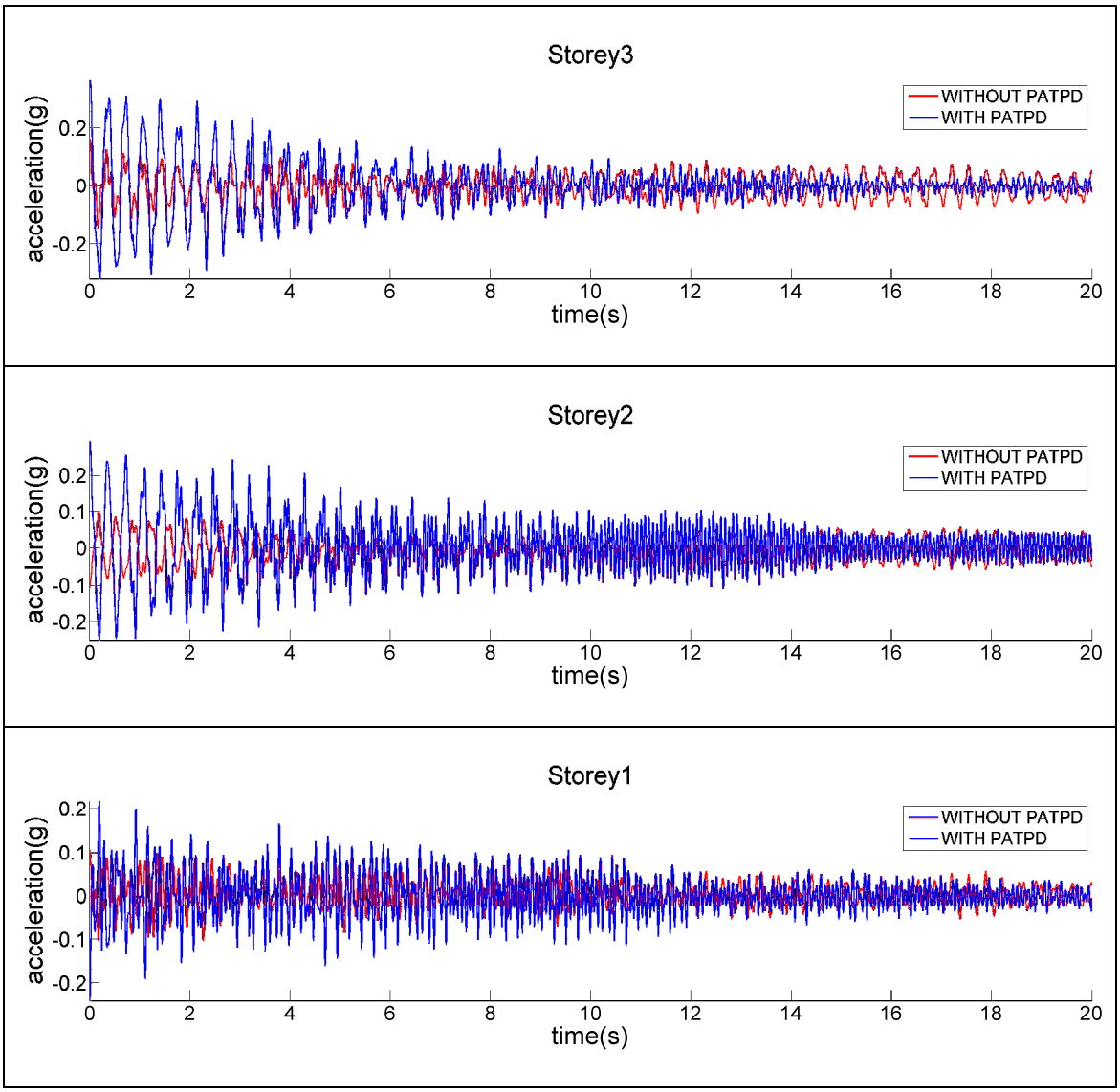

Figure 249: Time history of acceleration response per storey for free torsional vibration in the y-direction, model height 32cm

Figure 248 shows similarity to the results for the primary model[22], of height 37cm, as the PATPD started moving; the acceleration peaks generated in the damped model are as high as those generated in the undamped model. However, these high accelerations subside and the accelerations rapidly decrease compared to that of the undamped model. As is expected the accelerations experienced in storey 3 are highest and the positive damping effect of the PATPD is still significant. Figure 249 however, shows increased acceleration for all 3 storeys.

[22] Primary model (mass 42.09kg) figures can be found in Chapter 4 page 63 onwards

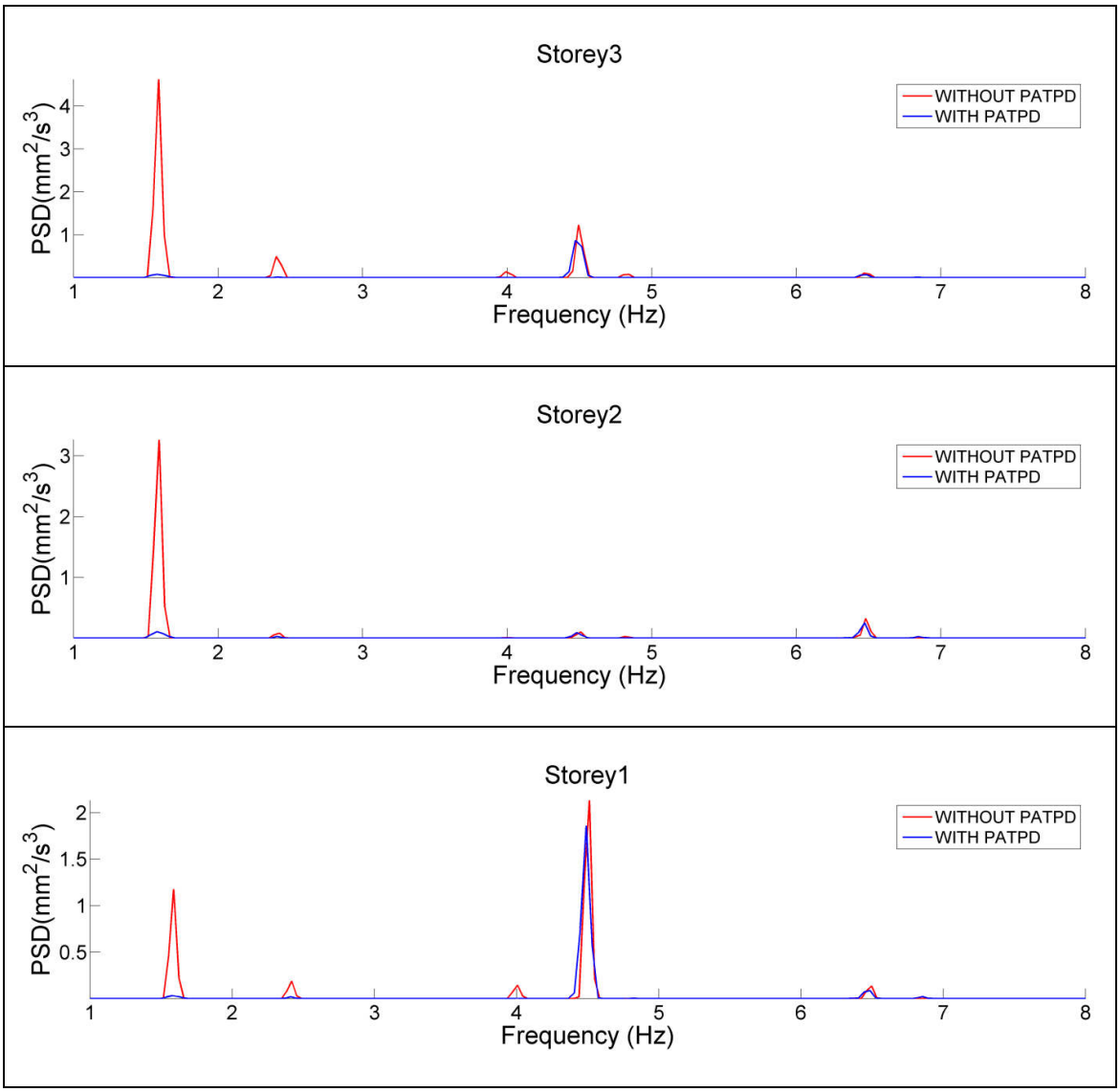

Figure 250: Power Spectral Density (PSD) per storey of the acceleration response for free torsional vibration in the y-direction, model height 27cm

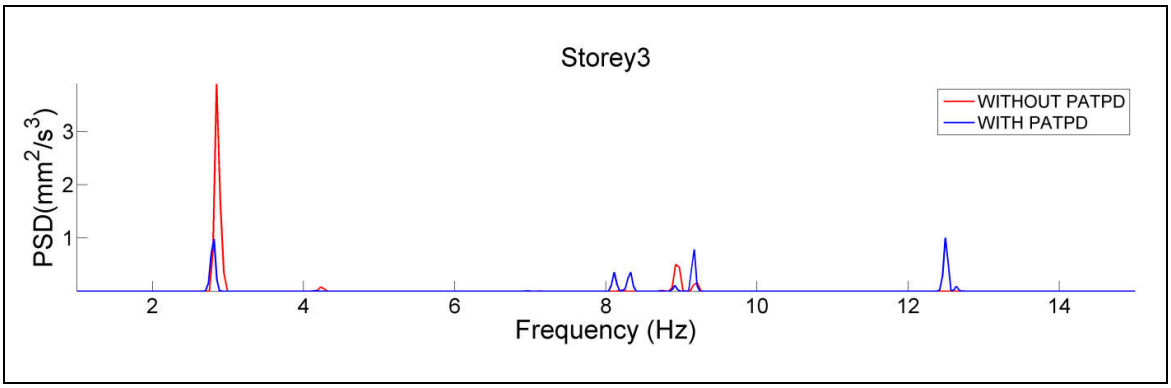

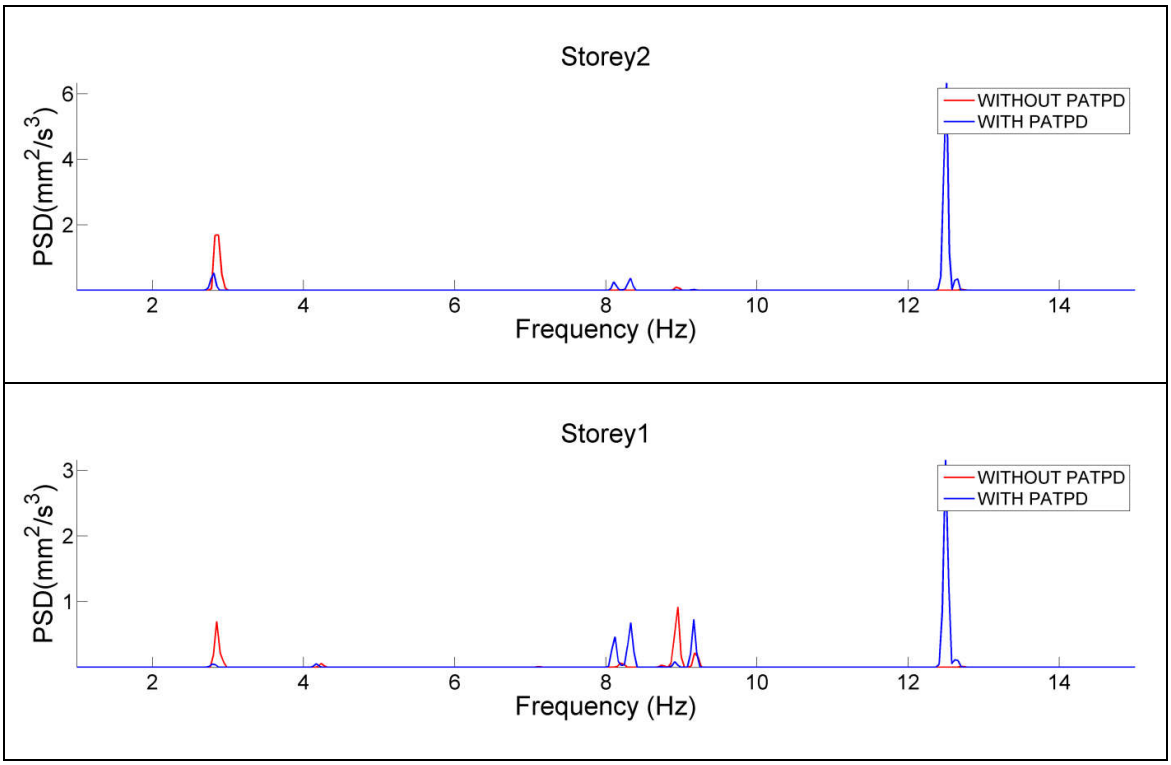

Figure 251: Power Spectral Density (PSD) per storey of the acceleration response for free torsional vibration in the y-direction, model height 32cm

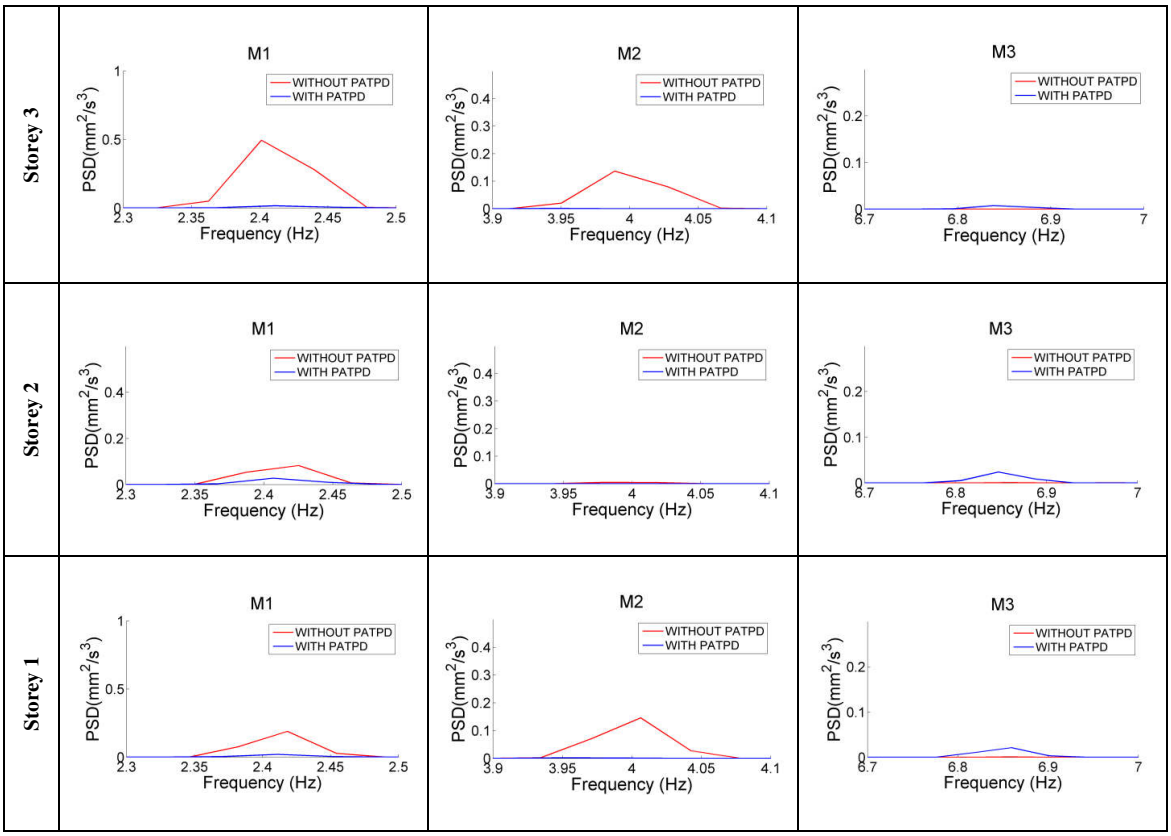

Figure 252: Magnified Power Spectral Density (PSD) of the acceleration response for free torsional vibration in the y-direction, model height 27cm

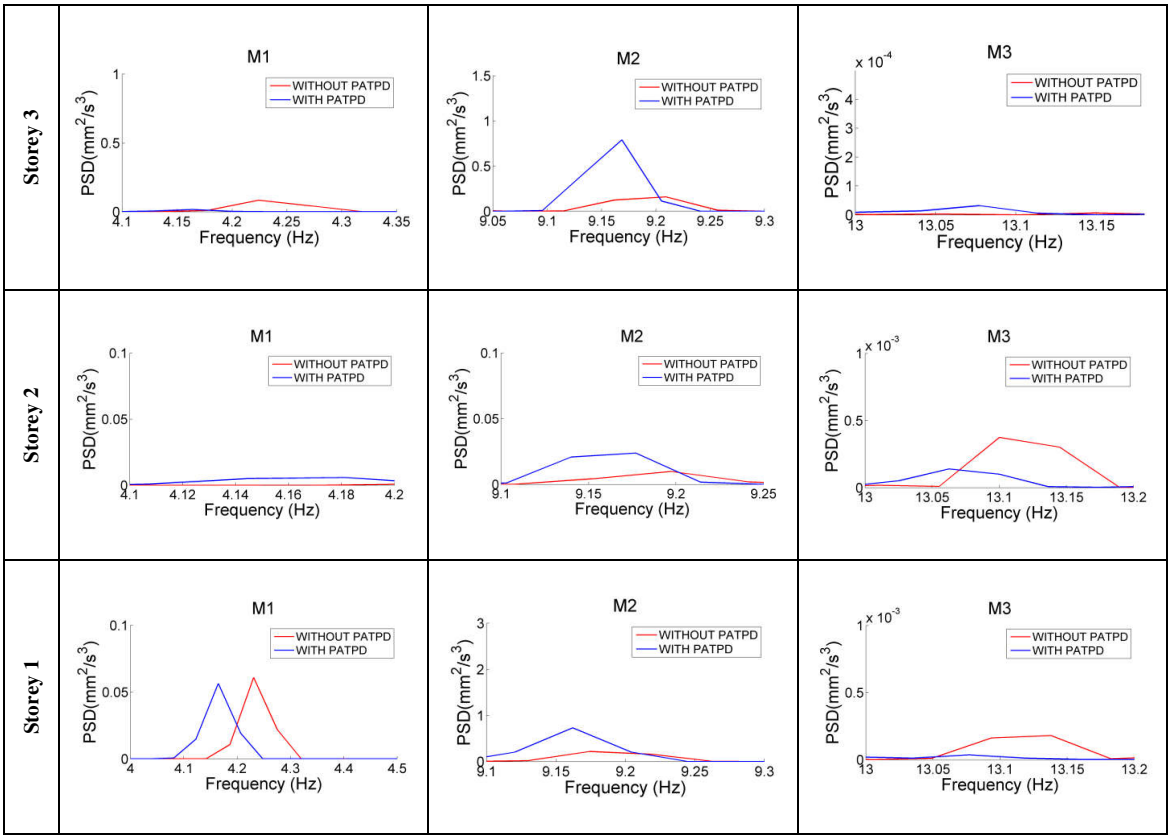

Figure 253: Magnified Power Spectral Density (PSD) of the acceleration response for free torsional vibration in the y-direction, model height 32cm

Figure 250 for storeys 3-1 with height 27cm shows a high peak at: 3.377Hz, 5.646Hz and 8.973Hz for the first, second and third natural torsional frequencies.

Figure 251 for storeys 3-1 with height 32cm shows a high peak at: 4.225Hz, 9.209Hz and 13.080Hz for the first, second and third natural torsional frequencies.

Peaks are also visible at natural frequencies for translation in the y-direction which is expected as the structure had some movement in the y-direction as well as torsionally. As is also evident all translational frequencies are controlled by at least 99% for height 27cm. For 32cm height only first natural frequency PSD peak is controlled, second and third natural frequency PSD peaks show significant increases.

As can be seen from Figure 252 and Figure 253, the PATPD provides at least 99% attenuation for all 3 storeys to the first and second natural frequency for height 27cm model. The third natural frequency PSD peak is slightly increased.

For the height 32cm model the PATPD does not provide significant control to torsional natural frequencies.

The PATPD has achieved attenuating the first natural frequency which has the greatest amplitude for torsional vibration in the y-direction for a height of 27cm but lacks control for the 32cm model showing a similar trend as with primary test model. The stiffer model has better torsional control as can be expected; further investigation is required to improve the control effect for less stiff models. It is also evident, as with the primary model, that the PATPD control in the x-direction is better than in the y-direction.

6.2.1.5 Coupled Vibration (translation in X-direction and torsion)

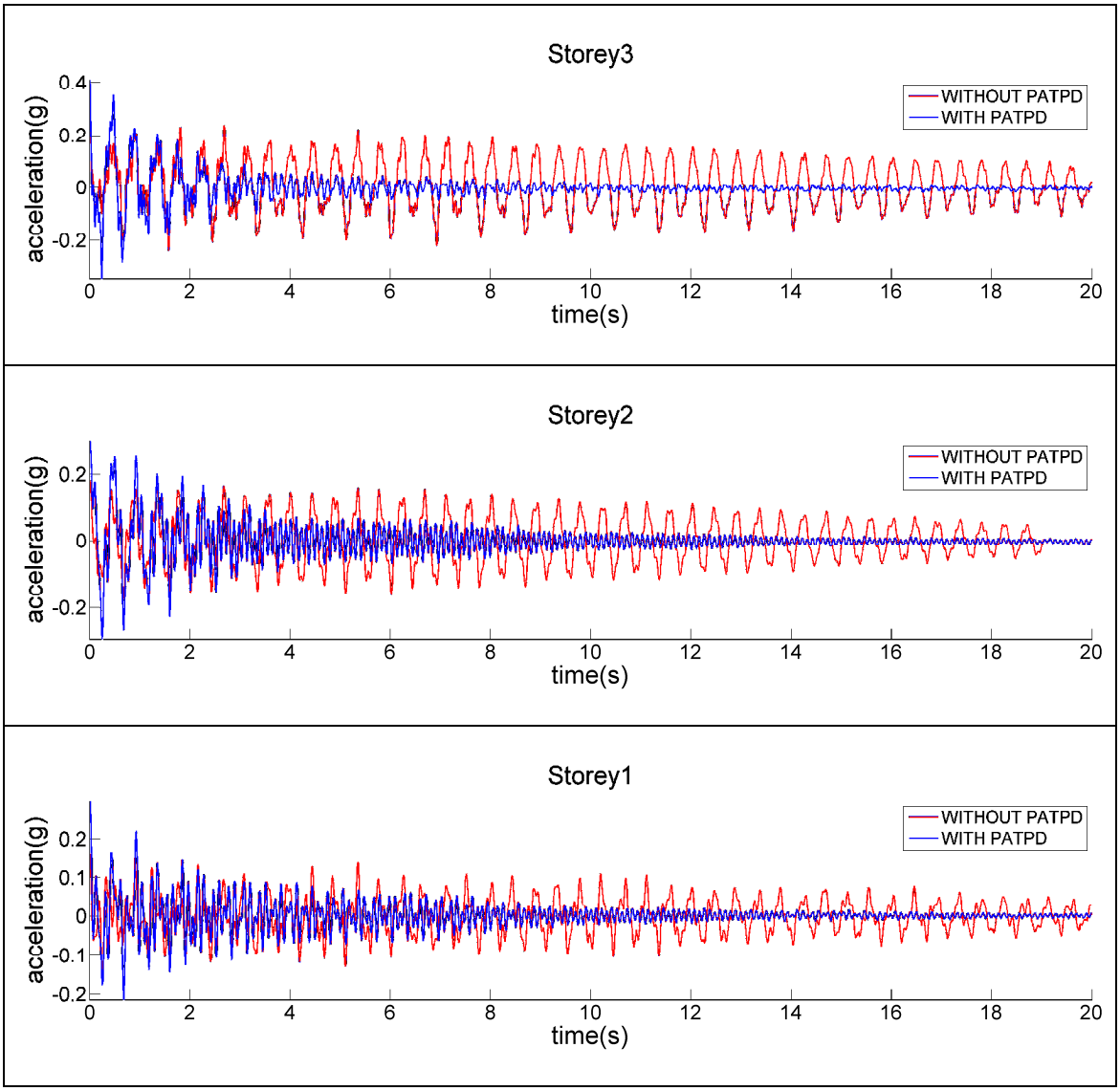

Figure 254: Time history of acceleration response per storey for free coupled vibration (translation in x-direction and torsion), model height 27cm

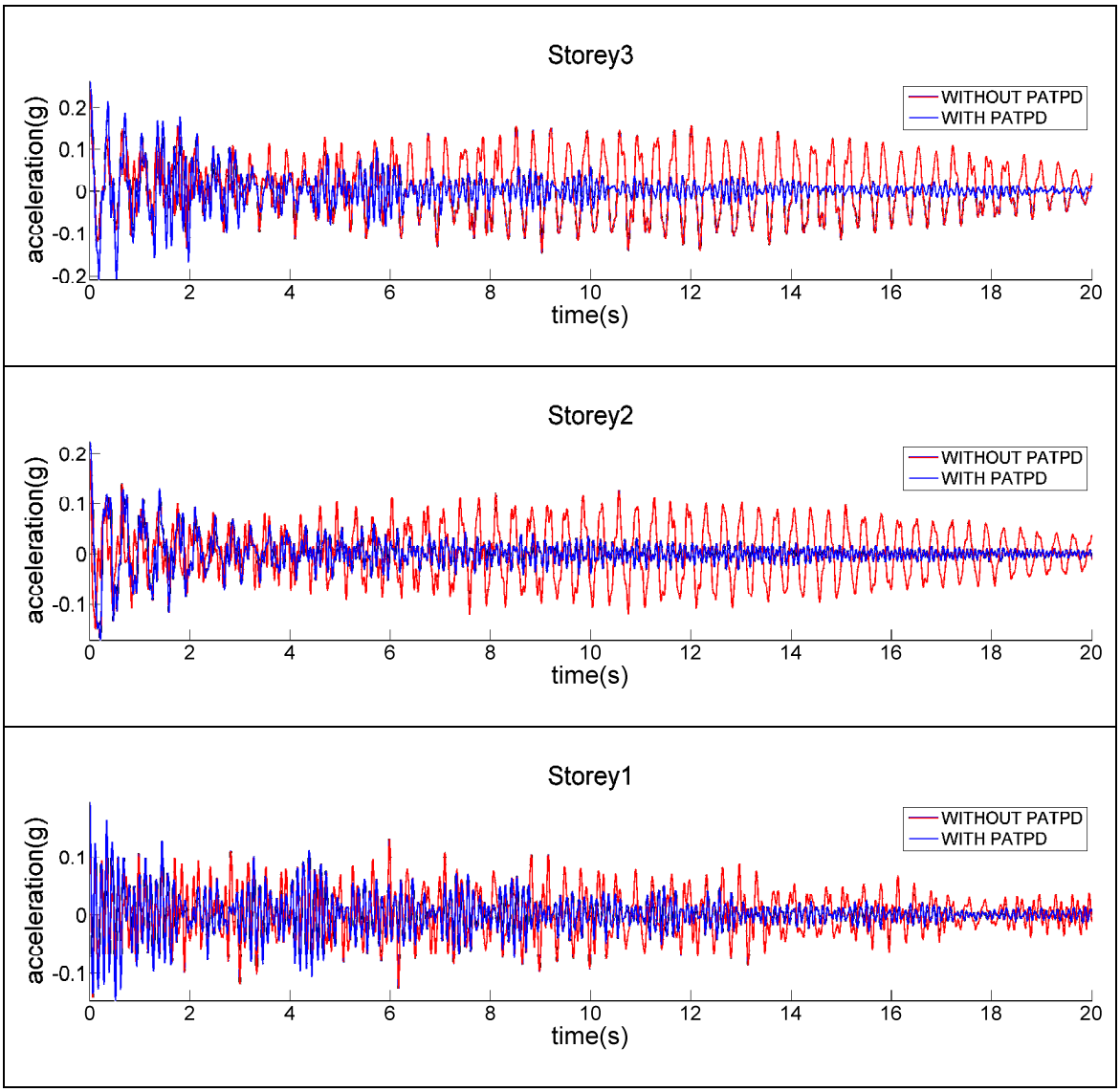

Figure 255: Time history of acceleration response per storey for free coupled vibration (translation in x-direction and torsion), model height 32cm

Figure 254 and Figure 255 shows similarity to the results for the primary model[23], of height 37cm per storey, as the PATPD started moving, the acceleration peaks generated in the damped model are as high as those generated in the undamped model. However, these high accelerations subside and the accelerations rapidly decrease compared to that of the undamped model. As is expected the accelerations experienced in storey 3 are highest and the positive damping effect of the PATPD is still significant.

[23] Primary model (mass 42.09kg) figures can be found in Chapter 4 page 63 onwards

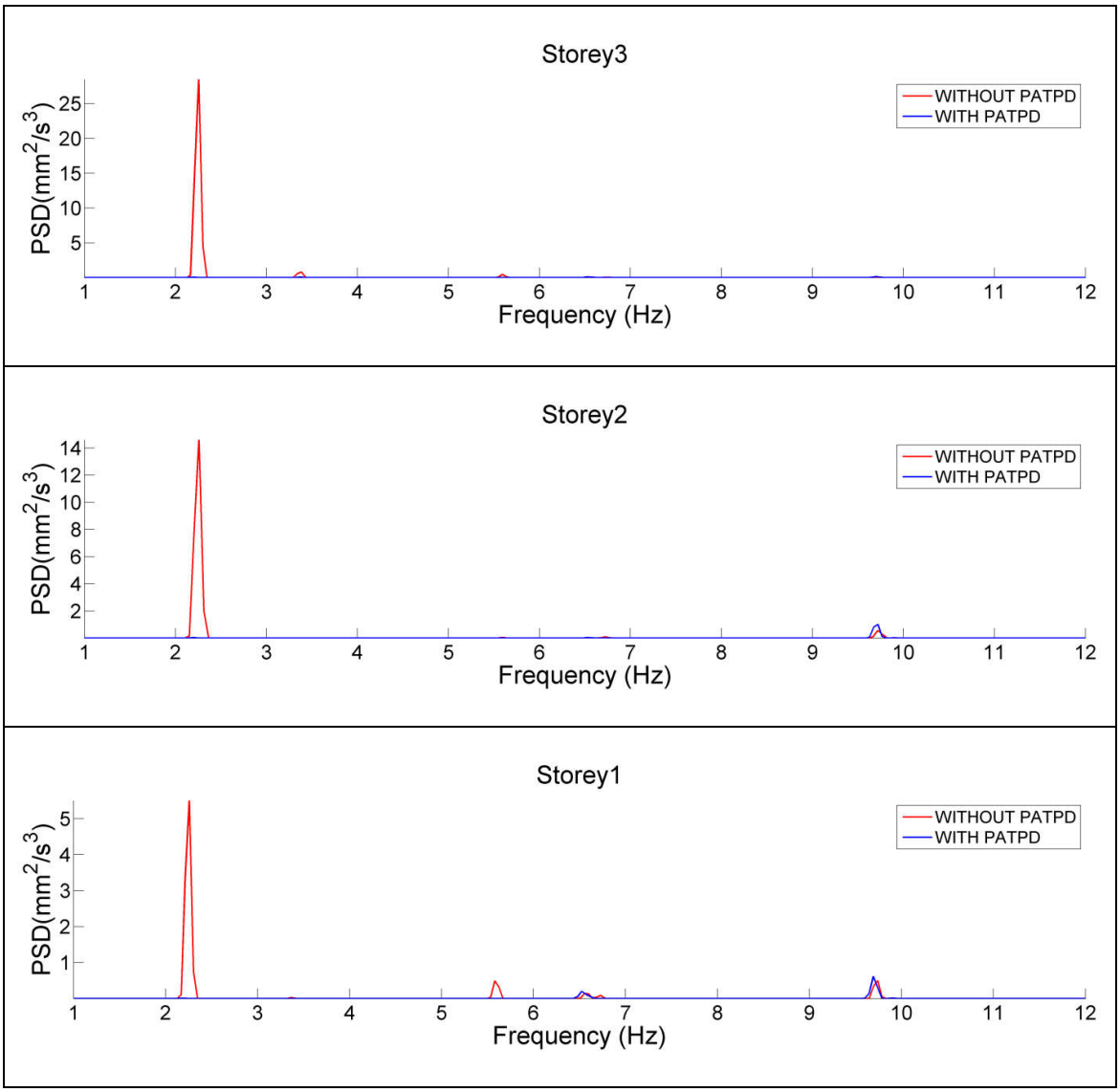

Figure 256: Power Spectral Density (PSD) per storey of the acceleration response for free coupled vibration (translation in x-direction and torsion), model height 27cm

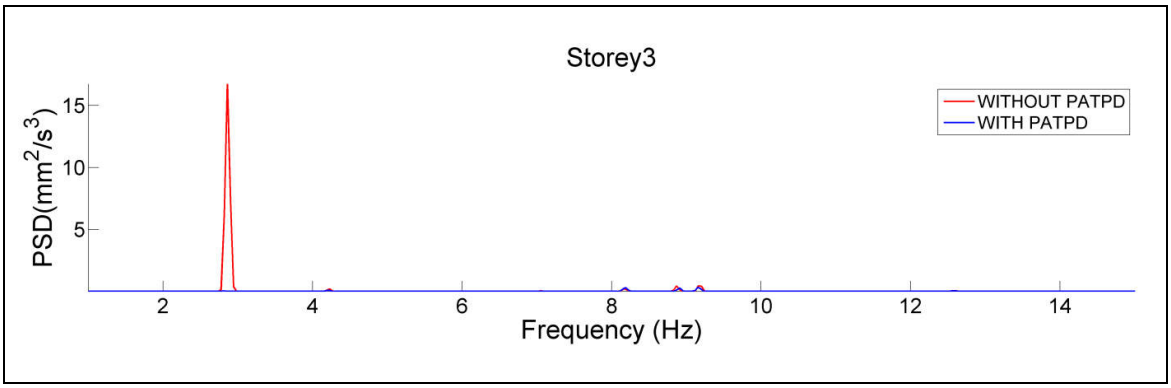

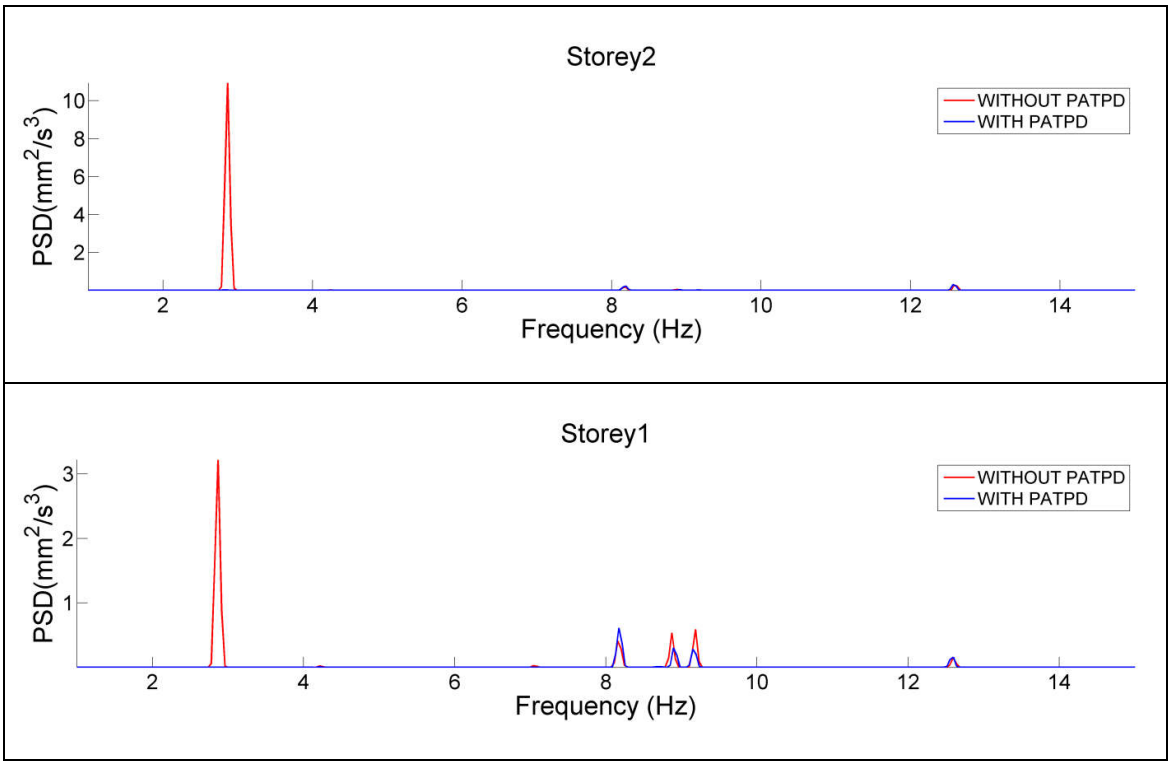

Figure 257: Power Spectral Density (PSD) per storey of the acceleration response for free coupled vibration (translation in x-direction and torsion), model height 32cm

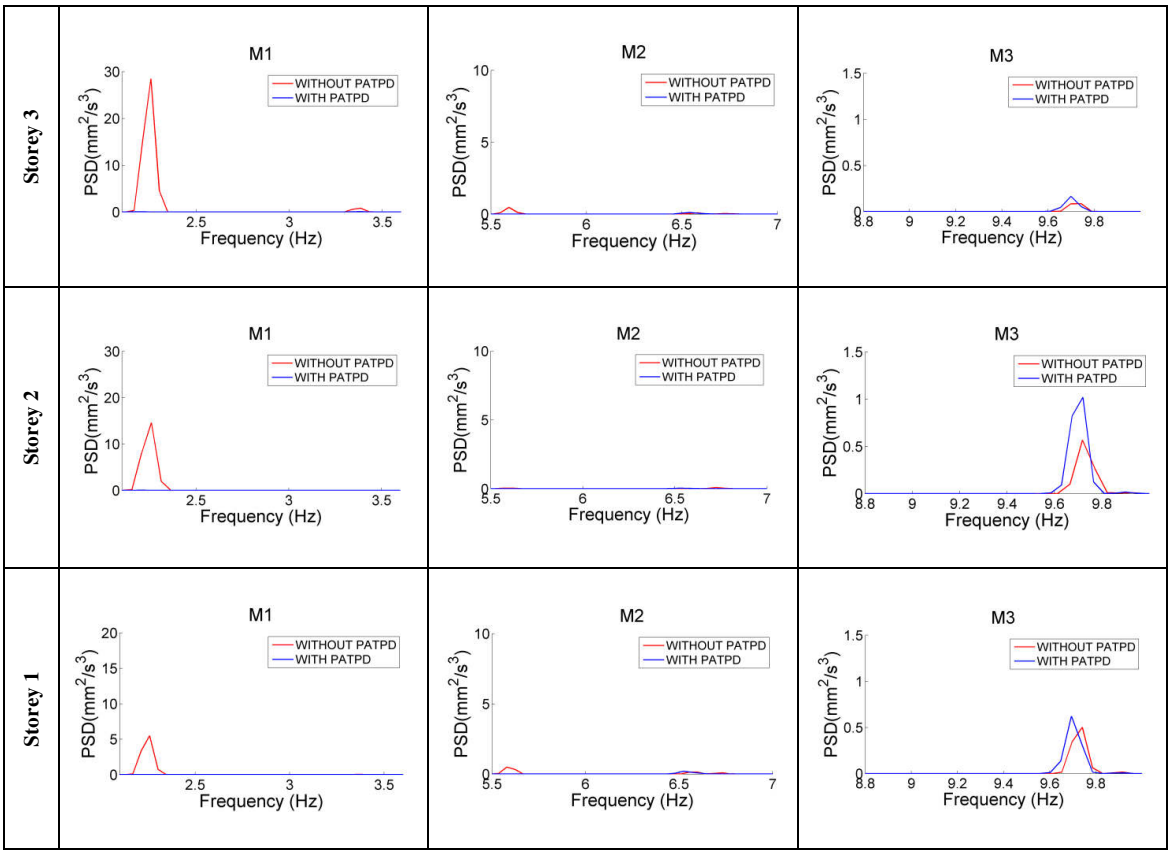

Figure 258: Magnified Power Spectral Density (PSD) of the acceleration response for free coupled vibration (translation in x-direction and torsion), model height 27cm

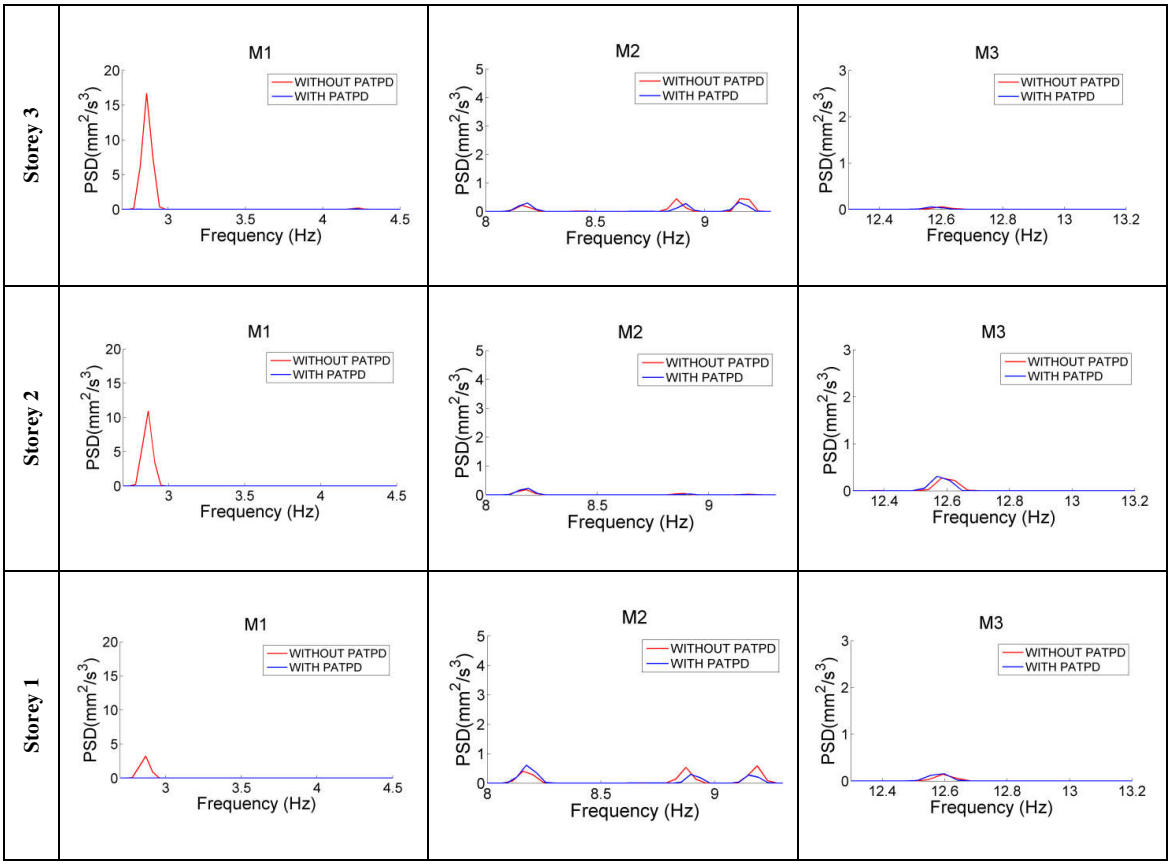

Figure 259: Magnified Power Spectral Density (PSD) of the acceleration response for free coupled vibration (translation in x-direction and torsion), model height 32cm

Figure 256 for storeys 3-1, with height 27cm, shows a high peak at: 2.272Hz and 3.354; 6.548Hz and 5.605; 9.707Hz and 9.003 first, second and third translational and torsional natural frequencies.

Figure 257 for storeys 3-1, with height 32cm, shows a high peak at: 2.885Hz and 4.204; 8.205Hz and 9.167; and 12.590Hz and 13.100 first, second and third translational and torsional natural frequencies.

As can be seen from Figure 258 and Figure 259, for both translation and torsion the PATPD provides at least 99% attenuation for all 3 storeys to the first natural frequency for both model heights.

For the 27cm height for all storeys, second torsional PSD peak for translation and torsion is attenuated by at least 99%, but for the third PSD peak there is only a slight attenuation to translation as torsion remains zero.

For the 32cm height for all storeys, second torsional PSD peak for translation and torsion, and third translational PSD peak, is attenuated slightly. Torsional PSD peak remains zero.

The PATPD has achieved attenuating the first natural frequency which has the greatest amplitude for coupled vibration in the x-direction covering a relatively wide range of frequencies, by adapting to dynamic changes i.e. change in the models stiffness.

6.2.1.6 Coupled Vibration (translation in Y-direction and torsion)

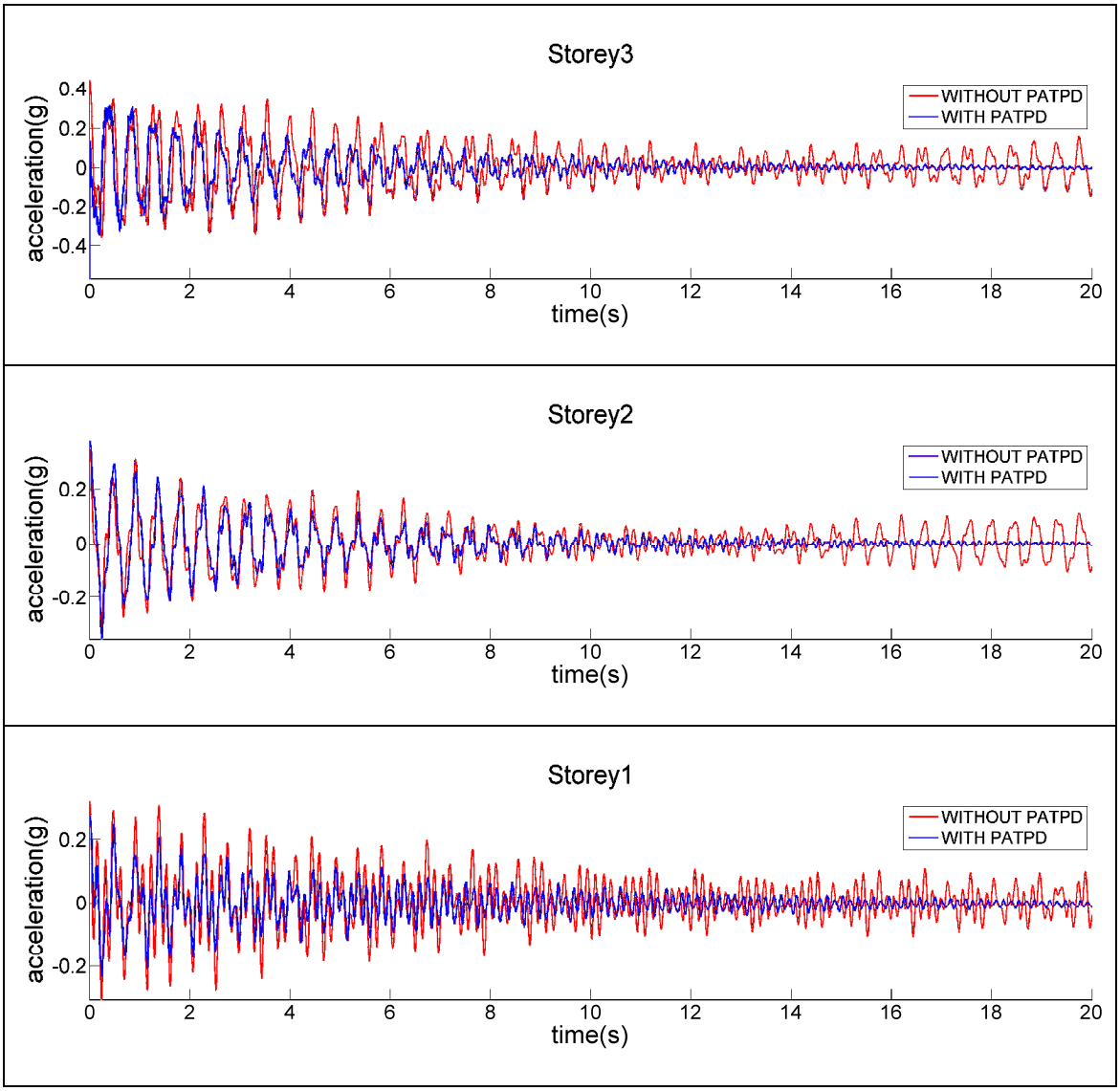

Figure 260: Time history of acceleration response per storey for free coupled vibration (translation in y-direction and torsion), model height 27cm

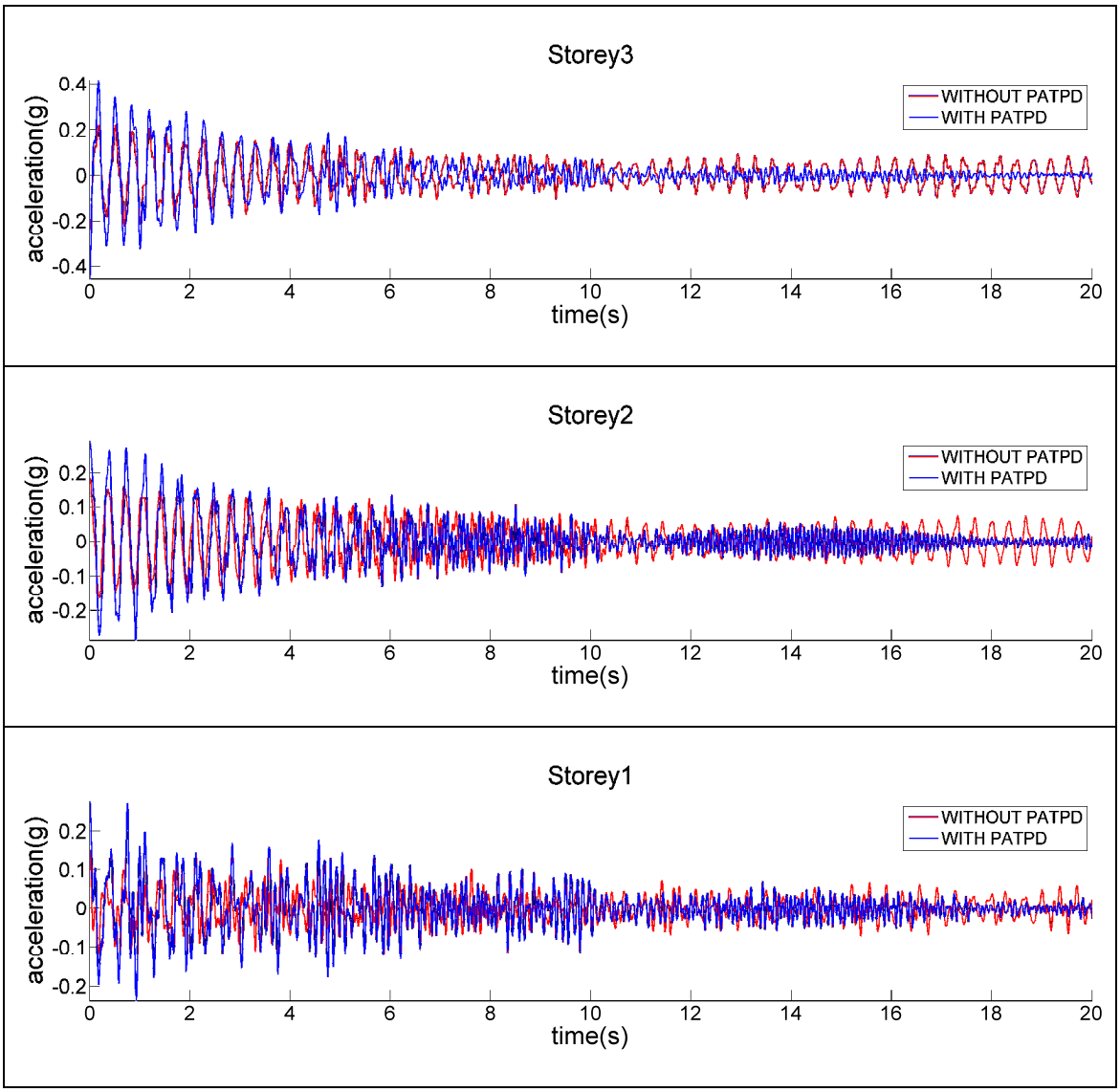

Figure 261: Time history of acceleration response per storey for free coupled vibration (translation in y-direction and torsion), model height 32cm

Figure 260 shows similarity to the results for the primary model[24], of height 37cm per storey, as the PATPD started moving; the acceleration peaks generated in the damped model are as high as those generated in the undamped model. However, these high accelerations subside and the accelerations rapidly decrease compared to that of the undamped model. As is expected the accelerations experienced in storey 3 are highest and the positive damping effect of the PATPD is still significant. Figure 261 however, shows increased acceleration until 10s for all 3 storeys, and then a gradual decrease.

[24] Primary model (mass 42.09kg) figures can be found in Chapter 4 page 63 onwards

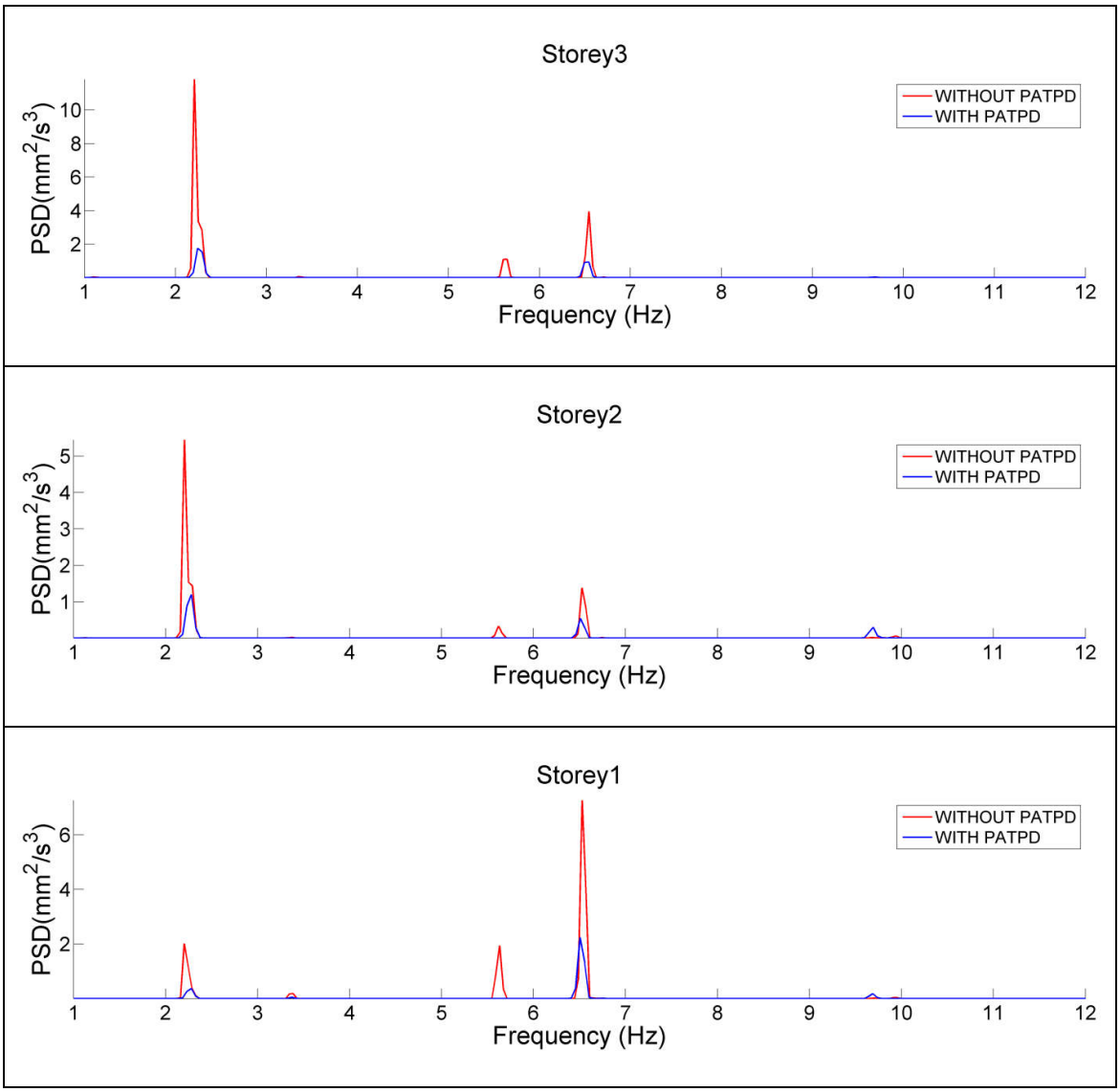

Figure 262: Power Spectral Density (PSD) per storey of the acceleration response for free coupled vibration (translation in y-direction and torsion), model height 27cm

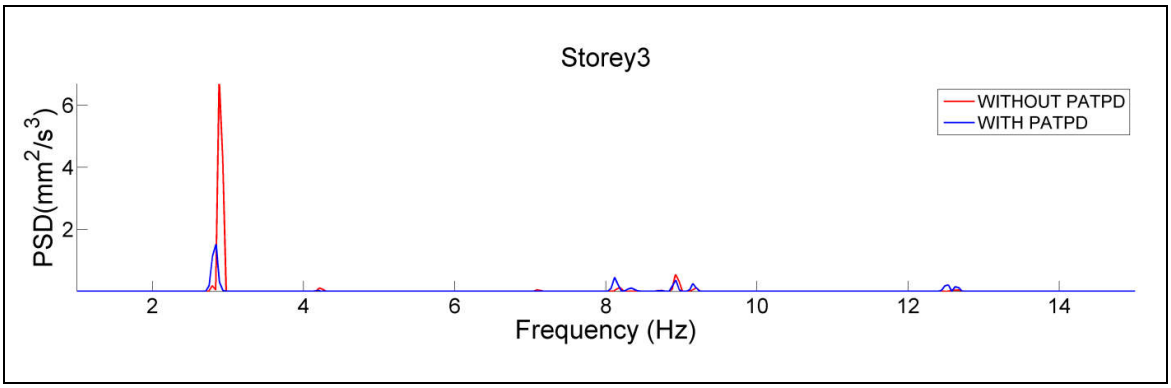

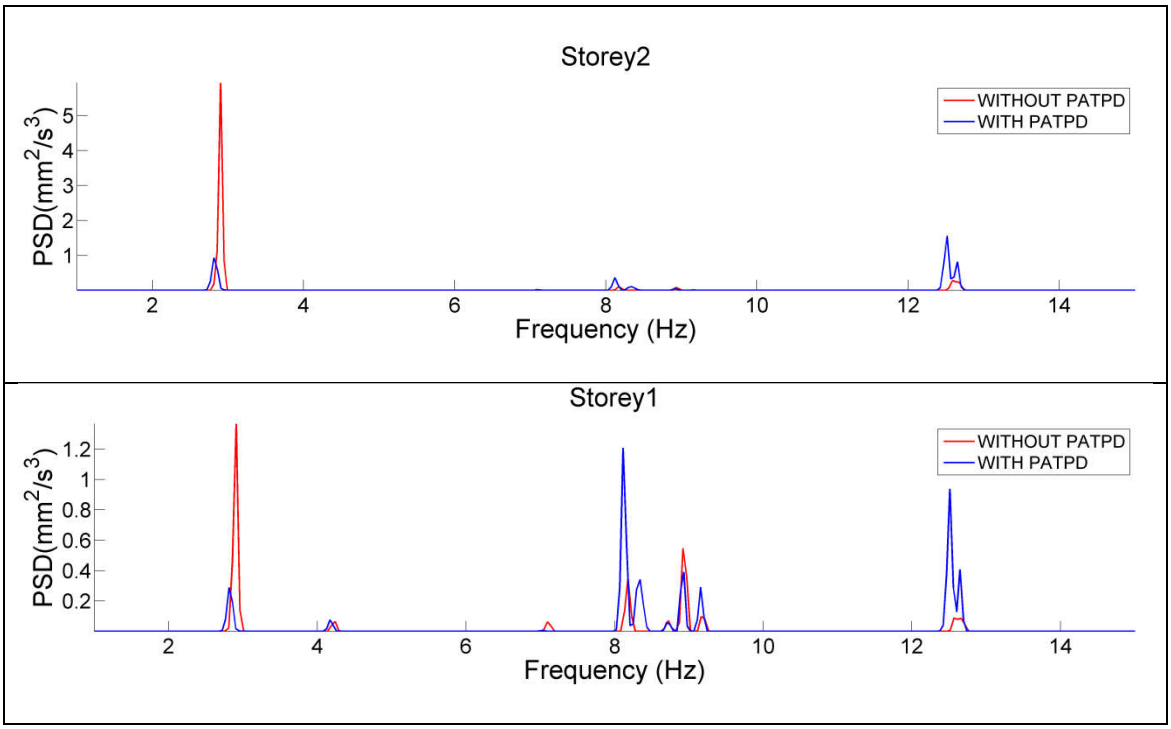

Figure 263: Power Spectral Density (PSD) per storey of the acceleration response for free coupled vibration (translation in y-direction and torsion), model height 32cm

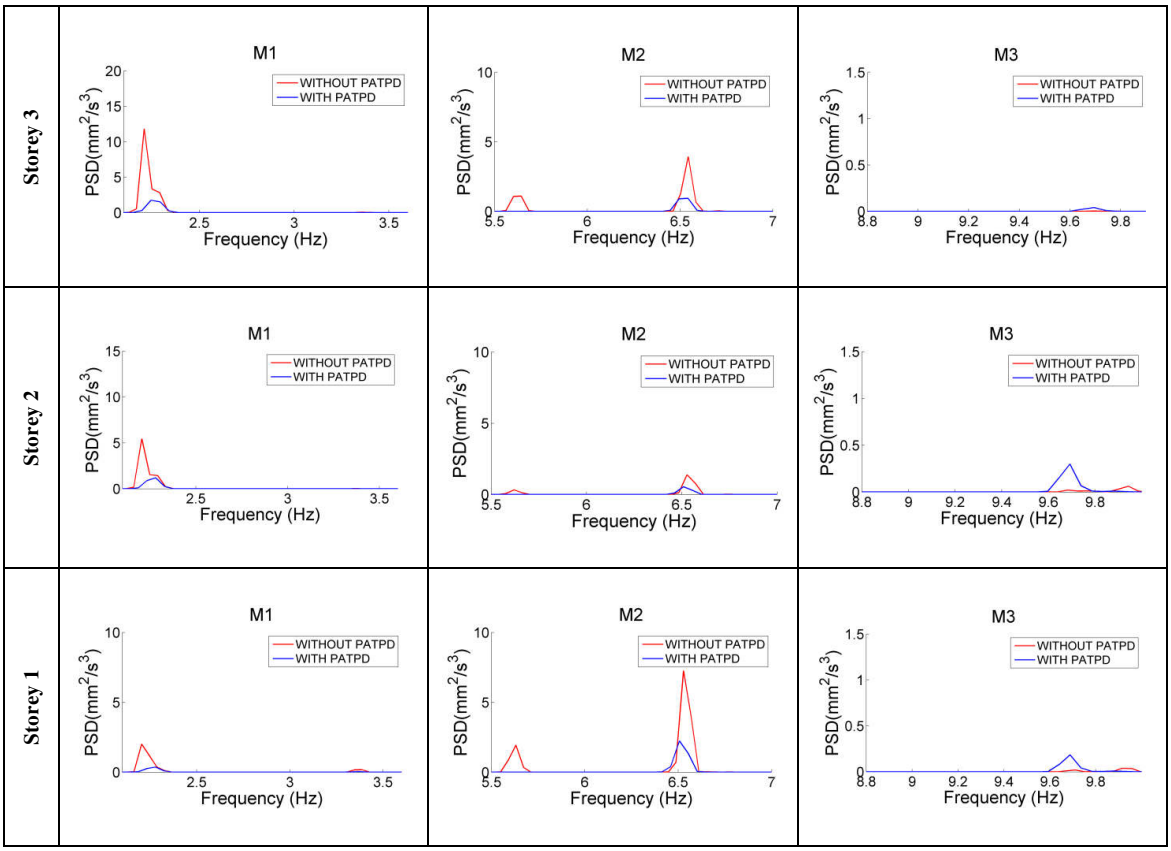

Figure 264: Magnified Power Spectral Density (PSD) of the acceleration response for free coupled vibration (translation in x-direction and torsion), model height 27cm

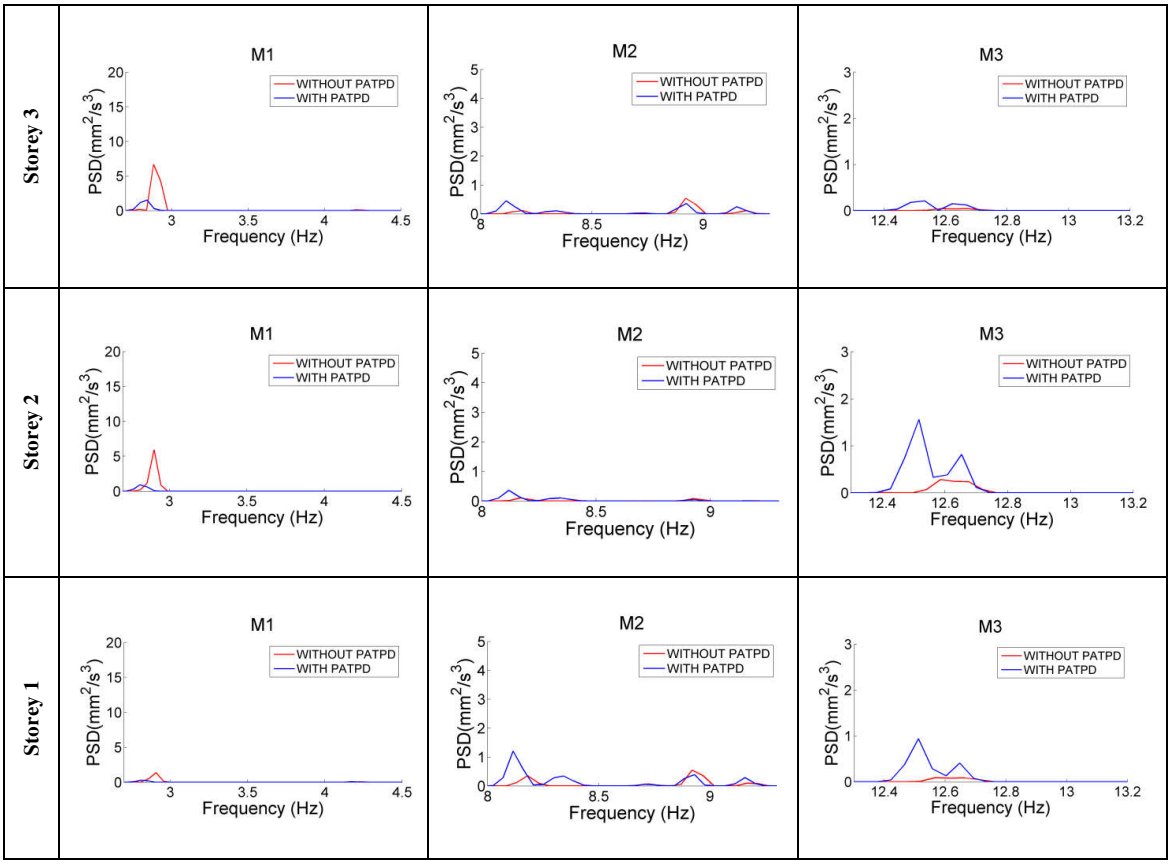

Figure 265: Magnified Power Spectral Density (PSD) of the acceleration response for free coupled vibration (translation in y-direction and torsion), model height 32cm

Figure 262 for storeys 3-1, with height 27cm, shows a high peak at: 2.243Hz and 3.377; 6.545Hz and 5.646; and 9.703Hz and 8973Hz for the first, second and third translational and torsional natural frequencies.

Figure 263 for storeys 3-1, with height 32cm, shows a high peak at: 2.855Hz and 4.255; 8.132Hz and 9.209; and 12.540Hz and 13.080 for the first, second and third translational and torsional natural frequencies.

As can be seen from Figure 264 and Figure 265 , for both translation and torsion the PATPD provides significant attenuation for all 3 storeys to the first natural frequency for both heights. The third natural frequencies for translation and torsion for height 27cm is also attenuated by at least 99%.

For height 27cm second torsional PSD peak is attenuated by at least 99% for all 3 storeys. The translational PSD peak is also significantly attenuated for all 3 storeys. For

the 32cm height M2 for translation and torsion shows slight increase in torsional PSD peak for all 3 storeys.

The third torsional PSD peak for the 32cm height shows a slight increase in frequency for all 3 storeys for translational vibration, but at least 99% attenuation to torsional vibration.

The PATPD has achieved attenuating the first natural frequency which has the greatest amplitude for coupled vibration in the y-direction covering a relatively wide range of frequencies, by adapting to dynamic changes i.e. change in the models stiffness.
It is also evident, as with the primary model, that the PATPD control in the x-direction is better than in the y-direction.

6.2.2.0 Forced Vibration

6.2.2.1 Translational Vibration in the X-Direction

The test model is orientated on the shake table so as to generate forced vibrations in the x-direction. The test model was chosen such that it would have the largest change from the primary model, thus the model with storey height of 27cm was used instead of 32. A frequency sweep was performed from 0Hz to 10Hz with and without the damper. The test duration was 120 seconds.

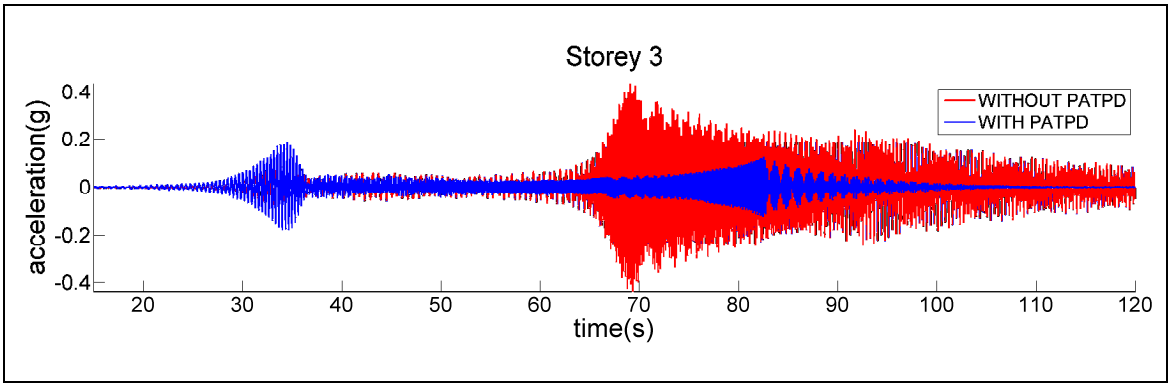

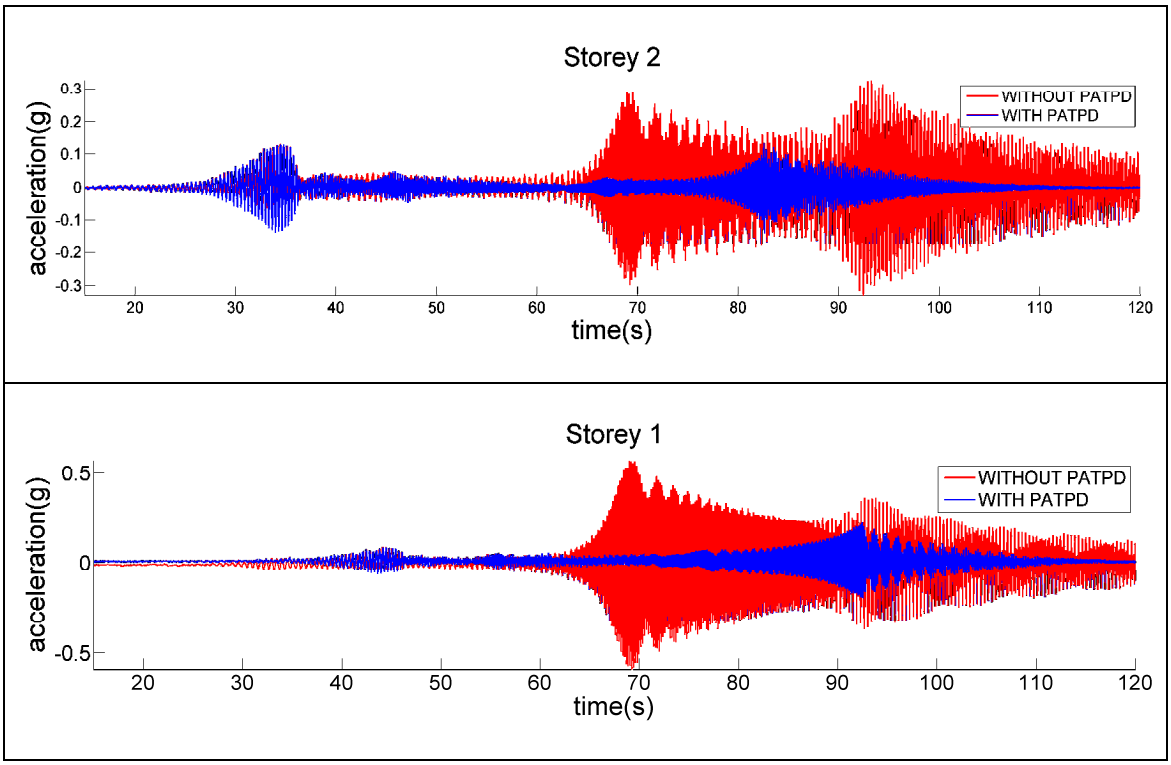

Figure 266: Time history of acceleration response per storey for forced translational vibration in x-direction, model height 27cm

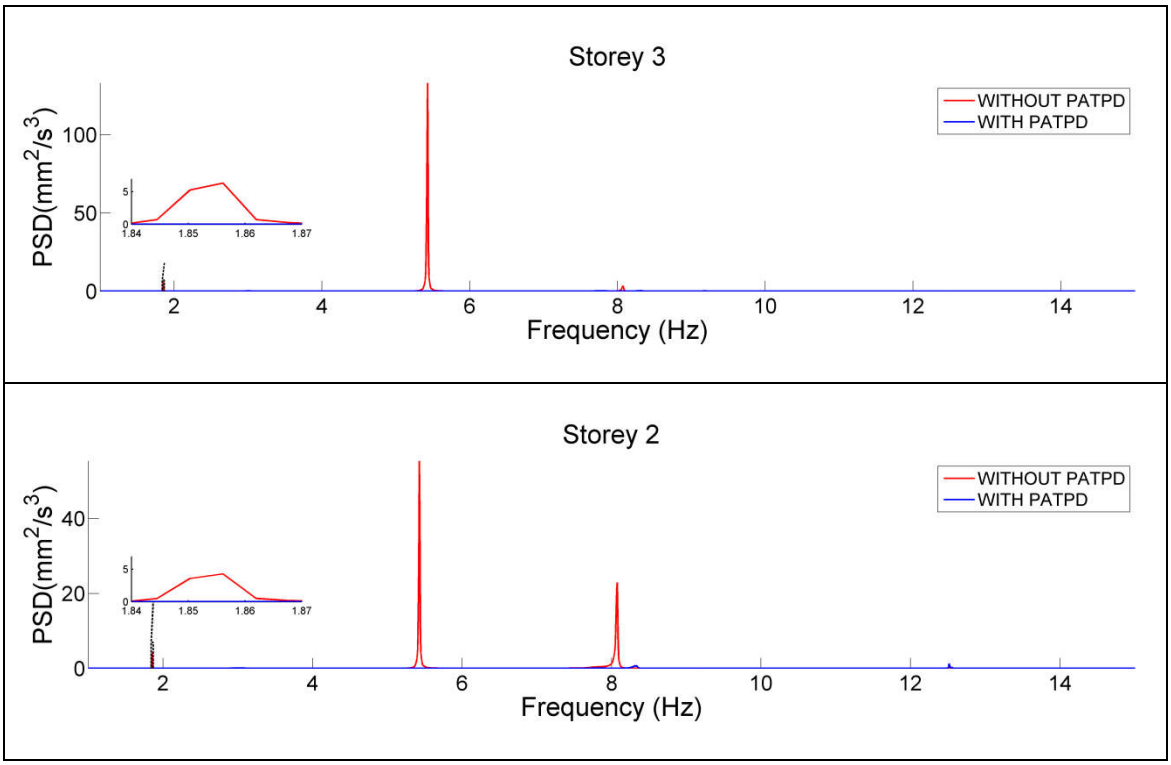

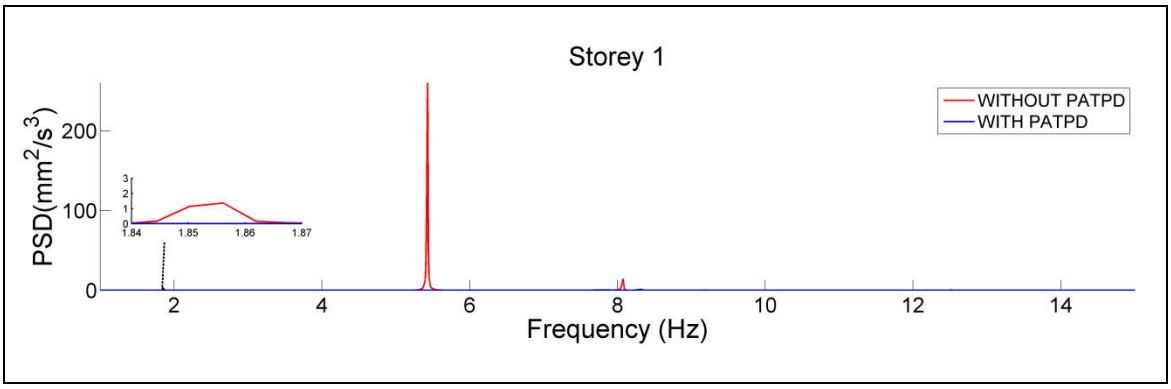

Figure 267: Power Spectral Density (PSD) of the acceleration response per storey under forced excitation in the x-direction, model height 32cm

Figure 266 shows for all 3 storeys that by adding the damper onto model the acceleration experience is significantly reduced.

Figure 267 shows PSD peaks at 1.856Hz, 5.429Hz and 8.074Hz. This corresponds to the models first, second and third frequencies. The positive control effect is evident as PSD peaks for all 3 frequencies are significantly reduced by at least 99%.

6.2.2.2 Translational Vibration in the Y-Direction

The test model is orientated on the shake table so as to generate forced vibrations in the y-direction on the model. The test duration was 120 seconds.

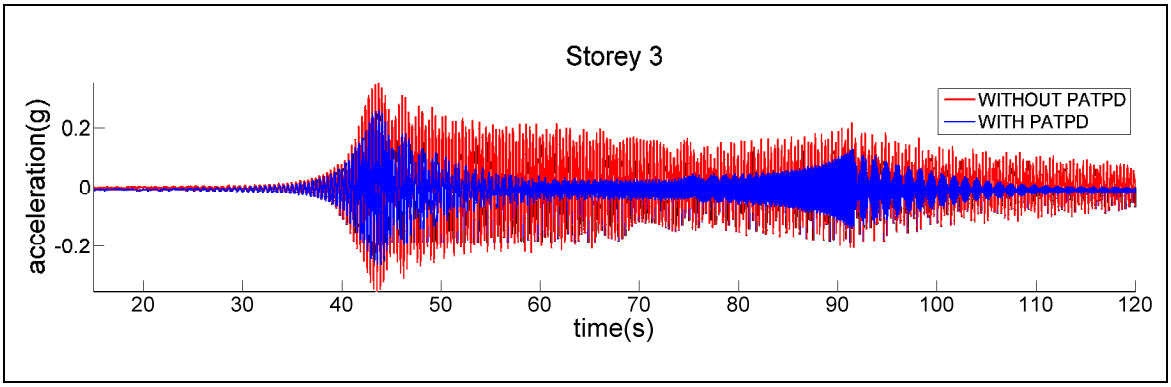

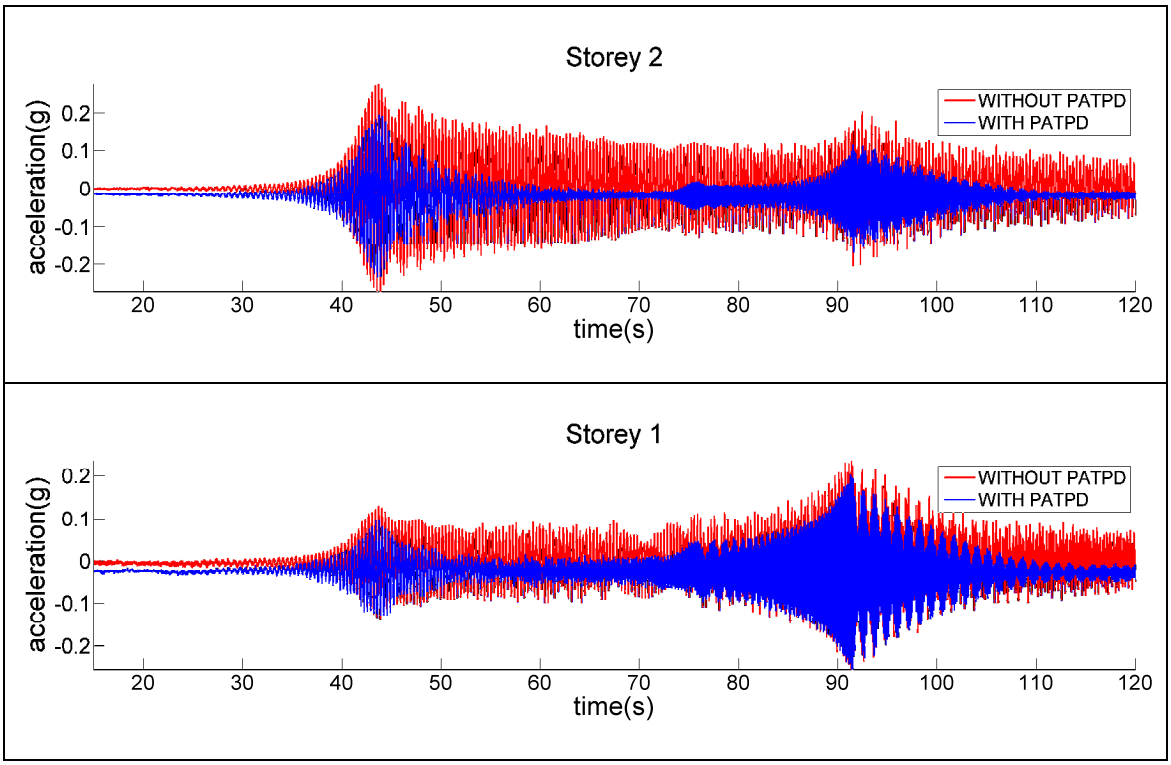

Figure 268: Time history of acceleration response per storey for forced translational vibration in y-direction, model height 27cm

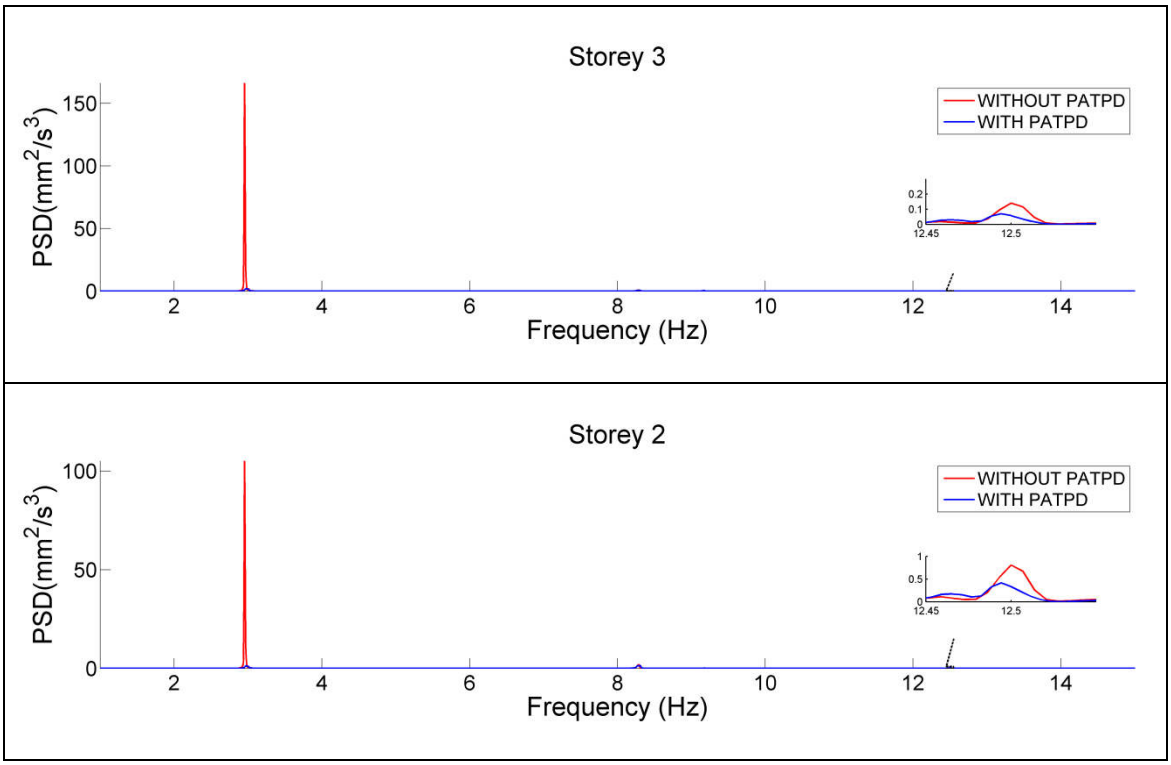

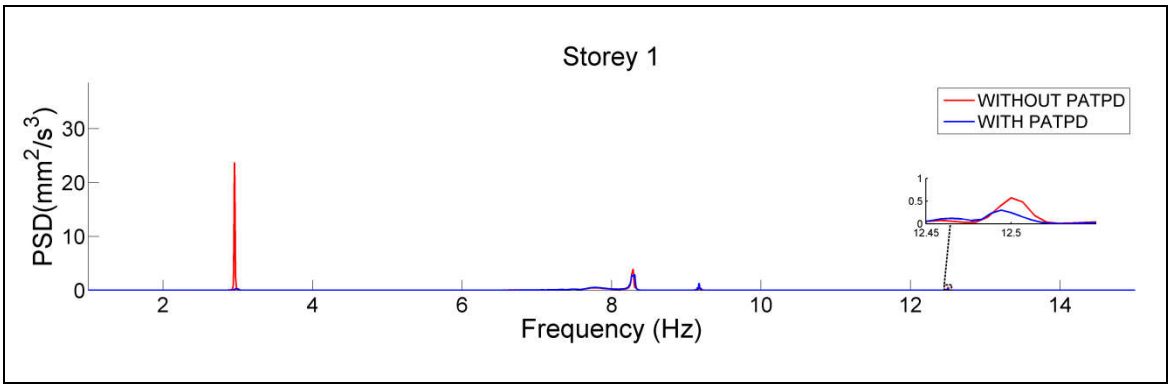

Figure 269: Power Spectral Density (PSD) of the acceleration response per storey under forced excitation in the y-direction, model height 32cm

Figure 268 shows for all 3 storeys that by adding the damper onto model the acceleration experience is significantly reduced.

Figure 269 shows PSD peaks at 2.955Hz, 8.285Hz and 12.50Hz. This corresponds to the models first, second and third frequencies. The positive control effect is evident as PSD peaks for all 3 frequencies are significantly reduced.

6.2.3.0 Summary and Conclusions

Free Vibration

For both heights, for translation and coupled, as the PATPD started moving, the acceleration peaks generated in the damped model are as high as those generated in the undamped model. However, these high accelerations subside and the accelerations rapidly decrease compared to that of the undamped model. As is expected the accelerations experienced in storey 3 are highest, the positive damping effect of the PATPD is still significant. An inconsistency exists with torsion in y-direction for the 32cm height which does not demonstrate significant control.

For translational vibration in the x directions the PATPD provides attenuation to all 3 natural frequency PSD peaks. However, in the y-direction the first natural frequency peak is attenuated for both, with a slight increase in the second and third PSD peak.

For torsion in the y-direction, the stiffer test model behaves better which is expected. The 27cm test model first and second natural frequency PSD peaks attenuated by the PATPD, with a slight increase in the third. However, the 32cm test model does not

show significant control for torsion with addition of damper, where translational frequencies are slightly increased and thus further investigation is required. In the x-direction first and second natural frequency PSD peaks for both are attenuated. The third PSD peak sees no change as damped and undamped frequency densities are similar.

For y-direction coupled vibration the translational and torsional frequency measured in y-direction for the first natural frequency PSD peak for all storeys is attenuated. The second and third natural frequency PSD peaks show torsional attenuation and for translational vibration show slight increase. In the x-direction all three natural frequency PSD peaks are attenuated for both translation and torsion for all storeys and both heights.

Table 2: Comparison of percentage change of PSD peak for the first natural frequency with and without PATPD for free vibration, for the 37cm (primary model), 32cm and 27cm model height

	Translation vibration		Torsion vibration		Coupled vibration			
					Translation		Torsion	
	x	**y**	**x**	**y**	**x**	**y**	**x**	**y**
37cm - first natural frequency	1.733	1.747	2.677	2.680	1.733	1.747	2.677	2.680
37cm - PSD peak % change	99.9 %	98.7 %	99.9 %	99.9 %	99.3 %	99.3 %	99.9 %	99.2 %
32cm - first natural frequency	1.573	1.593	2.418	2.401	1.573	1.593	2.418	2.401
32cm - PSD peak % change	76.1 %	99.3 %	50.5 %	80.3 %	99.9 %	77.3 %	53.2 %	69.0 %
27cm - first natural frequency	1.455	1.471	2.188	2.199	1.455	1.471	2.188	2.199
27cm - PSD peak % change	99.6 %	98.9 %	79.9 %	90.0 %	99.8 %	85.2 %	87.7 %	87.5 %

As is evident from Table 2 even though the storey height (or stiffness) changed, which resulted in the change of the structures' natural frequency, the control provided by the PATPD was still significant for all tests. Without any tuning or adjustment to the damper it still efficiently controlled vibration.

Forced Vibration

For Forced Vibration the PATPD provides significant control to all 3 frequencies for the dynamic property change of stiffness. This demonstrates the auto-tuning or adaptivity of the PATPD.

The results reveal that the PATPD performs better in translation the x –direction than the y-direction.

6.3 Changing Dynamic Properties: Comparison showing Auto-tuning characteristic of PATPD

The Auto-tuning effect of the PATPD can be seen directly from comparing models with different dynamic properties and observing the results.

The comparison is made for the Forced Vibration sweep test from 0.2Hz to 10Hz for 120 second duration in the x-direction (the y-direction shows similar trend and can be seen previously). Storey 1 is used for comparison (storey 2 and 3 shows similar trend and can be seen previously).

The primary model with mass of 42.09kg and storey height of 37cm is compared with (a) mass of 42.09kg and storey height of 27cm and (b) the test model with mass of 66.09kg and storey height of 37cm.

This comparison seeks to demonstrate the adaptability of the PATPD.

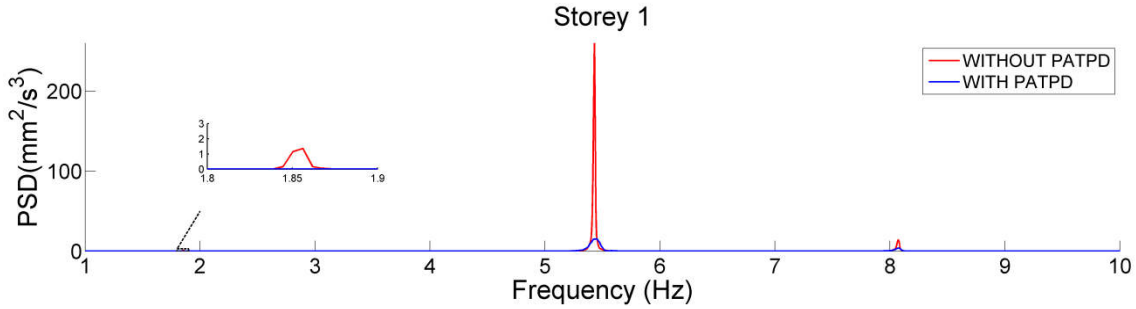

Figure 270: Power Spectral Density (PSD) of the acceleration response of the primary model with mass 42.09kg and storey height 37cm under forced excitation in the x-direction

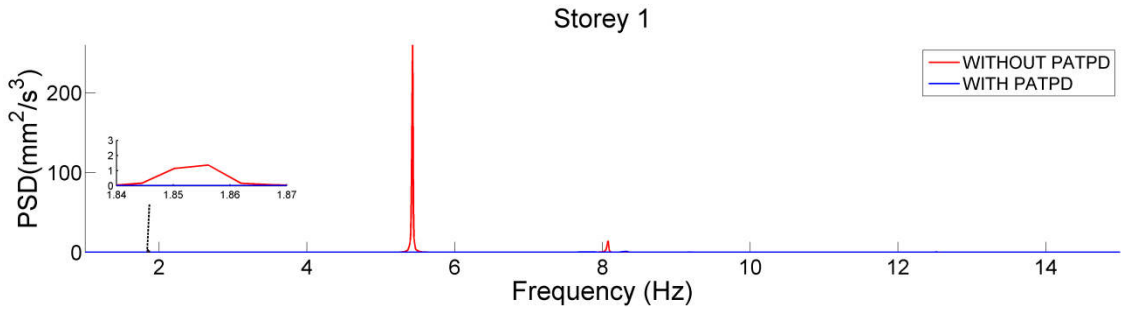

Figure 271: Power Spectral Density (PSD) of the acceleration response of the test model with mass 42.09kg and storey height 27cm under forced excitation in the x-direction

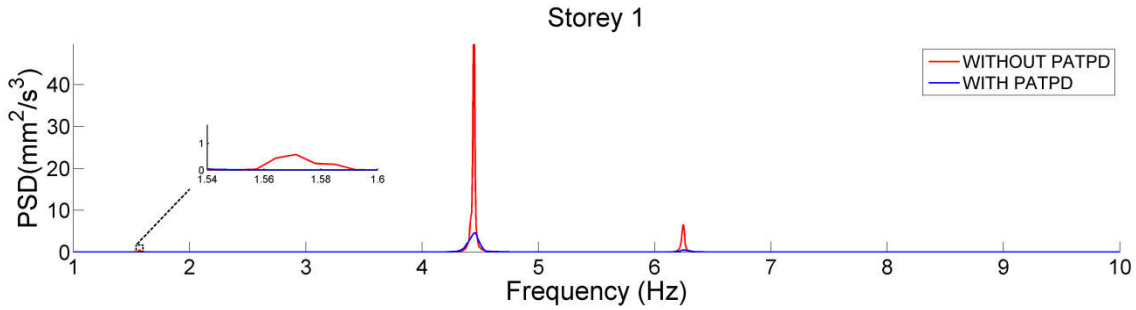

Figure 272: Power Spectral Density (PSD) of the acceleration response of the test model with mass 66.09kg and storey height 37cm under forced excitation in the x-direction

As can be seen in Figure 270, Figure 271 and Figure 272 the PATPD significantly controls all three frequencies for each model with different respective dynamic properties.

The first natural frequency band range is between 1.54Hz and 1.9Hz. The second natural frequency band range is between 4Hz and 6Hz. The third natural frequency band range is between 6Hz and 8.3Hz. Each frequency within this band is controlled significantly. This demonstrates the adaptability or auto-tuning capability of the PATPD.

CHAPTER 7

Experimental results: Additional Forced vibration tests

7.1 Tests under specific forced vibration frequency using sin curve wave shape

7.1.1 Forced frequency of 5.4Hz (structures second natural frequency for free vibration)

The primary test model is orientated on the shake table so as to generate forced vibrations in the x-direction. The actuator was set to the displacement control mode with stroke end levels of -1mm to 1mm. A sin waveform is used and tests were performed with and without the damper. The test duration was 40 seconds. The results are as follows:

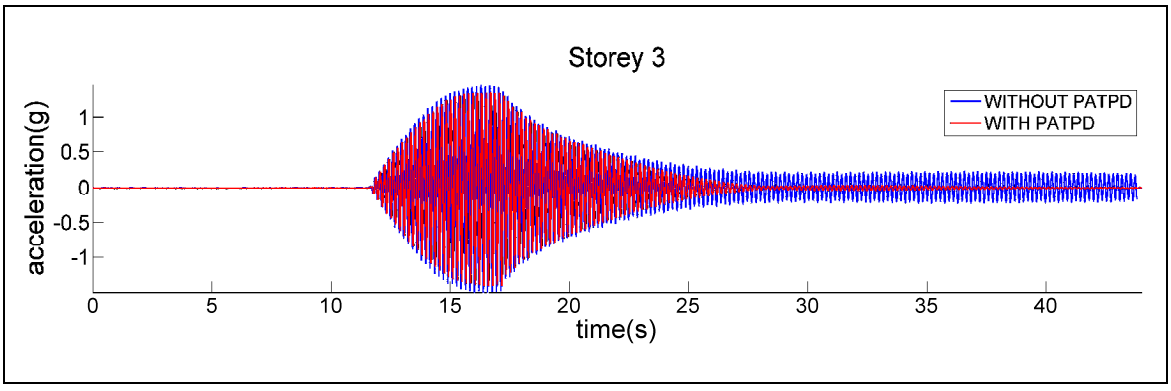

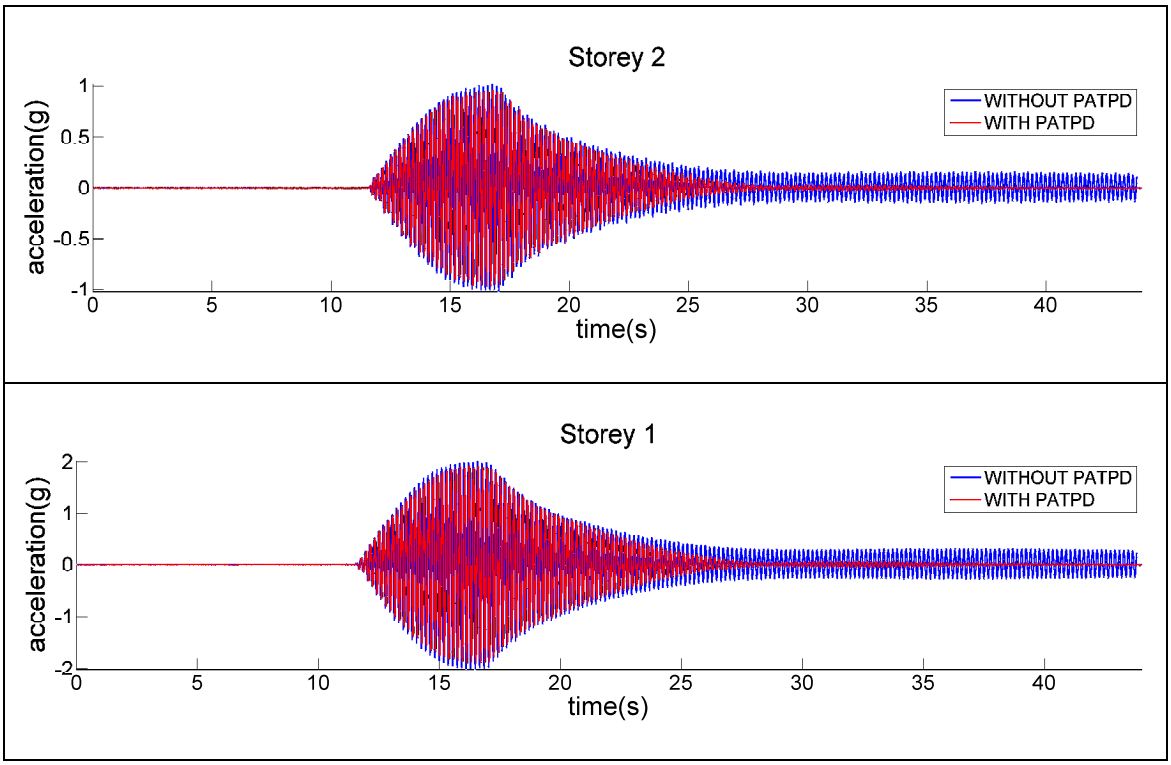

Figure 273: Time history of acceleration response per storey for forced translational vibration in x-direction

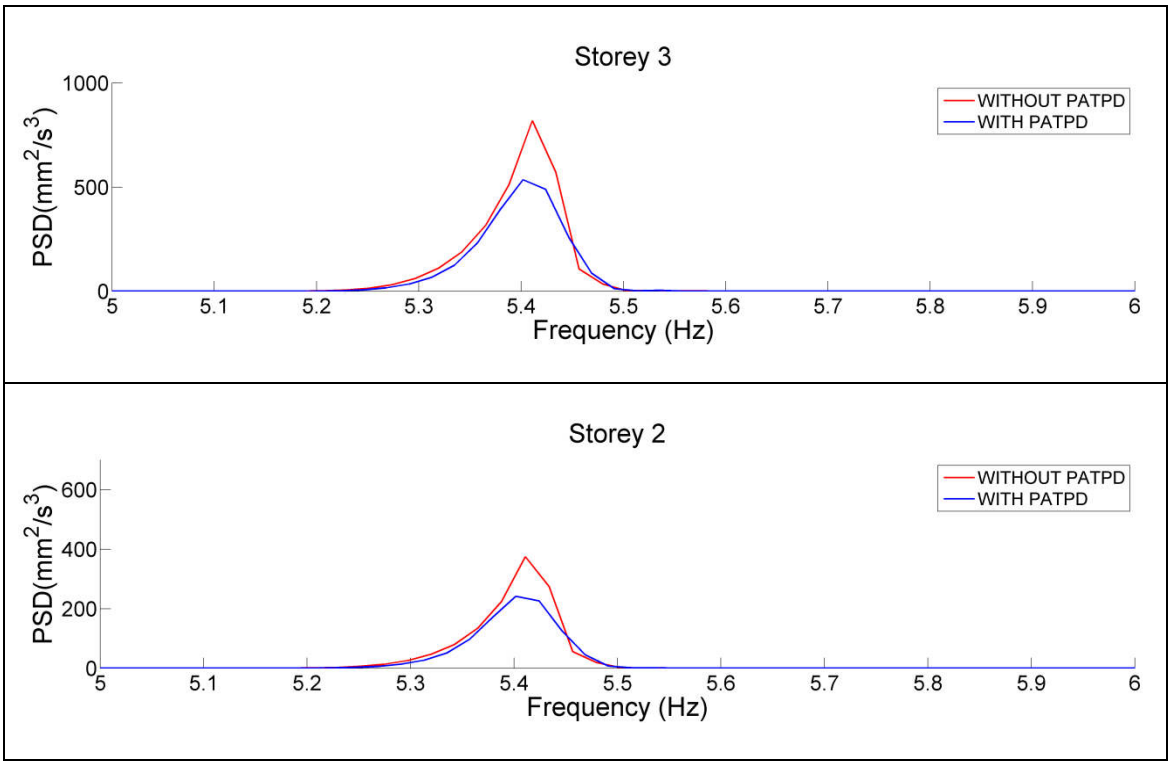

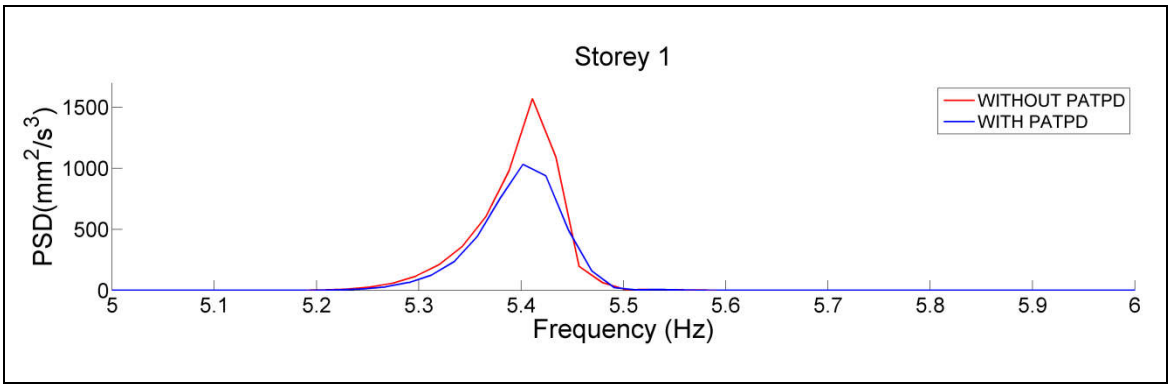

Figure 274: Power Spectral Density (PSD) of the acceleration response per storey under forced excitation in the x-direction

As is evident under an excitation close to the structures second natural frequency the PATPD still provides damping control to the structure reducing the PSD peak.

This attests to the PATPD efficiency.

7.1.2 Forced frequency of 15Hz (structures second natural frequency for free vibration)

The primary test model is orientated on the shake table so as to generate forced vibrations in the x-direction. The actuator was set to the displacement control mode with stroke end levels of -1mm to 1mm. A sin waveform is used and tests were performed with and without the damper. The test duration was 50 seconds. The results are as follows:

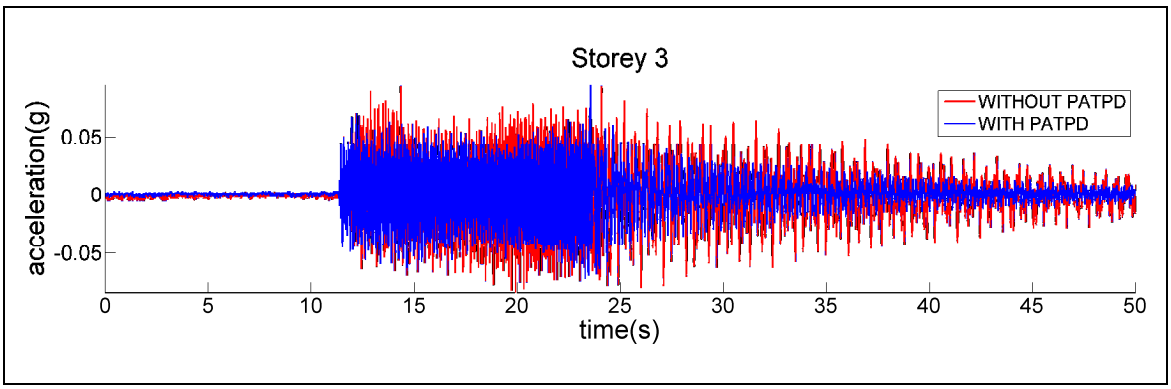

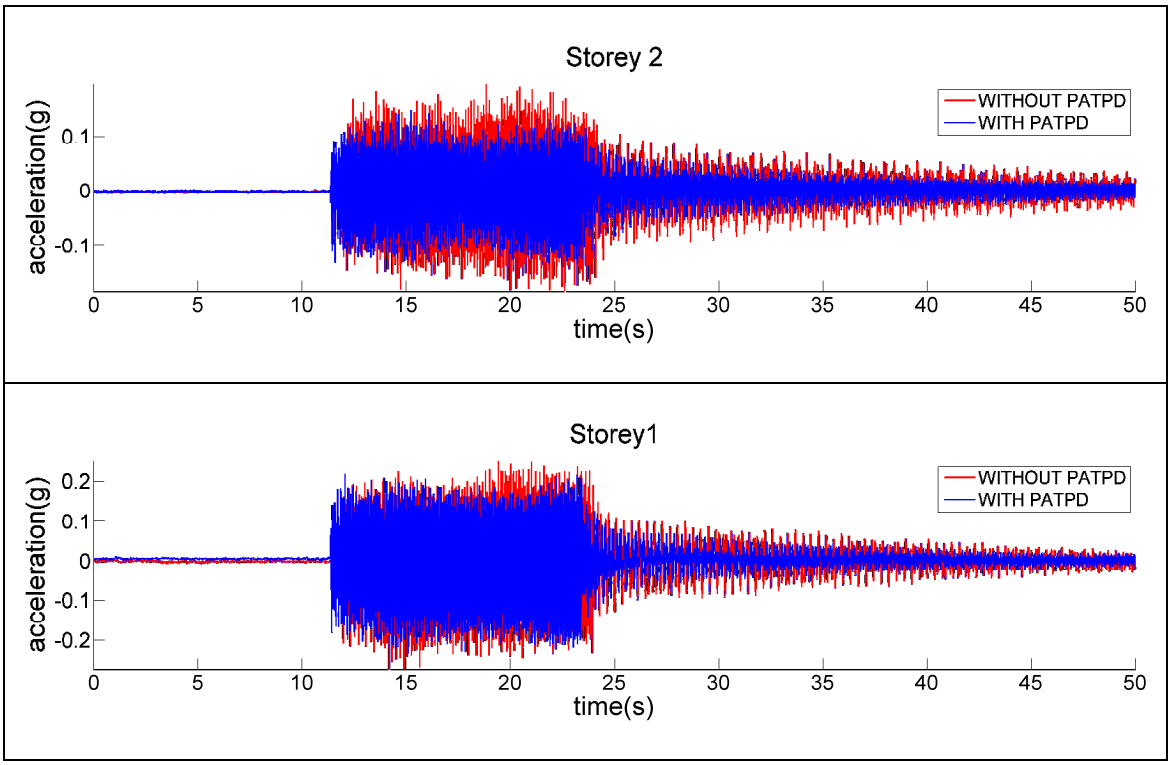

Figure 275: Time history of acceleration response per storey for forced translational vibration in x-direction

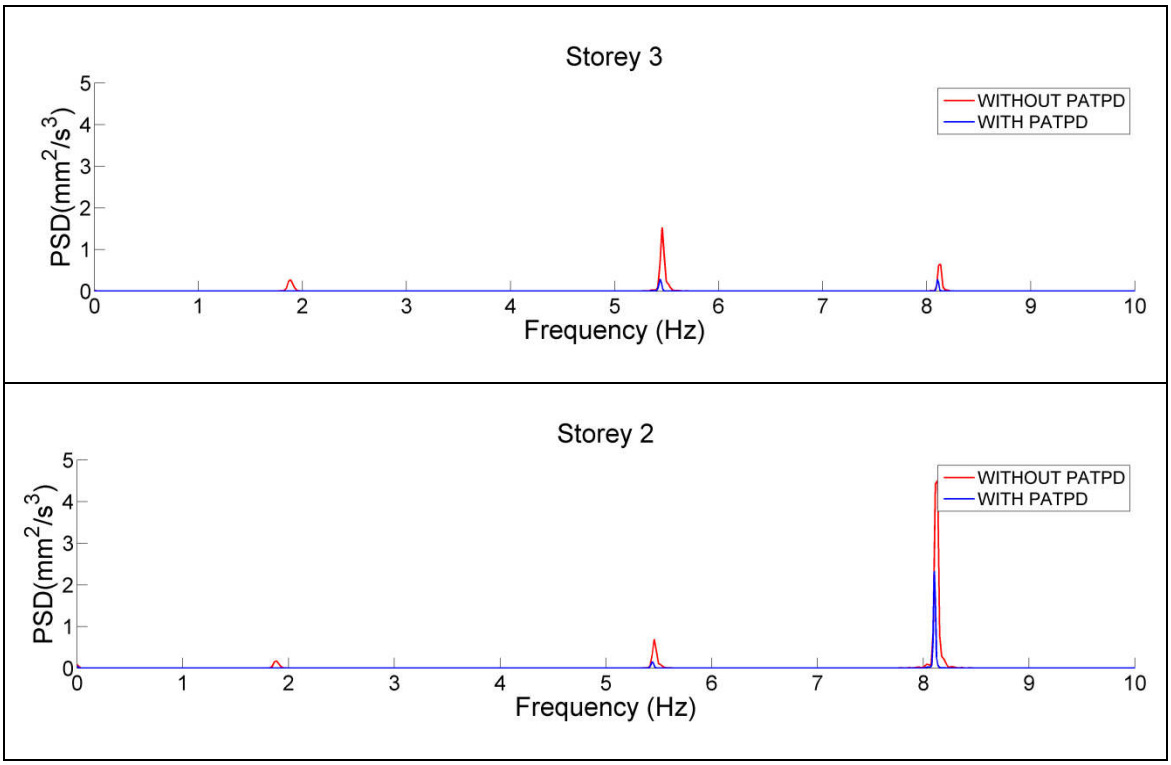

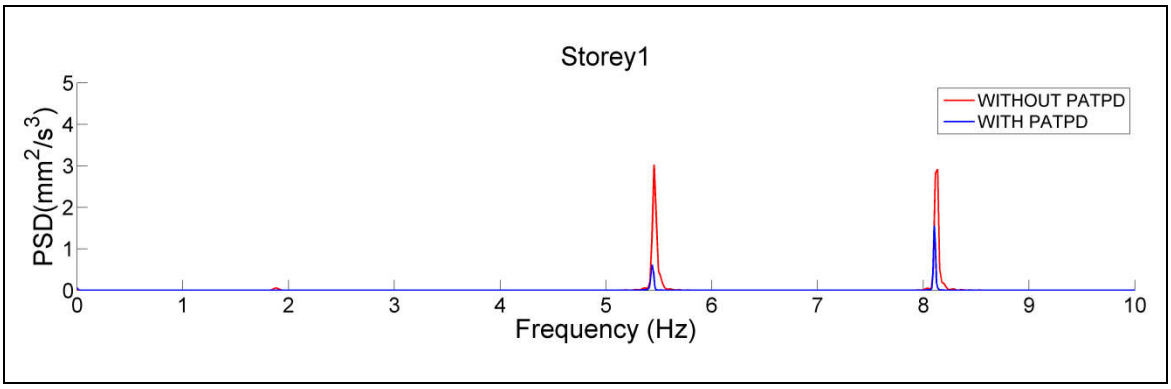

Figure 276: Power Spectral Density (PSD) of the acceleration response per storey under forced excitation in the x-direction

As is evident under an excitation far away from the structures third natural frequency the PATPD still provides damping control to the structure reducing all natural frequency PSD peaks.

This attests to the PATPD efficiency.

7.1.3 Random excitation

The primary test model is orientated on the shake table so as to generate random forced vibrations in the x-direction. The actuator was set to the displacement control mode and tests were performed with and without the damper. A profile[25] shape similar to the 1940 El Centro earthquake in Southern California was used for the random excitation profile. However the maximum values of the random excitation test were kept within the system limits with maximum displacement of 75mm (the El Centro NS maximum displacement was approximately 127mm).

The test duration was 59 seconds. The results are as follows:

[25] A detailed explanation of profile extrapolation can be found in Appendix C

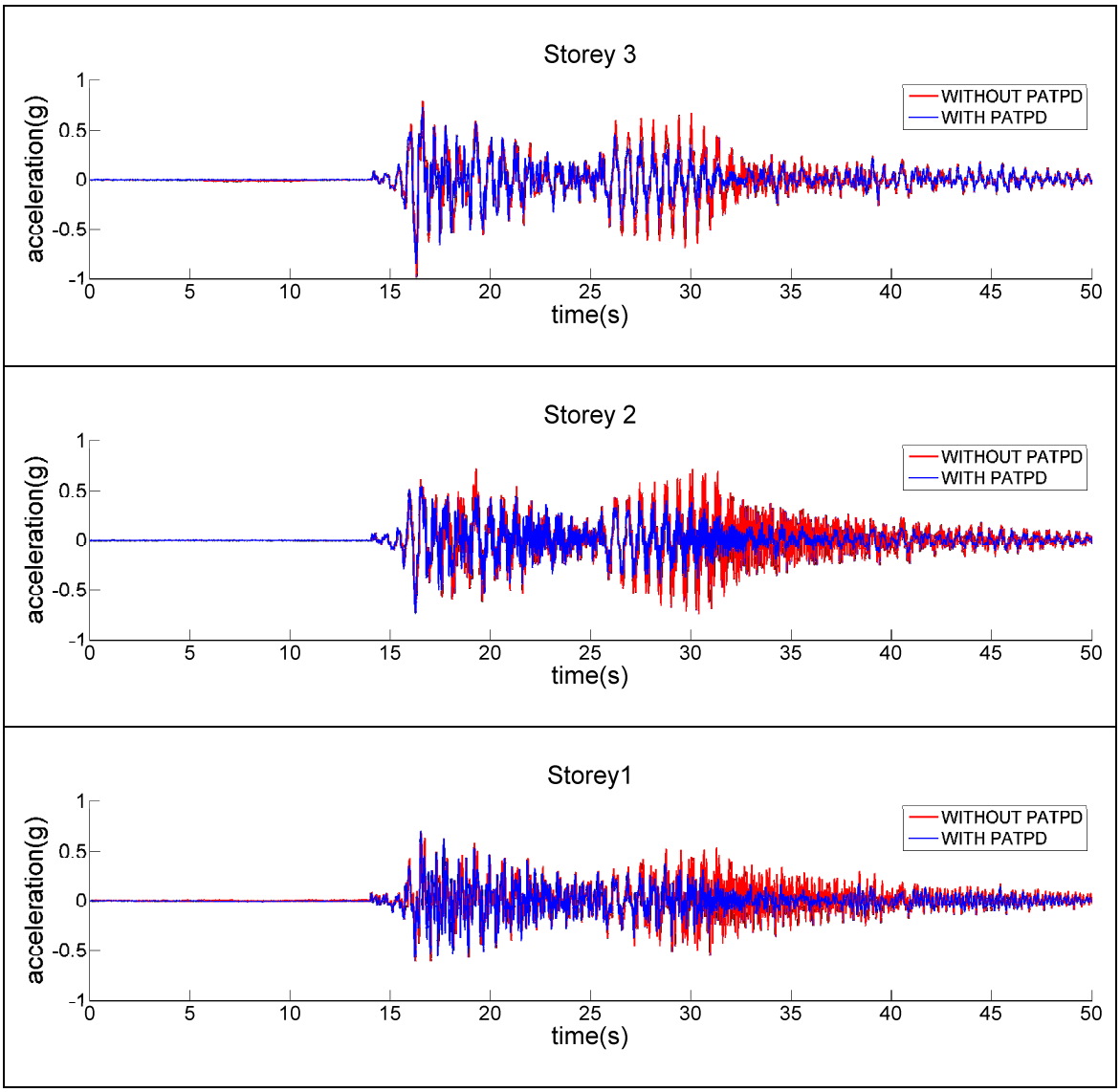

Figure 277: Time history of acceleration response per storey for forced translational vibration in x-direction

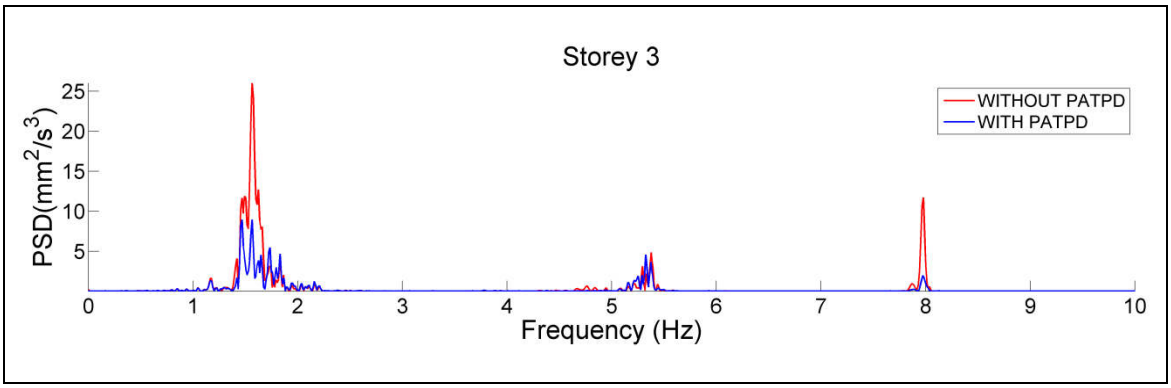

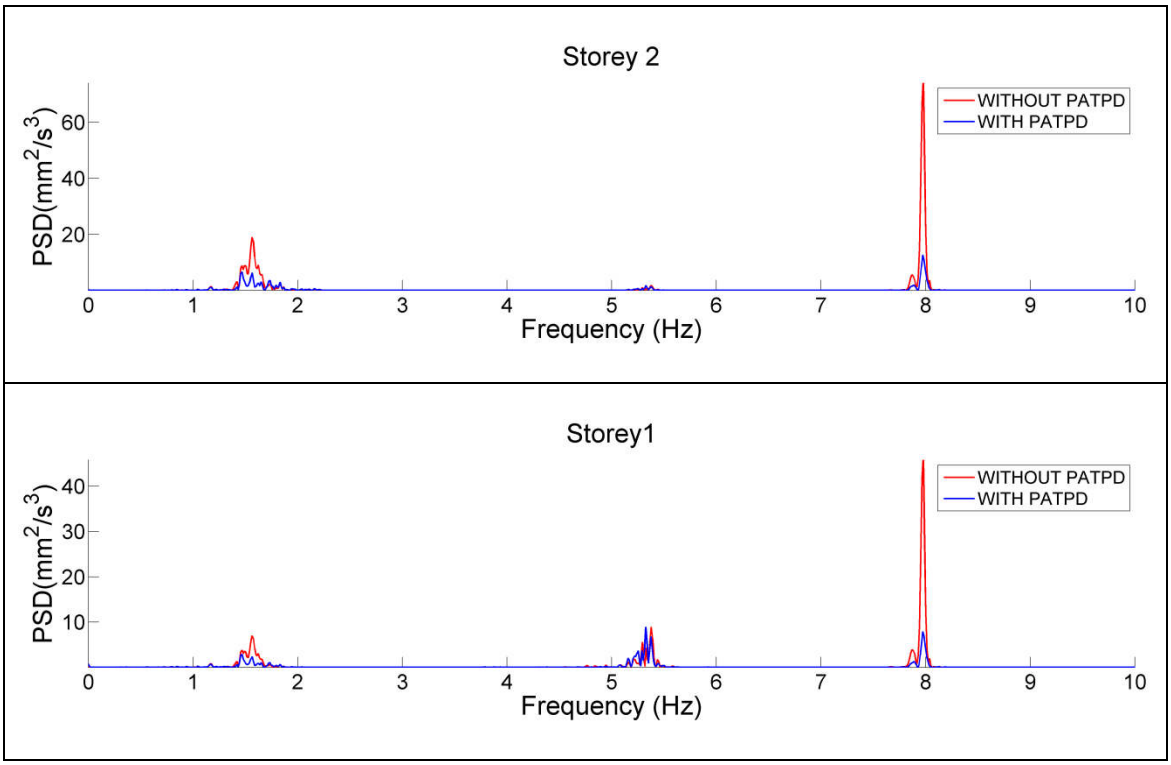

Figure 278: Power Spectral Density (PSD) of the acceleration response per storey under forced excitation in the x-direction

Figure 277 indicates that between the 15 to 25 second period the damper provided slight control effect, a more significant control effect is seen from the 25th second onwards. Figure 278 shows that under random excitation the PATPD provided significant PSD peak reduction for the first and third natural frequencies of the model, and even though the second natural frequency PSD peak is not reduced – it is not increased either.

The results from Figure 277 to Figure 278 indicate the efficiency of the PATPD under random excitation.

CHAPTER 8

8. 1 Conclusions

The continual increase in high-rise construction of residential and office buildings worldwide, mainly in urban areas, or economic hubs, have necessitated advances in technology and innovation in structural design as structures push the limits in terms of height, shape and slenderness. Thus modern high-rise buildings, or skyscrapers as they have become known, which are even taller and more slender, necessitate improved vibration control making research and application within the field vitally important. Many techniques have been developed over the years and many vibration control systems have been implemented successfully in some of the most ingenious buildings to date.

The passive TMD is one of the most common and widely accepted control strategies, which has been in use since the 1970s. However, the greatest drawback with the TMD is that it requires tuning to a specific frequency which limits its efficiency to a narrow band control; in addition it does not perform well under torsional and coupled vibration. The proposed auxiliary damping device, the PATPD, contained herein seeks to address the primary issue of detuning, and also investigates the dampers performance under torsional and coupled vibrations.

Efficiency tests on the PATPD for free translation, torsion and coupled vibrations revealed that the first natural frequency was significantly controlled with least control being 95%. The second and third natural frequencies were controlled in some cases and not in others – where there were slight increases in PSD peaks. However, these increases were minimal in comparison with the control effect provided to the first natural frequency. There is room for improvement with torsional control. For Forced translational vibration tests the PATPD provides significant control to all 3 frequencies. All PATPD tests performed indicated better overall control effect in x-direction than y-direction, with control in y-direction still being significant.

Parameter test for varying mass ratios indicates better control in x than in y direction. Even though a highest mass ratio is expected to perform better, these tests indicate otherwise. The highest mass ratio means that the sand has less ability to 'move' and thus does not perform as well, overall, as the 3% wherein the sand can do so was optimal. The 1.5% ratio did not perform as well, even though it had greatest sand mobility, since it was too light. All mass ratios provided control effect to the first natural frequency for all free vibration tests for all storeys. For Forced translational vibration the PATPD provides significant control to all 3 frequencies for all mass ratios and the PATPD performs better in translation in the x –direction than the y-direction.

Parameter test for varying friction indicates better control in y than in x direction. Steel and sandpaper demonstrates best control effect for first natural frequency. Rubber is worst under translational vibration. They all behave similarly under coupled vibrations. All friction surfaces provided control effect to the first natural frequency for all free vibration tests for all storeys. For Forced translational vibration the PATPD provides significant control to all 3 frequencies for all friction surfaces tested and the PATPD performs better in translation the x –direction than the y-direction.

Parameter test for varying connection type indicates better control in x than in y direction. Cotton and ski-rope demonstrates best control effect for first natural frequency. Nylon is poor in translation. All ropes provided control effect to the first natural frequency for all free vibration tests for all storeys, except Nylon which did not control the first natural frequency for storey 1 under torsional vibration (x-direction).
For Forced translational vibration the PATPD provides significant control to all 3 frequencies for all rope types tested and the PATPD performs better in translation the x –direction than the y-direction.

Parameter test for varying configurations indicates better control in x than in y direction. All configurations provided control effect to the first natural frequency for all free vibration tests for all storeys, except Configuration 3 (transverse only) which did not control first natural frequency for storey 1 under torsional vibration (y direction). Configuration 2 behaves best for control of natural frequency 1 and worst for 2 and 3.

Configuration 1 behaves consistently which is the primary model configuration. A greater number of connections improve behaviour. Also, having more connections along the x-axis spaced more closely together would improve imparting of inertia reaction force as well as the drive force from structure which is transferred through pulleys thus improving control. For Forced translational vibration the PATPD provides significant control to all 3 frequencies for all connection configurations tested and the PATPD performs better in translation the x –direction than the y-direction.

Parameter test for varying connection heights indicates better control in x than in y direction. All configurations provided control effect to the first natural frequency for all free vibration tests for all storeys, except height 15cm which did not control first natural frequency for storey 1 under torsional vibration (y direction). The lower height behaves best for control of natural frequency in most cases. The higher height means looser ropes as more slack is required for movement thus reducing the imparting of inertia reaction to the structure. The lower height performs better since the ropes are tighter and has less slack. For Forced translational vibration the PATPD provides significant control to all 3 frequencies for all connection heights tested and the PATPD performs better in translation the x –direction than the y-direction.

Dynamic property test for varying structure mass indicate similar trend to the primary model for both model masses. For translational vibration in the x directions the PATPD provides at least 93% attenuation to both first and third natural frequency PSD peaks. However, the second natural frequency PSD peak shows an increase in density for both model masses. Results in the y-direction are similar except that in addition to the increase to second natural frequency PSD peak, there is so too an increase in the third natural frequency PSD peak thus indicating better control effect in x-direction than y-direction for translation. Under Torsional vibration the PATPD provides at least 99% attenuation for all 3 storeys to the first and second natural frequency for both model masses. This applies to both the x and y directions. The third natural frequency PSD peak for both masses storey1-3 overall shows a slight increase in density of frequency, the increase is less than that of the y-direction thus again supporting the PATPDs better control in x-direction than y-direction. For coupled vibration the torsional frequency

measured in y-direction, for all 3 natural frequency PSD peaks, for all storeys is attenuated by at least 99%, with the translational frequencies also being attenuated slightly, albeit not completely. Torsion measured in y-direction shows same trend except that there is a slight increase in density of second translational frequency PSD peak. Even though the mass has changed, which resulted in the change of the structures' natural frequency, the control provided by the PATPD was still significant for all tests. Without any tuning or adjustment to the damper it still efficiently controlled vibration. For Forced translational vibration the PATPD provides significant control to all 3 frequencies for the dynamic property change of mass. This demonstrates the auto-tuning or adaptivity of the PATPD and the PATPD performs better in translation the x – direction than the y-direction.

Dynamic property test for varying structure stiffness indicates as is expected the accelerations experienced in storey 3 are highest; the positive damping effect of the PATPD is still significant. An inconsistency exists with torsion in y-direction for the 32cm height which does not demonstrate significant control. For translational vibration in the x directions the PATPD provides attenuation to all 3 natural frequency PSD peaks. However, in the y-direction the first natural frequency peak is attenuated for both, with a slight increase in the second and third PSD peak. For torsion in the y-direction, the stiffer test model behaves better which is expected. The 27cm test model first and second natural frequency PSD peaks attenuated by the PATPD, with a slight increase in the third. However, the 32cm test model does not show significant control for torsion with addition of damper, where translational frequencies are slightly increased and thus further investigation is required. In the x-direction first and second natural frequency PSD peaks for both are attenuated. The third PSD peak sees no change as damped and undamped frequency densities are similar. For y-direction coupled vibration the translational and torsional frequency measured in y-direction for the first natural frequency PSD peak for all storeys is attenuated. The second and third natural frequency PSD peaks show torsional attenuation and for translational vibration show slight increase. In the x-direction all three natural frequency PSD peaks are attenuated for both translation and torsion for all storeys and both heights. Even though the storey height (or stiffness) changed, which resulted in the change of the structures'

natural frequency, the control provided by the PATPD was still significant for all tests. Without any tuning or adjustment to the damper it still efficiently controlled vibration. For Forced translational vibration the PATPD provides significant control to all 3 frequencies for the dynamic property change of stiffness. This demonstrates the auto-tuning or adaptivity of the PATPD and the PATPD performs better in translation the x – direction than the y-direction.

Additional forced translational vibration tests demonstrated the adaptability and efficiency of the PATPD, even for random excitation such as earthquakes. Under an excitation close to the structures second natural frequency the PATPD still provides damping control to the structure reducing the PSD peak; under an excitation far away from the structures third natural frequency the PATPD still provides damping control to the structure reducing all natural frequency PSD peaks. A sweep test indicates that between the 15 to 25 second period the damper provided slight control effect, a more significant control effect is seen from the 25^{th} second onwards. Under random excitation (scaled El Centro profile) the PATPD provided significant PSD peak reduction for the first and third natural frequencies of the model, and even though the second natural frequency PSD peak is not reduced – it is not increased either.

The investigation contained herein reveals that the PATPD is simple, effective, robust and adaptable. It significantly controls translational, torsional and coupled vibration; does not require tuning to a specific frequency and works over a wide frequency band. All of which renders this proposed damper an appealing solution for engineering applications.

8.2 Further Research

In all tests the PATPD control in the x-direction was more significant than in the y-direction. Further research into improved control in the y-direction would be vital in improving the damper effectiveness.

Torsional control was not as significant as translational; the cause should be investigated and possibly rectified.

Connections, rope type and support surface all contributed differently to PATPD control effect; more research should be carried out to determine the PATPD connection configuration which provides the optimum amount of vibration control; the best location for the PATPD and the optimal type of sand used for the mass.

Mechanics of the damper was not a focus of this report but rather the effect of the damper on a MDOF system. As such in order for the PATPD to be a viable solution implementable in industry further research into the damper characteristics, design and optimization is necessary.

The PATPD was tested under random excitation and results indicate significant control effect for the first and third natural frequencies. However, the second natural frequency PSD peak remained the same with the addition of the PATPD. Further research into reducing this frequency as well would prove beneficial.

REFERENCES

Adhikari, S. & Ali, F., 2012. Energy harvesting dynamic vibration absorbers. *Journal of Applied Mechanics,* 80(4).

Al Saif, K., Aldakkan, K. & Foda, M., 2011. Modified liquid column damper for vibration control of structures. *International Journal of Mechanical Sciences,* Volume 53, pp. 505-512.

Alqado, T., Niolakopoulos, G. & Dritsas, L., 2016. Semi-active control of flexible structures using closed-loop input shaping techniques. *Structural control and Health Monitoring.*

Aly, M., Zasso, A. & Resta , F., 2011. Response reduction using MR damper with lever mechanism. *The Structural design of Tall and Special Builings ,* Volume 20, pp. 539-551.

Amin, J. A. & Ahuja, A. K., 2010. Aerodynamic modifications to the shape of buildings:A review of the state-of-the-art. *Asian Journal of Civil Engineering,* II(4), pp. 433-450.

Andrade, L. & Tuxworth, J., 2015. *Seismic Protection of Structures with Modern Base Isolation Technologies,* Pyrmont: Green Leaf Engineers .

Anon., s.d. *Habitables.* [En ligne]
Available at: http://www.habitables.co.uk/wp-content/uploads/2011/03/Kanto-1923.jpg
[Accès le 20 march 2013].

Anon., s.d. *Wikipedia.* [En ligne]
Available at: http://en.wikipedia.org/wiki/Seismic_analysis
[Accès le 20 March 2013].

Bekdas, G. & Nigdeli, S., n.d.. *Optimum Tuned Mass Dampers for Structures with Different Periods,* Istanbul: Istanbul University.

Belash, T., 2015. Dry Friction Dampers in Quake-proof Structures of Buildings. *Procedia Engineering,* Issue 117, pp. 397-403.

Bergman, L., MacFarland, D. & Kareem, A., 1991. *'Coupled passive control of buildings',* New York: Structural Abstracts ASCE.

Bhattacharyya, S., 2016. *Tuned sloshing damper in response control of Tall Building Structure.* Kharagpur, Proceedings National Academy of Sciences India.

Blogspot, 2012. *Blogspot.* [En ligne]
Available at: http://winddesign4.blogspot.co.za/
[Accès le 9 November 2015].

Buzznet, n.d.. *Buzznet.com.* [En ligne]
Available at: http://www.buzznet.com/404.html
[Accès le 9 November 2015].

Carlisle, M., 2013. *Experimental Investigations into a Passive Auto-Tuning Mass Damper,* Johannesburg: University of the Witwatersrand.

Carlisle, M. & Li, K., 2013. *Experimental Investigations into a Passive Auto-Tuning Mass Damper,* Johannesburg: University of the Witwatersrand.

Chang, C., 1999. "Mass Dampers and Their Optimal Designs for Building Vibration Control. *Engineering Structures,* 21(5), pp. 454-463.

Chang, C. & Spencer Jr, B., 2010. Active base isolation of buildings subjected to seismic excitations. *EARTHQUAKE ENGINEERING AND STRUCTURAL DYNAMICS,* Volume 39, p. 1493–1512.

Cha, Y., Trocha, P. & Büyüköztürk, O., 2016. *Field Measurement-Based System Identification and Dynamic Response Prediction of a Unique MIT Building,* Massachusetts: MIT.

Chen, G. & Wu, J., 2001. Optimal Placement of Multiple Tuned Mass Dampers for Seismic Structures. *Journal of Structural Engineering,* 9(127), pp. 1054-1062.

Chey, M., Rodgers, G., Chase, G. & Mander, J., 2010. Using upper storeys as semi-active tuned mass damper building systems- a case study. *Bulletin of The New Zealand Society of earhquake enginerring,* 43(2), pp. 126-133.

Cho, B., Jo, J. & Joo, S., 2012. Dynamic Parameter Identification of Secondary Mass Dampers Based on Full-Scale Tests. *Computer-Aided Civil and Infrastructure Engineering,* Volume 27, pp. 218-230.

Clark Aiken and Kelly, C. P. A. I. a. K. J., 1997. *'Ongoing studies of the Foothill Communities Law and Justice Center',* Portland, Oregon: s.n.

Clinton, F., Bradford, C., Heaton, T. & Favela, J., 2005. *The Observed Wander of the Natural Frequencies in a Structure,* California: s.n.

CTBUH, C. f. B. a. U. H., 2012. *Outrigger design for High Rise Buildings,* s.l.: s.n.

CTBUH, C. f. B. a. U. H., 2014. *Tall Trends of 2014, and Forecasts for 2015,* s.l.: s.n.

CUREE, C. o. U. f. R. i. E. E., 1998. *Historic Developments in the Evolution of Earthquake Engineering,* California: s.n.

Datta, D. T., 2003. 'A state-of-the-art review on active control of structures'. *ISET Journal of Earthquake Technology,* Issue 41(1), pp. 1-17.

Den Hartog, J., 1956. *Mechanical Vibrations.* 4 éd. New York: McGraw-Hill.

Denawa, M., 2005. *Brown University Library Center.* [En ligne]
Available at: http://library.brown.edu/cds/kanto/denewa.html
[Accès le February 2015].

Dhar, S., Das, S. & Saha, P., 2015. State of the art review of shape memory alloy used in civil structures as seismic control device. *Internation Journal of Research in Engineering and Technology,* 4(13), pp. 195-203.

Douglas, I., 2013. Cities. Dans: *Cities:An environmental history.* s.l.:I. B. Tauris & Co Ltd, pp. 211-252.

Dyke, S., Spencer Jr, B., Sain, M. & Carlson, J., n.d.. *An Experimental Study of MR Dampers for Seismic Protection,* Indiana: Purdue University.

Fu, T. & Johnson, E., 2016. Semi-active control for a distributed mass damper system. *Structural Health and Monitoring.*

Ghaffarzadeh, H. & Younespour, A., 2014. Active tendons control of structures using block pulse functions. *STRUCTURAL CONTROL AND HEALTH MONITORING,* Volume 21, p. 1453–1464.

Gonzalez-Buelga, A. et al., 2015. An electromagnetic vibration absorber with harvesting and tuning. *STRUCTURAL CONTROL AND HEALTH MONITORING,* Volume 22, pp. 1359-1372.

Heysami, A., 2015. Types of Dampers and their seismic performance. *Current World,* 10(1), pp. 1002-1014.

Ikago, K., Saito, K. & Inoue, N., 2009. *Seismic Control of Buildings using Tuned Viscous Mass Dampers.* Tokyo, Proceedings of JSSI 15th Anniversary International Symposium on Seismic Response Controlled Buildings for Sustainable Society.

Ikago, K., Saito, K. & Inoue, N., 2012. Seismic control of single-degree-of-freedom structure using tuned viscous mass damper. *EARTHQUAKE ENGINEERING AND STRUCTURAL DYNAMICS,* Volume 41, pp. 453-474.

Ikeda, Y., 2016. An active mass damper designed using ARX models of a building structure. *EARTHQUAKE ENGINEERING & STRUCTURAL DYNAMICS.*

Inaudi, I. & Kelly, J., 1990. Active isolation. *U.S. National Workshop on Structural Control Research,* pp. 125-130.

Ji, X., Hikino, T., Kasai, K. & Nakashima, M., 2013. Damping identification of a full-scale passively controlled five-story steel building structure. *EARTHQUAKE ENGINEERING & STRUCTURAL DYNAMICS,* Volume 42, pp. 277-295.

Kang, J., Kim, H.-s. & Lee, D.-G., 2011. Mitigation of wind response of tall building using semi-active mass dampers. *The structural design of Tall and Special Buildings,* 20(1), pp. 552-565.

Kareem, A. K., Kijewski, T. K. & Tamura, Y., 1999. *Mitigation of Motions of Tall Buildings with Specific Examples Mitigation of Motions of Tall Buildings with Specific Examples,* s.l.: s.n.

Kareem, A. & Kline, S., 1995. ‘Performance of multiple mass dampers under random loading'. *Journal of Structural Engineering,* Volume 121, pp. 348-361.

Katz, P., PEDERSON , K. & ROBERTSON, L., 2008. Shanghai World Financial center. *CTBUH Council on Tall Buildings and Urban Habitat,* Issue ii.

Khan, F., 1965. *Design of high-rise buildings.* Illinois, ASCE, AISC Chicago Fabricators.

Kijewski and Kareem, 2000. *Estimation and Modeling of Damping and Engineering Auxiliary Damping Systems in Civil EngineeringStructures: An Overview,* s.l.: University of Notre Dame.

Koss, L. & Melbourne, W., 2014. *A review of impact dampers to control cross wind vibration of.* Melbourne, inter.noise 2014.

Kwok and Isyumov, 1998. *Aerodynamic Measures to Reduce the Wind-Induced Response of Buildings,* San Francisco: s.n.

Lai, M., Lundsford, D., Kasai, K. & Chang, K., 1996. *Viscoelastic Damper: A damper with linear or non-linear material.* s.l., WCEE: ELSEVIER SCIENCE LTD.

Landau, I., Airimitoaie, T. & Silva, A., 2015. Adaptive attenuation of unknown and time-varying narrow band and broadband disturbances. *INTERNATIONAL JOURNAL OF ADAPTIVE CONTROL AND SIGNAL PROCESSING,* Volume 29, p. 1367–1390.

Lin, G.-L., Lin, C.-C., Chen, B.-C. & Soong, T.-T., 2015. Vibration control performance of tuned mass dampers with resettablevariable stiffness. *Engineering Structures*, pp. 187-197.

Lord, J. & Ventura, C., 2016. *MEASURED AND CALCULATED MODAL CHARACTERISTICS OF A 48-STOREY TUNED MASS SYSTEM BUILDING IN VANCOUVER,* British Columbia: The University of British Columbia.

Lourenco, R., 2011. *Design, Construction and Testing of an Adaptive Pendulum Tuned Mass Damper,* Ontario: University of Waterloo.

Lu, X. et al., 2016. Improving performance of a super tall building using a new-eddy current tuned mass damper. *Structural Control and Health monitoring.*

Lynch, J., 1998. *Active Structural Control Research at Kajima Corporation,* Japan: The National Science Foundation's Summer Institute in Japan Program.

Mendis, P. et al., 2007. Wind loadings on tall buildings. *EJSE Special Issue: Loading on Structures.*

Mondal, J., Nimmala, H., Abdulla, S. & Tafreshi, R., 2014. *Tuned Liquid Damper.* Prague, International Conference on Mechanical Engineering and Mechatronics.

Mori Building Co, L., n.d.. *Mori co.* [En ligne]
Available at: https://www.mori.co.jp/en/office/china/swfc/siteplan.html
[Accès le 8 November 2015].

Nagarajaiah, S., 2009. ‘Adaptive passive, semiactive, smart tuned mass dampers: identification and control using empirical mode decomposition, hilbert transform, and short-term fourier transform’. *Structural Control and Health Monitoring,* Issue 16, p. 800–841.

Nagarajaiah, S., Riley, M. & Reinhorn, A., 1993. Control of sliding-isolated bridge with absolute acceleration feedback. *Journal of Engineering Mechanics,* 119(1), p. 2317–2332..

Nagase, T., 2000. *Earthquake Records observed in Tall Buildings with Tuned Mass Damper.* s.l., WCEE.

Obata, T., Hayashikawa, T., Sato, K. & Shimoda, K., 1996. *Analytical study of Active Vibration control on Tall Buildings.* Japan, WCEE: Elsevier Science Ltd.

Ok, S., Song, J. & Park, K., 2008. 'Optimal performance design of bi-tuned mass damper systems using multi-objective optimization'. *KSCE Journal of Civil Engineering,* 12(5), pp. 313-322.

Patil, V. & Jangid, R., 2011. Optimum multiple tuned mass dampers for the wind excited benchmark building. *Journal of Civil enginerring and Management,* 17(4), pp. 540-557.

Preumont, P. A., n.d.. *ACTIVE VIBRATION CONTROL,* Brussels, Belgium: s.n.

Purdue University, 2002. Introduction to Structural vibration control, Chapter 4. Dans: *Structural Motion Control.* Indiana: University of Purdue, pp. 217-285.

Rana, N. & Rana, S., 2014. Structural forms systems for Tall Building Structures. *SSRG International Journal of Civil Engineering,* 1(4), pp. 33-35.

Raut, B. & Jangid, R., 2013. Seismic analysis of benchmark building installed with friction dampers. *The IES Journal Part A: Civil & Structural Engineering,* 7(1), p. 2013.

Reinhorn, A. & Valles, R., 1995. *Damage Evaluation in Inelastic Response of Structures: A Deterministic Approach,* Buffalo: National Centre for.

Ribakov, Y., 2011. Using viscous and variable friction dampers for improving structural seismic response. *The structural design for Tall and Special buildings,* Volume 20, pp. 579-593.

Ribakov, Y., Blostotsky, B. & Ishakov, I., 2006. Theoretical model and laboratory tests of a variable friction damper. *European Earthquake Engineering,* 20(1), pp. 43-47.

Rozas, L., Boroschek, R., Tamburrino, A. & Rojas, M., 2016. A bidirectional tuned liquid column damper for reducing the seismic response of buildings. *STRUCTURAL CONTROL AND HEALTH MONITORING,* Volume 23, pp. 621-640.

Saito, K. & Inoue, N., 2007. A study on optimum response control of passive control systems using viscous damper with inertial mass: Substituting equivalent nonlinear viscous elements for linear viscous elements in optimum control systems.. *Architectural Institute of Japan Journal of Technology and Design,* 23(26), pp. 457-462.

Saito, K., Kurita, S. & Inoue, N., 2007. ptimum response control of 1-DOF system using linear viscous damper with inertial mass and its Kelvin-type modeling. *Journal of Structural Construction Engineering Architectural Institute of Japan,* Volume 53B, pp. 53-66.

Sakai, F., Takeda, S. & Tamaki, T., 1989. *Tuned liquied column damper- new type device for suppression of building vibration.* Nanjing, Proceedings of the International Conference on High Rise Buildings.

Scheller, J. & Starossek, U., 2011. *A versatile active mass damper for structural vibration control.* Belgium, EURODYN 2011: .

Sgobba, S. & Marano, G., 2010. Optimum design of Linear Tuned Mass Damper for building vibration. *Mechanical Sytem Signal Processing,* 24(6), pp. 1739-1755.

Sharma, A., Kumar, R., Vaish, R. & Chauhan, V., 2015. Performance of K0.5 Na0.5 NbO3 (KNN)-based Lead-free Piezoelectric Materials in Active Vibration Control. *Journal of applied ceramic technology,* 12(s1), p. E64–E72.

Soliman, I., Tait, M. & Damatty, A., 2016. Modelling and Analysis of a structure semi-active tuned liquid damper system. *Structural Control and Health Monitoring.*

Soong, Soong, T. & Reinhorn, A., 1994. Recent structural applications of active control technology. *Journal of Structural Control,* 1(1-2), pp. 5-21.

Soong, T. & Spencer , B., 2000. *ACTIVE, SEMI-ACTIVE AND HYBRID CONTROL OF STRUCTURES.* s.l., WCEE: Elsevier Science Ltd.

Sourav, G., Koushik, R. & Mishra, S., 2015. Tuned liquid column ball damper for seismic vibration control. *STRUCTURAL CONTROL AND HEALTH MONITORING,* Volume 22, pp. 1325-1342.

Spencer, . B. & Sain, M., 1997. 'Controlling buildings: A new frontier in feedback'. *IEEE Control Systems Magazine,* Issue (17)6, pp. 9-35.

Spencer, J. & Soong , T., 1999. *New applications and development of active semi active and hybrid control techniques for seismic and non seismic vibration in the USA.* Korea, International Post-SMiRT Conference Seminar on Seismic Isolation.

Tamura, Y., 2009. *Wind and tall buildings,* Tokyo: Wind research center, Tokyo Polytechnic University.

Tang, X. & Zuo, L., 2012. Simultaneous energy harvesting and vibration control of structures with tuned mass dampers. *Journal of,* 23(18), p. 2117–2127.

Taylor and Constantinou, 1996. *Fluid Dampers for Applications of Seismic Energy Dissipation and,* s.l.: Publication of Taylor Devices, Inc.

Taylor, D. P., 2003. *History, Design, and applications of fluid dampers in structural engineering,* NY: Taylor Devices, Inc..

Thao, N. & Uchida, K., 2015. ACTIVE AND REACTIVE POWER CONTROL TECHNIQUES BASED ON FEEDBACK LINEARIZATION AND FUZZY LOGIC FOR THREE-PHASE GRID-CONNECTED PHOTOVOLTAIC INVERTERS. *Asian Journal of Control,* 17(5), p. 1522–1546.

Tuan, A. & Shang, G., 2014. Vibration Control in a 101-Storey Building Using a. *Journal of Applied Science and Engineering,* 17(No. 2), pp. 141-156.

Tuan, A. & Shang, G., 2014. Vibration control in a 101-storey building using a Tuned Mass Damper. *Journal of Applied Science and Engineering,* 17(2), pp. 141-156.

Verdirame, J., 2003. *Design of Multi-Degree-of-Freedom Tuned-Mass,* Massachusetts : Massachusetts Institute of Technology .

World Wondering, 2013. *World Wondering:Preview- CN Tower.* [En ligne]
Available at: http://www.nevworldwonders.com/2013/10/preview-cn-tower.html
[Accès le 9 November 2015].

World, V. a. o. t., n.d.. *Visit all of the World.* [En ligne]
Available at: http://vizts.com/burj-khalifa-world-tallest-skyscraper/
[Accès le 8 November 2015].

Wu, J. & Li, Q., 2003. STRUCTURAL PERFORMANCE OF MULTI-OUTRIGGERBRACED. *THE STRUCTURAL DESIGN OF TALL AND SPECIAL BUILDINGS,* Volume 12, pp. 155-176.

Wu, T., 2001. *DESIGN OF BASE ISOLATION SYSTEM FOR BUILDINGS,* MASSACHUSETTS: MASSACHUSETTS INSTITUTE OF TECHNOLOGY.

Xie, J., 2012. *Aerodynamic optimization in super-tall building designs ,* Shanghai: The Seventh International Colloquium on Bluff Body Aerodynamics and its Application.

Xu, K. & Igusa, T., 1992. 'Dynamic characteristics of multiple substructures with closely spaced frequencies'. *Earthquake Engineering and Structural Dynamics,* Volume 21, pp. 1059-1070.

Yamaguchi, H. & Harnpornchai , N., 1993. 'Fundamental characteristics of multiple tuned mass dampers for suppressing harmonically forced oscillations'. *Earthquake Engineering and Structural Dynamics,* Volume 22, pp. 51-62.

Yang, J., Wu, J., Reinhorn, A. & Riley, M., 1996. Control of sliding-isolated buildings using sliding-mode control. *Journal of Structural Engineering,* 122(2), p. 179–186.

Zemp, R., de la Llera, J. & Roschke, P., 2011. Tall building and vibration control using a TM-MR damper assembly. *Earthquake Engineering and Structural Dynamics,* Volume 40, pp. 257-271.

APPENDIX A: ADDITONAL PATPD PHOTOS

Figure 279: PATPD SUPPORT

Figure 280: SIDE VIEW PATPD

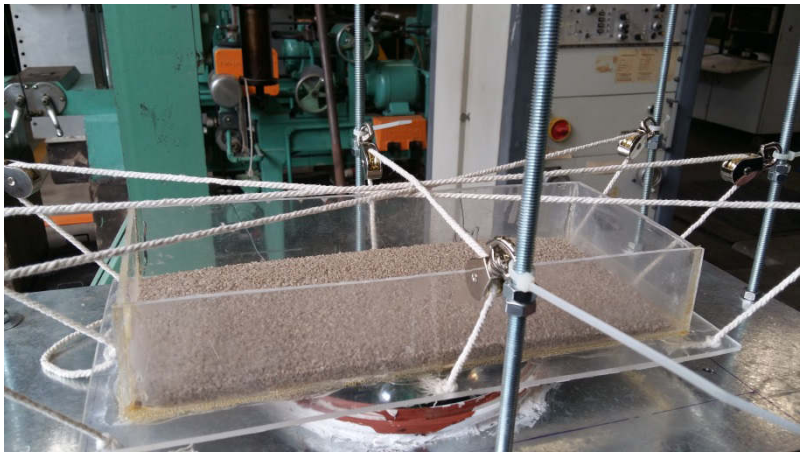

Figure 281: PATPD PULLEYS

Figure 282: STRAIN GAUGE USED IN TESTS

Figure 283: STRAIN GAUGE CONNECTION AND SET UP

APPENDIX B: SAP SIMULATION

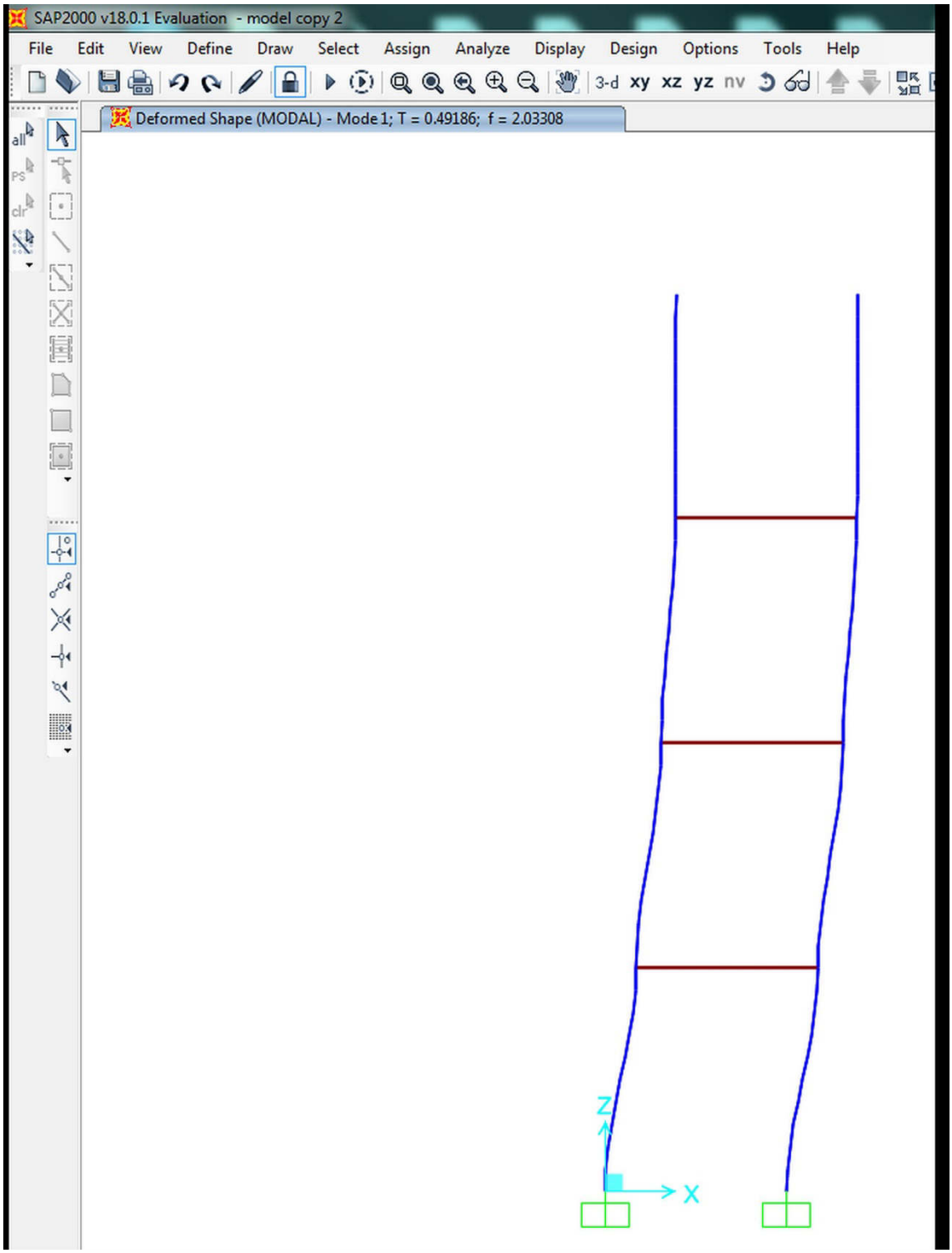

Figure 284: Translation Mode 1

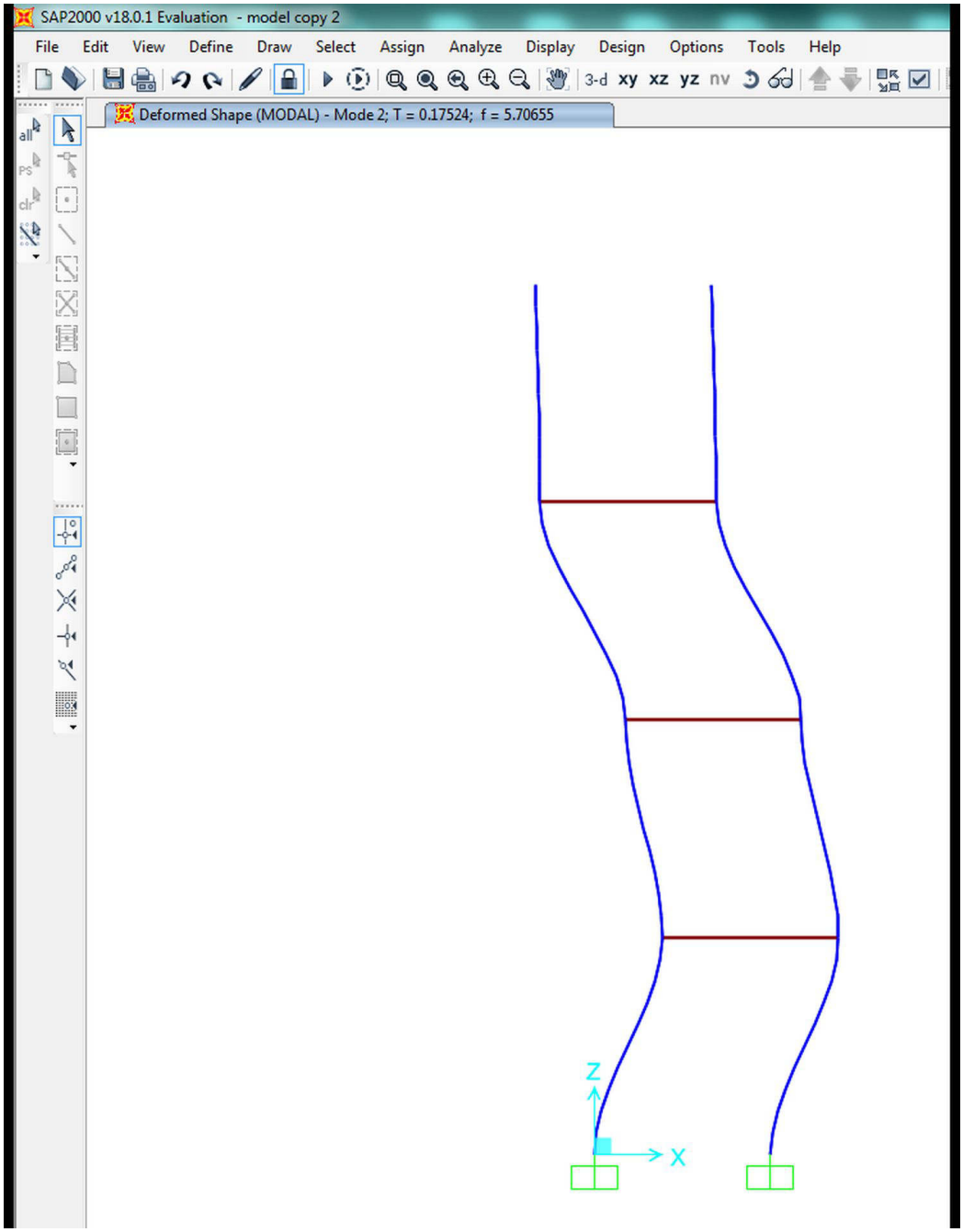

Figure 285: Translation Mode 2

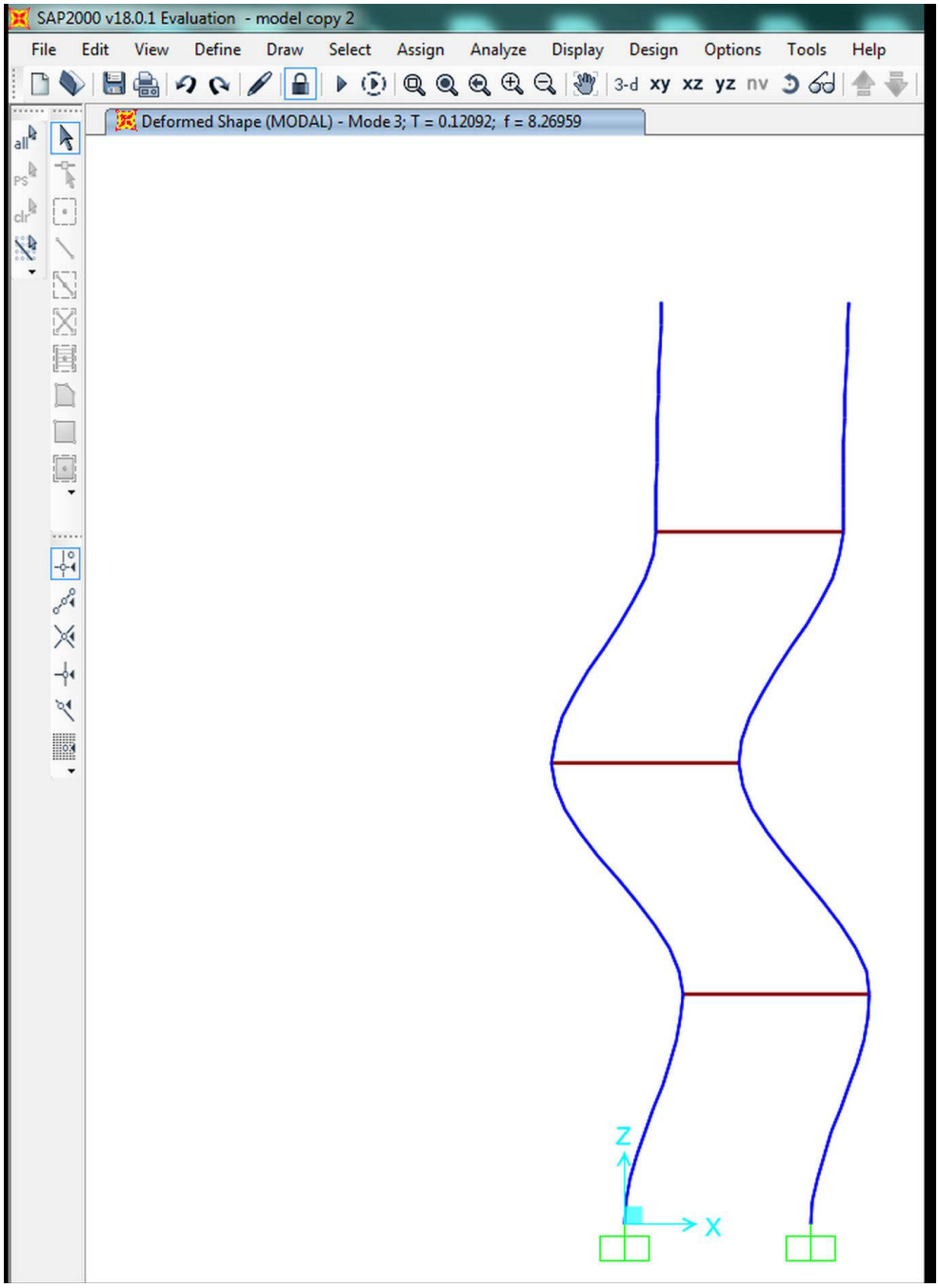

Figure 286: Translation Mode 3

APPENDIX C: Earthquake profile extrapolation

Code used for conversion of acceleration-time to displacement time (MATLAB):

```
%  earthquake-NS.m
%
%  Script which inputs, plots and analyzes the 1940 El Centro
%  earthquake north-south acceleration data.

%  Input the data
cd 'C:\Users\Nicole\Documents'
data = dlmread('elcentro_NS.csv',',');      %original
%  Column 1 time ; Column 2 acceleration G's
accel = 386.4*data(:,2);
time = data(:,1);
dt=time(2)-time(1);
%  Create the times that go with the acceleration.
%  Plot the time-accel data
%figure
subplot(3,1,1)
plot(time,accel,'r-')
grid
title('N-S Acceleration History 1940 El Centro EarthQuake')
xlabel('time (sec) ')
ylabel('accel. (in/s^2)')
axis([0 31 -150 150])

%  Find the maximum and minimum values of the acceleration data
%  and print them.

[amax,imax] = max(accel);
[amin,imin] = min(accel);
fprintf('\nThe max accel is %5.3f in/s^2 and occurs at time = %5.3f sec.\n
',amax,time(imax))
fprintf('The min accel is %5.3f in/s^2 and occurs at time = %5.3f sec.\n',amin,time(imin))

grd_disp(1)=0
grd_vel(1)=0
for count=1:(length(accel)-1)
   grd_vel(count+1)=grd_vel(count)+ accel(count)*dt;
   grd_disp(count+1)=grd_disp(count)+ grd_vel(count)*dt;
end

for count=1:(length(accel))
      grd_disp(count)=grd_disp(count)-100/53.75*(count-1)*dt;
end

%grd_disp=detrend(grd_disp)';
%grd_vel=detrend(grd_vel)';
%%grd_time = [0:0.02:(length(grd_disp)-1)*0.02];

subplot(3,1,2)
plot(time,grd_vel,'r-')
grid
title('N-S Velocity History 1940 El Centro EarthQuake')
xlabel('time (sec) ')
```

```
ylabel('vel. (in/s)')

subplot(3,1,3)
plot(time,grd_disp,'r-')
grid
title('N-S Displacement History 1940 El Centro EarthQuake')
xlabel('time (sec) ')
ylabel('position (in)')

displacment_NS = transpose(grd_disp);
```

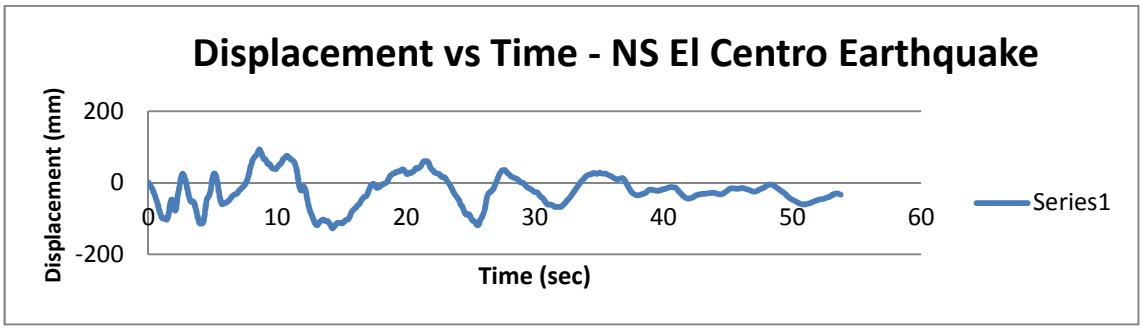

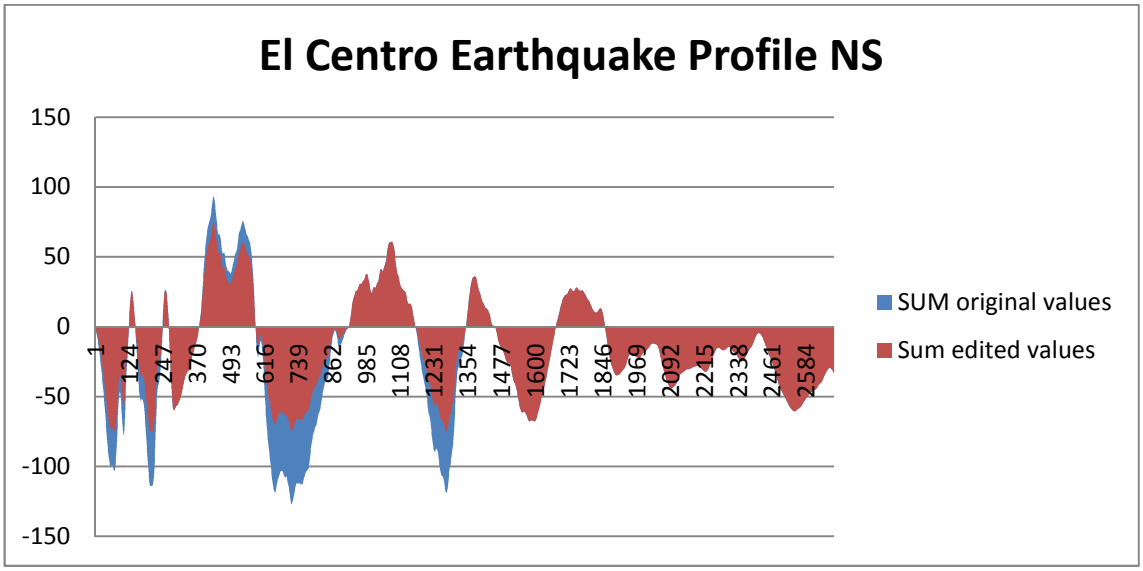

The only values edited were those which peaked above 75mm, these were adjusted manually to fall within the limit but still retain a similar profile shape as that of El Centro.

http://faculty.mercer.edu/jenkins_he/elcentro_NS.txt
http://faculty.mercer.edu/jenkins_he/
http://www.vibrationdata.com/elcentro.htm
Time History Data File Reference:
Pacific Earthquake Engineering Research Center
http://peer.berkeley.edu/research/motions/
CIT-SMARTS
http://www.eerl.caltech.edu/smarts/smarts.html
Type of Digital Strong-Motion Data: Corrected